THE UNIVERSITY
of EDINBURGH

Tenascin-C: A marker and driver of inflammation

James Ozanne

This thesis is presented for the degree of Doctor of Philosophy at The University of Edinburgh

2019

Declaration

I declare that this thesis has been composed entirely by the candidate, James Henry John Ozanne. This work has not previously been submitted for a Doctor of Philosophy, a degree or any professional qualification. I have done all the work, unless acknowledged otherwise. All sources of information have been acknowledged.

James Ozanne

Acknowledgments

First and foremost, I'd like to thank my primary supervisors, Prof. Colin Farquharson and Prof. Kim Midwood, for their fantastic support throughout my PhD. It is with their guidance and scientific knowledge that I have been able to compile this thesis and I thank them for that. The lessons they have taught will no doubt stay with me for the rest of my scientific career and beyond.

I would also like to thank my industrial collaborators and supervisors at Axis Shield Diagnostics Ltd. including Dr David Pritchard, Dr Jeff Brady and Dr Mel Lewis. Their supervision helped guide my work and gave me invaluable experience and appreciation of working outside an academic environment. I would like to thank Mel in particular for her patience, technical assistance, and guidance in the lab which allowed me to achieve all I did during my time in Dundee.

At the Roslin institute I would like to thank all of the technical and support staff who supported my research. In particular I would like to thank Elaine Seawright for her technical guidance and assistance, particularly in regard to teaching me a range of techniques including immunohistochemistry. I also thank my BSc honours project student Brandon Shek whose hard work under my supervision was a great aid. I also give thanks to Prof Elspeth Milne and the Easter Bush Pathology staff whose aid with the histopathological investigations of this thesis was invaluable. The work of this thesis also involved a substantial amount of animal work which was assisted by the staff of the institute's biological resource facility. In particular I'd like to thank Darren Smith whose excellent experimental assistance and day to day handling of my mice made my job a whole lot easier.

I also give my gratitude to the funders of this project, Medical Research Scotland (MRS) and Axis Shield Diagnostics Ltd, as without their generous financial support this PhD would not have been possible. In particular I also give thanks to Dr Alex Graham, scientific advisor at MRS, whose tireless efforts in organising the various opportunities and meetings MRS gave me was much appreciated.

I also thank the staff of the Easter Bush Science Outreach Centre (EBSOC) whose outreach opportunities broadened my skills and enriched my time at Roslin.

I'd also like to give thanks to my friends and family in Edinburgh and further afield who have supported me throughout my studies. This includes a special thank you to my parents and Amy Wieckowski, whose support and understanding has helped me get through the good and bad.

Abstract

Tenascin-C, the founding member of the matricellular tenascin family, is a large multifunctional hexameric extracellular matrix (ECM) glycoprotein. It is abundantly expressed in the developing embryo but its expression becomes tightly regulated in the adult. However, during inflammatory responses tenascin-C becomes highly upregulated where it acts to create a local pro-inflammatory 'niche'. In this pro-inflammatory role tenascin-C has been implicated in the pathogenesis of a variety of chronic inflammatory diseases including rheumatoid arthritis (RA) and inflammatory bowel disease (IBD), both of which are characterised by upregulated tenascin-C locally and systemically.

The work of this thesis has looked to expand upon this earlier work, identifying tenascin-C as a key driver as well as marker of inflammation, and further probe its mechanistic role in the inflammatory response and utility as a biomarker of inflammatory disease.

To answer the first question regarding tenascin-C's role in pathological inflammation a murine Dextran Sulphate Sodium (DSS) model of chemically induced colitis was utilised. This thesis details the spatial and temporal expression of tenascin-C in the colon under basal conditions as well as the inflammatory state of the DSS model. Tenascin-C demonstrated a marked upregulation within the inflamed mucosa coinciding with the upregulation of other pro-inflammatory mediators and immune cell infiltration.

Following this descriptive characterisation, subsequent studies probed the mechanistic relevance of this upregulation utilising the same model in combination with a tenascin-C knockout mouse. These studies showed a protective effect of tenascin-C's genetic ablation on the severity of the colitis induced. This included reductions in gross pathology as well as histopathology including lower inflammation and tissue damage observed during the acute stage.

Finally, with this mechanistic link clearly established between tenascin-C and the inflammatory diseased state this thesis aimed to explore tenascin-Cs utility as a

disease marker, with a focus on RA. To this end, a number of novel immunoassays were established and validated for the measurement of tenascin-C and autoantibodies against in human serum samples. Screening of serum samples with these assays showed significantly higher levels of tenascin-C or autoantibodies against it in the serum of RA patients compared to healthy controls. These changes were not entirely RA specific however with a number of other inflammatory diseases tested also showing higher serum tenascin-C levels.

The work described herein has utilised the DSS colitis model in combination with tenascin-C knockout mice to demonstrate the role of tenascin-C as a driver of inflammatory disease and has further shown translational relevance as a disease marker in human patients.

Publications & Awards

Published Abstracts

Ozanne J, Shek B, Milne E, McLachlan G, Midwood KS, Farquharson C (2019). Tenascin-C: A Driver of Inflammatory Bowel Disease. *International Journal of Experimental Pathology*, 100, A1-a45. British Society for Matrix Biology Spring 2019 Meeting: "Stroma, Niche, Repair", abstract 42, poster presentation.

Awards

British Society for Matrix Biology reporter bursary - 2019

Birrell-Gray travelling scholarship – 2019

British Society for Immunology travel award – 2019

Abbreviations

95% CI	95% Confidence interval
AAV	Antineutrophil cytoplasmic antibody-associated vasculitis
ACPA	Anti-citrullinated protein autoantibodies
ADAMTS	A disintegrin and metalloproteinase with thrombospondin motifs
AF488	Alexa Fluor 488
AF594	Alexa Fluor 594
ANOVA	Analysis of variance
APC	Antigen presenting cell
AS	Ankylosing spondylitis
AUC	Area under the curve
BLAST	Basic local alignment search tool
bp	Base pairs (nucleotides)
BRF	Biological resource facility
BSA	Bovine serum albumin
CARD	Caspase recruitment domain-containing protein
CCL	chemokine C-C motif ligand
CCN4	Cellular Communication Network Factor 4
CCP	Cyclic citrullinated peptide
CD	Crohn's disease
CD	Cluster of differentiation
cDNA	Complementary DNA
ColIV	Type IV collagen
CP	Colonic patch
CRP	C-reactive protein

Ct	Cycle threshold
cTNC	Citrillunated tenascin-C
cTNC5	Citrillunated tenascin-C peptide 5
CXCL	chemokine C-X-C motif ligand
Da	Daltons
DAI	Disease activity index
DAMP	Damage associated molecularl pattern
DAPI	4′,6-Diamidino-2-phenylindole
DAS28	Disease Activity Score 28 joints
DC	Dendritic cell
DC Assay	Detergent compatible assay
dH2O	Deionised water
DKK1	Dickkopf-1
DMEM	Dulbecco's modified Eagle's medium
DMSO	Dimethyl sulfoxide
DNA	Deoxyribonucleic acid
DNFB	Dinitrofluorobenzene
dNTP	Deoxyribonucleotide triphosphate
DSS	Dextran sulphate sodium
DTT	Dithiothreitol
ECM	Extracellular matrix
EDTA	Ethylenediaminetetraacetic acid
EGF-L	Epidermal growth factor-like
EGFR	Epidermal growth factor receptor
ELISA	Enzyme linked immunosorbent assay
EpCAM	Epithelial cell adhesion molecule

ESR	Erythrocyte sedimentation rate
EtOH	Ethanol
EVX1	Even-skipped homeobox 1
FAK	Focal adhesion kinase
FBG	Fibrinogen-like globe
FBS	Fetal bovine serum
FGF	Fibroblast growth factor
FMF	Familial Mediterranean fever
FNIII	Fibronective type 3
GALT	Gut associated lymphoid tissue
GI	Gastrointestinal
GM-CSF	Granulocyte-macrophage colony-stimulating factor
H&E	Haematoxylin and eosin
HGF	Hepatocyte growth factor
HIF	Hypoxia inducible factor
His-tag	Polyhistidine-tag
HMGB1	High mobility group box 1
HNK-1	Human natural killer-1
HPLC	High performance liquid chromatography
HRP	Horseradish peroxidase
IBD	Inflammatory bowel disease
IFN	Interferon
IgA	Immunoglobin A
IgE	Immunoglobin E
IgG	Immunoglobin G
IHC	Immunohistochemistry

IHH	Indian hedgehog
IIM	Idiopathic inflammatory myositis
IKK	Inhibitor of κB kinase
IL	Interleukin
ILF	Isolated lymphoid follicle
IMID	Immune-mediated inflammatory disease
IP	Immunoprecipitation
IRAK	IL-1R-associated kinase
ISPCR	in situ polymerase chain reaction
IκB	Inhibitor of κB
JIA	Juvenile idiopathic arthritis
KO	Knock out
LC-MS/MS	Liquid chromatography-tandem mass spectrometry
LDS	Lithium dodecyl sulfate
LN_2	Liquid nitrogen
LPS	Lipopolysaccharide
LYVE-1	Lymphatic vessel endothelial hyaluronan receptor 1
MAPK	Mitogen activated protein kinase
MDSC	Myeloid derived suppressor cell
MEF	Mouse embryonic fibroblasts
MMP	Matrix metalloproteinase
MPO	Myeloperoxidase
mRNA	Messanger RNA
mTOR	Mammalian target of rapamycin
MW	Molecular weight
MWCO	Molecular Weight Cut Off

MyD88	Myeloid differentiation factor 88
***Myd88*$^{-/-}$**	MyD88 knock out
NBF	Neutral buffered formalin
NCBI	National Center for Biotechnology Information
NFκB	Nuclear factor κB
NH4OAc	Ammonium acetate
NS IgG	Non-specific IgG
NTC	No template control
OA	Osteoarthritis
OA	Osteoarthritis
OCT	Optimal Cutting Temperature
OID	Other inflammatory disease
OTX2	orthodenticle homolog 2
PAGE	Polyacrylamide gel electrophoresis
PAMP	Pathogen asscoiated molecular pattern
PBS	Phosphate buffered saline
PBST	Phosphate buffered saline Tween 20
PCR	Polymerase chain reaction
PDGF	Platelet derived growth factor
PG	Prostaglandin
PKB	Protein kinase B
PMF	Proteomics and Metabolomics Facility
POU3F2	POU domain class 3 transcription factor 2
PR	Polymyalgia rheumatica
PRR	Pattern recognition receptor
PTM	Post-translational modification

qPCR	Quantitative polymerase chain reaction
RA	Rheumatoid arthritis
***Rag1*$^{-/-}$**	Rag1 knock out
RF	Rheumatoid factor
RIPA	Radioimmunoprecipitation assay
RNA	Ribonucleic acid
ROC	Receiver operating characteristic
ROS	Reactive oxygen species
RPM	Revolutions per minute
RT	Reverse transcription
rTNC5	Native tenascin-C peptide 5
SAGE	Serial analysis of gene expression
SDS	Sodium dodecyl sulphate
SILT	Solitary intestinal lymphoid tissues
SLE	Systemic lupus erythematosus
SNP	single nucleotide polymorphism
SPECT	Single-photon emission computed tomography
SPF	Specific pathogen free
STAT	Signal transducer and activator of transcription
StdDev	Standard deviation
TA	Tenascin assembly domain
TAE	Tris-acetate EDTA
TAK1	TGF-β activated kinase 1
Tc cell	Cytotoxic T cell
TCR	T cell receptor
TE	Tris-EDTA

TF	Transcription factor
TFA	Trifluoroacetic acid
TGFβ	Transforming growth factor β
Th cell	Helper T cell
TLR	Toll-like receptor
***Tlr4*$^{-/-}$**	TLR4 knock out
TMB	3,3',5,5'-Tetramethylbenzidine
Tnc	Tenascin-C
***Tnc*$^{-/-}$**	Tenascin-C knock out
TNF	Tumour necrosis factor
Treg cell	Regulatory T cell
UC	Ulcerative colitis
WB	Western blot
WT	Wild-type
αSMA	α-Smooth muscle actin

Table of contents

List of figures

List of tables

Chapter 1 Introduction

1.1 Inflammation

1.1.1 The inflammatory response

Inflammation, from the Latin *inflammare* (to set on fire), was first clinically described in the first century AD by the scholar Celsus in his medical encyclopaedia '*De Medicina*'. He classified inflammation symptomatically which formed the basis of its diagnosis, still in use today, using the five cardinal signs; redness, swelling, increased heat, pain, and loss of function (Scott et al., 2004). In more modern medical terms' inflammation is defined as the non-specific and largely immunovascular response launched by the body in response to a challenge to homeostasis, such as that caused by infection or tissue injury. The purpose of this response is to ultimately restore normal tissue function by repelling the threat, such as by eliminating an invading pathogen, and subsequently initiating tissue remodelling and repair (Medzhitov, 2008). The exact course of the response is complex and varied, reflecting the wide variety of insults which may present as a challenge and the accompanying variety of responses the body can deploy to counteract them. In its simplest terms however, a model acute inflammatory response can still be subdivided into three broad categories; initiation, propagation, and resolution (Chen et al., 2018).

1.1.2 Initiation

Inflammation begins with the initiation stage where the response is triggered by detection of either an extreme deviation of a homeostatic variable, eliciting a stress response, or a threat which could disrupt homeostasis, eliciting a defence response. This detection utilises a variety of mechanisms and can be carried out by the majority of cells although specialised sensory cells, such as sentinel innate immune cells, are the key orchestrators (Chovatiya and Medzhitov, 2014).

The defence response encompasses the classical inflammatory induction pathway with its sensors the pattern recognition receptors (PRRs). PRRs encompass several families of intra- and extracellular receptors which bind a wide variety of exogenous and endogenous ligands from nucleic acids to lipids and proteins (Takeuchi and Akira, 2010). The first of these, recognising exogenous ligands, follow Charles Janeway's

theory of the 'Infectious Non-self' and rely on recognition of non-self derived pathogen associated molecular patterns (PAMPs). PAMPs constitute conserved elements of pathogens which are distinguishable from the self and thus their presence within a normally sterile tissue would suggest a barrier breakdown or pathogenic invasion (Janeway, 1992, Broggi and Granucci, 2015). A prototypical example of this type of inducer and sensor would be lipopolysaccharide (LPS), a bacterial outer-membrane component not found on eukaryotic cells, which is recognised by the PRR Toll-like receptor 4 (TLR4) (Bryant et al., 2015). The second set of patterns recognised by PRRs are the endogenous damage associated molecular patterns (DAMPs) which follow Polly Matzinger's 'Danger Theory'. This theory correctly proposed the existence of a variety of endogenously derived patterns recognised by PRRs which only become available for detection upon cellular or tissue damage (Matzinger, 1994, Broggi and Granucci, 2015). DAMPs can be derived from a variety of cellular and tissue matrix sources which when damaged release detectable DAMPs as breakdown products or due to loss of compartmentalisation or sequestration away from sensors (Medzhitov, 2008). As their name would suggest the presence of these patterns signals that cellular or tissue injury has occurred and thus activates the inflammatory response in response to this. A prototypical example in this case is the protein High mobility group box 1 (HMGB1) which normally functions to stabilise nucleosomes and thus in healthy cells is safely sequestered in the nucleus (Celona et al., 2011). However, in the case of necrosis membrane integrity is lost and HMGB1 is released extracellular where it can act in a pro-inflammatory manner. This includes by acting as a ligand for the PRR TLR4 and demonstrates the cross-talk between these two arms of the PRR system (Broggi and Granucci, 2015).

In contrast to the defence response the stress response is triggered by sensing a direct deviation of a variable from a homeostatic set point. This deviation is detected by the sensors in the variety of homeostatic regulatory systems, for example elevated temperature detected by heat-shock factors (Buchman, 2002). This stress can be extra- or intracellular in nature and if it is extreme or persistent enough it can likewise lead to induction of inflammation in an attempt to restore homeostasis (Chovatiya and Medzhitov, 2014).

1.1.3 Propagation and effector function

Having initiated the response following inducer detection the inflammatory response is first propagated by the production, release, or activation of a range of pro-inflammatory mediators. These can be classified into seven broad groups which encompass; cytokines, chemokines, lipid mediators, vasoactive amines, vasoactive peptides, complement components, and proteolytic enzymes (Medzhitov, 2008). These mediators can be produced by many cell types under inflammatory conditions although they are primarily produced by immune cells such as resident macrophages early in the response. These mediators can act both locally and systemically on target effector cells to induce and activate a range of functions resulting in development of inflammation (Medzhitov, 2008).

As a primarily immunovascular response the immune system and vasculature are key effectors of inflammation. Mediators act to activate the local vasculature to dilate and increase in permeability resulting in localised oedema. This delivers a range of circulating plasma components which aid in both pathogen removal, such as complement and antibodies, and tissue repair, such as fibrin and coagulation factors, to the site of challenge (Medzhitov, 2008). These vascular changes additionally facilitate the recruitment of leukocytes from the blood with upregulation of expression of leukocyte adhesion molecules on the endothelium occurring as well. These changes synergise with the immune cell mobilising and chemotactic action of other mediators resulting in leukocyte extravasation and infiltration into the inflamed site (Medzhitov, 2008).

Immune cell recruitment initially consists primarily of neutrophils, followed by other myeloid cells such as monocytes, and finally the lymphocytes. The initial innate response functions primarily to eliminate pathogens, clear tissue debris, and release further inflammatory mediators to fine tune the response and local tissue to the threat being faced. This paves the way for the later arrival of lymphocytes which, further aided by antigen-presentation, mount the adaptive immune response alongside production of their own repertoires of pro-inflammatory mediators (Barton, 2008).

1.1.4 Resolution

As a correctional response to challenge the ultimate goal of the inflammatory response is to successful resolve with resumption of homeostasis and normal tissue function. This was once thought to be simply a passive process whereby elimination of the original threat resulted in the loss of pro-inflammatory inducers and thus the downregulation and eventual cessation of the response. It is now appreciated however that inflammatory resolution is in fact an active process with its own inducers, drivers, and regulators (Buckley et al., 2013).

The inducers of resolution are still being elucidated although it has been shown that they appear based on feedback loops from the initial signals and effectors of the inflammatory response (Serhan and Savill, 2005). The best example of this to date has been the discovery that efferocytosis of spent neutrophils, key early inflammatory effectors, by macrophages results in a promotion of a pro-resolution macrophage polarisation (Ortega-Gomez et al., 2013). In addition to induced pro-resolution cell types there are also intrinsic populations of immunomodulatory cell types such as myeloid derived suppressor cells (MDSCs) (Budhwar et al., 2018) and T regulatory (Treg) cells (Qiao et al., 2017). The recruitment of these anti-inflammatory cells to sites of inflammation therefore might likewise help promote resolution as the inflammatory response progresses.

Much like the initial pro-inflammatory response resolution likewise has a variety of its own, and even shared in some pleiotropic cases, signalling mediators. These include anti-inflammatory cytokines, such as interleukin (IL)-10, lipid mediators, such as resolvins, and hormones such as glucocorticoids (Headland and Norling, 2015). These mediators act to counteract their pro-inflammatory counterparts by supressing their signalling and production. They also act to promote immune cell deactivation via apoptosis or egress via vasculature and block further recruitment. Furthermore, they actively promote downregulation of damaging anti-microbial and degradative processes in favour of those of repair such as production of growth factors to promote parenchymal and stromal cell regeneration (Headland and Norling, 2015). Thus, with repair and resumption of normal function this stage successfully ends the model acute inflammatory response, the stages of which are finally summarised in figure 1.1.

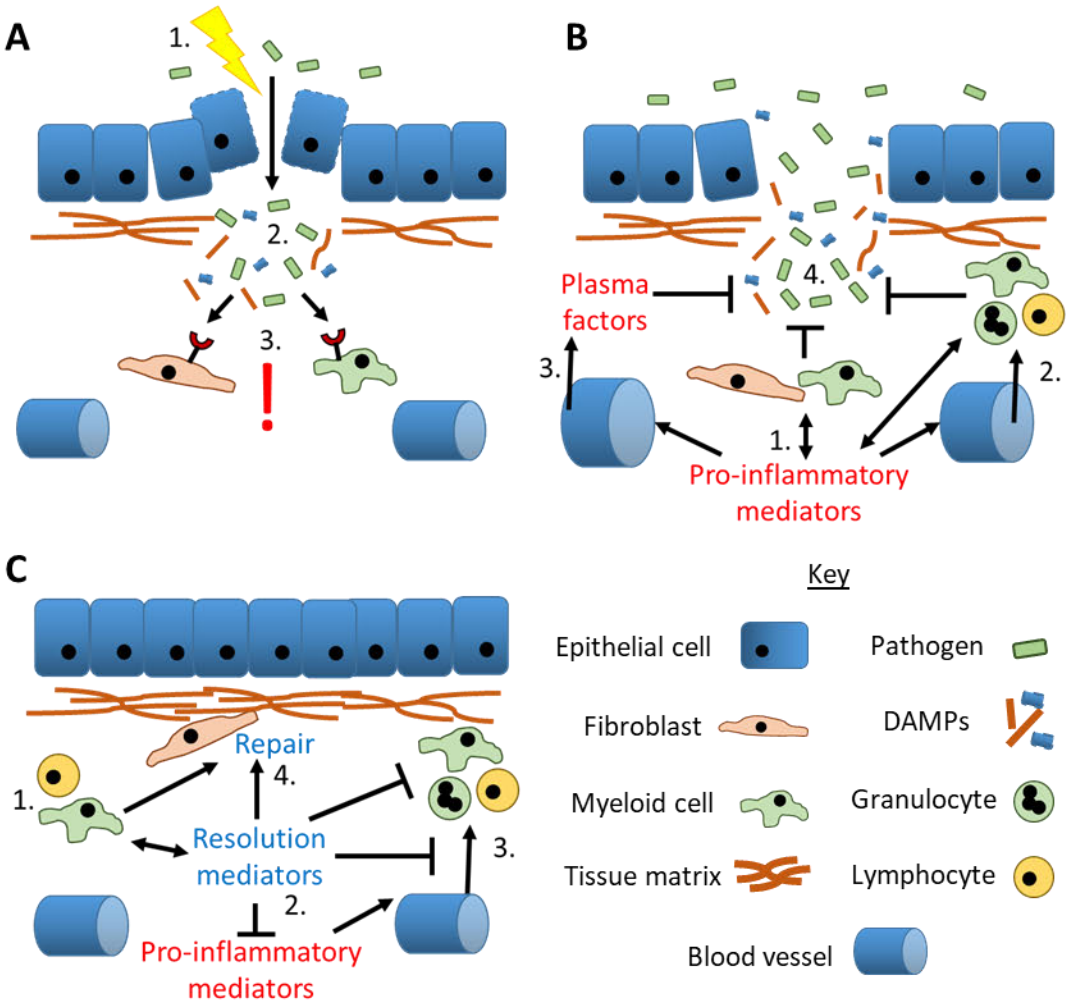

Figure 1.1 Outline of the stages of the acute inflammatory response

(A) Initiation: Tissue injury or pathogen invasion occurs (1.) which releases a variety of exogenous pathogen associated and endogenous damage associated molecular patterns (PAMP and DAMPs) into the underlying tissue (2.). These molecular patterns are detected by local stromal and immune cells by pattern recognition receptors triggering the inflammatory response (3.).
(B) Propagation and effector function: The activated local stromal and immune cell populations produce a variety of pro-inflammatory mediators in response to the challenge (1.). These act on the local vasculature to facility immune cell recruitment to the site as well as the activation of these cells (2.). Additionally, inflammatory plasma components also extravasate from the vasculature (3.). Together these effectors act to repel the challenge through functions such as pathogen entrapment and killing (4.).
(C) Resolution: With the elimination of the original threat immune cells adopt new resolving phenotypes and produce pro-resolution mediators (1.). These act to inhibit pro-inflammatory mediators (2.), as well as other immune cells inflammatory effector functions and recruitment (3.). Furthermore, resolving mediators also promote debris clearance and tissue repair by immune and stromal cells (4.) which leads to the resumption of homeostasis ending the response.

1.1.5 Chronic inflammation and disease

The inflammatory response clearly plays a positive role in normal physiology as a mechanism to counteract challenges. This is evidenced by the evolutionary conservation of the process (Straub and Schradin, 2016) and the increased morbidity and mortality, from infection and other complications, seen in those in which the process is deficient (Nathan, 2002). However, the inflammatory response is not always positive for health with a dysregulated response potentially severely damaging. This can be exemplified in the case of sepsis whereby a hyperactive response to a particularly potent pathogen derived inflammatory inducer causes rapid organ failure and subsequent death in the host (Cohen, 2002). This starkly demonstrates the severity of damage inflammation can self-inflict, far in excess of the original pathogen challenge, and thus the need to tightly regulate the process.

In recent decades a different type of inflammatory dysregulation has come to prominence however grouped under the umbrella term of chronic inflammatory diseases. Chronic inflammation as its name suggests is characterised by a continuous or recurrent response occurring over prolonged periods, from many months to years, far outlasting the classical acute response detailed above (Nathan and Ding, 2010). Chronic inflammation can occur simply due to a failure to eliminate the offending insult with persistent infection, such as that caused by *Mycobacterium tuberculosis*, or repeated irritation, such as that caused by silica dust inhalation, classic examples (Pahwa and Jialal, 2019). An increasing number of chronic inflammatory conditions have been characterised by the absence of obvious pathological challenge and instead appear a direct result of immune dysregulation and a failure of inflammatory resolution (Nathan and Ding, 2010).

These wide varying diseases, covering a range of organ systems and presentations, are broadly classified as immune-mediated inflammatory diseases (IMIDs) (Rahman et al., 2010). Matching their variety, a range of shared mechanisms can drive these disorders which can be sub-classified on a spectrum ranging from autoimmune to autoinflammatory mediated. Autoimmunity is characterised by a loss of tolerance with the development of a pathological immune response against the self (Doria et al., 2012). The disease systemic lupus erythematosus (SLE) is a classic example, being

characterised by the development of disease driving autoantibodies against a range of nuclear derived autoantigens (Rekvig et al., 2012). Autoinflammation in comparison is characterised by a breakdown in immune regulation with either overactivation of pro-inflammatory pathways or deficiencies in anti-inflammatory ones (Doria et al., 2012). A paradigm of these diseases would be familial Mediterranean fever (FMF) in which a deactivating mutation in a negative regulator of the inflammasome leads to spontaneous overproduction of the pro-inflammatory cytokine IL-1β and thus disease (Papin et al., 2007).

The rise to prominence of the IMIDs has been in part spurred by epidemiological changes with many of the diseases of rising prevalence globally. Indeed, prevalence while varying substantially by population studied is already high in the western world with estimates of an average prevalence between 5-7% (Kuek et al., 2007, El-Gabalawy et al., 2010). Their threat to health is further compounded by their usually high burden on both patients and society. For patients this is reflected in both their significantly impaired quality of life due to pain, disability, depression, and anxiety (Russell et al., 2011, Enns et al., 2018), as well as their heightened incidence of mortality and other comorbidities (El-Gabalawy et al., 2010). In terms of society the conditions chronic duration and disabling nature lead to high socioeconomic costs due to decreased work-related productivity (Jacobs et al., 2011) as well as the need for expensive extended health and social care (Baumgart et al., 2019).

The reasons for the increase in prevalence of IMIDs is an area of active research in which several theories have been posited. Most rest on a common base theory, stemming from the field of evolutionary biology, which proposes that humans are maladapted to their modern environment which leads to disease (Okin and Medzhitov, 2012). Sociological changes in recent decades which have hastened or are a result of these environmental factors have thus led to increased disease prevalence. The increase in lifespans due to modern medicine and resulting aging populations seen in most industrialised countries is one such sociological factor. IMID incidence increases with age and ageing is characterised by a gradual increase in systemic inflammation, termed inflammaging (Franceschi and Campisi, 2014). This is hypothesised to occur due to positive selection for pro-inflammatory systems occurring due to their ability to help

fend off challenge, such as infection, early in life. As the subsequent long term detrimental effects of these systems mainly become apparent at post-reproductive ages they are thus selected for in the population as they result in an increase in reproductive fitness (Straub and Schradin, 2016). Environmental sociological factors are also implicated in IMID pathogenesis with the comparative cleanliness of modern living conditions implicated. The detriments of this lifestyle is summarised in the hygiene hypothesis that states that the immune system is adapted to function in an unsterile environment and thus in the absence of microbial challenge becomes dysregulated resulting in IMIDs (Okada et al., 2010). In addition, modern environmental stressors are another factor implicated in IMID development with exposure to irritants from smoking and via pollution both associated with inflammatory diseases (Gawda et al., 2017). Finally, diet is another potential stressor with the western diet associated with IMIDs due to its propensity to lead to obesity and dysbiosis of the gut microbiota which can both cause inflammation aggravating stress (Versini et al., 2014).

In summary the chronic inflammatory IMIDs represent a growing threat to global health and already represent a large burden on both patients and societies as a whole. Their threat is further amplified by their often complex and uncertain aetiology which negatively impacts their medical management by for example hindering development of effective curative therapies. Going forward the work of this thesis will predominantly focus on the archetypal IMID inflammatory bowel disease, an umbrella term for inflammatory diseases of the gastrointestinal tract.

1.2 Inflammatory bowel disease (IBD)

Before delving into the pathology of IBD it is pertinent to first assess the context in which the disease arises in the gastrointestinal (GI) system, considering this major organ systems overall function as well as its immune components.

1.2.1 The gastrointestinal system

The human GI system is a major organ system responsible for the digestion of ingested foodstuffs so that nutrients can be extracted and adsorbed into the body. Multiple organs co-ordinate to achieve this goal and make up the GI tract, through which ingested food passes, as well as the accessory organs which aid digestion. The GI tract begins at the mouth where food first enters the tract and is mechanical broken down by mastication and by digestive enzymes produced by the salivary glands. Food is then passed through the pharynx and oesophagus to the stomach where it is mixed with gastric acid and digestive enzymes for further digestion. The digestate, called chyme, then passes, via the pyloric sphincter, into the duodenum, the first segment of the small intestine. In the small intestine the chyme is mixed with digestive enzymes and other secretions produced in the liver, gall bladder, and pancreas. This results in further breakdown and release of nutrients, including saccharides, amino acids, vitamins, and lipids, which are absorbed into the body across the intestinal epithelium. This process of digestion and absorption continue as the digestate passes through the remaining sections of the small intestine, the jejunum and ileum, before reaching the large intestine. Upon reaching the large intestine digestion has largely run its course and the digestate, now termed faeces, is prepared for excretion from the body. This largely involves the absorption of any remaining water and minerals from the faeces before it is finally excreted from the tract via the rectum and anus (Greenwood-Van Meerveld et al., 2017). A summary diagrammatic overview of the GI systems anatomy highlighting these key organs and their arrangement in the human body can be found in figure 1.2.

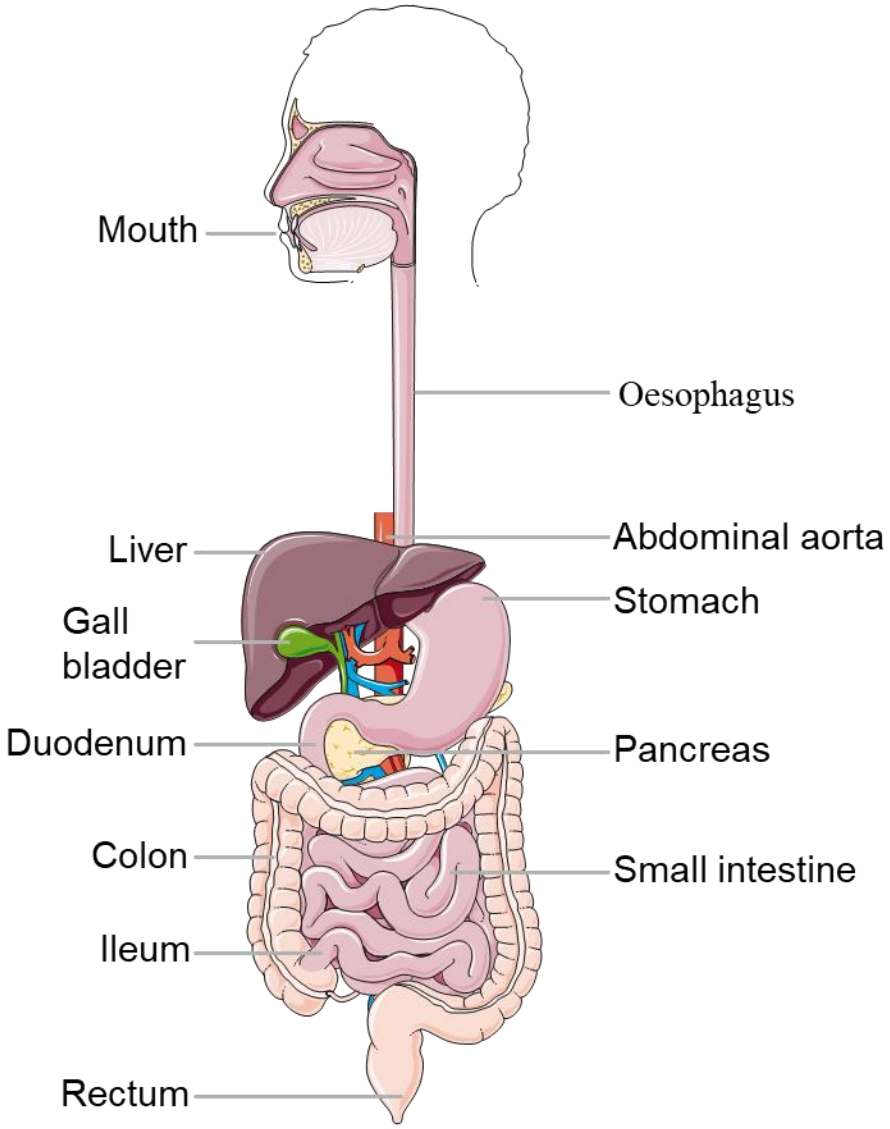

Figure 1.2 Diagrammatic representation of the anatomy of the human gastrointestinal system

The gastrointestinal tract beings at the mouth through which foodstuffs enter and are mechanically broken down before passing through the oesophagus to the stomach. In the stomach secreted stomach acids and digestive enzymes breakdown foodstuffs further before passing them into the small intestine as chyme. In the small intestine further enzymatic digestion occurs and the released nutrients absorbed into the body by the intestinal epithelium. This process is aided by factors secreted by the pancreas, liver, and gall bladder. After passing through the length of the small intestine the luminal contents enter the large intestine. Here any remaining nutrients and water are resorbed with the remaining waster excreted via the rectum.
The original author of the source image is Servier Medical Art (Servier Laboratories) and was provided under a creative commons attribution 3.0 unported (CC BY 3.0) licence.

1.2.2 The intestinal tract

The intestinal tract is composed of both the small and large intestine which form a continuous tube, approximately eight metres long in an adult human, from the outlet of the stomach to the anus (Mowat and Agace, 2014). The small intestine is narrow in diameter but long, at approximately six and a half metres in length, and is responsible for handling the majority of the digestion and nutrient absorption process. The large intestine in contrast is wider in diameter but shorter, at approximately one and a half metres in length, and is composed of the caecum, colon, and rectum (Mowat and Agace, 2014). The caecum is a blind-ended pouch present at the start of the large intestine at its junction with the small intestine. The caecum's function is as a store for the commensal microbiota, which is in highest numbers in the large intestine, which ferment foodstuffs not able to be digested by the small intestine. This function is mainly pertinent to herbivores, such as the house mouse *Mus musculus*, due to the need for fermentation to efficiently breakdown plant material and as such the caecum is largely vestigial in humans (Smith et al., 2009). The colon makes up the majority of the large intestine and carries out its primarily water reabsorption functions in preparation for excretion which occurs via the rectum an anal canal ending in expulsion through the anus (Greenwood-Van Meerveld et al., 2017).

In terms of histology a common layout of the intestinal wall is maintained along the length of the tract. This consists of an outer *muscularis externa*, which overlies the submucosa, which in turn overlies the inner luminal facing mucosa (Mowat and Agace, 2014). The *muscularis externa* is primarily composed of smooth muscle and functions in motility and segmentation of luminal contents ensuring their proper mixing and propulsion in an anterograde manner (Greenwood-Van Meerveld et al., 2017). The submucosa separating the muscularis externa from the mucosa serves a mainly connective tissue role containing major vascular vessels and nerves and thus is also an important site of interface with the rest of the body (Greenwood-Van Meerveld et al., 2017). The final layer is the mucosa which serves as the interface with the lumen from which it absorbs nutrients and fluid and secretes into a variety of protective and digestive factors. In terms of structure at its base the mucosa separates itself from the submucosa with a layer of smooth muscle termed the *muscularis mucosae.* Above this lies the connective tissue of the mucosa, the lamina propria, which contains a variety

of stromal cells, such as fibroblasts, and immune cells, such as macrophages as well as the mucosal vascular network. Covering the lamina propria and separating it from the lumen is the intestinal epithelium, composed primarily of a single layer of columnar epithelial cells, which displays a structure characterised by crypts, tubular invaginations which extend down into the mucosa (Mowat and Agace, 2014). At the base of these crypts are epithelial stems cells which replicate and differentiate moving up the crypt to replace epithelial cells which are shed into the lumen at the luminal surface at the tops of the crypts. Other fully differentiated epithelial cell types include goblet cells, which secrete mucus into the lumen, and a variety of enteroendocrine and immune related cell types with secretory, as well as sensing and signalling roles (Garrett et al., 2010). The major histological difference between the mucosa of the small and large intestine are the presence of intestinal villi which are present in the former and absent in the latter. Villi are long thin mucosal extensions, extending from the epithelium at the top of the crypts out further into the lumen. Villi serve to further increase the surface area of the small intestine to aid nutrient absorption (Mowat and Agace, 2014). To summarise a diagrammatic representation of histological layout of the colon wall in transverse cross section, as well as a labelled histological section of murine colon in the same orientation, are presented in figure 1.3.

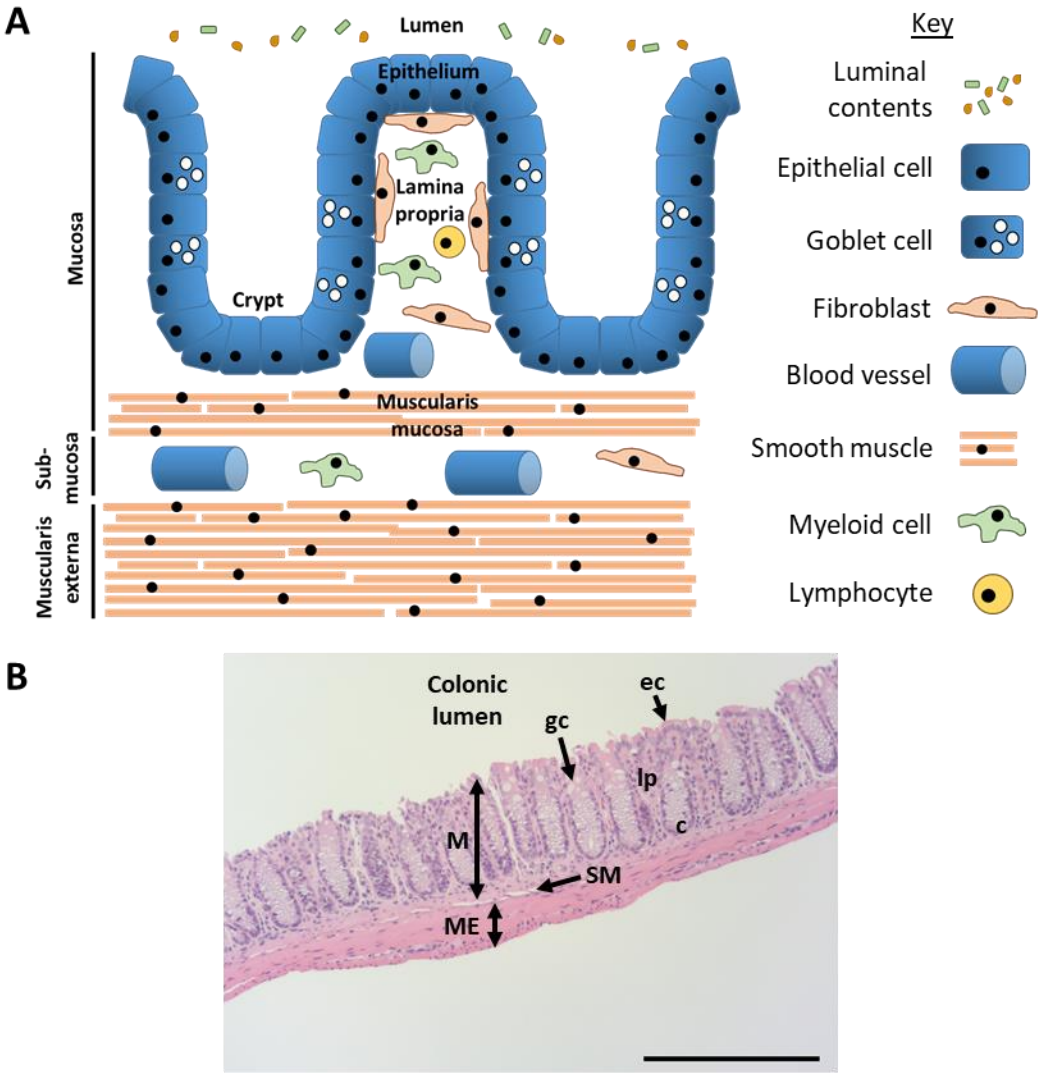

Figure 1.3 Histology of the colon

(A) Diagrammatic representation of the histology of the colonic wall which is composed of three major structures; the luminal facing mucosa; the underlying submucosa; and the outer muscularis externa. The mucosa has an overlying epithelial layer composed of columnar epithelial cells and goblet cells, the later of which are responsible for luminal mucus secretion. The mucosa displays a crypt architecture with regular tubular invaginations which extend down into it (crypts). At the base of the crypts lie epithelial stem cells responsible for the replacement of epithelial cells which are shed into the lumen at the top of the crypts. The lamina propria connective tissue underlies the epithelium and consists of stromal cells, such as fibroblasts, a large number of resident immune cells, as well as vasculature providing the local blood supply. Underneath the lamina propria is the muscularis mucosa, a layer of smooth muscle cells which separates the mucosa from the submucosa. The submucosa similarly to the lamina propria consists of vascular and connective tissue components. Finally, the last layer of the wall is the outer smooth muscle of the muscularis externa.
(B) A representative labelled haematoxylin and eosin (H&E) stained histology section of the mouse colonic wall in the same orientation as (A). M = mucosa, ec = epithelial cell, gc = goblet cell, lp = lamina propria, c = crypt, SM = submucosa, ME = muscularis externa. Scale bar = 500µm.

1.2.3 The mucosal immune system

As a major interface with the external environment, with a surface area of approximately 100m^2, the intestines are a major site of immunological challenge (Artis, 2008). As such, humans have evolved a robust GI mucosal immune system consisting of resident immune cell populations as well as distinct specialised lymphoid tissues which together make up the largest compartment of the body's immune system (Mowat and Agace, 2014).

The majority of the immune cells of the intestines reside diffusely distributed within the lamina propria of the mucosa and vary in number and variety along its length based on immunological function and need (Mowat and Agace, 2014). Macrophages of the innate immune mononuclear phagocytic system are the most abundant in the lamina propria and present along the entire length of the intestine (Mowat and Agace, 2014). Macrophages play a key local immunomodulatory role in managing maintenance of tolerance to the commensal microbiota while also acting as important immune sentinels for pathogenic threats (Bain and Schridde, 2018). In their first role intestinal resident macrophages help maintain tolerance via their secretion of the immunoregulatory cytokines IL-10 and transforming growth factor β (TGFβ) which help dampen local immune responses (Hadis et al., 2011). In their second major role macrophages act as a second line of defence following microbial breach of the epithelium with potent bactericidal phagocytic activity (Bujko et al., 2018). They also act to monitor the luminal microbiota, via extension of antigen sampling transepithelial dendrites, for potential threats which they can then present antigens of to the adaptive immune system (Niess et al., 2005). Macrophages are helped in this last role by dendritic cells (DCs), also of the mononuclear phagocytic system, which are also present along length of the intestine although at much lower abundance (Mowat and Agace, 2014). DCs play an important role in progressing the adaptive immune response via uptake of antigens, including those sampled from the lumen by macrophages, before migrating to local lymphoid tissues for antigen presentation to lymphocytes (Persson et al., 2013).

In terms of lymphocytes both cytotoxic and helper T cells are also present within the lamina propria although the latter predominates (Mowat and Agace, 2014). These cells

are predominantly of a resident effector memory phenotype which are primed to respond to a previously encountered antigen (Sathaliyawala et al., 2013). They additionally come in a variety of functional subtypes including the pro-inflammatory Th1 and Th17 polarisations which can function to counteract local pathogens (Tato and O'Shea, 2006). In addition, immunomodulatory Treg cells are also present and along with macrophages play an important role in dampening the local immune response via production of cytokines such as IL-10 (Zigmond et al., 2014). Alongside T cells B lymphocytes are also present in the lamina propria along the length of the intestinal tract largely as plasma cells which predominantly produce IgA class antibodies (Mowat and Agace, 2014). These antibodies are then trafficked into the lumen via overlying epithelial cells and act as another line of defence against microbial encroachment (Brandtzaeg, 1974).

In addition to their presence in the lamina propria lymphocytes are also reside within the organised lymphoid tissues of the intestine, termed gut associated lymphoid tissue (GALT). GALT exist as subepithelial lymphoid aggregates embedded in the mucosa and submucosa of the gut wall where, like other secondary lymphoid tissues, they function to aid the co-ordination of the immune response (Mowat and Agace, 2014). They carry out this role by acting as specialised collecting sites for mucosal derived antigens which are then efficiently presented to lymphocytes in a lymph node-like environment that supports the adaptive immune response (Randall and Mebius, 2014). In the intestinal tract GALT can be developmentally derived, as is the case for Peyer's patches in the small intestine (Veiga-Fernandes et al., 2007) and colonic patches in the large (Baptista et al., 2013). In addition, solitary intestinal lymphoid tissues (SILT), which includes the cryptopatch and isolated lymphoid follicle (ILF) GALTs, develop postnatally in response to antigenic challenge and inflammation (Buettner and Lochner, 2016).

The mucosal immune system must not only be able to efficiently mount a response against a perceived threat but must also exist in balance with the basal external environment. In doing this it must contend with a high load of innocuous foreign antigens derived from food and commensal organism which must be tolerated. When

this system of regulation is disrupted disease arises as in the case of IBD (Garrett et al., 2010).

1.2.4 Pathophysiology of IBD

IBD is the name given to a group of IMIDs characterised by idiopathic non-infectious pathological inflammation of gastrointestinal tract. The two main clinical subgroupings of IBD are ulcerative colitis (UC) and Crohn's Disease (CD) which while sharing some similarities both have their own distinct disease presentations and pathophysiology (de Souza and Fiocchi, 2016).

UC is clinically defined as a condition that causes non-infectious chronic mucosal inflammation that affects the rectum and colon in a continuous lesion and has a relapsing and remitting disease course (Magro et al., 2017). UC can be further subclassified based on the disease's distribution along the large intestine, as assessed by endoscopy, which produces the three subgroups of proctitis, left-sided, or extensive UC. These reflect the extension of the disease proximally, with proctitis affecting solely the rectum, left-sided UC restricted to the distal colon, and extensive UC extending even further proximally from the distal colon (Silverberg et al., 2005). Additionally, UC can also be sub-classified based on disease activity and severity as assessed by several clinical parameters. These include measures of systemic inflammation and toxicity including, erythrocyte sedimentation rate (ESR), body temperature, haemoglobin concentration, and pulse rate, as well as frequency of passing stools and presence of blood in faeces. This produces four subclasses of increasing severity from, asymptomatic remission, to mild, moderate, and severe disease activity (Silverberg et al., 2005). In terms of macroscopic pathology UC is characterised by an inflammatory vascular pattern, including erythema and loss of vascularity, as well as mucosal damage including bleeding and the presence of the eponymous superficial ulceration (Travis et al., 2012). Histologically UC pathology is generally superficial being restricted to the mucosa with only occasional extension into the submucosa. Mucosal damage presents in a continuous nature with widespread distortion of crypt architecture, including atrophy and branching, alongside luminal mucus depletion. Additionally, infiltrating neutrophils invade the crypt epithelium, termed cryptitis, as well as the crypt lumen forming crypt abscesses. This accompanies

the general diffuse inflammatory infiltration of the lamina propria which is primarily composed of neutrophils and lymphocytes, including plasma cells which are characteristically found around the base of the crypts (Magro et al., 2013).

Crohn's disease in contrast to UC is a more clinically heterogenous disease characterised by chronic non-infectious discontinuous granulomatous inflammation which may affect anywhere along the entire length of the GI tract (Gomollon et al., 2017). Like UC disease is also subclassified based on number of features which include age of diagnosis, location of disease, and disease behaviour. Age of diagnosis splits patients into three subgroups of early, common, and late onset CD based on the cut offs of 16 years or younger, 17-40 years, and over 40 years of age respectively (Silverberg et al., 2005). Disease location splits patients into a further four subcategories centred primarily on the most commonly affected areas of the ileum and colon. These categories include terminal ileum, colon, ileocolon in which disease affects both the colon and ileum, and upper GI tract. Additionally, the first three categories are not entirely mutually exclusive with the potential for upper GI involvement in each of these categories as well (Silverberg et al., 2005). Finally, disease can also be subclassified based on its behaviour which splits patients into an additional three groups. These include stricturing, in which constant obstructive luminal narrowing occurs, penetrating, in which intraabdominal fistulas or inflammatory masses and abscesses are present, and uncomplicated non-stricturing non-penetrating disease (Silverberg et al., 2005). In terms of macroscopic pathology CD is characterised by skip lesions whereby inflammation presents as patchily distributed lesions interspersed between areas of unaffected tissue, commonly giving a cobblestone like appearance. In addition, longitudinal serpinginous ulcers, fistulae, and strictures can also all potentially be present (Annese et al., 2013). Matching its macroscopic presentation histopathologically CD presents as focal discontinuous tissue damage and or inflammatory infiltration. Unlike UC this infiltrate and tissue damage is not restricted to the superficial mucosa and may extended through the entire width of the gut wall. Tissue damage typically presents as abnormal crypt architecture, including distortions in crypt morphology and branching, and in the small intestine irregular villous architecture. In terms of immune infiltration lymphocytes and plasma

cells are found diffusely infiltrating the tissue alongside granulomas consisting of monocytes and macrophages (Magro et al., 2013).

To summarise these two major IBD clinical groupings a diagrammatic overview of the common histopathological features of both UC and CD is presented in figure 1.4.

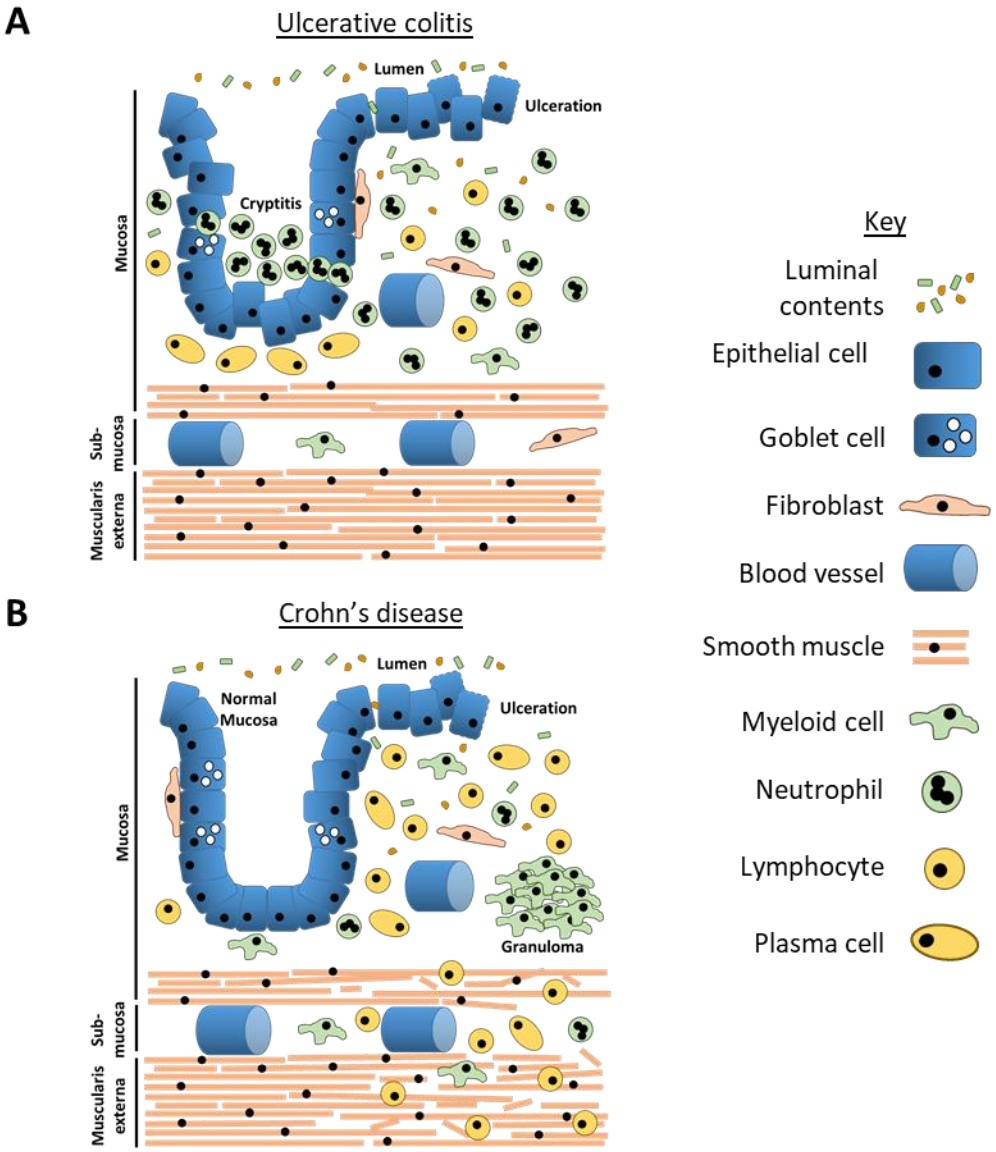

Figure 1.4 Presentation and pathological features of ulcerative colitis and Crohn's disease

(A) Diagrammatic representation of the histopathological features of ulcerative colitis (UC). The inflammatory lesion is continuous and restricted to the mucosa. The intestinal epithelial architecture is disrupted with loss of goblet cells and ulceration resulting in disrupted barrier function. There is oedema and immune cell infiltration of the lamina propria which predominantly consists of neutrophils and lymphocytes. There is characteristic neutrophilic cryptitis with some neutrophils exuding into the crypt lumen forming an abscess. Basal plasmacytosis is all present with plasma cells observed at the base of the crypts. **(B)** Diagrammatic representation of the histopathological features of Crohn's disease (CD). The inflammatory lesion is discontinuous with focal lesions present next to normal tissue. Additionally, lesions can occur transmurally with inflammation and tissue damage extending across the entire colonic wall. The intestinal epithelial architecture is disrupted with loss of goblet cells and ulceration resulting in disrupted barrier function. There is oedema and immune cell infiltration of the lamina propria which predominantly consists of lymphocytes as well as granulomas composed of myeloid cells.

1.2.5 Epidemiology of IBD

Like other IMIDs IBD is growing problem globally with increased incidence observed especially in countries with emerging economies and associated societal westernisation (Ng et al., 2018). In western countries, in which IBD is well established, prevalence is also high, around or exceeding 0.3% in many countries (Ng et al., 2018), including in the UK where prevalence has been estimated at 261 per 100,000 population (Lewis et al., 2002). Much like other IMIDs as well IBD has a high patient and societal burden. For patients this burden manifests as reduced quality of life due to abdominal pain, incontinence, GI bleeding, fatigue, and the associated impacts of these symptoms on their ability to function in society (Lonnfors et al., 2014). In terms of society, the loss of productivity and need for social care due to the disabling nature of these symptoms impacts social safety nets, with for example 20% of European IBD patients requiring disability benefits (Burisch et al., 2013). In addition, costs of treatment have risen in recent decades, primarily due to the introduction of highly costly biologic therapies, which combined with the need for long-term medical management has led to high IBD related health care expenditure (Click et al., 2019). This can be seen in Europe's IBD costs which have been estimated to account for the significant sum of €4.6-5.6 billion in direct healthcare expenditure per year (Burisch et al., 2013).

In terms of IBD patient demographics there is considerable geographic variation, as would be expected by the diverse array of potentially geographically influenced factors which are implicated in this multi-factorial disease (Cosnes et al., 2011). Typically though, in contrast to some other IMIDs, disease onset usually occurs in early to mid-life with peak occurrences from 20-30 and 30-40 years for CD and UC respectively (Ruel et al., 2014). In terms of sex UC occurs more frequently in men and CD more frequently in women, although these associations can be lost of reversed when looking at different subgroups categorised based on factors such as on age of onset (Cosnes et al., 2011). Patients suffering from IBD additionally often present with initially or develop other IMIDs as comorbidities at a higher incidence rate than the population average (Halling et al., 2017). IMID comorbidity in IBD is associated with worse quality of life for the patient as well as more severe IBD which often requires more intensive therapies (Conway et al., 2017, Burisch et al., 2019).

1.2.6 Aetiology of IBD

Like most IMIDs IBD is a complex multi-factorial disease with no definitive aetiological mechanisms defined, although a number of factors have been identified and theories based on them proposed (de Souza and Fiocchi, 2016).

As has been suggested for IMIDs in general and as the epidemiological data, showing geographic heterogeneity, would suggest a range of environmental factors have been proposed to influence the development of IBD (Bernstein, 2017). Of these it has been diet, antibiotic use, and by extension the gut microbiota these can alter which have received the most attention, with a potential microbial infectious origin of disease proposed since the diseases first medical description (Bosca-Watts et al., 2015). Indeed, dysbiosis of the GI microbiota is well characterised in IBD patients with reduced commensal diversity and higher number of mucosa associated pathogenic species (Chassaing and Darfeuille-Michaud, 2011). Furthermore, animal models have shown that transplant of IBD patient derived microbiotas can exacerbate colitis susceptibility (Britton et al., 2019). However, due in part to the immense diversity between and within individuals' microbiotas, a definitive causative microbe or microbes has so far remained elusive. Additionally, some argue that dysbiosis rather than a causative factor of IBD is actually just a secondary by-product of intrinsic inflammatory pathology of the gut (Chassaing and Darfeuille-Michaud, 2011).

Looking to host factors, similarly to other IMIDs, IBD has been shown by familial aggregation and genetic association studies to also be underpinned by a genetic component to disease (Ye and McGovern, 2016). Some of the first gene variants identified to predispose to IBD were for the PRR receptor caspase recruitment domain-containing protein 15 (CARD15), with predicted implications on its activation (Hugot et al., 2001). Since then a plethora of risk genes across different populations have been identified which are known to be involved in a range of diverse processes from *HLA* genes, involved in antigen presentation, to *ATG* genes, involved in autophagy (Liu et al., 2015). Additionally, some of these factors have been further linked to specific subtypes of disease, such as disease location in CD, further suggesting they play a role in specific aspects of disease pathogenesis (Cleynen et al., 2016). However, it should be noted that IBD is very much a polygenic disease with individual variants only

providing a minor contribution to disease heritability which even when combined only explain between 15-19% and 19-26% heritability for UC and CD respectively (Ye and McGovern, 2016). As such, current theories centre around the interactions of host genetics and the microbiota in combination. In these models genetic variants predisposes to auto-inflammatory overactivation of immunity and defective interactions with the microbiota. Combined with other complex environmental factors in reciprocal interactions it is theorised these factors jointly lead to the development of the inflammatory pathology and dysbiosis of IBD (de Souza and Fiocchi, 2016).

Despite these theories, which have in some cases have helped guide clinical practice, lack of a clarity in IBDs aetiology is still problematic from a clinical management and therapeutic development point of view. In particular, this knowledge gap prevents the development of causal therapies which, in targeting the cause of the disease, unlike all current treatments could prove to be potentially curative (de Souza and Fiocchi, 2016). As such, further work is needed to further identify and better understand the pathological mechanism in play in IBD. Regarding this aim, the work of this thesis will focus on dissecting the role of one such pathogenic mechanism based on the protein tenascin-C, which will potentially have broad applicability to other IMIDs as well.

1.3 Tenascin-C

1.3.1 The extracellular matrix (ECM)

The ECM, of which tenascin-C is a component, is the three-dimensional non-cellular macromolecular network found within all tissues of multicellular metazoan organisms. The ECM varies substantially by tissue type and sub-localisation, reflecting the different requirements of each site, and in most tissue is primarily composed of proteins and carbohydrates, often in combination as glycoproteins (Theocharis et al., 2016).

In terms of function the ECM has a clear integral role as a structural and mechanical component of tissues. This is exemplified by the fibrillar collagens, such as collagen type 1, which provide tensile strength to a range of tissues (Frantz et al., 2010). The ECM in this structural role also functions as a scaffold substrate for cells to adhere to,

with the basement membrane, which underlies all epitheliums and acts as an anchorage point for epithelial cells, a clear example (Jayadev and Sherwood, 2017). In addition to these structural roles it has also become appreciated in recent decades that the ECM can also act as an important modulator of cellular behaviour and tissue function. In the first instance this can be achieved by the ECMs function as a storage reservoir for a variety of biochemical and biological factors, including minerals and growth factors, whose controlled release can affect cells in a myriad of ways. Secondly, ECM components can carry out this role through their own direct or indirect interactions with cells. This includes their ability to function as co-receptors to a range of soluble signalling factors, as well as their ability to directly bind and activate a range of cell surface receptors (Hynes, 2009).

In regard to the matrix as a direct signalling modulator of cellular behaviour the matricellular family of proteins are probably the best-known example. A diverse family they were classically defined by their de-adhesive properties and non-structural roles in a range of processes from embryogenic cell differentiation to tissue remodelling in response to wounding. The family consists of several sub-families with a variety of distinct and overlapping structures, functions, and expression patterns. This includes the tenascin family of proteins of which tenascin-C is a member (Murphy-Ullrich and Sage, 2014).

1.3.2 The tenascin family of proteins

The tenascin family of proteins is composed of four members in mammals; tenascin-C, tenascin-R, tenascin-W, and tenascin-X. The family is believed to have evolved early in the chordate lineage with a single precursor tenascin gene present. This gene was subsequently conserved in future lineages and duplicated in vertebrates to produce the four members of the family found in tetrapods today (Tucker et al., 2006, Adams et al., 2015). The family is not unified by expression patterns or function which, while in some cases overlapping, overall differ substantial. Instead the family are characterised by their common unique domain structure consisting of, from N to C terminus, tenascin assembly (TA) domain, a series of epidermal growth factor-like (EGF-L) repeats, a series of fibronectin type 3 (FNIII)-like repeats, and finally a terminal fibrinogen-like globe (FBG) domain (Chiovaro et al., 2015).

1.3.3 Molecular structure of tenascin-C

Tenascin-C, originally just called tenascin among other names, was the founding member of the family, being first described in 1983 by Bourdon and colleagues (Bourdon et al., 1983), and is no exception from this domain structural organisation. The human tenascin-C polypeptide consists of an N terminal TA domain followed by 14.5 EGF-L repeats, up to 17 FNIII-like repeats, and a terminal FBG domain (Mighell et al., 1997). This domain structure for tenascin-C, as well as its amino acid sequence, is further conserved evolutionarily between organisms, including between humans and the common house mouse, *Mus musculus*. This can be revealed by aligning the protein sequences of human (UniProt identifier P24821) and mouse (UniProt identifier Q80YX1) using the multiple sequence alignment tool Clustal Omega (Sievers et al., 2011). Such an alignment shows the orthologs overall share a high amino acid sequence identity of approximately 88%, with the most major difference between the proteins being the presence of three fewer FNIII-like repeats in the murine version.

Indeed, the FNIII-like repeats are of particular note in tenascin-C as they are known to produce significant isoform diversity due to alternative splicing. In mice and humans eight of the FNIII-like repeats are constitutively expressed while six and nine, in humans and mice respectively, are subject to alternative splicing (Giblin and Midwood, 2015). In the tenascin-C gene each FNIII-like repeat is encoded individually by one or two exons with, from the N to C terminal, five constitutive repeats followed by all of the alternatively spliced repeats, before the sequence is finished by the three remaining constitutive repeats. As each repeat is encoded by separate exons, and thus able to be spliced independently, this allows for a wide range of potential alternative splicing combinations which are realised as a wide range of tenascin-C isoforms that have been found (Giblin and Midwood, 2015).

As well as being alternatively spliced each tenascin-C polypeptide does not exist in isolation with the mature protein secreted into the matrix as a homo-oligomer (Taylor et al., 1989). This takes the form of a hexamer with each of the six tenascin-C polypeptide monomers joined centrally by disulphide bonding within their N terminal TA domains (Kammerer et al., 1998). This adds another area of potential variation with the opportunity for homo- and hetero-typic oligomerisation of differentially

spliced or otherwise modified tenascin-C monomers (Giblin and Midwood, 2015), and even theoretically other tenascin family members (Jones and Jones, 2000).

A summary overview of the molecular structure of a tenascin-C monomer and its arrangement in its mature hexameric form are shown in figure 1.5a and 1.5b respectively.

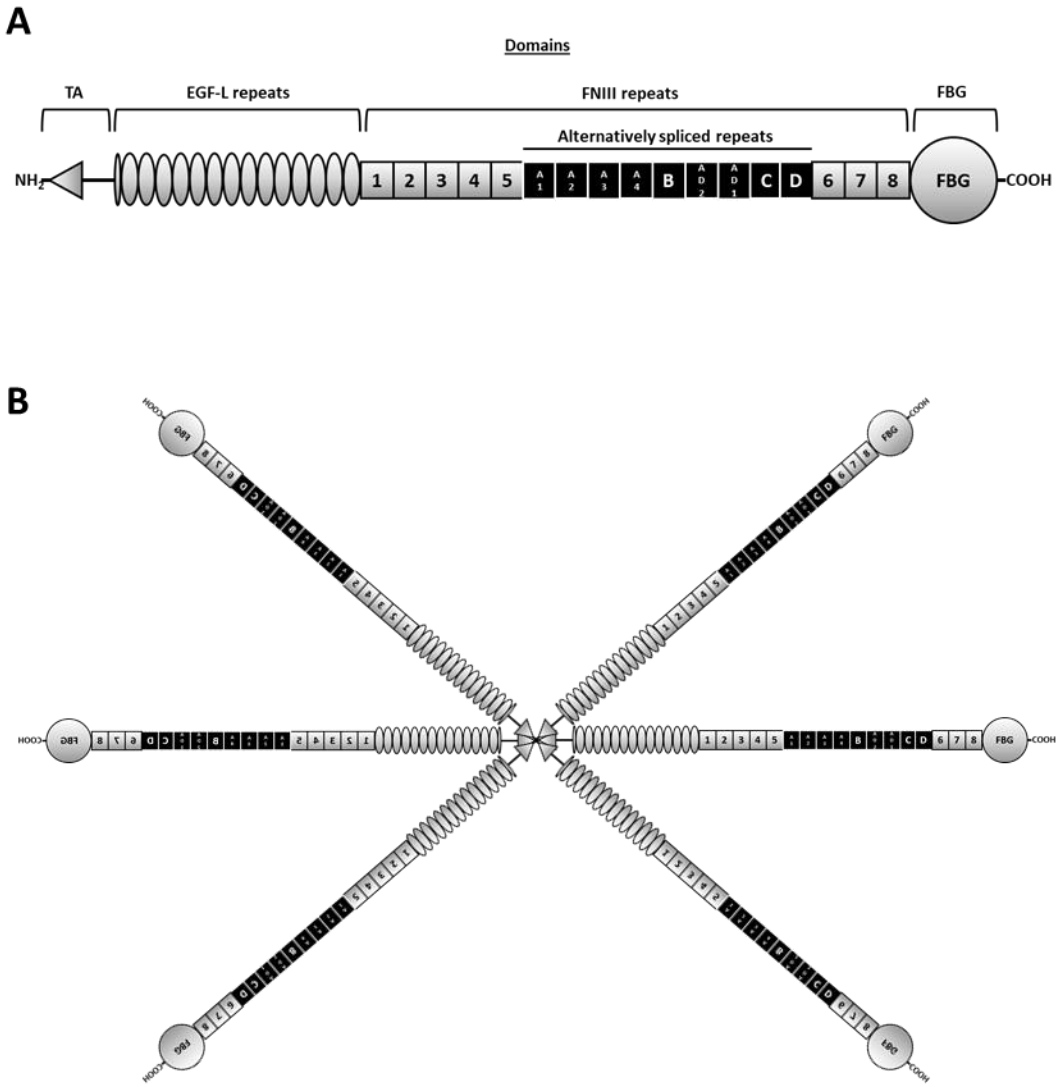

Figure 1.5 The domain and oligomeric structure of human tenascin-C

(A) Diagrammatic representation of a tenascin-C monomer with domains indicated above. The polypeptide starts on the left hand side with the N terminal tenascin assembly (TA) domain. This is followed by 14.5 epidermal growth factor-like (EGF-L) repeat domains after which come up to 17 fibronectin type III-like (FNIII) repeats domains. Of these FNIII repeats 8 are constitutively expressed (FNIII 1-8 in grey) while 9 are included subject to alternative splicing (FNIII A1-D in black). The molecule ends with the C terminal fibrinogen-like globe (FBG) domain.
(B) Representation of a tenascin-C hexamer made using the diagrammatic monomer presented in (A). Tenascin-C forms a homo-oligomeric hexamer with 6 monomers joined at their N termini by a series of inter-monomer disulphide bonds in their TA domains.

1.3.4 Post-translation modification (PTM) of tenascin-C

Further diversity is added, to the already described variability of tenascin-C, through a variety of known post-translational modifications. The best described of these is glycosylation, with tenascin-C shown to be a glycoprotein, like many ECM proteins, shortly after its first identification. These early studies proved tenascin-C's glycosylated status by treating the purified protein with different glycosidases, such as endoglycosidase F and neuraminidase. The proteins molecular weight was then determined and the loss weight, due to the loss of the carbohydrate moieties, assessed. This, along with other more indirect methods such as caesium chloride equilibrium sedimentation, demonstrated that tenascin-C had a significant carbohydrate component and was thus significantly glycosylated (Vaughan et al., 1987, Taylor et al., 1989). Subsequent studies using protein sequence interrogation and bioinformatic resources has revealed human tenascin-C has 26 and 34 predicted N-glycosylation and O-glycosylation sites respectively (Gulcher et al., 1989, Giblin and Midwood, 2015). Of these for the N-glycosylation sites the predominant number were found in the FNIII-repeat domains with 21 sites identified, including many within alternatively spliced domains. Of the remaining sites 2 were found in the TA domain, 2 in the EFG-L repeat region, 1 in the FBG domain (Giblin and Midwood, 2015). These *in silico* predictions have subsequently been largely validated by glycopeptide mass mapping with only two sites, one in the FNIII-like repeat region and one in the FBG domain, found not to be glycosylated (Mangan et al., 2019). These studies also confirmed the presence of significant variability in tenascin-C N-glycosylation dependent on the tissue or cellular source of the protein, including differences in sialyation, mannose content, and proportions of processed glycans (Mangan et al., 2019). For O-glycosylation, while no validating mapping has been undertaken, a similar pattern of predicted sites is seen with again the predominant number found in the FNIII-repeat domains with 24 sites identified including a number within alternatively spliced domains. Of the remaining sites 8 were found in the TA domain and 2 in the EFG-L repeat region, with none identified in the FBG domain (Giblin and Midwood, 2015). Despite these limited descriptive studies of tenascin-C's glycosylation status even less is known about the functional significance of these modifications with the most work to date focused on the human natural killer-1 (HNK-1) carbohydrate epitope. HNK-1

is a unique trisaccharide motif found on both O- and N-linked glycoconjugates of a number of glycoproteins expressed in the nervous system (Morise et al., 2017), including tenascin-C (Kruse et al., 1985, Grumet et al., 1985). While having a number of roles in the nervous system tenascin-C specific HNK-1 has been implicated in modulating the proliferation of neural stem cells (Yagi et al., 2010).

Besides glycosylation the other main PTM which has been studied in the case of tenascin-C is proteolytic processing. In regard to this a variety of proteases have been identified with the ability to cleave tenascin-C which include; matrix metalloproteinases (MMP) -1, -2, -3, -7, neutrophil elastase, cathepsins -B, -G, a disintegrin and metalloproteinase with thrombospondin motifs (ADAMTS) -5, and meprinβ (Imai et al., 1994, Siri et al., 1995, Mai et al., 2002, Zhen et al., 2008, Ambort et al., 2010). Proteolytic processing, as well as controlling the amounts of proteins in its classic degradative role, can also have functional consequences for proteins. This can be achieved by processing resulting in the exposure or release a novel functional site on the protein, termed a matricryptic site or if released as a fragment a matricryptin (Ricard-Blum and Salza, 2014). Such cryptic sites have been found in tenascin-C such as an integrin binding site in the third FNIII-like repeat which is only functional when presented to cells as part of a small fragment of the total protein (Denda et al., 1998). Additional functionality for subdomains, distinct from the full length tenascin-C protein, includes; inhibition of fibronectin fibrillogenesis (To and Midwood, 2010), syndecan-4 dependent β1 integrin activation (Saito et al., 2007), and induce apoptosis in smooth muscle cells (Wallner et al., 2004).

The combination of all of these PTMs with the post transcriptional splicing tenascin-C undergoes results in the potential production of a wide range of isoforms. In addition, a number of uncharacterised established, as well as yet to be discovered, PTMs may add further layers of complexity to tenascin-C. A prime example would be protein phosphorylation, with a recent study of publicly available human proteomic data finding evidence of four previously unrecognised putative phosphorylation sites in tenascin-C, three in the TA domain and one in the FNIII-like repeat region (Klement and Medzihradszky, 2017). Furthermore, as was mentioned earlier for glycosylation, there is evidence that splicing and PTMs occur in a cell type or tissue specific manner

suggesting there is likely multiple potential layers of regulation of tenascin-C function *in vivo* (Giblin, 2018). The functional impacts of much of this variation still remain to be determined although both splicing and PTMs are already been shown to impact a range of processes from cancer cell invasion to embryonic development (Giblin and Midwood, 2015).

1.3.5 Expression and role of tenascin-C in development

The first description of tenascin-C, by Bourdon and colleagues, characterised its presence in the ECM of human glioma cell lines and tissue (Bourdon et al., 1983). Tenascin-C was subsequently determined to be present in not only in the stroma of numerous tumour tissue types but also dynamically in a wide range of locations during embryogenesis (Midwood et al., 2016). This dynamic and diverse oncofetal expression pattern, as would be expected, was found to be regulated by an equally diverse range of transcription factors (TFs) and gene response elements (Chiovaro et al., 2015). These include classical developmentally important homeobox containing TFs such as, even-skipped homeobox 1 (EVX1) (Jones et al., 1992), orthodenticle homolog 2 (OTX2) (Briata et al., 1999), and POU domain class 3 transcription factor 2 (POU3F2) (Copertino et al., 1997).

This highly regulated expression provoked widespread research interest, particularly in the field of developmental biology, which subsequently attributed a variety of functions to tenascin-C based on its locality and findings of *in vitro* studies. This included roles for tenascin-C in embryological cell proliferation, differentiation, and migration in a range of tissues from the GI tract to the nervous system (Chiquet, 1992, End et al., 1992, Beaulieu et al., 1993, Chiquet and Wehrle-Haller, 1994). However, these theories largely fell apart in the early to late 1990s when two independent groups published the generation of tenascin-C knockout (*Tnc*$^{-/-}$) mice, which both demonstrated apparently normal embryonic development (Saga et al., 1992, Forsberg et al., 1996). Hopes were further dashed in subsequent studies which found no obvious mechanisms of compensation for loss of tenascin-C by other tenascin family members, suggesting tenascin-C plays a largely superfluous role in embryogenesis (Mackie and Tucker, 1999).

At this point in time, aside from in the field of oncology, tenascin-Cs role in mature adults had been largely neglected. This was due to the observation that, especially in comparison to its embryological expression, tenascin-C seemed sparsely expressed in most adult tissues (End et al., 1992). Subsequent studies have identified roles for this limited basal expression of tenascin-C in adult tissues, particularly as a component of stem cell niches where it can influence cell differentiation (Chiquet-Ehrismann et al., 2014). The subsequently most studied aspect of adult tenascin-C expression has not been this baseline expression however but its reactive expression, with tenascin-C shown to be induced by a variety of signals in the adult. Of most interest to this thesis was the observation that tenascin-C was found to be induced as part of the inflammatory response, it's expression and roles in which will now be discussed.

1.4 Tenascin-C and inflammation

1.4.1 Expression of tenascin-C in the inflammatory response

The first observation of inflammatory tenascin-C expression was identified in a model of dermal wounding where tenascin-C was found significantly upregulated at the wound edge and within granulation tissue. Of note was the fact this expression was transient and, like the inflammatory response itself, as the wound healed and resolution finalised so too did tenascin-C expression subside to negligible basal levels (Mackie et al., 1988, Murakami et al., 1989). Subsequent studies in a range of tissue and injury types, from human patients as well as animal models, have found similar patterns of transient inflammatory upregulation of tenascin-C (Udalova et al., 2011). This included in infectious inflammation induced by bacterial; such as tuberculosis (Kaarteenaho-Wiik et al., 2000) and *H. pylori* (Tiitta et al., 1994); viral; such as human rhinovirus 16 (Proud et al., 2008) and hepatitis B (Lebensztejn et al., 2006); and fungal; such as candidaosis (Tiitta et al., 1995); pathogens. Likewise, tenascin-C was also found upregulated in sterile inflammatory responses as well, such as in cases of dermal photodamage (Filsell et al., 1999), tendon and joint injury (Riley et al., 1996, Chockalingam et al., 2013), and asbestos induced lung damage (Kaarteenaho-Wiik et al., 2000).

This reactive expression has been shown to be driven and regulated by a number of different signalling pathways and TFs involved in responses to cellular stress,

cytokines, and growth factors (Chiovaro et al., 2015). In regard to cellular stressors a range of exogenous derived noxious stimuli, discussed earlier as inducers of the inflammatory response, have been found to also induce tenascin-C expression. This includes PAMP signalling via PRRs, such as LPS and flagellin signalling via TLR4 and TLR5, and by extension via DAMPs which engage the same receptors (Goh et al., 2010). These receptors engage a variety of signalling pathways, with the best described for tenascin-C induction being that of inhibitor of κB kinase (IKK) which activates the tenascin-C inducing TF nuclear factor κB (NFκB) (Goh et al., 2010). Besides PRR signalling other noxious environmental stimuli present in inflammatory lesions can also result in tenascin-C expression. This includes hypoxia, with the oxygen sensing TF hypoxia inducible factor (HIF)1α able to induce tenascin-C expression (Miroshnikova et al., 2016), as well as reactive oxygen species (ROS) which can also activate NFκB (Yamamoto et al., 1999).

In addition to these cellular stressors endogenous pro-inflammatory cytokines and other growth factors, induced to propagate and guide the inflammatory response, can also induce tenascin-C expression. For example, in the case of pro-inflammatory cytokines both IL-1β and tumour necrosis factor (TNF) have been shown to induce tenascin-C expression, with the later shown to be in an NFκB dependent manner (McCachren and Lightner, 1992, Nakoshi et al., 2008). In terms of growth factors TGFβ and platelet derived growth factor (PDGF) have both been shown to induce tenascin-C expression in SMAD3/4 and ETS1/2 TF dependent manners respectively (Jinnin et al., 2004). These tenascin-C inducing mediators also do not act in isolation during the inflammatory response. For example, it has been shown that hypoxia can enhance tenascin-C production in response to the pro-inflammatory cytokine IL-1β (Tojyo et al., 2008). This reflects the complex network of factors which can interact at sites of inflammation to induce tenascin-C's dynamic spatiotemporal production.

1.4.2 Tenascin-C as an endogenous pro-inflammatory factor

Once produced at sites of inflammation tenascin-C has been found to act as a pro-inflammatory factor with two major classes of receptors thus far identified as mediating this function; the PRR TLRs and the adhesion modulating integrins.

The best described of these is the former with tenascin identified as a ligand for TLR4 (Midwood et al., 2009). TLR4 is best known as the PRR for the bacterially derived PAMP LPS, although in recent years a number of endogenous molecules alongside tenascin-C have been found activate it as well. These include a diverse range of proteins from fibrinogen to HMGB1, and biglycan (Bryant et al., 2015). Subsequent studies mapped the TLR4 activating site on tenascin-C to the FBG domain with the exact interacting site made up of three loops forming a non-contiguous cationic ridge (Zuliani-Alvarez et al., 2017). Engagement of the receptor leads to recruitment of the adaptor molecule myeloid differentiation factor 88 (MyD88) to the intracellular TIR domain of the receptor, followed by the kinases IL-1R-associated kinase (IRAK)4 and IRAK1 along with the pseudokinase IRAK2. This signalling complex, termed the myddosome, recruits and activates the ubiquitin ligase TNF receptor-associated factor 6 (TRAF6) which through generation of atypical ubiquitin chains recruits and activates the TGF-β activated kinase 1 (TAK1) complex. TAK1 is subsequently responsible for the phosphorylation based activation of the mitogen activated protein kinase (MAPK) cascade as well as the IKK complex. These pathways both ultimately lead to the activation of a pro-inflammatory TF program with the NFκB, AP-1, and CREB factors key master regulators (Balka and De Nardo, 2019). Despite these signalling events appearing to occur in a broadly similar manner for tenascin-C and LPS some differences for tenascin-C have been noted which result in distinct effector outcomes (Piccinini et al., 2016). Additionally, also in contrast with LPS it has been shown that tenascin-C does not share the requirement for the CD14 and MD-2 co-receptors which are essential for LPS stimulation of TLR4 (Midwood et al., 2009).

Besides TLR4 the other major pro-inflammatory signalling mechanism described for tenascin-C is mediated by integrins. Integrins are a family of transmembrane cell adhesion receptors best known for their functions in signalling and linking the ECM and cytoskeleton, with important roles in development as well as immune responses. Integrins exist as heterodimers of one alpha (α) and one beta (β) subunit, with 18 α and 8 β subunits found in humans which together generate 24 different integrin receptors (Barczyk et al., 2010). In terms of tenascin-C pro-inflammatory signalling it is the α9β1 and αVβ3 integrins which have been identified as responsible (Kanayama et al., 2011, Shimojo et al., 2015). The α9β1 binding site has been mapped to the FNIII-like

repeat 3 of tenascin-C (Yokosaki et al., 1994). Binding, and thus recruitment of the receptor to a focal adhesion, subsequently results in activation of the intracellular adaptor focal adhesion kinase (FAK) complex which can trigger a number of downstream signalling pathways. This includes the MAPK and IKK pathways which can activate pro-inflammatory TF programs such as that of NFκB (Yokosaki et al., 1996, Kanayama et al., 2011). In terms of the αVβ3 integrin two binding sites for it in tenascin-C have been identified with one, distinct from the α9β1 site, in the FNIII-like repeat 3 (Sriramarao et al., 1993) and the other in the FBG domain (Yokoyama et al., 2000). Similarly to α9β1 the FAK complex was implicated in activating downstream signalling pathways which resulted in activation of the pro-inflammatory TF NFκB (Shimojo et al., 2015).

In addition to these pathways which have been validated and most studied there is the theoretical possibility for tenascin-C to influence the inflammatory response via a variety of other interactions as well. In terms of direct cellular signalling interactions the EGF-L repeats of human tenascin-C have been found to bind and activate the EGF receptor (EGFR) (Swindle et al., 2001). The functional *in vivo* relevance of this interaction has been further demonstrated with tenascin-C EGF-L able to activated the MAPK pathway and protect cells from death induced by pro-apoptotic ligands (Rodrigues et al., 2013). While not in the context of tenascin-C stimulation this same MAPK EGFR signalling pathway has also been implicated as a driver of both sterile (Rayego-Mateos et al., 2018) and infectious (Hardbower et al., 2016) inflammation. In both of these cases, which included chronic kidney disease and *H. pylori* infection, these affects were found to be driven by the AP-1 and NFκB TFs and thus this provides another potential mechanism by which tenascin-C may activate these factors.

Aside from these direct receptor interactions tenascin-C can also potentially modulate the response via crosstalk and indirect interactions with other pro-inflammatory pathways. This could be mediated by the wide range of secreted signalling factors tenascin-C has been shown to bind and interact with which include mediators such as Wnt ligands, fibroblast growth factors (FGF), and TGFβ (Giblin and Midwood, 2015). In the case of Wnt ligands tenascin-C has been shown to directly bind and facilitate Wnt3a signalling promoting β-catenin mediated TF programs (Hendaoui et al., 2014).

In addition, tenascin-C can further accentuate Wnt signalling by its ability to downregulate the Wnt inhibitor Dickkopf-1 (DKK1) by blocking actin stress fibre formation (Saupe et al., 2013). Wnt signalling has been shown to have pro-inflammatory affects as well as displaying crosstalk with numerous other pro-inflammatory signalling pathways (Moparthi and Koch, 2019). For example Wnt3a stimulation is able to directly induce pro-inflammatory cytokine production in some cell types (Aumiller et al., 2013). In addition, Wnt3a is known to upregulate signal transducer and activator of transcription (STAT)3 expression which functions in IL-6 signalling (Hao et al., 2006, Fan et al., 2013).

Together these pro-inflammatory mechanisms, the most well characterised and validated of which are summarised in figure 1.6, demonstrate the diverse range of ways tenascin-C may act to help drive the inflammatory response.

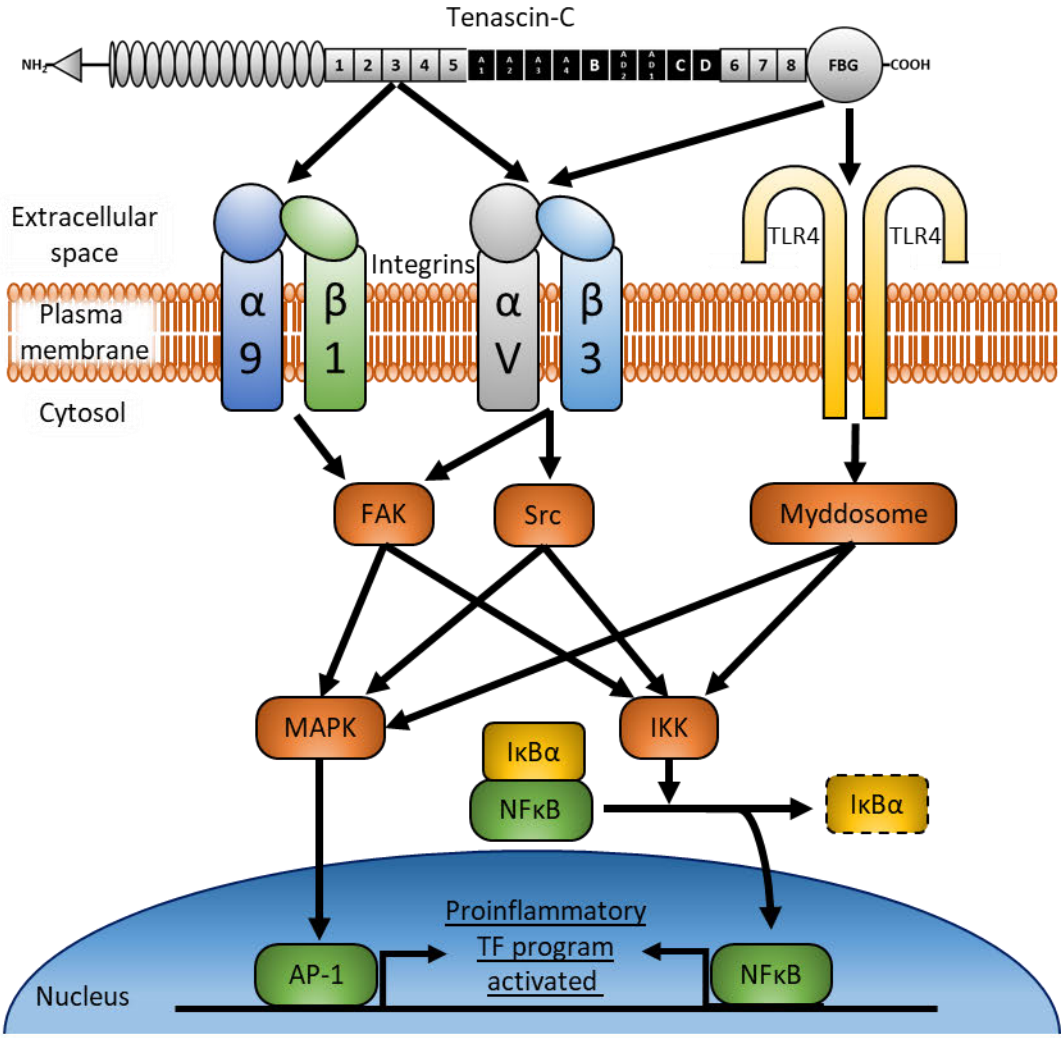

Figure 1.6 Summary of the major validated pro-inflammatory cell signalling mechanisms of tenascin-C

The two major validated pro-inflammatory signalling mechanisms utilised by tenascin-C are via the pattern recognition receptor toll-like receptor (TLR)4 and the integrins αVβ3 and α9β1. TLR4 is activated by the fibrinogen-like globe (FBG) domain of tenascin-C which leads to recruitment and activation of intracellular adaptor proteins. These form the myddosome signalling complex which activates the mitogen activated protein kinase (MAPK) and inhibitor of κB (IκB) kinase (IKK) downstream signalling pathways. The integrin receptors are both activated by distinct epitopes in the FNIII-like repeat 3 of tenascin-C as well as an epitope in the FBG domain for αVβ3. Both receptors activation lead to activation of the intracellular focal adhesion kinase (FAK) as well as the Src kinase for αVβ3. As with TLR these both activate the MAPK and IKK downstream signalling pathways. The MAPK pathway ends with phosphorylation based activation of the proteins that form the activator protein (AP)-1 transcription factor (TF) in the nucleus. The IKK pathway meanwhile terminates with the phosphorylation directed ubiquitination and resulting proteasomal degradation of the IκBα. Degradation of IκBα leads to the release of the TF nuclear factor κB (NFκB) which is then able to translocate to the nucleus. Both of these key TFs then drive the transcription of a variety of key pro-inflammatory mediators and effector proteins.

1.4.3 Impact of tenascin-C on innate immune cells

The innate immune system comprises a range of leukocytes of primarily myeloid origin as well as lymphocytic natural killer cells. The myeloid cells comprise of two main subgroups which include the mononuclear phagocytes; consisting of monocytes, macrophages, and DC; and the granulocytes; consisting of neutrophils, basophils, eosinophils, and mast cells. These varied cell types play important roles in pathogen recognition and the initiation of the inflammatory responses, as well as acting as key effectors through their phagocytic activity and production a myriad of anti-microbials, proteases, and ECM molecules (Delves et al., 2006).

Research on tenascin-Cs impact on the innate immune system have primarily focused on its effects on the cells of the mononuclear phagocyte system. This focus has been in part because it is this lineage which has been implicated as the primary immune cell source of tenascin-C at sites of inflammation with macrophages in particular show to be able to secrete significant quantities of the protein (Goh et al., 2010, Giblin, 2018). Tenascin-C stimulation has been shown to drive macrophages, which display wide ranging phenotypic plasticity (Mosser and Edwards, 2008), to adopt a pro-inflammatory M1 polarisation classically shown to be induced in response to PAMPs (Kimura et al., 2019). In terms of effector outcomes this has been shown to result induction of pro-inflammatory cytokine production in both macrophages and DC, including the production of TNF, IL-6, IL-1α, IL-1β, and IL-23 (Midwood et al., 2009, Kanayama et al., 2011, Machino-Ohtsuka et al., 2014). As well as directly driving production, tenascin-C also acts to enhance production with tenascin-C signalling upregulating the microRNA miR-155 which is known to aid TNF synthesis by stabilising the TNF mRNA transcript (Bala et al., 2011, Piccinini and Midwood, 2012). In addition to cytokines tenascin-C also induces macrophages and DC to produce a raft of chemokines, including IL-8, chemokine C-C motif ligand (CCL)2, CCL3, CCL4, chemokine C-X-C motif ligand (CXCL)2, and CXCL5, which are important for the recruitment of various immune cell types to sites of inflammation (Kanayama et al., 2009, Midwood et al., 2009). Aside from mediator production tenascin-C can also induce the production of tissue remodelling effector molecules. This includes proteases such as; MMP1, 3, 9, and 14; as well as ECM molecules such as collagens (Tremble et al., 1994, Piccinini et al., 2016)

In terms of the granulocytes much less work has been done to characterise the impact of tenascin-C stimulation. Indeed, the most numerous granulocyte, the neutrophil, has been shown in *in vitro* studies to be incapable of producing tenascin-C under basal or pro-inflammatory stimulated conditions (Giblin, 2018). However, tenascin-C has been shown to be able to act on neutrophils via its stimulation of TLR4 which has been shown to upregulate production of the extracellular protease MMP9. This is believed to aid in immune cell recruitment to sites of inflammation in tissues by helping to breakdown ECM barriers in the vasculature during endothelial transmigration (Kuriyama et al., 2011, Coito, 2011). Tenascin-C has also been shown to play a role in eosinophil biology by acting as a growth factor that promotes eosinophil precursor proliferation while also blocking their complete maturation. As such, via these mechanisms tenascin-C is implicated in aiding progenitors in the local generation of eosinophils at sites of inflammation (Doan et al., 2018).

Together these studies show a clear pro-inflammatory role for tenascin-C in innate immunity, especially for cells within the mononuclear phagocytic system, although roles in other innate cell types remains to be properly characterised.

1.4.4 Impact of tenascin-C on adaptive immune cells

The cells of the adaptive immune system include T and B cells. T cells are split into two broad subgroups of CD4+ helper T (Th) cells, responsible for orchestrating immune responses through cytokine production and B cell activation, and CD8+ cytotoxic T (Tc) cells, responsible for antigen targeted cell killing. B cells meanwhile are primarily responsible for the adaptive humoral immune response through their production of antibodies (Delves et al., 2006).

In terms of tenascin-C signalling there is less literature characterising its interactions with the adaptive immune system, and of that which there it has predominantly focused on T cells. Indeed, like the neutrophil both the Th and Tc cell subtypes have been shown to be incapable of secreting tenascin-C themselves and thus any affects must occur in a paracrine rather than autocrine signalling manner (Giblin, 2018). The best characterised of these interactions is the ability for tenascin-C to inhibit T cell activation in response to a range of activators, including T cell receptor (TCR) specific

activation with tetanus toxoid C fragment, with tenascin-C reducing the proliferative response (Ruegg et al., 1989). Most work however has taken place using TCR non-specific activation methods, utilising either anti-CD3 and anti-CD28 antibodies or the mitogen concanavalin A, which similarly showed, irrespective of co-stimulation, reduced proliferation as well as reduced IL-2 and interferon (IFN)-γ production (Hemesath et al., 1994, Hibino et al., 1998, Parekh et al., 2005, Mirzaei et al., 2018). These affects were mapped to a region spanning the alternatively spliced FNIII-like repeats A1 to A3 of tenascin-C (Puente Navazo et al., 2001). Further mechanistic studies demonstrated that this inhibition is mediated at least partially by α5β1 and αvβ6 integrin signalling which results in reduced activation of the key signalling kinases mammalian target of rapamycin (mTOR) and protein kinase B (PKB) (Mirzaei et al., 2018). In the case of α5β1 this was shown to be mediated by inhibiting reorganisations of the actin cytoskeletal required for efficient TCR activation (Jachetti et al., 2015)

In contrast to these findings other studies have shown that attachment of the Jurkat T cell line to tenascin-C results in significant calcium ion influx which is known to be an important second messenger signal in T cell activation (Weismann et al., 1997, Christo et al., 2015). Additionally, while tenascin-C itself may directly inhibit T cell activation studies in more physiological co-culture settings with APC myeloid cells have shown tenascin-C can promote T cell activation, potentially indirectly via its stimulation of the innate immune cells. This includes studies which have shown that tenascin-C produced by DCs drives the paracrine production of IL-23 which is needed for efficient polarisation of the Th17 T cell subtype which produces the pro-inflammatory cytokine IL-17 (Ruhmann et al., 2012). In addition, loss of tenascin-C *in vivo* results in decreased numbers of Th1 polarised T cells which are characterised by production of the pro-inflammatory cytokine IFN-γ, during the inflammatory response (Momcilovic et al., 2017). Additionally, culture of crudely extracted splenic lymphocytes with tenascin-C was shown to result in elevated production of the Th2 T cell associated cytokines IL-5 and IL-13, as well as IFN-γ. Additionally in these cultures elevated B cell antibody production was observed with tenascin-C treatment with increased levels of IgE found in the medium (Nakahara et al., 2006).

As well as activation some studies have also investigated tenascin-C ability to influence lymphocyte migration and trafficking. The earliest of these identified a role for tenascin-C as acting as a ligand supporting lymphocyte rolling adhesion which occurs as part of T cells extravasation from the vasculature into an inflammatory site (Clark et al., 1997). In contrast to this study another using an *in vitro* glioblastoma model found tenascin-C inhibited T cell migration, in part by activation of FAK by integrin signalling (Huang et al., 2010). As such, the current impact of tenascin-C as a substrate for lymphocyte migration appears inconclusive.

Overall these studies show that tenascin-C appears to be pleotropic mediator of adaptive immunity able to exert both inhibitory and activating action via direct and indirect mechanisms.

1.4.5 Impact of tenascin-C on non-immune cells

While not classically considered part of what was thought to be a purely immunovascular phenomenon stromal cells have recently become more greatly appreciated for their role in the inflammatory response. Of these fibroblasts, spindle shaped adherent cells with roles in ECM production and organising, are the most common non-immune cell types found in most tissues stroma (Patel et al., 2014). Of particular note is that fact that owing to their ECM producing function, fibroblasts derived from a variety of sources have been identified as some of the highest tenascin-C producing cell types to date under both basal as well as pro-inflammatory conditions (Goh et al., 2010, Giblin, 2018). As such, a large proportion of the tenascin-C found at sites of inflammation is likely to be of fibroblastic origin.

In regard to the impact of tenascin-C stimulation on fibroblasts a number of pro-inflammatory and tissue remodelling effector functions have been identified. Firstly, as for innate immune cells tenascin-C has been shown to induce pro-inflammatory mediator production in fibroblasts, derived from both the synovium and myocardium, with IL-6 and IL-1α both found to be upregulated (Midwood et al., 2009, Kanayama et al., 2009, Maqbool et al., 2016). In addition, fibroblast are also able to produce chemokines with CCL2, CCL4, CXCL5, and CXCL12 all found to be produced in response to tenascin-C stimulation (Kanayama et al., 2009). In terms of tissue

remodelling effector functions, as with myeloid cells, tenascin-C can induce extracellular protease production, including MMP3 and 9, as well as production of ECM components, including type 1 and type 3 collagens (Bhattacharyya et al., 2016, Kanayama et al., 2009, Maqbool et al., 2016).

Besides fibroblasts other non-immune stromal cells have also demonstrated pro-inflammatory activity in response to tenascin-C. This includes chondrocytes of cartilaginous tissue which have been shown to produce IL-6, IL-8, and the protease ADAMTS-4 in response to tenascin-C (Patel et al., 2011). It has also been recently demonstrated that epithelial cells can also respond to tenascin-C with its stimulation of a lung epithelial cell line resulting in production of IL-8 (Mills et al., 2019). Together these studies demonstrate the wide range of different cell types which can act as pro-inflammatory and tissue remodelling effectors in response to tenascin-C stimulation.

Through all of the cell types discussed in this section tenascin-C is believed to play an important pro-inflammatory role *in vivo* which has been implicated in mediating protection from microbial infection (Piccinini and Midwood, 2012). However, while tenascin-C may in some instances play a positive role in the acute inflammatory response it has been most widely investigated for its apparent and proven roles in mediating chronic inflammatory disease.

1.5 Tenascin-C and inflammatory disease

1.5.1 Tenascin-C expression is increased in inflammatory disease

After the initial discovery of tenascin-Cs upregulation in response to wounding it was not long before tenascin-C was also identified at sites of pathological chronic inflammation. The first reported instance in the literature for a bona fide IMID was in 1991 by Schalkwijk and colleagues who showed by immunohistochemistry elevated tenascin-C staining in skin lesions from psoriasis patients (Schalkwijk et al., 1991). Since then tenascin-C has been identified as being upregulated in a wide range of IMIDs from the inflamed synovia of rheumatoid arthritis (RA) patients (Cutolo et al., 1992), the ulcerated intestinal mucosa of those with IBD (Geboes et al., 2001). A summary of these, as well as a range of other major IMIDs identified thus far in the

literature to be characterised by elevated tenascin-C expression is presented in table 1.1. Additional information is also provided on the functional implications for tenascin-C in disease interpreted from either human patient samples or animal models. Of particular note is the fact that in these animal models genetic ablation or treatment with inhibitors of tenascin-C results in a marked reduction in inflammation and associated pathology attesting to tenascin-C's pro-inflammatory role *in vivo*.

Table 1.1: Summary table of published data on tenascin-C's involvement in a range of major immune mediated inflammatory diseases (IMIDs), including the nature of its upregulation and, if known, its functional significance to disease pathogenesis. References and an indication as to whether the data arises from studies of human patients (p) or animal models (am) are also provided.

IMID (Primary site/s of disease)	Nature of upregulation and functional significance
Ankylosing spondylitis (Axial joints)	Tenascin-C found elevated in the serum and correlated with markers of disease activity (p) (Page et al., 2012, Gupta et al., 2018).
Hashimoto's thryroiditis (Thyroid gland)	Tenascin-C found elevated surrounding lymphocytic aggregates in the thyroid by IHC (p) (Back et al., 1997)
Idiopathic inflammatory myositis (Muscle)	Tenascin-C found in immune infiltrated inflammatory muscle lesions by IHC (p) (Gullberg et al., 1997, Muller-Felber et al., 1998). Tenascin-C found elevated in the serum (p) (Page et al., 2012).
Inflammatory bowel disease (GI tract)	IBD associated SNP identified in the tenascin-C gene (p) (Brant et al., 2017) Increased tenascin-C observed by IHC within the inflamed mucosa in UC, CD, and microscopic colitis. Infliximab treatment of CD results in a reduction of this mucosal tenascin-C staining (p) (Geboes et al., 2001, Salas et al., 2003, Geboes et al., 2005, Ambort et al., 2010). Mass spectrometry and western blotting shows increased tenascin-C in intestinal epithelial cell extracts from patients with active UC (p) (Moriggi et al., 2017) Tenascin-C found elevated in the serum and correlated with disease activity and stricture forming disease. For UC levels decreased in response to successful treatment by proctocolectomy surgery or with the drug infliximab (p) (Riedl et al., 2001, Erdem et al., 2014, Magnusson et al., 2015)
Juvenile arthritis (appendicular joints)	Tenascin-C found elevated in the serum which correlated with disease activity (p) (Shukla et al., 2015)

Table continued on next page

Table 1.1: Table continued from preceding page

IMID (Primary site/s of disease)	Nature of upregulation and functional significance
Kawasaki disease (Cardiovascular system)	Increased tenascin-C observed by IHC within vascular inflammatory lesions which correlated with degree of inflammation (p) (Yokouchi et al., 2019)
	Tenascin-C found elevated in the serum which correlated with disease parameters and poor response to intravenous immunoglobulin (p) (Okuma et al., 2016)
	Elevated tenascin-C protein in vascular lesions as observed by IHC staining in the murine *Candida albicans* induced Kawasaki disease model (am) (Suzuki et al., 2017)
Multiple sclerosis (Brain and spinal cord)	Tenascin-C IHC staining localises to subacute and chronic plaque lesions in the brain and is elevated in serum samples (p) (Gutowski et al., 1999, Harada et al., 2015).
	Tenascin-C found elevated in the brain at the mRNA level in the murine EAE, cuprizone, TMEV MS models. Elevated protein also found in brain lesions by IHC in the TMEV model (am) (Haist et al., 2012, Harada et al., 2015, Zendedel et al., 2016).
	The EAE MS model was attenuated in *Tnc*$^{-/-}$ mice (am) (Momcilovic et al., 2017).
Psoriasis (Skin)	Increased tenascin-C observed within psoriatic skin lesions by IHC (p) (Schalkwijk et al., 1991, Gerritsen et al., 1997, Latijnhouwers et al., 1998a).
Psoriatic arthritis (Skin and joints)	Tenascin-C found elevated in the serum (p) (Page et al., 2012).
Rheumatoid arthritis (Appendicular joints)	Tenascin-C found elevated in the synovium at the mRNA level as observed by in situ hybridisation (p) (McCachren and Lightner, 1992).
	Tenascin-C found elevated in the inflamed synovium and cartilage as observed by IHC, especially in early disease (p) (Cutolo et al., 1992, Salter, 1993, Aungier et al., 2019).
	Tenascin-C found elevated in synovial fluid by WB and ELISA (p) (Hasegawa et al., 2007).
	Tenascin-C found elevated in serum by ELISA which correlated with increased disease duration and erosive joint damage. (p) (Page et al., 2012).
	Elevated tenascin-C at the mRNA and protein level as observed by IHC staining of the joints in a murine collagen antibody induced arthritis model. An antibody against tenascin-C reduces it's expression and attenuates disease (am) (Kanayama et al., 2009, Mehta et al., 2018).

Table continued on next page

Table 1.1: Table continued from preceding page

IMID (Primary site/s of disease)	Nature of upregulation and functional significance
Rheumatoid arthritis - List continued from previous page	Elevated tenascin-C at the protein level in the joint and serum as observed by ELISA in a murine collagen induced arthritis model. Serum tenascin-C correlated with clinical score (am) (Kiyeko et al., 2016). Murine zymosan and antigen induced arthritis models were both attenuated in *Tnc*$^{-/-}$ mice (am) (Midwood et al., 2009). Tenascin-C was found elevated at the mRNA level in the joints of a murine cytokine induced arthritis model. Pathology was attenuated with administration of antibodies or shRNA against tenascin-C (am) (Harada et al., 2015). Rat CIA arthritis model showed attenuated pathology in a dose dependent manner in response to treatment with an antibody against tenascin-C (am) (Aungier et al., 2019)
Sarcoidosis (Lungs, skin, and lymph nodes)	Tenascin-C observed surrounding cutaneous and pulmonary granulomatous lesions by IHC (p) (Kaarteenaho-Wiik et al., 1996, Hasibuan et al., 2015). Tenascin-C found elevated in serum and lung epithelial lining fluid by ELISA (p) (Kaarteenaho-Wiik et al., 1998).
Scleroderma (Connective tissue systemically)	Tenascin-C increased in dermal and pulmonary lesions observed by IHC. This was reduced by methotrexate treatment (p) (Lacour et al., 1992, Seyger et al., 2001, Brissett et al., 2012). Tenascin-C found elevated in serum (p) (Brissett et al., 2012, Inoue et al., 2013, Bhattacharyya et al., 2016). Tenascin-C found to drive fibrotic pathology in a variety of murine models in which it was also elevated. Disease was attenuated in *Tnc*$^{-/-}$ mice (am) (Bhattacharyya et al., 2016).
Sjögren's syndrome (Mouth and eye glands)	Increased subepithelial tenascin-C deposition found in bronchial biopsies (p) (Amin et al., 2001).
Systemic lupus erythematosus (skin, joints, and muscle)	Tenascin-C increased in lupus nephritis kidney lesions as observed by IHC (p) (Assad et al., 1993). Tenascin-C found elevated in the serum and correlated with disease activity (p) (Page et al., 2012, Zavada et al., 2015).

1.5.2 Proposed role of tenascin-C in inflammatory disease

The collective data in table 1.1, showing that tenascin-C is implicated in inflammatory diseases in near all the major organ systems of the human body, suggests that tenascin-C may play a common pathological role in IMIDs. Indeed, common pathological mechanisms have already been proposed to mediate IMIDs due to their shared risk

factors, propensity to occur as comorbidities, and responsiveness to similar targeted therapies (Kuek et al., 2007).

For tenascin-C the current mechanism proposed centres on its role in helping drive the persistence of pathological chronic inflammation as part of what has been termed the pro-inflammatory niche (Ruhmann and Midwood, 2013). The role of the ECM in creating specialised microenvironments that locally support and modulates cell behaviour is a well-known phenomenon, with the stem cell niche a prime example (Hynes, 2009). Tenascin-C's deposition at sites of inflammation and its ability to drive pro-inflammatory signalling pathways suggest it could function similarly to create a pro-inflammatory permissive microenvironment at sites of disease (Ruhmann and Midwood, 2013). Additionally, certain features of tenascin-C might also make it well suited to drive inflammation persistently in comparison to other pro-inflammatory factors.

In regard to this firstly tenascin-C's simple nature as a relatively large ECM glycoprotein might mean that turning off its pro-inflammatory signalling might be more difficult than for other mediators. For example, receptor internalisation and subsequent intracellular ligand degradation is a well-established mechanism for downregulating extracellular signalling pathways, including those for TLRs (Wells et al., 2005). Tenascin-C in contrast, due to its bulky and ECM anchored nature, would be more resistant to this mechanism and thus could theoretically persist in the local ECM continually stimulating its pro-inflammatory signalling receptors. Additionally, the nature of tenascin-C's induction in inflammation might also help it act as a persistence driver as it has been shown to be able to self-induce its own expression (Kanayama et al., 2009, Goh et al., 2010). This could be either directly, through its own pro-inflammatory signalling, or indirectly, by inducing mediators such as cytokines which themselves induce tenascin-C production. In either case this positive feedback loop thus creates a mechanism whereby autocrine or paracrine tenascin-C signalling could promote persistent tenascin-C expression at the chronically inflamed site.

In summary this model, diagrammatical illustrated in figure 1.7, proposes that the microenvironment created by tenascin-C at sites of chronic inflammation helps

propagate the local inflammatory response by forming a persistent pro-inflammatory positive feedback loop.

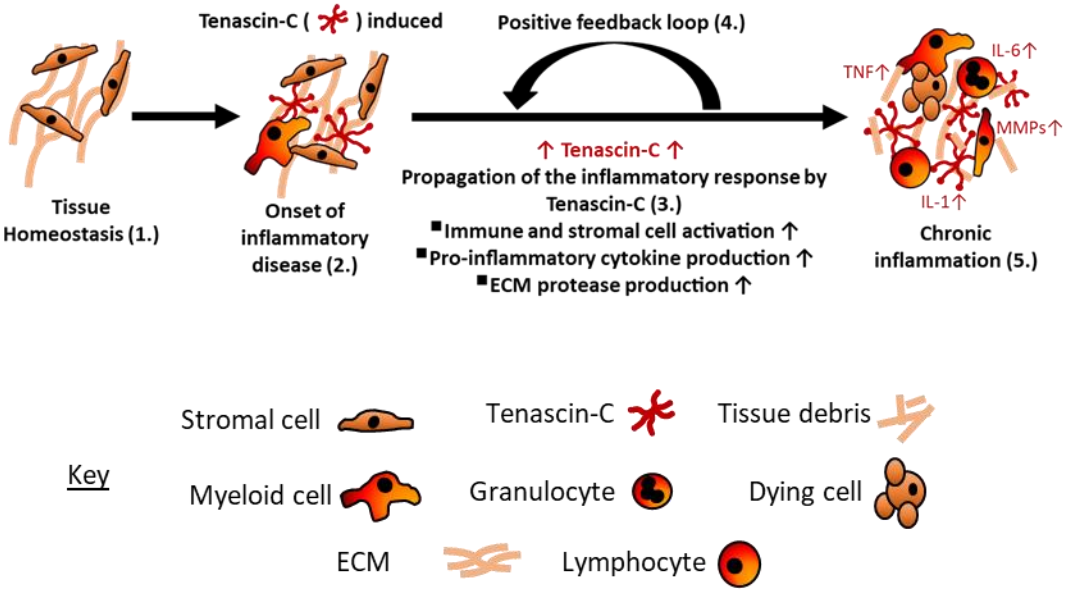

Figure 1.7 Inflammatory niche model of tenascin-C in inflammatory disease

Theoretical model for how tenascin-C functions as a key driver of pathological chronic inflammation in diseases such as inflammatory bowel disease. Basal expression of tenascin-C is low or negligible in the majority of post-natal tissues at homeostasis (1.). However, in the context of tissue insult or inflammatory disease tenascin-C becomes locally upregulated and deposited in the extracellular matrix (ECM) at the site of inflammation (2.). Tenascin-C then acts to create a pro-inflammatory niche at the site of inflammation by re-enforcing the pathological inflammatory response via its pro-inflammatory signalling mechanisms, such as activation of TLR4. This pro-inflammatory signalling induces inflammatory effector functions in stromal and immune cells such as production of tissue damaging extracellular proteases like matrix metalloproteases (MMPs). Additionally, it also drives production of other pro-inflammatory mediators such as the potent pro-inflammatory cytokines tumour necrosis factor (TNF), interleukin (IL)-1, and IL-6 (3.). This pro-inflammatory signalling by tenascin-C is then further enforced in a positive feedback loop with it's own signalling as well as that of the mediators it induces acting to induce further tenascin-C production (4.). In this manner tenascin-C plays a key role in the deregulated inflammatory response by blocking resolution and aiding in its continuing propagation to chronicity. The chronic response ultimately leads to the tissue succumbing to dysfunction and destruction and thus causing the pathology seen in chronic inflammatory diseases (5.).

1.5.3 Tenascin-C as a biomarker of disease

With the above highlighted body of literature supporting the notion that tenascin-C is inextricably associated with inflammatory disease it is of no surprise that tenascin-C has been investigated for potential clinical utility. These investigations have included studies into its value as a biomarker.

Biomarker, a portmanteau of biological and marker, is the term used to describe a characteristic that can be objectively measured as an indicator of normal or pathological biological processes, or responsiveness to a therapeutic intervention (Group, 2001). Biomarkers are measured in clinical practice as tools for identifying and classifying diseases in patients at diagnosis, as well as for informing predictions of disease course when considering prognosis. In recent years these processes have all become more critical with the development of the precision medicine approach to patient management where treatment is aimed to be tailored more closely to a patient's specific presentation of disease (Committee, 2011). Biomarkers have a clear role in this approach in aiding in the better subclassification of disease, in terms of specific disease mechanisms and prognosis, to which tailoring of treatment can be applied.

Tenascin-C presents a potentially attractive biomarker of inflammatory disease based on its characteristics described previously. This includes its limited expression in the adult outside of the context of inflammation making it a specific marker of the process. Additionally, with its implicated roles in disease pathogenesis tenascin-C would be classified as a mechanistic biomarker which display superior utility over simple descriptive surrogate markers (Robinson et al., 2013). As such, it is not surprising that numerous studies have already been undertaken to investigate tenascin-C's utility as an inflammatory disease biomarker in a range of contexts, which are summarised in table 1.2 below.

Table 1.2: Summary table of published data on tenascin-C as a biomarker of inflammatory disease. References and detail on the methodology employed to measure tenascin-C in the study are also provided. Disease and assay abbreviations detailed at the end of the table.

Disease	Methodology employed	Key findings	Reference
AAV	ELISA of serum tenascin-C (FN III-C splice specific)	Tenascin-C was higher in active disease compared to healthy controls and patients in remission and correlated with disease activity and occurrence of lung infiltration.	(Ishizaki et al., 2017)
Asthma	ELISA of serum tenascin-C (FN III-C splice specific)	Tenascin-C was higher in severe asthma compared to mild asthma and was associated with clinical features such as more severe airflow limitation	(Yasuda et al., 2018)
Ankylosing spondylitis	ELISA of serum tenascin-C (FN III-C splice specific)	Tenascin-C was elevated in patients compared to healthy controls and correlated with markers of disease activity. Levels also correlated with response to treatment	(Gupta et al., 2018)
IBD	ELISA of serum tenascin-C	Tenascin-C was higher in IBD patients compared to healthy controls and correlated with measures of disease activity. A treatment responsive decrease was also observed.	(Riedl et al., 2001)
	IHC for tenascin-C in colon biopsies	Thickened subepithelial tenascin-C staining shown to be an accurate marker for diagnosis of collagenous colitis	(Muller et al., 2001)
IIM	IHC of tenascin-C in muscle biopsies	Tenascin-C staining pattern was shown to distinguish dermatomyositis from polymyositis	(Muller-Felber et al., 1998)
IgA nephropathy	IHC and ISPCR for tenascin-C in kidney biopsies	Tenascin-C protein staining was associated with disease chronicity while mRNA expression was associated with disease activity	(Masaki et al., 1998)
JIA	ELISA of serum tenascin-C (FN III-C splice specific)	Tenascin-C was elevated in active disease compared to inactive disease and healthy controls. Levels correlated with markers of disease activity and decreased with therapy.	(Shukla et al., 2015)
Kawasaki disease	ELISA of serum tenascin-C (FN III-C splice specific)	Tenascin-C found elevated in the serum compared to healthy controls and recovering patients. Levels correlated with disease parameters and poor response to intravenous immunoglobulin.	(Okuma et al., 2016)

Table continued on next page

Table 1.2: Table continued from preceding page

Disease	Methodology employed	Key findings	Reference
Myocarditis	IHC for tenascin-C in myocardial biopsies	Tenascin-C staining was elevated in cases with active myocarditis and discriminated from patients with non-inflammatory dilated cardiomyopathy. Staining correlated with severity of histological lesions.	(Morimoto et al., 2005, Tsukada et al., 2009)
Psoriasis	IHC of skin biopsies	Tenascin-C was shown elevated in psoriatic skin lesions although it did not correlate with disease activity	(Latijnhouwers et al., 1998a)
RA	ELISA of serum tenascin-C (FN III-C splice specific)	Tenascin-C was elevated in patients compared to healthy controls and further increased with longer disease duration. Levels also correlated with joint erosion severity and decreased in response to therapy. Baseline tenascin-C was predictive of treatment responsiveness.	(Page et al., 2012)
	ELISA of serum autoantibodies targeting citrullinated tenascin-C	Autoantibodies against citrullinated tenascin-C (cTNC) had high diagnostic specificity for RA and were found in ~50% of patients. cTNC autoantibodies were found to pre-date disease development and in undifferentiated disease were associated with the development of RA. cTNC autoantibodies also associated with a subset of patients with periodontitis.	(Schwenzer et al., 2015, Raza et al., 2016, Schwenzer et al., 2017)
Scleroderma	ELISA of serum tenascin-C (FN III-C splice specific)	Tenascin-C was higher in scleroderma patients compared to healthy controls. Patients with pulmonary fibrosis involvement had the highest levels.	(Brissett et al., 2012)
SLE	ELISA of serum tenascin-C (FN III-B splice specific)	Serum tenascin-C was higher in patients with active disease compared to those with inactive disease and healthy controls. Elevated levels predicted need to escalate therapy in response to disease flare.	(Zavada et al., 2015)

AS, ankylosing spondylitis; SLE, systemic lupus erythematosus; RA, rheumatoid arthritis; IIM, idiopathic inflammatory myositis; AAV, antineutrophil cytoplasmic antibody (ANCA)-associated vasculitis; JIA, juvenile idiopathic arthritis; IHC, immunohistochemistry; ISPCR, *in situ* polymerase chain reaction; ELISA, Enzyme-linked immunosorbent assay; SPECT, single-photon emission computed tomography

These publications highlight the broad range of conditions which have been studied in the context of tenascin-C. Additionally, they also highlight the range of methodologies employed to detect tenascin-C. This includes direct observation of tenascin-C *in situ* as in the case of immunohistochemical detection of the protein in biopsy samples as in the case of Muller and colleagues' study of tenascin-C in collagenous colitis diagnosis (Muller et al., 2001). Enzyme-linked immunosorbent assay (ELISA) for the detection of tenascin-C in solution was by far the most commonly used methodology with tenascin-C having been detected in a variety of bodily fluids. This has included synovial fluid (Hasegawa et al., 2004), lung epithelial lining fluid (Kaarteenaho-Wiik et al., 1998), cerebrospinal fluid (Yoshida et al., 1994), as well as in the serum of the circulatory system.

Tenascin-C was first reported to be found in human serum in 1991 in a study by Herlyn and colleagues (Herlyn et al., 1991). Shortly after this discovery Schenk and colleagues demonstrated the link between systemic tenascin-C and inflammation by showing its correlation with other circulating inflammatory markers (Schenk et al., 1995). Since these early observations unsurprisingly, due it's to more ubiquitous availability for testing in the clinical setting, it is this systemic tenascin-C on which the majority of inflammatory biomarker work has focused. Of note are the number of studies which demonstrate a link between systemic tenascin-C and disease activity as well as other specific aspects of disease pathology. Additionally, the studies of Závada and Page and their respective colleagues are of particular interest due to their demonstration that measurement of systemic tenascin-C has prognostic value. In the case of the Závada study this was shown in SLE, a disease characterised by periods of flare and remission, which showed that elevated tenascin-C levels were predictive of initiation of a flare (Zavada et al., 2015). The Page study conversely focused on the inflammatory joint disease rheumatoid arthritis and showed that high tenascin-C levels were predictive of poor response to the biologic anti-TNF therapy infliximab (Page et al., 2012). As such, both of these studies suggest that tenascin-C could have utility as part of a companion diagnostic, a diagnostic tool which accompanies a specific treatment and allows tailoring of its application for maximum clinical benefit to patients (Jorgensen, 2015).

In summary these studies collectively demonstrate that measurement of tenascin-C by a variety of methodologies presents a variety of potential uses as diagnostic tool in a range of inflammatory diseases. In particular measurement of systemic tenascin-C, while not specific enough to be of use in diagnosis, could yet find utility in clinical practice for monitoring disease activity and assessing disease prognosis.

1.6 Aims and strategy

This introduction has summarised the previous work which has established tenascin-C as a pathological driver of inflammation implicated in many different IMIDs, including IBD.

In regard to this the first arm of this project aimed to further the understanding of the role of tenascin-C in IBD *in vivo*, building on this previous work which has been primarily of a descriptive rather than mechanistic nature. To do this the murine dextran sulphate sodium (DSS) model of colitis was identified as a valid model in which to study IBD in a controlled setting (Wirtz et al., 2017). In addition, the *Tnc*$^{-/-}$ mouse was also identified as a useful tool which in combination with this model would allow the dissection of tenascin-Cs contribution to colitis pathology.

The second arm of this project has focused upon a more immediate clinical application of tenascin-C as a potential systemic biomarker of inflammatory disease. As well as in IBD, tenascin-C is also found elevated in many other IMIDs. However, further investigations of the nature of this circulating tenascin-C have been limited by the tools available, with no sensitive, robust, and reliable commercially ELISA able to detect all forms of the protein in biological samples. As such, in partnership with the company Axis Shield Diagnostic Ltd, it was determined that the development of assays to measure tenascin-C in human serum would be undertaken. These assays were then aimed to be characterised and used to determine the nature of tenascin-C in a healthy control and IMID patient serum samples.

Towards both these goals the following aims have been achieved:

I. Characterise the expression of tenascin-C in a murine colitis model
II. Examine the effect of tenascin-Cs genetic ablation in a murine colitis model
III. Design novel tenascin-C based assays and assess their use as inflammatory disease diagnostics.

Chapter 2 Materials and Methods

2.1 Reagents and solutions

All chemicals and buffers were purchased from Sigma-Aldrich (Dorset, UK) unless otherwise stated. Commercial buffer recipes are shown in Appendix I. All primers and antibodies used are shown in Appendices II, III, and IV.

2.2 Bioinformatics

Tenascin-C expression data was obtained from the online gene expression databases Bio-GPS (http://biogps.org) (Wu et al., 2009) and SAGE-genie (http://cgap.nci.nih.gov/SAGE) (Boon et al., 2002). The bio-GPS data obtained was from the MOE430 Gene Atlas Data set (Lattin et al., 2008) which subjected a variety of tissue samples from 8-10 week old male C57BL/6 mice to MOE430_2 to microarray analysis. The SAGE-genie data comprised serial analysis of gene expression (SAGE) libraries of tissues taken from 84 day old mice of unspecified sex and strain. This was with the exception of the lung library which was obtained from a 109d old mouse and the MEF library which was of embryonic origin.

2.3 *In vivo* studies

2.3.1 Animal welfare

Mice were maintained under conventional specific pathogen free (SPF) conditions in the Biological Resource Facility (BRF; Roslin Institute, University of Edinburgh, Midlothian, UK) with a 12 hour light/dark cycle. All animal experiments were approved by the Roslin Institute's Animal Users Committee and the animals were maintained in accordance with Home Office guidelines for the care and use of laboratory animals.

2.3.2 Maintenance of tenascin-C knockout mice

All mice used in this thesis were on a 129sv genetic background strain from established colonies. Tenascin-C knockout (*Tnc*$^{-/-}$) mice were generated as previously described (Saga et al., 1992) whereby the second exon of the *Tnc* gene, containing the translation start site, was replaced using homologous recombination with a *LacZ* gene, thus deleting the tenascin-C protein. The colony was established with mice provided by my

Oxford based supervisor Prof. Kim Midwood, with knockout (KO) and wild-type (WT) mice maintained through homozygous pair matings. To distinguish WT mice from this *Tnc*$^{-/-}$ Oxford derived colony from WT mice obtained from a separate Roslin Institute colony the *Tnc*$^{-/-}$ colony WT mice will be referred to as WT(Ox) mice.

2.3.3 Genotyping

For DNA extraction, ear clip samples were taken from new born mice and digested in 200µl genotyping lysis buffer (1% SDS, 20mM EDTA, 0.1M NaCl, 50mM Tris-HCl pH8) supplemented with 1mg/ml proteinase K (recombinant PCR Grade; Roche, Mannheim, Germany) overnight at 55°C. The following day the tubes were cooled to room temperature and a 100µl of 3.75M NH_4OAc added. Tubes were vortexed and then centrifuged at 14,000 rpm for five minutes at 4°C. Following centrifugation, 100µl of chloroform was added before centrifugation at 14,000 rpm for five minutes at room temperature. The supernatant was then transferred to a new tube containing 500µl of 100% ethanol which was subsequently mixed by inverting. The tube was then centrifuged at 14,000 rpm for five minutes at room temperature after which the supernatant was removed and the DNA pellet left to air dry. Once dry the pellet was resuspended in 30µl TE buffer and left overnight at 4°C to fully dissolve. DNA concentration and purity was measured using a NanoDrop 1000 spectrophotometer (Thermo Fisher Scientific, Waltham, USA) ensuring that the A260/280 ratio was in the expected 1.8 to 2 range for pure DNA.

Two primer pairs were previously designed to amplify either the WT or the *Tnc*$^{-/-}$ (*LacZ*) alleles (Saga et al., 1992) and both were used in separate reactions to determine genotypes (for primer sequences see Appendix IV). Reactions were set up using components from a *Taq* DNA polymerase kit (Thermo Fisher Scientific). Reactions consisted of 100-200ng of template DNA in 1x PCR buffer, 5mM $MgCl_2$, 0.2mM dNTPs, 1% DMSO, 0.5µM forward primer, 0.5µM reverse primer, and 1.5 units *Taq* DNA polymerase made up to a 20µl final reaction volume with nuclease free water. No template control (NTC) reactions were prepared and ran alongside every PCR run for both primer sets. PCR was carried out on a DNA Engine DYAD (Peltier Thermal Cycler; Bio-Rad Laboratories, Hertfordshire, UK) using the following protocol: 95°C for five minutes, followed by 35 cycles of 94°C for one minute, 63°C for two minutes,

and 72°C for two minutes, with a final step to finish the reaction of 72°C for ten minutes.

After the reaction was completed, 5µl of 5X DNA loading buffer red (Bioline, London, UK) was added to each reaction and 20µl loaded onto a 1.5% agarose/TAE gel supplemented with 1x SYBR Safe DNA gel stain (Thermo Fisher Scientific). A 1Kb Hyperladder (Bioline) was loaded alongside samples as a molecular weight marker. Gels were electrophoresed at 140V for 60 minutes in a gel tank containing 1x TAE. Gels were imaged on a Gel Doc XR system with Quantity One 1-D Analysis Software (Bio-Rad Laboratories). An example genotyping result is shown in figure 2.1.

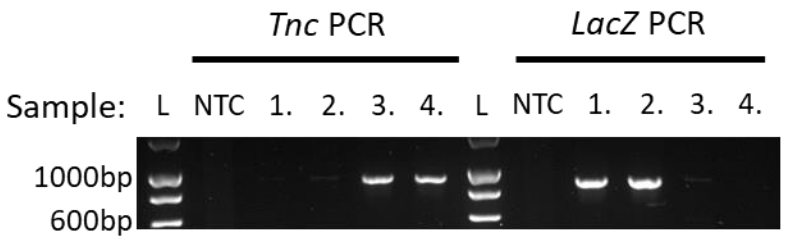

Figure 2.1 Example genotyping gel result

An example *Tnc* genotyping result for four mice with two (samples 1 and 2) identified as homozygous knockouts and two (samples 3 and 4) as homozygous wild-types. The ladders (L) show the PCR products are of the expected ~1000bp size (ladder bp sizes indicated on the right of the figure). The no template control (NTC) samples show no product for either PCR reaction.

2.3.4 Dextran Sulphate Sodium (DSS) murine model of colitis

Male mice of 7 - 9 weeks of age were used for all experiments. To induce colitis, Colitis Grade 36,000-50,000 MW DSS (MP Biomedicals, Santa Ana, USA) was administered in the drinking water *ad libitum* at a concentration of 2-3% (w/v) for five days. DSS was then withdrawn and the mice returned to regular drinking water for the remaining days before cull. In the acute model the mice were left for 3 days following DSS withdrawal and in the recovery model the mice were left for 17 days (Wirtz et al., 2007, Wirtz et al., 2017). Control age and sex matched mice received normal drinking water for the duration of the experiment. To control for potential genotypic

differences in water consumption between *Tnc*$^{-/-}$ and WT mice, water intake was monitored during the DSS dosing period as well by daily weighing of water bottles.

Throughout the protocol, general welfare monitoring was carried out daily and included weighing the mice as well as scoring for general health parameters and disease activity. General health scoring included monitoring for changes in appearance such as coat staring, hunching, and change in gait; and behavioural changes such as reluctance to move, and restlessness. Additionally, the colitis specific changes in stool consistency and presence of faecal blood were also scored for. A daily disease activity index (DAI) score for each mouse was produced by summing these scoring parameters. The study scoring sheet is included in Appendix V. Mice that exhibited severe adverse reactions, met DAI scoring severity thresholds, and/or lost more than 20% body weight before the study end point were euthanized on humanitarian grounds in compliance with home office regulations and were not included for analysis. For presentation of body weight loss data, percentage body weight loss relative to the day zero time point at the start of the experiment were calculated, with data presented as the mean of this percentage ± standard deviation. For presentation of DAI scoring data, a DAI sum score was calculated as the sum of all parameters scored for which is then presented in this thesis as median score ± interquartile range.

At the endpoint of all experiments the mice were culled by exsanguination by cardiac puncture while under terminal isoflurane induced anaesthesia to provide a terminal blood sample.

2.3.5 Tissue harvesting

Immediately following cull as detailed in section 2.3.4, blood samples and cadavers were collected. Blood samples were left to clot at room temperature for 30 minutes before centrifugation for 10 minutes, at 1000g, at 4°C. The serum supernatant was then transferred to another tube and flash frozen in LN_2 before storage at -70°C until use.

Colons were transected at the colorectal and colonocecal margins and resected with as much mesenteric tissue removed as possible. Colons were then inspected for gross pathology such as luminal blood, stool consistency, and enlarged lymph tissue before forceps were used to remove colonic contents. The colon was then flushed with PBS

to help remove any remaining faeces. Following flushing the colon length was measured and based on this it was transected into 3 equal segments corresponding to the proximal, middle, and distal portions of colon. These segments were further subdivided and processed for RNA extraction (see section 2.5.1), histology (see sections 2.4.1 to 2.4.2), protein extraction (see section 2.6.1), or myeloperoxidase assay (see section 2.7).

2.4 Histology

2.4.1 Paraffin embedded tissue processing and sectioning

Colon segments obtained in section 2.3.5 were flushed with 10% neutral buffered formalin (NBF; CellPath, Powys, UK) and then placed in histology cassettes (Simport, Beloeil, Canada) and incubated in 10% NBF for a minimum of 48hrs with agitation at 4°C. Cassettes were then transferred and stored in 70% ethanol before there transfer to the Easter Bush Pathology Department (Midlothian, UK) who carried out the wax embedding, sectioning, and staining (see section 2.4.3). Tissue processing used the following protocol: one wash in 95% ethanol for 1 hour, 5 washes in absolute ethanol for 1 hour each, 3 washes in xylene for 1 hour each, and embedding in paraffin wax for 4 hours with a wax change every 1 hour 20 minutes. Colon segments were embedded transversely and then sectioned at 5µm using a RM2155 microtome (Leica Biosystems, Milton Keynes, UK) before mounting on Superfrost slides (Thermo Fisher Scientific).

2.4.2 Cryo-embedded tissue processing and sectioning

Colon segments obtained in section 2.3.5 were placed in Surgipath embedding moulds (Leica Biosystems) in a transverse orientation and covered with Optimal Cutting Temperature (OCT) embedding compound (Cellpath). Blocks were then snap frozen in an ethanol-dry ice slurry cooled hexane bath for approximately one minute. Blocks were placed on dry ice for the hexane to evaporate before storage at -70°C until use. Cryosections were cut at 7µm on an OTF5000 cryostat (Bright Instruments, Bedfordshire, UK) and mounted on Superfrost slides (Thermo Fisher Scientific). Slides were allowed to air dry at room temperature for 30 minutes before storage at -70°C until use.

2.4.3 Haematoxylin and eosin (H&E) staining

The staining of paraffin embedded tissue sections (section 2.4.1) was performed by the Easter Bush Pathology Department (Midlothian, UK). Slides were dewaxed with xylene before rehydration through graded alcohol solutions. Slides were stained with Harris haematoxylin, washed, and further stained in 1% eosin. Stained slides were then dehydrated through graded alcohol solutions and cleared with xylene before mounting with coverslips using DePeX mountant (VWR, Radnor, USA).

H&E staining was performed on cryo-embedded tissue sections (section 2.4.2). Briefly, slides were removed from the -70°C and allowed to equilibrate to room temperature for approximately ten minutes. Sections were then fixed in ice cold methanol for two minutes before a brief wash in tap water. Staining was then performed on an Autostainer XL (Leica) with the following steps. Firstly, sections were stained with Harris haematoxylin, washed, and then blued in Scott's Tap Water. Slides were then washed and further stained with 1% eosin before dehydration through graded alcohol solutions and clearing with xylene. Finally slides were mounted with coverslips using Clearvue mountant Xyl (Thermo Fisher Scientific).

2.4.4 Light microscopy imaging

H&E stained sections stained as described in section 2.4.3 were visualised using an Eclipse E600 upright brightfield microscope (Nikon Instruments, Melville, USA) and images captured using an Axiocam 105 colour camera (Zeiss, Oberkochen, Germany) with Zen 2 software (Zeiss). Image processing, including adding scale bars and adjusting brightness, was performed using Zen lite software (Zeiss).

2.4.5 Colitis histopathology grading

H&E stained paraffin embedded and cryo-embedded sections which had been stained as described in section 2.4.3 were used for colon histopathology grading. Grading was performed blind by Professor Elspeth Milne (The Royal (Dick) School of Veterinary Studies, Midlothian, UK) using a published colitis grading system (Dieleman et al., 1998), which had been used previously in our lab (Dobie et al., 2018) (table 2.1). Pathology was scored for at least one section of proximal, middle, and distal colon per mouse. The scoring system assessed inflammation severity, inflammatory extent

through the tissue, tissue regeneration, and crypt damage. Additionally, a grade was also given for each of these parameters based on the percentage of the tissue which was affected by it. Final scores for the individual scoring parameters, inflammation severity, inflammation extent, crypt damage, and regeneration, were calculated as the parameters score multiplied by its percentage involvement grade. Sum histopathology scores were then calculated as the sum of each of these individual scoring parameters. Data for individual parameters as well as the sum score are presented as median score ± interquartile range throughout this thesis.

Table 2.1: Scheme used for colitis histopathology grading.

Feature Graded	Grade	Description
Inflammation	0	None
	1	Slight
	2	Moderate
	3	Severe
Extent	0	None
	1	Mucosa
	2	Mucosa and submucosa
	3	Transmural
Regeneration	4	No tissue repair
	3	Surface epithelium not intact
	2	Regeneration with crypt depletion
	1	Almost complete regeneration
	0	Complete regeneration or normal tissue
Crypt Damage	0	None
	1	Basal 1/3 damaged
	2	Basal 2/3 damaged
	3	Only surface epithelium intact
	4	Entire crypt and epithelium lost
Percentage Involvement	1	1-25%
	2	26-50%
	3	51-75%
	4	76-100%

2.4.6 Immunohistochemistry

Cryo-embedded tissue sections which had been processed as described in section 2.4.2 were removed from -70°C and allowed to equilibrate to room temperature for approximately ten minutes. Slides were washed with phosphate buffered saline-tween 20 (PBST; 0.05%) for 5 minutes before blocking with blocking solution constituting: 10% secondary antibody matched normal serum, 1% BSA, 0.1% Triton X-100 in PBST for one hour at room temperature. For CD11c staining, blocking solution was not used and PBST was used in its place for all steps. For CD3 staining, where a biotinylated secondary antibody was used, post blocking using an avidin biotin block was also performed (Vector Laboratories, Peterborough, UK). This was performed by first washing the slides in PBST briefly for one minute before applying Avidin D solution for 15 minutes. Another brief PBST wash was performed and the slides were then incubated with biotin solution for 15 minutes. Another brief PBST wash was performed before proceeding with primary antibody incubation. Sections were incubated with primary antibodies (see Appendix II) at appropriate concentrations diluted in blocking solution overnight at 4°C in a humidity chamber. The following day slides were washed with PBST 3 x 5 minutes, before application of appropriate fluorescent or biotin conjugated secondary antibodies at 2µg/ml diluted in PBST (see Appendix III). Slides were incubated for one hour at room temperature shielded from light. Slides which were incubated with biotinylated secondary antibodies were washed with PBST 3 x 5 minutes and followed with a 1 hour incubation with streptavidin conjugated to AF594 at 2µg/ml in PBST, followed by another 3 x 5 minutes PBST wash. All slides were then counterstained by incubation with DAPI (Thermo Fisher Scientific) nuclear stain at 0.1µg/ml in PBS for five minutes. Following a final 3 x 5 minutes PBS wash slides were mounted with coverslips using ProLong Gold Antifade Mountant (Thermo Fisher Scientific) and left to cure overnight at room temperature before imaging.

2.4.7 Fluorescent microscopy imaging

Fluorescently stained sections generated as described in section 2.4.6 were visualised using a DMLB upright fluorescent microscope (Leica) with a quad pass filter excitation wheel (Zaber, Vancouver, Canada), and SOLA source (Lumencor, Beaverton, USA). Images were captured with a Coolsnap MYO low light monochrome

CCD camera (Teledyne Photometrics, Tuscon, USA) using ImageJ2 software (Rueden et al., 2017) with the µManager plugin (Edelstein et al., 2014). Image processing, including standardisation of colour balance and addition of scale bars, was performed using the Fiji distribution of ImageJ 1.52e software (Schindelin et al., 2012).

2.5 RNA methods

2.5.1 Tissue RNA extraction

Tissue was extracted as described in section 2.3.5 and flash frozen in LN_2 before storage at -70°C until use. RNA was extracted using the acid guanidinium thiocyanate-phenol-chloroform method (Chomczynski and Sacchi, 1987). All surfaces and instruments coming into contact with the tissue was cleaned with RNAse Zap (Thermo Fisher Scientific) to remove any contaminating RNAses. Tissue was thawed on ice and at least 20mg added to 1ml of QIAzol Lysis Reagent (Qiagen, Hilden, Germany) in an Eppendorf. For RNA extraction from OCT embedded tissue processed as described in section 2.4.2 cryosections were cut at 10µm thickness and 5 sections per block were pooled and added to 1ml of QIAzol Lysis Reagent in an Eppendorf.

Tissue was homogenised in QIAzol with 3 x 10 second bursts of a T10 basic ultra-turrax handheld tissue homogeniser with an S10N 5G dispersing tool (IKA England, Oxford, UK). Following warming to room temperature 200µl of chloroform was added to the homogenate before 15 seconds vigorous mixing. Phases were then separated by centrifugation at 12,000 rpm for 15 minutes at 4°C after which the upper aqueous phase was taken off and transferred to a separate tube.

RNA was then purified using an RNeasy spin column kit (Qiagen) following the manufacturer's instructions. Briefly, an equal volume of ethanol was added to the aqueous phase before transfer to the RNeasy column. The column was then centrifuged to run samples through its silica membrane which selectively bound the sample RNA with contaminants discarded in the run through. An on column DNase treatment using an RNase-free DNase kit (Qiagen) was carried out to remove residual contaminating DNA before washing with wash buffers (provided with kit) to remove any remaining contaminants. Finally, RNase free water was passed through the column to elute the purified RNA.

RNA concentration and purity was assessed using a NanoDrop 1000 spectrophotometer (Thermo Fisher Scientific) checking that the A260/A280 and the A260/230 ratios were both approximately 2.0 indicating low protein and organic compound contamination respectively. Samples below 100ng/ml were left undiluted while those with a higher RNA concentration were diluted to 100ng/ml with RNAse free water.

2.5.2 Reverse Transcription

Complementary DNA (cDNA) was generated from extracted RNA as described in section 2.5.1. Superscript II reverse transcriptase (RT) kit (Thermo Fisher Scientific) was used following the manufacturer's instructions. Firstly, 10µl of RNA at or below 100ng/ml was incubated with 100ng of random primers (mostly hexamers; Thermo Fisher Scientific) for ten minutes at 70°C in a DNA Engine DYAD thermalcycler (Bio-Rad Laboratories). Following primer annealing, tubes were cooled on ice and 8µl of RT master mix was added to each for a 20µl total reaction volume containing 1x first strand buffer, 10mM Dithiothreitol (DTT), 0.5mM dNTPs, and 200U Superscript II RNase H. Tubes were returned to the DNA Engine DYAD thermalcycler and the following program ran: 25°C for 10 minutes, 42ºC for 50 minutes, 70°C for 15 minutes, and finally held at 4°C. cDNA samples were stored at -20°C until used.

2.5.3 Quantitative polymerase chain reaction (qPCR)

qPCR was carried out using cDNA generated as described in section 2.5.2 in a 96 well plate (Thermo Fisher Scientific) format using the SYBR green method (Ponchel et al., 2003). All qPCR reactions were run in technical duplicates with a NTC, where cDNA was replaced with RNase free water, also run alongside as a negative control. All cDNA was diluted to 5ng/µl with RNAse free water. For reactions using primers supplied by Sigma-Aldrich, the master mix (PrecisionPLUS mastermix, Primerdesign, Southampton, UK), was prepared in RNase free water and 20µl was added per well together with 5µl (25ng) diluted cDNA for a final reaction concentration of 1x SYBR green mastermix, 200nM forward primer, and 200nM reverse primer. For Tnc primers supplied by Primerdesign, 15µl of mastermix was added per well along with 5µl (25ng) diluted cDNA for a final reaction concentration of 1x SYBR green mastermix,

300nM forward primer, and 300nM reverse primer. All primer sequences used are listed in Appendix IV.

qPCR reactions were carried out on a MX3000P qPCR system (Stratagene, San Diego, USA) using the following program: 95°C for 2 minutes, followed by 40 cycles of 95ºC for 15 seconds, 60°C for 1 minutes, before a final melt curve of all PCR products from 55°C to 95ºC was generated.

2.5.4 qPCR Data Analysis

MxPro Mx3000P software (Stratagene) was used to calculate an arbitrary amplification-based threshold which was then used to assign each reaction a Ct (cycle threshold) value denoting the cycle number it reached this fluorescence threshold value. For further processing the Ct data was extracted and transferred to Microsoft Excel 2016 (Microsoft, Redmond, USA). For assessment of raw expression of genes in samples $2^{-\Delta CT}$ values were calculated where ΔCT relates to the gene's relative expression to the housekeeping 18s rRNA, calculated by subtracting the samples 18s rRNA CT value from the gene of interests CT value. For calculation of relative gene expression between test conditions the ΔΔCt method was used (Livak and Schmittgen, 2001). This method similarly initially calculated a ΔCT value relative to the 18s housekeeping gene to normalise the samples account for any slight variations in cDNA concentration. The ΔΔCt was then subsequently calculated with normalisation carried out to a selected control condition, which was set to 1, so that all other test condition values are presented as fold change relative to this value.

2.5.5 Primer quality control assessment

All primer sequences used were inputted into the NCBI Primer-BLAST webtool (Ye et al., 2012) initially to determine that the predicted specificity, GC% content, and self-complementarity were all acceptable. Tests for specificity and efficiency were also performed. To do this serial dilutions of cDNA from a sample known to express the transcript of interest were prepared and used to carry out qPCR, as detailed in section 2.5.3, to generate a standard curve. Firstly, to determine that the reactions had been successful the amplification plots for each primer were assessed to check amplification had taken place producing regular sigmoid curves. Additionally, Ct values were

checked to ensure they fell in the range for reliable detection below 35 cycles. Next specificity was assessed by checking the melt dissociation curve to ensure only one distinct peak and thus one distinct product had been produced. Specificity was further confirmed by running the qPCR product on an agarose gel as in section 2.3.3 to check the singular product detected was of the predicted length for that produced by the primer pair. Efficiency was assessed by checking the R^2 value produced by the standard curve, which if >0.9 indicates a near perfect linear correlation and at least >90% primer efficiency. An example primer optimisation result is shown in figure 2.2.

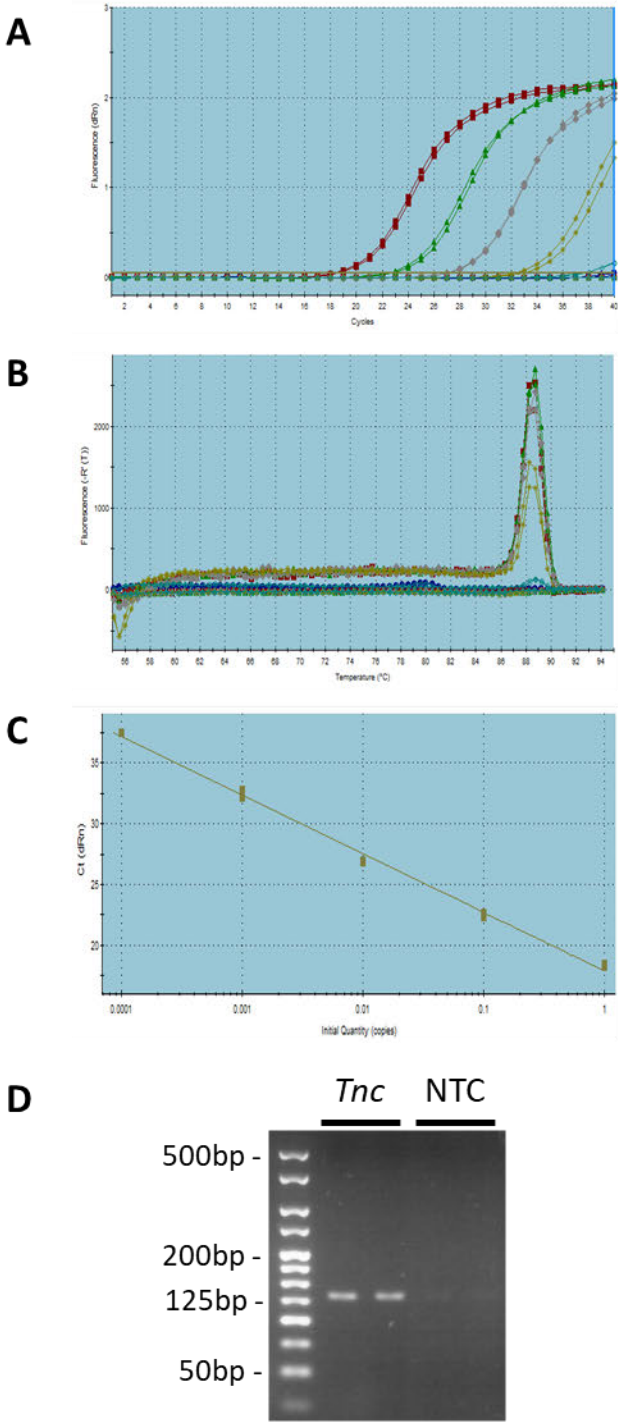

Figure 2.2 Primer optimisation example for *Tnc* primers

Example of primer quality control testing results for the *Tnc* qPCR primers.
(**A**) The standard sigmoidal amplification curves for the primers with cycle thresholds within the limits of detection.
(B) The melt dissociation curve showing a single peak and thus product is produced.
(C) The standard curve produced by setting up reactions of serially diluted cDNA with the primers.
(D) *Tnc* primer qPCR reaction products ran on an agarose gel showing just one product of the predicted 127 base pairs (bp) size. No bands are evident in the no template control (NTC) reactions. A 25bp hyperladder was ran alongside with band sizes in bp marked as indicated.

2.6 Protein methods

2.6.1 Protein extraction

Tissue was extracted as described in section 2.3.5 and flash frozen in LN_2 before storage at -70°C until use. Tissue was thawed on ice and a minimum of 35mg added to 300µl of RIPA buffer (Thermo Fisher Scientific) supplemented with 1x cOmplete mini EDTA-free protease inhibitor cocktail (Roche). Tissue was homogenised by 3 x 10 second bursts of a T10 basic ultra-turrax handheld tissue homogeniser with an S10N 5G dispersing tool (IKA England). Samples were then clarified by centrifugation at 13,000 rpm for ten minutes at 4°C. The supernatant was then taken off and stored at -20°C before use.

2.6.2 Quantification of protein

Protein concentration was determined using a DC Protein Assay kit (Bio-Rad Laboratories) using a 96 well plate format. Initially, Reagent A' was prepared by adding 20µl of reagent S per 1ml of Reagent A and 25µl of Reagent A' added per plate well. A 1/10 dilution of the sample prepared as described in section 2.6.1 was then made up in RIPA buffer and 5µl added per plate well with two technical replicate wells prepared for each sample. A standard curve of known protein concentrations was also prepared on the plate utilising bovine plasma gamma globulin diluted in RIPA buffer. Reagent B was then added to the plate with 200µl dispensed per well. The plate was mixed and then left to develop at room temperature for at least 15 minutes, during which time the alkaline copper tartrate and Folin reagent in the kit reagents reacted with the protein in solution to produce a blue product proportional to the protein concentration. The colour change was then quantified by measuring the plate's absorbance at 750nm on a Synergy HT Multi-Mode Microplate Reader (BioTek Instruments, Winooski, USA). The Gen5 microplate reader software (BioTek) was then used to fit a standard curve, using a four parameters logistic regression, to the gamma globulin standards. The protein concentration of the samples was then interpolated from this standard curve.

2.6.3 Polyacrylamide Gel Electrophoresis (PAGE)

Samples were electrophoresed using a NuPAGE Novex PAGE system under denaturing conditions with buffers and equipment all provided by Thermo Fisher

Scientific unless otherwise specified. Sample loading mixes were prepared containing 1x NuPAGE LDS (lithium dodecyl sulphate) sample buffer, 1x NuPAGE reducing agent, and 1mg/ml protein sample (from section 2.6.1 and using concentrations calculated in section 2.6.2) diluted with distilled water (dH_2O) if required. Loading mixes were then denatured by incubation at 70°C for 10 minutes before cooling at room temperature. Samples were then loaded onto NuPAGE pre-cast 10% Bis-Tris, 4-12% Bis-Tris, or 3-8% Tris-Acetate protein gels in a Novex XCell SureLock Mini-Cell gel tank. A pre-stained molecular weight marker (Precision Plus Protein All Blue Prestained Protein Standards; Bio-Rad Laboratories) was also loaded onto all gels alongside the samples. Bis-Tris gels were run with 1x NuPAGE MOPS SDS running buffer at constant 200V until desired protein separation was achieved. Tris-acetate gels were run with 1x NuPAGE Tris-acetate SDS running buffer at constant 150V until desired protein separation was achieved.

2.6.4 Western blotting

Following gel electrophoresis as described in section 2.6.3 proteins were wet transferred onto Amersham Protran nitrocellulose membranes (GE Healthcare Life Sciences, Buckinghamshire, UK). Transfer was carried out in a Novex XCell II Blot Module (Thermo Fisher Scientific) filled with 1x transfer buffer (20% methanol, 0.04% SDS, 39mM glycine, 50mM Tris) with the gel and membrane sandwiched together between filter paper and sponges. Transfer was carried out with the tank on ice at 30V for 90 minutes. Immediately after transfer the membrane was briefly washed in dH_2O before staining with Ponceau S solution to confirm transfer success and uniform sample loading. Membranes were then washed in PBST (0.05%) to de-stain before blocking in Odyssey PBS Blocking Buffer (LI-COR Biotechnology, Cambridge, UK) for one hour at room temperature with agitation. Following blocking the blocking buffer was discarded and primary antibodies applied to the membrane at the indicated concentrations (see Appendix II) in Odyssey PBS Blocking Buffer. Membranes were incubated with primary antibody overnight at 4°C with agitation. The following day primary antibody solution was tipped off and the membrane washed 3 x 5 minutes in PBST (0.1%) at room temperature with agitation. Appropriate secondary antibodies were then applied to the membrane at the indicated concentrations (see Appendix III) in Odyssey PBS Blocking Buffer and incubated for

one hour at room temperature with agitation. As secondary antibodies were conjugated to near infrared dyes the membrane was protected from light exposure for all subsequent steps. Secondary antibody solution was then discarded and the membrane washed for 3 x 5 minutes in PBST (0.1%) at room temperature with agitation. Blots were then visualised using an Odyssey imaging system (LI-COR Biotechnology) and captured scans analysed using Image Studio Lite Ver 5.2 software (LI-COR Biotechnology). Blots were stored in PBS at 4°C after scanning until re-probing, if necessary.

2.6.5 Protein gel silver staining

Samples were run on an SDS-PAGE gel as detailed in section 2.6.3 and immediately after running transferred to a gel dish containing gel fixer solution (40% ethanol, 10% acetic acid in dH_2O) and incubated with agitation for one hour. The gel was then washed with dH_2O overnight with multiple changes of the dH_2O. The gel was then sensitised to staining by incubating with 0.02% sodium thiosulphate solution for one minute followed by three quick washes with dH_2O. The gel was then stained with cooled (4°C) silver nitrate solution (0.1% silver nitrate, 0.02% formaldehyde) for 20 minutes with agitation followed by washing four times briefly with dH_2O to ensure any residual silver nitrate was removed. Stain was then developed by incubating the gel with sodium carbonate solution (3% sodium carbonate, 0.05% formaldehyde). Once protein was sufficiently stained the staining was terminated by first washing the gel briefly in dH_2O before incubating it with 5% acetic acid solution for five minutes. The gel was then stored in 1% acetic acid solution at 4°C until use.

2.7 Myeloperoxidase (MPO) Assay

MPO enzymatic activity, a surrogate marker of neutrophil infiltration (Krawisz et al., 1984), was assessed according to a published protocol (Kim et al., 2012). Tissue was extracted as described in section 2.3.5 and flash frozen in LN_2 before storage at -70°C until use. Tissue was thawed on ice, weighed, and at least 25mg placed in an Eppendorf tube. Hexadecyltrimethylammonium bromide (HTAB) buffer (0.5% HTAB, 50mM potassium phosphate pH 6.0) was then added to the tissue at a ratio of 25mg tissue per ml of HTAB buffer. The tissue was then homogenised by 3 x 10 second bursts of a T10 basic ultra-turrax handheld tissue homogeniser with an S10N 5G dispersing tool

(IKA England). Homogenate was then clarified by centrifugation for 6 minutes at 13400g at 4°C. The supernatant was then taken off and stored at -70°C before use.

The assay was carried out in a 96 well plate format with all samples tested in triplicate as technical replicates. To begin, 7µl of HTAB tissue homogenate was added per test well followed by 200µl of o-dianisidine buffer (0.5mM o-dianisidine dihydrochloride, 0.0006% H_2O_2, 5mM potassium phosphate buffer pH 6.0). O-dianisidine is catalysed to produce a yellow-orange substrate by the MPO in the homogenate. This colour change was quantified by measuring the plate's absorbance at 450nm on a Synergy HT Multi-Mode Microplate Reader (BioTek) using Gen5 microplate reader software (BioTek). Three measurements were taken over a one minute period at 0 seconds, 30 seconds, and 60 seconds. The MPO activity in units (U; the amount of MPO needed to degrade 1µmol of H_2O_2 per minute at room temperature) per mg of tissue was then determined using the following equation:

$$U/mg\ \ of\ tissue = \left(\frac{\Delta Absorbance}{\Delta \min\, x\, 1.13x10^{-2}}\right)/0.175\, mg$$

ΔAbsorbance: The change in 450nm absorbance which was calculated by subtracting the starting absorbance read from the end absorbance read.

Δmin: The change in minutes between each absorbance reading used to calculate the ΔAbsorbance.

$1.13x10^{-2}$: The change in absorbance that 1µmol of H_2O_2 gives per minute.

0.175mg: The amount of tissue homogenate added per well.

U/mg was calculated using the average ΔAbsorbance of the technical replicates for both the 0 to 30 seconds time point and the 30 to 60 seconds time point. The MPO activity for each sample was then taken as the average of both of these time points activity.

2.8 Human cTNC autoantibody enzyme-linked immunosorbent assay (ELISA)

2.8.1 Plate washing and coating

Streptavidin Immobilizer 96 well plates (Nunc, Thermo Fisher Scientific) were used for all experiments. All washes were carried out using a Stat-Matic II plate washer (Sigma-Aldrich). Wells were filled with cTNC wash buffer (PBS-T (0.05%)) followed by inverting to remove wash buffer. Washes were repeated as indicated. After the final wash the plates were dried by blotting onto paper towels to remove residual buffer.

Biotinylated peptides used for coating the plates were cyclic citrullinated peptide (CCP; second generation; Axis-Shield Diagnostics Ltd, Dundee, UK), non-citrullinated TNC5 (rTNC5), and citrullinated TNC5 (cTNC5) (both peptides produced by Pepceuticals Ltd (Leicester, UK)). The CCP2 peptide is a component of Axis Shield's commercial anti-CCP assays and its amino acid sequence is confidential. The rTNC5 and cTNC5 peptides, have the amino acid sequences EHSIQFAEMKLRPSNFRNLEGRRKR and EHSIQFAEMKL-cit-PSNF-cit-NLEG-cit-cit-KR respectively and were derived from the human tenascin-C protein as previously described (Schwenzer et al., 2015). For plate coating, peptides were prepared at 0.3µg/ml in cTNC peptide buffer (PBST (0.05%), 0.1% BSA). Plates were washed three times before the addition of 100µl/well of the peptide coat solutions. For the no peptide control wells, 100µl/well of cTNC peptide buffer alone was added. The plates were incubated for one hour at room temperature on an orbital plate shaker at 200 rpm. Peptide coating solution was then decanted, and the plates washed three times before sample loading.

2.8.2 Sample preparation

Human serum or plasma samples were diluted 1/100 in cTNC sample buffer (1M NaCl, 4.9mM disodium phosphate, 0.5% Tween 20, 2% BSA, pH 7.2) for all assays. Every plate included three control samples diluted in the same manner as the test samples. These included a negative control individual normal serum sample (Access Biologicals, Vista, USA), as well as the intermediate (QC2) and high (QC5) positive control samples from a commercial Architect CCP assay (Axis-Shield Diagnostics Ltd).

Plates prepared as described in section 2.8.1 were loaded with 100µl/well of each control and test sample in duplicate. Plates were incubated for one hour at room temperature on an orbital plate shaker at 200 rpm after which the sample solutions were decanted and plates washed three times prior to autoantibody detection.

2.8.3 Autoantibody detection

Detection antibodies were conjugated to horseradish peroxidase (HRP) for enzymatic colourimetric detection and were diluted in cTNC conjugate buffer (PBS, 0.05% Tween 20, 1% BSA) to a working concentration of 0.1µg/ml. For detection of IgG class autoantibodies a goat anti-human IgG (γ-chain)-HRP detection antibody (catalogue number: 074-1002) was used and for detection of IgA a goat anti-human IgA (α-chain)-HRP detection antibody (catalogue number: 14-10-01) was used, both from Kirkegaard & Perry Laboratories (KPL; Gaithersburg, USA).

Plates from section 2.8.2 were incubated with 100µl/well of detection antibody for one hour at room temperature on an orbital plate shaker at 200 rpm after which the detection antibody solutions were decanted and plates washed three times. For colourimetric detection 3,3',5,5'-tetramethylbenzidine (TMB) HRP substrate (Moss Inc, Pasadena, USA), a clear solution which produces a blue product upon incubation with HRP, was added to the plate at 100µl/well. The plate was incubated at room temperature for five minutes and then colour change was quantified by measuring absorbance at 650nm using a Varioskan Flash Multimode Reader with SkanIt Microplate Reader software (both Thermo Fisher Scientific). Raw absorbance data was exported to Microsoft Excel 2016 (Microsoft) for analysis.

2.9 Human tenascin-C sandwich ELISA

The below protocol detailed in sections 2.10.1 to 2.10.3 is the final assay protocol developed. However, while this basic scheme of work was followed during assay development some steps or materials were later amended during optimisation. This includes during initial antibody screening in which 1% BSA PBST was used as the block, sample, and antibody dilution buffer instead of the respective buffers detailed below. Additionally, during screening differing antibody concentrations were

investigated with detection antibodies used in a range from 5 to 0.001µg/ml while all capture antibodies were kept constant and coated at 1µg/ml.

2.9.1 Plate coating and washing

High binding capacity 96 well plates (Biomat, Trento, Italy) were used for all experiments. All washes were carried out as specified in section 2.8.1.

Mouse anti-tenascin-C monoclonal antibody, clone 9F8 (MAB1911; Merck, Darmstadt, Germany) was used as capture antibody. For coating, antibody was prepared at 2µg/ml in carbonate buffer (15mM sodium carbonate, 35mM sodium bicarbonate, pH 9.6) and then 100µl/well was added to the plate. Plates were coated overnight at 2-8°C. The following day the coating solution was decanted, and plates washed three times before proceeding with blocking.

2.9.2 Plate blocking and sample preparation

Coated plates from section 2.9.1 were blocked by adding 200µl/well of blocking buffer (PBS, 0.05% Tween 20, 2% BSA) and incubating for one hour at room temperature on an orbital plate shaker at 200 rpm.

Human serum and plasma samples were diluted 1/200 in cTNC sample buffer. A standard curve (0 to 50 ng/ml tenascin-C) was prepared using human tenascin-C purified from a glioma cell line (Merck) diluted in cTNC sample buffer. The 0ng/ml standard was cTNC sample buffer alone. A standard curve was included on all plates. After blocking, the plate was washed four times before samples and standards were added to the plate at 100µl/well in duplicate. The plates were then incubated for one hour at room temperature on an orbital plate shaker at 200 rpm. Following incubation, the sample solutions were decanted and the plates washed four times before proceeding with detection.

2.9.3 Tenascin-C detection

Tenascin-C specific detection antibody, NSCT-121 (kindly provided by Nascient Ltd, Cambridge, UK), was conjugated to biotin (kindly carried out by Dr Mel Lewis, see section 2.12.1) and diluted in cTNC conjugate buffer to a working concentration of 5ng/ml. Plates from section 2.9.2 were incubated with 100µl/well of detection

antibody for one hour at room temperature on an orbital plate shaker at 200 rpm. Following incubation, the detection antibody was decanted and plates washed four times. High sensitivity streptavidin-HRP conjugate (Thermo Fisher Scientific) was used as a secondary detection reagent. This was diluted to a working concentration of 0.2µg/ml in cTNC conjugate buffer before use. Plates were incubated with 100µl/well of streptavidin-HRP for one hour at room temperature on an orbital plate shaker at 200 rpm. Following incubation streptavidin-HRP was decanted and the plates washed three times. Colourimetric detection was carried out using TMB solution as described in section 2.8.3. Raw absorbance data was exported to Microsoft Excel 2016 (Microsoft) and sample tenascin-C concentrations interpolated from the standard curves as detailed in section 2.14.3.

2.10 Human tenascin-C competition assay

2.10.1 Plate coating

Nunc Immuno-Module F8 MaxiSorp plates (Thermo Fisher Scientific) were used for all experiments. All washes were carried out as specified in section 2.8.1.

Plates were coated with 100µl/well 0.5µg/ml of his-tagged recombinant human tenascin-C fibrinogen-like globe domain (his-FBG; kindly provided by Nascient Ltd) in carbonate buffer overnight at 2-8°C. The following day coating solution was decanted, and plates washed three times before proceeding with blocking.

2.10.2 Sample and antibody competitor preparation

Coated plates from section 2.10.1 were blocked as described in section 2.9.2 and after blocking, washed three times before addition of samples.

Human serum and plasma samples were diluted 1/100 in blocking buffer. A standard curve (0 to 100 ng/ml tenascin-C) prepared as described in section 2.9.2 was included on all plates. Biotinylated detection antibody, NSCT-121 (kindly provided by Nascient Ltd) was prepared to 1.25ng/ml in blocking buffer.

Samples and standards were mixed with the detection antibody solution in a 1:1 (v/v) ratio (100µl:100µl) and then incubated for one hour at room temperature on an orbital plate shaker at 200 rpm. Following the co-incubation, 150µl /well of each standard and

sample in triplicate was transferred to his-FBG coated plates. The plate was then incubated for one hour at room temperature on an orbital plate shaker at 200 rpm.

2.10.3 Detection

Secondary detection and colourimetric development were carried out with a streptavidin-HRP conjugate and TMB substrate solution as described in section 2.9.3 except that streptavidin-HRP was used at 0.1µg/ml. Raw absorbance data was exported to Microsoft Excel 2016 (Microsoft) and sample tenascin-C and sample tenascin-C concentrations interpolated from the standard curves as detailed in section 2.14.3.

2.11 Tenascin-C Large FnIII-B and FnIII-C ELISAs

The tenascin-C large FnIII-B and FnIII-C ELISA kits (IBL International, Hamburg, Germany) were used to quantify tenascin-C FnIII-B or FnIII-C splice variants respectively. Both ELISAs were performed according to the manufacturer's instructions with samples and standards run in duplicate. Sample dilutions for human serum and plasma samples was determined by titration with samples diluted 1/400 for the FnIII-B assay and 1/10 for the FnIII-C assay using the EIA sample dilution buffer provided by the kits. For chromogenic development plates were left at room temperature in the dark for 30 minutes before addition of stop solution. Absorbance was then measured at 450nm using a Varioskan plate reader as described in section 2.8.3. Raw absorbance data was exported to Microsoft Excel 2016 (Microsoft) and sample tenascin-C FnIII-B and FnIII-C concentrations interpolated from the standard curves as detailed in section 2.14.3.

2.12 Tenascin-C immunoprecipitation (IP)

2.12.1 Antibody biotinylation and bead coupling

Prior to biotintylation, antibody was buffer exchanged into PBS using a Zeba Spin Desalting Column with a 7000Da molecular weight cut off (MWCO) (Thermo Fisher Scientific) according to the manufacturer's instructions. In brief, the column's storage buffer was removed and then PBS was passed through the column resin three times. This consisted of applying 300µl of PBS to the top of the column and then centrifuging the column at 1500g for one minute. After the final PBS wash, the antibody was

applied to the column followed by centrifugation at 1500g for two minutes with the antibody in PBS obtained in the run through.

Antibody was biotinylated using EZ-Link NHS-PEG_4-biotin (Thermo Fisher Scientific) according to the manufacturer's instructions. In brief, the NHS-PEG_4-biotin was rehydrated in dH_2O and then added to the antibody at a 12mmol excess. The biotinylation reaction was then left to occur for 30 minutes at room temperature. Biotinylated antibody was dialysed into PBS overnight at 4°C to remove non-reacted biotin using a 7000Da MWCO Slide-A-Lyzer MINI Dialysis Unit (Thermo Fisher Scientific) Using the IgG extinction coefficient of 1.35 and the antibody solutions absorbance at 280nm, measured against a PBS blank using a Varian Cary 50 UV-Vis Spectrophotometer (Agilent Technologies, Santa Clara, USA), the final concentration of the dialysed antibody was determined.

Biotinylated antibodies were coupled to magnetic M-270 streptavidin Dynabeads (Thermo Fisher Scientific). Raw microparticles were first resuspended by mixing on a roller mixer. The appropriate volume of resuspended raw microparticles were transferred to a centrifuge tube and PBS-10% Tween 20 was added to a final concentration of 0.05% Tween 20. Microparticles were washed by rotating for ten minutes using an end over end mixer. After washing particles were immobilised to a magnet and the supernatant removed. This wash protocol was repeated, and the particles were finally resuspended in PBST (0.05%). Biotinylated antibody was added to the microparticles at a ratio of 1 mg antibody per 40 mg of microparticles. Microparticles were incubated with antibody using an end over end mixer for one hour to allow binding of biotinylated antibody to the streptavidin on the surface of the microparticle. Following coupling the microparticles were washed in PBST (1%) using a magnet and end over end mixer as described above. This wash was carried out with rotation for ten minutes and was repeated twice. Following the final wash microparticles were finally resuspended in microparticle storage solution (100mM Tris, 150mM NaCl, 20mM EDTA, 0.1% Tween 20, 0.1% Proclin) at 20mg/ml and stored at 4°C.

2.12.2 Human serum and plasma tenascin-C IP

To immunoprecipitate tenascin-C, Dynabeads coupled to the tenascin-C specific NSCT-121 antibody (Nascient Ltd) were used. For all samples a matched control IP was also carried out using Dynabeads coated with an antibody to an irrelevant target. Uncoupled dynabeads were also used for pre-clearing the samples. All dynabead preparations were made up as described in section 2.12.1 with antibody omitted for uncoupled dynabeads.

The Dynabead preparations were initially washed three times with an excess volume of PBS using an end over end mixer and magnet before resuspension in their original volume with PBS. Serum and plasma samples were diluted 1/5 in PBS (200µl sample + 800µl PBS) before addition of 2mg of uncoupled beads which were then left to roll for at least one hour to pre-clear. Following pre-clearing, the particles were brought to a magnet and the supernatant equally split between two tubes, one for tenascin-C IP and one for the control IP. For both the control and tenascin-C IP 1mg of Dynabeads, prepared in PBS as above, were added to the IP tubes and left on a roller mixer at 4°C overnight. The following day the dynabeads were washed three times with an excess volume of PBS using a tube rotator and magnet. After the final wash, the dynabeads were brought to the magnet and as much fluid drained as possible before immediate elution or storage at -20°C for later use.

To elute tenascin-C from the beads for measurement in the tenascin-C sandwich ELISA beads were incubated with 20µl of 50mM Glycine pH 2.5 (elution solution) for approximately one minute. The tube was then placed to the magnet to remove the beads from solution and the eluent transferred to another tube. The eluent was then neutralised with the addition of 1M Tris-HCl pH 7 till a neutral pH was achieved as determined using litmus paper (Sigma-Aldrich). Eluents were then diluted 1/25 and supernatants 1/100 in cTNC sample buffer, while IP waste wash buffer was left undiluted, prior to analysis in the sandwich ELISA as detailed in section 2.9.

For western blot and gel band mass spectrometry analysis proteins were eluted from dynabeads beads in 20µl 1x NuPAGE sample buffer supplemented with 1x NuPAGE

reducing agent and then processed for gel electrophoresis as described in section 2.6.3. For on bead digestion for mass spectrometry analysis see section 2.13.1.

2.13 Mass spectrometry (MS)

Mass spectrometry was carried out with the assistance of Dr Dominic Kurian of the Roslin Proteomics and Metabolomics Facility (PMF) at the Roslin Institute unless otherwise stated.

2.13.1 On bead protein digestion

IP Dynabeads prepared as described in section 2.12.2 were resuspended in 70µl of MS buffer 1 (2M Urea, 50mM ammonium bicarbonate, 1mM DTT) supplemented with 5µg/ml sequencing grade modified trypsin (Promega, Madison, USA). Tubes were then left to digest on a thermomixer at 29°C for 30 minutes at 1200 rpm. After digestion a magnet was used to separate the beads and the supernatant was taken off and transferred to another tube. The IP Dynabeads were then resuspended in 60µl of MS buffer 2 (2M urea, 50mM ammonium bicarbonate, 5mM iodoacetamide), mixed, separated using a magnet, and the supernatant taken off. This second supernatant was pooled with the first supernatant and was then left to digest overnight protected from light on a thermomixer at 37°C and at 800 rpm. To stop the reaction the next day the sample was acidified by addition of trifluoroacetic acid (TFA) for final sample concentration of 0.5%.

2.13.2 In gel protein digestion

Gels silver stained as detailed in section 2.6.5 were washed three times for ten minutes in dH_2O to remove any residual acetic acid. Bands were then cut out with sterile scalpel blade and diced into 1mm cubes which were placed in Protein Low bind tubes (Eppendorf, Hamburg, Germany). In gel protein digestion was then carried out by the Roslin PMF staff. In brief, the gel bands were dehydrated with acetonitrile to shrink them and enhance solution penetration. The proteins in the gel were then reduced and alkylated with incubations in 10mM DTT and 55mM iodoacetamide respectively, before overnight digestion with trypsin. Formic acid was then added the next day to stop digestion and peptide extraction buffer (50% Acetonitrile, 0.001% formic acid) was added to fully extract peptides from the gel.

2.13.3 Peptide purification

Before mass spectrometric analysis peptides from protein digests as detailed in sections 2.13.1 and 2.13.2 were first purified using C18 HyperSep SpinTip Microscale SPE Extraction Tips (Thermo Fisher Scientific). The column was washed by passing 70µl of acetonitrile buffer (80% Acetonitrile, 0.05% TFA) through the column, by spinning it at 2000 rpm for one minute, three times. The column was then equilibrated by washing three times in a similar manner with 0.05% TFA. The peptide samples were then loaded onto the column and passed through with the run through, collected and passed through a second time. The column was then washed twice with 100µl of 0.05% TFA before elution by passing 60µl of acetonitrile buffer through. This elution step was repeated and the eluents pooled before sample drying in a Savant SPD 2010P1 speedvac (Thermo Fisher Scientific). Once dried the sample was dissolved in formic acid and stored at -20°C until use.

2.13.4 Liquid chromatography- tandem mass spectrometry (LC-MS/MS) analysis

Peptides obtained as in section 2.13.3 were analysed by mass spectrometry by Roslin PMF staff. Analysis was carried out using an UltiMate HPLC system (Thermo Fisher Scientific) coupled to a micrOTOF-Q II ESI-Qq-TOF mass spectrometer (Bruker, Billerica, USA). Spectra were analysed using ProteinScape software (Bruker) in combination with the Mascot database search engine (Matrix Science, London, UK) for protein identification.

2.14 Statistical analysis

2.14.1 Significance tests and data presentation

Statistical analysis was carried out using Prism 8 statistical software (Graphpad Software, San Diego, USA). Data was checked for normal distribution, to inform statistical test choice, using the Shapiro–Wilk test. For normally distributed continuous data direct comparisons were carried out using the Student's t-test or a one-way analysis of variance (ANOVA). For multiple comparisons a two-way ANOVA with Sidak's multiple comparisons test was used. For direct comparisons of non-parametric data the Mann-Whitney U test was used. For multiple comparisons the Kruskal-Wallis test with Dunn's multiple comparisons test was used. $P<0.05$ was considered to be

significant for all tests carried out. All continuous data are presented as the mean ± the standard deviation (StdDev) and ordinal data as the median ± the interquartile range.

2.14.2 Assessment of correlation and prevalence

Both correlation and prevalence were graphed and statistically assessed utilising Prism 8 statistical software (Graphpad Software).

Correlation between two variables was assessed using the non-parametric Spearman's rank correlation test providing a correlation coefficient (ρ) describing the relationship between the variables with 1 indicating a perfect positive and -1 a perfect negative correlation. A p value was also computed testing the null hypothesis that the two variables were not correlated, with significance ($p<0.05$) indicating that they do display some correlation.

Prevalence of a variable was calculated and graphed as the percentage of total animals exhibiting the variable over time. Statistical significance of differences in prevalence between groups was then assessed for each time point using Fisher's exact test.

2.14.3 ELISA standard curve interpolation and signal to noise ratio calculations

Standard curves were fitted using a quadratic polynomial regression for the IBL and sandwich ELISAs (described in sections 2.9 and 2.11) while a cubic polynomial regression was used for the competition assay (described in section 2.10). A new standard curve was calculated based on the on-plate standards for every plate from which interpolation of that plates unknown sample concentrations was then carried out either manually in Microsoft Excel 2016 (Microsoft) or using the Prism 8 statistical software (Graphpad Software).

To calculate a signal to noise ratio the absorbance of the highest standard concentration was divided by the lowest standard concentration on the assay plate. This was done for at least three plates with the mean signal to noise ratio calculated across the plates given.

2.14.4 Receiver operating characteristic (ROC) curve calculation and assessment of diagnostic ability

ROC curves, calculated using the Prism 8 statistical software (Graphpad Software), were used to assess test diagnostic ability by plotting sensitivity (percentage of true positives identified) against test specificity (percentage of false positives identified) across a range of assay cut offs. Area under the curve (AUC) values calculated from the ROC curve reflect the ability of the test to discriminate between controls and patients. A p value was also calculated alongside the curve generation based on the AUC value testing the null hypothesis that the diagnoses are made no better than random chance. This was done by assessing if the AUC value calculated was significantly different from 0.5, the AUC value expected if a test is not able to discriminate true positives from true negatives. Likelihood ratios were also computed during curve generation which indicate how much more likely a patient with a positive test result is to be a true positive compared to a patient with a negative result.

2.14.5 Survival analysis

Survival was analysed using Prism 8 statistical software (Graphpad Software) and was first assessed by using the product limit method of Kaplan and Meier to generate Kaplan-Meier survival curves. Significant difference in survival between groups was then assessed using the logrank test which tests whether the median survival between the groups differed significantly.

Chapter 3 Profiling tenascin-C in murine dextran sulphate sodium colitis

3.1 Introduction

Tenascin-C is expressed dynamically at numerous sites during embryonic development, including during epithelial morphogenesis (Chiquet, 1992), neurogenesis (Faissner, 1997), and developing connective tissues (Tucker and Chiquet-Ehrismann, 2009). In the adult this expression becomes more sparse and restricted, narrowing to a few tissues under tensile stress, such as muscle (Fluck et al., 2000), underlying some epithelia, such as blood vessels (Hedin et al., 1991), and within a number of stem cell niches (Chiquet-Ehrismann et al., 2014).

In the response to tissue injury however, tenascin-C has been shown to become markedly upregulated as part of the inflammatory response. This has been demonstrated in in a variety of different tissues, and in response to a wide range of insults (Midwood and Orend, 2009). In these scenarios tenascin-C acts as a damage associated molecular pattern (DAMP), a class of endogenous molecules which promote and drive inflammation through their interactions with immune and stromal cells (Schaefer, 2014). In the case of tenascin-C this interaction has been shown to be mediated by the pattern recognition receptor (PRR) Toll-Like Receptor 4 (TLR4) (Zuliani-Alvarez et al., 2017) as well as the integrins α9β1 (Asano et al., 2014) and αVβ3 (Shimojo et al., 2015), whose engagement by tenascin-C promotes cell activation and often the production of a variety of pro-inflammatory mediators. While this pro-inflammatory action may be beneficial in the normal physiological response to injury it has become increasingly appreciated in recent years that DAMPs also play a role in the pathogenesis of inflammatory disease (Piccinini and Midwood, 2010). In this context tenascin-C itself has already been implicated in a diverse range of chronic inflammatory conditions such as rheumatoid arthritis (Midwood et al., 2009), systemic lupus erythematosus (Zavada et al., 2015), as well as Inflammatory Bowel Disease (IBD).

IBD encompasses a group of conditions in which an aberrant chronic inflammatory response of unknown aetiology targets the intestinal tract which results in its

progressive dysfunction and destruction. It presents clinically as two main subtypes which are ulcerative colitis (UC) and Crohn's disease (CD). UC is characterised by continuous mucosal inflammatory lesions affecting only the colon whereas CD presents as patchy transmural inflammation potentially affecting any region along the alimentary tract, although most commonly found in the distal small intestine (Neurath, 2019). Both of these conditions are chronic with no medically curative therapies available except for major surgical intervention, with its own potentially serious complications, in extreme cases of UC (Mowat et al., 2011). This is particularly problematic when considering disease burden has been increasing globally in recent decades with prevalence now surpassing 0.3% in most of Europe and North America (Ng et al., 2018). It is thus apparent that further work on understanding the pathogenesis and drivers of the disease is needed to aid in the development of effective tools for its clinical management and treatment.

In terms of tenascin-C's involvement in IBD a genome wide association study has previously identified a SNP linked to the tenascin-C gene as being associated with IBD. This was found within an intronic region of the gene between the alternative spliced FNIII repeats A4 and B with the impact on tenascin-C expression or function as yet unknown (Brant et al., 2017). At the protein level it has been demonstrated that systemic levels of circulating tenascin-C are increased in IBD patients compared to healthy controls (Riedl et al., 2001). Furthermore, these levels were shown to correlate with disease activity and showed responsiveness to therapy with proctocolectomy surgery and successful biologic therapy resulting in a significant decrease in tenascin-C levels (Magnusson et al., 2015). This systemic increase is also reflected at the local level with a number of histological studies showing high levels of tenascin-C staining in the inflamed gut tissue of patients with UC (Geboes et al., 2001), CD (Ambort et al., 2010), and microscopic colitis (Salas et al., 2003). Collectively these largely descriptive studies indicate that tenascin-C is potentially an inflammatory driver of interest in IBD. However, additional work is needed to further validate and characterise the functional role tenascin-C may be playing.

With a myriad of confounding factors to consider in IBD, including variations in genetics and gut microflora, murine models of colitis provide a useful controlled

setting for studying the underlying mechanisms of disease (Kolios, 2016). A number of models of colitis exist which can be broadly broken down into chemically induced models, cell transfer models, spontaneous models, and genetically engineered models. Out of these, owing to their relative simplicity and adaptability, the chemically induced models, including Dextran Sulphate Sodium (DSS) induced colitis, are the most commonly used. The DSS model involves the dosing of mice with commonly between 1-5% DSS in their drinking water for four to eight days to induce acute colitis. Alternatively, repeated cycles of DSS dosing to induce colitis followed by brief recovery periods can be used to induce a self-perpetuating chronic colitis (Wirtz et al., 2017). The exact mode of action by which DSS induces colitis is not fully clear although it has been suggested that DSS forms lipocomplexes with fatty acids in the colon. These lipocomplexes are believed to be partially toxic to the colonic epithelial cells inducing inflammatory signalling and cell death which compromises epithelial barrier integrity. The resulting injury and exposure of sub-epithelial immune cells to luminal antigens is thus believed to trigger the acute inflammatory response observed (Laroui et al., 2012). With this proposed mechanism the genetic background of the host would be expected to influence the colitic response and this is seen with susceptibility as well as the area of colon affected varying among inbred mouse strains. Additionally, the microbiota is another variable that must be taken into account with the type of luminal antigens and pathogens of obvious importance to disease development (Perse and Cerar, 2012). As such, local optimisation of colitis induction protocols is required to account for each of these factors which will vary by facility.

3.2 Hypothesis

Tenascin-C will have restricted expression in adult mice but will become upregulated with the induction of an inflammatory state such as in the DSS model of colitis.

3.3 Aims

I. Profile tenascin-C's expression in the mouse under basal conditions with a focus on the colon.
II. Establish and optimise the DSS model of colitis for use with the 129sv mouse strain.
III. Profile the gross and histopathological features of DSS colitis in this strain of mice.
IV. Study tenascin-C's spatiotemporal expression in control and colitic mice relating this back to the gross and histopathology observed.
V. Further map tenascin-C's expression in relation to a range of inflammatory mediators and cell types.

3.4 Materials and methods

3.4.1 Tissue culture

All tissue culture reagents were acquired from Thermo Fisher Scientific unless otherwise indicated. Passage one mouse embryonic fibroblasts (MEFs) isolated from E13.5 CD1 mouse embryos were acquired frozen from Elisabeth Thornton (McLachlan group, Roslin Institute).

MEFs were thawed in a 37°C water bath before drop wise addition of 5mls culture medium (high glucose Dulbecco's modified Eagle medium (Sigma Aldrich) supplemented with 10% heat inactivated foetal bovine serum, 1% GlutaMAX and 50µg/ml gentamicin). The cells were then transferred to a 30ml universal tube and centrifuged at 1000g for five minutes to pellet the cells. The supernatant was then taken off and the cells resuspended in fresh culture medium before transfer to tissue culture flasks. MEFs were cultured in a humidified atmosphere (37°C, 5% CO2) with media changed every two to three days. MEFs were passaged when they reached ~80% confluency.

To passage cells they were initially rinsed in sterile Dulbecco's PBS before addition of trypsin-EDTA (0.25%) cell dissociation reagent. After a five minute incubation at 37°C the flasks were gently tapped to aid the detachment of cells from the culture flask. Culture medium was then added to the dissociated cells which were then transferred to a universal tube and pelleted by centrifugation at 1000g for five minutes. The supernatant was then removed, and the pellet resuspended in fresh culture medium. Cells were counted using a haemocytometer and then either transferred to fresh flasks at the desired cell number for continued culture or seeded at $1x10^4$ cells/cm^2 in multi-well plates for use in experiments. Cells were rested for a minimum of 24 hours after seeding before use in experiments and were not used past passage 5.

3.4.2 Tissue and cell gene expression analysis

Bio-GPS and SAGE-genie gene expression data, expressed as arbitrary units and tags per 200,000 tags respectively, were obtained as detailed in section 2.2.

RNA extraction from tissue and RT-qPCR analysis carried out as detailed in section 2.5. For profiling *Tnc* expression a range of tissues were harvested and snap frozen from three 8 week old male 129sv WT mice for later RNA extraction. Data for this analysis is presented as $2^{-\Delta CT}$ values relative to the housekeeping 18s rRNA. For initial colon region gene expression analysis in the DSS model RNA was similarly extracted from snap frozen colon tissue segments. For gene expression analysis for DSS time course samples the RNA was extracted from cryosections containing multiple segments across the full length of the colon. In both cases analysis of DSS colon data is presented as fold change compared to control non-colitic samples calculated using the ΔΔCt method as detailed in section 2.5.4.

For extraction of RNA from MEF cells seeded in 6 well plates the culture media was first aspirated and the cells lysed with the addition of 350µl RLT lysis buffer (Qiagen) supplemented with 10µl per millilitre β-mercaptoethanol. Wells were then scraped, and the lysate transferred to an Eppendorf tube which was vigorously vortexed to aid complete cell lysis. RNA was then extracted as detailed in section 2.5.1, starting from the addition of an equal volume of 70% ethanol step, utilising an RNeasy spin column kit (Qiagen).

3.4.3 Western blotting

Colon tissue from 7-9 week old male WT and *Tnc*$^{-/-}$ mice was dissected as detailed in section 2.3.5 and flash frozen in LN_2. Neonate lungs were dissected from five day old WT mice. Protein was extracted from approximately 40mg of tissue. Following quantitation, 20µg of each tissue homogenate was run on a 10% Bis-Tris SDS-PAGE gel and western blotted using the MTn-12 anti-tenascin-C and 13E5 anti-β-actin (Cell Signalling Technology) antibodies, the former of which was a kind gift from Dr. Gertraud Orend (INSERM, Strasbourg, France). All western blotting procedures were carried out as detailed in section 2.6.

3.4.4 Immunohistochemistry (IHC)

Cryosections of tenascin-C rich murine tumour tissue, cut at 7µm, were a kind gift from Dr. Gertraud Orend (INSERM, Strasbourg, France). Colon tissue was harvested for IHC analysis as detailed in section 2.3.5. Proximal, middle, and distal sections from one mouse were embedded together in the same OCT block for cryosectioning, immunostaining, and imaging together. All IHC staining procedures were carried out as detailed in sections 2.4.2, 2.4.6, and 2.4.7. Negative controls were performed where the primary antibody was either omitted (no primary) or replaced with non-specific IgG from the animal the primary antibody was raised in (Sigma Aldrich).

3.4.5 DSS murine model of colitis

DSS colitis was induced, as detailed in section 2.3.4, in 7-9 week old male 129sv mice, provided as a kind gift from a colony belonging to Prof. Bernadette Dutia (Roslin Institute). Initial DSS titration experiments were carried out utilising a more simplistic disease activity index (DAI) scoring scheme where only faecal blood and stool consistency were scored for. The final scoring sheet, as shown in Appendix V, was subsequently developed and was used for all other experiments. Body weight data are presented as mean percentage body weight loss ± standard deviation and DAI sum score data is presented as median score ± interquartile range, as specified in section 2.3.4. Mice that exhibited severe adverse reactions or exceeded study severity limits, as described in section 2.3.4, were immediately euthanized and were not included for analysis.

3.4.6 Colitis histopathology grading

H&E staining of paraffin and cryo-embedded colon tissue sections was carried out as detailed in section 2.4.3 and colons graded for histopathology as described in section 2.4.3. For the DSS titration experiments histopathology was graded using paraffin embedded sections and for the DSS time course experiment cryo-embedded sections were scored.

3.4.7 Statistical Analysis

Statistical analysis was carried out as detailed in section 2.14. Continuous data, including body weight loss, colon length, and qPCR results, were analysed using Student's t-test, a one-way ANOVA, or a two-way ANOVA with Sidak's multiple comparisons test unless found to be not normally distributed. Non-normally distributed continuous data or ordinal data, such as DAI and histopathology scoring, were analysed using the appropriate non-parametric Mann-Whitney U or Kruskal-Wallis with Dunn's multiple comparisons tests.

3.5 Results

3.5.1 Tenascin-C's gene expression profile in adult mice

Tenascin-C is reported not to be expressed, or to be expressed at low levels, in the majority of adult tissues (Midwood et al., 2016). However, no single systematic study of tenascin-C expression covering multiple tissues has been carried out. To confirm this observation a review of published expression data as well in-house profiling was carried out. The BioGPS database of microarray data was the first resource to be interrogated with the data extracted presented in figure 3.1a. The SAGE-genie database of SAGE library data was the next source of expression data utilised, with the data extracted shown in figure 3.1b. Finally, to confirm the data generated by these high-throughput screening methods tenascin-C expression was analysed by RT-qPCR in a similar array of tissues extracted from adult 129sv mice, shown in figure 3.1c. Alongside the major tissues investigated MEF cells, an embryonic stromal cell type known to produce high levels of tenascin-C (Brellier et al., 2011), were also analysed as a benchmark for high tenascin-C expression.

Each of the approaches utilised, while showing some differences, broadly confirmed that tenascin-C is comparatively lowly expressed at the mRNA level in most murine adult tissues. This included no expression found in spleen, liver, and heart, while only low levels of mRNA were detected in brain, bone, and the intestines, including the colon. This was particularly clear when comparing tissue expression levels with the MEF cells, which displayed by far the highest tenascin-C expression across all methods.

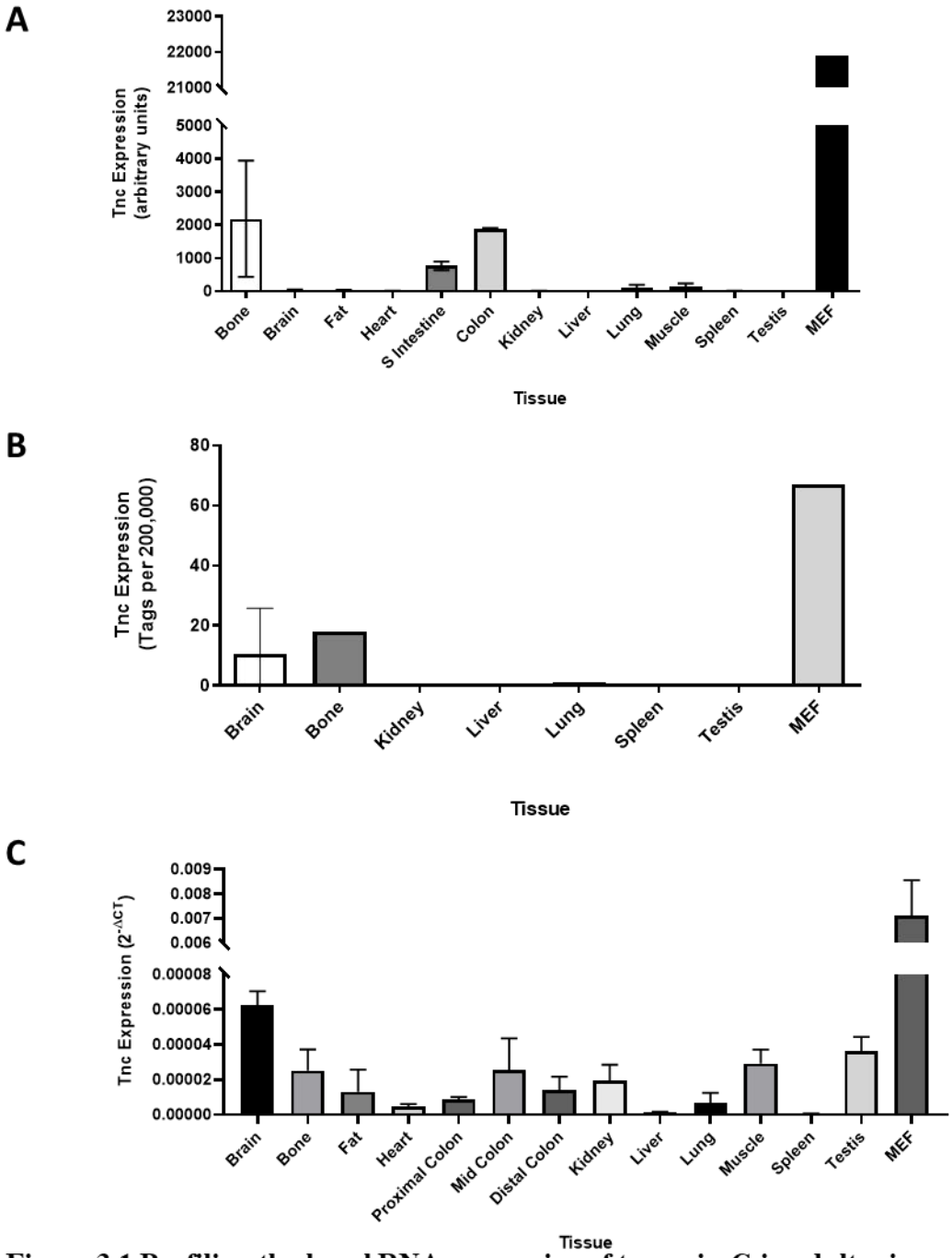

Figure 3.1 Profiling the basal RNA expression of tenascin-C in adult mice

(A) Microarray gene expression data for tenascin-C in a variety of tissues from 8-10 week old male C57BL/6 mice and mouse embryonic fibroblasts (MEF). Data extracted from the BioGPS gene expression database and presented in arbitrary units.
(B) Serial analysis of gene expression (SAGE) library data for tenascin-C gene expression in number of tissues taken from 84 and 109 day old mice of unspecified sex and strain as well as MEFs. Data extracted from the SAGE-genie gene expression database and presented as tenascin-C tags per 200,000.
(C) Tenascin-C gene expression data determined by RT-qPCR for a variety of tissues harvested from male 8 week old 129sv mice and MEFs. Data presented as mean ± SD, n = 3.
Muscle = skeletal muscle, S intestine = small intestine.

3.5.2 Expression of tenascin-C at the protein level in the colon of adult mice

With the identification of the adult colon as an expression site of tenascin-C it was next decided to validate this mRNA data at the protein level. To do this protein lysates of colon samples were prepared and western blotted for tenascin-C with the result shown in figure 3.2. Supporting the gene expression data tenascin-C was found to be expressed in the colon with a major band seen at approximately 200kDa as well as a minor band at 280kDa. The positive control of a known expression site, five day old neonate lung (Saga et al., 1992), showed the presence of the same bands although at higher levels. Also conversely compared to the colon, a predominance of the higher molecular weight form of tenascin-C was observed in lung lysate suggestive of differential splicing and/or of differential glycosylation of tenascin-C between the tissues. The negative control of colon tissue from a *Tnc*$^{-/-}$ mouse produced no bands as expected.

Having demonstrated protein expression in the colon its localisation within the tissue was next investigated. To do this an immunohistochemistry protocol using the MTn-12 antibody against tenascin-C was optimised with cryosections of murine tumour tissue which express high levels of tenascin-C. Strong staining with MTn-12, shown in figure 3.3, was observed in the matrix of the tumour and this was demonstrated to be specific with no staining observed in the matched negative controls.

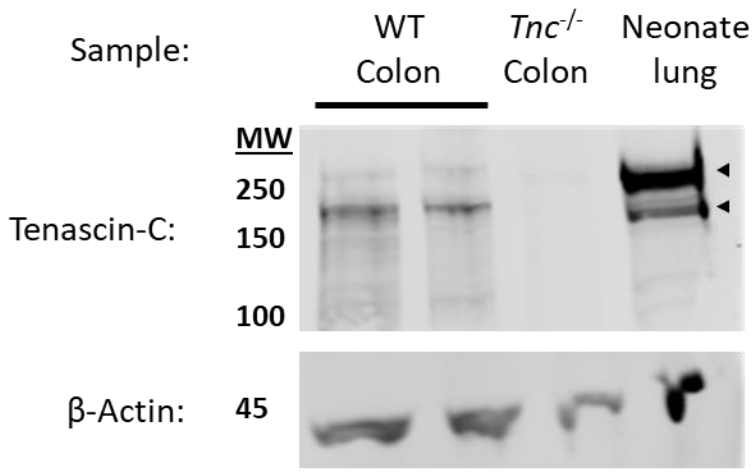

Figure 3.2 Tenascin-C is expressed at the protein level in the colon of 129sv mice

Protein extracts from wild-type (WT) adult colon and neonate lung as well as tenascin-C knockout (*Tnc*$^{-/-}$) colon were run on a 10% SDS-PAGE gel and western blotted for tenascin-C with β-actin used as a loading control. Two tenascin-C bands are identified at approximately 200 and 280kDa (indicated with black arrowheads) in WT colon and neonate lung samples. Despite comparable loading no bands are observed in a colon sample from a *Tnc*$^{-/-}$ mouse. Molecular weight (MW) in kDa is indicated at the side of the blots.

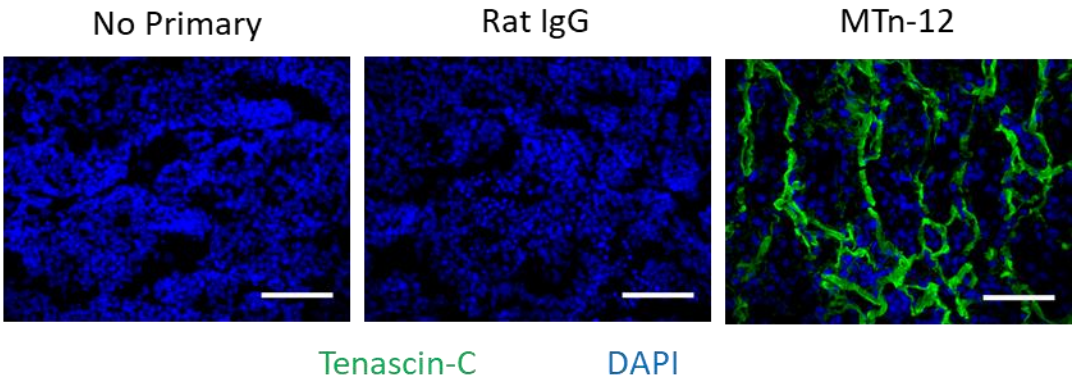

Figure 3.3 Validation of tenascin-C immunohistochemistry

Murine tumour tissue with a tenascin-C rich extracellular matrix was IHC stained using the MTn-12 anti-tenascin-C antibody using an anti-rat-Alexa Fluor 488 (green) secondary antibody for detection. Accompanying no primary, in which the primary antibody was omitted, and non-specific rat IgG controls are also shown. All slides were counterstained with DAPI nuclear stain (blue). Slides were imaged using a Leica DMLB microscope. Scale bars = 100μm.

Having optimised tenascin-C IHC staining, cryosections were generated covering the length of the colon of eight-week-old male mice which were then immunostained for tenascin-C, shown in figure 3.4a. This further confirmed the basal expression of tenascin-C protein in the colon with staining observed along the length of the colon. Additionally, despite morphological differences in different regions of the colon, the staining followed broadly the same staining pattern in each region. This included tenascin-C staining in the outer muscle layer of the colon, the muscularis externa, as well as a subepithelial band in the lamina propria directly underlying the surface epithelium. Specific to the middle colon, some additional tenascin-C staining appeared to be present in the lamina propria extending further down the crypts from this subepithelial band. Higher magnification images also revealed tenascin-C immunoreactivity present in the muscularis mucosa, although this was less apparent in the proximal colon compared to the middle and distal segments. To further confirm this was the result of specific tenascin-C staining a second tenascin-C specific antibody, NSCT-121, recognising a different epitope of tenascin-C was also used for colon IHC staining, shown in figure 3.4b. The same pattern of staining was again observed with this antibody as was seen by MTn-12, confirming its specificity.

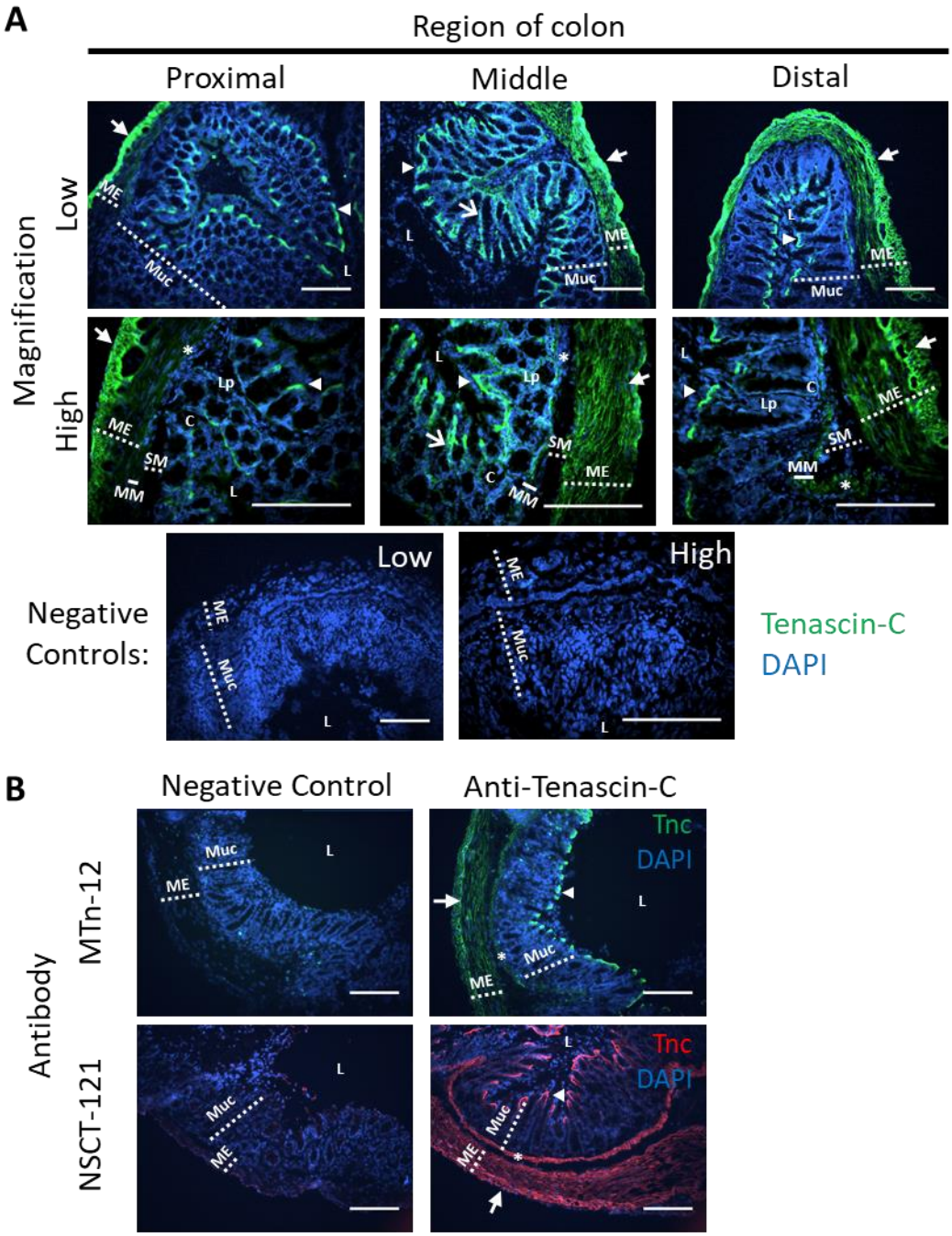

Figure 3.4 Immunohistochemical profiling of basal tenascin-C expression in the murine colon

(A) IHC staining of proximal, middle, and distal colon for tenascin-C (green) imaged at a low (upper panel) and high magnification (lower panel). Staining is observed in the muscularis externa (closed arrows), in a subepithelial band underlying the surface epithelium (arrowheads), lamina propria (open arrows), and in the muscularis mucosa (asterisks). Negative controls showed no staining. **(B)** Validation of tenascin-C staining in the distal colon with two antibodies, MTn-12 (green) and NSCT-121 (red). Specific tenascin-C staining indicated as in (A). Negative controls showed no staining. All slides were imaged using a Leica DMLB microscope and counterstained with the nuclear stain DAPI (blue). Scale bars = 250μm. ME = muscularis externa, Muc = mucosa, L = lumen, MM = muscularis mucosa, SM = submucosa, LP = lamina propria, C = crypts.

3.5.3 129sv mice develop acute colitis upon dosing with DSS

Following the profiling of tenascin-C under basal conditions in the colon the next aim of the project was to profile tenascin-C under inflammatory conditions. To do this the DSS chemically induced colitis model was established in the lab for 129sv strain mice. This mouse strain was chosen as it is the background strain for the *Tnc*$^{-/-}$ mouse colony which was utilised in future experiments. As well as DSS dosing concentration and duration the genetic background and local gut microflora are known to impact colitis induction and severity (Perse and Cerar, 2012). As such, a titration experiment was required to optimise DSS dosing for this 129sv colony to ensure robust induction of colitis which remained within animal welfare severity limits as mandated by home office regulations.

The most common doses used in the literature range between one to five percent DSS (Perse and Cerar, 2012). As such, for the titration experiment groups of mice were dosed with between one to five percent DSS in their drinking water for five days. They were then returned to normal drinking water before cull on day seven. As expected, a dose response was seen with presentation of gross pathology, with increasing doses of DSS inducing more severe colitis. This was first demonstrated using body weight loss and DAI readouts of animal health, the data for which is shown in figure 3.5a and figure 3.5b respectively. Control animals, which were not dosed with DSS, showed no DAI scoring or weight loss over the duration of the experiment. Mice dosed with the lowest DSS concentration of 1% also displayed no significant bodyweight loss although they showed a significant increase in DAI scoring on day 6 of the protocol. All of the dosages tested above 1% conversely did show significant body weight loss for at least one time point with the trend in body weight loss beginning at around day 5-6. For the higher doses of 4-5% this weight loss became significant from day five itself whereas for the lower doses of 2-3% while a trend down was apparent this only achieved significance on the final day 7. These changes were likewise reflected in the DAI which also showed scoring for all these doses from day five onwards. It was apparent however that the basic scoring sheet used for these initial experiments didn't capture the full picture of observable animal health however as it only recorded stool-based symptoms. This prompted the development of the final more holistic health monitoring which was used for all future experiments.

Overall based on these gross health parameters the two higher doses were judged to be too severe, with mice culled on humane grounds on day five and six, resulting in no mice from these groups reaching the experimental end point. The 3% dosage, while reaching the study end point, was also judged by the facility named veterinary surgeon to be too severe. Thus, the 2% DSS dosage appeared to be the most appropriate and this was confirmed by the final gross parameter examined, the colon length at cull which is shown in figure 3.5c. One of the hallmarks of DSS induced colitis is a shortening of the colon due to tissue wastage associated with the pathology (Chassaing et al., 2014). As such, the observation that the colon length in the 2% group showed a significant shortening compared to control mice provided further evidence that colitis had been successfully induced. Additional observations at cull, including that 2% DSS treated mice had loose stool and in some cases faecal blood present, further supported the conclusion that colitis had been successfully induced. In comparison and in line with the other parameters examined no difference in colon length or other gross features at cull was observed between the control and 1% DSS groups.

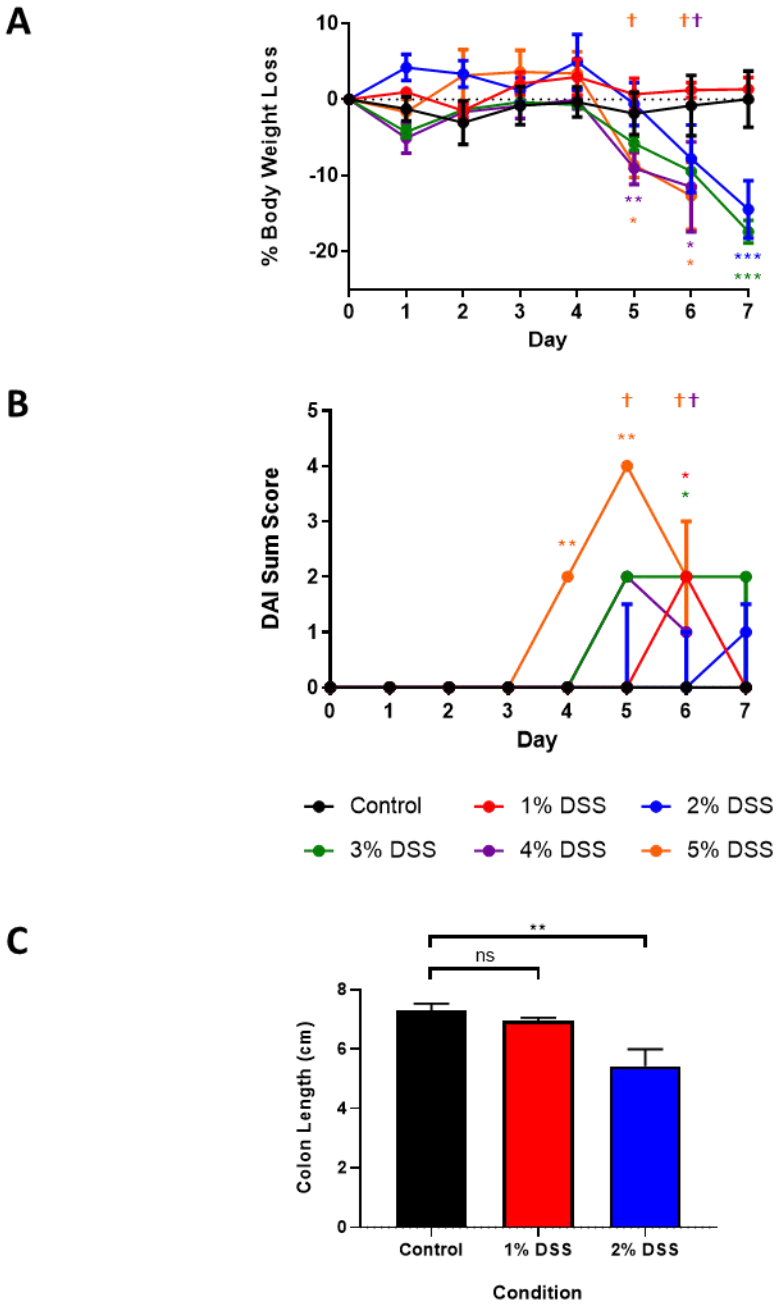

Figure 3.5 Gross pathology of different DSS dosing concentrations

(A) Percentage body weight loss compared to day 0 of control mice or mice treated with varying concentrations of DSS supplemented water. Mice treated with 2% DSS or over suffer significant body weight loss by day 7. Crosses (†) indicate days at which mice in the corresponding colour group were culled due to severity limit breaches. Data presented as mean ± SD, n≥3 per group at day 0, significance determined by one-way ANOVA.
(B) Disease activity index (DAI) scoring data for the same mice as in (A). Data presented as median ± interquartile range, n≥3 per group at day 0, Significance determined by Kruskal-Wallis test.
(C) Colon length at cull on day 7 of control or 1 and 2% DSS treated animals. Data presented as mean ± SD, n ≥3 per group, significance determined by Kruskal-Wallis test.
** = $p<0.01$, * = $p<0.05$, ns = not significant.

Based on the gross pathology it was thus decided to go forward with the 2% DSS dose and confirm the induction of colitis at the histopathological level. Histological analysis of H&E stained colon sections showed normal colonic architecture and little inflammation in control mice. In comparison DSS treated mice showed significant inflammatory pathology which was predominantly localised to the middle and distal colon. As reported by trained histopathologist Elspeth Milne; Professor of Veterinary Clinical Pathology, University of Edinburgh; this included significant mixed infiltration of macrophages and neutrophils into the submucosa and which occasionally extended transmurally across the entire colonic wall. Additionally, moderate to severe oedema, another marker of inflammation, was also commonly observed in the submucosa. Tissue damage was also apparent with ulceration and crypt loss present alongside hyperplastic epithelial tissue, indicative of atypical tissue regeneration in response to damage.

These changes were quantified by blinded histopathology scoring, which was also carried out by Prof. Elspeth Milne, with the results presented in figure 3.6a. This confirmed the above observations with the proximal colon appearing unaffected by DSS treatment while a significant increase in pathology score was observed for the distal colon. The middle colon in comparison exhibited a more variable intermediate pathology score which was still significant increased compared to control samples. Scoring breakdown for the distal portion of colon, shown in figure 3.6b, demonstrated a significant increase compared to the control for all the parameters scored for. This included showing a marked increase in inflammation with the inflammatory severity and extent measures, representing the severity of the inflammatory pathology, such as degree of immune cell infiltration, and the extent of its penetration into the gut wall respectively, both showing significant increases. Additionally, the crypt damage and regeneration parameters, measuring damage to the mucosa and the presence of tissue repair processes, such as epithelial hyperplasia, respectively, likewise also showed significant increases.

To confirm the greater degree of inflammatory pathology in the distal colon myeloperoxidase (MPO) activity was assayed in each of the colonic regions. Myeloperoxidase is expressed in neutrophils and is often used as a surrogate marker

for their infiltration into the intestines in inflammatory models (Krawisz et al., 1984). The results of this assay, presented in figure 3.6c, again supported the histological observations that DSS pathology was worse in the distal colon with significant increase in MPO activity only observed in the distal segments. Conversely, just a non-significant trend towards increase was seen in the mid colon while no significant difference was observed in the proximal colon. This matches with previously reported data that the distal portion of the colon is often the most affected by DSS treatment (Perse and Cerar, 2012).

3.5.4 Upregulation of tenascin-C in the distal colons of DSS treated colitic mice

Having established the DSS colitis model in 129sv mice, work began to characterise tenascin-C's expression in this murine inflammatory model. This was initially done at the gene expression level by carrying out RT-qPCR on RNA extracted from colon tissue from the control or 2% DSS treated mice. The results of this analysis, shown in figure 3.7a, demonstrated a significant upregulation in tenascin-C mRNA expression in the distal colon of DSS treated mice compared to controls. No significant difference in tenascin-C mRNA expression between the groups was observed in either the proximal or middle colon.

To confirm this increase at the protein level IHC was carried out on distal colon samples from control and 2% DSS treated mice, with representative images shown in figure 3.7b. Control mice exhibited the same tenascin-C staining pattern in the mucosa and muscularis externa as shown previously, with mucosal expression restricted to a distinct subepithelial band. As the histopathology scoring suggested tissue architecture in the DSS treated mice appeared perturbed with oedema and immune cell infiltration evident in the submucosa, alongside significant mucosal damage including crypt loss. In terms of tenascin-C expression compared to the controls an increase in staining was observed in the mucosa of DSS treated mice. This presented as expression which was no longer restricted to a distinct subepithelial band but was now found as diffuse staining throughout the entire width of the damaged mucosa. Additionally, a thickening of the muscularis mucosa was observed in some areas with a matching increase in the tenascin-C staining for this structure.

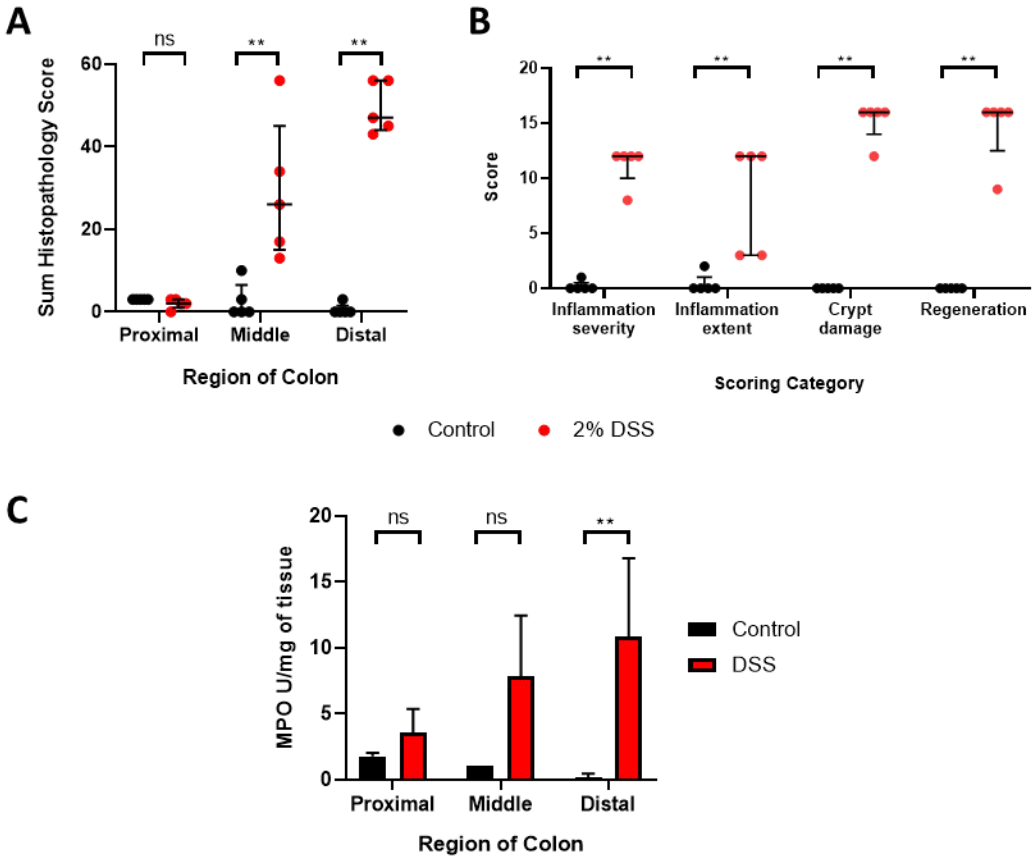

Figure 3.6 The 2% DSS dose induces acute inflammatory histopathology in the distal colon by day 7

(A) Sum histopathology scores for proximal, middle, and distal colon sections from control and 7 day 2% DSS treated mice. Middle and distal colon sections show significantly increased scoring compared to controls upon DSS treatment. **(B)** Histopathology scores for individual scoring parameters in distal colon segments from control and 7 day 2% DSS treated mice. All parameters show significant elevation in the DSS treated condition.
Data points represent scores for individual mice with bars marking the median ± interquartile range, n = 5 per group, significance compared to control determined by Mann-Whitney U test, ** = $p<0.01$, ns = not significant.
(C) Myeloperoxidase (MPO) assay results for proximal, middle, and distal colon segments from control and 7 day 2% DSS treated mice. Significantly elevated myeloperoxidase levels, a read out of inflammatory neutrophil infiltration, are seen in the distal colon of DSS treated mice compared to controls. Data presented as mean ± standard deviation, n = 3 per group, significance compared to region matched control determined by two-way ANOVA, ** = $p<0.01$, ns = not significant.

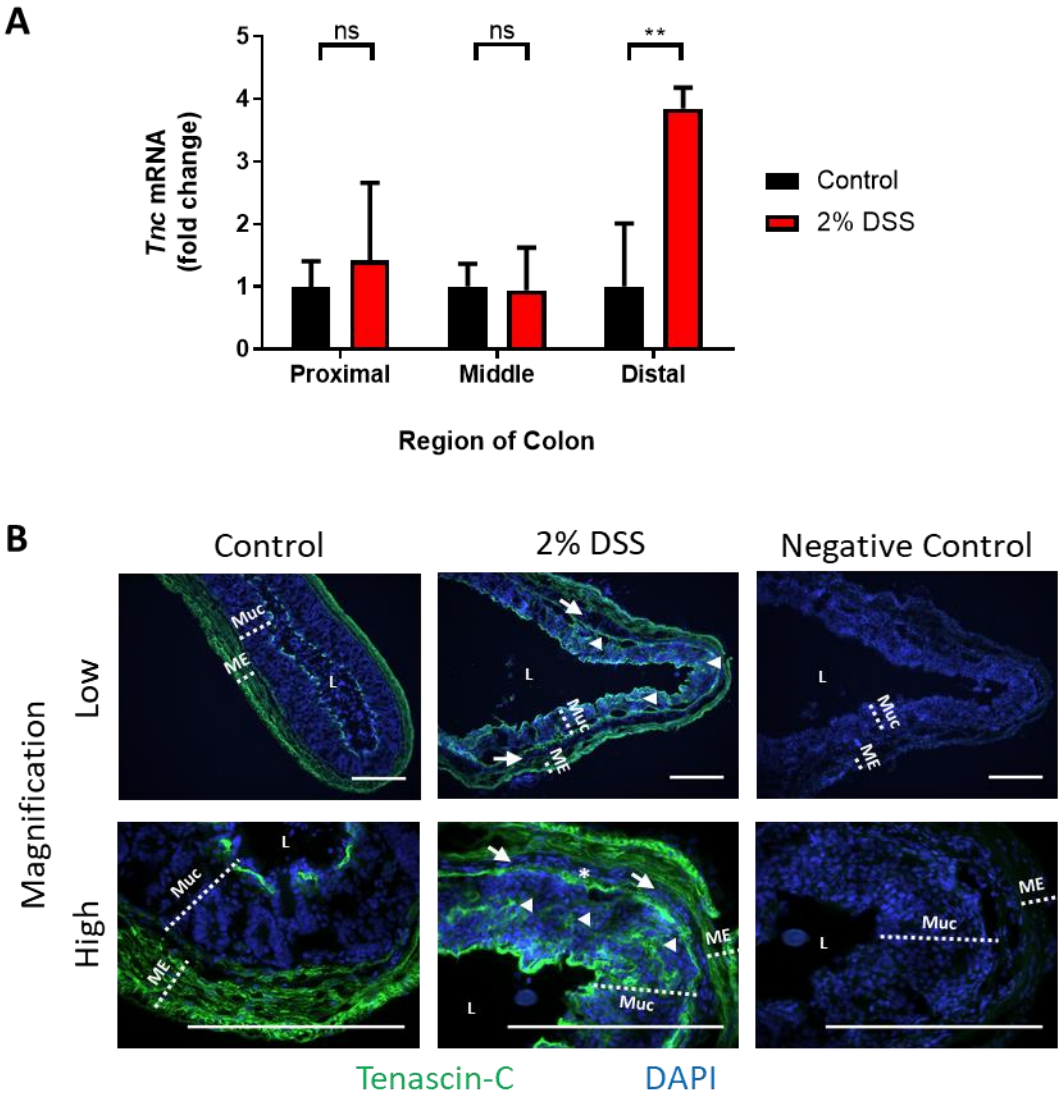

Figure 3.7 Tenascin-C is upregulated at day 7 in the distal colon of 2% DSS treated colitic mice

(A) RT-qPCR analysis shows significant tenascin-C (*Tnc*) gene expression upregulation in the distal colon of 7 day 2% DSS treated mice compared to non-DSS treated controls. Data presented as mean fold change compared to matching control region ± SD, n=4-5 per group, significance determined by Student's t-test, ** = $p<0.01$, ns = not significant.
(B) IHC analysis of the distal colons of control and 7 day 2% DSS treated mice shows an increase in tenascin-C staining (green) in inflamed damaged mucosa (arrowheads) and muscularis mucosa (asterisks) of the colitic mice. Alongside the mucosal architectural disruption submucosal oedema and immune cell infilitration is also apparent (closed arrows). No staining was observed in the negative controls. Slides were imaged using a Leica DMLB microscope. All slides were counterstained with the nuclear stain DAPI (blue). Scale bars = 250µm. ME = muscularis externa, Muc = mucosa, L = lumen

3.5.5 Temporal profiling of acute DSS coltis pathology

Having demonstrated tenascin-C's upregulation at the acute stage of inflammation it was next decided to interrogate the temporal nature of this increase. To do this a DSS time course experiment, outlined in figure 3.8a, was carried out in which mice were culled at two-day intervals throughout the now established DSS colitis protocol. To accommodate this chosen time point interval it was decided to increase the study end point from day seven to day eight at which acute colitis should still be firmly maintained. The same gross and histological pathological readouts were chosen to be monitored as well as collecting colon tissue for further gene expression and IHC analysis at each cull time point.

Initial assessment of gross pathological readouts confirmed successful colitis induction. This included body weight loss, presented in figure 3.8b, mimicking the titration experiment with a significant decrease compared to controls observed from day seven onwards. The improved DAI scoring scheme, better capturing observable mouse health, likewise showed a significant increase in pathology, with the results shown in figure 3.8c. This showed the development of symptoms, such as the presence of pasty stools and faecal blood, preceding the weight loss starting from as early as day four and become significantly established at day five. Finally, at cull the last gross parameter presented in figure 3.8d, colon length, also demonstrated colitis induction at the roughly the same time point with a trend towards decreasing length which became significant from day six.

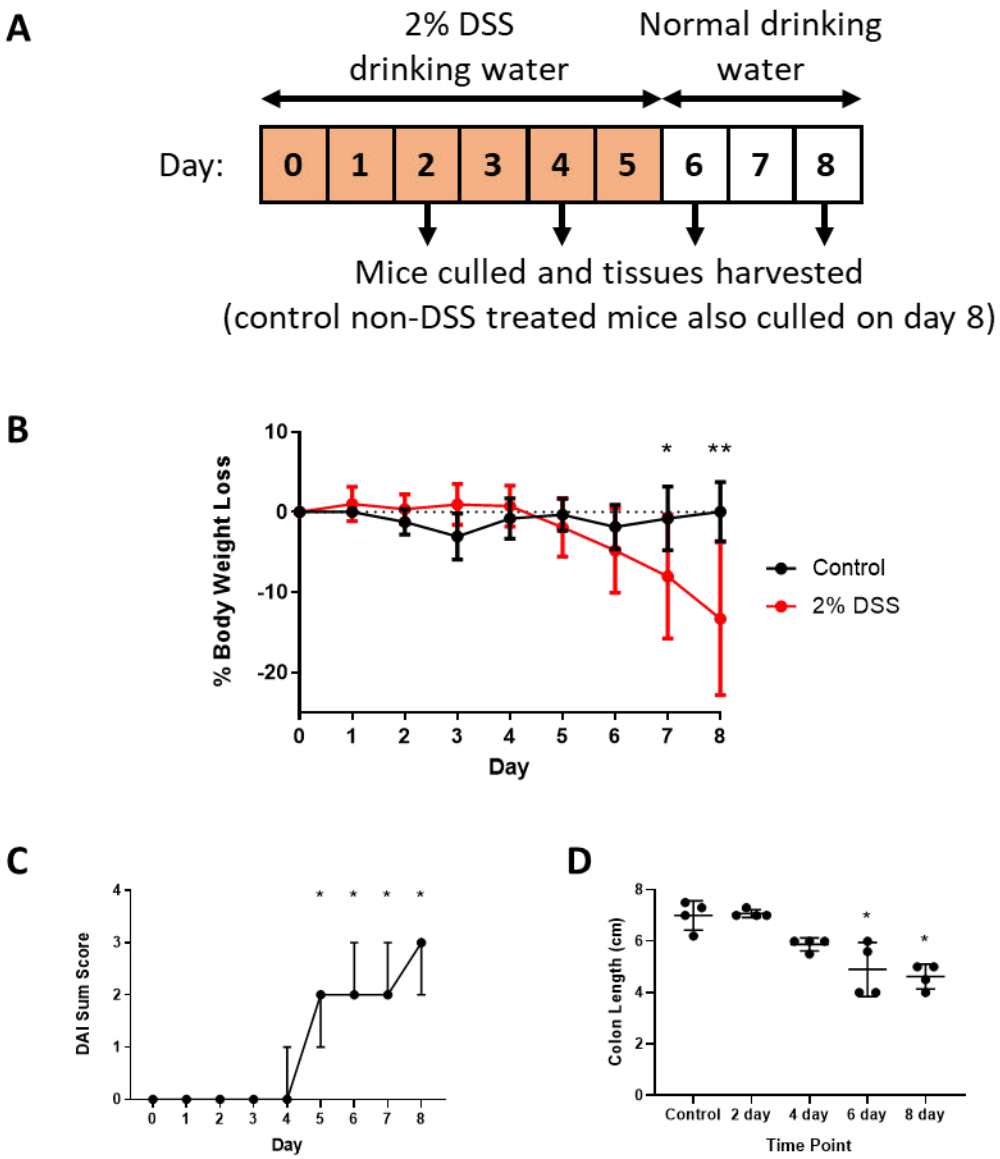

Figure 3.8 DSS colitis time course experiment outline and gross pathology

(A) Experimental outline of the DSS time course experiment carried out indicating the DSS dosing regime as well as the time points mice were culled and tissues harvested for analysis.
(B) Significant body weight loss compared to control mice is observed with 2% DSS treatment over the time course. Data presented as mean body weight loss compared to day 0 ± SD, n=3≤ per group at each time point, significance compared to control determined by two-way ANOVA.
(C) Disease activity index (DAI) sum scoring is significantly increased in DSS treated mice from day five onwards. No scoring was observed for control mice. Data presented as median ± interquartile range, n=4≤ per time point, significance compared to day 0 baseline determined by Kruskal-Wallis test.
(D) Colon length at cull compared to control mice is significantly decreased from day 6 of DSS treatment. Data presented as mean ± SD, n=3-4 per group, significance determined by Kruskal-Wallis test.
** = $p<0.01$, * = $p<0.05$

To definitively determine induction of colitis histological analysis of H&E stained colon sections, shown in figure 3.9, was again carried out. Control mice (plotted as day zero indicating zero days DSS treatment) displayed normal colonic architecture and little evidence of any inflammation present along the length of the colon. Likewise, day two time point DSS mice also showed no signs of any pathology along the length of the colon, which appeared indistinguishable from control mice. From day four of DSS treatment some evidence of pathological changes began to become apparent with minor immune infiltration seen in some sections for the middle and distal colon. Tissue damage was not apparent at this stage however, with tissue architecture appearing largely normal. This dramatically changed when moving on to the day six time point tissues where significant pathological changes were now readily apparent in the middle and distal colon of all mice assessed. This included inflammatory changes such as marked submucosal oedema and now significant immune cell infiltration by mainly neutrophils as well as occasionally mononuclear cells. Additionally, tissue damage, including disrupted mucosal architecture with extensive ulceration, loss of crypts, and hyperplasia, was now also readily apparent in all mice assessed. From this time point till the final time point on day eight this pathology was maintained and presented similarly in all in the day eight mice assessed.

These changes were additionally quantified and confirmed using the blinded histopathology scoring scheme. Sum scores, presented in figure 3.10a, again demonstrated the focus of pathology towards the distal end. This also confirmed the time point for colitis initiation with scores beginning to raise above background levels at around day four. It also confirmed the establishment of acute colitis at day six at which point both middle and distal scores appeared elevated, although this was only significant for the former colonic region. From day six to eight only a moderate increase was observed at which point both the middle and distal colons showed significant scoring increases. Breakdown by scoring parameter, shown in figure 3.10b, for the distal colon further supported earlier observations that the early pathology seen at day four was due solely to inflammatory changes. Tissue damage conversely only began to appear at day six before achieving significance at day eight.

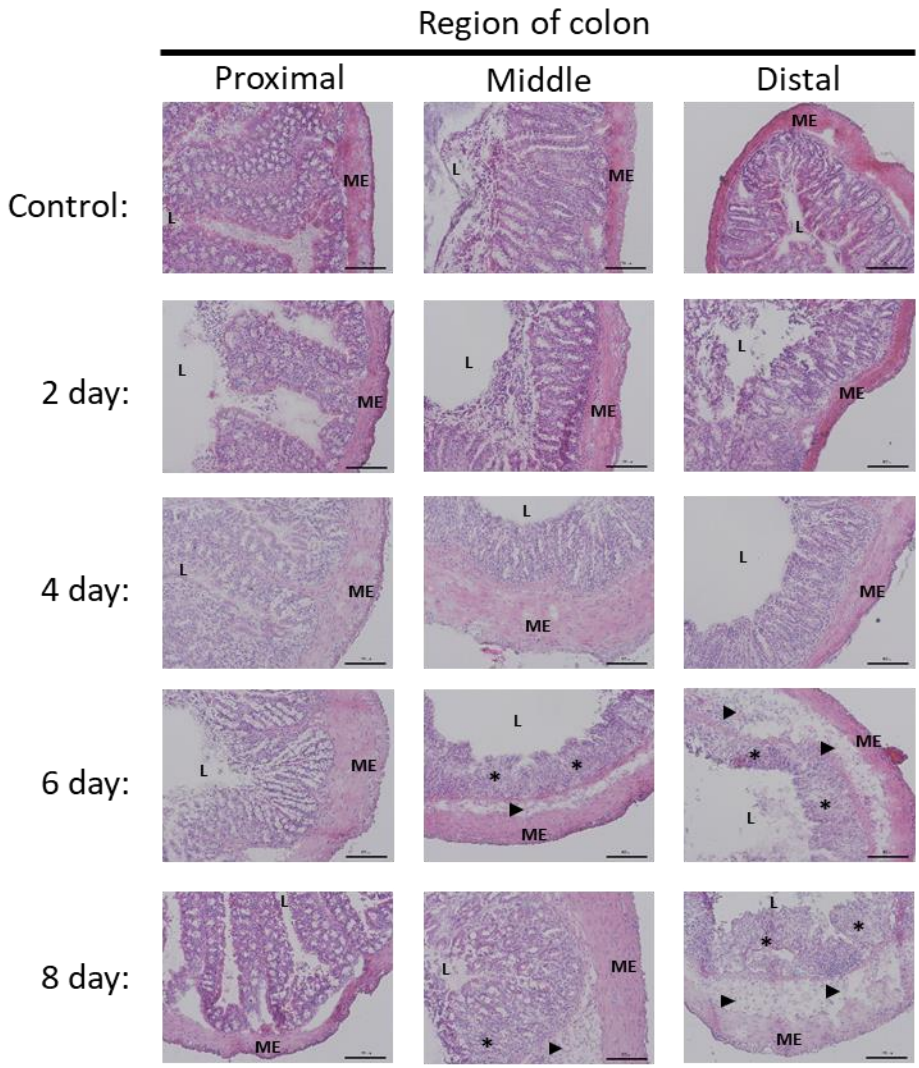

Figure 3.9 Representative H&E stained colon sections from 2% DSS colitis time course mice

Representative H&E stained proximal, middle, and distal colon sections from control and at time points throughout a 2% DSS treatment time course. Mixed immune cell infiltration and submucosal oedema (arrowheads), ulceration (asterisks), and epithelial hyperplasia (arrows) are indicated. Legend continued on following page-

Figure 3.9 Continued

Enlarged images of the distal colon sections at each time point (right) to more clearly show the histopathology induced by DSS treatment in this region of the colon.

Images captured using a Nikon E600 brightfield microscope. Scale bars = 100µm. ME = muscularis externa, L = lumen.

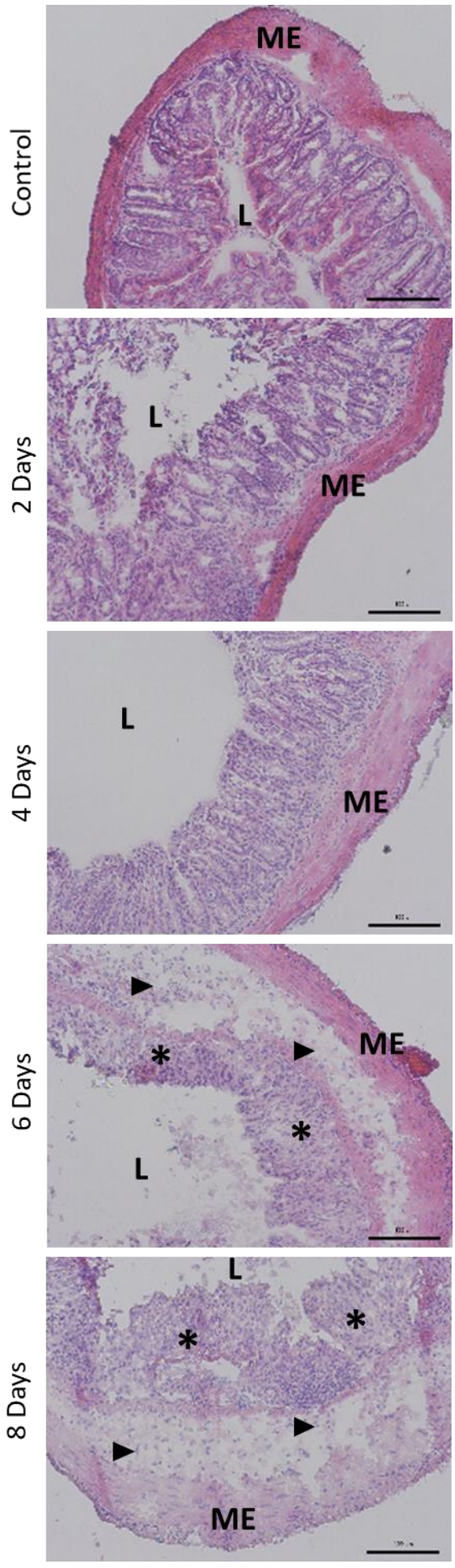

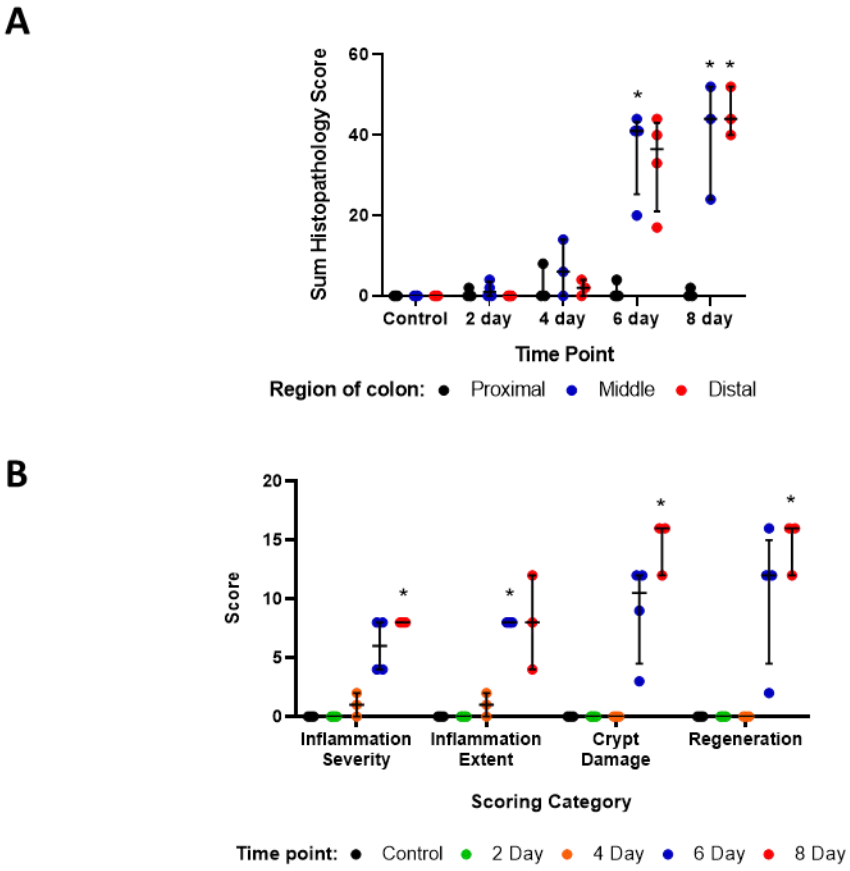

Figure 3.10 DSS colitis time course colon histopathology scoring confirms induction of pathology from day six.

(A) Sum histopathology scores for proximal, middle, and distal colon sections from control as well as each 2% DSS treated mouse time point . DSS treatment results in increased scoring compared to controls from day 6 in the middle colon and day 8 in the distal.
(B) Histopathology scores for individual scoring parameters in distal colon segments from control as well as each 2% DSS treated mouse time point. All parameters, except inflammatory extent, show significant elevation in the DSS treated condition at day 8.
Data points represent scores for individual mice with bars marking the median ± interquartile range, n = 3-4 per group, significance compared to control determined by Kruskal-Wallis test, * = $p<0.05$.

3.5.6 Pro-inflammatory mediators are increased from day six of the DSS colitis protocol

Having shown establishment of pathology at day six gene expression analysis for tenascin-C as well as other key inflammatory regulators was carried out on RNA from cryosections containing colon segments covering the full length of the colon. This strategy of extracting RNA from cryosections rather than snap frozen individual colonic segments was required to accommodate for the lack of tissue due to shortening of the colon with colitis. The result of this for tenascin-C, presented in figure 3.11a, showed that unlike seen previously when colon RNA was isolated from separate colonic regions (figure 3.7a) a statistically significant increase in expression was not observed at any time point, although a upwards trend was seen from day six. In terms of other mediators, the classical pro-inflammatory cytokines interleukin (*Il*)-*6*, *Il-1β*, tumour necrosis factor (*Tnf*), and *Il-12a* were also analysed with the results shown in figures 3.11b, 3.11c, 3.11d, and 3.11e, respectively. *Il-6*, *Il-1β*, and *Tnf* all showed higher fold inductions compared with tenascin-C and conversely demonstrated significance in their upregulation from day six. *Il-12a* by comparison did not demonstrate significance at any time point with only a trend upwards seen on day eight. Additionally, the non-classical pro-inflammatory cytokine *Il-17*, related to the Th17 response implicated in IBD pathogenesis (Fujino et al., 2003), was also analysed and the result shown in figure 3.11f. Like the classical pro-inflammatory mediators high fold inductions were observed for *Il-17a* and differentially while a trend was evident at day six significance of this increase was only achieved at day eight. The final gene analysed, presented in figure 3.11g, was the immunomodulatory cytokine *Il-10*, which is associated with immune down regulation and anti-inflammatory processes. While a trend to increase was seen from day six, matching the pro-inflammatory cytokines profile, this was not determined to be significant.

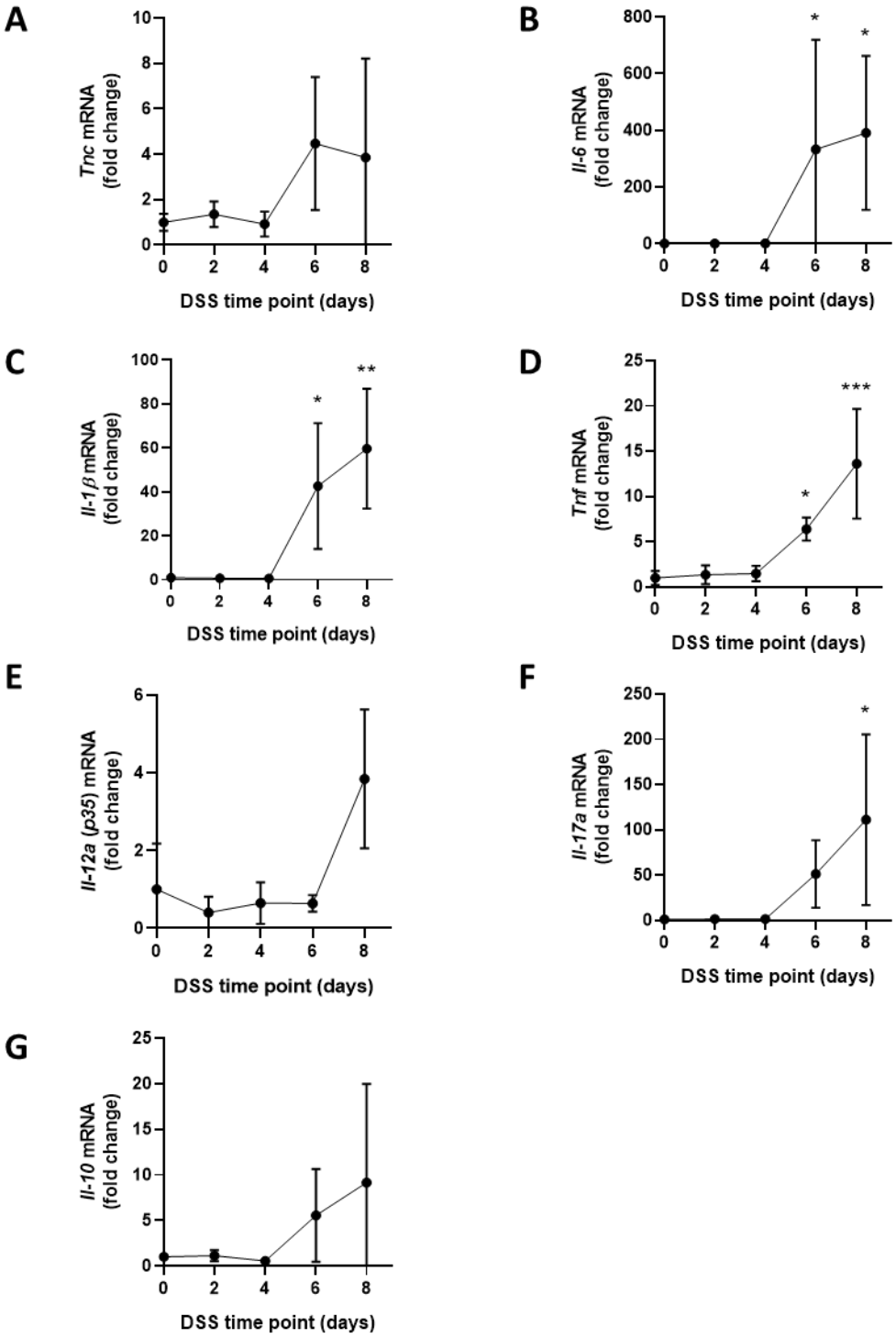

Figure 3.11 DSS time course colonic gene expression analysis

RT-qPCR analysis of colonic gene expression in control (set as day zero) or at the indicated time points in the DSS time course. Genes assayed for included **(A)** tenascin-C (*Tnc*), **(B)** Interleukin (*IL*)*-6*, **(C)** *IL-1β*, **(D)** Tumour necrosis factor (*Tnf*), **(E)** *IL-12a* (*p35*), **(F)** *IL-17a*, and **(G)** *IL-10*.
Data presented as mean fold change compared to control ± SD, n=3-4 per timepoint, significance determined by One-way ANOVA or for nonparametric data Kruksal-Wallis test, *** = $p<0.001$, ** = $p<0.01$, * = $p<0.05$

3.5.7 Tenascin-C is elevated at the protein level in the colitic mucosa from day six

With the gene expression analysis for tenascin-C conflicting with previous results (figure 3.7a), likely due to the methodological changes resulting in the mixing of tissue from proximal, middle and distal parts of the colon it was decided to profile tenascin-C at the protein level by IHC as well. The results of this IHC analysis, shown in figure 3.12, did corroborate previous results with an increase in tenascin-C staining in the middle and distal colonic mucosa evident with the induction of colitis. Additionally, matching the development of the tissue damage pathology this increase was seen from the day six time point, where it appeared tenascin-C stained more prominently in the areas with heightened damage.

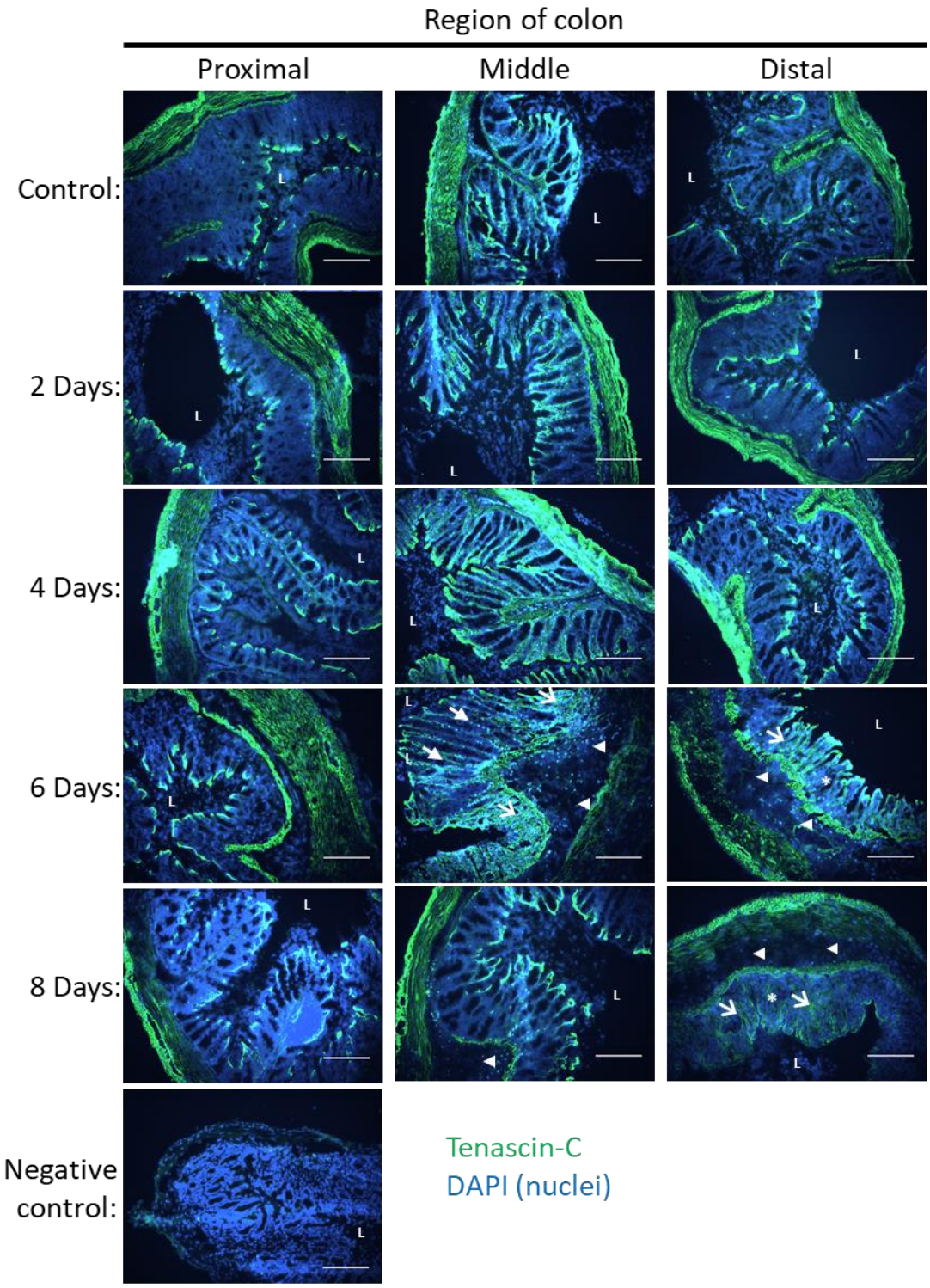

Figure 3.12 Temporal profiling of tenascin-C expression in 2% DSS induced colitis

IHC staining for tenascin-C (green) of proximal, middle, and distal colon sections from control mice or those from the indicated time points in the DSS time course. Tenascin-C is shown to be increased (open arrows) from day six of 2% DSS treatment in the damaged middle and distal colonic mucosa. Mixed immune cell infiltration and submucosal oedema (arrowheads), ulceration (asterisks), epithelial hyperplasia (closed arrows) are also indicated. Legend continued on following page-

Figure 3.12 Continued

Enlarged images of the distal colon sections at each time point (right) to more clearly show the increased levels of tenascin-C staining in the damaged mucosa at the later time points.

The negative control, in which the primary antibody was replaced by non-specific rat IgG, displays no staining. All slides were counterstained with the nuclear stain DAPI (blue) and imaged using a Leica DMLB microscope. Scale bars = 250µm. L = lumen

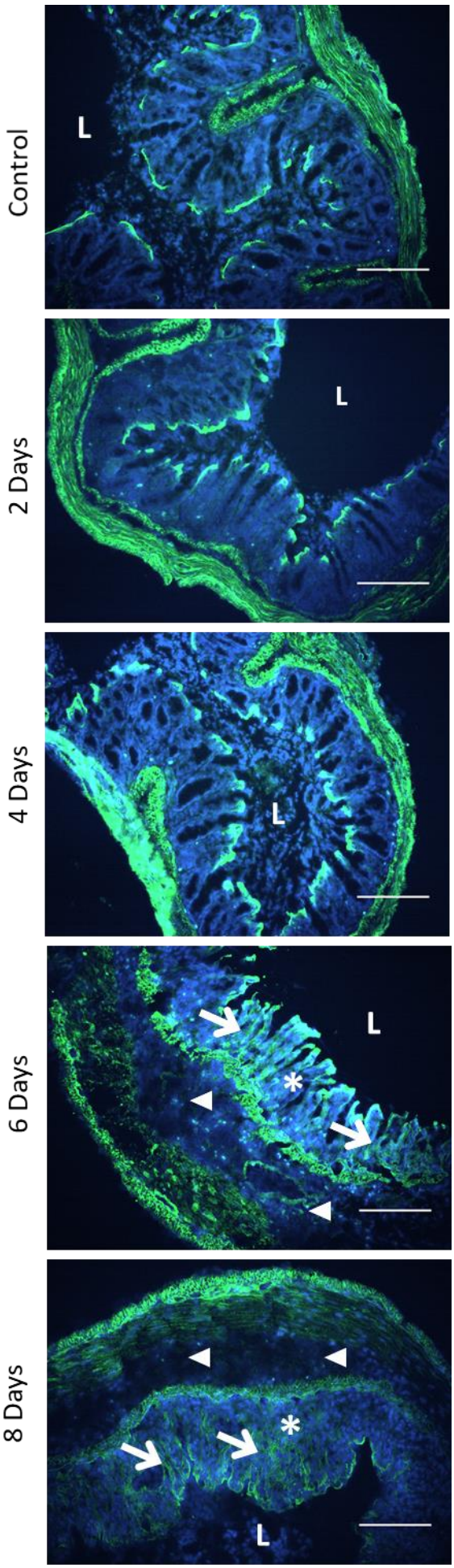

3.5.8 Co-localisation of tenascin-C and α-smooth muscle actin (αSMA) under basal conditions

To probe tenascin-C's association with various histological features of the healthy and inflamed gut, dual IHC staining for a variety of other markers was performed alongside tenascin-C. Initially, based on the observation that tenascin-C appeared to localise to the muscularis externa and muscularis mucosa staining was carried out for αSMA, a marker of smooth muscle and myofibroblasts. This staining, presented in figure 3.13a, showed that under basal conditions αSMA stained the muscularis externa and muscularis mucosa predominantly as expected. Additionally, tenascin-C co-localised largely with these same areas showing a close association in the matrix around the αSMA positive cells. The exception for this appeared to be the subepithelial mucosal tenascin-C staining which did not show any αSMA positivity (see arrow heads in the proximal, middle and distal portions of the control tissue).

Under colitic conditions αSMA localisation remained unchanged, staining to the same smooth muscle structures as under basal conditions. These structures likewise appeared largely similar to basal conditions with the exception of a slight thickening of the muscularis mucosa in the distal colon of the DSS treated mice from day six. Co-staining with tenascin-C likewise remained similar to basal conditions with αSMA also absent from the colitis induced mucosal tenascin-C staining (see asterisk in the middle and distal portions of the colitic tissue).

Additional chance observations were also made during staining with the identification of gut associated lymphoid tissue (GALT), including a colonic patch (CP) and a putative isolated lymphoid follicle (ILF). These were identified morphologically as aggregates embedded in the mucosa and submucosa of the gut wall with the ILFs distinguishable due to their solely mucosal localisation. The identity of these aggregates as CPs was confirmed by staining for B and T lymphocytes, as shown in figure 3.13b and c respectively, which confirmed their lymphoid tissue nature. Interestingly while the ILFs did not appear to show strong tenascin-C staining in their matrix colonic patches did. This staining localised around the periphery of the patch with some matrix staining also extending into and sounding cells within the patch as well (see middle portion of the control tissue).

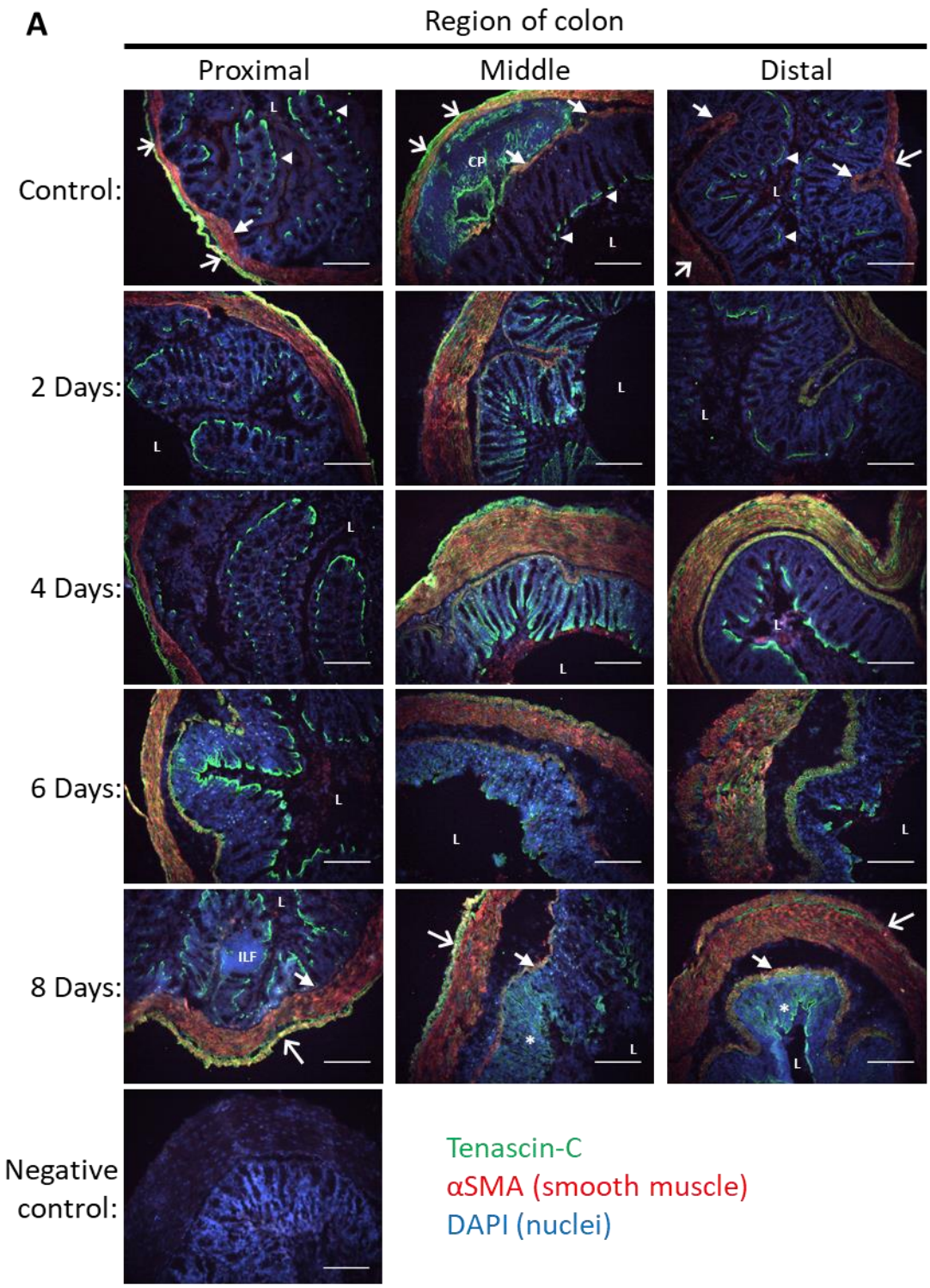

Figure 3.13 Basal tenascin-C localises with smooth muscle marker staining

(A) IHC dual staining for tenascin-C (green) and α-smooth muscle actin (αSMA, red) of proximal, middle, and distal colon sections from control mice or those from the indicated time points in the 2% DSS time course. Tenascin-C co-localises with the αSMA staining in the muscularis mucosa (closed arrows) and muscularis externa (open arrows). Basal (arrowheads) and colitis induced (asterisks) mucosal tenascin-C does not display this co-localisation. Legend continued on following page-

Figure 3.13 Continued

Enlarged images of the distal colon sections at each time point (right) to more clearly show the co-staining for tenascin-C and αSMA in the muscularis externa. This co-staining is not observed for the colitis induced tenascin-C present in the damaged mucosa. The negative control, in which the primary antibody was omitted, displays no staining.

CPs were identified by their morphology with their identities confirmed by additional staining carried out using the B cell marker B220 (B) and the T cell marker CD3 (C). This confirmed that the mucosal aggregates observed were composed primarily of both these lymphocyte populations confirming their identity as gut associated lymphoid tissue.

All slides were counterstained with the nuclear stain DAPI (blue) and imaged using a Leica DMLB microscope. Scale bars = 250µm. L = lumen, CP = colonic patch, ILF = isolated lymphoid follicle.

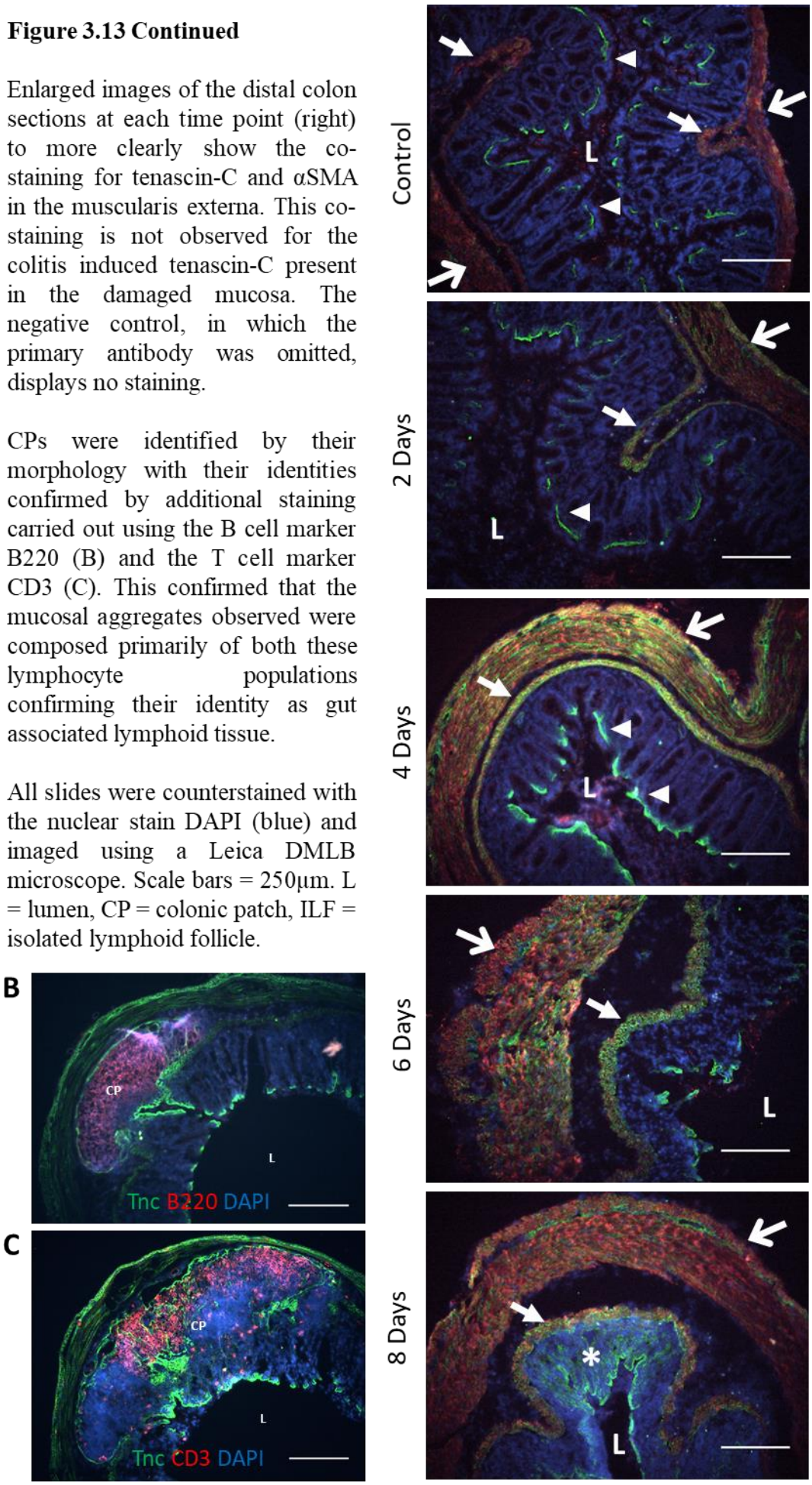

3.5.9 Tenascin-C associates with areas of ulceration in the colonic mucosa of DSS treated mice

Having observed tenascin-C's upregulation appearing to coincide with the onset of mucosal damage, the colonic epithelium was the next structural feature to be studied. To do this the tenascin-C staining was performed alongside the epithelial cell marker, CD326, which is also known as epithelial cell adhesion molecule (EpCAM). This dual IHC staining, shown in figure 3.14, demonstrated strong CD326 staining for the mucosal epithelium along the length of the colon in control tissue. This staining was maintained in the proximal colon throughout the induction of colitis corroborating the observed lack of tissue damage in this region. For the middle and distal colon however ulceration, evidenced by loss of CD326 mucosal staining, was observed which exposed the underlying connective tissue and subepithelial tenascin-C to the lumen. In some cases, the epithelial debris from the sloughed epithelium was also present in the colonic lumen overlying these areas. In terms of colitis induced tenascin-C staining this appeared to predominantly occur in these damaged ulcerated areas. In contrast, areas maintaining at least some CD326 expression showed reduced or absent mucosal tenascin-C staining suggesting tenascin-C was being deposited directly at the sites of mucosal injury.

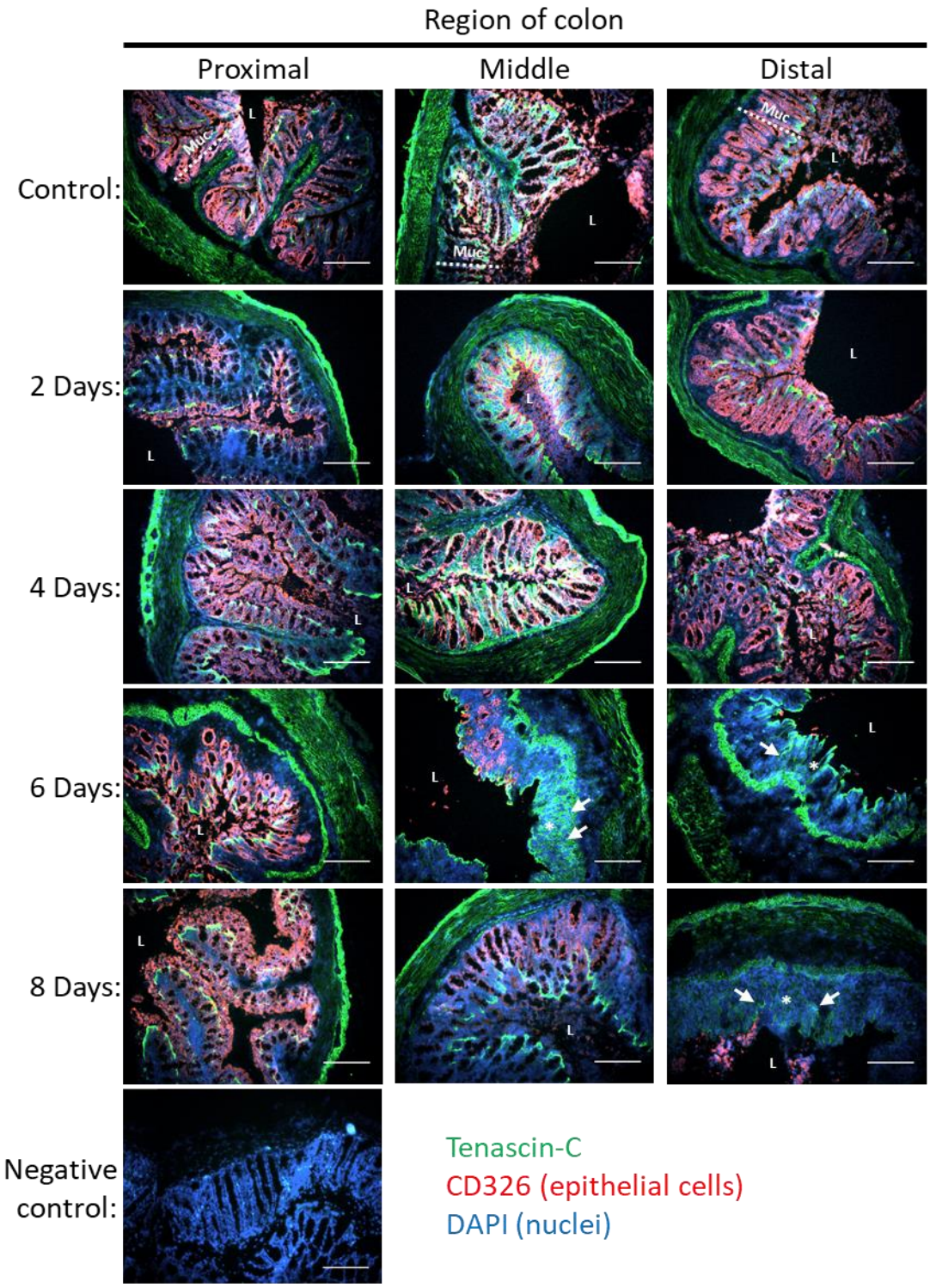

Figure 3.14 2% DSS induced tenascin-C localises to areas of ulceration

IHC dual staining for tenascin-C (green) and CD326 (red) of proximal, middle, and distal colon sections from control mice or those from the indicated time points in the DSS time course. CD326 strongly stains all of the colonic epithelium in control tissue. From day six in the 2% DSS treated mice ulceration, shown by loss of CD326 staining (asterisks), becomes apparent with tenascin-C localising to these areas of damage (closed arrows).

Figure 3.14 Continued

Enlarged images of the distal colon sections at each time point (right) to emphasise the loss of epithelial CD326 staining due to ulceration from day 6 of DSS treatment. Tenascin-C preferential localises to these areas of damaged mucosa highlighted particularly in the enlarged image of the day six middle colon (below). Note the tenascin-C staining in the damaged mucosa predominates to areas of ulceration, lacking CD326 staining, compared to adjacent less damaged areas where some CD326 staining, and thus intact epithelium, remains (open arrows).

The negative control, in which the primary antibody was omitted, displays no staining. All slides were counterstained with the nuclear stain DAPI (blue) and imaged using a Leica DMLB microscope. Scale bars = 250µm. L = lumen, Muc = mucosa.

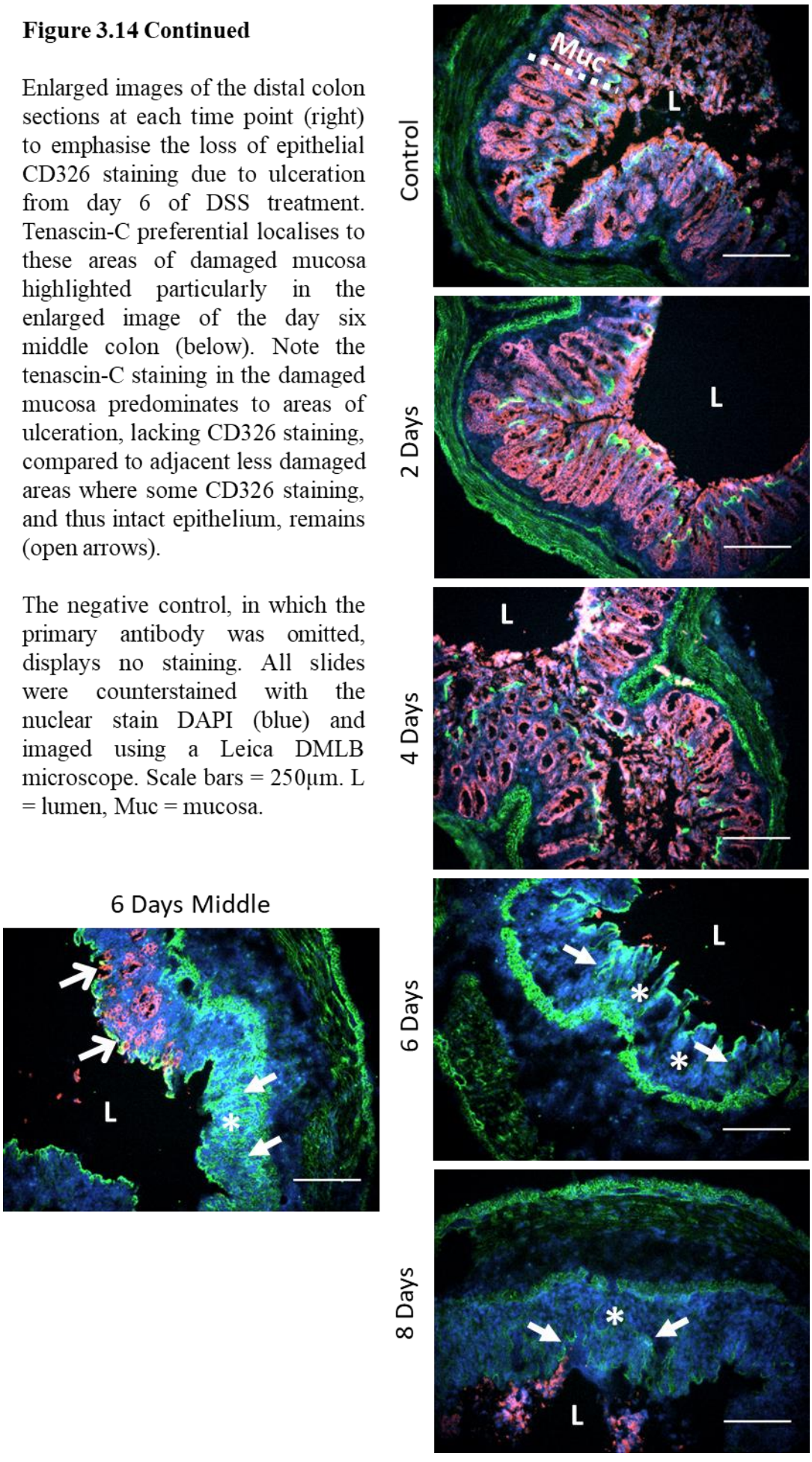

3.5.10 Tenascin-C localisation in relation to the vascular system

The vasculature is of obvious inflammatory importance with vasodilation and immune cell trafficking among the key events in any response. As tenascin-C has been reported to localise to blood vessels in other tissues (Mackie et al., 1992) these vessels were the first to be stained for using the endothelial cell marker CD31, shown in figure 3.15. Normal blood vessel architecture was observed in control tissue along the length of the colon with discrete vessels clearly present in the submucosa and extending into the lamina propria. In terms of tenascin-C staining this did not appear to co-localise with these vessels in the submucosa although the apical tips of the mucosal vessels did appear in some cases to co-localise with subepithelial tenascin-C staining. From day six of DSS treatment, alongside the inflammatory disruption of the mucosal architecture, the vascular network likewise became distorted. In hyperplastic epithelial regions the mucosal blood vessels expanded matching the increased thickness of the mucosa. In damaged areas of the mucosa, rich in tenascin-C, endothelial staining was also still observed although now as a disrupted microvascular network in the granulation tissue.

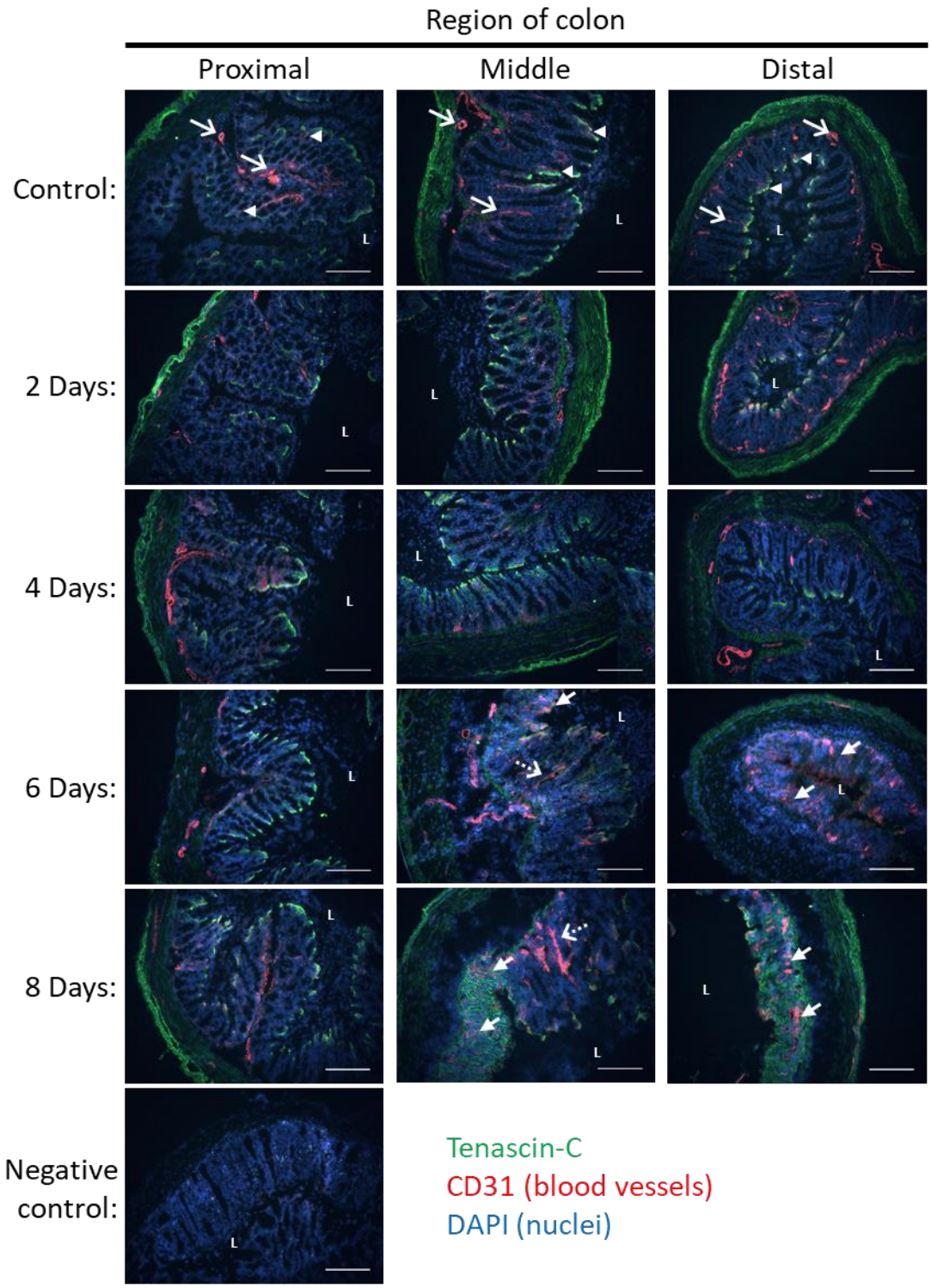

Figure 3.15 Disrupted blood vessel architecture is present in 2% DSS colitis

IHC dual staining for tenascin-C (green) and CD31 (red) of proximal, middle, and distal colon sections from control mice or those from the indicated time points in the 2% DSS time course. Normal vessels are observed along the length of the colon under basal conditions (open arrows) including below the subepithelial tenascin-C band (arrowheads; see following page for enlarged image to aid visualisation). An increase in blood vessels with aberrant architecture is observed in the damaged (closed arrows) and hyperplastic (dashed arrows) mucosa of DSS treated mice from day six. Legend continued on following page-

Figure 3.15 Continued

Enlarged images of the distal colon sections at each time point (right) in particular to emphasise the subepithelial mucosal blood vessel staining in close proximity to subepithelial tenascin-C staining present in the control colon tissue.

The negative control, in which the primary antibody was replaced with non-specific rat IgG, displays no staining. All slides were counterstained with the nuclear stain DAPI (blue) and imaged using a Leica DMLB microscope. Scale bars = 250µm. L = lumen

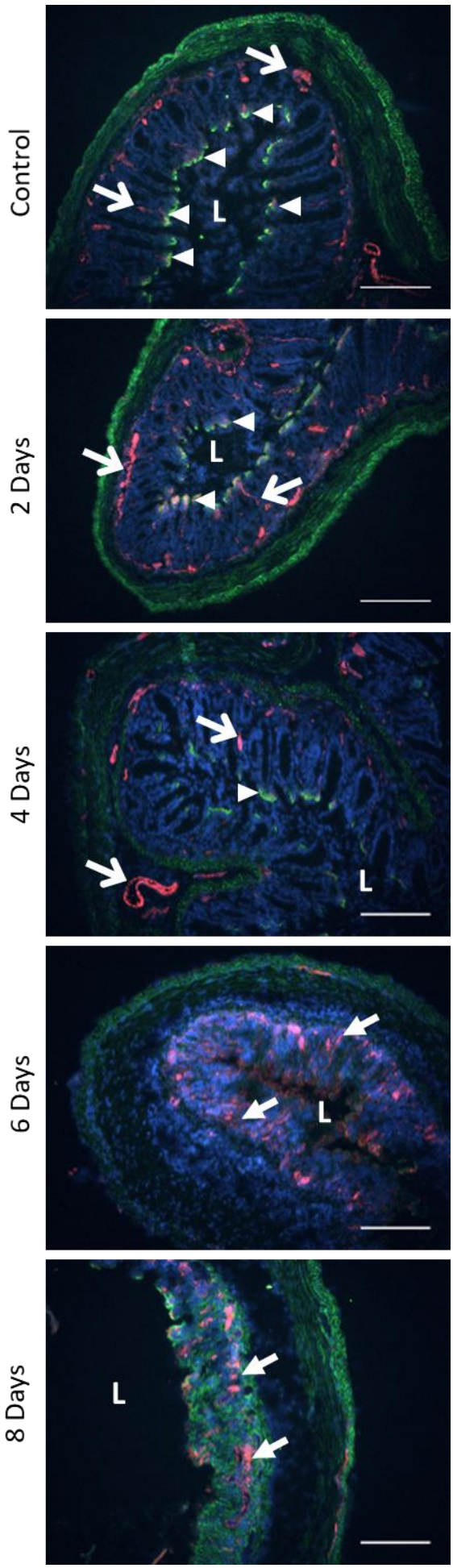

Besides the cardiovascular system the other component of the body's vasculature is the lymphatic system. To investigate the spatial relationship between the lymphatic system and tenascin-C IHC was performed for the lymphatic endothelium specific marker lymphatic vessel endothelial hyaluronan receptor 1 (LYVE-1), as shown in figure 3.16. In control tissue, lymphatic vessels were observed in the mucosa along the length of the colon. In the proximal colon, staining was localised to a band of vessels just overlying the muscularis mucosa as well as vessels extending into the lamina propria of the mucosal folds. A similar pattern was seen with the middle and distal colon although here the vessels extending into the lamina propria were far less prominent. This localisation positioned LYVE-1 in close association with tenascin-C which stained the underlying muscularis mucosa. Also, in contrast to the CD31 staining the lymphatics in the lamina propria did not extend as far apically and thus did not appear to contact the subepithelial tenascin-C staining.

From day six of DSS treatment the apically extending vessels appeared to be lost with the breakdown of mucosal architecture with some staining only appearing to remain in hyperplastic regions. Vessels overlying the now thickened tenascin-C staining muscularis mucosa remained however and appeared dilated with enlarged lumens, presumptively as a result of the marked oedema observed.

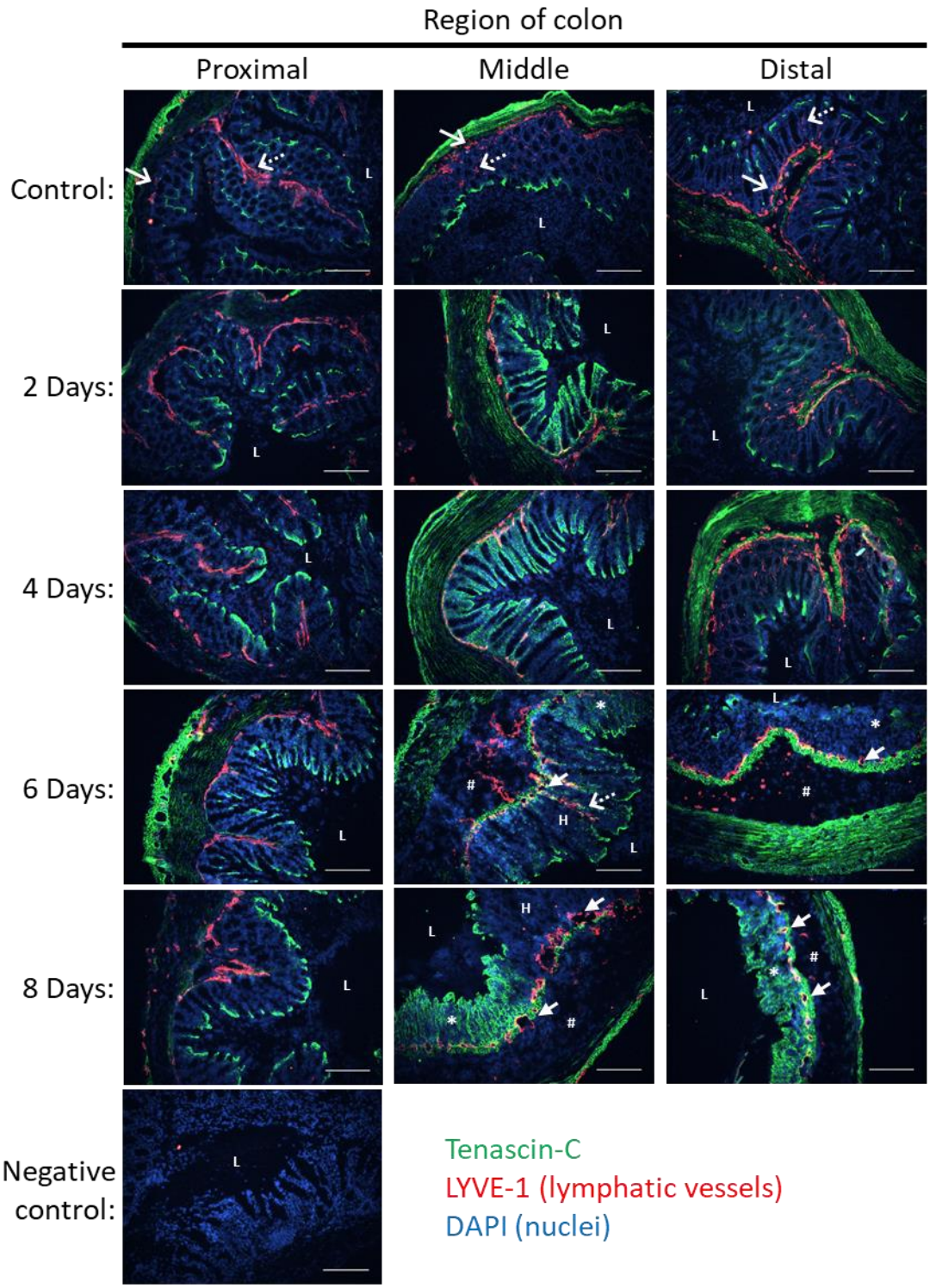

Figure 3.16 Lymphatic vessels localise adjacent to the tenascin-C positive muscularis mucosa

IHC dual staining for tenascin-C (green) and LYVE-1 (red) of proximal, middle, and distal colon sections from control mice or those from the indicated time points in the 2% DSS time course. Lymphatics are present at the base of the mucosa (open arrows) and within the lamina propria (dashed arrows). Vessels in the middle and distal colon appear dilated from day six of DSS treatment (closed arrows). Legend continued on following page-

Figure 3.16 Continued

Enlarged images of the distal colon sections at each time point (right) to more clearly show the detail of the mucosal lymphatic staining.

The negative control, in which the primary antibody was omitted, displays no staining. All slides were counterstained with the nuclear stain DAPI (blue) and imaged using a Leica DMLB microscope. Scale bars = 250µm. L = lumen, * = ulceration, H = hyperplastic mucosa, # = oedema

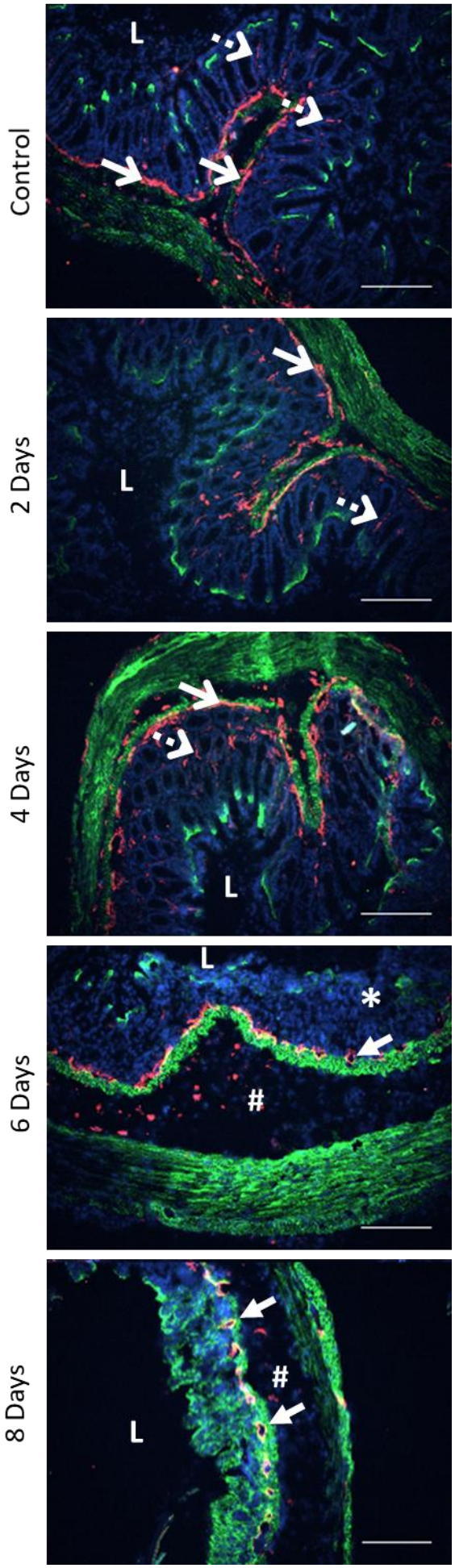

3.5.11 Tissue resident macrophages underlie the band of subepithelial tenascin-C staining

Having examined several structural features of the colon it was next decided to interrogate the immune compartment in more detail. To begin the lamina propria resident macrophage population was investigate by IHC using the integrin CD11c as a marker, the results of this shown in figure 3.17. In control mice resident macrophages were found throughout the lamina propria, tending to localise more towards the upper apical regions closer to the lumen. The macrophages occupying these apical locations were thus found to closely associate with the band of subepithelial tenascin-C staining also found in this region.

With the onset of obvious colitic damage at day six of DSS treatment numbers of resident macrophages did not appear to change from the basal state. The cells remained within the damaged mucosa and were found in both tenascin-C rich ulcerated regions as well as and non-staining areas, such as less damaged hyperplastic regions.

3.5.12 Mucosal tenascin-C upregulation is concurrent with immune infiltration by T-cells

Following from the investigation of the innate tissue resident macrophages the final cell type to be examined was the T cells of the adaptive arm of the immune system. Staining for the T cell marker CD3, a component of the T cell receptor, was carried out along with staining for tenascin-C with representative images of staining shown in figure 3.18. In control tissue, T cells were found to sparsely distributed along the length of the colon within the lamina propria. This was similar to the resident macrophages albeit in lower numbers and with no apical preference in location observed. Despite this however, some T cells were still observed to localise to the same apical locations underlying tenascin-C staining which the resident macrophages were shown to occupy.

Unlike the resident macrophages however, upon establishment of colitis on day six of the time course a significant increase in T cell numbers was observed. This increase was largely seen as infiltrating cells within the mucosa in damaged ulcerated and hyperplastic regions. A small number of T cells were additionally observed among the cells infiltrating within the oedematous submucosa.

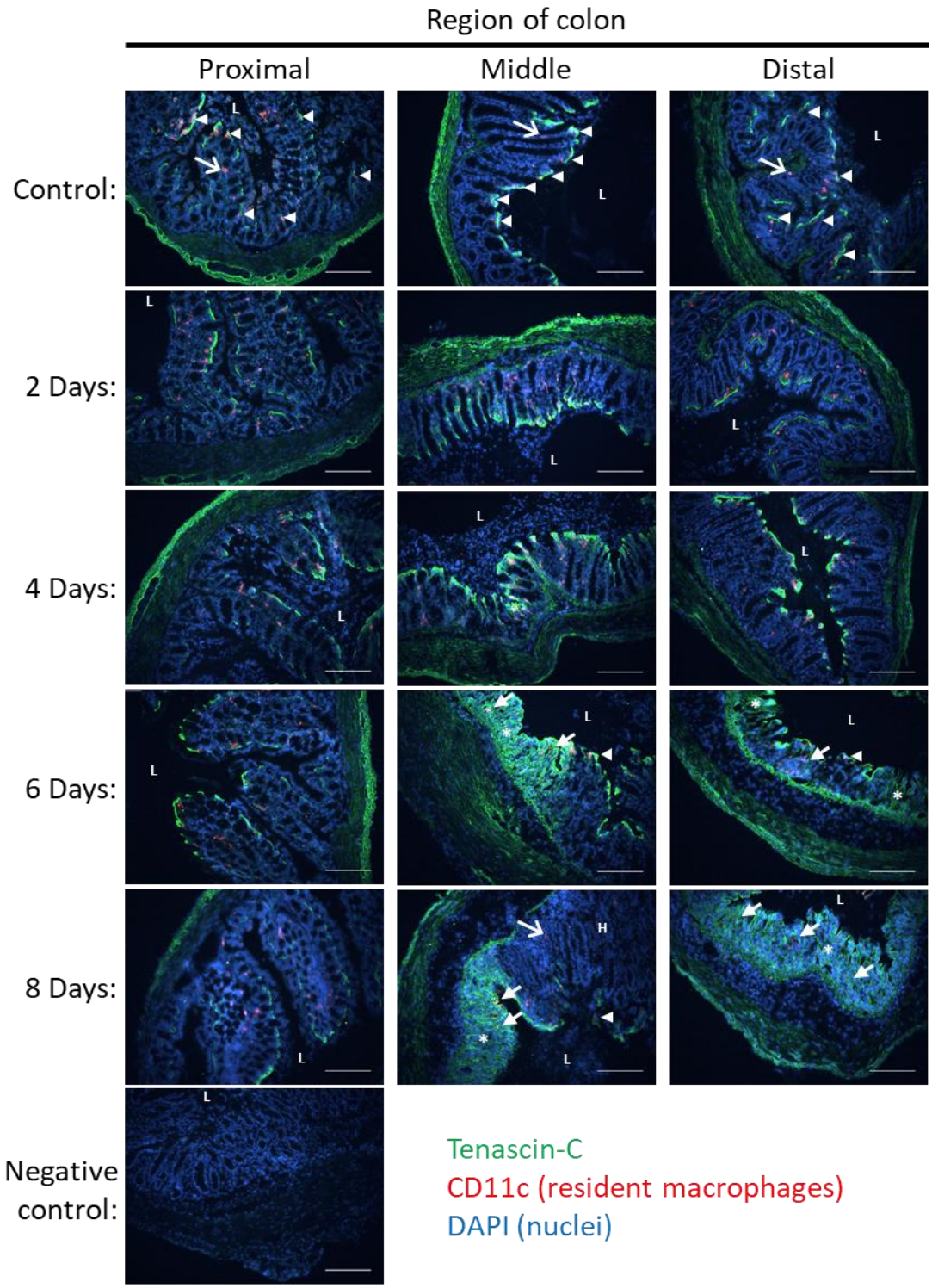

Figure 3.17 Lamina propria macrophages underlie subepithelial tenascin-C

IHC dual staining for tenascin-C (green) and CD11c (red) of proximal, middle, and distal colon sections from control mice or those from the indicated time points in the 2% DSS time course. Resident macrophages (open arrows) are found throughout the lamina propria, particularly apically underlying tenascin-C staining (arrowheads). Under colitic conditions similar numbers of macrophages were observed in the damaged tissue (arrows; see following page for enlarged image to aid visualisation). Legend continued on following page-

Figure 3.17 Continued

Enlarged images of the distal colon sections at each time point (right) to highlight resident macrophages underlying subepithelial tenascin-C staining and within the colitic damaged mucosa from day six of DSS treatment.

The negative control, in which the primary antibody was omitted, displays no staining. All slides were counterstained with the nuclear stain DAPI (blue) and imaged using a Leica DMLB microscope. Scale bars = 250µm. L = lumen, * = ulceration, H = hyperplastic mucosa.

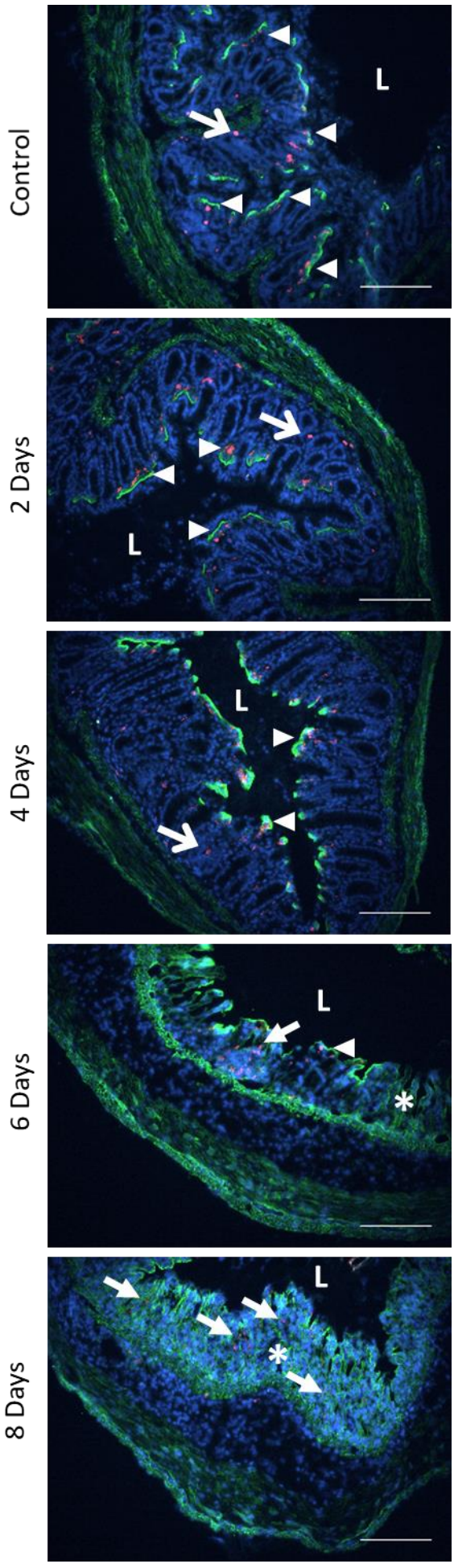

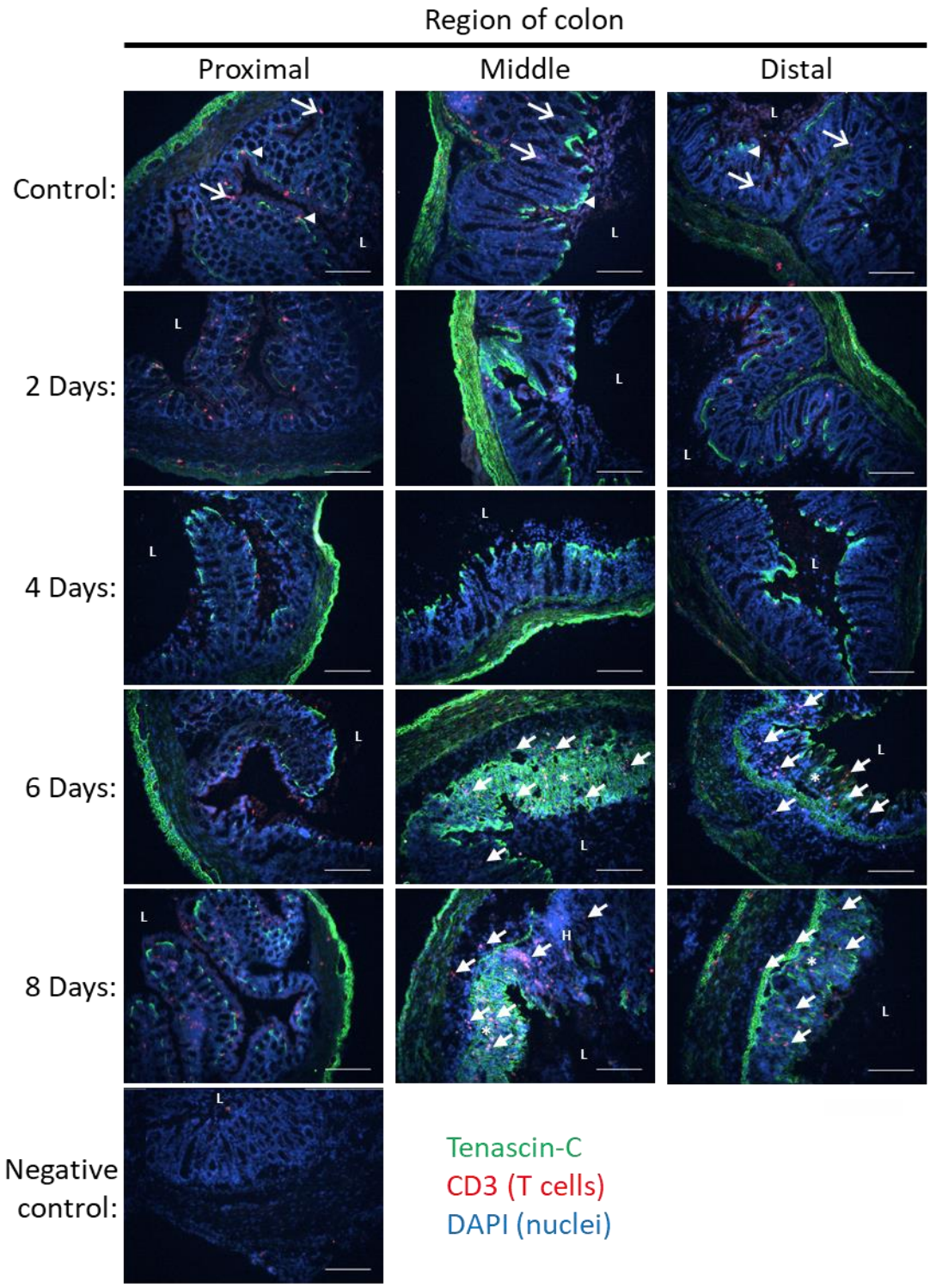

Figure 3.18 T cells infiltrate the colitic colon on day six of 2% DSS treatment

IHC dual staining for tenascin-C (green) and CD3 (red) of proximal, middle, and distal colon sections from control mice or those from the indicated time points in the 2% DSS time course. T cells (open arrows) are found throughout the lamina propria in control tissue including occasionally occupying positions underlying subepithelial tenascin-C staining (arrowheads). Increased T cell numbers are seen in the colitic mucosa of DSS treated mice from day six (closed arrows). Legend continued on following page-

Figure 3.18 Continued

Enlarged images of the distal colon sections at each time point (right) to better highlight the numerous CD3 positive T cells infiltrating the damaged colitic mucosa alongside tenascin-C staining.

The negative control, in which the primary antibody was omitted, displays no staining. All slides were counterstained with the nuclear stain DAPI (blue) and imaged using a Leica DMLB microscope. Scale bars = 250µm. L = lumen, * = ulceration, H = hyperplastic mucosa.

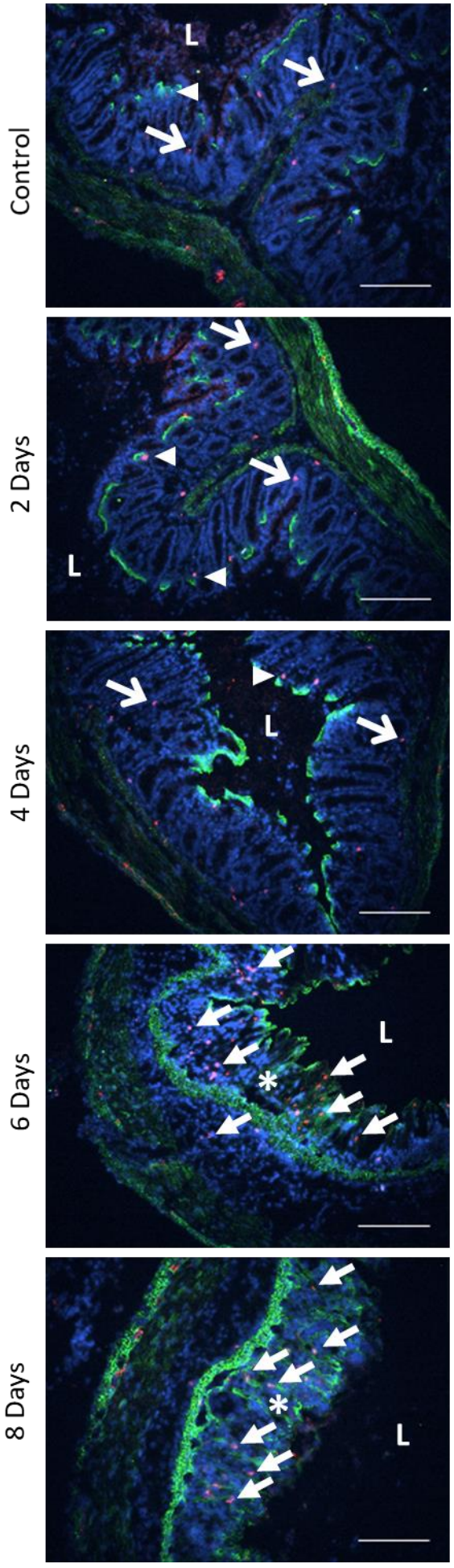

3.6 Discussion

In summary in this chapter I have systematically profiled the basal expression of tenascin-C in the healthy murine colon and then followed its induction and localisation at this site during DSS induced colitis. The significance of these findings and the hypothetical roles and mechanism by which tenascin-C may be acting, in both health and disease, will now be discussed.

3.6.1 Expression pattern of tenascin-C in the adult mouse

All the methods investigated, including microarray, SAGE, and qPCR, broadly confirmed tenascin-C's restricted adult expression with the majority of tissues showing low to negligible expression, especially in relation to embryonic MEF cells. The less sensitive high throughput microarray and SAGE screening data largely corroborated with each other. This included the identification of bone as an expression site although this was more variable in the BioGPS data owing to the pooling of data for bone and bone marrow samples. The majority of the remaining common tissues analysed were also in agreement with comparatively low levels of mRNA expression observed. The one exception observed was brain tissue which showed some expression in the SAGE-genie dataset but little expression in the BioGPS dataset. This could be explained by the fact that the expression for brain was calculated in both datasets by pooling data from a number of microdissected regions. This included the cerebellum, cerebral cortex, prefrontal cerebral cortex, amygdala, hippocampus, hypothalamus, nucleus accumbens, olfactory bulb, and pituitary gland in the BioGPS dataset. Conversely, the data available in the SAGE-genie set was much more limited and only included the hippocampus, amygdala, and thalamus, with the thalamus, which was not included in the BioGPS dataset, accounting for the majority of the tags identified. Indeed, even within the regions pooled in the BioGPS dataset variation was observed with cerebellum for example appearing to express far more tenascin-C than the other brain areas sample. This thus supports the notion that tenascin-C's expression is tightly restricted down to the level of sub-localisation within tissues.

In comparison, the RT-qPCR data showed a generally similar pattern of low expression for most tissues. This included the brain, like for the SAGE genie dataset, being identified as the highest tissue expressing tenascin-C alongside bone and colon

which were also picked up as expressers in the BioGPS dataset. Unlike, the above methods however the testis, kidney, and muscle were also identified as expressers. This could potentially be a sensitivity issue however as some expression within the testis (Paranko et al., 1995), kidney (Aufderheide et al., 1987) and muscle tissue (Fluck et al., 2000) has been reported previously. Additionally, differences in the methodology of RNA extraction used as well as mouse strains and age may also explain some of the observed discrepancies.

3.6.2 Basal expression of tenascin-C in the murine colon

Focusing in on the colon it was clear by all the gene expression methods utilised that it was one of the more prominent tenascin-C expressing tissues. Additionally, it was apparent that the expression varied along its length, with the highest expression seen in the mid colon, followed by the distal, and then the proximal segments respectively.

This basal gene expression in the adult colon was further found to have relevance at the protein level. Initially, western blotting of adult colon tissue extracts revealed two molecular weight variants present with a predominance of the small form. This corroborated with published data reporting RNA splice variants of tenascin-C in the developing and adult colon. Early in development both variants were found but in the adult the small variant predominated (Saga et al., 1991). This contrasts with what was observed in neonate lung samples in which higher levels of tenascin-C were seen with a predominance for the large variant, as has been previously reported (Young et al., 1994). As such, it appears the colon seems to follow a similar expression pattern as has been observed in a variety of other tissues, including in the brain (Dorries and Schachner, 1994) and kidney (Weller et al., 1991), whereby expression of large tenascin-C variants decreases with age (Giblin and Midwood, 2015). This potentially contrasts with what has been reported for the small intestine in which equal expression between the small and large variants as well as an increase in expression of the large variant with age has been reported (Aufderheide and Ekblom, 1988, Weller et al., 1991). However, other reports appear to contradict this observation and instead, like in the colon, have reported a predominance of the small tenascin-C variant (Probstmeier et al., 1990b) and a reduction of expression with age (Saga et al., 1991). This observed tissue specific variation in molecular weights could have a number of

explanations including alternative splicing or post translational modification such as glycosylation, both of which have been shown to vary by cell or tissue source (Giblin and Midwood, 2015, Mangan et al., 2019).

In terms of localisation within the colon tenascin-C was found in the lamina propria as well as the muscularis mucosa and externa along the length of the colon. Supporting the gene expression data, the mid colon was also found to contain the highest amount of tenascin-C staining where in the lamina propria it expanded beyond the tight subepithelial staining seen in the proximal and distal colon. This expression pattern is similar to what has been observed in the murine small intestine (Aufderheide and Ekblom, 1988, Probstmeier et al., 1990a) and stomach (Scherberich et al., 2004) where tenascin-C has been shown in the smooth muscle tissue as well as in the mucosal lamina propria. More similarly to the mid colon the mucosal staining is more prominent along the length of the villus co-localising with its core and subepithelial sheath with, as in the colon, increasing expression towards the apical surface. This difference is potentially developmentally rooted as tenascin-C staining of the embryonic small intestine likewise showed strong mucosal villus core staining while the colonic mucosa showed none (Desloges et al., 1994). Additionally, this same expression pattern in the small intestine and colon has also been reported in adult human samples, suggesting this is a conserved aspect of tenascin-C biology not unique to the mouse (Sakai et al., 1993, Beaulieu, 1997).

Having demonstrated tenascin-C's presence in the colon under basal conditions the identification of the tenascin-C producing cells from which it originates is of obvious interest. For the muscularis mucosa and externa tenascin-C this appears to be of smooth muscle cell origin as demonstrated by the clear overlap with αSMA staining at these sites. This is similar to what has been observed in other tissues with basal expression of tenascin-C also observed surrounding vascular smooth muscle cells of the aorta (Kimura et al., 2014) and pulmonary smooth muscles cells of the bronchi (Kaarteenaho-Wiik et al., 2002). While IHC staining does not confirm the smooth muscle cells as the source of the tenascin-C its close association by co-staining with this cell type across a number of tissues does lend credence to this theory. Future studies should aim to confirm these findings by micro-dissection or isolation of the

smooth muscle cell population specifically to examine their expression of tenascin-C by qPCR. The subepithelial tenascin-C by contrast had a number of potential origins the first of which was postulated as production by resident macrophages, whose marker staining was shown in close proximity to these subepithelial sites. Macrophages are known to be able to produce tenascin-C, being among some of the significant sources in pathological conditions such as in the inflamed synovium of rheumatoid arthritis patients (Goh et al., 2010). Another potential candidate were epithelial cells potentially laying down tenascin-C within their basement membrane. However, studies in the developing small intestine have shown the tenascin-C appears to be produced by cells of mesenchymal rather than epithelial origin (Perreault et al., 1998). Additionally, studies utilising immuno-electron microscopy in the murine small intestine have also showed that subepithelial tenascin-C was not found within the basement membrane but was located below it associated with fibroblast like cells (Probstmeier et al., 1990a).

The identity of these fibroblast like cell was not confirmed in this publication however and so the exact type of stromal cell remains to be determined. Myofibroblasts were a potential candidate as their differentiation and activation has been closely linked to tenascin-C in other settings (Bhattacharyya et al., 2016), and in the cases of colonic adenomas they have already been proposed as producers of tumour related tenascin-C (Hanamura et al., 1997). However, the observed lack of αSMA staining, a marker of myofibroblasts, at the apical epithelium would appear to discount this cell type as a potential source. A similar lack of overlap has also been observed in human samples where myofibroblasts were found to be more prevalent towards the base of the crypts away from apical tenascin-C staining (Salas et al., 2003). Further stromal cell subtype information has been gleaned from a single cell RNA sequencing study of ileal tissue from Crohn's disease patients which identified fibroblasts, smooth muscles cells, and pericytes as the main tenascin-C producing cells present (Martin et al., 2019). Following from this, the fibroblasts of the colon have recently been further broken down into a number of subtypes based on gene expression analysis. Reviewing the data in this study it was found that tenascin-C was expressed in the stromal 2 subtype which was characterised as colonic crypt niche mesenchymal cells with functions implicated in epithelial support and maintenance. In this role the stromal 2 population

was found to localise to the subepithelial space thus adding strength to its claim to be the source of the subepithelial tenascin-C also found in this location (Kinchen et al., 2018). Why these cells produce tenascin-C preferentially at the apical surface remains to be determined although one potential mechanism hypothesised would be induction of tenascin-C expression by indian hedgehog (IHH) signalling. In regards to this, IHH has been found to be preferentially expressed by apically located mature colonic epithelial cells (van den Brink et al., 2004) and has additionally been shown to induce tenascin-C expression in some cell types (Liu et al., 2013, Foley et al., 2017).

3.6.3 Potential functional roles of basal tenascin-C

The exact role of tenascin-C in the gut under basal conditions remains to fully be determined although the apparent normality of *Tnc*$^{-/-}$ mice would suggest it is not essential for normal gut development (Saga et al., 1992). In terms of the muscularis related tenascin-C in other tissues it has been implicated as a smooth muscle cell survival factor. This has been shown predominantly for vascular smooth muscle cells which show enhanced proliferation in response to growth factors in the presence of tenascin-C (Jones et al., 1997). Work in the developing small intestine likewise supports this potential role in the gut context where tenascin-C is seen to localise to areas of smooth muscle generation (Beaulieu et al., 1993) suggesting it may be playing a supportive proliferative role here too.

For the role of the subepithelial tenascin-C two main potential functions could be suggested. The first of these is that tenascin-C may be playing a role at sites of lumen immune surveillance, as suggested by its close proximity to the immune cells highlighted in this study. In regard to this, the fibroblasts suggested above as the primary source of this tenascin-C are known to have immunological roles. This includes expression of innate immune receptors, such as TLR4 (Kurahashi et al., 2013), and limited antigen presentation abilities (Saada et al., 2006, Owens et al., 2013). As such, tenascin-C might form a part of these cells immunomodulatory niche influencing their own as well as accompanying immune cell interactions at the epithelial-lumen interface.

The second role postulated was tenascin-C may be playing a role in the support and maintenance of the colonic epithelium. Indeed, in the case of the dermal epithelium under wounding conditions a number of studies have implicated tenascin-C in epithelial differentiation, proliferation, and migration (Midwood and Orend, 2009). In the small intestine it has also been suggested that tenascin-C may aid in maintenance of the epithelial by promoting terminal epithelial cell shedding (Probstmeier et al., 1990a). Tenascin-C could also influence the epithelium in an indirect manner by binding soluble factors for sequestration or presentation. A potential example would be hepatocyte growth factor (HGF), which can bind the FNIII 1-5 repeats of tenascin-C (De Laporte et al., 2013), and has been suggested as a key epithelial repair promoting factor secreted by colonic macrophages (D'Angelo et al., 2013). This immune and barrier maintenance cross talk additionally demonstrates the potentially non-mutually exclusive role tenascin-C may be playing at this location.

3.6.4 Evaluation of the DSS model of colitis

To study tenascin-C under inflammatory conditions the DSS model of colitis was established and shown to behave in a similar manner as has previously been reported in the literature. This included the predominantly distal nature of the colitis induced as well as its gross and histopathological features (Perse and Cerar, 2012).

A number of chemically induced as well as genetic models of IBD have been developed over the years. Of these the DSS model has proved popular as it provides a relatively rapid and reproducible platform for studying colonic inflammation in immunocompetent wild-type mice (Wirtz et al., 2017). The model additionally successfully recapitulates a number of pathological changes observed in ulcerative colitis patients. This includes gross parameters such as weight loss, diarrhoea and colonic bleeding as well as histological features such as, epithelial ulceration, crypt abscesses, and mucosal immune cell infiltration. (Okayasu et al., 1990). The epithelial barrier integrity disruption induced by DSS also likewise mimics the defective barrier function which is seen in both ulcerative colitis and Crohn’s disease (Antoni et al., 2014). Further bolstering the translational credentials of the model DSS has additionally been shown to recapitulate the therapeutic responses seen with some drugs in use clinically for the treatment of IBD (Melgar et al., 2008).

Despite these advantages however the limitations of the model should also be taken into account. In particular, the disease mechanism of acute mass barrier disruption, while mimicking some features of IBD, is unlikely to be the main disease mechanism present in IBD patients (Kiesler et al., 2015). Additionally, due to this mechanism of action and the acute nature of the protocol DSS colitis is primarily a model of innate immune driven pathology. The innate cell types macrophages and granulocytes in this case are the key inflammatory pathology drivers constituting the primary cell type detecting the initial barrier disruption and then infiltrating the tissue in response respectively. This is evidenced by the fact that the adaptive immune system has been previously found to not be required for colitis induction (Dieleman et al., 1994). As such it's mechanism of action may underestimate the contributions of the adaptive system to IBD pathology.

3.6.5 Tenascin-C expression in DSS induced colitis

Tenascin-C has been shown in this study to be upregulated in the colitic colon at the mRNA and protein level. This increase is in line with previously reported omic studies of DSS colitis which have also showed tenascin-C upregulation in the colitic colon by gene expression microarray (Fang et al., 2011) and mass spectrometry (Zhang et al., 2019). Additionally, tenascin-C has also been shown to be elevated at the protein level in the colitic colons of *Il-10*$^{-/-}$ mice, a genetic model of IBD, suggesting this upregulation is not simply a quirk of the DSS colitis model (Shimshoni et al., 2019). This increase of tenascin-C in animal models likewise matches what has been observed in human samples, with increased tenascin-C detected in inflamed UC colon tissue compared to uninflamed and control samples (Moriggi et al., 2017). Likewise, the distribution of tenascin-C within the colon of the DSS colitic mice also matched what has been reported in human samples. This includes an observed general increases in disorganised tenascin-C deposition within the lamina propria outside of its normal apical localisation in both UC and Crohn's disease samples (Riedl et al., 1992, Ambort et al., 2010). Additionally, as in the DSS model, this increase has been reported to be particularly prominent within the granulation tissue stroma of ulcerations (Geboes et al., 2001).

Besides inflammatory pathology the IBDs are also associated with fibrosis such as thickening of muscularis mucosa which is observed in both CD (Lee et al., 1991) and UC (Gordon et al., 2018). As shown in this study, as well previously in the literature (Forbes et al., 2004), DSS colitis likewise replicates this muscularis mucosal thickening pathology. With tenascin-C's strong localisation to the muscularis mucosa and its known pro-fibrotic properties (Bhattacharyya et al., 2016) this potentially implicates tenascin-C in another aspect of IBD pathology. Indeed, findings from patients with the less common microscopic collagenous colitis may provide additional evidence for this pro-fibrotic hypothesis. Collagenous colitis is characterised by an absence of gross colonic pathology, such as ulceration, with only the presence of histological inflammation alongside deposition of a thick subepithelial collagen band (Miehlke et al., 2019). This subepithelial collagen band coincides with the localisation of the basal apical mucosal tenascin-C staining which is shown to be significantly increased in collagenous colitis patients (Aigner et al., 1997). As such, this again places tenascin-C at a site of colonic inflammatory associated fibrosis suggesting further its involvement.

Together these observations suggest that tenascin-C's upregulation in colitis is conserved across disease models and types as well as species, implicating it in a common colitis promoting role. Additionally, this indicates that the DSS model is appropriate for studying tenascin-C in IBD and that the conclusions gained will be potentially translationally relevant.

3.6.6 Kinetics of tenascin-C upregulation in colitis

In terms of the kinetics of the *Tnc* mRNA upregulation in colitis a trend towards an increase was observed from day six alongside a variety of other pro-inflammatory mediators. This analysis was likely abrogated however due to sampling constraints which resulted in the full length colon being analysed rather than just solely the colitic distal colon. Inclusion of the uninflamed sites potentially introduced additional variation into the mRNA samples resulting in the modest approximately four fold increase seen in earlier experiments being diluted out. This explanation is supported by the observation that other genes which have previously been shown to be upregulated in acute DSS colitis, such as *Il-10* and *Il-12a* (Egger et al., 2000, Yan et

al., 2009), also only displayed a non-significant trend to increase in this analysis. Other pro-inflammatory mediators, including *Tnf*, *Il-6*, and *Il-1β*, did show robust increases from day six however, although their significance was likely preserved due to their many fold higher induction compared to *Tnc*, *Il-10*, and *Il-12a*. These genes were likely many fold higher induced due to the fact that, unlike tenascin-C, as potently pro-inflammatory cytokines they are likely very lowly expressed under basal conditions resulting in higher induction from the resting state. Indeed, this could be observed at the level of the CT values which for *Tnc* in control samples was approximately 23 cycles, contrasting with for example *Il-6* which in the same samples was only present at the much lower 29 cycles. This difference in upregulation likewise might be expected as higher amounts of cytokines, which are more readily cleared locally by diffusion, degradation, and internalisation, are likely needed to be produced compared to a large ECM molecule which likely persists more readily.

Considering the protein level, the trend in upregulation seen at the mRNA level was found to be likewise present with tenascin-C staining increased from day six. This mimicked the development of significant histological pathology in the mice which, as reported by others (Nunes et al., 2018), developed by day six of initial DSS dosing. As such, this would suggest that as expected tenascin-C is not an early inducer of the inflammatory response but instead only becomes increased at sites of established inflammation and tissue damage.

One potential mechanism of induction may involve the microbiome, which has been shown to be essential in the establishment of DSS colitis (Hudcovic et al., 2001). Early in DSS dosing, colonic permeability has been shown to increase significantly by as early as day three and increase further by day five (Yan et al., 2009). This would thus result in luminal bacterial content leaking into the underlying lamina propria and activate PRRs on the resident stromal and immune cell populations. A variety of bacterial components acting via various different PRRs, including the TLRs 1, 2, 4, and 5, have previously been shown to drive tenascin-C production in human dendritic cells (Goh et al., 2010).

An endogenous mechanism may also potentially be responsible with the observation that the earliest observed pathological sign was limited immune cell infiltration seen

on day four. These cells were likely neutrophils as they have previously been identified in the literature as the earliest immune cell type recruited to the colon in DSS colitis (Hall et al., 2011). Neutrophils display limited ability to produce tenascin-C and thus are unlikely the source of the tenascin-C subsequently found at day six (Giblin, 2018). However, neutrophils can produce significant amounts of the pro-inflammatory cytokine TNF (Tecchio et al., 2014) which in turn has been shown to induce the expression of tenascin-C in a number of cells types (Latijnhouwers et al., 1998b, Nakoshi et al., 2008).

These two pathways thus both present themselves as potential mechanisms of tenascin-C induction in DSS colitis.

3.6.7 Identity of the tenascin-C producing cells of the inflamed colon

Having shown the upregulation of tenascin-C at sites of mucosal damage this raises the question of what cells are responsible for its deposition. In regard to this stromal cells, such as fibroblasts, with the capacity to produce large amounts of ECM culture have been implicated in the production of tenascin-C in other inflammatory contexts. This includes within the inflamed synovium in a murine model of rheumatoid arthritis in which the stromal synovial fibroblasts were shown to be the main cell type responsible for tenascin-C production (Goh et al., 2010). In the case of DSS colitis a previous publication suggested myofibroblasts as the tenascin-C producing cells (Islam et al., 2014) of the colitic colon. However, in this present study little expression of the myofibroblast marker αSMA was observed in the colitic mucosa and thus these findings do not corroborate this. Also, in contrast, single cell RNA sequencing of mesenchymal cells from DSS treated mice has also highlighted increased tenascin-C expression in a non-myofibroblast stromal cell subset. This subset, termed stromal 4, was significantly expanded in colitic mice and was characterised as having an expression profile associated with responses to bacteria and TNF (Kinchen et al., 2018). As such, it is likely that this fibroblast subset is the primary source of tenascin-C in colitis.

As mentioned previously macrophages are also well known producers of tenascin-C at sites of inflammation (Goh et al., 2010) and thus could also potentially contribute to

the elevated levels seen in DSS colitis. In this current study only the colonic resident macrophage population was analysed by IHC. This population is known for its anergic anti-inflammatory phenotype (Bain and Schridde, 2018) and thus while retained throughout the induction of colitis, as seen in the present study, it is unlikely the source of the pro-inflammatory tenascin-C. Instead newly recruited infiltrating monocytes and their immediate progeny, previously shown to become the predominant macrophage subset in colitis (Jones et al., 2018) but not investigated in this current study, would likely be the myeloid source of some of the tenascin-C produced.

3.6.8 Putative roles for tenascin-C in DSS colitis pathology

A number of potential roles for tenascin-C in colitis can be postulated based on the findings in this study. One potential role could be, as seen in other inflammatory disease models (Midwood et al., 2009), as a local modulator of the inflammatory process. For example, it was observed that tenascin-C upregulation at the protein level appeared to occur prior to upregulation of the pro-inflammatory cytokine IL-17 at the mRNA level. Tenascin-C has previously been shown to promote the polarisation of T cells to the key IL-17 producing Th17 subtype and thus this is a potential role it may be playing in the colitic colon as well (Ruhmann et al., 2012).

As well as directly activating immune cells tenascin-C may also impact the inflammatory response by regulating immune cell recruitment to the colon. T cells and neutrophils were both shown to be major infiltrating immune cell types in the DSS model, and the trafficking of both cell types has previously been shown to be impacted by tenascin-C. For T cells tenascin-C has been shown to promote lymphocyte tethering and rolling adhesion and thus is potentially promoting T cell migration into the colitic colon (Clark et al., 1997). In terms of neutrophils in a mouse model of hepatic injury tenascin-C was shown to upregulate the chemokine CXCL2 a chemoattractant for neutrophils. Additionally, tenascin-C was also shown to upregulate matrix metalloproteinase 9 (MMP9) which has been shown degrade the vascular ECM and thus aid leukocyte transmigration (Kuriyama et al., 2011).

Besides these impacts on the infiltrating immune cells tenascin-C could also potentially shape the inflammatory response by influencing local stromal remodelling

such as in the case of the vasculature. Neovascularisation is important for the inflammatory response and has been shown to worsen pathology in DSS model presumably by aiding immune cell infiltration (Scaldaferri et al., 2009). Previous publications have highlighted a pro-angiogenic role for tenascin-C, including a promotion of endothelial cell migration and enhancement of proliferation in response to vascular growth factors (Chung et al., 1996). This pro-angiogenic role has been shown to be particularly important in the early stages vessel formation (Radwanska et al., 2017), which would be occurring within the newly deposited granulation tissue of the damaged colonic mucosa where tenascin-C is also expressed.

These potential roles for tenascin-C in driving the inflammatory response, as well as its basal expression and mechanism for induction in colitis, are summarised in figure 3.19.

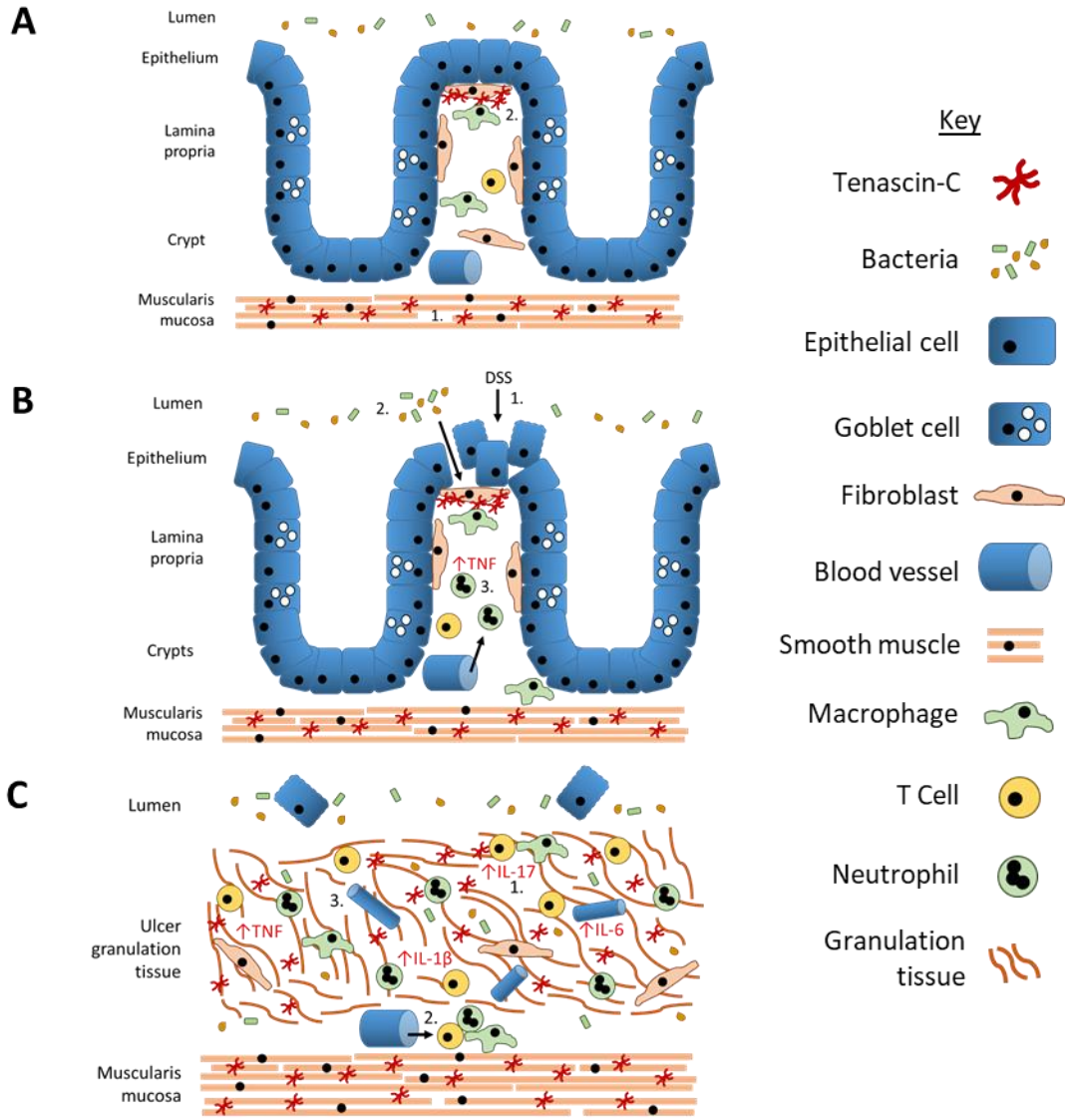

Figure 3.19 Known expression and hypothetical roles for tenascin-C in DSS colitis

(A) In healthy adult colon tenascin-C expression in the mucosa has been shown to be restricted to smooth muscle tissue (1.) and a subepithelial band at the luminal surface (2.).
(B) Dextran sulphate sodium dosing induces colitis by disrupting epithelial barrier integrity by selectively damaging colonic epithelial cells (1.). An inflammatory response is launched against the luminal contents entering the lamina propria potentially resulting in production of tenascin-C (2.). This response also results in early neutrophil recruitment to the tissues which produce pro-inflammatory cytokines which could also potentially upregulate tenascin-C expression (3.).
(C) Acute colitis results in mucosal tissue ulceration and destruction with tenascin-C shown to be strongly upregulated in the resulting granulation tissue. Here tenascin-C can potentially act as a driver of the inflammatory response by activating immune and stromal cells (1.). Tenascin-C may additionally influence immune cell recruitment or retention to the mucosa via its migratory modifying properties (2.). Additionally, tenascin-C could impact tissue remodelling including the neovascularisation of the granulation tissue (3.).

Chapter 4 Tenascin-C knockout mice are protected from DSS colitis

4.1 Introduction

Upon the development of gene knockout technologies in the late 1980s tenascin-C was among some of the first genes to be targeted for ablation, with the first *Tnc*$^{-/-}$ mouse generated in 1992 (Saga et al., 1992). Its selection for targeting was due in part to its wide-ranging expression at sites of interest during embryonic development leading many to infer it to be performing key developmental roles. In contrast to these predictions however, the mice generated, harbouring a homozygous insertion of the *lacZ* reporter gene into the tenascin-C locus, were obtained according to Mendelian laws with no gross developmental defects (Saga et al., 1992). This lack of an obvious phenotype was so surprising that a second independent *Tnc*$^{-/-}$ mouse was generated which likewise confirmed that mice lacking tenascin-C undergo normal development (Forsberg et al., 1996).

In light of these findings' subsequent studies of *Tnc*$^{-/-}$ mice shifted emphasis from embryonic development to more subtle phenotypes which were found to occur postnatally (Mackie and Tucker, 1999). These have ranged from neurological behavioural phenotypes, such as hyperlocomotion linked to changes in neurotransmission (Fukamauchi et al., 1996), to abnormalities in the cellularity of whisker follicles resulting from dysregulated stem cell differentiation (Hendaoui et al., 2014). The area of study which has garnered most interest however has stemmed from studies probing the sometimes stark phenotypes *Tnc*$^{-/-}$ mice have displayed in models of pathological stress, inflammation, and tissue injury.

On the back of early observations that tenascin-C was significantly upregulated at sites of tissue injury it was postulated that tenascin-C played a role in the inflammatory response (Schenk et al., 1995). *Tnc*$^{-/-}$ mice provided a useful tool to interrogate this hypothesis further *in vivo* with the first study to this end carried out using a model of contact dermatitis which showed *Tnc*$^{-/-}$ mice exhibited an aberrant inflammatory response (Koyama et al., 1998). Subsequent studies utilising other disease models, employing a wide variety of different mechanisms and targeting numerous different

tissue types, have found similar phenotypes of altered responses (Marzeda and Midwood, 2018). In the majority of these models this alteration has shown that while an acute response can still be initiated the loss of tenascin-C proves protective of progression to more serious chronic disease. Models of rheumatoid arthritis (RA) prove a good example of this paradigm with both acute zymosan induced and erosive antigen induced models demonstrating favourable outcomes in *Tnc*$^{-/-}$ mice. In both cases an initial immune response in the joint was found to have been mounted, suggesting no severe intrinsic immunological deficits in the mice. However, these initial responses failed to progress further in *Tnc*$^{-/-}$ mice with accelerated inflammatory resolution and thus reduced joint damage observed instead (Midwood et al., 2009). Likewise, similar findings were found with an experimental autoimmune encephalitis (EAE) model of multiple sclerosis in which *Tnc*$^{-/-}$ mice showed significantly reduced clinical scores and duration of symptoms than seen in wild-type (WT) mice (Momcilovic et al., 2017). As a final example, a model of autoimmune myocarditis has also shown the protective effects of tenascin-C deficiency with *Tnc*$^{-/-}$ mice showing reduced histopathology scoring and retained heart function in comparison to WT mice (Machino-Ohtsuka et al., 2014). In each of these systems this protection in the knockout mouse was attributed to tenascin-Cs ability to drive the production of pro-inflammatory cytokines as well as the induction of pathological Th1 and Th17 T cell responses resulting in more severe disease in its presence (Ruhmann et al., 2012, Machino-Ohtsuka et al., 2014, Momcilovic et al., 2017).

Besides these inflammatory autoimmune driven examples other diseases characterised by other aspects of immunological dysregulation have also shown protection in *Tnc*$^{-/-}$ mice. This includes pathological allergic type 2 immunity such as seen in the ovalbumin induced model of bronchial asthma. In this case *Tnc*$^{-/-}$ mice showed reduced lung inflammation, with decreased pathological Th2 cytokines and IgE antibodies observed, resulting in increased lung function compared to WT mice (Nakahara et al., 2006). Aberrant tissue remodelling and fibrosis related to immune responses, such as seen in disease such as systemic sclerosis, is another area in which tenascin-C's ablation has been shown to be protective. For example, in a bleomycin induced model of pulmonary fibrosis *Tnc*$^{-/-}$ mice showed reduced fibroblast activation and collagen deposition (Carey et al., 2010). Similarly, in a model of bleomycin induced skin

fibrosis *Tnc*$^{-/-}$ mice were also protected showing reduced immune cell infiltration and accelerated fibrotic resolution as measured by dermal thickness (Bhattacharyya et al., 2016).

Despite these examples however not all trauma and inflammation models have shown a protective phenotype in *Tnc*$^{-/-}$ mice. The first study mentioned investigating contact dermatitis found that the haptenizing agent dinitrofluorobenzene (DNFB) produced a more severe response in *Tnc*$^{-/-}$ mice. This manifested as increased and prolonged neutrophil infiltration alongside aberrant tissue remodelling (Koyama et al., 1998). Another early study of a model of acute kidney injury, habu snake venom induced glomerulonephritis, likewise showed a more severe non-resolving phenotype in *Tnc*$^{-/-}$ mice as measured by histological damage and assays of kidney function (Nakao et al., 1998). More recently studies utilising both spontaneous and surgical osteoarthritis models have found more severe joint degeneration develops in *Tnc*$^{-/-}$ mice with cartilage regeneration appearing disrupted (Okamura et al., 2010). In all these cases it appeared that lack of tenascin-C perturbed tissue repair in response to the initial insult. What causes this perturbation to occur in some model systems while benefit is seen in others is unknown.

The gastrointestinal system is one of the few remaining systems in which tenascin-C's role in inflammatory pathology has yet to be investigated thoroughly utilising *Tnc*$^{-/-}$ mice. This is despite tenascin-Cs known association with IBD at the genetic (Brant et al., 2017) as well as the protein level (Geboes et al., 2001). As was demonstrated in the preceding chapter, mimicking to some extent these changes found in IBD patients, tenascin-C was likewise found to be upregulated in a chemically induced DSS colitis model. As such, this model would appear appropriate for further interrogation utilising *Tnc*$^{-/-}$ mice to assess the impact of tenascin-C deficiency on the colitis and thus infer to some degree tenascin-C's role in the model.

4.2 Hypothesis

Genetic ablation of tenascin-C will impact the inflammatory response and prove protective in the murine DSS model of colitis.

4.3 Aims

I. Assess the basal colonic phenotype of *Tnc*$^{-/-}$ mice.

II. Optimise the DSS protocol and confirm its ability to induce colitis in mice from the *Tnc*$^{-/-}$ colony.

III. Compare the gross and histopathological features of DSS colitis in WT and *Tnc*$^{-/-}$ mice.

IV. Profile a range of cell types and structural markers in the colons of control and colitic WT and *Tnc*$^{-/-}$ mice.

V. Compare the gross and histopathological features of a colitis recovery model in WT and *Tnc*$^{-/-}$ mice.

4.4 Materials and methods

4.4.1 DSS murine model of colitis

Colitis was induced following the standard protocol, described in section 2.3.4, in 7-9 week old male WT or *Tnc*$^{-/-}$ mice from the *Tnc*$^{-/-}$ colony, originally from the University of Oxford, maintained at the Roslin Institute, University of Edinburgh. To distinguish the WT mice from this colony from those from the RI colony used in Chapter 3 they will be referred to as WT(Ox) in this chapter. To study acute colitis the DSS protocol was followed with mice culled at day eight. To study recovery after the acute period the DSS protocol was again followed with the mice culled at the later time point of day twenty-two. During the DSS dosing period to control for potential genotypic differences in water consumption water intake was monitored by daily water bottle weighing. Body weight data are presented as mean percentage body weight loss ± standard deviation and DAI sum score data is presented as median score ± interquartile range, as specified in section 2.3.4. Mice that exhibited severe adverse reactions or exceeded study severity limits, as described in section 2.3.4, were immediately euthanized and were not included for analysis, except when calculating survival.

4.4.2 Colon histology and colitis histopathology grading

H&E staining of paraffin embedded colon tissue sections was carried out as detailed in section 2.4.3 and colons graded for histopathology using these paraffin stained sections as described in section 2.4.3.

4.4.3 Immunohistochemistry (IHC)

The IHC work in this chapter was carried out with the assistance of University of Edinburgh undergraduate honours project student Brandon Shek. Colon tissue was harvested for IHC analysis as detailed in section 2.3.5. Proximal, middle, and distal sections from one mouse were embedded together in the same OCT block for cryosectioning, immunostaining, and imaging together. All IHC procedures were carried out as detailed in sections 2.4.2, 2.4.6, and 2.4.7. Negative controls were performed where the primary antibody was either omitted (no primary) or replaced with non-specific IgG from the animal the primary antibody was raised in (Sigma Aldrich).

4.4.4 Statistical Analysis

Statistical analysis was carried out as detailed in section 2.14. Continuous data, including body weight, body weight loss, colon length, and water consumption were analysed using Student's t-test, a one-way ANOVA, or a two-way ANOVA with Sidak's multiple comparisons test unless found to be not normally distributed. Non-normally distributed continuous data or ordinal data, such as DAI and histopathology scoring, were analysed using the appropriate non-parametric Mann-Whitney U or Kruskal-Wallis with Dunn's multiple comparisons tests.

4.5 Results

4.5.1 The *Tnc*$^{-/-}$ mouse colon is grossly and histologically indistinguishable from that of WT(Ox) mice

To confirm the *Tnc*$^{-/-}$ mouse was appropriate for modelling colitis their colonic phenotype under basal conditions was first assessed. Tenascin-C has been reported to be present at high levels in the developing intestinal tract including in the colon (Beaulieu, 1997). As such, this profiling was necessary to ensure no developmental defects or other abnormalities in comparison to WT mice were present which may have confounded future analysis.

To begin, *Tnc*$^{-/-}$ mice appeared to have normal gastrointestinal function with passage of firm faecal pellets of a similar size to those observed in age matched WT(Ox) mice. At cull, dissection of the colon revealed it to likewise be of similar gross appearance,

including in morphology and length, to WT(Ox) mice. To confirm these observations at the histological level paraffin-embedded sections covering the length of the colon from WT(Ox) and *Tnc*$^{-/-}$ mice were taken for H&E staining, representative images of which are shown in figure 4.1a. Additional supplementary representative images of both genotypes' colon tissue are provided in Appendix VI. Examination of these sections revealed normal colonic architecture present in *Tnc*$^{-/-}$ mice which was the same as that in WT(Ox) mice. This included a morphologically normal mucosa, with an enterocyte lined epithelium facing the lumen interspersed with goblet cell lined crypts, with an underlying submucosa separating the mucosa from the outer muscularis externa smooth muscle tissue. Regional specific features of the colonic architecture were also preserved such as the prominent mucosal folds of the proximal colon which were absent in the middle and distal colon of both genotypes. To confirm these observations the slides were examined by a qualified pathologist, Elspeth Milne, Professor of Veterinary Clinical Pathology, University of Edinburgh, who likewise found no differences between *Tnc*$^{-/-}$ and WT(Ox) mouse tissue.

Having confirmed the presence of normal colonic architecture the ablation of tenascin-C expression in the *Tnc*$^{-/-}$ mice was confirmed by immunohistochemistry, the results of which are presented in figure 4.1b. As seen previously colon tissue from WT(Ox) mice exhibited tenascin-C staining present in the smooth muscle of the muscularis mucosae and the muscularis externa, as well as underlying the luminal epithelium of the mucosa. In contrast and as expected no staining, comparable to negative control, was observed in *Tnc*$^{-/-}$ mouse tissue along the length of the colon, indicating that tenascin-C protein expression was indeed ablated.

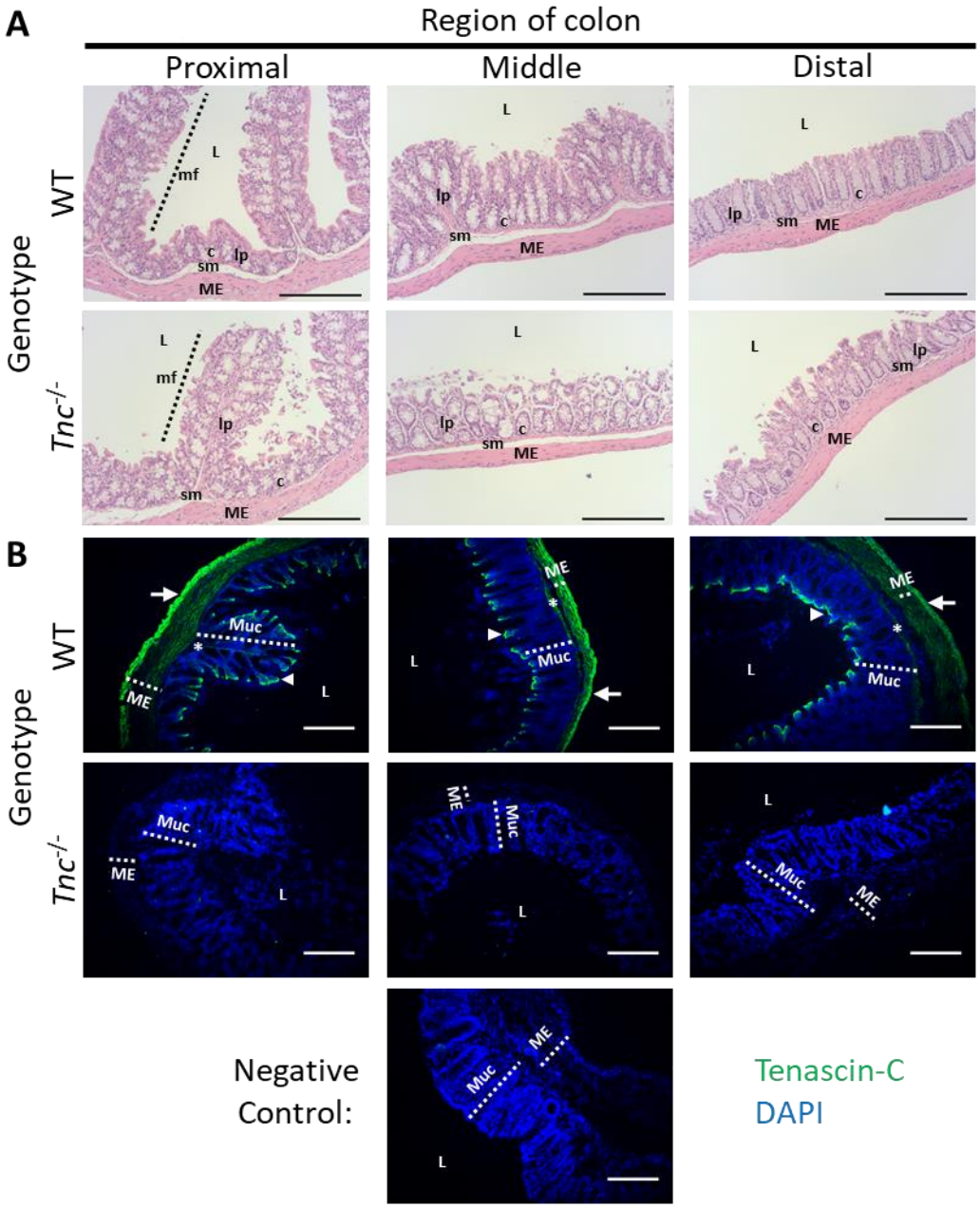

Figure 4.1 *Tnc*$^{-/-}$ mice have histologically normal colon tissue

(A) Representative H&E stained proximal, middle, and distal colon sections from WT(Ox) and *Tnc*$^{-/-}$ mice. Histologically along it's full length the colon tissue from *Tnc*$^{-/-}$ mice appears the same as that from WT(Ox) mice. No abnormalities were observed in the tissue taken from either genotype. Images captured using a Nikon E600 brightfield microscope. Scale bars = 500µm.
(B) IHC staining for tenascin-C (green) of proximal, middle, and distal colon sections from WT(Ox) and *Tnc*$^{-/-}$ mice. Staining is observed in WT(Ox) mice in the muscularis externa (closed arrows), in a subepithelial band (arrowheads), and in the muscularis mucosa (asterisks) along the length of the colon. *Tnc*$^{-/-}$ mouse tissue shows no staining confirming genetic ablation of the protein. A negative control of WT(Ox) distal colon tissue, in which the primary antibody was omitted, also displays no staining. Slides were imaged using a Leica DMLB microscope and counterstained with the nuclear stain DAPI (blue). Scale bars = 250µm. L = lumen, Muc = mucosa, mf = mucosal fold, lp = lamina propria, c = crypt, sm = submucosa, ME = muscularis externa.

4.5.2 Optimisation of DSS colitis in the *Tnc*$^{-/-}$ mouse colony

The DSS colitis model was established in 129sv mice in the previous chapter with a dosing regime of 2% DSS administered for five days. The *Tnc*$^{-/-}$ mouse colony while on the same genetic background was setup utilising animals imported from the Kennedy Institute of Rheumatology at the University of Oxford. It was initially apparent that these mice, including the WT(Ox)s, differed from the 129sv mice at the Roslin Institute with much heavier weights observed. This was postulated to likely be due to dietary differences, with the mice at the Kennedy Institute found to be on a diet with higher fat content, as well as possible genetic drift. Local environment (Tasnim et al., 2017) as well as diet (Tremaroli and Backhed, 2012) are known to affect the makeup of the gut microbiota, which is vertically transmitted to offspring during birth and weaning (Moeller et al., 2018). As such, this founding population of mice as well as potentially being genetically distinct from the Roslin 129sv would also likely impart a differential microbiota onto their offspring as well. Commercial health screening (Envigo, Huntingdon, UK) of these imported mice did however confirm their specific pathogen free status and thus no highly pathogenic gut microbes, such as rotavirus or *Salmonella* species, which could confound results were present.

As both genetic and microbiota factors are known to influence the course of DSS induced colitis (Perse and Cerar, 2012) it was thus deemed necessary to trial the 2% DSS regime previously employed with this colony. This trial revealed the WT(Ox) and knockout mice of the *Tnc*$^{-/-}$ colony to be seemingly resistant to this dose of DSS. This was seen in the gross health parameter of body weight loss, data for which is presented in figure 4.2a, which showed that both genotypes displayed minimal to no weight loss over the eight days of dosing. Disease activity scoring, presented in figure 4.2b, likewise showed minimal change over the eight days with most mice showing little to no colitis symptoms in contrast to previous experiments with the Roslin 129sv colony. In addition to these observations indicating lack of colitis induction no significant differences in gross parameters were observed between the genotypes. This included body weight at the start of DSS dosing, as shown in figure 4.2c, which showed that both WT(Ox) and *Tnc*$^{-/-}$ mice did not initially differ significantly in weight.

To confirm the lack of colitis induction the gold standard of histopathology scoring was carried out, the results of which are displayed in figure 4.2d. This revealed some signs of colitis were present in the 2% DSS mice with significant increases in scores compared to controls seen in the middle and distal colon. Although the n numbers were low these also indicated that the colitis in the *Tnc*$^{-/-}$ mice was less severe in the distal colon as, in contrast to the WT(Ox)s, the increase in pathological scoring was not deemed to be significantly higher compared to the matched control. As expected, based on the gross parameters results however, these increases were all much reduced compared to those seen with the 129sv Roslin colony in which with distal colon sum scores ranged from 45 to 56 compared to the scores of 0 to 28 seen in this experiment. This scoring also highlighted that while inflammatory infiltration was present tissue damage appeared reduced and less severe of submucosal oedema present than observed in previous experiments. These all indicated that while the DSS did have some effect on the *Tnc*$^{-/-}$ colony mice it was not as significant at this dose as seen previously.

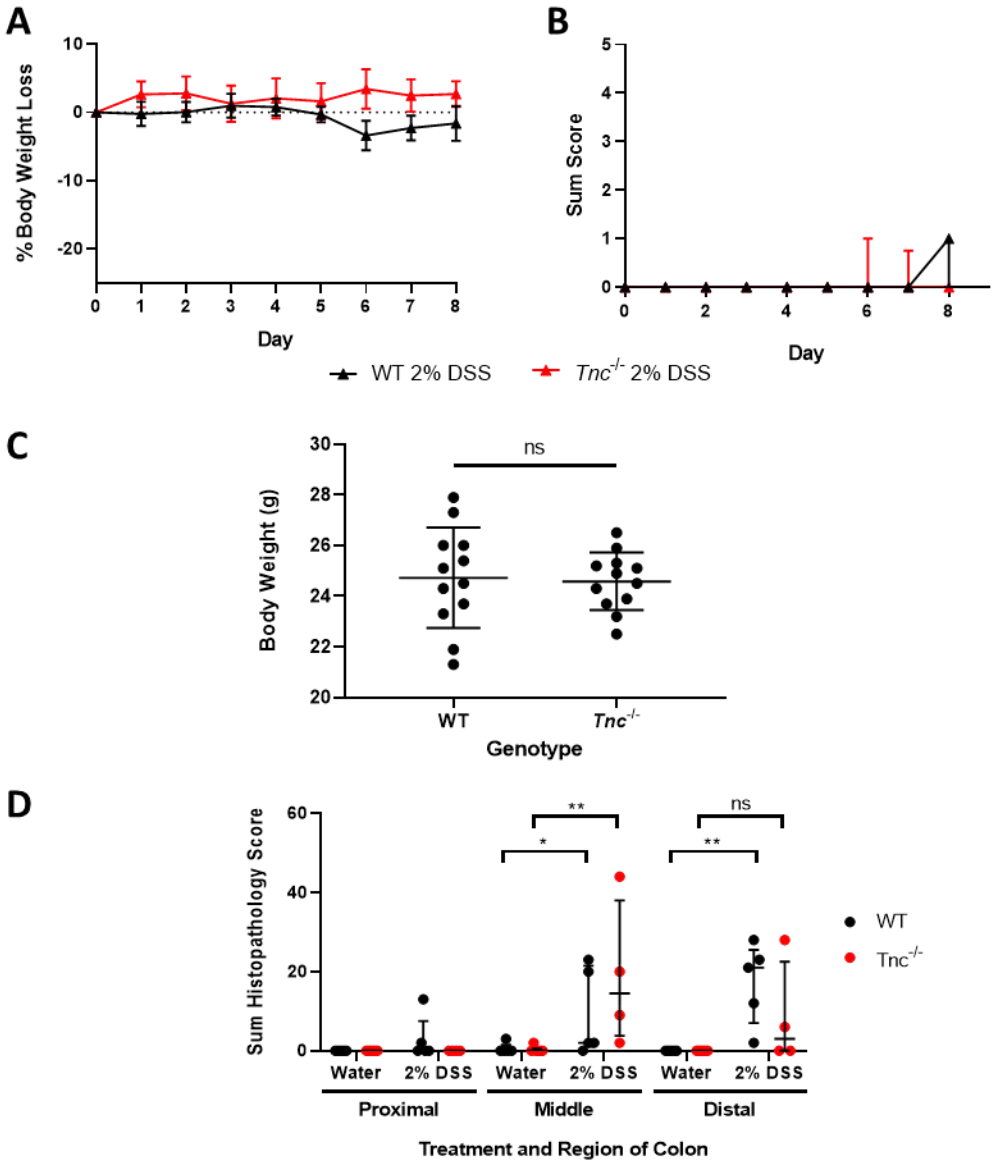

Figure 4.2 The 2% DSS dosing regime is not sufficient to induce colitis in WT or knockout mice from the *Tnc*$^{-/-}$ colony

(A) Baseline weights of 7-9 week old WT(Ox) or *Tnc*$^{-/-}$ mice. Data presented as data points representing weights for individual mice overlaid with the group mean ± SD, n = 12 per group, significance determined by Student's T-Test, ns = not significant.
(B) Minimal colitis disease activity index (DAI) scoring is observed with 2% DSS dosing of WT(Ox) and *Tnc*$^{-/-}$ mice from the *Tnc*$^{-/-}$ colony. Data presented as median ± interquartile range, n=7≤ per group.
(C) Body weight loss is not observed with 2% DSS treatment in WT(Ox) or *Tnc*$^{-/-}$ mice from the *Tnc*$^{-/-}$ colony. Data presented as mean body weight loss compared to day 0 ± SD, n=7≤ per group.
(D) Sum histopathology scores for proximal, middle, and distal colon sections from day eight control and 2% DSS treated WT(Ox) and *Tnc*$^{-/-}$ mice. 2% DSS treatment results in a significant increase in scoring compared to controls in both genotypes, although to a lesser degree than seen in previous experiments. Data presented as data points representing individual mouse scores overlaid with the median ± interquartile range, n=4-6 per group.

4.5.3 *Tnc*$^{-/-}$ mice develop acute DSS colitis with reduced severity as measured by gross pathological readouts

With the optimisation experiment concluding the 2% DSS dose did not robustly induce colitis it was decided to increase the DSS dose to 3% in the *Tnc*$^{-/-}$ colony for future experiments. Thus, with this new regime, WT(Ox) and *Tnc*$^{-/-}$ mice were administered 3% DSS for five days followed by three days of normal tap water before cull on day eight. Control mice of both genotypes were given normal tap water for the duration of the experiment before cull on day eight.

Gross pathology was first assessed with survival initially considered for the six *Tnc*$^{-/-}$ and eight WT(Ox) mice which underwent DSS treatment. No *Tnc*$^{-/-}$ mice were lost due to adverse events or severity limit breaches. Likewise, no WT(Ox) were lost due to adverse events, although one mouse was lost from the group as it breached body weight loss and DAI severity limits. Based on these observations statistical analysis determined that both groups showed no significant difference in survival of DSS treatment.

Body weight loss was the next parameter examined, the data for which is shown in figure 4.3a. This revealed that for both WT(Ox) and *Tnc*$^{-/-}$ mice the 3% DSS dose appeared sufficient to induce colitis with both showing significant weight loss compared to their genotype matched controls. This reached significance from day six in the *Tnc*$^{-/-}$ mice and from day seven in the WT(Ox). A significant difference was registered earlier at day one for the DSS treated *Tnc*$^{-/-}$ mice compared to their matched controls although this appeared mainly due to an aberrant increase in the control groups weight, potentially due to mis-weighing, rather than a decrease in the DSS treated groups weight. At the end point of the study on day eight a protective effect seemed apparent for the *Tnc*$^{-/-}$ mice which showed significantly less body weight at this time point compared to DSS treated WT(Ox) mice.

Disease activity index scoring, presented in figure 4.3b, likewise showed that colitis appeared to be successful induced with the higher DSS dose with all the mice of both genotypes developing colitic symptoms. A protective effect of the loss of tenascin-C was not evident using this metric however with both genotypes displaying a similar degree of scoring, which in both cases was significantly different from matched

controls, by day eight. In fact, in contrast to the body weight data, it appeared by this measure that more *Tnc*$^{-/-}$ mice developed colitic symptoms before WT(Ox) mice, with a significant difference between the groups observed at day four.

The final gross pathological feature measured was colon length at cull, shown in figure 4.3c. Again, this measure suggested successful induction of colitis in both genotypes with a significant decrease in colon length seen for both. No difference in length was observed between the control groups of both genotypes. However, supporting the body weight loss data *Tnc*$^{-/-}$ mice appeared protected with DSS treatment resulting in significantly less colon shortening compared to DSS treated WT(Ox) mice.

To ensure that these differences in gross pathology were not simply due to differential dosing resulting from genotype differences in water consumption during the five day treatment period water consumption was recorded. From these data average water consumption per mouse over this time period was calculated with the data presented in figure 4.3d. No significant difference was found between any of the groups with a rough average of around five millilitres of water, regardless of DSS supplementation, consumed per mouse per day for both genotypes.

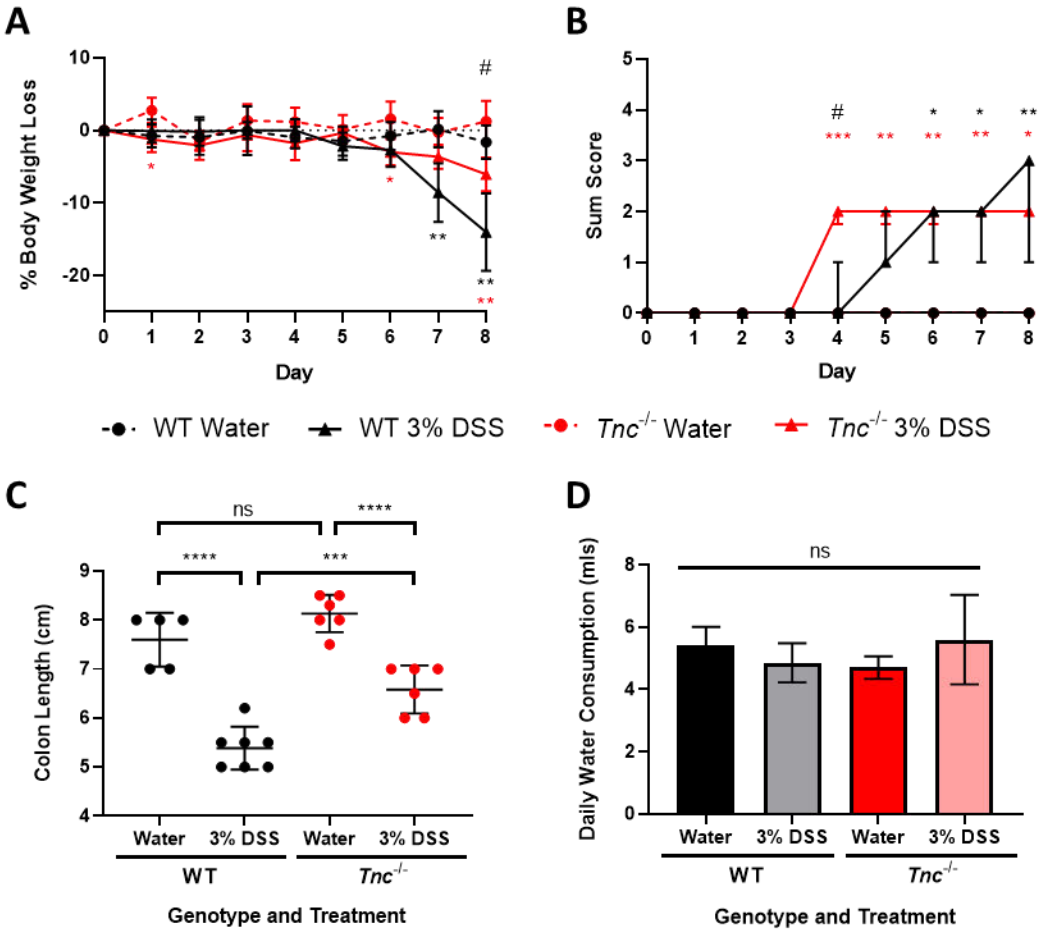

Figure 4.3 *Tnc*$^{-/-}$ mice show reduced 3% DSS colitis gross pathology compared to WT(Ox) mice

(A) Percentage body weight loss compared to day 0 of WT(Ox) or *Tnc*$^{-/-}$ mice dosed with normal drinking water or drinking water supplemented with 3% DSS. Both genotypes significantly lost weight compared to control mice by day 8 of DSS treatment. DSS treated *Tnc*$^{-/-}$ mice lost significantly less weight than DSS treated WT(Ox) mice. Data presented as mean ± SD, n= 5-7 per group, significance calculated between groups by two-way ANOVA. Significance compared to genotype matched controls (indicated by colour) shown with asterisks. # = $p<0.05$ for DSS *Tnc*$^{-/-}$ compared to DSS WT(Ox).
(B) Disease activity index (DAI) scoring data for the same mice as in (A). Both genotypes showed a significant increase in score by day 8 upon DSS dosing. Data presented as median ± interquartile range, n= 5-7 per group, Significance compared to matched genotype control (indicated by colour) determined by Kruskal-Wallis test. # = $p<0.05$ for DSS *Tnc*$^{-/-}$ compared to DSS WT(Ox).
(C) Colon length at cull on day 8 of the same mice as in (A). DSS treatment results in colon shortening for both genotypes although this is more pronounced in the WT mice. Data presented individual data points per mouse overlaid with mean ± SD, n= 5-7 per group, significance determined by one-way ANOVA.
(D) Daily water consumption during DSS dosing did not differ significantly between genotypes or with DSS treatment. Data presented as mean daily water consumption ± SD, n= 5-7 per group, significance determined by one-way ANOVA.
**** = $p<0.0001$, *** = $p<0.001$, ** = $p<0.01$, * = $p<0.05$, ns = not significant.

4.5.4 Reduced inflammation and tissue damage are found in *Tnc*$^{-/-}$ mice with acute DSS induced colitis

To confirm the reduction in colitis severity in *Tnc*$^{-/-}$ mice H&E stained paraffin-embedded tissue sections of colon tissue, representative images of which are shown in figure 4.4, were generated for histological analysis. Control mice of both genotypes showed normal colonic architecture and minimal to no inflammation along the length of the colon. Likewise, the proximal tissues of the DSS treated mice of both genotypes appeared similarly unperturbed with minimal inflammation present. Conversely, the middle and distal colon of these DSS treated mice showed marked colitic histopathology. This included inflammation such as mixed immune cell infiltration of the mucosa and submucosa. This infiltrate appeared in most cases to be composed predominantly of macrophages and lymphocytes as well as to a lesser extent neutrophils, although focal areas of neutrophilic infiltration were observed. Additionally, in contrast to the 2% DSS dosage submucosal oedema, another marker of inflammation, was observed in nearly all the slides examined. In terms of tissue damage again severe histopathology was noted with mucosal ulceration and crypt loss seen in both genotypes. Epithelial hyperplasia was also present in both groups resulting in crypt elongation and thus mucosal thickening. It did appear that tissue damage was reduced in the *Tnc*$^{-/-}$ mice with greater preservation of normal morphology such as areas of normal crypt architecture, absent in WT(Ox) tissue, observed.

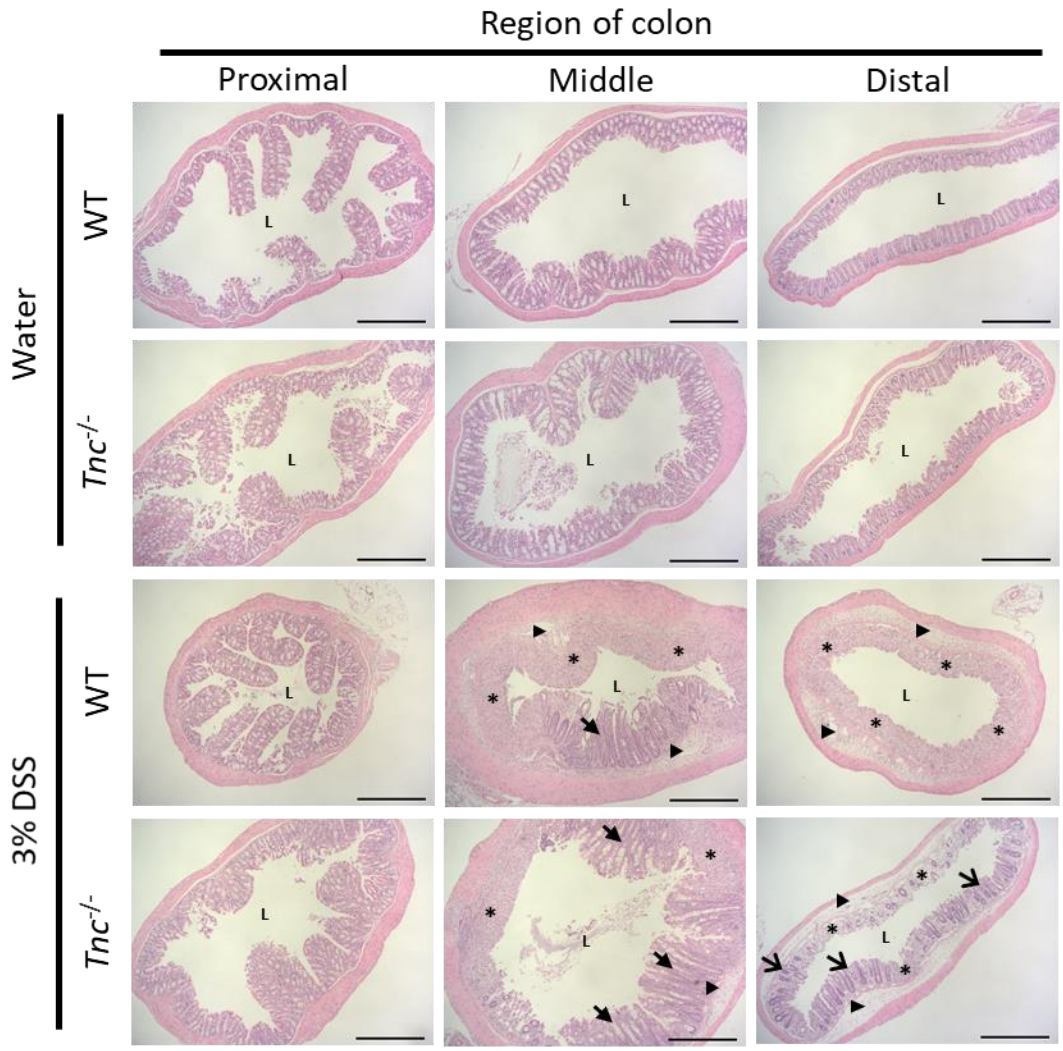

Figure 4.4 Representative H&E stained colon sections from control and 8 day 3% DSS colitic WT(Ox) and *Tnc*$^{-/-}$ mice

Representative images of H&E stained transverse proximal, middle, and distal colon sections from control and 3% DSS dosed WT(Ox) and *Tnc*$^{-/-}$ mice. Significant colonic inflammation is observed in both genotypes with DSS treatment, including mixed immune cell infiltration and submucosal oedema (arrowheads). Tissue damage, including ulceration (asterisks) and epithelial hyperplasia (closed arrows), is also present in both genotypes although greater preservation of crypt architecture (open arrows) is seen in *Tnc*$^{-/-}$ mice compared to WT(Ox) mice. Legend continued on following page-

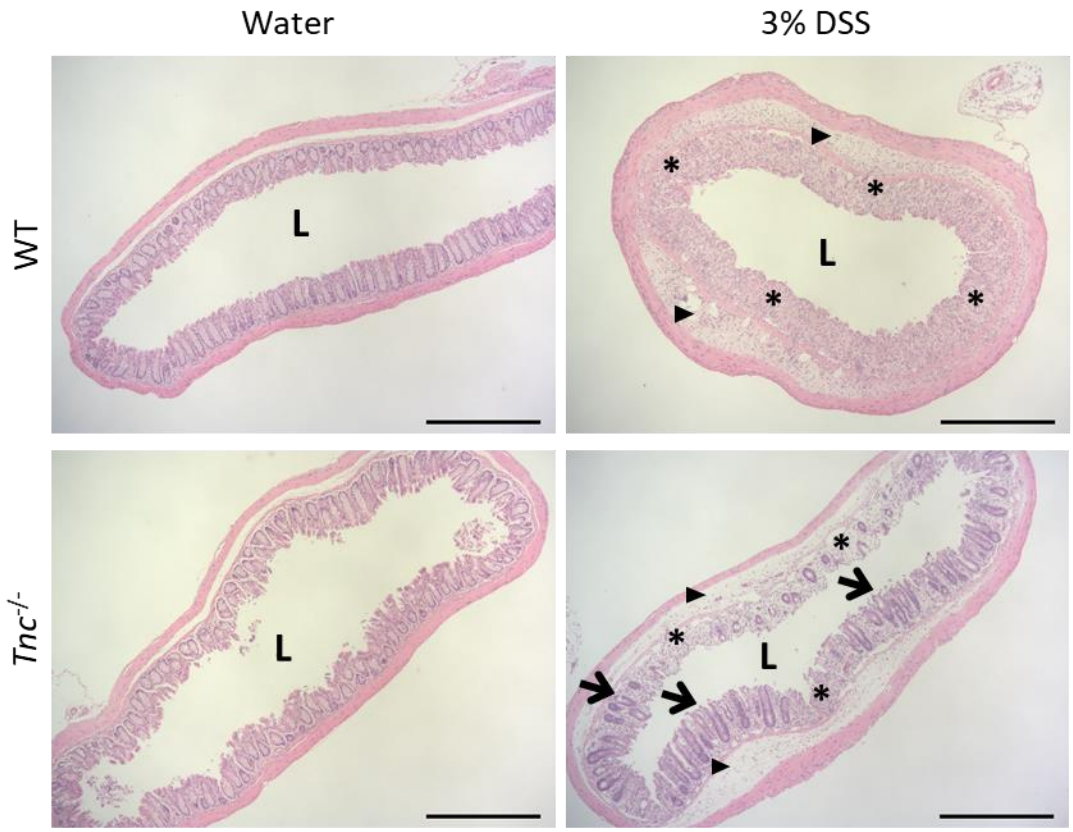

Figure 4.4 Continued

Enlarged images (above) of the control and DSS treated distal colon sections from both genotypes to better show the histopathology induced by DSS treatment.

Images captured using a Nikon E600 brightfield microscope. Scale bars = 1000μm. L = lumen.

To quantify these observations and confirm the apparent genotypic differences blinded histopathology scoring was undertaken by Elspeth Milne, Professor of Veterinary Clinical Pathology, University of Edinburgh. The sum scores of this scoring, presented in figure 4.5a, as expected confirmed the observation that treatment with DSS induced colitis in both genotypes. Additionally, the pathology was found to be regionally restricted with no increase observed in the proximal colon whereas a significant increase was observed in both the middle and distal colon for both genotypes. These middle and distal scores as expected were also elevated compared to the 2% dosing regime and thus more in line with those seen previously. Furthermore, as in the 2% dosing pilot, the DSS treated distal colon appeared to be protected in the *Tnc*$^{-/-}$ mice with a significantly lower score compared to the WT(Ox) mice found. Similarly, as in the 2% experiment the DSS treated middle colon conversely showed no differences in score between the genotypes, potentially due to, as seen previously, the pathology here being more variable.

A breakdown of the distal score of the DSS treated mice by scoring parameter, presented in figure 4.5b, revealed the contribution of each of these parameters to this apparent overall reduction in *Tnc*$^{-/-}$ score. In terms of inflammatory pathology this showed that inflammatory severity was significantly reduced in *Tnc*$^{-/-}$ mice while inflammatory extent showed no difference. This shows that while the level of inflammation, such as the amount of immune infiltration, appears reduced in *Tnc*$^{-/-}$ mice it is still locally confined within the same areas of predominantly the mucosa and submucosa. In terms of tissue damage the crypt damage and regeneration parameters showed even greater decreases in *Tnc*$^{-/-}$ score compared to WT(Ox) mice which were likewise both significant. This confirmed the earlier observations that the *Tnc*$^{-/-}$ tissue appeared to have better preserved architecture and morphology compared to the WT(Ox)s. Indeed, confirming the focal nature of the damage and preservation a large contributing factor to the crypt damage score difference was the much lower scores recorded for percentage involvement for this parameter in the *Tnc*$^{-/-}$ samples.

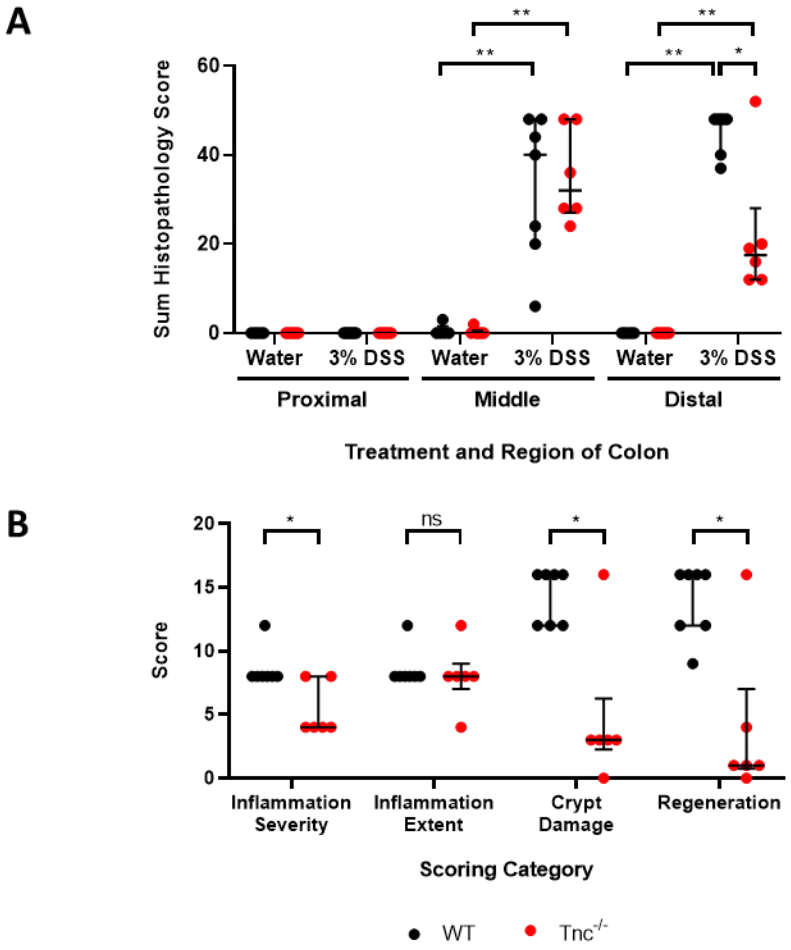

Figure 4.5 Colitis histopathology scoring for day 8 WT(Ox) and *Tnc*$^{-/-}$ mice shows reduced distal pathology in the knockouts

(A) Sum histopathology scores for proximal, middle, and distal colon sections from control and 3% DSS treated WT(Ox) and *Tnc*$^{-/-}$ mice. For both genotypes DSS treatment results in increased scoring compared to controls in the middle and distal colon with significantly reduced scores seen for *Tnc*$^{-/-}$ mice in the distal colon.
(B) Scores for individual histopathology scoring parameters in distal colon segments from 3% DSS treated WT(Ox) and *Tnc*$^{-/-}$ mice. Knockout mice show significantly reduced scoring compared controls for all parameters except inflammatory extent. Data points represent scores for individual mice with bars marking the median ± interquartile range, n = 5-7 per group, significance determined by Mann-Whitney U test, ** = $p<0.01$, * = $p<0.05$.

4.5.5 Confirmation of tenascin-C upregulation in the colitic colon of WT(Ox) mice using the 3% DSS regime

Having demonstrated a difference in pathology between the genotypes it was necessary to confirm the upregulation of tenascin-C in the colitic mucosa of the *Tnc*$^{-/-}$ colonies WT(Ox) mice. To do this IHC staining was carried out for tenascin-C with representative images displayed in figure 4.6. As seen previously under basal conditions the WT(Ox) mice showed normal smooth muscle and subepithelial tenascin-C staining while *Tnc*$^{-/-}$ mice showed only background staining similar to that present in the negative control. This same staining pattern for both genotypes was also found in the unaffected proximal colon of the DSS treated mice. However, confirming previous observations in the damaged mucosa of the middle and distal colon tenascin-C was found to be upregulated in the WT(Ox) mice. As expected in the same regions from the DSS treated *Tnc*$^{-/-}$ mice no staining was again observed.

4.5.6 *Tnc*$^{-/-}$ mice have normal colonic smooth muscle architecture

To identify any histological or cellular differences between the WT(Ox) and *Tnc*$^{-/-}$ mice, which could potentially explain the differences in pathology observed, IHC staining for a variety of markers was carried out. To start with, sections from control and DSS treated WT(Ox) and *Tnc*$^{-/-}$ mice were stained for the smooth muscle marker α-smooth muscle actin (αSMA), the results of which are shown in figure 4.7. In control and DSS treated tissue from both genotypes this staining clearly labelled the muscularis mucosae and the muscularis externa. In the control tissue these structures appeared morphologically normal and comparable between the genotypes. As observed previously in WT mice (figure 3.13) αSMA staining changed minimally with DSS dosing with only a slight thickening of the muscularis mucosae observed in the colitic middle and distal colon. These same minimal changes were likewise also observed in the DSS treated *Tnc*$^{-/-}$ tissue. Negative control sections showed largely absent staining except for some diffuse staining at the mucosal surface, also observed in some αSMA stained sections, which was judged to be due to non-specific secondary antibody binding to luminal mucus. Overall, this staining appeared to confirm that the lack of tenascin-C did not appear to impact the smooth musculature of the colon under basal or colitic conditions.

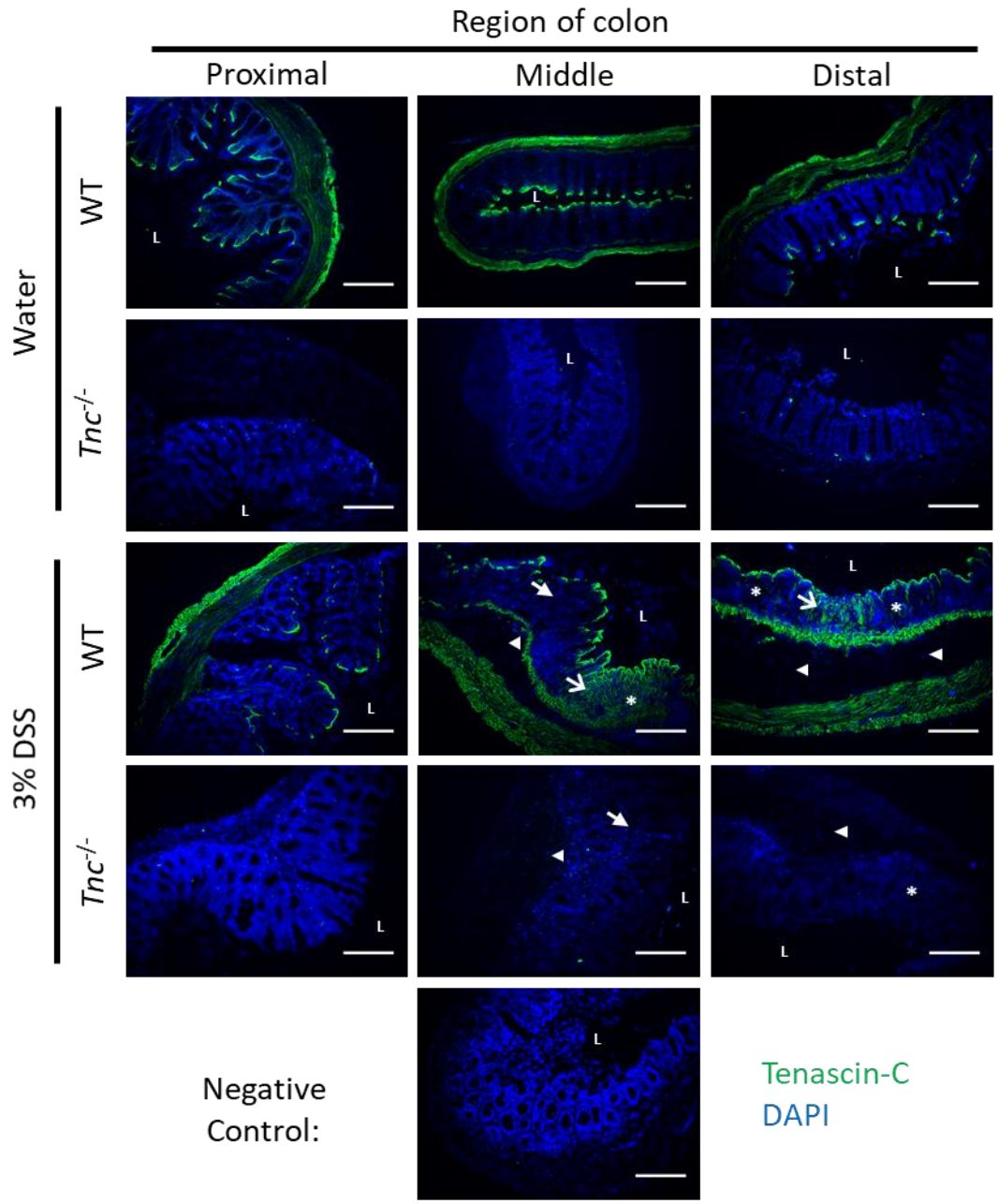

Figure 4.6 Tenascin-C is upregulated in the inflamed colon of 3% DSS treated WT(Ox) mice at day 8 but absent in *Tnc*$^{-/-}$ mice

IHC staining for tenascin-C (green) of proximal, middle, and distal colon sections from control and day eight 3% DSS dosed WT(Ox) and *Tnc*$^{-/-}$ mice. An increase in tenascin-C staining is observed in the mucosa of WT(Ox) mice localising to areas of damage in the middle and distal colon (open arrows). No tenascin-C staining is observed in control or DSS treated *Tnc*$^{-/-}$ mice. For both genotypes DSS treatment also results in mixed immune cell infiltration and submucosal oedema (arrowheads), ulceration (asterisks), and epithelial hyperplasia (closed arrows). Legend continued on following page-

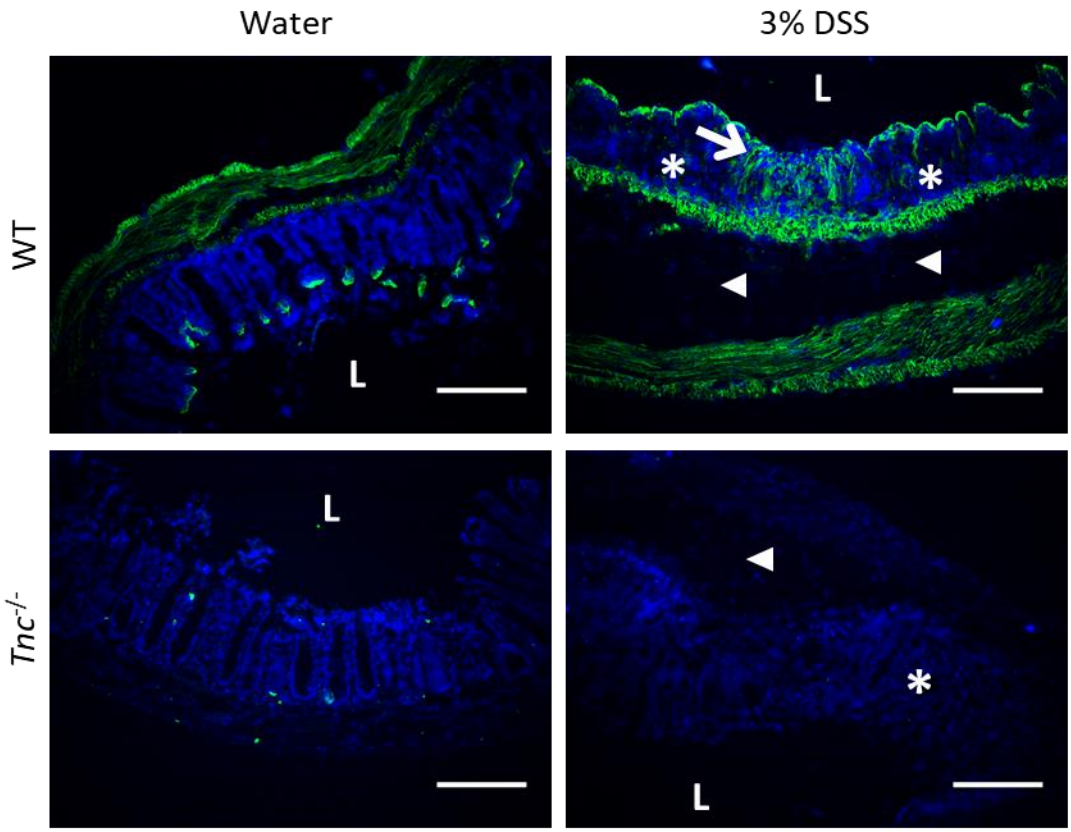

Figure 4.6 Continued

Enlarged images (above) of the control and DSS treated distal colon sections from both genotypes to emphasise the tenascin-C staining in the damaged mucosa of the WT(Ox) mice with DSS treatment.

The negative control, in which the primary antibody was omitted, of WT(Ox) distal colon displays no staining. All slides were counterstained with the nuclear stain DAPI (blue) and imaged using a Leica DMLB microscope. Scale bars = 250µm. L = lumen

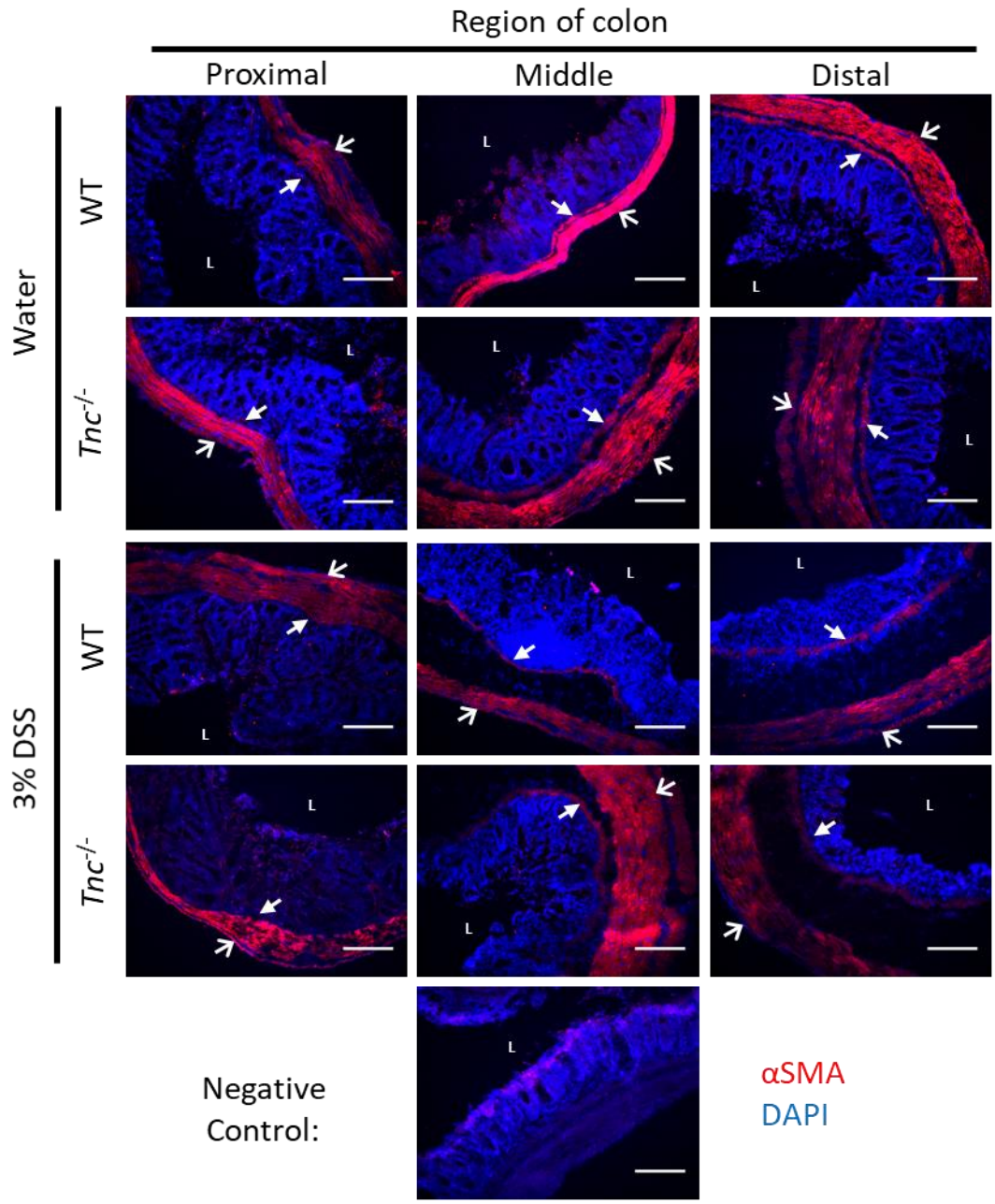

Figure 4.7 Muscularis externa and muscularis mucosa colonic smooth muscle is normal in *Tnc*$^{-/-}$ mice

α-Smooth muscle actin (αSMA) staining (red) of proximal, middle, and distal colon sections from control and day eight 3% DSS dosed WT(Ox) and *Tnc*$^{-/-}$ mice. αSMA staining localises to the muscularis mucosa (closed arrows) and muscularis externa (open arrows) along the length of the colon in both genotypes with and without DSS treatment. Legend continued on following page-

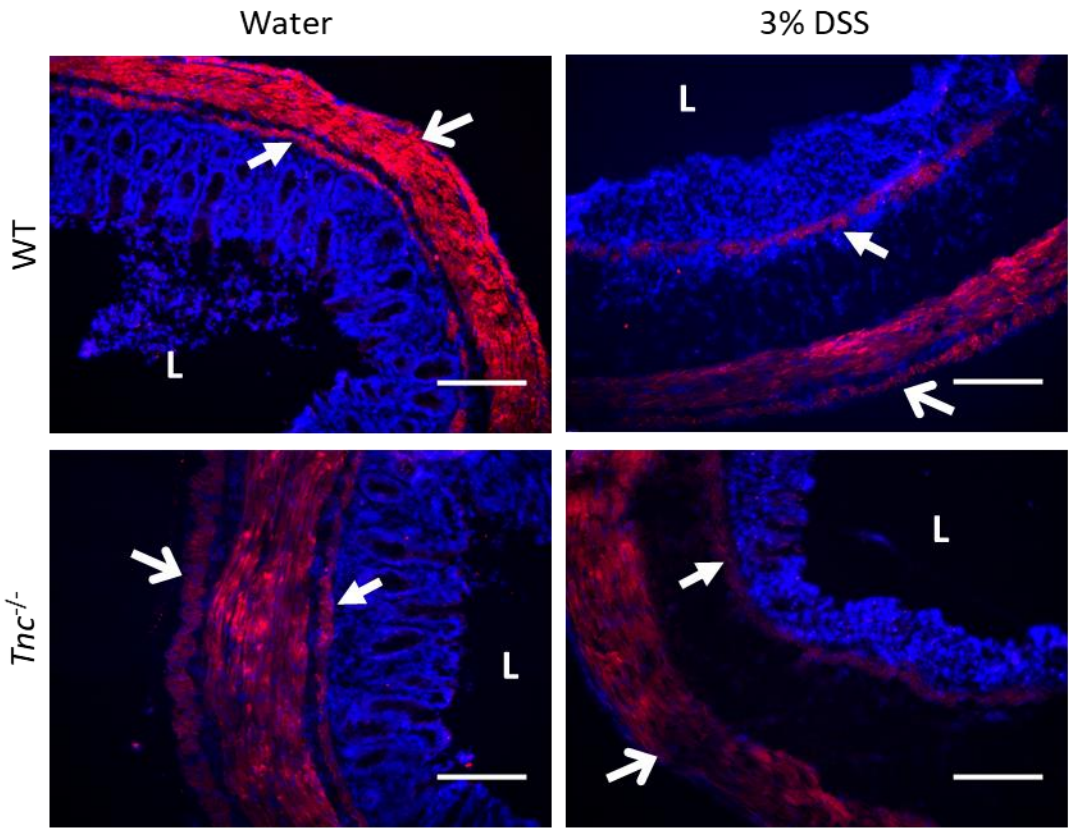

Figure 4.7 Continued

Enlarged images (above) of the control and DSS treated distal colon sections from both genotypes to more clearly show the indistinguishable αSMA staining of the muscularis mucosa and externa in both genotypes.

The negative control, in which the primary antibody was omitted, of WT(Ox) distal colon displays no staining expect for a non-specific band at the luminal surface of the mucosa. This was hypothesised to be likely due to non-specific secondary antibody binding to luminal mucus. All slides were counterstained with the nuclear stain DAPI (blue) and imaged using a Leica DMLB microscope. Scale bars = 250µm. L = lumen

4.5.7 Vascular markers are the same in *Tnc*$^{-/-}$ and WT(Ox) mice

The vasculature was the next feature of the colon to be examined this time utilising IHC dual staining for the blood vessel marker CD31 and the lymphatic vessel marker LYVE-1. Representative images of this staining are presented in figure 4.8 and show normal vascular architecture is present in along the length of the colon of control WT(Ox) and *Tnc*$^{-/-}$ mice. This includes evenly distributed vessel like staining of CD31 showing diffuse blood vessel distribution throughout the mucosa and muscularis. LYVE-1 staining in contrast shows predominant staining present in a main lymphatic vessel running along the base of the mucosa just overlying the muscularis mucosae. This vessel co-stains albeit more weakly for CD31 which is known to also be expressed weakly on the lymphatic endothelium (Baluk and McDonald, 2008). As seen previously additional LYVE-1 staining lymphatics are also found extending up into the mucosa which seemed to stain less strongly for CD31.

Similarly, with the induction of colitis with DSS treatment similar vascular changes were observed in both WT(Ox) and *Tnc*$^{-/-}$ mouse colons. No changes were observed in the unaffected proximal colon of either genotype. However, in the middle and distal colon colitic changes were apparent with marked oedema observed with accompanying dilation of the mucosal lymphatics. Severe mucosal damage was also seen, particularly in the distal colon, where granulation tissue was observed with accompanying microvascularisation of blood vessels.

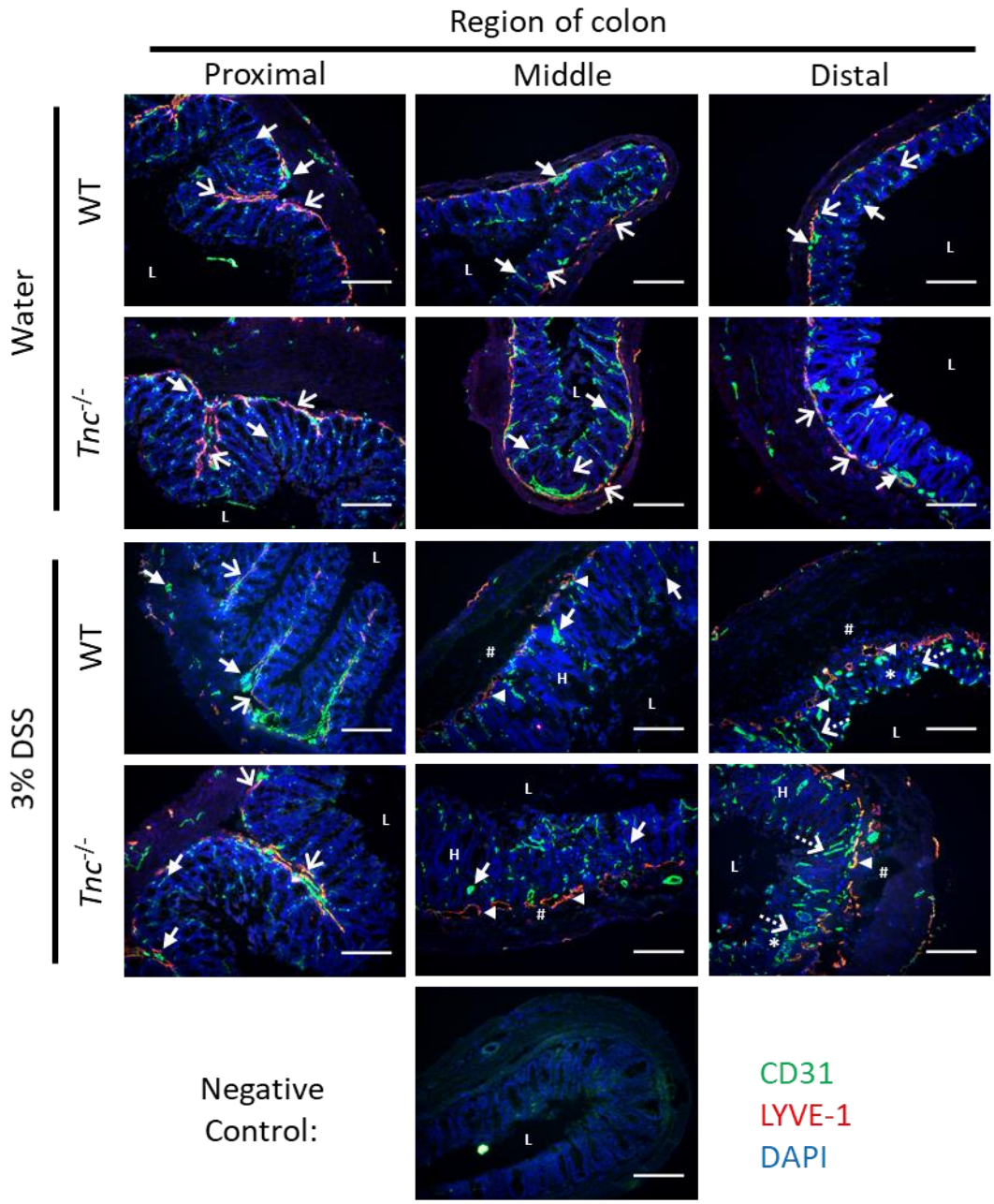

Figure 4.8 No difference in blood or lymphatic vessels is observed between WT(Ox) and *Tnc*$^{-/-}$ mouse colons under resting or colitic conditions

IHC dual staining for blood (CD31; green) and lymphatic (LYVE-1; red) vessels of proximal, middle, and distal colon sections from control and day eight 3% DSS dosed WT(Ox) and *Tnc*$^{-/-}$ mice. Blood (closed arrows) and lymphatics (open arrows) in the mucosa and submucosa appear normal in both genotypes under basal conditions. Colitis results in an upregulation of blood vessels in the damaged mucosa (dashed arrows) and dilated lymphatics (arrowheads) alongside submucosal oedema (hash) in the middle and distal colon of both genotypes. Legend continued on following page-

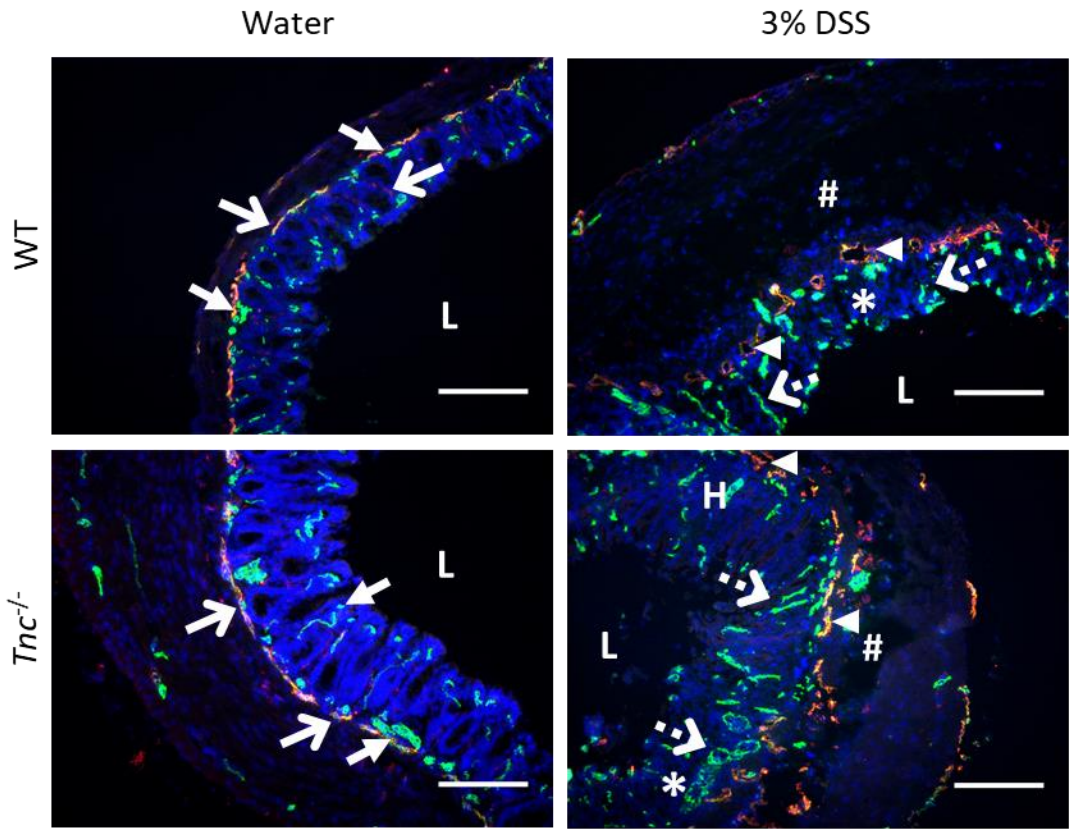

Figure 4.8 Continued

Enlarged images (above) of the control and DSS treated distal colon sections from both genotypes. These more clearly demonstrate how the vasculature found in *Tnc*$^{-/-}$ mice appears normal under basal conditions as well as how it mimics the changes which occur in WT(Ox) mice with DSS treatment.

The negative control, in which the primary antibody was omitted, of WT(Ox) distal colon displays only weak diffuse background in the green channel. All slides were counterstained with the nuclear stain DAPI (blue) and imaged using a Leica DMLB microscope. Scale bars = 250µm. L = lumen, * = mucosal granulation tissue, H = hyperplastic epithelium.

4.5.8 Tenascin-C loss modulates epithelial & crypt architectural damage

Following, from the observation that *Tnc*$^{-/-}$ mice suffered less tissue damage in response to DSS treatment the next markers chosen for investigation focused on the mucosal architecture. Colon sections from all groups were dual IHC stained for CD326, an epithelial cell marker, and type IV collagen (ColIV) a connective tissue marker to aid in delineating the structure of the mucosa. Representative images of this staining are shown in figure 4.9. In the control animals from both genotypes along the length of the colon the intact mucosal epithelium stained positive for CD326. Additionally, the ColIV staining allowed visualisation of the mucosa's structure which showed it to have normal architectural appearance with clearly delineated crypts in both genotypes.

With DSS treatment in both genotypes no changes were observed in the proximal colon. In contrast in the colitic distal colon of the WT(Ox) mice ulceration is apparent with loss of CD326 staining of the luminal surface of the mucosa. Furthermore, the damage to the mucosa has resulted in the loss of its normal structure with crypts no longer able to be delineated. In contrast, in the distal colon of the DSS treated *Tnc*$^{-/-}$ mice while these same changes are also still present areas of normal mucosal structure are also still present as well. These protected epithelial areas show preserved CD326 staining showing that epithelial integrity has been maintained. Additionally, these areas also showed preserved structural architecture with normal crypts still clearly present.

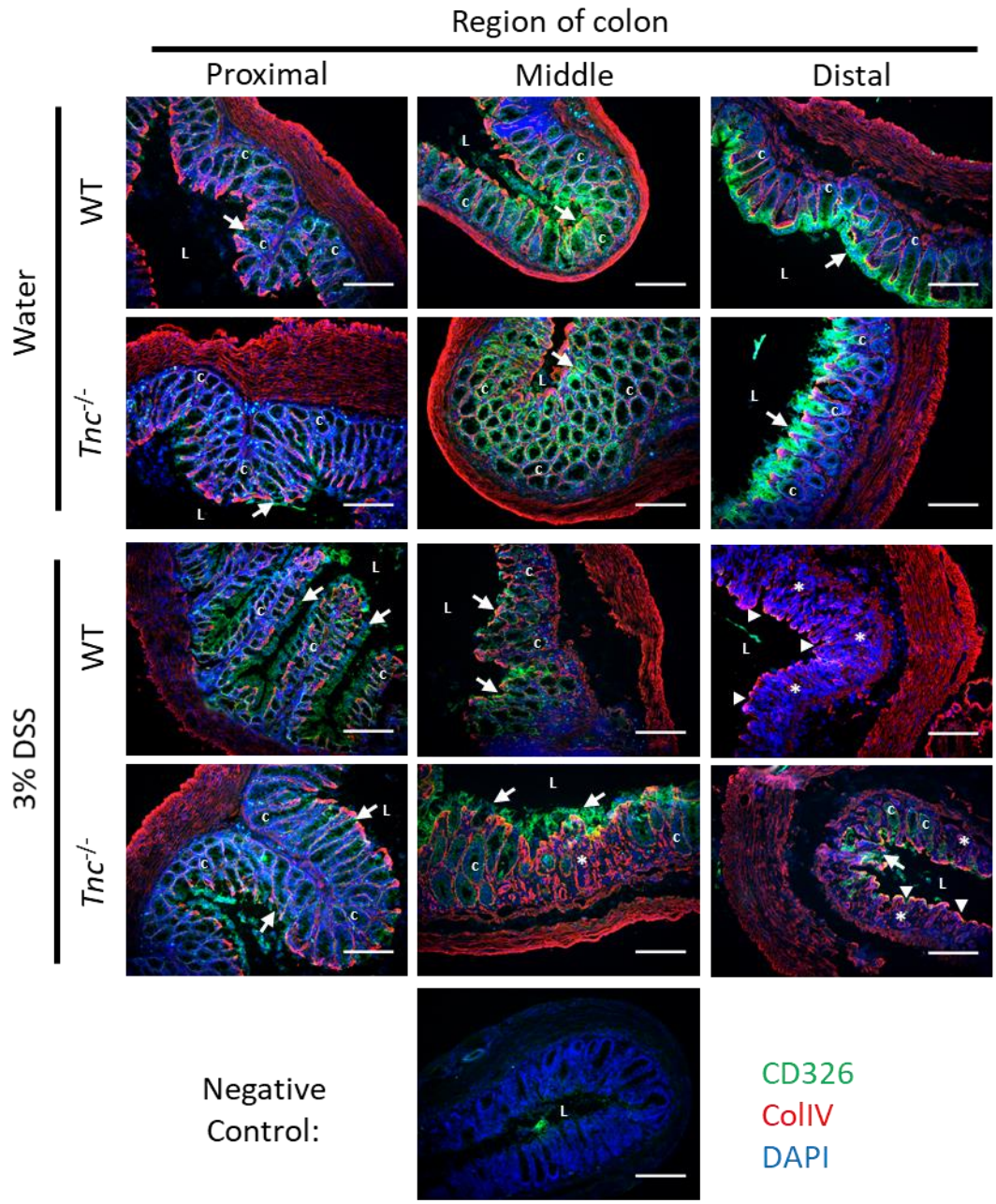

Figure 4.9 Mucosal architecture and epithelial integrity are protected in 3% DSS treated *Tnc*$^{-/-}$ mice at day 8

IHC dual staining for epithelial cells (CD326; green) and basement membranes (ColIV; red) of proximal, middle, and distal colon sections from control and day eight 3% DSS dosed WT(Ox) and *Tnc*$^{-/-}$ mice. Under basal conditions epithelial cells (closed arrows) cover the mucosal surface with normal crypt architecture observed along the length of the colon in both WT(Ox) and *Tnc*$^{-/-}$ mice. With DSS treatment in WT(Ox) mice the mucosa is damaged with the epithelium becoming ulcerated (arrowheads) and crypt architecture abrogated (asterisks) in the middle and distal colon. In *Tnc*$^{-/-}$ mice with DSS treatment similar changes are observed although partial protection of the epithelium and crypt architecture is also seen. Legend continued on following page-

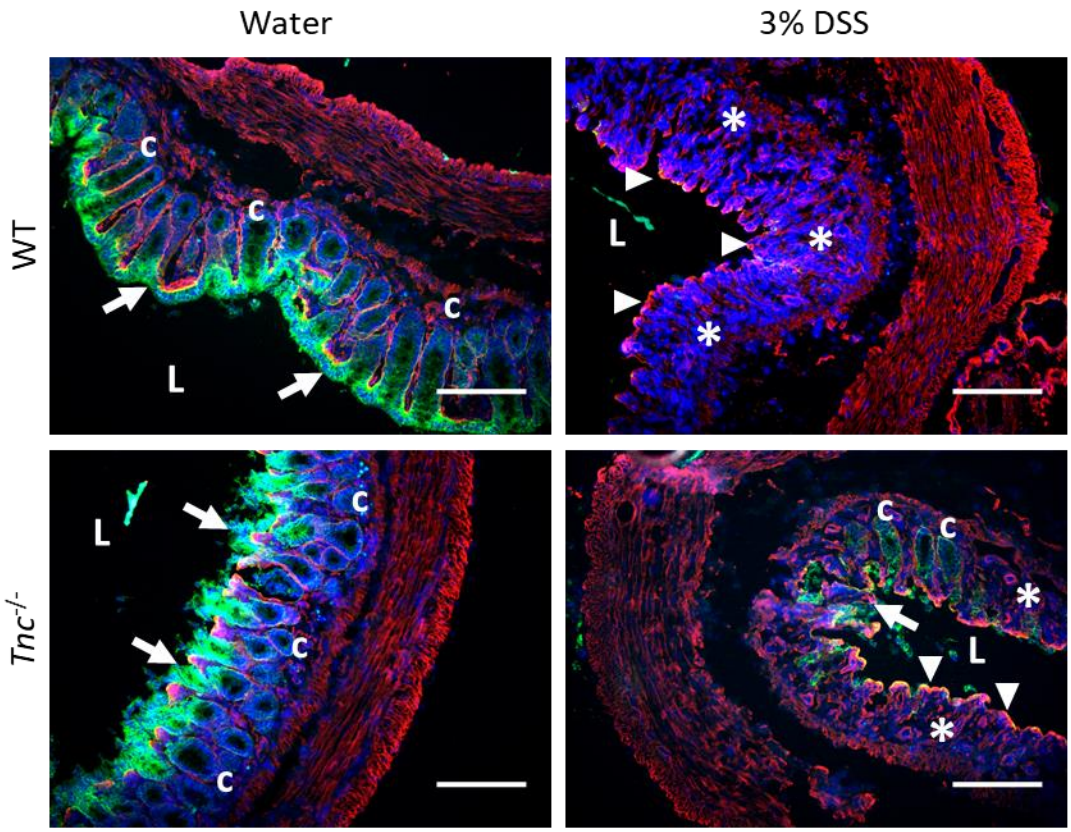

Figure 4.9 Continued

Enlarged images (above) of the control and DSS treated distal colon sections from both genotypes. These more clearly show that in the control groups normal crypt architecture and CD326 staining is observed in both genotypes which is abrogated with DSS treatment, although to a lesser degree in *Tnc*$^{-/-}$ mice.

The negative control, in which the primary antibody was omitted, of WT(Ox) distal colon shows only weak background staining. All slides were counterstained with the nuclear stain DAPI (blue) and imaged using a Leica DMLB microscope. Scale bars = 250μm. L = lumen, c = crypt

4.5.9 Colitis induced immune cell changes appear the same in WT(Ox) and *Tnc*$^{-/-}$ mice

To attempt to identify the cause of this increase in damage profiling of immune cell types was undertaken to determine the impact, if any, of tenascin-C's deletion on this facet of the colitis pathology. This initially involved IHC staining for the resident macrophage population using the marker CD11c, the results of which are shown in figure 4.10. In control tissue samples from both genotypes this macrophage population was found liberally dispersed throughout the mucosal lamina lamina propria along the length of the colon. This included a population that was found localised in the subepithelial space below the luminal facing epithelium. Previous dual staining for tenascin-C identified this subepithelial populations as being in close contact with deposits of tenascin-C found in this same area. Similar numbers and localisation of CD11c positive cells in the *Tnc*$^{-/-}$ samples would suggest that tenascin-C in these locations does not appear to mediate macrophage recruitment or retention.

With DSS treatment no major changes in proximal macrophage staining were observed with either genotype. In the damaged mucosa of the colitic distal colon macrophages were likewise still present within and around the granulation tissue. Again, no robust differences between the genotypes in macrophage number or localisation were observed here.

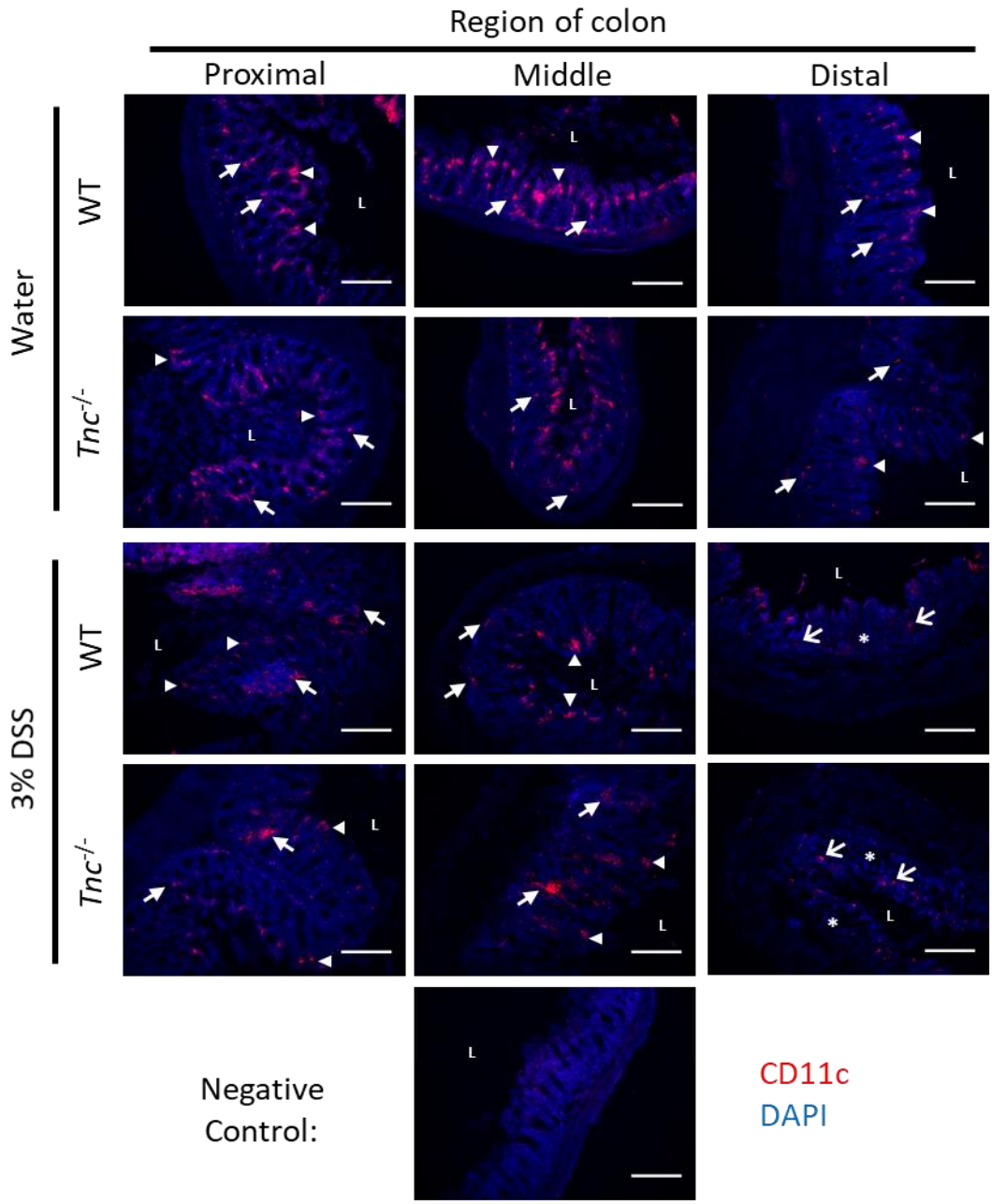

Figure 4.10 Colonic tissue resident macrophage localisation appears unaffected by loss of tenascin-C

IHC staining for colonic tissue resident macrophages (CD11c; red) of proximal, middle, and distal colon sections from control and day eight 3% DSS dosed WT(Ox) and *Tnc*$^{-/-}$ mice. Macrophages (closed arrows) are found throughout the lamina propria, including at apical subepithelial sites (arrowheads), along the length of the colon in both genotypes. Under colitic conditions similar numbers of resident macrophages are found within the damaged mucosa (open arrows). Legend continued on following page-

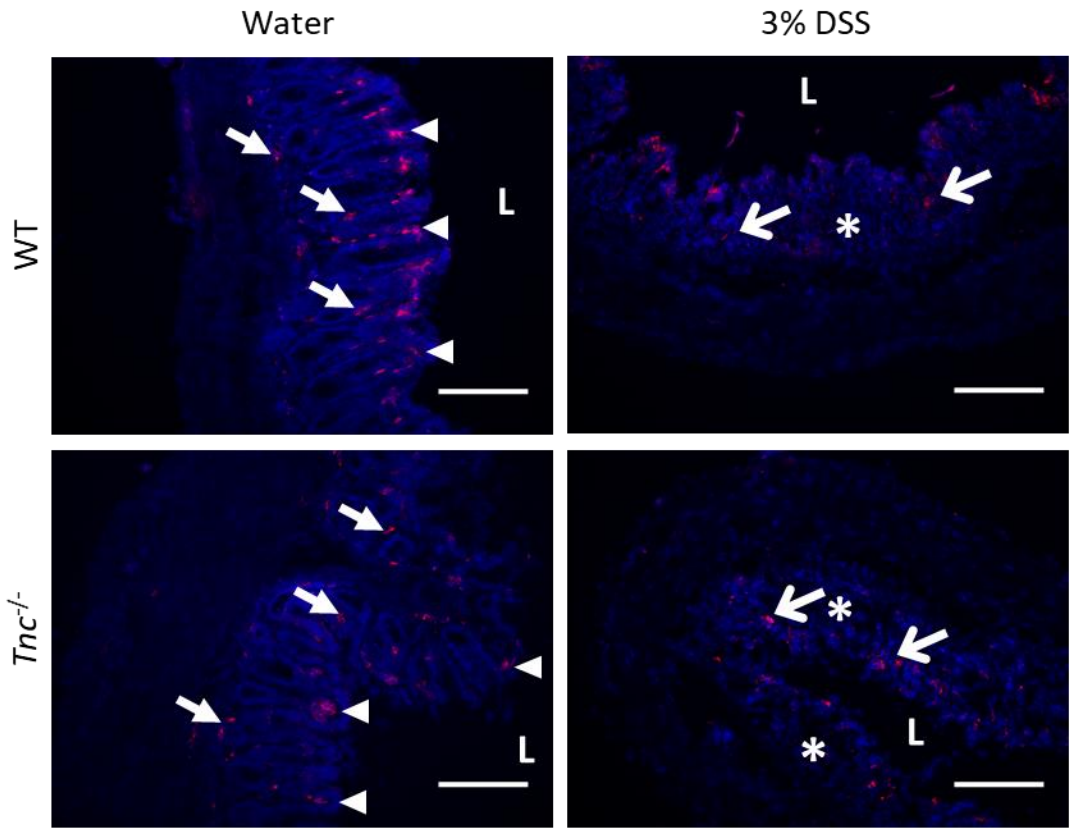

Figure 4.10 Continued

Enlarged images (above) of the control and DSS treated distal colon sections from both genotypes to better show the individual cell staining. CD11c positive macrophages in the colon tissue appear similar between the genotypes with and without DSS treatment.

The negative control, in which the primary antibody was omitted, of WT(Ox) distal colon displays no staining. All slides were counterstained with the nuclear stain DAPI (blue) and imaged using a Leica DMLB microscope. Scale bars = 250µm. L = lumen, * = damaged mucosa

The final cell type to be interrogated by IHC were the T cells of the adaptive immune system which were detected by staining for CD3, representative images of which are shown in figure 4.11. In colon tissue from WT(Ox) control mice, T cells were found in low numbers scattered throughout the lamina propria and muscularis. Similar numbers and distribution of T cells were found in samples from *Tnc*$^{-/-}$ mice suggesting that lack of tenascin-C did not influence basal T cell recruitment and retention in the colon.

Inducing colitis with DSS treatment in WT(Ox) mice resulted in a marked increase in the numbers of T cells observed in the colitic middle and distal colon. T cells while still seen within the muscularis were now found predominantly infiltrating the hyperplastic or damaged mucosa. Showing that in this instance T cell infiltration did not appear to be impacted by loss of tenascin-C similar numbers and distribution of CD3 staining were likewise observed in the colitic colon sections from *Tnc*$^{-/-}$ mice. As seen with other markers no changes from levels seen in control tissue were observed in the unaffected proximal colon in both genotypes.

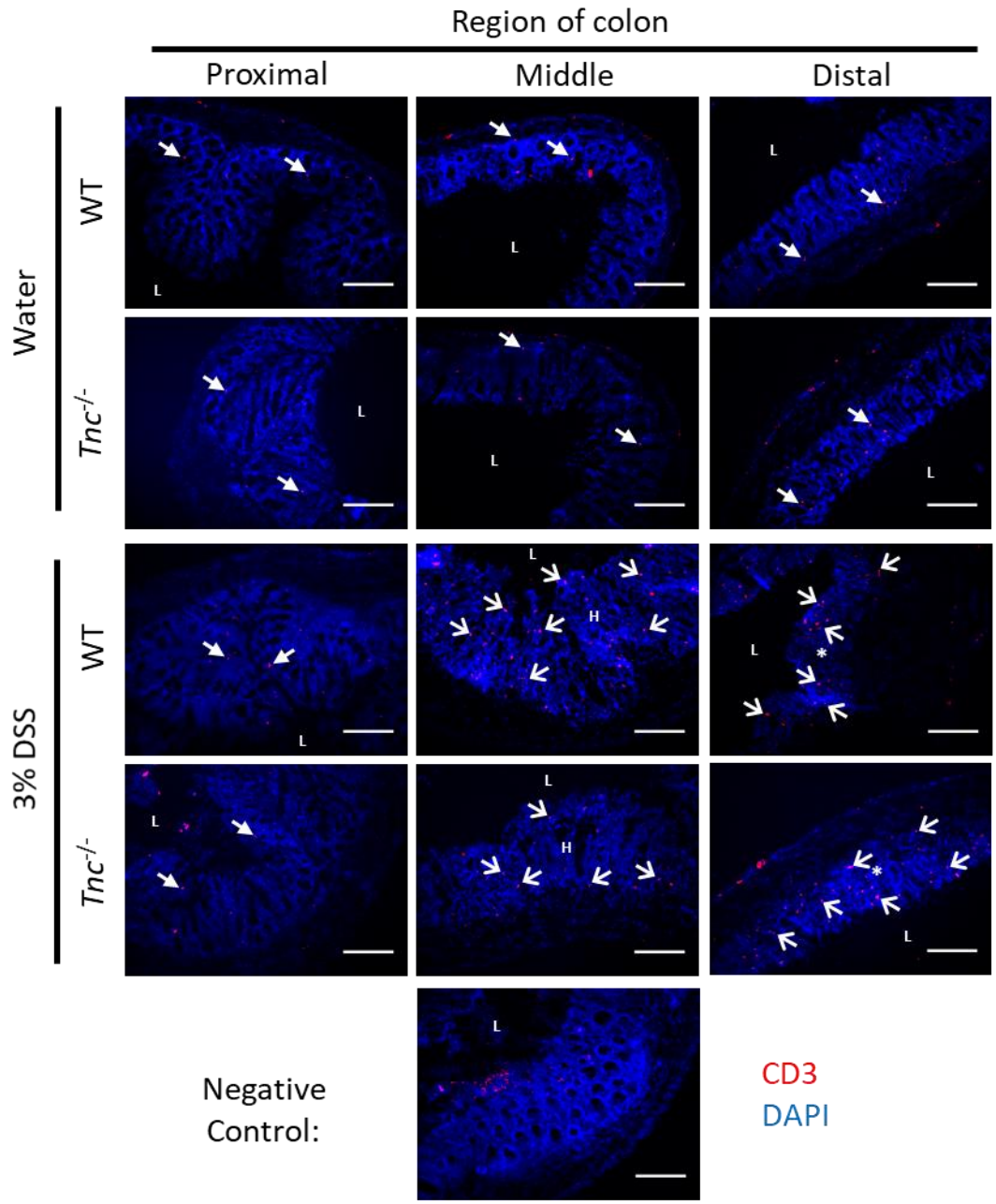

Figure 4.11 T cell infiltration of the colitic colon is observed in both WT(Ox) and *Tnc*$^{-/-}$ mice at day 8

IHC staining for T cells (CD3; red) of proximal, middle, and distal colon sections from control and day eight 3% DSS dosed WT(Ox) and *Tnc*$^{-/-}$ mice. Under basal conditions low numbers of T cells (closed arrows) are found within the lamina propria and muscularis externa along the length of the colon in both genotypes. Likewise, in both genotypes with DSS dosing elevated numbers of T cells are observed infiltrating the damaged mucosa of the middle and distal colon. Legend continued on following page-

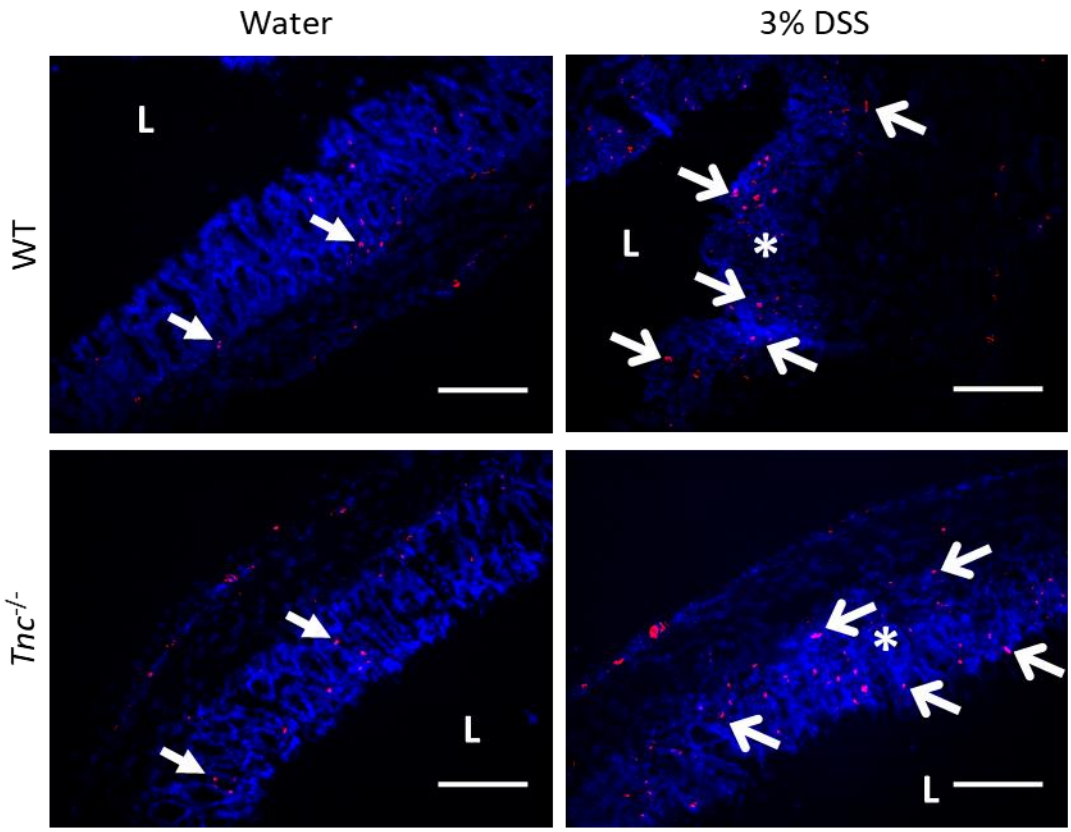

Figure 4.11 Continued

Enlarged images (above) of the control and DSS treated distal colon sections from both genotypes to better show the individual cell staining. Few CD3 positive T cells are present in the colon tissue of control mice in comparison to those following DSS treatment where significant infiltration is evident in both genotypes.

The negative control, in which the primary antibody was omitted, of WT(Ox) distal colon displays no staining except for some weak patches at the mucosal luminal surface. This was likely due to secondary antibody non-specific binding to luminal contents such as mucus. All slides were counterstained with the nuclear stain DAPI (blue) and imaged using a Leica DMLB microscope. Scale bars = 250μm. L = lumen, * = damaged mucosa, H = hyperplastic epithelium.

4.5.10 No significant difference in gross pathology is seen between *Tnc*$^{-/-}$ and WT(Ox) mice during colitis recovery

Having shown that *Tnc*$^{-/-}$ mice appeared partially protected at an acute time point in the DSS colitis model and considering tenascin-Cs known roles in wound repair it was next decided to study the colitis recovery phase in *Tnc*$^{-/-}$ mice. In this recovery version of the DSS protocol acute colitis was similarly induced by dosing for five days with 3% DSS before transfer over to normal drinking water. In this case however instead of culling the mice three days later at day eight the mice were now left for a further seventeen days for cull on day twenty-two, at which point colitis symptoms should have resolved and recovery commenced.

Following this revised protocol WT(Ox) and *Tnc*$^{-/-}$ mice were assigned to either the control or DSS treatment groups and gross pathology tracked as in previous experiments. As in the acute model survival was the first parameter assessed with increased loss of mice expected due to the potential of further decline after the acute time point resulting in mice breaching severity limits. This was observed in the *Tnc*$^{-/-}$ group which in this experiment lost three mice out a total of eleven administered DSS compared to no mice being lost in the earlier acute model. Two of these mice were lost to due to breaches of severity limit and thus were culled on humane grounds. The third was lost in an apparent adverse event as it was found dead in its cage after apparently suffering a severe colonic haemorrhage as evidenced by large amounts of fresh loose bloody stool present in the cage and on the fur near its anus. Necropsy supported this finding with large amounts of bloody stool found in the colon which appeared bloated suggesting it have potentially been suffering from a stool blockage as well. As for the WT(Ox) mice no change in survival was found compared to the acute model with again only one mouse out of seven lost due to breaching severity limits resulting in cull on humane grounds. Based on these low numbers of mice lost as in the acute model statistical analysis determined that both groups showed no significant difference in survival of DSS treatment.

Body weight loss was the second parameter analysed with the data presented in figure 4.12a. As expected, this showed both genotypes again suffered from significant body weight loss with DSS dosing compared to controls. As in the acute experiment this

began from day six for the DSS treated *Tnc*$^{-/-}$ group and in this experiment for the DSS treated WT(Ox) group as well. This significant difference between the *Tnc*$^{-/-}$ DSS and control groups was maintained consistently until the study end point on day twenty-two. A similar trend was observed with the WT(Ox) mice although significance was lost briefly at day ten partially due to a sporadic decrease in the control groups weight. Significance was also lost at the later time points of day eighteen, twenty, and twenty-one although this time seemingly more due to weight gain due to recovery in the DSS treated group. Unlike in the acute experiment the protective effect in the *Tnc*$^{-/-}$ mice was not apparent by this measure at day eight. Indeed, throughout the entire experiment no significant difference between the DSS treated WT(Ox) and *Tnc*$^{-/-}$ groups was noted for any time point.

The DAI was the next gross pathological measure scrutinised with the scoring data shown in figure 4.12b. In line with the body weight data again significant increases in sum score were observed for the DSS treated groups of both genotypes with a median score of two achieved at day eight for both genotypes.

In a reversal of what was seen in the acute experiment a significant difference compared to the genotype matched control was first achieved by the DSS treated WT(Ox) group at day four. From this point onwards the WT(Ox) mice retained a median score of two or one until day thirteen after which median scoring began to fall back to zero. Significance of these scores was not retained completely throughout this period although this was potentially due to the low power provided by the comparative control group which only contained four mice. In contrast, although some *Tnc*$^{-/-}$ mice began scoring from day four as well this did not reach significance until day six. From this point like the WT(Ox) mice a median score of two or one was maintained with significance seen throughout until day twelve. Subsequence significant scoring was then also seen on day fourteen and sixteen as a median score of one was maintained until day seventeen after which scores began to fall back to zero. Examining the breakdown of the scoring parameters stool consistency scoring appeared to follow a similar trend in both genotypes with reductions in score and number of mice scoring seen at a similar rate. In contrast the faecal blood score appeared to differ between the genotypes with scoring for it completely stopping in all WT(Ox) mice from day

fourteen while it was still seen in some *Tnc*$^{-/-}$ mice up until day nineteen. Despite these apparent temporal differences in scoring overall no significant differences in sum DAI scores were found between the DSS treated WT(Ox) or *Tnc*$^{-/-}$ groups at any time point. Additionally, no significant difference in median max sum score, as determined by Kruskal-Wallis test, was found between the DSS treated groups with a median max of recorded 2 for the WT(Ox)s and 2.5 for the *Tnc*$^{-/-}$ mice.

To assesses the apparent temporal difference in symptom presentation between the genotypes shown in the sum scoring data the prevalence of mice displaying symptoms in each group was also calculated. These data, presented in figure 4.12c, showed that from day five onwards all of the DSS treated WT(Ox) mice scored for at least one DAI parameter until day thirteen when symptoms began to subside. The majority of the WT(Ox) mice ceased scoring by day fifteen with all WT(Ox) mice no longer scoring for the remained of the experiment from day nineteen. In comparison it took until day seven until all of the *Tnc*$^{-/-}$ mice were displaying colitis symptoms although these continued for longer than seen with the WT(Ox) mice taking until day nineteen until the majority stopped displaying symptoms. From this point most *Tnc*$^{-/-}$ mice no longer displayed any symptoms aside for one which again registered soft stool consistency scoring on day twenty and twenty-one. Despite these trends being observable however, they were not found to be statistically significant as determined by Fisher's exact test, with no significant difference in prevalence between the genotypes found at any time point.

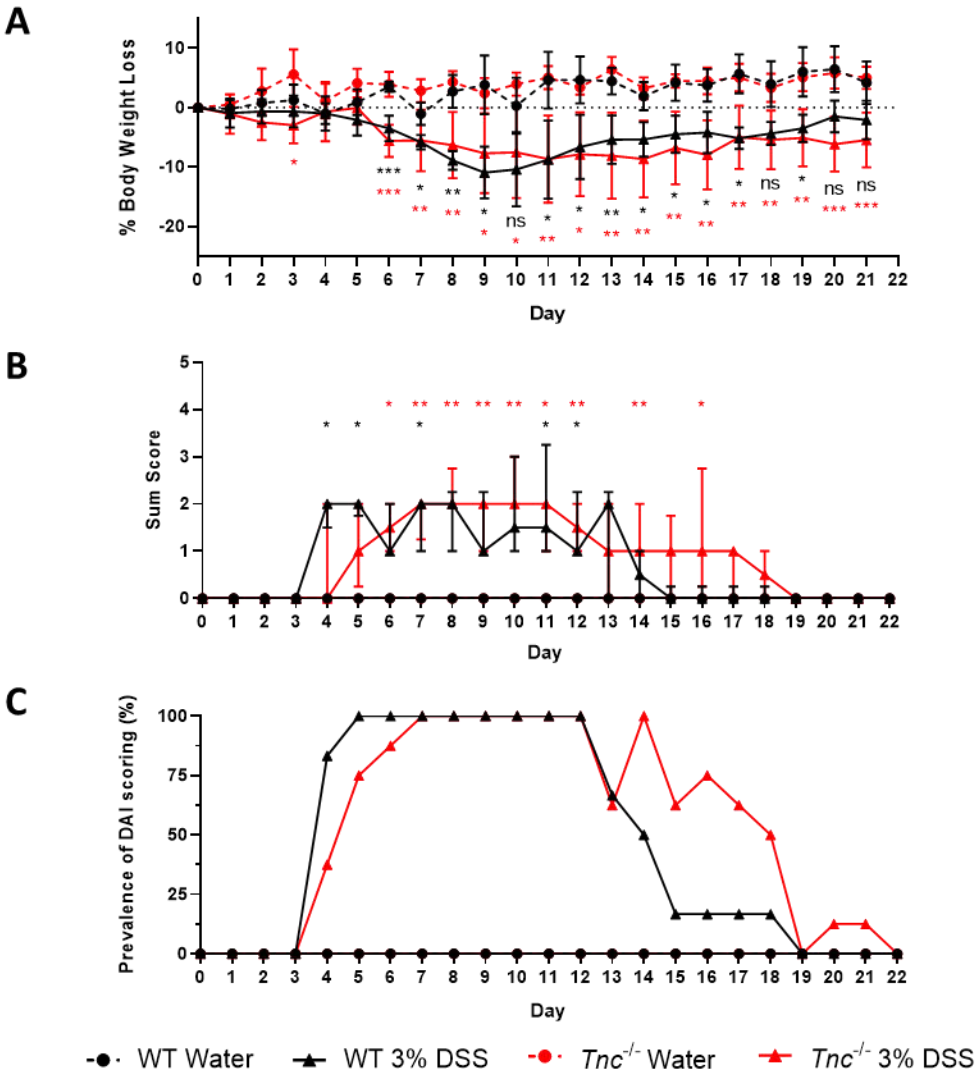

Figure 4.12 Gross pathology of WT(Ox) and *Tnc*$^{-/-}$ mice in the 3% DSS colitis recovery protocol

(A) Percentage body weight loss compared to day 0 of WT(Ox) or *Tnc*$^{-/-}$ mice given normal drinking water or drinking water supplemented with 3% DSS. Mice were dosed with DSS for the first five days to induce acute colitis by day eight before being left to recover for two weeks. Weights were measured daily except for on the day of cull at day 22. Both genotypes significantly lost weight with DSS treatment compared to control mice from day six. Data presented as mean ± SD, n= 4-8 per group, significance calculated between control and DSS treated mice of matching genotype by two-way ANOVA.
(B) Disease activity index (DAI) scoring data for the same mice as in (A). Both genotypes showed a significant increased DAI scoring compared to controls with DSS dosing. Data presented as median ± interquartile range, n= 4-8 per group, Significance compared to matched genotype control (indicated by colour) determined by Kruskal-Wallis test.
(C) Prevalence of symptoms as measured by DAI scoring for the same mice as in (A). Data presented as percentage of total mice in the group with a DAI sum score above zero, n= 4-8 per group, Significance between DSS treated groups assessed by Fisher's exact test.
*** = p<0.001, ** = p<0.01, * = p<0.05, ns = not significant.

4.5.11 Histopathology shows *Tnc*$^{-/-}$ mice retain their partial protective phenotype at the colitis recovery time point

To interrogate the colons post-colitis recovery further histological analysis was carried out on H&E stained paraffin embedded tissue sections, representative images of which are shown in figure 4.13. As observed previously tissue from control mice of both genotypes showed normal colonic architecture and minimal inflammation along the length of the colon. In the DSS treated groups of both genotypes the proximal colon likewise showed the presence of normal colonic architecture and no pathology. The middle and distal colon from both these groups in comparison still had moderate histopathology detectable.

In the mid colon for both genotypes this manifested as mainly the presence of residual immune cell infiltration in the lamina propria of the mucosa. This infiltrate now consisted, in contrast to the acute model, predominantly of just lymphocytes with less innate macrophages and neutrophils observed. Additionally, focal aggregates of immune cells were also observed in the mucosa which were potentially isolated lymphoid follicles (ILFs) produced in response to the earlier immunological challenge. This change would be expected as the immune response would be expected to be at a more advanced stage at which the adaptive immune system was playing a bigger role. The lack of submucosal infiltrate and oedema also contrasted strongly with what was observed at the acute time point indicating that the inflammatory response at this later time has subsided in this region of the colon. Finally, in terms of tissue damage this appeared to be largely resolved compared to what was seen at the acute time point with the epithelium appearing intact without ulceration and normal crypt architecture with goblet cells observed.

In comparison to the mid colon the distal colon showed more severe histopathology, in line with it being worse affected by DSS treatment. Regeneration was still apparent with intact epithelium and crypt architecture with goblet cells present to a greater degree compared to the acute time point. However, compared to the mid colon this repair was less advanced with areas of aberrant architecture, epithelial hyperplasia, and occasional focal ulceration still present. The inflammatory pathology while reduced and now predominantly lymphocytic as in the mid colon was also likewise still more

severe in appearance. Mucosal infiltration was still present to a seemingly greater degree, particularly in or around areas of worse tissue damage such as areas of continued ulceration. In addition, putative ILF like immune cell aggregates, as observed in the mid colon, were also observed in this region. In contrast to the mid colon however submucosal immune infiltration with oedema was also still present.

Comparing between the DSS treated genotypes the tissue appeared similar in the mid colon with no obvious difference observable. In the distal colon, as in the acute model, the tissue from the *Tnc*$^{-/-}$ mice appeared to display reduced pathology in comparison to that from WT(Ox) mice. This manifested as *Tnc*$^{-/-}$ mice appearing to have less aberrant mucosal architecture with more normal epithelium with goblet cell lined crypts present. Additionally, the inflammation in the *Tnc*$^{-/-}$ samples seemed somewhat reduced, particularly in terms of reduced submucosal oedema which appeared more common and severe in the WT(Ox) mice.

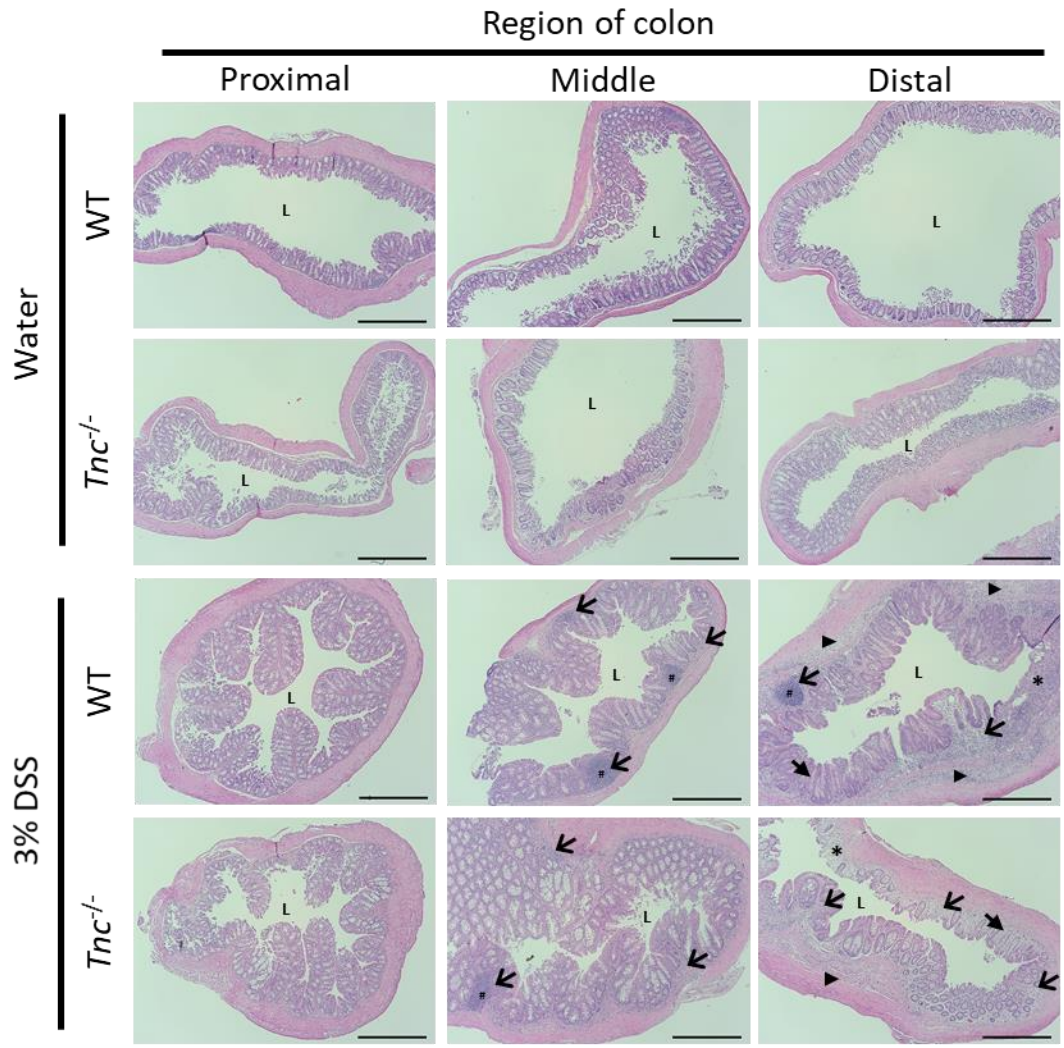

Figure 4.13 Representative H&E stained colon sections from 3% DSS recovery mice at day 22

Representative H&E stained transverse proximal, middle, and distal colon sections from control and day 22 recovered 3% DSS treated WT(Ox) and *Tnc*$^{-/-}$ mice. DSS treated mice of both genotypes show residual colitis pathology in the middle and distal colon. This includes inflammation such as mucosal immune cell infiltration (open arrows) and submucosal infiltration with oedema (arrowheads). This infiltrate is predominantly lymphocytic in nature and is observed forming mucosal aggregates (hashes), which are potentially inflammation induced isolated lymphoid follicles. Tissue damage and repair is also present including patches of ulceration (asterisks) and epithelial hyperplasia (arrows). Legend continued on following page-

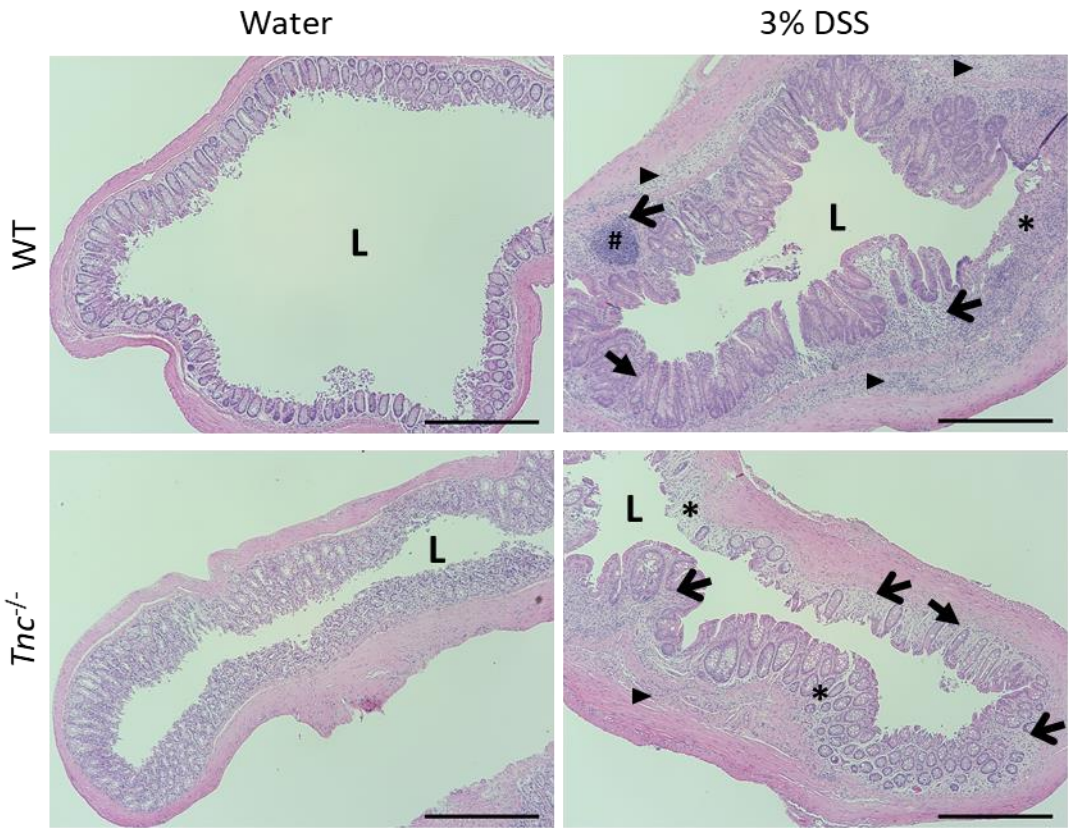

Figure 4.13 Continued

Enlarged images (above) of the control and DSS treated distal colon sections from both genotypes to better show the histopathology in the mice recovering from DSS induced colitis.

Images captured using a Nikon E600 brightfield microscope. Scale bars = 1000μm. L = lumen.

To quantify these observations in an objective manner blinded histopathology scoring was undertaken by Elspeth Milne, Professor of Veterinary Clinical Pathology, University of Edinburgh. The sum score results for the different regions of the colon, presented in figure 4.14a, largely confirmed the observations made above. Firstly, it was apparent that some degree of recovery had taken place by this time point with the sum histopathology scores for the middle and distal colon both appearing reduced compared to those seen at the acute time point. Additionally, as in the acute experiment and as noted above it confirmed that *Tnc*$^{-/-}$ mice retained their protective phenotype with significantly reduced scores observed in their distal colon in comparison to WT(Ox) mice. To further interrogate this difference further the distal colon scores were delved into in more detail by breaking them down by individual scoring parameter as presented in figure 4.14b. This revealed that while a trend in decrease was seen for the inflammatory severity and extent parameters for *Tnc*$^{-/-}$ mice compared to WT(Ox)s this was not statistically significant. The biggest contributor in score difference was thus found to be the tissue damage parameters of crypt damage and regeneration which were both significantly reduced in *Tnc*$^{-/-}$ mice compared to WT(Ox)s. The reduction in these scores appeared to be due to concomitant reductions in both the severity and percentage involvement components of the score. This contrasted with what was observed at the acute time point at which the major contributing factor to the score reduction in the *Tnc*$^{-/-}$ samples was the reduction in the percentage involvement component. This shows that at this time point *Tnc*$^{-/-}$ mice displayed less severe colitic damage compared to WT(Ox) mice rather than a similar degree of damage which affected a smaller area of the colon.

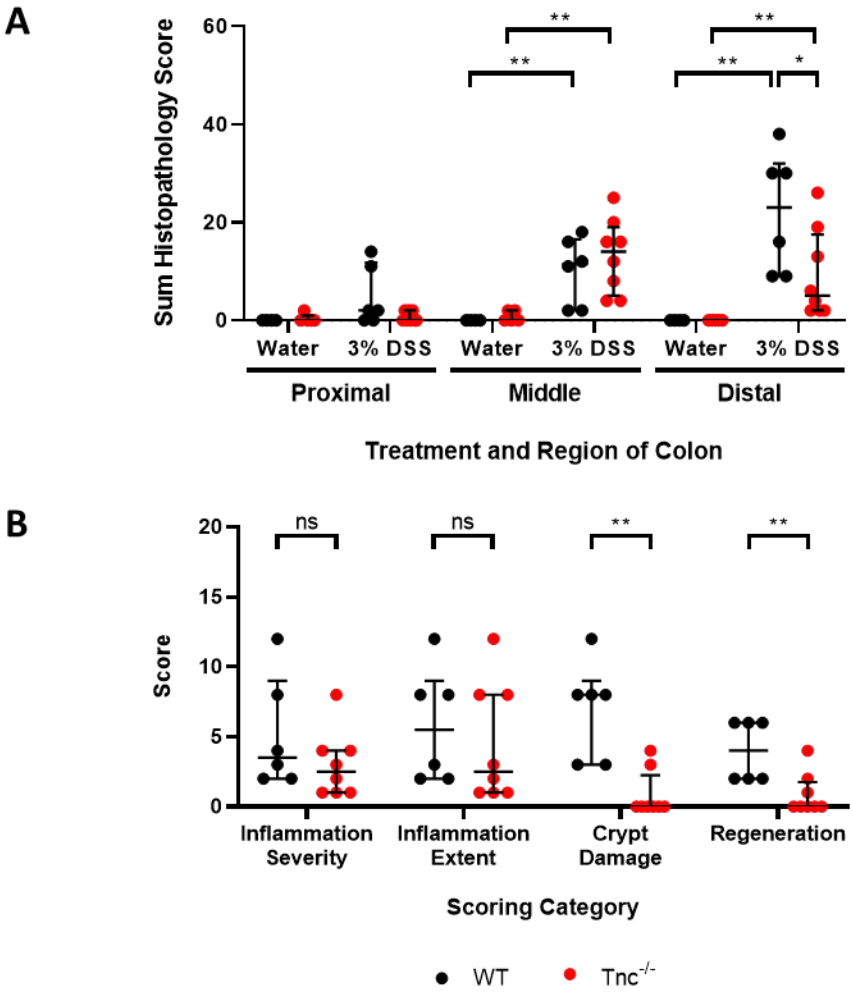

Figure 4.14 Colitis histopathology scoring of day twenty-two 3% DSS recovered WT(Ox) and *Tnc*$^{-/-}$ mice mirrors changes seen at the acute time point

(A) Sum histopathology scores for proximal, middle, and distal colon sections from control and day 22 recovered 3% DSS treated WT(Ox) and *Tnc*$^{-/-}$ mice. DSS treated mice of both genotypes show scoring compared to controls in the middle and distal colon, although to a lesser extent than seen at the acute time point. *Tnc*$^{-/-}$ mice show significantly reduced colitis scoring in the distal colon. **(B)** Scores for individual histopathology scoring parameters in distal colon segments from day 22 recovered 3% DSS treated WT(Ox) and *Tnc*$^{-/-}$ mice. *Tnc*$^{-/-}$ mice display less severe tissue damage compared to controls as measured by the crypt damage and regeneration categories. No significant difference in terms of inflammatory pathology was found between the genotypes as measured by the inflammation severity and extent categories. Data points represent scores for individual mice with bars marking the median ± interquartile range, n = 4-8 per group, significance determined by Mann-Whitney U test, ** = $p<0.01$, * = $p<0.05$, ns = no significance.

4.6 Discussion

4.6.1 Loss of tenascin-C has no impact on colonic development and tissue maintenance

In line with previous studies *Tnc*$^{-/-}$ mice were found to have undergone normal gastrointestinal development with no gross or histological abnormalities found in the adult colon (Saga et al., 1992, Forsberg et al., 1996). This is despite tenascin-Cs expression in the presumptive colon in the embryo (Beaulieu, 1997) as well as its continued expression postnatally through to adulthood. At these sites' tenascin-C has been implicated, based mainly on *in vitro* experimental evidence, in a variety of processes. This has included in the developmental context mediating cell migrations (Aufderheide and Ekblom, 1988), smooth muscle cell survival (Jones et al., 1997), and epithelial-mesenchymal interactions (Belanger and Beaulieu, 2000). Despite these hypothesised roles, *Tnc*$^{-/-}$ mice showed no obvious changes from WT mice under basal conditions as shown by H&E staining as well as staining for a variety of specific features by IHC. In particular the colonic epithelium and enteric musculature appeared by all measures to be comparable to WT mice, both of which would have likely been significantly impacted if the above-mentioned developmental processes were affected.

In the adult again due to its localisation and *in vitro* attributed functions a number of roles had been suggested for tenascin-C. One of the first to be attributed to tenascin-C was a potential role in epithelial homeostasis and in particular functioning in the important epithelial crypt migration and shedding cycle (Patterson and Watson, 2017). This was postulated due to its subepithelial expression pattern and apparent adhesion modulating properties which suggested it could either promote epithelial detachment during shedding (Probstmeier et al., 1990a) or allow for epithelial migration up the crypt (Hashimoto and Kusakabe, 1997). The lack of any abrogation of the epithelium or the mucosal crypt architecture in *Tnc*$^{-/-}$ mice which would occur with disruption to these processes key to epithelial maintenance brings into question these theories.

4.6.2 Immunological roles for tenascin-C under basal conditions in the colon

The next intestinal compartment potentially impacted by tenascin-C would be the immune system and in particular the innate arm within the lamina propria.

Subepithelial macrophages within the colon are known to be a key barrier to invasion by the luminal microbiota that have breached the epithelium, acting to mount a rapid response which results in the infringing microorganisms containment and destruction (Rubio et al., 2018). With tenascin-C's localisation at the subepithelial sites as well as it's known ability to stimulate myeloid cells (Midwood et al., 2009) it is thus not unfeasible that tenascin-C may influence the innate immune system at these sites. Additionally, via its effects on innate immune cells or direct interactions, such as those suggested by *in vitro* experiments (Weismann et al., 1997), tenascin-C could also impact the adaptive immune system in the colon as well. In this study no apparent basal aberrations in either cell number or localisation were observed for the resident macrophage or T cell populations in any compartment found along or across the colon wall. This suggests that tenascin-C, despite its ability to influence both innate (Abbadi et al., 2017) and adaptive (Clark et al., 1997) immune cell migration, does not appear to do so under resting conditions in the colon. Likewise, these observations also support previous studies on immune cell development that found no abnormalities in blood immune cell development and number (Ohta et al., 1998) or myeloid cell differentiation (Ruhmann et al., 2012) in *Tnc*$^{-/-}$ mice.

These analyses may prove too simplistic to rule out an immunological role of the gut tenascin-C however as it's affects could likely be subtler influencing immune cell polarisation rather than absolute numbers and location. Indeed, it has already been shown that tenascin-C can aid in polarising innate cells such as in the case of macrophages driving them towards the M1 polarity at the expense of the M2 polarity (Kimura et al., 2019). Via its interactions with dendritic cells tenascin-C has also been shown to modulate polarisation of the adaptive immune system by for example promoting polarisation of T cells towards the Th17 subtype (Ruhmann et al., 2012). Studies of immune cell polarisation under basal conditions in *Tnc*$^{-/-}$ mice in lymph node and spleen, which also maintain tenascin-C expression in the adult (Ocklind et al., 1993), have demonstrated no difference in numbers of proportions of a variety of adaptive (Machino-Ohtsuka et al., 2014, Momcilovic et al., 2017) and innate (Kimura et al., 2019) subtypes. However, it cannot be assumed that the same is true for the gastrointestinal immune system where the continual immunological challenge of the microbiota results in its own distinct immune landscape (Mowat and Agace, 2014). As

such, further detailed analysis is needed of the colonic immune compartment in *Tnc*$^{-/-}$ mice to rule out any other more subtle changes.

It could be argued that the health and seemingly normal immune status of *Tnc*$^{-/-}$ mice under homeostatic conditions would suggest that these differences do not exist or are functionally irrelevant. However, it should be stressed that, especially in terms of gut immunology, the *Tnc*$^{-/-}$ mice by nature of their specific pathogen free (SPF) housing are not kept under what should be considered normal conditions. It has been shown that the gut microbiota of laboratory mice differs significantly from their wild counterparts and this impacts upon host fitness (Rosshart et al., 2017). The evolutionary conservation of tenascin-C (Tucker et al., 2006) would suggest that it confers some evolutionary advantage and thus it might be these are only realised under the normal pressures exerted by the microbiota on the host.

4.6.3 Potential for compensation of loss of tenascin-C in *Tnc*$^{-/-}$ mice

Since the generation of the original *Tnc*$^{-/-}$ mouse, researchers have looked for mechanisms of compensation to account for the largely normal phenotype observed. These initially focused on the possibility of functional redundancy (Tautz, 1992) of tenascin-C, and in particular the potential of other members of the nascent tenascin family to compensate for tenascin-C's loss (Chiquet-Ehrismann et al., 1994). This was found to be unlikely in the case for tenascin-R which has a very restricted expression pattern to the nervous system during both development and postnatal life (Brellier et al., 2009). Tenascin-W more similarly to tenascin-C shows more fluctuating and wide-ranging expression where it has been implicated in smooth muscle development. In the colon however it was found to be absent in both development and in the adult (Scherberich et al., 2004). Tenascin-X conversely has shown to be expressed in the developing gastrointestinal tract including the colon (Geffrotin et al., 1995). While the colon has not been examined in the developing small intestine tenascin-X was found at similar sites of smooth muscle cell development, such as the presumptive muscularis mucosae, as tenascin-C (Matsumoto et al., 1994). Unlike tenascin-C this expression was not preserved in the adult however with tenascin-X found restricted to sensory and motor neurones of the enteric nervous system of the colon (Aktar et al., 2018). As

such, while tenascin-X may serve some compensatory role in development it does not appear to substitute for tenascin-C in the adult. With these spatiotemporal differences it was postulated that a compensatory upregulation of another tenascin may occur in *Tnc*$^{-/-}$ mice. Evidence for this hypothesis has been found lacking however with both tenascin-X (Saga et al., 1992) and tenascin-R (Steindler et al., 1995) found to maintain their same expression levels and patterns, while tenascin-W remains to be studied.

Besides compensation by other members of the tenascin family other genetic mechanisms for compensatory modulation of gene expression exist by which loss of tenascin-C could be mitigated (El-Brolosy and Stainier, 2017). In particular, transcriptional adaptation whereby the mRNA degradatory machinery's targeting of mutant mRNA transcripts results in compensatory upregulation of other genes could be of relevance (El-Brolosy et al., 2019). This is because the genetic knockout strategy employed in the generation of the in the *Tnc*$^{-/-}$ mouse (Saga et al., 1992) while abrogating protein expression still produces a mutant tenascin-C mRNA transcript. As such, this compensatory mechanism could be engaged, and gene expression modulated to broadly accommodate for tenascin-Cs loss resulting in more subtle phenotypes than expected.

4.6.4 Acute colonic inflammation in *Tnc*$^{-/-}$ mice

Despite no basal colonic differences observed the induction of acute colitis revealed genotypic differences with *Tnc*$^{-/-}$ mice showing reduced colitis severity. Due to tenascin-Cs known role in driving inflammatory pathology in other disease models this presents a clear mechanism by which DSS pathology might be mitigated in *Tnc*$^{-/-}$ mice (Marzeda and Midwood, 2018). These pro-inflammatory effects have been shown to be primarily mediated by tenascin-Cs activation of TLR4 (Midwood et al., 2009) as well as the integrins α9β1 (Kanayama et al., 2011) and αVβ3 (Shimojo et al., 2015). Activation of these receptors results in production of a wide variety of pro-inflammatory mediators with relevance to colitis pathology. These include the classical pro-inflammatory cytokines IL-6 and TNF which have been shown to be upregulated at the transcriptional and post-transcriptional level via tenascin-C's induction of histone deacetylase (HDAC) 1 (Haage et al., 2019) and the micro RNA miR-155(Piccinini and Midwood, 2012) respectively. The pro-inflammatory cytokine

IL-23 has also likewise been shown to be upregulated by tenascin-C although the exact mechanism has yet to be established (Kanayama et al., 2011).

All of these cytokines are known to be upregulated and act as important drivers in colitis (Neurath, 2014). For example, TNF is upregulated in the colon of mice in the chronic DSS model and neutralising antibody treatment results in a reduction in inflammation (Kojouharoff et al., 1997). Similarly, IL-6 is likewise upregulated in the colon of DSS treated mice and mice with IL-6 genetically ablated show attenuated colonic injury and immune infiltration (Naito et al., 2004). IL-23 meanwhile has been shown to be instrumental in driving inflammation to chronicity in a separate model of colitis resulting from intestinal barrier impairment (Eftychi et al., 2019). IL-23 is known to be key for Th17 T cell polarisation (Toussirot, 2012) and indeed in this model a pathological Th17 response was implicated. *Tnc*$^{-/-}$ mice with reduced IL-23 production are known to show deficiencies in Th17 responses (Ruhmann et al., 2012) and thus this presents another manner in which tenascin-C deficiency may confer protection in colitis.

Further supporting the translational relevance of these studies these cytokines have or are currently being developed as the targets of IBD therapeutics. Therapies targeting TNF have proven strong clinical efficacy which demonstrates its mechanistic relevance with TNF neutralising antibody therapies in regular clinical use (Jarnerot et al., 2005). Therapies targeting IL-6 meanwhile are in an early stage of development although again have shown some benefit in patients confirming this cytokines role in disease (Danese et al., 2019). Likewise, therapies targeting IL-23 in IBD are also currently undergoing clinical trials for the treatment of Crohn's disease (Ma et al., 2018) with promising case reports of successful treatment already published (Grossberg, 2019).

In terms of the cell types tenascin-C is likely mediating these pro-inflammatory signals through innate immune myeloid cells are a likely target as they have been identified as the primary cell types responsible for the production of these cytokines in IBD (Kamada et al., 2008). Indeed it is known that macrophages are key for the induction of DSS colitis as severe combined immunodeficient mice which lack adaptive immune cells still develop pathology and produce ample amounts of these pro-inflammatory

cytokines (Dieleman et al., 1994). These cells are unlikely the resident gut macrophages however as these are known to suppress their pro-inflammatory activity and display TLR hyporesponsiveness through co-receptor downregulation and chromatin remodelling (Bain and Schridde, 2018). As such, it is likely recruited circulating pro-inflammatory myeloid cells interacting with the colonic tenascin-C to and adopting a pro-inflammatory M1 polarisation resulting in production of pro-inflammatory mediators (Kimura et al., 2019).

Aside from regulating the phenotype of cells in the colon tenascin-C deficiency could also affect immune cell recruitment and migration via regulation of chemokines. For example, it has been shown that the neutrophil attracting chemokines CXCL1 and CXCL2 are produced at reduced levels in *Tnc*$^{-/-}$ mice (Piccinini and Midwood, 2012, Matsumoto et al., 2017). Additionally, the myeloid attracting chemokine CCL2, has likewise shown to be decreased in *Tnc*$^{-/-}$ mice in a number of inflammatory models (Nakahara et al., 2006, Bhattacharyya et al., 2016). All of these chemokines have previously been shown to be increased in DSS colitis (te Velde et al., 2007) and are also increased in IBD patients (Banks et al., 2003, Alzoghaibi et al., 2008) suggesting they are relevant to IBD pathogenesis. In terms of functional outcomes while no differences in two broad immune cell populations were found in this study these investigations were far from extensive and thus warrants further investigation.

Finally, tenascin-C deficiency may also potentially impact upon pathological remodelling of the colonic ECM. For example, unlike other TLR4 ligands tenascin-C has been shown to upregulate the membrane bound extracellular protease MMP14 (Piccinini et al., 2016). MMPs are well known to be increased in IBD where through ECM degradation they mediate a variety of pathological processes (O'Sullivan et al., 2015). In regards to MMP14 specifically it has been found at increased levels in the DSS model of colitis (te Velde et al., 2007) as well as in the inflamed mucosa of IBD patients (von Lampe et al., 2000). Additionally, a SNP in the MMP14 gene has been shown to be associated with IBD in certain cohorts (Morgan et al., 2011). As such, MMP14 is clearly implicated in the pathogenesis of IBD and thus with tenascin-C's known link to its expression shows another potential mechanism by which tenascin-C deficiency may be protective in colitis.

4.6.5 Tenascin-C in resolution of colonic inflammation

Having shown reduced colitis severity during the acute phase of the DSS model in *Tnc*$^{-/-}$ mice the observation period was extended by two weeks to study the impact of tenascin-C on colitis resolution. This was undertaken as tenascin-C as well as having known roles in supporting the initial inflammatory responses has also been shown to have roles in the later repair phases (Midwood and Orend, 2009). This study while not recapitulating the earlier acute findings entirely, including not showing the same protection from weight loss, did still find that *Tnc*$^{-/-}$ mice had reduced histopathology compared to WT mice. While it could be speculated that this may simply be a result of a reduction in initial inflammation and thus damage in the knockouts it cannot be ruled out that loss of tenascin-C is not positively impacting the wound healing response as well. These observations contrasted with a previous report in the literature which proposed tenascin-C as a protective factor in DSS colitis which mediated epithelial healing (Islam et al., 2014). This would appear to be supported in part by some work done on dermal wound healing models which have implicated tenascin-C in promoting keratinocyte proliferation and migration (Mackie et al., 1988). The findings in the current study of reduced tissue damage, including reduced ulceration, in *Tnc*$^{-/-}$ mice however would suggest that this is not the case in the gut.

Besides impacting directly upon mucosal repair loss tenascin-C may also have promoted enhanced healing by leading to an upregulation of the pro-resolution immune response. For example, it has been shown that bone marrow derived macrophages from *Tnc*$^{-/-}$ mice show enhanced production of the anti-inflammatory cytokine IL-10 (Piccinini and Midwood, 2012). This bias has been shown to be preserved *in vivo* in murine models of Alzheimer's disease (Xie et al., 2013) and cardiac injury (Kimura et al., 2019) which both showed increased levels of IL-10 in *Tnc*$^{-/-}$ mice. IL-10 is of particular importance in the gut where it is a key mediator for maintaining gut immune homeostasis as evidenced by the spontaneous development of chronic colitis in IL-10 deficient mice (Kuhn et al., 1993). To achieve this immune control IL-10 acts on a variety of immune cell types including T cells for which it is known to inhibit Th17 functions while supporting anti-inflammatory regulatory T cell functions (Murai et al., 2009, Chaudhry et al., 2011). It is probably best known for its action on myeloid cells however, with its ability to polarise macrophages towards an

anti-inflammatory reparative M2 phenotype (Mosser and Edwards, 2008). This action was apparent in the above mentioned disease models which alongside the increased levels of IL-10 also saw increases in the expression of the M2 macrophage marker MRC1 (Xie et al., 2013, Kimura et al., 2019).

In addition to helping dampen the inflammatory response an increase in M2 macrophages in *Tnc*$^{-/-}$ mice would likely also result in the promotion of mucosal tissue repair. This has been demonstrated in cell transfer experiments of M2 macrophages into DSS treated animals which show enhanced ulcer repair (Enderlin Vaz da Silva et al., 2014). This repair is likely mediated by several mechanisms which may include M2 macrophages enhanced ability to clear apoptotic cells debris (Zizzo et al., 2012) or ability to synthesise new ECM (Novak and Koh, 2013). M2 macrophages biggest impact on the repair process is likely in a trophic manner however by promoting repair by other stromal cell types. For example, M2 macrophages are known to produce growth factors such as TGFβ to promote fibroblast matrix synthesis and VEGF to promote angiogenesis by vascular endothelial cells (Brancato and Albina, 2011). In regard to colonic regeneration specifically M2 macrophages have been shown to secrete Wnt ligands which promote epithelial proliferation and differentiation as part of the reepithelialisation repair process (Cosin-Roger et al., 2016). Additionally, macrophage derived IL-10 was shown to promote epithelial secretion of CCN4 which acts in autocrine manner to promote epithelial wound healing in part by enhancing Wnt signalling (Quiros et al., 2017). As such, enhanced M2 macrophage activity in *Tnc*$^{-/-}$ mice presents another mechanism by which colonic damage is reduced in DSS colitis.

A summary of all of the proposed protective mechanisms in DSS colitis is presented in figure 4.15 highlighting the anti-inflammatory and pro-repair affects that loss of tenascin-C mediates in *Tnc*$^{-/-}$ mice.

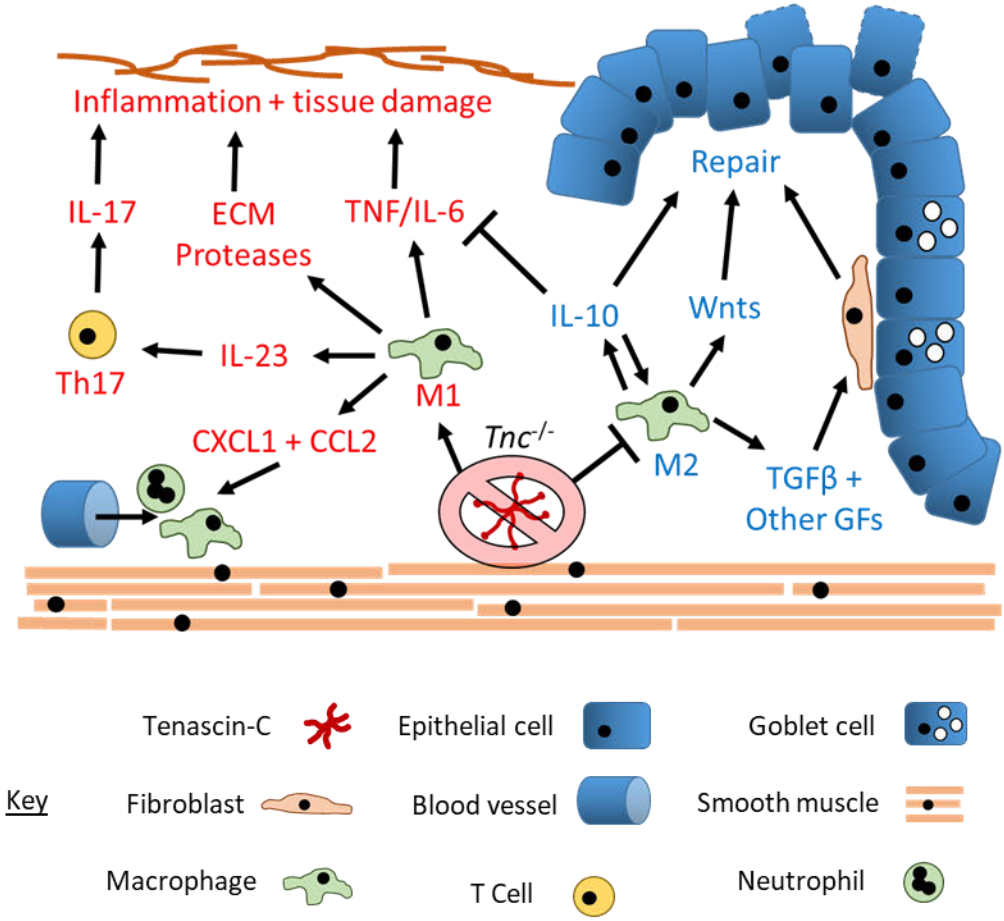

Figure 4.15 Summary hypothetical model of the protective mechanisms of genetic ablation of tenascin-C in DSS colitis

Genetic ablation of tenascin-C results in downregulation of pro-inflammatory processes (red) and promotion of anti-inflammatory and pro-repair processes (blue). Tenascin-C engages pro-inflammatory receptors on macrophages and stromal cells to drive pro-inflammatory cytokine and ECM protease production. These cytokines drive the pathological inflammatory process including promoting pathological adaptative immune processes such as the differentiation of IL-17 producing Th17 T cells. Tenascin-C also drives further immune cell recruitment to the colon via promoting the production of chemokines such as CXCL1 and CCL2. These processes all contribute to the excessive tissue damaging inflammatory response and are mitigated by tenascin-Cs loss in *Tnc*$^{-/-}$ mice. Furthermore, loss of tenascin-C results in the promotion of anti-inflammatory immune responses such as the polarisation of macrophages to an M2 phenotype. These cells produce the potent anti-inflammatory cytokine IL-10 which inhibits inflammatory processes such as pro-inflammatory cytokine production and promotes epithelial repair. M2 macrophages additionally promote tissue repair by secretion of a variety of other growth factors such as TGFβ and Wnts which act of stromal and epithelial cells to promote tissue regeneration.

Chapter 5 Development of assays to assess the clinical utility of tenascin-C expression

5.1 Introduction

A large body of literature, including the preceding studies in this thesis, have shown tenascin-C is mechanistically associated with the inflammatory process (Marzeda and Midwood, 2018). Moreover, it is well described that tenascin-C expression in healthy adults is tissue restricted, with most tissues expressing low to negligible levels of the protein (Udalova et al., 2011). As such, tenascin-C may have utility as a potential biomarker of inflammation and more specifically of chronic inflammatory disease, a category of diseases where clinically useful markers are in great need.

In regard to this it has been the systemic circulating form of tenascin-C which, due to its ease of sampling, has gained the most attention for potential use in a diagnostic tool. Indeed, systemic tenascin-C has been studied in a variety of inflammatory conditions with elevated levels having been demonstrated in conditions as diverse as IBD (Riedl et al., 2001), ankylosing spondylitis (Gupta et al., 2018), and systemic lupus erythematosus (Zavada et al., 2015). Furthermore, these studies have likewise shown clinical applicability with tenascin-C levels associated with disease activity in SLE (Zavada et al., 2015) and responsiveness to biologic therapy in IBD (Magnusson et al., 2015). The studies of this thesis chapter will focus on adding to this body of work with the development of novel assays for the detection of tenascin-C in human serum samples. These assays it is envisaged could eventually be applied to a variety of inflammatory diseases with the above variety of conditions in which tenascin-C is implicated in indicating a potential common mechanism of action in disease.

With this broad applicability in mind for the development and validation work of this chapter these assays were primarily applied to the inflammatory disease rheumatoid arthritis (RA). RA was chosen as a focus for three prime reasons the first of which was that it is this condition which has received the most characterisation in terms of tenascin-C's role in disease in the literature, as will be outlined below. This has included some work on systemic tenascin-C and its potential clinical application,

which will also be described below. The second consideration was the current clinical diagnostic landscape with specific blood tests used regularly in the diagnosis of RA already (Allen et al., 2018). This contrasts with some other IMIDs, including IBD, in which diagnosis is currently carried out without specific serological tests with in the case of IBD a greater focus on symptoms, imaging, and histopathology (Magro et al., 2017, Gomollon et al., 2017). As such, initial adoption of a serological test in the clinical setting might be more easily managed in the context of RA, in which they are already readily used, compared to these other conditions. The final consideration was a more practical one, relating to the availability of serum samples, with primarily those of RA patients initially identified at the commencement of the project.

RA is a chronic inflammatory disease of the joints for which reliable diagnostic biomarkers, as well as markers of disease progression and treatment response, are few. Due to its heterogeneous nature, current diagnosis of RA is based on composite scoring systems, which, among other physical assessments, take into account four serological markers. These include testing for rheumatoid factor (RF) and anti-citrullinated protein autoantibodies (ACPA), as well as the more general inflammation markers of C-reactive protein (CRP) and erythrocyte sedimentation rate (Aletaha et al., 2010). Both RF and ACPA are types of self-reacting antibodies, termed autoantibodies, which are produced due to loss of self-tolerance in autoimmune diseases. Autoantibodies are categorised by the specific self-antigens, termed autoantigens, which they recognise with RF for example constituting autoantibodies which target the Fc portion of IgG (Song and Kang, 2010). ACPA in particular are considered a highly specific serological marker of RA and consist of a heterogenous pool of autoantibodies which target autoantigens which have been post-translationally modified to include the non-standard amino acid citrulline (Demoruelle and Deane, 2011). The current clinical gold standard test for ACPA is the cyclic citrullinated peptide (CCP)2 assay which utilises a pool of synthetic citrullinated peptides to capture citrulline specific autoantibodies in patient serum samples for detection (van Venrooij and Zendman, 2008).

Overall, the CCP2 test in combination with the other available markers and diagnostic criteria has proven reasonably successful for the diagnosis of RA. However, the sensitivity and specificity of these measures is still only estimated at around 70% when

used in the diagnosis of patients presenting with synovitis suggesting that they still do not detect a significant proportion of patients (Alves et al., 2011, Cader et al., 2011). This is particularly problematic when considering the proposed existence of a 'window of opportunity' for treatment early in disease where intervention is associated with better long term patient outcomes (Espinoza et al., 2016). Any delay in diagnosis would thus result in delayed treatment and therefore worse patient outcomes. In addition, the absence of reliable prognostic and theranostic markers for RA presents a significant challenge for the clinical management of RA patients (Cuppen et al., 2016). For example, 30-40% of patients do not respond, or respond poorly, to the biologic therapies introduced in recent years (Bansard et al., 2009). Reliable biomarkers for the stratification of patients prior to treatment would improve patient wellbeing and decrease cost by ensuring that patients receive treatment with the highest efficacy (Isaacs and Ferraccioli, 2011).

Tenascin-C has a long association with RA, with early reports detailing its upregulation in the inflamed synovium of patients (Cutolo et al., 1992). More recent work has expanded on this association and demonstrated that tenascin-C is a driver of joint inflammation in murine models (Midwood et al., 2009) and may have potential as a target in therapeutic applications (Aungier et al., 2019). In addition to local upregulation of tenascin C, as with the other inflammatory conditions listed above, elevated levels of the tenascin-C have been shown in the serum of RA patients (Page et al., 2012). These preliminary studies have demonstrated that serum tenascin-C positively correlates with disease duration and degree of joint erosion, and was negatively correlated with response to anti-TNF biologic therapy (Page et al., 2012). This may reflect that tenascin-C is intrinsically involved in the disease process and as such is an example of a mechanistic biomarker, in contrast to the mainly descriptive biomarkers currently used for RA management (Robinson and Mao, 2016).

Besides acting as a disease driver and biomarker, tenascin-C has been implicated in the ACPA response in RA. As mentioned earlier the ACPA in RA consist of a heterogenous population of autoantibodies which have been identified as targeting a range of citrullinated autoantigens which has included proteins such as fibrinogen (Masson-Bessiere et al., 2001) and vimentin (Vossenaar et al., 2004). Recently

tenascin-C was also identified in a subset of patients as an ACPA autoantigen by using citrullinated peptides derived from the protein to capture autoantibodies in patient serum. This approach identified a number of epitopes located in the FBG domain which were specifically recognised by RA patient autoantibodies when citrullinated. The most robust of the FBG domain derived peptides was called cTNC5 with an amino acid sequence of EHSIQFAEMKL-cit-PSNF-cit-NLEG-cit-cit-KR, with 'cit' indicating the citrulline residues in the peptide (Schwenzer et al., 2015). These autoantibodies were apparent in some cases many years before clinical disease manifested and were associated with the development of RA in patients presenting with early undifferentiated disease (Raza et al., 2016). This suggests that tenascin-C is involved in the very early stages of the disease and highlights that its measurement may be clinically informative.

The full diversity of tenascin-C's molecular forms has not been investigated in the studies of systemic tenascin-C owing to limitations of the assays used. Human tenascin-C contains 9 alternatively spliced fibronectin type III repeats, which produce a significant diversity in isoforms (Giblin and Midwood, 2015). The most commonly used assay in the literature for tenascin-C quantification is the tenascin-C large FNIII-B ELISA kit produced by IBL, due in part to its high specificity and linear range (Giblin et al., 2018). However, the kit, as its name might suggest, detects only isoforms of tenascin-C containing the alternatively spliced FNIII type repeat B domain. The mechanism and impact of tenascin-C alternative splicing are still being investigated, although cell type and disease specific difference have been observed (Giblin and Midwood, 2015). Therefore, the impact of the measurement of one alternative splice variant rather than total tenascin-C levels is currently unknown. Some commercial assays do claim to detect all forms of tenascin-C but these are not well described in the literature and in some cases have shown poor assay performance (Giblin, 2018).

5.2 Hypothesis

Tenascin-C, or autoantibodies against tenascin-C, are associated with inflammatory disease, particularly rheumatoid arthritis, and its measurement in the blood could be clinically informative.

5.3 Aims

I. Establish a commercially viable ELISA for measuring anti-citrullinated tenascin-C autoantibodies.

II. Screen control, RA, and other inflammatory disease patient blood samples for citrullinated tenascin-C specific autoantibodies and compare to results obtained with the anti-CCP2 test.

III. Develop and characterise an ELISA for measurement of total tenascin-C, including all splice variants, in human blood samples.

IV. Screen control, RA, and other inflammatory disease patient blood samples to characterise the amount and molecular forms of tenascin-C in human blood under healthy and diseased conditions.

V. Analysis of the diagnostic and prognostic potential of the ELISA tests developed and identify potential clinical utility.

5.4 Materials and methods

Assay development and sample screening was carried out at Axis Shield Diagnostics Ltd alongside principal research scientist Dr Mel Lewis and with supervision from Dr David Pritchard and Dr Jeff Brady.

5.4.1 Patient cohorts

All human blood samples were provided by Axis Shield Diagnostics Ltd and consisted of four main cohorts. The main control sample cohort was lithium heparin plasma samples from 114 healthy Swiss donors. Donors ranged from 19 to 74 years old with a mean age of 49 years. In terms of sex it was composed 40% of males and 60% of females. Additional control samples were provided from Axis Shield's own in-house plasma and serum sample stocks.

For diseased samples the first cohort was of 40 RA patients from Mexico. Patients ranged from 28 to 78 years old with a mean age of 55. In terms of sex it was composed 15% of males and 85% of females. The second cohort was of 190 patients with inflammatory disease from Ipswich, UK. This included 103 RA patients of which 73 were rheumatoid factor (RF) positive and 30 RF negative. Additional non-RA inflammatory disease patients included 9 scleroderma patients, 9 osteoarthritis (OA) patients, 24 psoriatic arthritis patients, 14 ankylosing spondylitis patients, 7 systemic lupus erythematosus (SLE) patients, 4 polymyalgia rheumatic, 6 vasculitis, and 8 suffering from other miscellaneous rheumatic diseases. Patients in this cohort ranged from 12 to 87 years old with a mean age of 58. In terms of sex it was composed 32% of males and 68% of females. Additional RA samples were also provided from Axis Shield's own in-house plasma and serum sample stocks. All samples were collected with informed consent in accordance with local ethical committee guidelines for the collection of research samples from human patients or donors.

5.4.2 cTNC autoantibody ELISA

The final ELISA format used for all sample screening was carried out as described in section 2.8. All cTNC5 screening was carried out with no peptide (streptavidin alone), CCP, and rTNC coating conditions run alongside on the same plate. Data for cTNC is presented as absorbance minus the absorbance value obtained for the rTNC coat. Data

for CCP are presented as absorbance minus the absorbance value obtained for the no peptide coat.

5.4.3 Tenascin-C sandwich ELISA

The final sandwich ELISA, used for all sample screening, was carried out as described in section 2.9 respectively. The final format of a tenascin-C competition ELISA, for which development and sample screening was carried out by Dr Mel Lewis at Axis Shield Diagnostics, is also included as results from this assay will be discussed in this chapter. The competition ELISA was carried out as described in section 2.10. Data are presented as ng/ml of tenascin-C as interpolated from the standard curve included on each plate and corrected for sample dilution factor.

For ELISA assays detection antibodies were either biotinylated or conjugated to HRP. This was carried out by Dr Mel Lewis of Axis Shield Diagnostics, with biotinylation performed as detailed in section 2.12.1 and HRP conjugation carried out using a Lightning-Link HRP conjugation kit (Expedeon, San Diego, USA).

5.4.4 Mass spectrometry

With the assistance of Roslin Proteomics and Metabolomics Facility staff, mass spectrometry was carried out, as described in section 2.13, on tenascin-C IP samples produced as described in section 2.12.2. To account for protein hits produced due to non-specific bead binding a control non-specific IgG IP was analysed for each sample alongside the tenascin-C specific IP for the in solution digested samples. Protein lists between these two were compared and all hits of a similar or higher score in the non-specific IP were filtered out of the tenascin-C IP results. Additional filtering of the lowest scoring protein hits was also carried out to remove low abundance potential contaminants.

5.4.5 Statistical Analysis

Statistical analysis was carried out as described in section 2.14. For the analysis of assay screen results involving multiple groups, significance was determined using the Kruskal-Wallis test with Dunn's post-test for multiple comparisons. For comparisons between just two conditions significance was determined using a Student's t-test for

normally distributed data or Mann-Whitney U test for not normally distributed data. Normal distribution was assessed using the Shapiro Wilk normality test.

5.5 Results

5.5.1 cTNC5 autoantibody ELISA detects IgG and IgA autoantibodies specifically in RA patients

A cTNC5 autoantibody ELISA was developed and optimised wherein biotinylated cTNC5 peptides were immobilised onto streptavidin coated plates and used to capture autoantibodies within patient samples that recognized this epitope. Bound IgG or IgA autoantibodies were detected using HRP conjugated detection antibodies binding to the isotype specific γ heavy chain for IgG or α heavy chain for IgA. The same ELISA format was also optimised for detection of CCP2 autoantibodies for comparative purposes. Non-citrullinated TNC5 (rTNC5) peptide was used as a control for non-specific binding. A schematic of the final ELISA design is shown in Figure 5.1a. The blue colour change of the TMB HRP substrate was measured at 650nm for autoantibody quantification.

As a small pilot study, used to optimize conditions, I screened serum samples in this assay including commercial CCP2 assay standards as positive controls and a healthy donor sample as a negative control. Representative results for the IgG and the IgA assays are shown in Figure 5.1b and 5.1c respectively. For the IgG assay the healthy control sample gives the anticipated negative result with no signal observed in any condition. Both of the positive controls likewise gave their anticipated result for CCP with a strong high and weaker low signal observed. For the test serum samples both the RA samples were CCP positive and neither of the normal sera tested were. Additionally, RA serum sample 2 shows cTNC autoantibody positivity. The result is confirmed with the low background absorbance readings obtained for the no peptide and rTNC control conditions suggesting the binding to CCP and cTNC is specific. For the IgA assay just one positive control RA sera, identified in an earlier screening experiment, was used which again showed its expected strong signal for CCP autoantibodies. In this case the RA serum sample 2 was identified as CCP IgA positive while the RA serum sample 1 and both healthy control samples were negative. None of the samples were found to be cTNC IgA positive in this example.

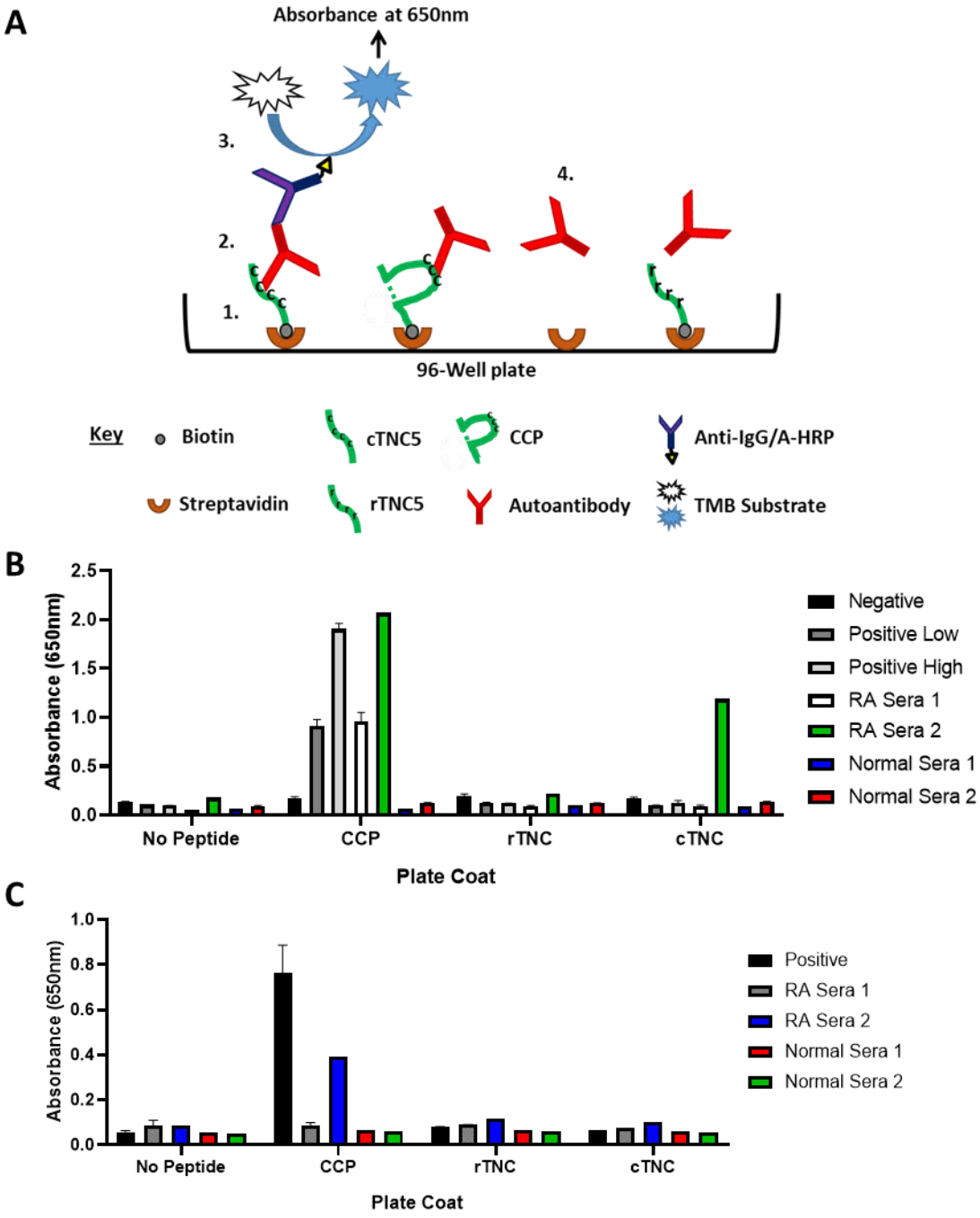

Figure 5.1 Development of a sandwich ELISA for cTNC specific IgG and IgA autoantibodies

(A) A schematic of the cTNC autoantibody ELISA. Biotinylated cTNC5 peptide is captured onto streptavidin coated 96 well plates (1.) and then incubated with diluted sera samples, allowing autoantibodies to bind to the peptide (2.). Autoantibodies are detected using HRP-conjugated detection antibodies against either IgG or IgA combined with TMB for colourimetric detection (3.). CCP peptide and rTNC5 peptides were also tested and a no peptide negative control was included as well (4.).
(B) Representative results of an IgG autoantibody assay and **(C)** an IgA autoantibody assay. Data presented as duplicate mean ± SD.

5.5.2 cTNC5 IgG autoantibodies are specifically detected in RA patients

In total 318 human blood samples were screened in the cTNC5 ELISA including 82 healthy donors, 150 confirmed RA patients, and 86 patients suffering from other rheumatic diseases. Patients with confirmed RA but not those with other rheumatic diseases showed a significant difference in both cTNC, see figure 5.2a, and CCP, see figure 5.2b, autoantibody response compared to the healthy control group. Using an arbitrary absorbance cut off of 0.2, estimated as a lower limit of positive detection for the assay, 14/318 samples were positive in the absence of peptide and 12/318 were rTNC positive. This indicated that the assay was not unduly hindered by non-specific plate or peptide binding and thus the majority of binding observed in the assay can be attributed to the specific recognition of the CCP or cTNC peptides.

Attempts were made to stratify patients based on their cTNC or CCP levels, such as by RF positivity as is shown in figure 5.2c for cTNC and figure 5.2d for CCP. The majority of cTNC positive samples came from the RF+ group with no significant difference compared to healthy controls seen for the for the RF- samples. A similar trend was seen for CCP, although a significant difference was also observed between the RF- samples and the control albeit to a much lesser to degree than for RF+ samples. However, the number of RF- samples was far lower than the RF+ samples within the RA cohort, which may have reduced the power of the analysis.

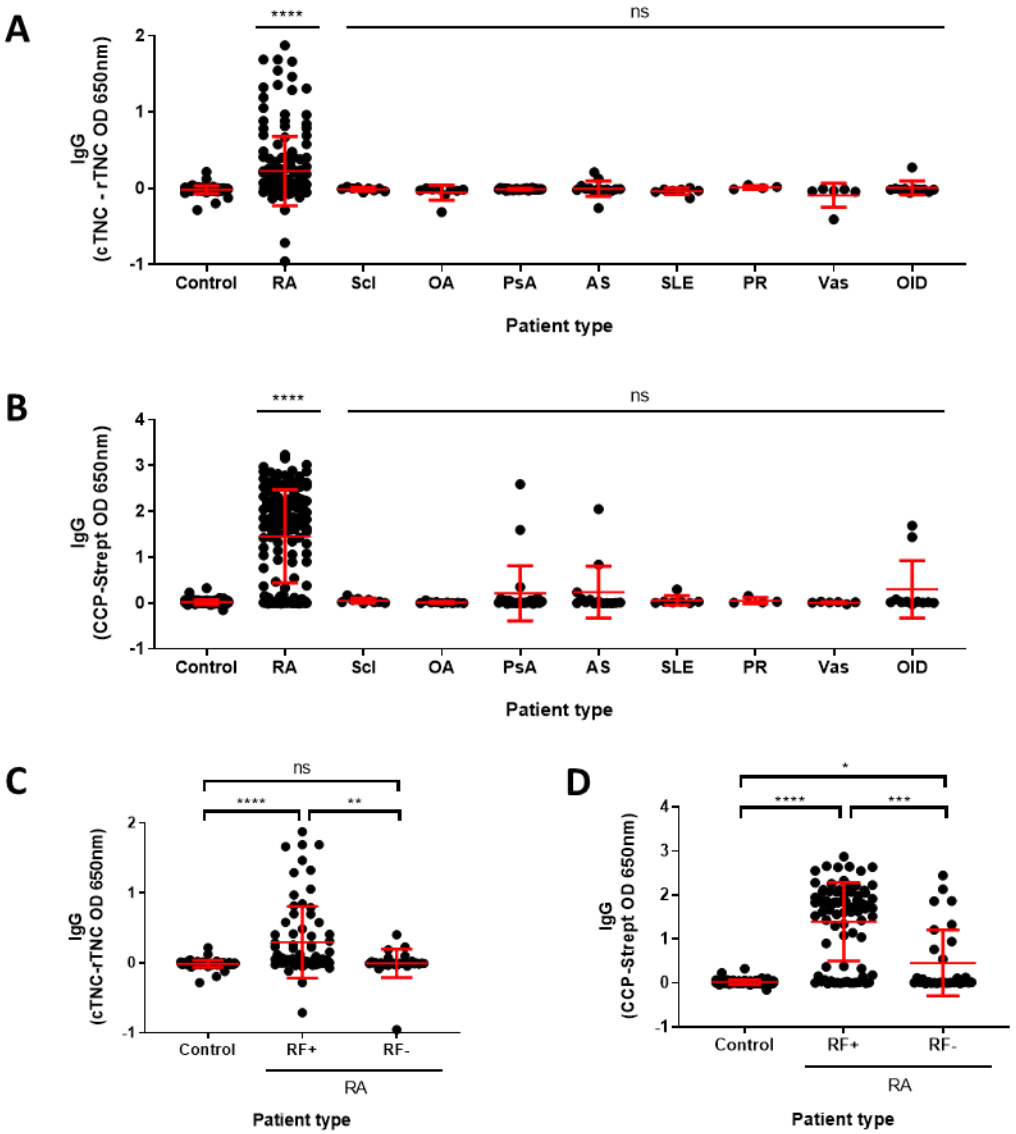

Figure 5.2 The cTNC ELISA detects cTNC specific IgG autoantibodies in RA patients

(A) Human blood samples screened for cTNC specific IgG autoantibodies and **(B)** for CCP specific IgG autoantibodies. Samples came from healthy donors (control) as well as, rheumatoid arthritis (RA), scleroderma (Scl), osteoarthritis (OA), psoriatic arthritis (PsA), ankylosing spondylitis (AS), systemic lupus erythematosus (SLE), polymyalgia rheumatica (PR), vasculitis (Vas) and other inflammatory disease (OID) patients. Data presented as data points representing the mean of the individual sample duplicates overlaid by the group mean ± SD, n: Control = 82, RA = 150, Scl = 9, OA = 9, PsA = 24, AS = 14, SLE = 7, PR = 4, Vas = 6, OID = 11, significance compared to control determined by Kruskal-Wallis test, **** = $p<0.0001$, ns = not significant.
(C) Results of the cTNC and **(D)** CCP IgG autoantibody assays stratified by rheumatoid factor (RF) positivity. Data presented as data points representing the mean of the individual sample duplicates overlaid by the group mean ± SD. n: Control = 82, RF+ = 82, RF- = 30, significance determined by Kruskal-Wallis test, **** = $p<0.0001$, *** = $p<0.001$, ** = $p<0.01$, * = $p<0.05$, ns = not significant.

5.5.3 cTNC5 IgG autoantibodies are less sensitive than CCP autoantibodies for diagnosis of RA

With the established tests able to robustly detect cTNC autoantibodies, further analysis was carried out to test its diagnostic ability. To do this the cTNC and CCP assay results were subject to receiver operating characteristic (ROC) curve analysis to determine whether they could discriminate between the RA patient cohort and the healthy donor controls, the results of which are shown in figure 5.3a. Both the cTNC and CCP assays could significantly discriminate healthy samples from RA patients with area under the curve (AUC) values of 0.7933 (95% CI 0.7355 to 0.8510) for cTNC and 0.8851 (95% CI 0.8432 to 0.9270) for CCP which were both significantly different from the no discrimination value of 0.5. However, as the higher AUC value would suggest the CCP test was more sensitive than the cTNC assay, with the sensitivities of the assays using a 95% specificity cut off being 78.7% (95% CI 71.44% to 84.46%) and 52% (95% CI 44.06% to 59.84%) for CCP and cTNC respectively. This translated into 77/150 (51.3%) RA patients testing positive for cTNC specific IgG autoantibodies and 110/150 (73.3%) for CCP IgG autoantibodies. This gave the cTNC assay a likelihood ratio of 10.66, indicating that a patient with a positive result was 10.66 times more likely to have RA than someone with a negative result. For the CCP assay the likelihood ratio was 16.13.

In clinical practice, a diagnostic test for RA must identify patients with RA from those with other rheumatic diseases with similar clinical disease presentation. As such, these analyses of ideal conditions, comparing confirmed RA patients with healthy controls, is not truly reflective of clinical practice. To this end a further ROC analysis was carried out to compare the cTNC5 ELISAs ability to discriminate between the RA patient cohort and a non-RA group which combined the healthy control results with those obtained from patients suffering from a variety of rheumatic diseases. The results of this analysis are shown in figure 5.3b. Under these conditions both tests can still significantly discriminate the RA patients from the non-RA group. However, as might be expected a drop in diagnostic ability is observed with AUC values of 0.7927 (95% CI 0.7392 to 0.8461) and 0.8586 (95% CI 0.8146 to 0.9026) for cTNC and CCP respectively. Furthermore, the CCP test is still more sensitive than the cTNC assay with a sensitivity of 73.3% (95% CI 65.74% to 79.76%) as opposed to 51.33% (95%

CI 43.40% to 59.20%) when using a 95% specificity cut off. This gave the cTNC assay a likelihood ratio of 10.65 while the CCP assay had a likelihood ratio of 15.49. A summary of the results for all samples tested, broken down by disease type and cohort, along with the percentage testing positives using these cut offs is shown in table 5.1 below.

As multiple tests are usually employed to confirm an RA diagnosis it was next assessed whether the addition of cTNC alongside CCP for diagnosis had any additional benefit. Assigning cTNC and CCP positivity based on the 95% specificity cut off limit determined by the RA versus non-RA ROC curve analysis 110/150 (73.3%) of RA patients were correctly diagnosed by the CCP assay and 77/150 (51.3%) by the cTNC assay. No incremental benefit was seen with addition of the cTNC assay alongside the CCP assay with all cTNC positive RA patients in the cohorts also being CCP positive.

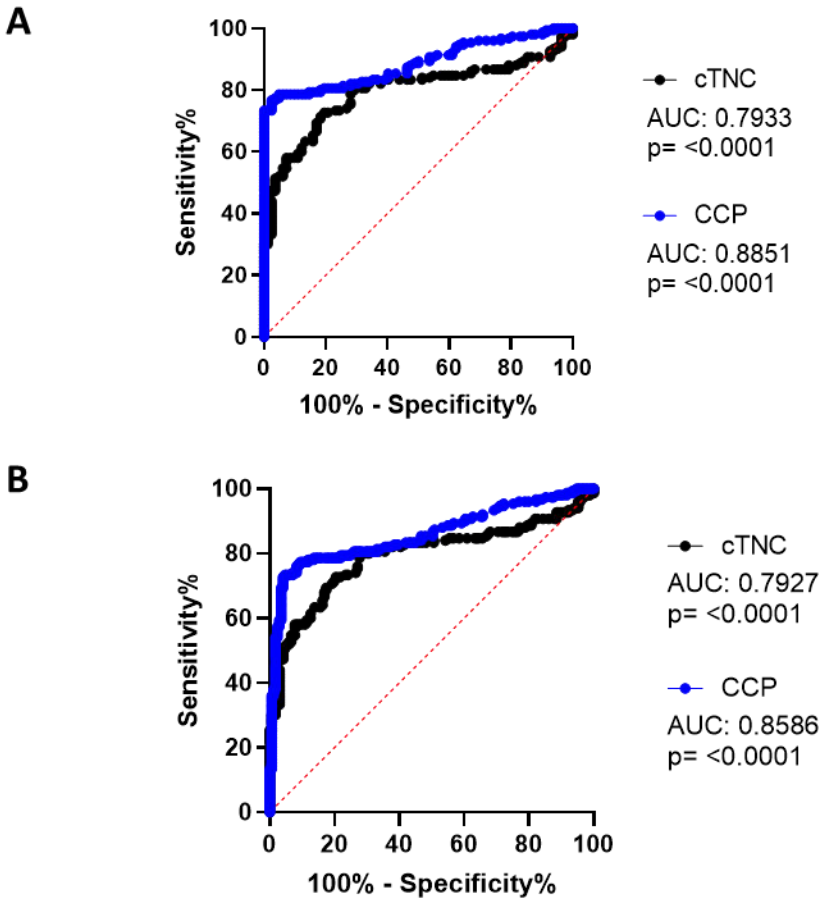

Figure 5.3 cTNC is able to discriminate RA patients from healthy controls and other inflammatory diseases but is less sensitive than CCP

(A) Receiver operating characteristics (ROC) curve analysis for the diagnosis of RA patients (n=150) versus solely healthy controls (n=82) or **(B)** healthy controls and patients with non-RA rheumatic diseases (n=169) using either the cTNC5 or CCP IgG autoantibody ELISAs. Data are presented as percentage sensitivity and specificity. Red dotted lines indicate no discrimination. Area under the curve (AUC) values and p values testing significance of curves from no discrimination are given.

Table 5.1: Summary of CCP and cTNC assay screening results. Patients classified as positive for cTNC5 or CCP based on ROC curve analysis to obtain a cut off giving 95% specificity of the assay. Early synovitis was not used for any of the non-RA grouped analysis due to the lack of definitive diagnosis. Significance was calculated compared to healthy donor controls using the Kruskal-Wallis test, ns = not significant. For groups with low n numbers significance was not determine (-).

		cTNC5		CCP	
Group	**n**	**Positive (%)**	**p value**	**Positive (%)**	**p value**
Healthy donors	82	3 (3.7)		0 (0)	
Rheumatoid arthritis	150	77 (51.3)	<0.0001	110 (73.3)	<0.0001
Ipswich RF+	73	44 (60.3)	<0.0001	61 (83.6)	<0.0001
Ipswich RF-	30	5 (16.7)	ns	9 (30.0)	ns
Mexico	40	28 (70.0)	<0.0001	40 (100.0)	<0.0001
Other	7	0 (0.0)	ns	0 (0.0)	ns
Scleroderma	9	0 (0.0)	ns	0 (0.0)	ns
Osteoarthritis	8	0 (0.0)	ns	0 (0.0)	ns
Psoriatic arthritis	23	0 (0.0)	ns	3 (12.5)	ns
Ankylosing spondylitis	14	3 (21.4)	ns	2 (14.3)	ns
SLE	7	0 (0.0)	ns	0 (0.0)	ns
PR	4	1 (25.0)	ns	0 (0.0)	ns
Vasculitis	6	0 (0.0)	ns	0 (0.0)	ns
OID	11	2 (18.2)	ns	2 (18.2)	ns
Sjögren's syndrome	2	1 (50.0)	-	1 (50.0)	-
Dermatomyositis	2	0 (0.0)	-	0 (0.0)	-
Polymyositis	1	0 (0.0)	-	0 (0.0)	-
Fibromyalgia	2	0 (0.0)	-	0 (0.0)	-
JIA	2	0 (0.0)	-	1 (50.0)	-
Reactive arthritis	1	0 (0.0)	-	0 (0.0)	-
Sarcoidosis	1	0 (0.0)	-	0 (0.0)	-
Early synovitis	3	1 (33.3)	-	1 (33.3)	-
Non-RA diseased (all)	86	8 (9.3)	ns	6 (7.0)	ns
Non-RA (all)	168	11 (6.6)		6 (3.6)	

AS, ankylosing spondylitis; SLE, systemic lupus erythematosus; PR, polymyalgia rheumatica; OID, other inflammatory disease; JIA, Juvenile idiopathic arthritis.

5.5.4 cTNC5 IgA autoantibodies are present in a fraction of RA patients

IgG autoantibodies are the main isotype detected for most ACPA tests, although other isotypes have also been studied including IgA. In common with other citrillunated peptide autoantigens the cTNC5 ELISA was also able to detect cTNC5 specific IgA autoantibodies in RA serum samples. This is shown in figure 5.4a where a significant difference in cTNC5 IgA autoantibody levels is shown between the RA and healthy donor groups. Similar to previous results in the literature (Verpoort et al., 2006), a subgroup of patients were also identified in the cohorts tested that had CCP specific IgA autoantibodies. This is shown in figure 5.4b where like for cTNC a significant difference between the RA and healthy donor group was found.

Based on the average background reading of 0.06 (StdDev ± 0.02) an arbitrary cut off of 0.10 for CCP-streptavidin and cTNC-rTNC absorbance readings was set to determine autoantibody positivity. For the RA serums this resulted in 53/112 (47.3%) testing positive for CCP specific IgA autoantibodies and 5/112 (4.5%) for cTNC IgA autoantibodies. IgA anti-cTNC or CCP autoantibodies were not detected in any of the healthy controls tested (0/33). As for the IgG autoantibodies stratification was also attempted by RF status. For CCP most of the positive samples came from the RF+ patients with no significant difference observed between the RF- patients and controls. In total 49/53 of the CCP IgA autoantibody samples were RF positive whilst only 4/53 were RF negative. No trends were observed with the cTNC assay which was unsurprising given the low number of positives detected overall. All 5 cTNC specific IgA positive samples were RF positive as well as positive for CCP specific IgA autoantibodies.

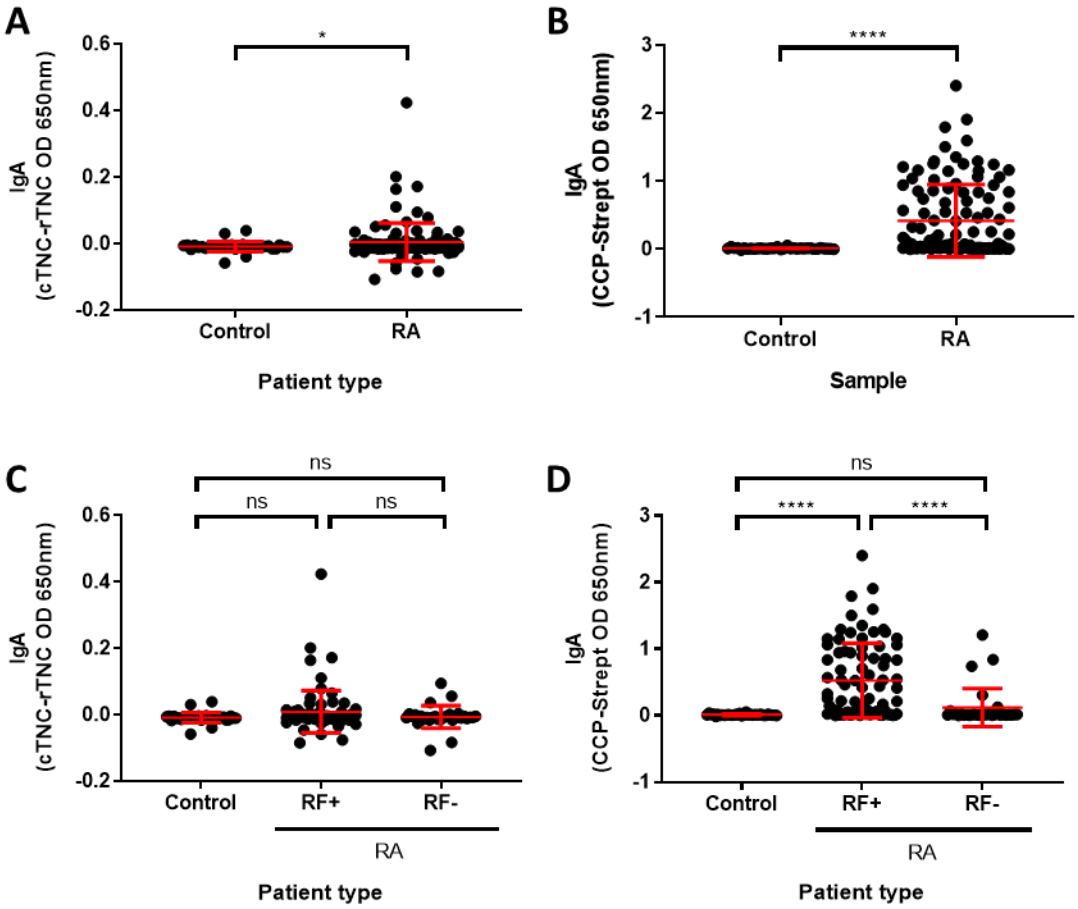

Figure 5.4 The cTNC ELISA detects cTNC specific IgA autoantibodies in RA patients

(A) Human blood samples screened for cTNC specific IgA autoantibodies and **(B)** for CCP specific IgA autoantibodies. Samples came from healthy donors (control) and rheumatoid arthritis (RA) patients. Data presented as data points representing the mean of the individual sample's technical duplicate overlaid by the group mean ± SD. n: Control = 33, RA = 112, significance determined by Mann-Whitney U test, **** = $p<0.0001$, * = $p<0.05$,
(C) Results of the cTNC and **(D)** CCP IgG autoantibody assays stratified by rheumatoid factor (RF) positivity.
Data presented as data points representing the mean of the individual sample's technical duplicate overlaid by the group mean ± SD. n: Control = 33, RF+ = 82, RF- = 30, significance determined by Kruskal-Wallis test, **** = $p<0.0001$, ns = not significant.

5.5.5 Antibody selection for total tenascin-C ELISAs

In addition to the autoantibody ELISAs, development of an assay to measure tenascin-C protein levels in human blood samples was also carried out. In aid of this, a review of a range of a range of commercially available anti-tenascin-C antibodies was carried out by Tara Kayser and Dr Mel Lewis of Axis Shield Diagnostics. Details of the antibodies identified are summarised in table 5.2.

Table 5.2: Summary of the commercially available antibodies identified for the detection of tenascin-C

Antibody	Supplier	Species & isotype	Immunogen	Epitope	Reference
19C4MS	IBL	Mouse IgG1κ	Recombinant FNIII A4-D	FNIIIC	(Hasegawa et al., 2004)
4C8MS	IBL	Mouse IgG1κ	Recombinant FNIII A4-D	FNIIIB	(Imanaka-Yoshida et al., 2002)
4F10TT	IBL	Mouse IgG1	Purified glioma cell line tenascin-C	EGF-like repeats	(Tsunoda et al., 2003)
4F8	Merck Millipore	Mouse IgG1κ	Unknown	FNIII 4-5	-
9F8	Merck Millipore	Mouse IgG1κ	Unknown	FNIII 1-3	(Ljubimov et al., 1998)
NSCT-121	Nascient	Human IgG4κ	Recombinant FBG	FBG	(Aungier et al., 2019)
BC-24	Sigma-Aldrich	Mouse IgG1	Purified melanoma cell line tenascin-C	EGF-like repeats	(Siri et al., 1991)
DB7	Merck Millipore	Mouse IgG2a	Purified foetal fibroblast tenascin-C	FBG	(Tiitta et al., 1992)
EB2	Abcam	Mouse IgG1	Purified foetal fibroblast tenascin-C	FNIII 4-5	(Tervo et al., 1989)
EPR4219	Abcam	Rabbit IgG	Recombinant FBG derived peptide	FBG	-
T2H5	Abcam	Mouse IgG1	Human mammary tumour homogenate	unknown	(Verstraeten et al., 1992)

After identifying available antibodies, a selection was screened for their compatibility to detect tenascin-C in a 96 well plate sandwich ELISA format. As part of this initial antibody screen two methods of detection, conjugation of detection antibody to HRP

or biotinylation of detection antibody with utilisation of HRP-conjugated streptavidin as a secondary detection reagent, were also evaluated. The results of this testing are summarised in table 5.3. Antibodies were ranked on an arbitrary scale on their ability to specifically detect purified tenascin-C.

Table 5.3: Summary of antibody pair screening results. Antibody pairings were ranked on an arbitrary scale, indicated below, based on the specific absorbance signal they produced detecting purified tenascin-C. Some pairings were not tested and are marked as not determined. The results for the 4F10TT with 4C8MS and 19C4MS pairings reflect those obtained using commercial kits by IBL. The 9F8 and EPR4219 antibody screens were carried out by myself while all other antibody pair screening was carried out by Tara Kayser and Dr Mel Lewis.

Scale:	Not determined ND	No reactivity -	V. weak reactivity -/+	Weak reactivity +	Mild reactivity ++	Strong reactivity +++	V. strong reactivity ++++

	Detection (HRP or biotin conjugated)							
Capture	NSCT121 -HRP	NSCT121 -bio	9F8-HRP	4F10TT-HRP	T2H5-HRP	DB7-HRP	4C8MS-HRP	EPR4219 -HRP
NSCT121	-	-	++	++++	-	-	+/-	-
9F8	++	+++	-	++++	-	-	-	-
4F10TT	+	++	-	+	-	-	-	ND
T2H5	++	ND	+/-	ND	-	-	-	ND
DB7	+	ND	+/-	ND	-	-	+/-	ND
4C8MS	++	ND	+/-	++++ (kit)	-	-	-	ND
EPR4219	ND	-/+	+	ND	ND	ND	ND	ND
19C4MS	ND	+	ND	++++ (kit)	ND	ND	ND	ND

As the aim of this study was to create an assay detecting all isoforms of tenascin-C, selection of antibodies based on the epitope they recognised was critically important. Figure 5.5 summarises published or supplier data mapping the antibodies to the domains they recognise. This shows that the majority of the antibodies tested recognise conserved epitopes and thus could potentially be used in the total tenascin-C assay. The only two antibodies ruled out were 4C8MS and 19C4MS which recognised the alternatively spliced FNIII repeats B and C respectively.

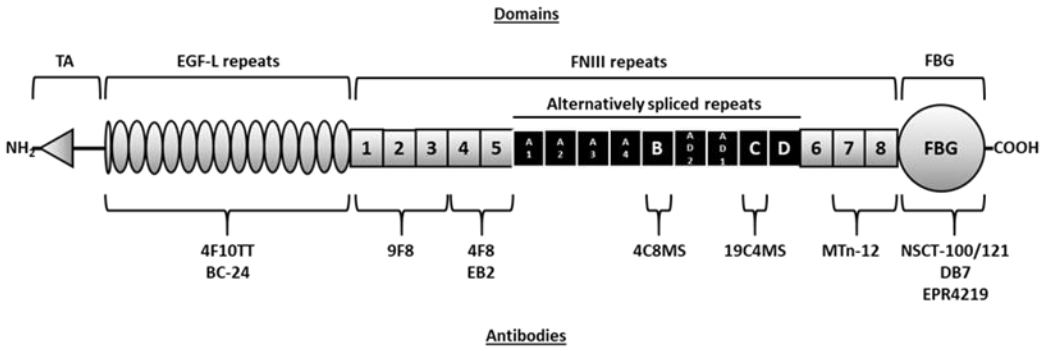

Figure 5.5 Epitopes recognised by anti-tenascin-C antibodies

A diagrammatic representation of a human tenascin-C monomer with the tenascin assembly (TA), epidermal growth factor-like (EGF-L) repeats, fibronectin type III-like (FNIII) repeats, and fibrinogen globe (FBG) domains indicated. A variety of commercially available antibodies and the regions they recognise are indicated below. The MTn-12 antibody is included for reference despite only recognising murine and not human tenascin-C.

Due to its availability, as a kind gift from Nascient Ltd, and based on the screening results showing its robustness, working in the most pairings in detection or capture roles, the NSCT-121 antibody was selected for further use. Furthermore, due to its greater availability at a high concentration, which would aid in conjugation reactions, it was also decided that NSCT-121 would be used as the detection antibody in the prospective pairing. In picking a capture antibody to pair with it a number of factors were considered which resulted in the final selection of the 9F8 antibody. These factors included the good performance of the pairing, which showed it to be one of the more sensitive and low background pairings for the detection of tenascin-C. Additionally, the 9F8 antibody proved economically favourable as it was available in bulk from the supplier Merck Millipore and at a price that was cost efficient to allow for maximal sample screening. This pairing would also, as aimed, detect total tenascin-C levels as the epitopes for both antibodies, in the FBG domain for NSCT-121 and the FNIII repeats 1-3 for 9F8, are constitutive domains and thus should be present in all forms of tenascin-C regardless of alternative splicing.

Further work was carried out to verify the specificity of the NSCT-121 antibody. Purified tenascin-C or fibrinogen were coated onto 96 well plate wells and blocked with 2% BSA. The biotinylated antibody was titrated against it, from 50 to 0.78ng/ml, and detected with streptavidin-HRP. Fibrinogen was chosen as an appropriate non-specific protein as NSCT-121 recognises the fibrinogen like globe (FBG) domain of tenascin-C which shares homology with terminal globular domains of fibrinogen (Doolittle, 1992). As such, it was essential to rule out cross-reactivity with this serum protein. The results of this assay, shown in figure 5.6a, show that NSCT-121 was able to detect tenascin-C at low ng/ml concentrations without any cross reactivity with fibrinogen. Further work was then carried out to develop the final sandwich assay, schematically outlined in figure 5.6b and methodologically described in section 2.9.

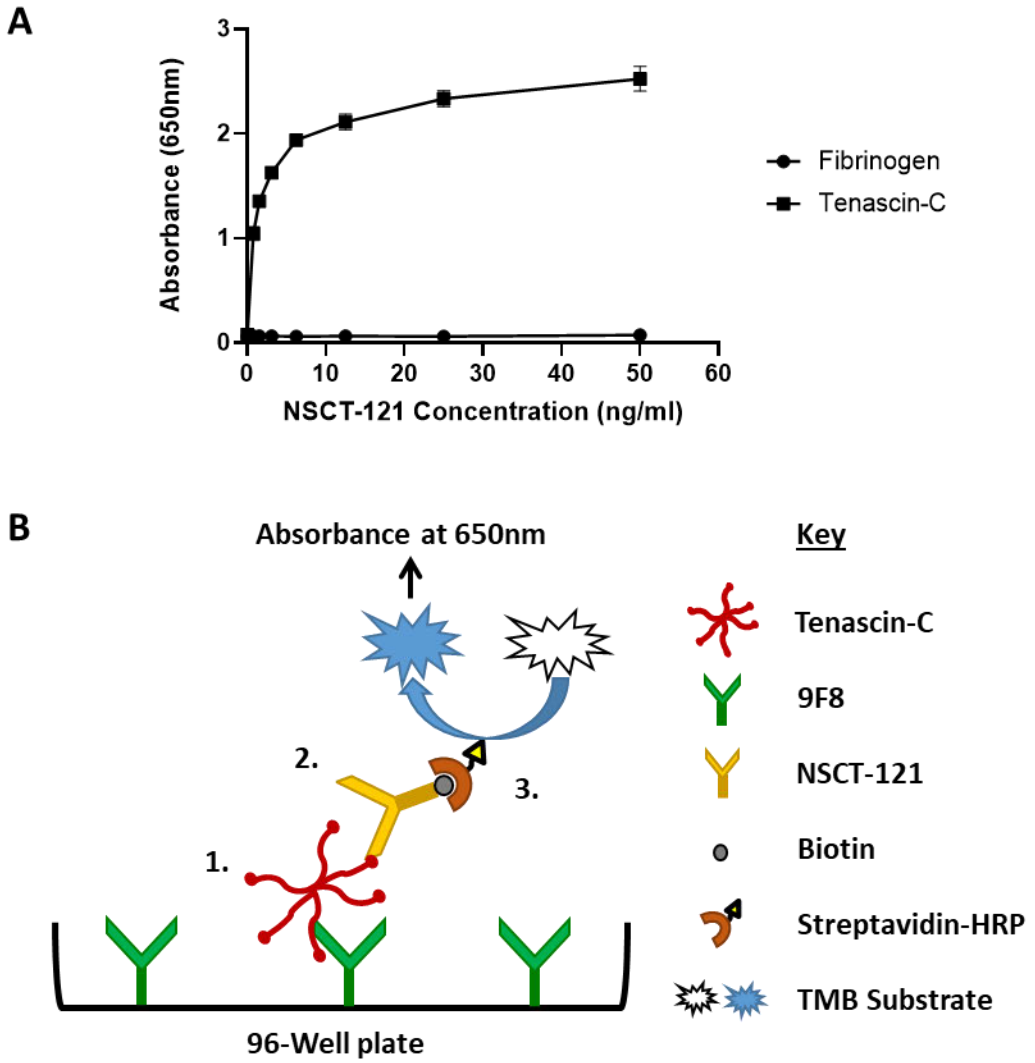

Figure 5.6 The 9F8 and NSCT-121 antibodies specifically recognise human tenascin-C

(A) Titration of the biotinylated NSCT-121 antibody using 96 well plates coated with 1µg/ml of human tenascin-C or fibrinogen, showing strong and no antibody binding respectively. Data presented as duplicate mean ± SD.
(B) A schematic of the final 9F8-NSCT-121 tenascin-C sandwich ELISA. Sample is incubated on 96 well plates coated with 9F8 which binds to the 1-3 FNIII repeat region, of tenascin-C (1.). Bound tenascin-C is then detected using the tenascin-C FBG domain specific NSCT-121 biotinylated antibody (2.) which is then detected using a streptavidin-HRP with TMB substrate solution detection system (3.).

5.5.6 9F8-NSCT-121 tenascin-C sandwich ELISA validation

The tenascin-C sandwich assay was then evaluated for detection of tenascin-C in serum samples. First, serum samples with or without 50 ng/ml purified tenascin-C added, were tested in a 'swap out' experiment. This involved systematically removing or replacing components of the assay with non-specific reagents, to ensure that signal obtained from tenascin-C spiked serum samples was specific and not the consequence of non-specific binding of the serum matrix. The results of this assay, shown in figure 5.7a, demonstrate that a signal above background was observed only when both tenascin-C specific antibodies were used in the presence of tenascin-C spiked serum, tenascin-C prepared in buffer or serum on its own. This indicates that the assay specifically recognises the exogenous purified tenascin-C spiked into the samples, as well as endogenous tenascin-C present in the serum samples. No signal was detectable when using either NSCT-121 or 9F8 in combination with a non-specific IgG, and no reactivity with any other component of the assay, including plate or block, was detected. Additionally, the spike-recovery component of the assay also showed analyte recovery was not affected by the serum matrix. This was evident as compared to 50ng/ml purified tenascin-C in buffer alone recovery of tenascin-C from the spiked 1/50 and 1/100 diluted serum was calculated as 98.5% ± 2.9% and 106.3% ± 4.2% respectively. This approximately 100% recovery for both dilutions demonstrates that the assay is not significantly affected adversely by the non-tenascin-C components of the serum which make up the sample matrix in the assay along with the diluent.

In order to confirm that basal levels of tenascin-C observed in normal serum samples was the result of specific detection, normal serum samples were subject to a tenascin-C depletion step prior to analysis in the tenascin-C ELISA. Samples were either prepared as normal or were preincubated in 96-well plates coated with tenascin-C specific NSCT-121 or a non-specific IgG. The result of this experiment, shown in figure 5.7b, demonstrated that pre-incubation with NSCT-121 resulted in a reduction in signal compared to the untreated control, whilst only a slight decrease was seen in samples pre-adsorbed with non-specific IgG. This suggested that signal obtained from normal serum samples in the tenascin-C sandwich ELISA was the result of a basal level of tenascin-C which could be depleted through pre-adsorption with tenascin-C specific antibody.

A third antibody-based inhibition assay was carried out as a final validation of tenascin-C sandwich assay specificity. Unlabelled 9F8, NSCT-121, or non-specific IgG were titrated into the assay samples in a concentration range from 5 to 0.07ng/ml. The result shown in figure 5.7c, showed that 9F8 and NSCT-121 dose-dependently reduced absorbance signal for both serum samples and buffer spiked with tenascin-C, whereas non-specific IgG had no effect on any of the samples tested. This strongly suggests that signal obtained in the tenascin-C sandwich assay was the result of specific binding of 9F8 and NSCT-121 to tenascin-C.

Overall, the assays described above robustly demonstrate that the tenascin-C sandwich ELISA specifically recognises tenascin-C in tenascin-C spiked buffer and serum samples and that pooled serum from normal individuals contains a basal level of tenascin-C.

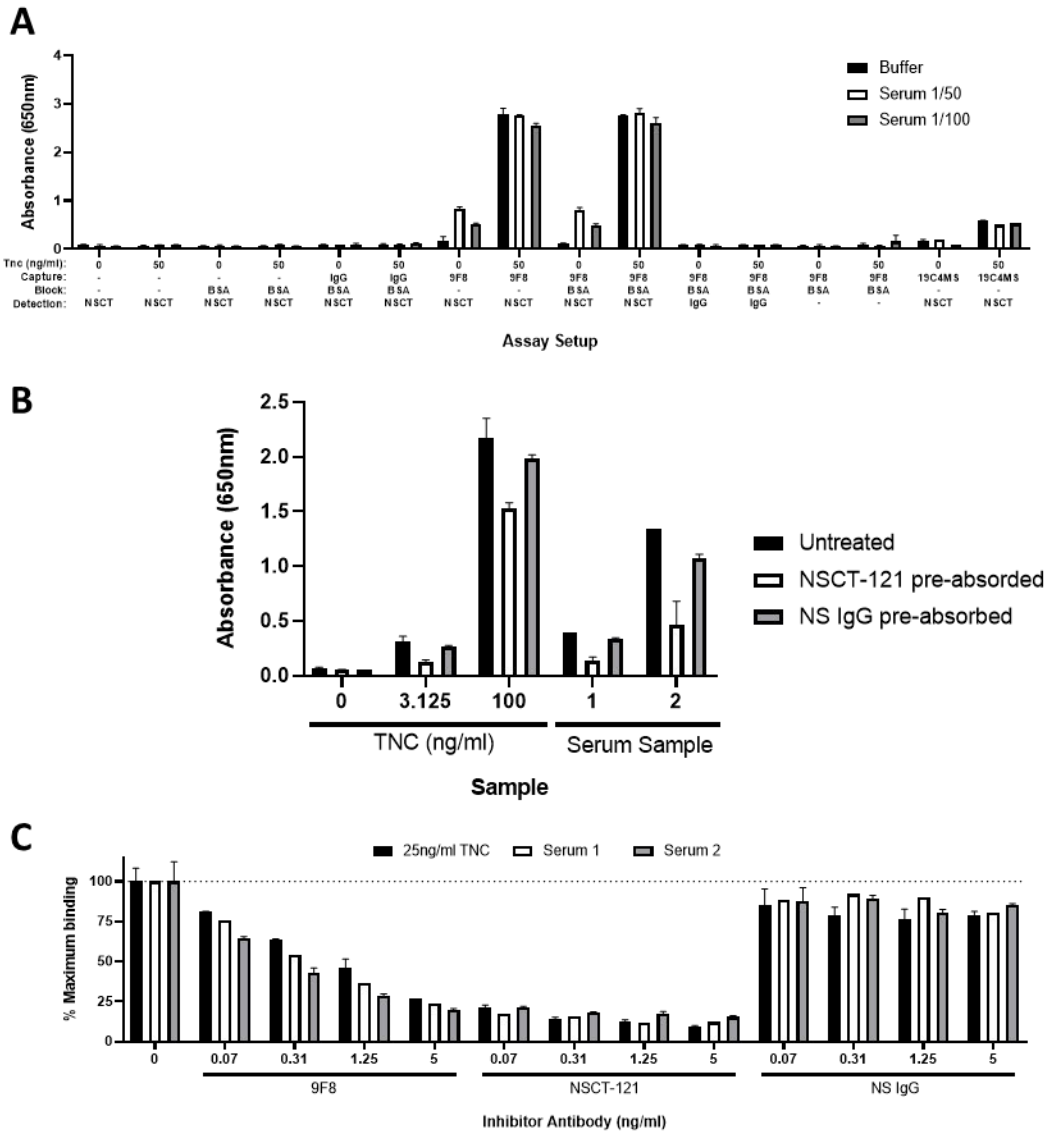

Figure 5.7 The 9F8-NSCT121 sandwich ELISA specifically recognises tenascin-C in human serum samples

(A) Swap out experiment where different components of the 9F8-NSCT121 sandwich ELISA were removed or swapped out to identify the source of the positive signal observed in the assay. Only when tenascin-C specific capture and detection antibodies are paired is a specific signal observed. Data presented as duplicate mean ± SD.
(B) Pre-absorbtion experiment where sandwich ELISA samples were run as normal or with pre-incubation on plates coated with either tenascin-C specific NSCT-121 or non-specific IgG (NS IgG). Pre-absorbtion with NSCT-121 results in a reduction in signal compared to both the non-preabsorbed and the NS IgG pre-absorbed samples. Data presented as duplicate mean ± SD.
(C) Antibody competitor experiment whereby samples were either run as normal or in the presence of unlabelled competitor antibodies at the indicated concentrations. Only the tenascin-C specific 9F8 or NSCT121 antibodies abrogated recognition of tenascin-C in the serum samples or purified tenascin-C control, with addition of the NS IgG having little affect. Data calculated as percentage inhibition with the no inhibitor control set as 100%. Data presented as duplicate mean ± SD.

5.5.7 Tenascin-C sandwich ELISA characterisation

Next, the sensitivity and dynamic range of the assay was assessed with a titration of purified tenascin-C from 100ng/ml to 0ng/ml, shown in figure 5.8a. A lower limit of detection of 0.78ng/ml was determined beyond which the tenascin-C dilutions were not reliably distinguishable from background levels. The linear dynamic range was determined to be between 0.78 to 50ng/ml and this was chosen as the concentration range for the assay standard curve going forward. From standard curves run across a number of plates an average signal to noise ratio of 29:1 was calculated by dividing the absorbance signal of the highest standard by the background buffer only readings.

The sample dilution factor for the assay was also assessed to ensure samples would fall within the standard curve range and to mitigate any matrix effects. To do this a selection of normal serums containing varying basal levels of tenascin-C were serially diluted from 1/50 to 1/6400, the results for which are shown in figure 5.8b. Serum samples showed reasonable linearity of dilution and all fell below the 25ng/ml standard at a 1/50 dilution. As it had been used in previous optimisation it was thus determined that 1/200 was an appropriate sample dilution factor for the assay.

As well as sample dilution, blood sample tube type was assessed. Work so far had utilised serum samples, which are produced by allowing the blood sample to clot before removing the clot and cells by centrifugation. However, plasma samples, to which anti-coagulation factors are added on sample collection to prevent clotting before centrifugation to remove cells, were also available. Several different anti-coagulants exist with some of the most common including lithium heparin and EDTA. Separator tubes, containing a gel which prevents the cell pellet from mixing with the supernatant after centrifugation, also exist for both plasma and serum samples. These sample types can potentially impact assay results and thus screening was carried out of a selection of normal serums of different blood tube types to determine if any affects were observable. The results of this screen are shown in figure 5.8c and demonstrate that for all the tube types tested no significant difference in levels or distribution of tenascin-C were seen. Thus, tube type does not appear to significantly affect or confound tenascin-C detection by the assay.

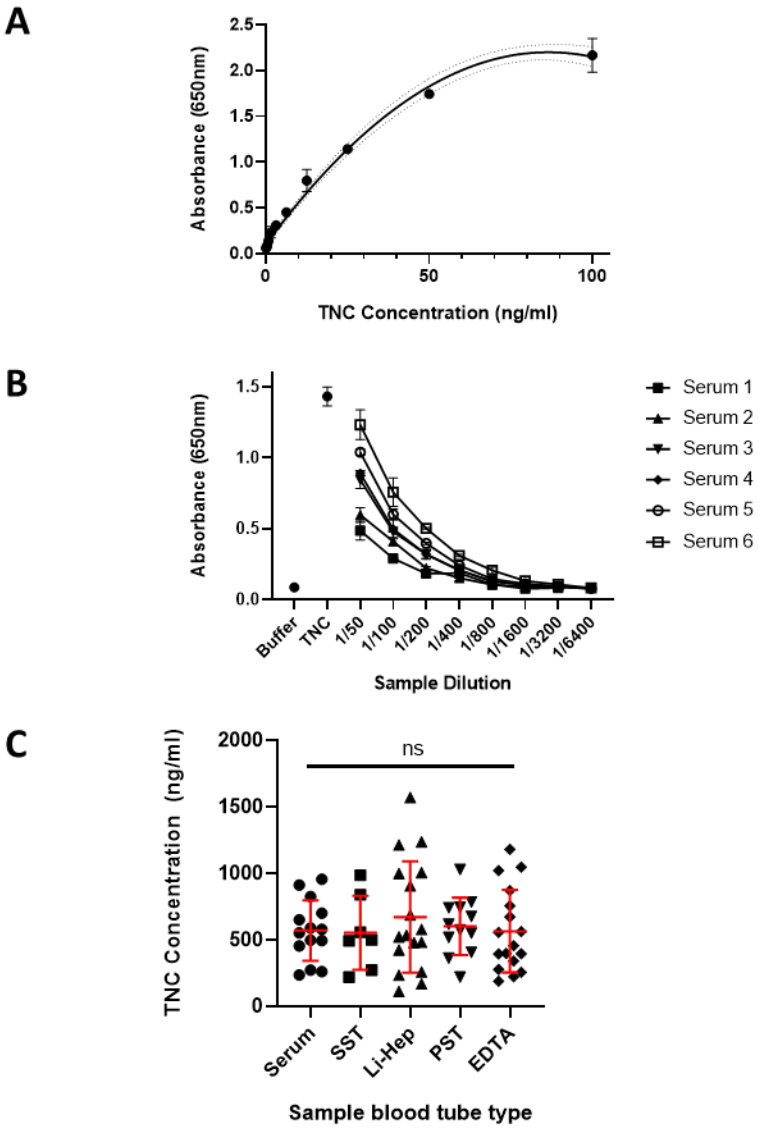

Figure 5.8 The 9F8-NSCT121 sandwich ELISA is sensitive and robust for detecting tenascin-C in human serum.

(**A**) An extended standard curve for the 9F8-NSCT121 sandwich ELISA showing detection of purified tenascin-C from 0 to 100ng/ml. A linear dynamic range is observed between 0.78ng/ml to 50ng/ml. Data presented as duplicate mean ± SD, dotted lines represent the 95% confidence limits.
(B) Titration of 6 normal donor control serums in the 9F8-NSCT121 sandwich ELISA to demonstrate dilution linearity. Buffer alone and 25ng/ml purified tenascin-C were used as negative and positive controls respectively. Data presented as duplicate mean ± SD.
(C) Normal healthy donor samples were collected using different blood tube types, including serum (n=7), serum separator tube (SST; n=7), lithium heparin plasma (Li-Hep; n=17), plasma separator tube (PST; n=12), and EDTA plasma (n=17). Results show a similar mean and distribution suggesting that blood tube type does not impact the assay. Data presented as data points representing the mean of the individual sample's duplicate overlaid by the group mean ± SD. Significance assessed by one-way ANOVA with Tukey's Multiple comparisons test, ns = not significant.

Having shown good performance with human serum samples the ELISA was also tested for its compatibility for use with murine serum samples collected from the colitis experiments covered in chapters 3 and 4. However, murine serum diluted at the assay standard 1/200 or at 1/100, from both colitic and control mice, failed to produce a signal above background and was comparable to readings obtained for serum from *Tnc*$^{-/-}$ mice. This result was not entirely unexpected as the 9F8 capture antibody utilised in the assay was generated using human tenascin-C in a murine host. It is therefore unlikely that antibodies cross-reactive with murine tenascin-C would have been generated due to their autoreactivity to the host. In line with this the supplier did not recommend its use for the detection of murine tenascin-C with detection of human tenascin-C is only validated use.

Alongside development of the tenascin-C sandwich assay carried out by myself a tenascin-C competition ELISA was also developed by Dr Mel Lewis at Axis Shield Diagnostics. A representative standard curve and the diagrammatic representation of the format of the assay are shown in figure 5.9a and 5.9b. In brief this competition assay involved the pre-mixing of labelled NSCT-121 and diluted sample before applying it to a recombinant FBG domain coated plate. Any tenascin-C in the sample would bind the tenascin-C during the pre-incubation and thus block its binding to the FBG domain on the plate. Thus, detection of the labelled NSCT-121 on the plate would provide an inverse readout of the amount of tenascin-C in the sample which the exact concentration of which could be calculated by utilising a standard curve of purified tenascin-C as in the sandwich ELISA. As this competition format of assay only utilises the binding of one antibody it can potentially detect distinct forms of tenascin-C, such as those in which the FBG domain and FNIII-repeat domains 1-3 have become detached, from the sandwich ELISA. As such, for comparative purposes the results from the screening of patient cohorts with this assay, also carried out by Dr Mel Lewis, are included for analysis in the sections below.

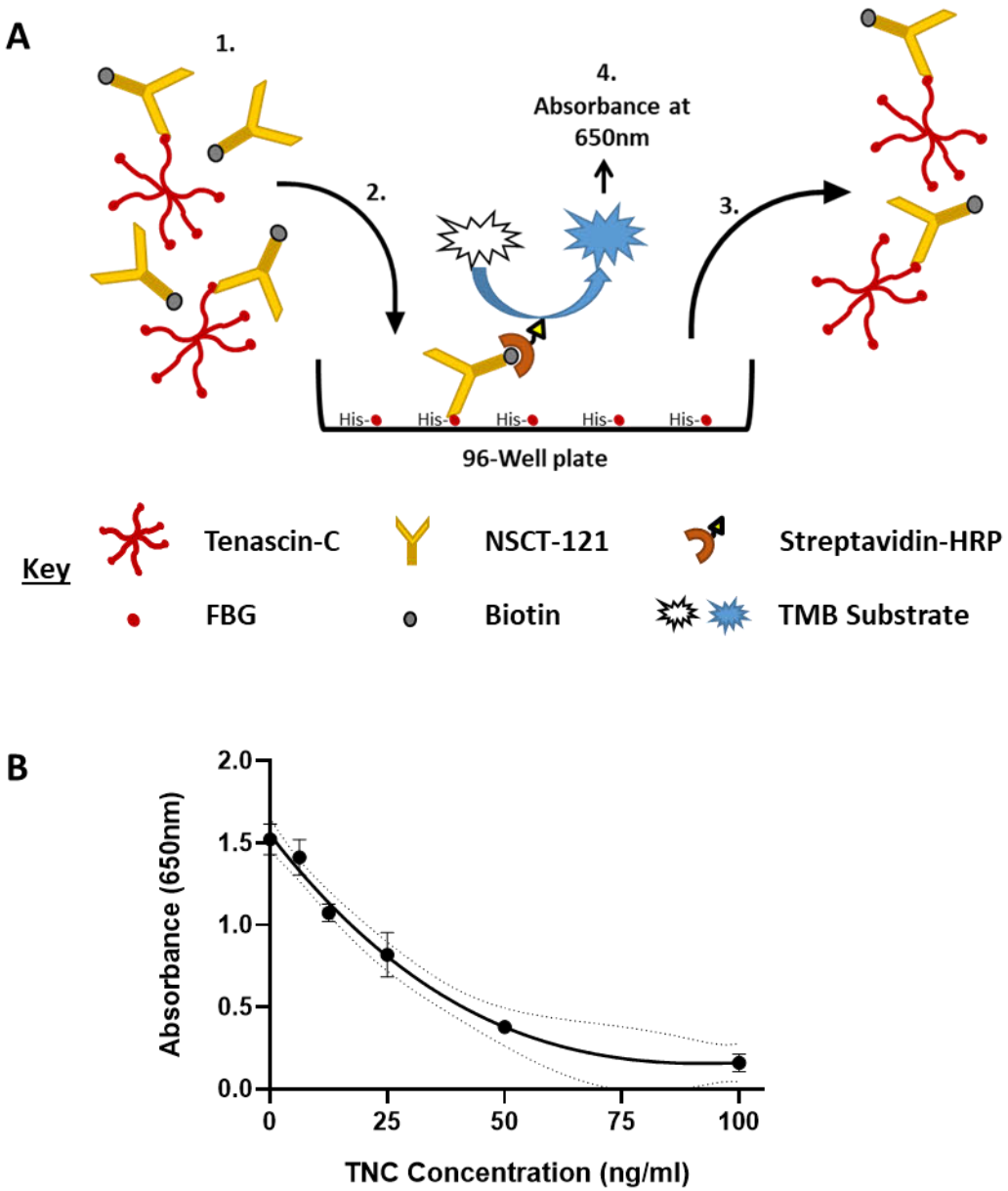

Figure 5.9 Tenascin-C competition ELISA schematic outline and representative standard curve demonstrating sensitivity

(A) The his-FBG coat format involved coating 96 well plates with recombinant his-tagged tenascin-C FBG domain. Samples were then pre-incubated with the biotinylated NSCT-121 detection antibody which recognises the FBG domain (1.). Following pre-incubation the sample is applied to the plate which free NSCT-121 binds to (2.). NSCT-121 bound to tenascin-C in the sample does not bind to the plate and is washed away (3.) and thus the amount of NSCT-121 bound to the plate is inversely proportional to the amount of tenascin-C in the sample. Plate bound NSCT-121 is detected with a streptavidin-HRP and TMB substrate system for colourimetric detection (4.).
(B) A representative standard curve from the competition ELISA ranging from 0ng/ml to 100ng/ml purified tenascin-C. Data presented as duplicate mean ± SD, dotted lines represent the 95% confidence limits.

5.5.8 Total serum tenascin-C is significantly elevated in RA patient blood samples

The tenascin-C sandwich ELISA was used to screen control, RA, and inflammatory diseased serum samples with the results shown in figure 5.10a. Results obtained from the screening the same cohorts with the tenascin-C competition ELISA, carried out by Dr Mel Lewis, are shown in figure 5.10b for comparison. Results for both assays are also summarised in table 5.4. Demonstrating a significant impact of assay format both assays detected a moderate amount of tenascin-C in the serum of healthy controls, with an average of 447ng/ml detected with the sandwich ELISA and 2164ng/ml with the competition ELISA. However, levels of tenascin-C detected by both assays were significantly higher in the serum of RA patients with average values of 768ng/ml and 4112ng/ml in the sandwich and competition ELISAs respectively. For non-RA rheumatic diseases tested with the sandwich ELISA, although some patient groups showed a trend towards increased tenascin-C levels, none were significantly elevated compared to healthy controls. Conversely, for the competition ELISA, non-RA rheumatic disease cohorts showed significantly increased tenascin-C levels compared to controls, with the only exception being polymyalgia rheumatica patients. Using these screen results concordance between the two assays was also assessed, as shown in figure 5.10c, which demonstrated a significant moderate positive correlation ($\rho = 0.55$, $p<0.0001$) in competition and sandwich ELISA tenascin-C levels.

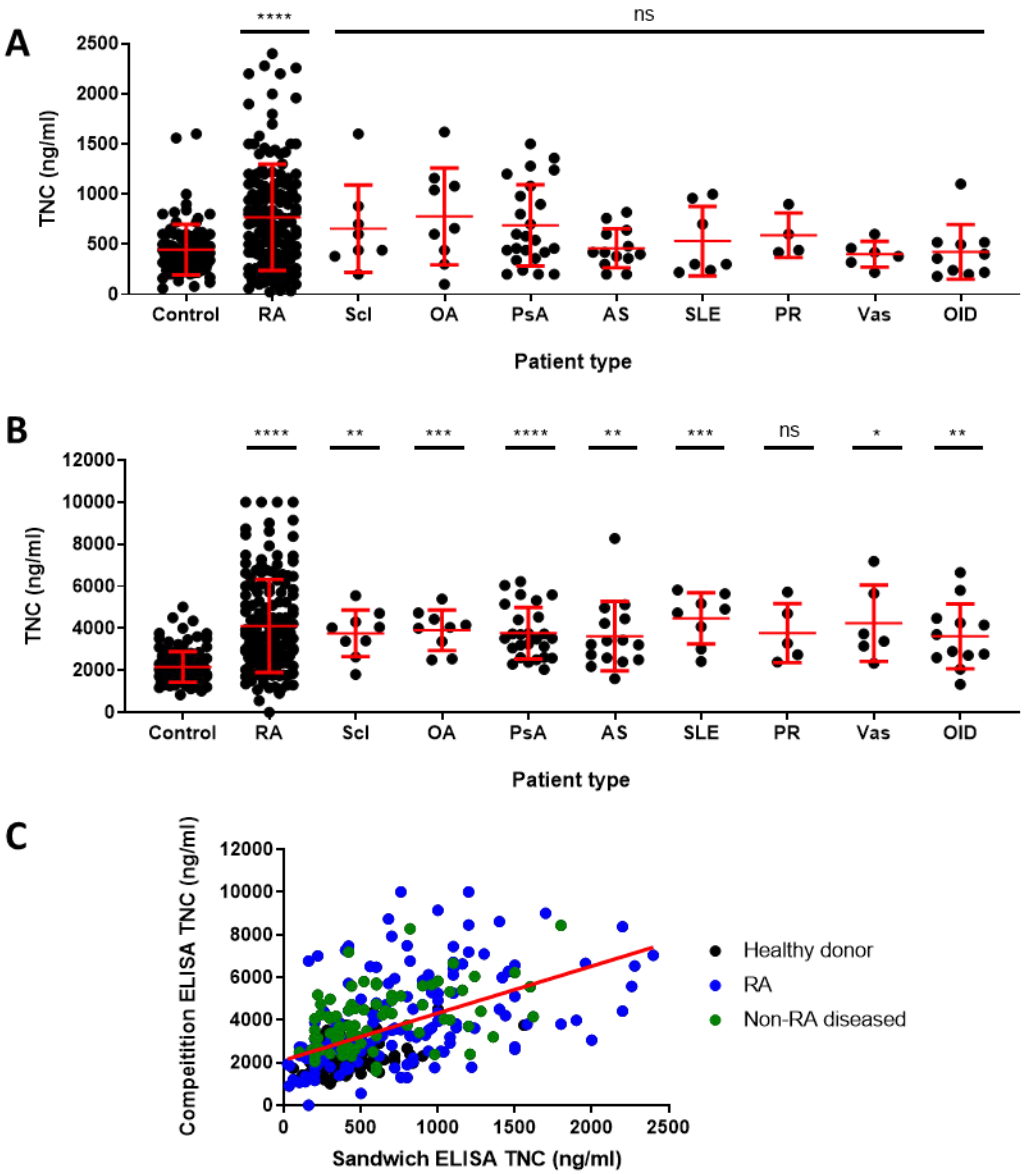

Figure 5.10 Total tenascin-C measured by ELISA is elevated in blood samples from RA patients compared to healthy controls

(A) Human blood samples screened for tenascin-C using the 9F8-NSCT121 sandwich or **(B)** competition ELISAs. Samples came from healthy donors (control) as well as, rheumatoid arthritis (RA), scleroderma (Scl), osteoarthritis (OA), psoriatic arthritis (PsA), ankylosing spondylitis (AS), systemic lupus erythematosus (SLE), polymyalgia rheumatica (PR), vasculitis (Vas) and other inflammatory disease (OID) patients. Data presented as data points representing the mean of the individual sample's technical duplicate overlaid by the group mean ± SD, n: Control = 93, RA = 150, Scl = 8, OA = 9, PsA = 24, AS = 13, SLE = 7, PR = 4, Vas = 6, significance compared to control determined by Kruskal-Wallis test, **** = $p<0.0001$, *** = $p<0.001$, ** = $p<0.01$, * = $p<0.05$, ns = not significant.
(C) Direct comparison of results obtained from the sandwich and competition ELISAs, with the three major patient groups highlighted. Data presented as data points representing the mean of the individual sample's technical duplicate overlaid with a linear regression (red line), n = 310, Spearman's rank correlation coefficient (ρ) = 0.5508, two tailed $p<0.0001$.

Table 5.4: Summary total tenascin-C sandwich ELISA screen results alongside competition ELISA results, provided by Dr Mel Lewis. Shown are the number of samples screened with each assay per group as well as the group's average tenascin-C concentration in both assays. Early synovitis was not used for any of the non-RA grouped analysis due to the lack of definitive diagnosis. Significance was calculated compared to healthy donor controls using the Kruskal-Wallis test, ns = not significant. For groups with low n numbers significance was not determined (-).

	Sandwich ELISA			Competition ELISA		
Group	**n**	**Mean TNC (ng/ml)**	**p value**	**n**	**Mean TNC (ng/ml)**	**p value**
Healthy donors	93	447		124	2164	
Rheumatoid arthritis	150	768	<0.0001	156	4112	<0.0001
Ipswich RF+	73	895	<0.0001	82	4840	<0.0001
Ipswich RF-	30	877	<0.0001	34	4800	<0.0001
Mexico	40	521	ns	40	2034	ns
Other	7	394	ns			
Scleroderma	8	655	ns	9	3766	0.0041
Osteoarthritis	9	778	ns	9	3910	0.001
Psoriatic arthritis	24	688	ns	26	3820	<0.0001
Ankylosing spondylitis	13	460	ns	15	3626	0.0018
SLE	7	531	ns	8	4477	0.0002
PR	4	590	ns	5	3770	ns
Vasculitis	6	400	ns	6	4243	0.0116
OID	10	424	ns	12	3619	0.0057
Sjögren's syndrome	2	210	-	3	2730	-
Dermatomyositis	2	310	-	2	2744	-
Polymyositis	1	360	-	1	3706	-
Fibromyalgia	2	360	-	2	3927	-
JIA	1	520	-	2	4315	-
Reactive arthritis	1	1100	-	1	6660	-
Sarcoidosis	1	500	-	1	2904	-
Early synovitis	3	810	ns	4	5081	0.0064
Non-RA diseased (all)	81	586	ns	90	3834	<0.0001
Non-RA (all)	174	512		214	2866	

AS, ankylosing spondylitis; SLE, systemic lupus erythematosus; PR, polymyalgia rheumatica; OID, other inflammatory disease; JIA, Juvenile idiopathic arthritis.

As with the ACPA assays stratification was attempted to determine if either assay was able to discriminate RA patient subgroups defined by either RF, CCP, or cTNC assay positivity. For the sandwich assay no significant differences in tenascin-C levels were seen for any of these stratification variables as shown in figure 5.11a. The result for the competition assay, shown in figure 5.11b, were similar although a significant increase ($p=0.045$) was seen in the CCP positive (average concentration 3880 ± 2161ng/ml) compared to the negative (average concentration 4710 ± 2119ng/ml) subgroup. Further analysis demonstrated no significant correlation between either the absorbance levels in the CCP or cTNC assays and tenascin-C concentration in the sandwich ELISA (CCP $\rho = -0.16$, $p=0.0527$; cTNC $\rho = -0.08$, $p=0.36$). The analysis was similar for the competition assay with no significant correlation seen between cTNC levels and competition assay tenascin-C concentration (cTNC $\rho = -0.11$, $p=0.20$). However, in this case significance was found for a weak negative correlation with the CCP assay absorbance's (CCP $\rho = 0.28$, $p=0.0006$).

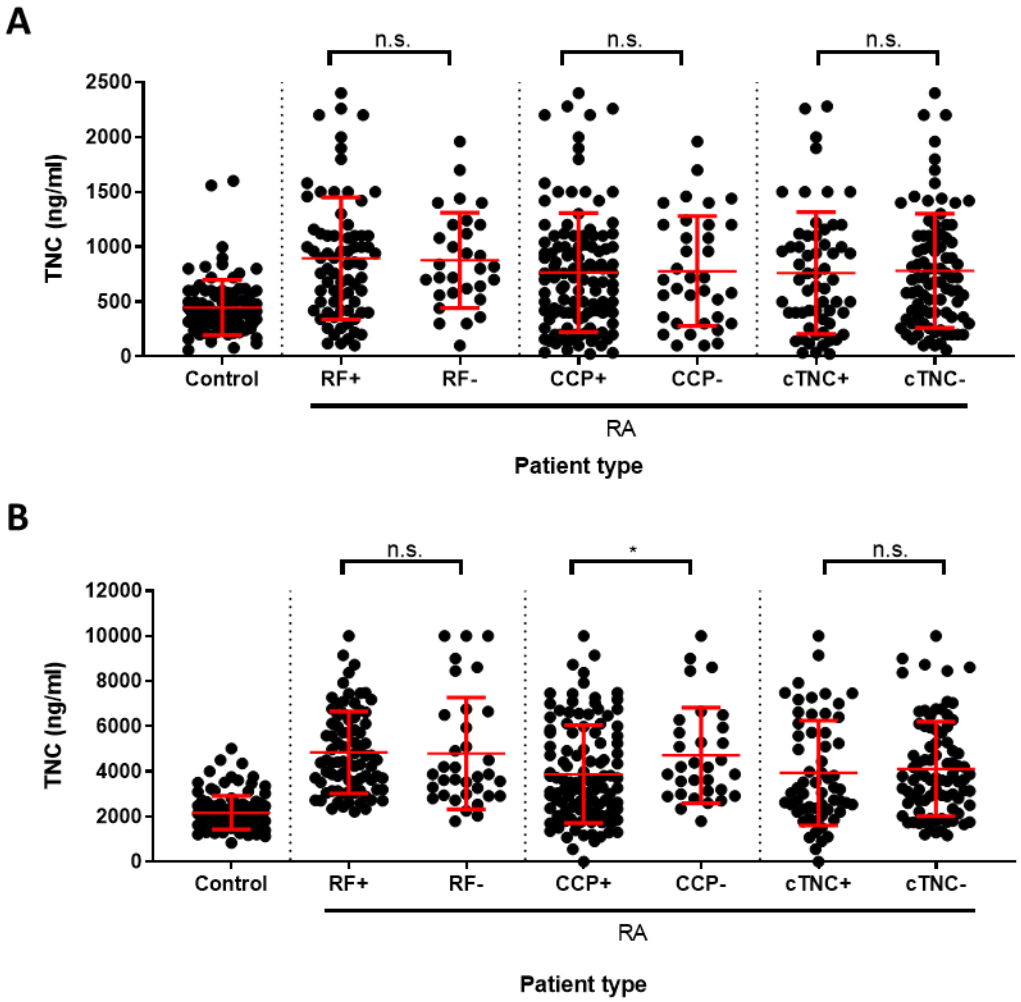

Figure 5.11 Total Tenascin-C levels significantly differ in patients stratified by CCP positivity but not by RF or cTNC positivity

(A) Results of the tenascin-C sandwich ELISA for healthy donor controls or rheumatoid arthritis (RA) patients stratified by either rheumatoid factor (RF), cyclic citrullinated peptide (CCP) autoantibody, or cTNC5 peptide autoantibody positivity. Data presented as data points representing the mean of the individual sample's technical duplicate overlaid by the group mean ± SD. n: control = 93, RF+ = 73, RF- = 30, CCP+ = 115, CCP- = 35, cTNC+ = 59, cTNC- = 88. Significance determined by Kruskal-Wallis test, ns = not significant.
(B) Results of the tenascin-C competition ELISA for healthy donor controls or rheumatoid arthritis (RA) patients stratified by either rheumatoid factor (RF), cyclic citrullinated peptide (CCP) autoantibody, or cTNC5 peptide autoantibody positivity. Data presented as data points representing the mean of the individual sample's technical duplicate overlaid by the group mean ± SD, n: control =114, RF+ = 82, RF- = 34, CCP+ = 115, CCP- = 31, cTNC+ = 59, cTNC- = 84; Significance determined by Kruskal-Wallis test, * = $p<0.05$, ns = not significant.

5.5.9 Comparison of tenascin-C levels in total and splice variant specific assays

Many studies investigating tenascin-C in blood samples have utilised splice variant specific assays. Therefore, the levels of tenascin-C detected using the total tenascin-C sandwich ELISA were compared to those obtained using assays that detect specific splice variants. Two of the most commonly used splice variant specific assays, the tenascin-C large FNIII-B or FNIII-C ELISA kits, produced by IBL International were selected for comparison. The FNIII-B kit utilises the alternatively spliced FNIII repeat B specific antibody, 4C8MS, for capture while the FNIII-C kit utilises the alternatively splice FNIII repeat C specific antibody, 19C4MS for capture. Both assays utilise the same detection antibody, 4F10TT, which recognises the conserved EGF-like repeat domain. The epitopes of the antibodies used in these assays are shown in figure 5.5.

Both assays are performed as standard sandwich ELISAs, as outlined in section 2.11, and utilise as detection antibody; a mouse IgG1 Fab fragment conjugated to HRP for colourimetric detection utilising TMB. The FNIII-B assay standard covers 12.5 to 0.20ng/ml whereas the FNIII-C assay from 24 to 0.38ng/ml. Representative standard curves for both assays are shown in figure 5.12a for FNIII-B and figure 5.12b for FNIII-C, which both showed good linearity. The bottom two standards were omitted to allow for additional sample quantification. In total 18 controls and 62 RA samples were screened with FNIII-B kit, and 8 controls and 30 RA samples were screened with the FNIII-C kit. The results for both the FNIII-B and FNIII-C kits, shown in figure 5.12c and figure 5.12d respectively, showed a significant increase in tenascin-C levels in the RA groups compared to the healthy controls. For the FNIII-B ELISA the mean concentration of the controls was 121.4 ± 239.4ng/ml and this was elevated to 557.8 ± 332.3ng/ml in the RA patients. For the FNIII-C ELISA the control average was 25.7 ± 23.4ng/ml and this increased to 77.3 ± 46.6ng/ml in the RA patients.

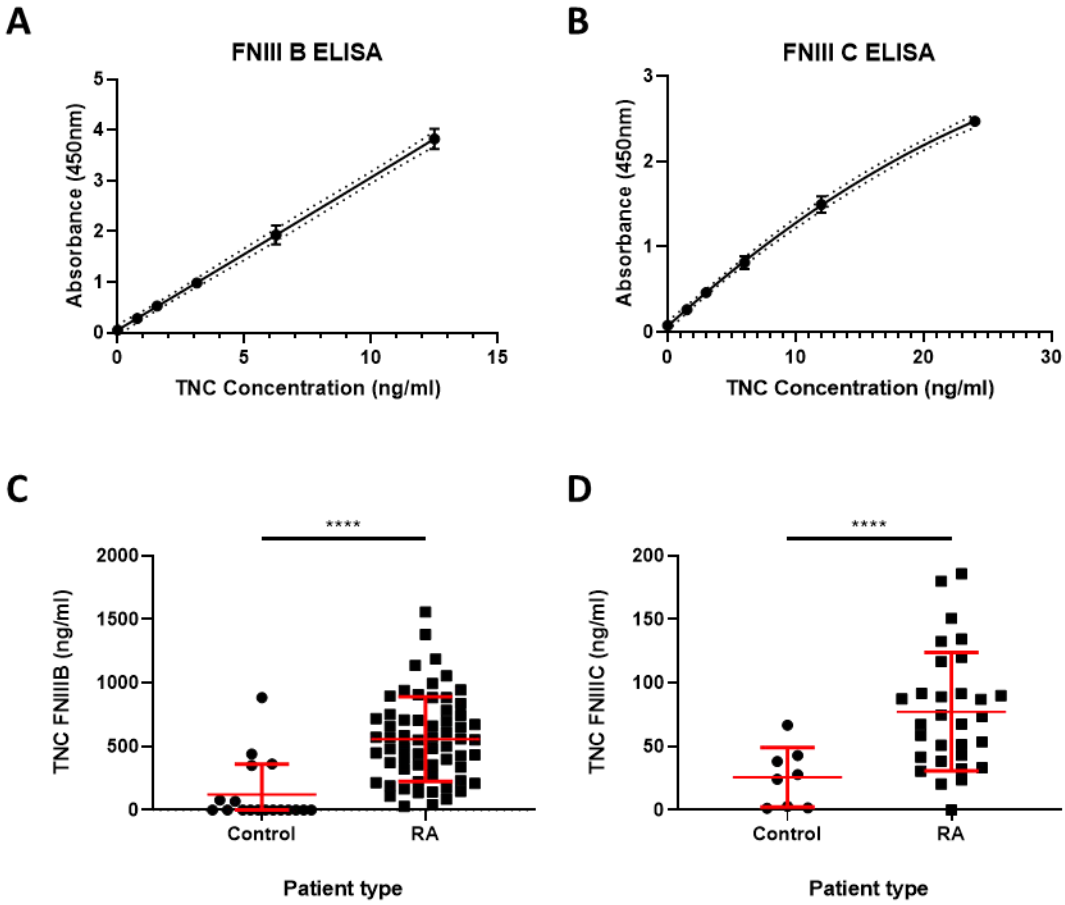

Figure 5.12 Tenascin-C FNIIIB and FNIIIC are significantly elevated in RA patients

(A) Representative standard curves obtained for the tenascin-C FNIII B and **(B)** FNIII C sandwich ELISAs. Data presented as mean ± SD, dotted lines represent the 95% confidence limits.
(C) Results for blood samples obtained from healthy donor (control) and RA patients for the tenascin-C FNIII B ELISA. Data presented as data points representing the mean of the individual sample's technical duplicate overlaid by the group mean ± SD, n: control = 18, RA = 62; Significance determined by Mann-Whitney U test, **** = $p<0.0001$.
(D) Results for blood samples obtained from healthy donor (control) and RA patients for the tenascin-C FNIII C ELISA. Data presented as data points representing the mean of the individual sample's technical duplicate overlaid by the group mean ± SD, n: control = 8, RA = 30; Significance determined by Student's t-test, **** = $p<0.0001$.

Results for samples tested with the IBL ELISAs were compared with the results obtained using the competition and sandwich ELISAs. For the sandwich ELISA a weak but significant positive correlation (ρ=0.3556, p=0.0012) was seen with the FNIII-B ELISA, as shown in figure 5.13a. A significant stronger positive correlation (ρ=0.7812, p<0.0001) was seen with the FNIII-C ELISA, shown in figure 5.13b. For the competition assay a significant moderate correlation (ρ=0.5086, p<0.0001) was seen with the FNIII-B assay, shown in figure 5.13c. Unlike the sandwich ELISA a similar moderate correlation (ρ=0.5795, p=0.0001) was also seen with the FNIII-C assay, shown in figure 5.13d. Finally, to compare the splice variants present a comparison was also made between the results from the FNIII-B and FNIII-C assays. This demonstrated a moderate significant positive correlation (ρ=0.4885, p=0.0019), as shown in figure 5.13e.

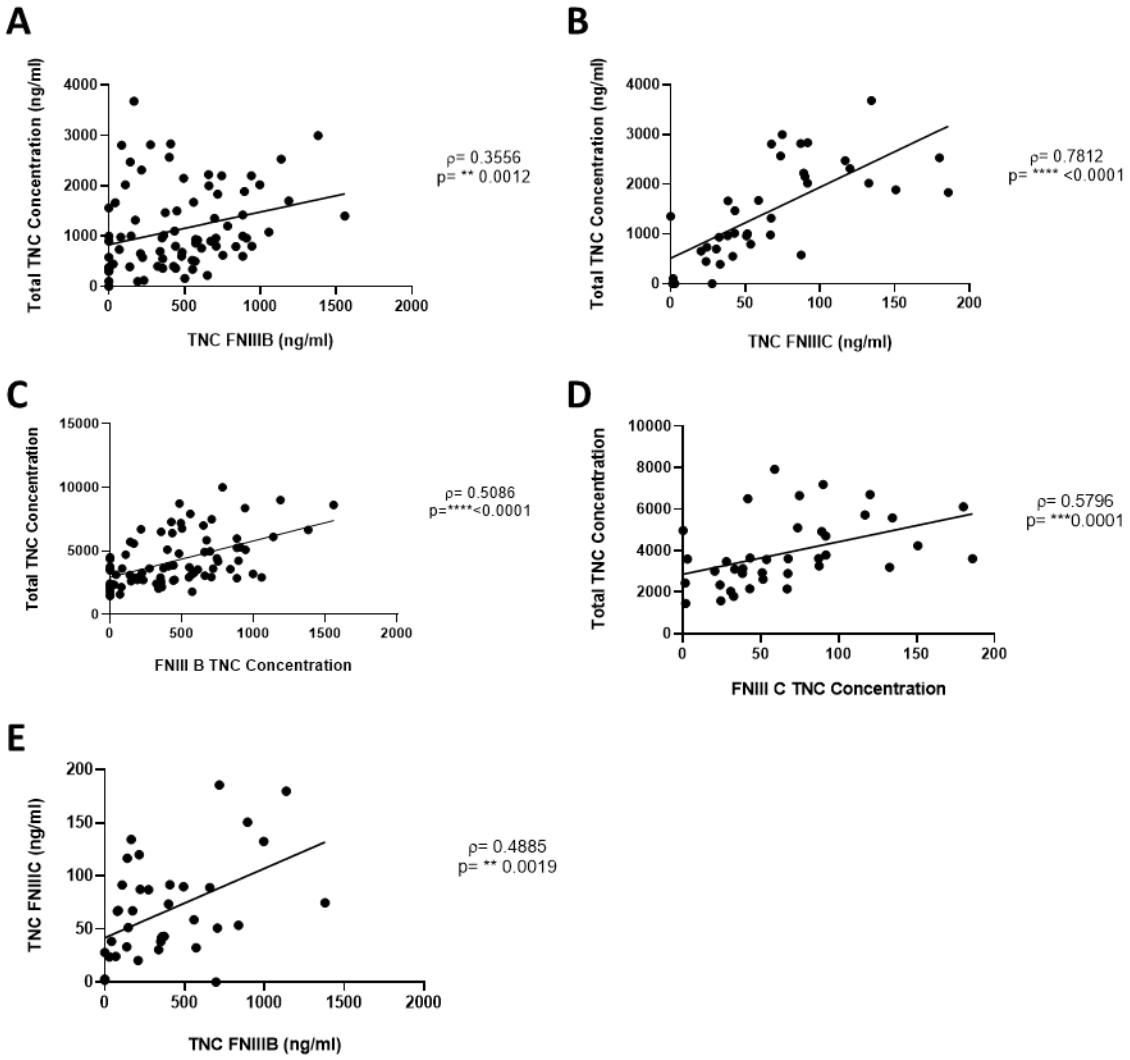

Figure 5.13 There is variable agreement between total and splice variant specific tenascin-C in human blood samples

(A) Direct comparison of the 9F8-NSCT sandwich ELISA with the results obtained with the FNIIIB (n=80) or the **(B)** FNIIIC (n=38) ELISAs.
(C) Direct comparison of the competition ELISA with the results obtained with the FNIIIB (n=80) or the **(D)** FNIIIC (n=38) ELISAs.
(E) Direct comparison between the FNIIIB and FNIIIC ELISAs results (n=38)
Data presented as data points representing the mean of the individual sample's technical duplicate, significance determined by Spearman's rank correlation analysis.

5.5.10 Total serum tenascin-C may be useful in the diagnosis of RA

To test the clinical utility of serum total tenascin-C levels, ROC curves were generated from the screening data. The result for the sandwich ELISA, shown in figure 5.14a, demonstrated that the assay was able to discriminate RA patients from healthy controls with an AUC of 0.6835 (95% CI 0.6170 to 0.7501). Furthermore, this discrimination was shown to be statistically significant with $p<0.0001$. When other inflammatory diseases were included along with the healthy controls (non-RA group) in the analysis the sandwich assay retained the ability to discriminate RA patients from non-RA patients and healthy controls at a statistically significant level with $p<0.0001$. However, specificity was impacted with a decrease in the AUC to 0.6394 (95% CI 0.5761 to 0.7027). Statistically the assay was still able to discriminate the RA patients from other rheumatic diseased patients with $p=0.0262$. However, the specificity of the assay was very poor with a low AUC of 0.5887 (95% CI 0.5149 to 0.6625) indicating a very limited ability for discrimination. To achieve a 95% specificity for RA diagnosis, cut off in tenascin-C levels was set to 850ng/ml when comparing to healthy controls and 1210ng/ml when comparing to the non-RA group. Using these cut offs the sensitivity of the assay was 38% (95% CI 30.62% to 45.98%) with a likelihood ratio of 8.83, and 16% (95% CI 10.99% to 22.70%) with a likelihood ratio of 3.48 for both group comparisons respectively.

The same ROC analysis was carried out for the competition assay as shown in figure 5.14b. Much like the sandwich ELISA the assay was able to significantly discriminate RA patients from both the healthy controls and non-RA groups (both $p<0.0001$). Additionally, for both groups the assay performed better than the sandwich assay with increased AUCs in both instances. However, the AUC of 0.7978 (95% CI 0.7449 to 0.8508) obtained just the healthy donors as controls suffered a much bigger loss of specificity with the addition of the non-RA rheumatic disease group as reflected by a greater decrease in the AUC to 0.6738 (95% CI 0.6167 to 0.7309). Furthermore, unlike the sandwich assay the competition assay was not able to discriminate the non-RA rheumatic diseased patients on their own from the RA patients with an AUC of 0.5028 (95% CI 0.4316 to 0.5741) and $p=0.9414$. To achieve a 95% specificity for RA diagnosis cut off in tenascin-C levels was set to 3606ng/ml when comparing to healthy

controls and 5622ng/ml when comparing against the non-RA group. Using these cut offs the sensitivity of the assay was 53% (95% CI 44.76% to 60.24%) with a likelihood ratio of 10.86, and 25% (95% CI 18.86% to 32.34%) with a likelihood ratio of 5.35 for both group comparisons respectively.

Finally, based on the healthy donor and RA patient group which was screened with the IBL splice variant assays a diagnostic comparison was made between all of the assays. Both of the IBL assays performed well being able to significantly discriminate the healthy donors from the RA patients with statistical significance at $P<0.0001$. The assays had AUCs of 0.8978 (95% CI 0.7981 to 0.9976) for FNIII-B and 0.85 (95% CI 0.7205 to 0.9795) for the FNIII-C respectively. In this limited cohort this outperformed both the total tenascin-C sandwich and competition ELISAs which had lower AUCs of 0.7451 (95% CI 0.6260 to 0.8642) and 0.8378 (95% CI 0.7357 to 0.9399) respectively. It should be noted that due to less samples being screened in the FNIII-C assay this comparison is not perfect and more samples are needed to be screened with this assay to determine if it is truly superior.

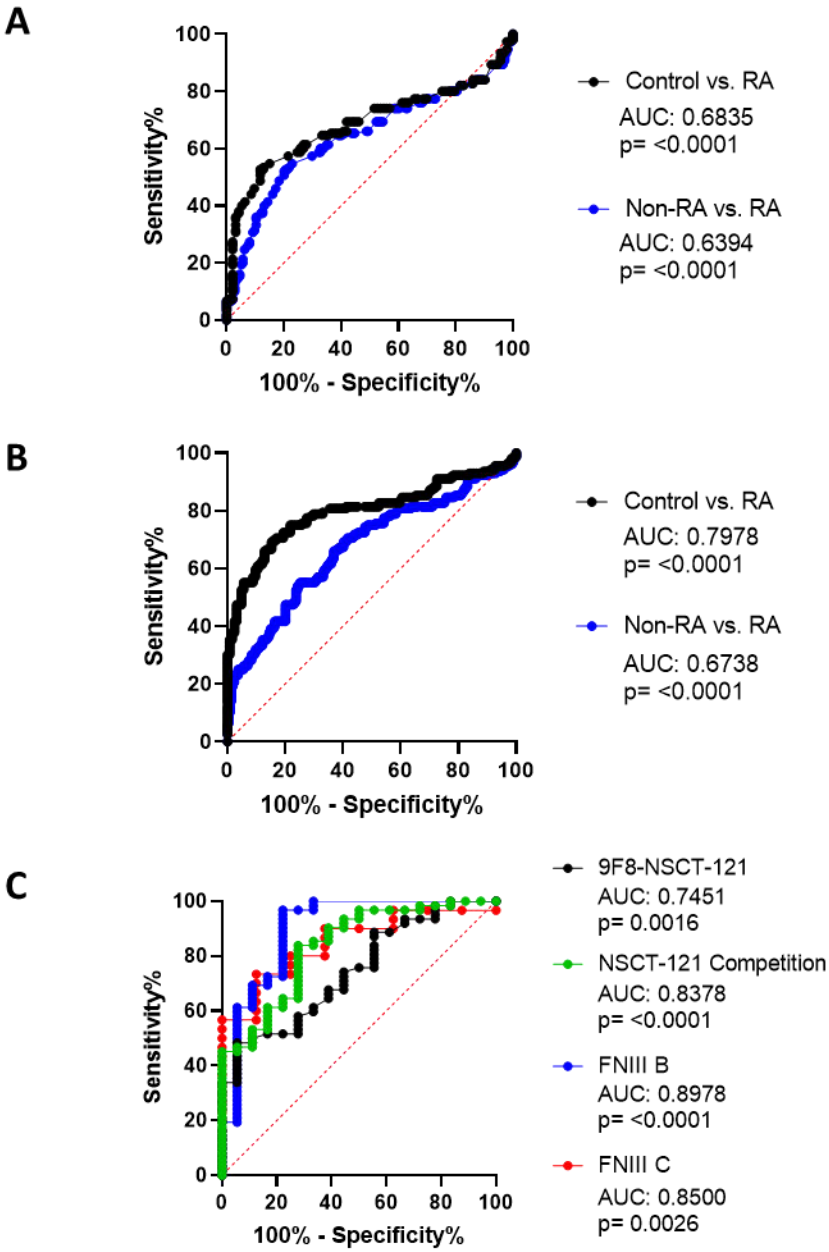

Figure 5.14 Total tenascin-C levels discriminate healthy controls from rheumatoid arthritis patients

(A)) Receiver operating characteristics (ROC) curve analysis for the diagnosis of RA patients (n=150) compared to healthy control (n=93) or healthy control and other rheumatic disease patients (non-RA; n=177) using the 9F8-NSCT121 sandwich ELISA.
(B) ROC curve analysis for the diagnosis of RA patients (n=156) compared to healthy control (n=124) or healthy control and other rheumatic disease patients (non-RA; n=219) using the tenascin-C competition ELISA.
(C) Direct comparison between ROC curves obtained for the diagnosis of RA compared to healthy controls with the 9F8-NSCT121 sandwich ELISA, competition ELISA, FNIII B ELISA (n=control 18, RA = 62) or FNIII C ELISA (n = 8, RA = 30)
Dashed red line indicates the line of no discrimination.

5.5.11 Molecular forms of tenascin-C in healthy and diseased human serum

The preceding sections of this chapter outline a sandwich ELISA I developed as well as a competition assay developed by a collaborator for the detection of tenascin-C in human serums samples. Both of these assays are robust tools for the detection of tenascin-C although due to methodological differences detect potentially differing forms of the protein due to potential fragmentation. Importantly for both these assays, unlike their commercial competition which were also tested, they detect total tenascin-C levels irrespective of splice forms. The weak concordance and differing diagnostic performance of all these various assays suggests that increasing levels of certain subtypes, such as splice variants, does not simply reflect an increase in total tenascin-C levels. As such, this would suggest that differing forms of tenascin-C must be present in human blood and that their abundance can vary independently of total tenascin-C levels. To investigate this further it was decided to attempt to purify and concentrate tenascin-C from human serum so that further biochemical analyses could be carried out. Current tenascin-C purification protocols generally rely on high volume, expensive, and lengthy chromatographic column-based methods and thus were deemed unsuitable for extraction of tenascin-C from the low volume and concentration serum samples available. As such, development of a novel IP protocol for tenascin-C using the NSCT-121 antibody was undertaken to allow for the future extraction and interrogation of tenascin-C from biological samples, including samples that had been tested in the tenascin-C ELISAs.

Initially, to test the IP protocol, an RA serum sample was immunoprecipitated with NSCT-121 or non-specific IgG coated Dynabeads. The supernatants from these IPs were further immunoprecipitated with NSCT-121 to test the efficiency of the first IP. The eluents of all of the IPs as well as the washes were then tested in the total tenascin-C sandwich ELISA the result of which is shown in figure 5.15a. This showed the successful IP of tenascin-C with clear enrichment in the NSCT-121 IP eluent and no tenascin-C present in the NS IgG IP eluent. Furthermore, low amounts of tenascin-C were detected in the NSCT-121 IPs wash and or supernatant suggesting the majority of tenascin-C was successfully captured. This was not observed for the NS IgG IP with significant amounts of tenascin-C still able to be depleted from its supernatant

suggesting no binding to this control occurred. The original serum sample was also ran in the assay as normal or supplemented with glycine to simulate the elution conditions. No difference was seen between the normal or glycine supplemented serum sample demonstrating that the elution conditions did not impact the ELISA results.

To investigate the immunopreciptate further the NSCT-121 precipitate from a normal and RA patient sera was run on an SDS-PAGE gel alongside purified tenascin-C. Silver staining was then used to visualise the protein on the gel as shown in figure 5.15b. The purified tenascin-C produced clear bands at 230 and 280 kDa as expected, whereas both of the IP samples produced a protein smear suggesting that the IP carried through other serum protein contaminants as well as tenascin-C. To confirm the presence of tenascin-C in the IP samples mass spectrometric analysis was performed on a gel band cut from the RA patient IP sample. This was cut at the same height as the high molecular weight (~280kDa) tenascin-C variant present in the purified samples which was also excised as a control for tenascin-C detection. The results of this analysis are shown in table 5.5 which showed that tenascin-C was readily detectable from purified tenascin-C gel band with it clearly the highest scoring hit. A few other ECM proteins were also detected which were suggested to be minor contaminants of the cell line purified prep. For the RA sera IP sample as expected contamination of abundant serum proteins was found with apolipoprotein B-100 and serum albumin featuring as top hits. However, tenascin-C itself was also identified as a top hit suggesting enough had been captured for detection.

Table 5.5: Proteins identified in mass spectrometric analysis of purified tenascin-C and RA sera tenascin-C IP gel bands (see figure 5.15b). The top 3 scoring proteins are listed for each. A total of 12 proteins were identified in the band 1 sample, and a total of 17 in the band 2 sample.

Protein ID	Protein name, species, and gene	Mascot Score
Band 1	**280kDa band of purified tenascin-C**	
P24821-4	Tenascin OS=Homo sapiens GN=TNC	9593
O00468	Agrin OS=Homo sapiens GN=AGRN	273
D6RGG3	Collagen alpha-1(XII) chain OS=Homo sapiens GN=COL12A1	234
Band 2	**280kDa band of RA sera IP**	
P04114	Apolipoprotein B-100 OS=Homo sapiens GN=APOB	7802
P24821	Tenascin OS=Homo sapiens GN=TNC	970
P02768	Serum albumin OS=Homo sapiens GN=ALB	682

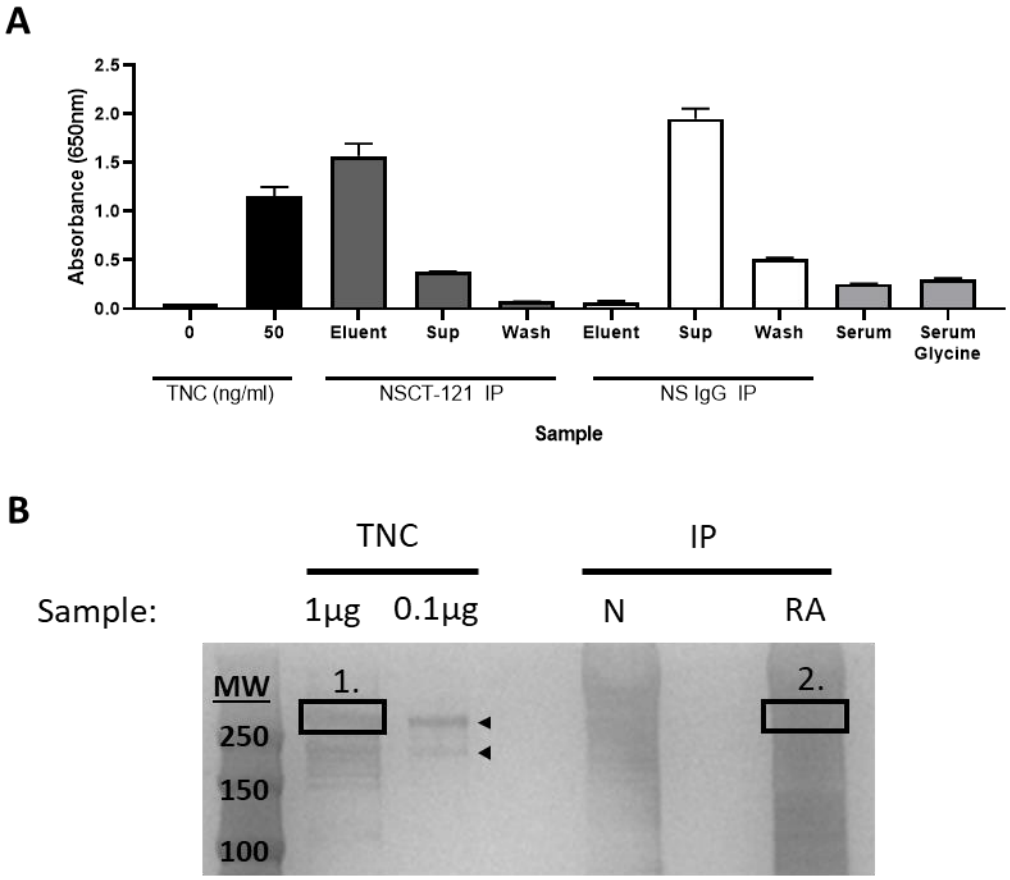

Figure 5.15 Validation of tenascin-C immunoprecipitation from sera using NSCT-121 coated dynabeads by ELISA and mass spectrometry

(A) A serum sample was immunoprecipitated (IP'd) with NSCT-121 or control non-specific IgG coated Dynabeads. Serum with and without glycine, to control for elution conditions, as well as IP eluents from two rounds of elution as well as the washes were analysed with the 9F8-NSCT121 tenascin-C sandwich ELISA. Additionally, the IP supernatants (Sup) were themselves IP'd again with NSCT-121 beads before running the eluent in the ELISA as well. Buffer and purified tenascin-C (TNC) were run along side as controls. Data presented as mean ± SD.
(B) Silver stained SDS-PAGE gel of 1 or 0.1µg of purified tenascin-C (TNC) or tenascin-C specific IPs of normal (N) or RA patient serum. Tenascin-C bands at approximately 230 and 280kDa in the purified tenascin-C samples are indicated with arrowheads. Boxes indicate bands 1 and 2 which were excised for mass spectrometry analysis. Molecular weight (MW) in kDa is indicated on the stained molecular weight marker.

Following from this preliminary gel band analysis these experiments were repeated with additional normal and tenascin-C high RA serum samples. This time however, the IP beads were subjected to in solution trypsin digestion to avoid bias toward a specific molecular weight and so identify all forms of tenascin-C present, as well as any potential interacting partners. Using this approach tenascin-C was identified in all the NSCT-121 IPs from both normal and RA samples and in in none of the corresponding control IPs. As the gel digest had suggested however, the IPs were not pure with many serum proteins pulled down with the beads as well. The non-specific IgG control IPs confirmed these proteins as non-specific interactors and thus they were filtered from the analysis. The final protein list produced post filtering is shown in table 5.6. Other than tenascin-C the protein fibronectin was the only other protein identified in the samples screened. Fibronectin was identified in the control IPs but it did appear enriched in the NSCT-121 IPs consistently attaining much higher mascot scores in these samples. This suggested fibronectin is a potential interactor with tenascin-C in serum. Tenascin-C consistently attained a higher mascot score in the RA patient samples compared to the healthy donors suggesting, as expected, a higher concentration of tenascin-C present and thus more robust detection.

Table 5.6: Proteins identified in mass spectrometric analysis of normal and RA sera tenascin-C IPs. Results were filtered by mascot score, a measure of confidence of identification, and by comparison to a non-specific IgG control IP.

Protein ID	Protein name, species, and gene	Mascot Score
Sample 1	**Normal donor serum 1**	
F8W7G7	Fibronectin OS=Homo sapiens GN=FN1	1541
J3QSU6	Tenascin OS=Homo sapiens GN=TNC	595
Sample 2	**Normal donor serum 2**	
P02751	Fibronectin OS=Homo sapiens GN=FN1	2275
J3QSU6	Tenascin OS=Homo sapiens GN=TNC	190
Sample 3	**RA patient serum 1**	
J3QSU6	Tenascin OS=Homo sapiens GN=TNC	2073
P02751	Fibronectin OS=Homo sapiens GN=FN1	3045
Sample 4	**RA patient serum 2**	
J3QSU6	Tenascin OS=Homo sapiens GN=TNC	1361
F8W7G7	Fibronectin OS=Homo sapiens GN=FN1	307
Sample 5	**RA patient serum 3**	
P24821	Tenascin OS=Homo sapiens GN=TNC	2146
P02751	Fibronectin OS=Homo sapiens GN=FN1	798

To validate these findings western blotting of the IPs was carried out. Firstly, RA and normal serum NSCT-121 and control IPs were western blotted for tenascin-C alongside 0.1µg of purified protein. This blot, shown in figure 5.16a, demonstrated that the two major bands at approximately 200 and 280kDa seen with the purified protein are also present in both the normal and RA patient samples. Also like the purified protein in both cases the higher weight form appears to pre-dominate over the smaller isoform. Confirming the ELISA and mass spectrometry analysis, additionally a greater amount of tenascin-C is seen present in the RA sample compared to the normal sample. For both the control IgG IPs a strong smear is seen although this was hypothesised to be due to cross reactivity of the non-specific IgG present in the IP,

which was a mouse antibody, with the anti-mouse secondary used in the blot. A similar problem is not seen for the NSCT-121 IP as the NSCT-121 antibody is a human IgG and thus not recognised by the anti-mouse secondary.

To check that both forms of tenascin-C were depleted equally the supernatants from the first IPs were subjected to an additional NSCT-121 IP and western blotted again for tenascin-C. As shown in figure 5.16b the first NSCT-121 IP was clearly sufficient to deplete both forms of tenascin-C with no bands seen in the NSCT-121 depleted supernatants from control or RA patients. As expected, the IgG IP did not deplete the sample tenascin-C and thus the follow up NSCT-121 IP was able to pull out tenascin-C from these supernatants. The amount did appear slightly reduced however compared to the first NSCT-121 IPs. This could likely be due to incomplete supernatant recovery from the beads and subsequent loss of some tenascin-C in the wash steps due to weak non-specific bead binding.

Having confirmed tenascin-C depletion, the fibronectin interaction was next investigated. To do this the first membrane presented in figure 5.16a was re-probed with an anti-fibronectin antibody, presented in figure 5.16c. This revealed fibronectin was present in all the IPs including the non-specific IgG IPs although this appeared enriched in the NSCT-121 IPs, corroborating with the mass spectrometry results. Comparing between the patient groups the form of fibronectin present appeared to differ with a major band at approximately 260kDa present in the control sample while a lighter form of around 250kDa seen in the RA sample. Additionally, less fibronectin seemed to be present in the RA patient sample compared to the healthy control. As the predicted band size of fibronectin was 263kDa it was hypothesised that this result for the RA patient sample may be due to proteolysis which may have also impacted antibody recognition or tenascin-C binding and thus resulted in the seemingly low levels detected in this sample. To investigate this further the original serum samples or an equivalent amount of the supernatant from the NSCT-121 depleted samples was blotted for fibronectin, as shown in figure 5.16d. This showed relatively equal amounts of fibronectin present in the original samples for the major 260kDa band although there was again differential banding seen in the RA sample. This took the form of an additional two bands at 250kDa, and 160kDa. The 260kDa band was the only major

band seen in the normal sample. This differences between the samples may have arose due to differential sample storage and freeze thaw cycles during previous usage, which has been shown to impact fibronectin fragmentation and western blotting (Griffiths et al., 1989). Overall, the NSCT-121 depleted supernatants both showed a slight reduction in fibronectin compared to the original serum samples although complete depletion like with tenascin-C was not observed.

These preliminary findings on the forms and functions of tenascin-C in human serum will need further validation and characterisation in future. Furthermore, as well as the still unanswered questions on the forms of tenascin-C posed earlier in this chapter they additionally raise further questions, such as those around the nature of the tenascin-C and fibronectin interaction in serum. The IP protocol developed provides a good platform for answering these questions. Additionally, with tenascin-C's often relatively low abundance in most other tissues this also provides a useful method applicable to a range of other biological sample sources as well.

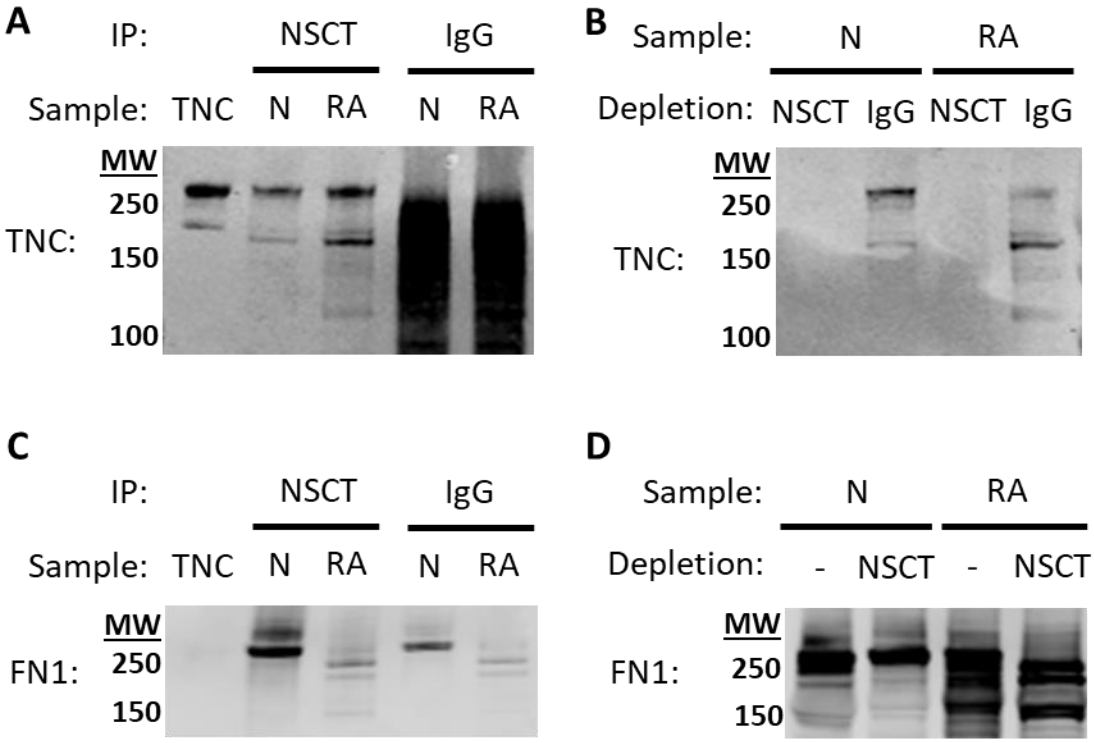

Figure 5.16 NSCT-121 immunoprecipitation and mass spectrometry western blotting validation

(A) NSCT-121 and control IgG IPs of normal (N) and RA serum were western blotted alongside 0.1µg purified tenascin-C (TNC) for tenascin-C using the B12 antibody. Two major bands of corresponding heights to those seen in the purified tenascin-C are also seen in both the normal and RA IPs. More tenascin-C is seen in the RA sample compared to the normal sample. A smear is detected in the IgG IPs, potentially due to cross reactivity of the mouse IgG present in the IP reacting with the anti-mouse secondary antibody used in the blot.
(B) The run through of the NSCT-121 and IgG IPs was further immunoprecipitated with NSCT-121 and western blotted using the B12 anti-tenascin-C antibody as an additional check for depletion. No further tenascin-C is able to be pulled out of the NSCT-121 depleted samples but tenascin-C is still able to be depleted from the non-specific samples.
(C) The blot shown in (A) was reprobed using the F14 anti-fibronectin (FN1) antibody. FN1 was detected in both the control and NSCT-121 IPs although some additional enrichment is seen in the NSCT-121 IP.
(D) To check the abundance of FN1 in the original serum samples 1µl of normal and RA sera or a comparable amount of NSCT-121 IP run through from both was western blotted for fibronectin with the F14 antibody. Similar abundance is seen in the normal and RA patient samples although different molecular weight forms are seen in the RA patient sample. Tenascin-C IP while appearing to reduce the amount of FN1 present does not fully deplete it suggesting that not all serum FN1 is tenascin-C bound.
All samples were run on 10% Bis-Tris SDS-PAGE gels under reducing conditions. Molecular weight (MW) in kDa indicated at the side of each blot.

5.6 Discussion

5.6.1 cTNC5 assay performance and screen results

The cTNC assay developed in this chapter specifically detected cTNC5 specific autoantibodies in human serum samples. This ELISA improved upon the protocol previously employed by Schwenzer and colleagues (Schwenzer et al., 2015) as it was less time intensive and had reduced complexity of assay buffers. Time saving steps included using commercially available streptavidin coated plates and biotin conjugated peptides which reduced plate coating from an overnight step to an hour incubation, and reduction in the sample and detection antibody incubation steps to one hour each from 1.5 to 2 hours for the Schwenzer assay. Buffers were simplified from the RIA buffer (1% BSA, 350 mM NaCl, 10 mM Tris–HCl, 1% Triton X-100, 0.5% Na-deoxycholate, and 0.1% SDS) used by Schwenzer et al for the sample and detection antibody steps. This was replaced with the more simplified buffers, cTNC sample buffer (1M NaCl, 4.9mM disodium phosphate, 0.5% Tween 20, 2% BSA) and cTNC conjugate buffer (PBS, 0.05% Tween 20, 1% BSA), both made up of with less individual components. In terms of assay performance, low background was observed with most negative samples reading close to the absorbance observed for the no peptide control coat. Non-specific binding was noted for several samples, however, this was controlled for in the results by subtracting the absorbance obtained from the no peptide and rTNC5 coat controls. Only a small fraction of samples in the IgG anti-cTNC5 assay, accounting for 3.6% of all samples tested, were rTNC5 positive. This was similar to the levels seen by Schwenzer and colleagues who found 2.5% of the RA sera samples they tested were rTNC5 positive.

Results obtained from sample screening of the cohorts in this study were similar to those described by Schwenzer et al (2015). In their study of two confirmed RA cohorts they detected cTNC5 autoantibodies in 47% and 51% of patients which was similar to the percentage of anti-cTNC5 positive samples (51%) detected in the current study. Furthermore, the high specificity of cTNC5 autoantibodies to RA patients with very few observed in the healthy controls tested was common to both studies. The CCP results were also similar with 73.3% sensitivity in the current cohorts compared to 63.2 and 83.6% seen in both the Schwenzer cohorts, which was in line with the 67-83%

range of sensitivities reported in the literature (Mathsson Alm et al., 2018). Likewise, CCP autoantibodies displayed high specificity for RA with no healthy controls testing positive. A mixed cohort of patients with non-RA rheumatic diseases was also included in the current study. This cohort had low levels of cTNC5 autoantibody positive samples (9.3%), emphasising the specificity of the anti-cTNC5 autoantibody biomarker for RA. However, slightly more positive results (9.3% versus 3.7%) were detected in this group than in the healthy controls suggesting that a small proportion of non-RA rheumatic disease patients may have cTNC5 autoantibodies. A similar result was seen with CCP with a small proportion (7%) of non-RA rheumatic disease patients categorised as CCP positive.

In addition to the IgG ACPA isotype, the cTNC5 and CCP assays were adapted for the detection of IgA autoantibodies, which have been shown to be present in some RA patients (Verpoort et al., 2006). Like the IgG assay, IgA was specific for RA patients and none of the healthy donors tested positive for either CCP or cTNC autoantibodies. A significant proportion of the RA patients tested were positive for IgA autoantibodies, at 47.3%, and this was in line with other studies in the literature which have reported a prevalence of 52.9% (Lakos et al., 2008). However, this was a lower sensitivity than seen with the IgG assay and all of the IgA positive samples were also CCP IgG positive, similar to what has been reported in the literature (Verpoort et al., 2006). cTNC IgA autoantibodies were much less prevalent with only 4.5% of RA patients positive, although again high specificity was observed with none of the healthy donors tested as positive. Interestingly, unlike for CCP, one of the cTNC IgA positive samples was not cTNC IgG positive although it was positive for both CCP IgA and IgG autoantibodies.

5.6.2 Clinical utility of cTNC5 in diagnosis

Overall the cTNC5 IgG assay exhibited a good diagnostic performance for RA in the cohorts tested although it was less sensitive than the CCP assay. In contrast to the studies by Schwenzer and colleagues (Schwenzer et al., 2015, Schwenzer et al., 2019), in the current study all anti-cTNC5 positive patients were also positive for anti-CCP autoantibodies. Therefore, there appeared to be no added benefit for additional testing for anti-cTNC5 alongside anti-CCP. The reported proportions of patients who are

CCP2 negative but cTNC5 positive is low at 1.7 (Schwenzer et al., 2017) to 4.9% (Schwenzer et al., 2015) and so it is possible that our cohort was not large enough to detect this small population. cTNC5 has also been investigated for its diagnostic potential in patients presenting with early synovitis as, like CCP autoantibodies (Nielen et al., 2004), cTNC5 autoantibodies have been shown to pre-date RA disease development, in some cases up to a decade before clinical symptoms appear (Schwenzer et al., 2015). The current study had a limited number of early synovitis samples, with only three analysed. However, one of these early synovitis patient samples was positive for cTNC5 and CCP suggesting that this individual was likely to develop RA. Recent studies in other clearly defined early synovitis cohorts have demonstrated that anti-cTNC5 autoantibodies can predict RA development, although in a less sensitive and largely overlapping manner to the CCP assay (Raza et al., 2016).

These results might be anticipated in light of the fact the CCP assay contains a mix of artificially engineered peptides designed to capture the majority of ACPA for maximum sensitivity (van Venrooij et al., 2011). Thus, it is likely that the majority of cTNC5 specific autoantibodies are detected in the CCP assay as well. Similar results have been seen with other specific autoantigen ACPA assays which generally show reduced sensitivity compared to CCP (Bizzaro et al., 2007) and similar low frequencies in CCP negative patients (van Heemst et al., 2015).

The diagnostic potential of detecting IgA autoantibodies should also be considered, as in recent years it has been recognised that determining autoantibody isotype may be diagnostically beneficial (Sieghart et al., 2018). The clinically used CCP3.1 assay is based on this principle, detecting both IgG and IgA CCP autoantibodies, with some evidence of improved sensitivity (dos Anjos et al., 2009). Whilst in the current cohorts studied a significant number of CCP IgA RA patients were identified there was no added benefit to observed sensitivity. This was also the case when taking the RF negative RA patients in isolation, in contrast to more recent literature reports that IgA detection may be particularly beneficial for the diagnosis of this group (Szekanecz et al., 2013). This likely reflects the low prevalence of CCP IgG negativity with IgA positivity that has been reported in the literature (Lakos et al., 2008, Svard et al., 2015). In contrast, a very slight diagnostic benefit was seen for IgA anti-cTNC5

autoantibodies with one RF negative RA patient tested as cTNC positive. This should be cautioned however as recent studies have suggested that IgA ACPAs increase with age in RA patients as well as healthy controls suggesting that the addition of IgA autoantibody detection may produce specificity problems (Berens et al., 2019). This was not observed in the current cohort tested with high specificity observed although more control samples as well as non-RA diseased samples would need to be tested to confirm this.

5.6.3 Clinical utility of cTNC5 in patient stratification

The benefit of detecting of ACPA fine specificities may not lie with diagnosis but in patient stratification. It is has already been shown that anti-CCP autoantibodies display some limited prognostic ability. This has included associations between CCP levels or positivity and aggressiveness of disease (Kastbom et al., 2004), mortality risk (Sihvonen et al., 2005), responsiveness to anti-TNF biologic therapy (Klaasen et al., 2011), and rate of joint destruction (de Rooy et al., 2011). However, some of these associations are weak or with low predictive value and can vary by cohort making them of limited routine clinical use. It could also be argued that when looking solely at CCP positivity, a diagnosis that includes >70% of all patients, is not particularly informative for clinicians, especially given the heterogeneous nature of RA even within these groups (Montgomery et al., 2013). As such, it has been proposed that further subdividing patients by ACPA fine-specificity may prove clinically informative. This is especially appealing if, in light of the heterogeneity of the condition, you consider RA as a syndrome encompassing a range of different aetiologies but a common clinical endpoint (Stanich et al., 2009). If such a view is taken it could be postulated that differing ACPA's could be generated by different disease subsets and thus reflect differences in underlying disease mechanisms with prognostic implications.

In this study cTNC5 was found to stratify patients by RF status. This is in agreement with other studies which have also shown an association between RF and cTNC5 positivity (Raza et al., 2016). Likewise, an association between RF and CCP positivity has been previously reported in the literature (Murphy et al., 2017) and was also found in the current study. As such, the cTNC5 assay showed no added benefit for the

identification of seronegative patients. Additionally, in this study no other factors including age or treatment were found to correlate with cTNC5 positivity. This analysis was limited however by the differing or lacking clinical information available for the cohorts used. The heterogeneity of the patients further complicated analysis and made it harder to identify potential confounding factors when isolating sub groups. Previous studies have shown cTNC5 positivity is associated with smoking, the HLA shared epitope, and disease activity in the form of DAS28-CRP scoring (Schwenzer et al., 2015). Similar associations with smoking, the shared epitope (Krol et al., 2015) and DAS28 scoring (Fisher et al., 2011) have been observed for CCP as well. No other clinical characteristics, such as swollen joint counts, were found to correlate with cTNC5 levels and this finding is similar to studies of other fine-specificity ACPAs (Willemze et al., 2012).

In light of this it has been hypothesised that ACPA fine specificities may associate more with extra-articular disease parameters relating to their potential association with different disease aetiologies or mechanisms (Montgomery et al., 2013). As expected based on this hypothesis the CCP test has shown no correlation with a range of extra-articular disease parameters (Gonzalez-Lopez et al., 2014). Conversely, associations have already been found for some fine-specificities, for example ACPAs to citrullinated fibrinogen and vimentin have been found to be associated with increased atherosclerotic plaque burden (Sokolove et al., 2013). In regards to cTNC5 ACPA, an association has already been identified with a subgroup of RA patients suffering from periodontitis caused by the pathogen *prevotella intermedia* (Schwenzer et al., 2017). Periodontitis is a known risk factor for RA and it is hypothesised as a possible initiator of disease with the citrullination of host proteins by periodontal bacteria leading to ACPA generation and RA (Rosenstein et al., 2004). As such, it could be hypothesised that cTNC5 positivity may identify an RA subgroup in which treating periodontal disease may have particular benefit, although a recent small scale trial using this approach found no added benefit (Moller et al., 2019).

Another angle of approach to patient stratification comes in the form of measuring specific ACPAs isotypes. In this study only a very small fraction of CCP IgA positivity was explained by cTNC5 suggesting it is not the primary target of the IgA response in

RA patients. CCP IgA positivity has previously been linked to smoking and it has been suggested it indicates a mucosal origin of the initiation of disease in these patients (Svard et al., 2015). As such, this result would suggest that cTNC5 is likely not a relevant autoantigen in this potential mucosal mode of pathogenesis.

Overall these findings highlight the need for further studies of cTNC5 and other, perhaps yet unidentified, ACPA fine specificities in larger fully clinically described cohorts to determine if further serological stratification is possible.

5.6.4 Performance of total tenascin-C ELISAs

As well as the auto-antibody assays I also developed a sandwich ELISA to quantify levels of total tenascin-C in biological samples, that I examined in parallel with a competition assay developed by a collaborator. The total tenascin-C sandwich ELISA demonstrated good assay specificity, sensitivity, and linear range in comparison to competitors. Additionally, the assay was also benefited from compatibility of use with a variety of different blood tube types. This contrasts with some alternative assays such as the IBL tenascin-C FNIII-C assay for which the manufacturer states that lower results will be obtained for EDTA, citrate, and NaF plasma compared to serum or heparin plasma samples.

Results from the anti-tenascin-C sandwich and competition ELISAs showed a reasonable correlation but the concentration range of tenascin-C detected with the competition assay was much higher than the sandwich ELISA. This was not particularly surprising as the use of a single antibody for recognition in the competition ELISA allows detection of proteolytically cleaved fragments of tenascin-C containing the intact FBG epitope. Whereas, in the sandwich ELISA both the 9F8 and NSCT-121 epitope must be linked for recognition in the assay. Therefore, proteolytic cleavage in the intervening FNIII domains would result in loss of detection. A number of cleavage sites for various proteases have been mapped within this area, including MMP-2, MMP-7 (Siri et al., 1995), and meprinβ (Ambort et al., 2010), and thus cleavage by any of these would result in lack of recognition in the sandwich ELISA. Additionally, estimation of tenascin-C concentration could be further reduced in the sandwich ELISA as these cleaved fragments could also act as inhibitors in the assay. This could

occur as the fragments could occupy capture antibody binding sites and thus prevent non-cleaved fragments, which would be recognised by the assay, from binding. These potential cleavage affects are summarised in figure 5.17a. Furthermore, these cleavage issues are further complicated as the alternative spliced domains of tenascin-C are subject to differential cleavage and this therefore provides another variable influencing tenascin-C processing and thus potentially recognition.

Another explanation of variation between the two assays could be due to the different binding modes of antibody to tenascin-C that can potentially occur. Antibodies have two antigen binding sites and tenascin-C as a hexamer would have potentially six antibody binding sites per oligomer. As such, in combination with proteolytically cleaved fragments a wide variety of binding can potentially occur including multiple antibodies binding per hexamer and crosslinking of hexamers by antibodies. The impact of these different binding modes on the ratio of antibody bound per tenascin-C hexamer are illustrated in figures 5.17b, c, and d. Additional complexity could also arise from the hypothesised oligomerisation of different splice variants or even with different tenascin family members (Jones and Jones, 2000). Together all of these factors could affect the amount of antibody sequestered in the competition assay as well as antibody:tenascin-C binding ratios in the sandwich ELISA and do so to differential degrees.

The tenascin-C in the standard curve used for calculating concentration should also be considered in light of these potential differential form effects. HPLC analysis, performed by Dr Mel Lewis, indicated that the standard tenascin-C, which was purified from tissue cultured glioma cells, was oligomeric in nature. It has been shown that tenascin-C can differ by cell source (Giblin, 2018) and thus it is unknown whether this form accurately reflects the form or forms of tenascin-C present in the blood. Due to the issues highlighted above the commutability of this standard in either assay may be different and thus differential affect assay readout. Overall though it would be expected that the competition assay would have a greater variety of forms of tenascin-C to detect which would thus explain its higher estimation of total tenascin-C concentrations.

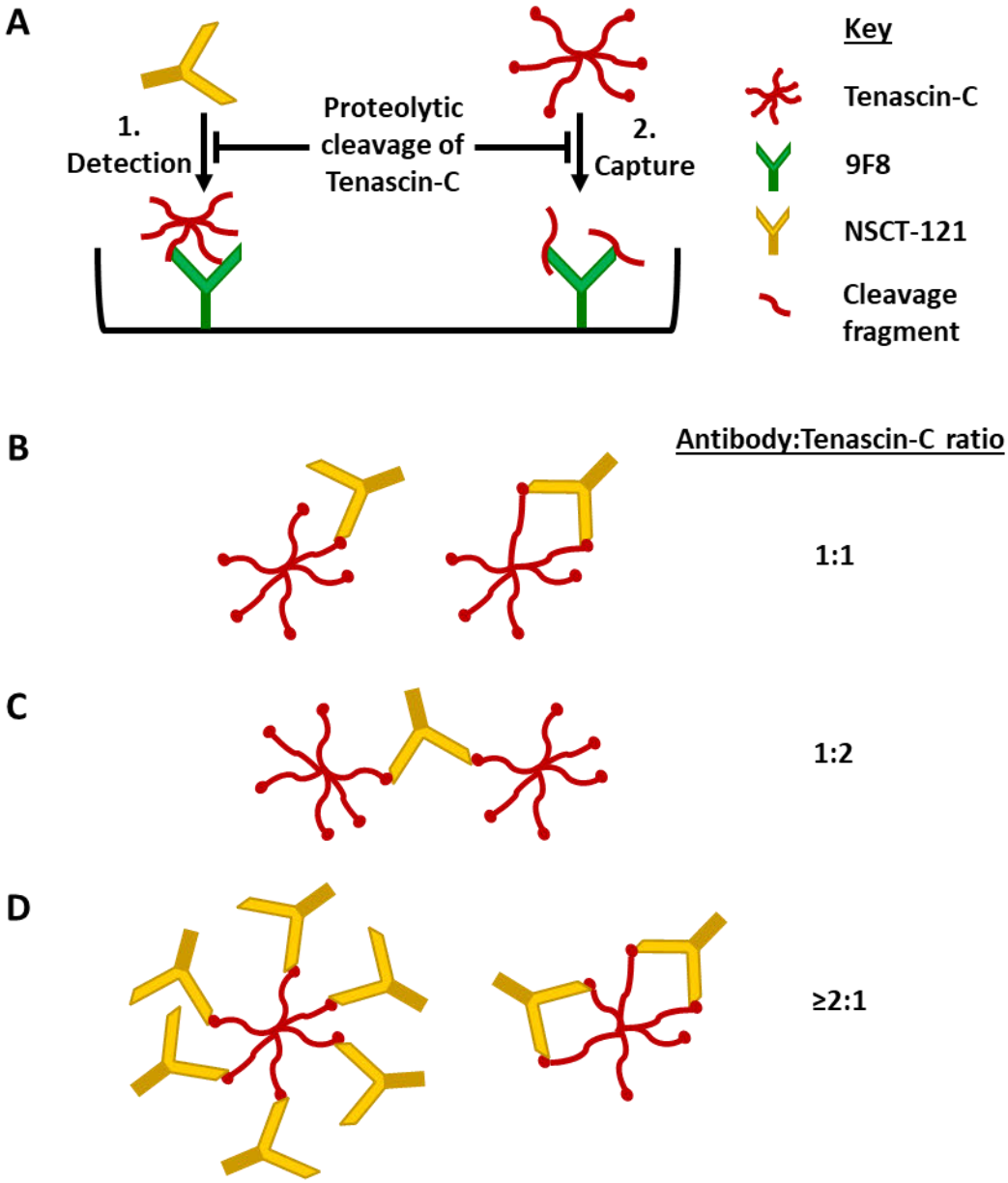

Figure 5.17 Effects of tenascin-C proteolytic cleavage and different modes of antibody binding upon ELISA recognition

(A) Proteolytic cleavage of tenascin-C can inhibit its detection by sandwich ELISA. This can due to removal of the FBG domain resulting in loss of detection antibody binding (1.) as well as cleaved fragments containing the FNIII-3 repeat blocking tenascin-C capture (2.).
Different potential modes of binding of detection antibody to tenascin-C. These result in different ratios of antibody:tenascin-C binding and thus potentially different sandwich ELISA readout for the same amount of tenascin-C present.
(B) 1:1 binding whereby one antibody binds one hexamer via one or both antigen recognition domains.
(C) 1:2 binding where one antibody binds to multiple hexamers.
(D) 2:1 to 6:1 antibody:tenascin-C binding whereby multiple antibodies bind to one tenascin-C hexamer via either one or both antigen recognition domains.

5.6.5 Basal levels of total tenascin-C in human serum

A wide range of total serum tenascin-C concentrations in health and disease obtained using various different assays have been reported in the literature. These are summarised in table 5.5. Concentrations range from as low as 0.09ng/ml, reported for the USCN ELISA, to as high as 33800ng/ml for the BIOABB ELISA. However, the majority of studies report an average tenascin-C concentration for healthy controls of 696 ± 314ng/ml. This concentration is in reasonable agreement with the range of tenascin-C concentrations observed using the 9F8-NSCT-121 sandwich ELISA and far greater than those observed with both IBL splice variant specific ELISAs. Tenascin-C assays reported in the literature were all in a sandwich immunoassay format and therefore differences in concentrations between the sandwich and competition ELISA formats, as previously discussed, are applicable to these assays as well. Together, information from the current study and the literature suggest that a notable amount of tenascin-C is expressed and transferred into the blood in normal healthy individuals. The tissue or cellular source and functional significance of this serum tenascin-C remains to be elucidated.

Those assays that differed substantially from the range described above and from each other were the BIOABB, USCN, and CusaBio commercial ELISAs. The BIOABB assay was described in a single publication and gave extremely high concentrations of tenascin-C concentration. In contrast, the CusaBio and USCN ELISAs gave much lower concentrations of tenascin-C. It is likely that poor assay performance or specificity were a potential cause of this low tenascin-C level and this has already been suggested as a problem with the USCN ELISA (Giblin, 2018). It is possible that these assays are not detecting total tenascin-C and, like many of the commercial assays identified, the epitopes of the antibodies used were not specified. Therefore, tenascin-C splicing or other modifications may be affecting the results of the CusaBio and USCN ELISAs. However, results obtained using both of the IBL splice variant specific ELISAs were much higher than obtained with these assays.

Table 5.7: Summary of total serum tenascin-C levels reported in the literature in healthy and diseased patients. Results presented as median or mean serum concentration of tenascin-C in ng/ml ± standard deviation (SD) or standard error (SE) depending upon the published data available. The in house ELISAs comprise five distinct assays with differing methodologies and antibody combinations.

Assay	Reference	Condition	Tenascin-C concentration (ng/ml)
In house ELISA 1	(Yamauchi et al., 1994)	Healthy control	Mean 860 ± 152 SD
		Hepatitis	Mean 1371 ± 333 SD
		Liver cirrhosis	Mean 1818 ± 484 SD
		Hepatocellular carcinoma	Mean 2455 ± 1153 SD
In house ELISA 2	(Ylatupa et al., 1995)	Healthy control	Mean 730 ± 310 SD
	(Kaarteenaho-Wiik et al., 1998)	Healthy control	Mean 750 ± 400 SD
		Sarcoidosis	Mean 1390 ± 580 SD
		Interstitial pneumonia	Mean 2810 ± 2970 SD
		Bronchioloalveolitis	Mean 950 ± 500 SD
In house ELISA 3	(Riedl et al., 1995)	Healthy control	Mean 320 ± 170 SD
		Colorectal cancer	Mean 500 ± 420 SD
	(Riedl et al., 2001)	Healthy control	Mean 320 ± 170 SD
		Ulcerative colitis	Mean 1720 ± 1460 SD
In house ELISA 4	(Kimura et al., 1993)	Healthy control	Mean 897 ± 250 SD
		Carcinoma	Mean 2546 ± 1746 SD
	(Washizu et al., 1993)	Healthy control	Mean 837 ± 162
		Carcinoma	Mean 2039 ± 1969
	(Yoshida et al., 1994)	Healthy control	Mean 1396 ± 368
		Brain tumour	Mean 1819 ± 1264
In house ELISA 5	(Latijnhouwers et al., 1998a)	Healthy control	Mean 1110 ± 390
		Psoriasis	Mean 1270 ± 790
Bayer Immuno 1 analyzer assay	(Ropers et al., 2000)	Healthy control	Mean 457 ± 176 SD
	(Burchardt et al., 2003)	Healthy control	Mean 444 ± 171 SD
		Melanoma	Mean 783 ± 630 SD
USCN (Cloud-Clone) ELISA	(Didem et al., 2014)	Healthy controls	Median 0.09
		Ovarian cancer	Median 0.13
	(Tastekin et al., 2014)	Healthy control	Mean 0.137 ± 0.026 SE
		Breast cancer	Mean 0.344 ± 0.042 SE
	(Clancy et al., 2014)	Healthy control	Median 1131
		Stroke	Median 1277

Table continued on next page

Table 5.7: Table continued from preceding page

Assay	Reference	Condition	Tenascin-C concentration (ng/ml)
CusaBio ELISA	(Karatas et al., 2013)	Healthy control	Mean 4.72 ± 1.77 SD
		Rheumatic heart valve disease	Median 9.09
	(Peng et al., 2018)	Healthy control	Mean 6.87 ± 2.63 SD
		Depression	Mean 14.37 ± 6.07 SD
BIOABB ELISA	(Orak et al., 2016)	Healthy pregnant	Mean 5020 ± 400 SE
		Preeclampsia	Mean 33800 ± 11700 SE
Myriad RBM immunoassay	(Bertenshaw et al., 2008)	Healthy control	Median 1090
		Ovarian cancer	Median 1910
	(Bhattacharyya et al., 2016)	Healthy control	Mean 410.1 ± 150.4 SD
		Systemic sclerosis	Mean 731.2 ± 371.5 SD
	(van den Ham et al., 2018)	Healthy control	Mean 488 ± 149 SD
Mesoscale immunoassay	(O'Bryant et al., 2016)	Healthy control	Mean 44.1 ± 13.1 SD
		Alzheimer's disease	Mean 37.7 ± 10.3 SD

5.6.6 Levels of total tenascin-C in human serum with inflammatory disease

In common with previous reports in the literature for splice variant specific tenascin-C (Schenk et al., 1995, Page et al., 2012) screening patient samples for total tenascin-C showed elevated serum tenascin-C levels within the inflammatory disease cohorts studied. However, the significance of tenascin-C levels varied by assay used with the sandwich ELISA showing elevation within the RA cohort only whereas the competition assay demonstrated significantly higher tenascin-C levels in all inflammatory diseases tested except for polymyalgia rheumatica. This may reflect the higher number of RA samples tested which would give this group more power for statistical analysis versus the control group. The highest levels of tenascin-C for both assays were observed for the RA group suggesting that tenascin-C plays a greater role in this inflammatory disease than the others tested. Proteolytic cleavage resulting in loss of recognition in the sandwich ELISA, (as discussed above) may be another reason for the discrepancy between sandwich and competition assay results. Tenascin-C alternative splicing (Giblin and Midwood, 2015) as well as protease expression and activation, such as that of MMPs (Nissinen and Kahari, 2014), is known to be affected by disease states. Therefore, the differences between tenascin-C levels in the non-RA

diseased group obtained from the sandwich versus competition ELISAs may reflect the greater likelihood of epitope loss for the sandwich assay.

For comparison, as in the healthy control samples the total tenascin-C levels of RA patients were found to be far greater than the specific splice variants detected by the IBL ELISAs. The correlations between splice specific variants and total tenascin-C were also found to be quite variable and in most cases weak. This suggests that splice specific tenascin-C is not a good read out of total tenascin-C levels in serum and this should be taken into account when considering the results of the IBL assays. Additionally, stark differences were also observed between the two IBL assays and thus between the levels of the different splice variants. This was evident with both assays results only showing a moderate correlation with the amount of the FNIII-C splice variant detected found to be much lower than the FNIII-B variant. While perhaps a reflection of differential assay performance, this could also suggest that the two exons are part of differential splicing modules resulting in different incorporation rates into tenascin-C and thus abundance. Alternatively, this could also suggest differential ability of the spliceoforms to make it into the circulation, perhaps due to the splicing conferring differential binding abilities or proteolytic processing.

Consideration should also be given to how accurately tenascin-C levels in the serum actually mirror the tenascin-C found at the pathological site as no current studies have characterised how tenascin-C ends up in circulation. This is additionally hampered by the fact the majority of studies carried out on the tenascin-C found at the inflammatory site utilise non-quantitative methods of tenascin-C measurement such as IHC or western blotting. RA is one of the few diseases in fact where local amounts of tenascin-C have been quantified with a studies investigating tenascin-C concentrations in knee synovial fluid utilising the IBL FNIII-C ELISA. These have revealed that control joints as expect contain very low amounts of tenascin-C with a median level of 7.7ng/ml whereas joints from RA patients have much higher levels with a median of 166.8ng/ml (Hasegawa et al., 2004, Hasegawa et al., 2007). While these studies did not investigate systemic tenascin-C the data presented above for the FNIII-C ELISA found that control and RA patients had lower average systemic tenascin-C concentrations of 25.7 and 77.3ng/ml respectively. While this might not be representative for other diseases

or total tenascin-C this does indicate that systemic tenascin-C does not necessarily completely mirror the tissue levels of tenascin-C in disease.

5.6.7 Clinical utility of total tenascin-C

Both the competition and sandwich ELISAs were able to discriminate RA patients from healthy controls. However, they were both outperformed by the splice variant specific IBL assays in the limited amount of patients and donors tested with the IBL kits. This suggests that the FNIII-B and FNIII-C splice variants are more closely associated with the RA diseased state, fitting with the observation that differential tenascin-C splicing is seen with inflammatory disease (Giblin and Midwood, 2015). The ability of the total tenascin-C assays to diagnose RA also suffered with the inclusion of non-RA inflammatory disease group which significantly impacted both assays specificity. This reflects the general increase of tenascin-C seen in inflammatory disease suggesting it is more a marker of general inflammation than of a specific disease such as RA. This is supported by previous studies of splice specific tenascin-C which showed it correlated with the levels of the acute phase protein CRP, a general systemic marker of inflammatory responses (Schenk et al., 1995).

In terms of RA patient subgroups using the tenascin-C levels measured in the sandwich assay no association between any of the groups for which data was available was identified. For the competition assay one subgroup association was found with seemingly higher levels of tenascin-C measured by this assay found in CCP negative patients. While this might simply be a reflection of the lower numbers of CCP negative patients in our cohort it could also due to a number of known differences between CCP positive and negative patients. For example, it is known that differences in synovial immune cell infiltration are seen with less lymphocytes and more extensive fibrosis seen in CCP negative patients (van Oosterhout et al., 2008). RA driven more weakly by lymphocytic infiltration would fit with heighted tenascin-C levels as it has it been shown that lymphocytes express lower levels of tenascin-C compared to other leukocytes, such as macrophages (Giblin, 2018). It has also been shown that tenascin-C is able to drive fibrosis (Bhattacharyya et al., 2016) and so this may correlate with the increased fibrosis seen in the CCP negative patients. Other studies have shown that CCP negative RA patients achieve less disease remission than positive patients when

treated with the conventional disease modifying anti-rheumatic drug methotrexate (Wevers-de Boer et al., 2012, van Dongen et al., 2007). Previous studies have shown that methotrexate, unlike biologic therapies, was unable to reduce tenascin-C FNIII-C levels in RA patients (Page et al., 2012). Thus, it could be postulated that CCP negative patients have a more tenascin-C driven form of disease which is less receptive to methotrexate treatment. FNIII-C tenascin-C levels have also been shown to correlate with disease severity and response to biologic therapies, with some prognostic ability for predicting responsiveness to the biologic therapeutic infliximab shown (Page et al., 2012). Future work with better clinically described cohorts would be is needed to see if this association is true for total tenascin-C as well.

5.6.8 Forms of tenascin-C in human serum

The results of the various assay formats, detecting different forms of tenascin-C, presented in this chapter highlight the heterogeneity of serum tenascin-C. The differences in isoforms of tenascin-C present in RA and healthy controls, as suggested by the IBL ELISAs, was also shown by western blotting. In both healthy control and RA patients two major molecular weight forms were seen at 200 and 280kDa. In addition, another, albeit less abundant, band was also observed in RA sera alone at approximately 210kDa suggesting the presence of a disease specific splice variant. Tenascin-C splicing is known to be regulated and promoted in a number of disease conditions including, inflammation, with functional consequences (Giblin and Midwood, 2015, Giblin, 2018). As such, further investigation of the forms identified here are warranted.

Another, form of variation investigated in this chapter was the presence of tenascin-C interacting partners in serum. As a large multi-modular ECM molecule tenascin-C is known to bind a wide array of partners, from other ECM molecules, to soluble signalling factors, as well as a variety of cell surface proteins (Midwood et al., 2016). As such, its ability to retain binding to these factors and accompany them while circulating was of interest. Mass spectrometric analysis identified fibronectin as a serum binding partner in both healthy control and RA serum. Fibronectin is a ubiquitously expressed ECM component but is also secreted into the blood by liver hepatocytes to exist as a distinct form in the circulation (To and Midwood, 2011b).

Plasma fibronectin has been previously described as a tenascin-C interactor *in vitro* (Chung et al., 1995) and the data in this chapter would support that this interaction has *in vivo* relevance. The functional implications of this interaction remain to be elucidated; however, plasma fibronectin is known to form part of fibrin clots formed in response to tissue injury. Tenascin-C likewise has been shown to accumulate adjacent to tissue wounds less than 24hrs after wounding (Mackie et al., 1988). Moreover, tenascin-C has also been shown to promote fibrin accumulation and localise in close proximity to it in pulmonary fibrotic lesions (Brellier et al., 2011). As such, recruitment of circulating tenascin-C could present another means by which the protein is upregulated and plays a role at sites of tissue injury. The association with circulating fibronectin in this scenario may also aid in the rapid deposition of the protein as it has been shown fibronectin is needed for tenascin-C incorporation into the matrix (Ramos et al., 1998). Furthermore, a reciprocal aspect of this relationship has also been observed with less fibronectin accumulating in the granulation tissue of tenascin-C KO mice after dermal wounding (Forsberg et al., 1996).

The fibronectin interaction may also have implications for the 9F8-NSCT-121 sandwich ELISA, with the binding site of plasma fibronectin mapped to the 1-5 FNIII-type repeats of fibronectin (To and Midwood, 2011a). This overlaps with the 9F8 epitope on tenascin-C, which is located within the 1-3 FNIII-type repeats. As such, fibronectin binding to tenascin-C may compete with or completely inhibit recognition of tenascin-C by 9F8. This may be further affected by tenascin-C alternative splicing as the inclusion of additional FNIII-type repeats was shown to result in lower affinity to plasma fibronectin (To and Midwood, 2011a).

Besides splicing and binding partners, additional aspects of tenascin-C variation while not directly investigated here should also be considered. This includes post translational modifications such as glycosylation, which has already been shown to vary by cell type (Mangan et al., 2019). This has potential implications for the molecular weight variant isoforms observed, which may have additionally been affected by their state of glycosylation. Citrullination may be another modification worth probing, as other RA citrullinated autoantigens such as fibrinogen have been detected in the circulation as part of immune complexes (Zhao et al., 2008). No

citrullination of circulating tenascin-C was detected in the current study although this may simply reflect technical limitations of the techniques employed.

5.6.9 Study considerations and limitations

Interpreting the results in this chapter a number of limitations and considerations should be made. Firstly, the patient and control cohorts investigated must be considered. Ascertainment bias could be a factor in the study, as CCP based assays are present in diagnostic guidelines and used routinely in the clinic for diagnosis of RA (Aletaha et al., 2010). Therefore, recruitment and classification as an RA patient within the cohorts studied is likely biased towards the CCP assay. This affect has been suggested in other studies using cohorts that recruited patients early in diagnosis before the CCP assay was used and showed a higher proportion of cTNC5 positive samples in the CCP negative groups (Schwenzer et al., 2019). In addition, when making comparisons of the current study to studies reported in the literature, the differences between study design and patient inclusion should be considered. For example, different results will be obtained when diagnostic accuracy is assessed in a study in which healthy donors are used as negative controls, versus a study using a more clinically representative population (Usher-Smith et al., 2016). This variation in test performance between different settings, referred to as the spectrum effect, were demonstrated in this study itself, with inclusion of non-RA diseased patients affecting the diagnostic ability of all the assays investigated.

The general characteristics of the patients cohorts studied should also be considered. For example, the RA cohorts utilised in this study comprised mainly elderly patients with well-established disease. This likely impacted results as the CCP test is known to perform differentially in early versus established disease (Demoruelle et al., 2013). Likewise, age of disease onset is another factor known to influence ACPA prevalence which could also have impacted results (Boeters et al., 2017). Differences have also been observed between different geographic populations, for example differences in ACPA fine specificities has been shown between Malaysian and Swedish RA patients (Too et al., 2017). These regional differences suggest that while overall disease characteristics may be similar, different underlying genetic or environmental factors may be in play. This is of note due to the inclusion of geographically separated cohorts

in this study with samples derived from patient populations in Mexico, the UK, and Switzerland. No overt differences were observed between the RA cohorts investigated and the cTNC5 autoantibody response. In contrast differences were observed with the total tenascin-C ELISAs, with lower tenascin-C levels seen in Mexican versus UK RA patients, suggesting the potential influence of a regional environmental factor. A final uncontrolled variable in the cohorts was patient treatment or disease activity which is likely to have had a major impact on anti-cTNC5 and anti-tenascin-C assay results. For example, it has been reported that treatment with the steroid prednisolone abrogated the CCP assays ability to predict radiographic joint damage (Hafstrom et al., 2014). Tenascin-C FNIII-C concentrations were likewise shown to be impacted by therapy with a decrease in tenascin-C levels observed with administration of biologic therapy (Page et al., 2012). Therefore, it is possible that the heterogeneity of patient treatment and disease activity could have affected the results.

Chapter 6 Final discussion and future research

6.1 General discussion

6.1.1 Role of tenascin-C in IBD

Immune mediated inflammatory diseases (IMIDs) represent a growing medical problem globally with a high burden on both patients as well as society as a whole (Russell et al., 2011, Baumgart et al., 2019). Inflammatory bowel disease (IBD), as one of the most common IMIDs, is no different in this regard with increasing incidence and prevalence in the UK (Molodecky et al., 2012), with rising associated costs to the National Health Service, which are estimated to already be in excess of £1 billion per year (Ghosh and Premchand, 2015). As such, with health services faced by this mounting challenge, the need to properly understand the aetiology and disease drivers of this enigmatic condition is greater than ever.

Much progress has been made in regard to this in recent decades with the identification of perturbations in epithelial barrier integrity and microbial dysbiosis which are now among some of the key factors implicated in disease pathogenesis (Chassaing and Darfeuille-Michaud, 2011, Antoni et al., 2014). In terms of disease drivers much progress has also been made with the identification of the key role of the pro-inflammatory cytokine TNF being arguably the biggest landmark finding in recent decades (Neurath, 2014). However, the puzzle is still very much incomplete with other factors contributing to this complex disease still yet to be identified and characterised. The work of this thesis has focused on one such potential factor, the ECM glycoprotein tenascin-C.

The ECM was once thought of as a static scaffold but is now well recognised as key modulator of cellular behaviour and function (Hynes, 2009). This includes behaviour in inflammatory disease as well as in health, with the recognition of its importance leading to research which is now opening up this previously untapped reserve of pathophysiologically relevant factors (Korpos et al., 2009, Sorokin, 2010). IBD is no exception to this with the role of the ECM and it's pathological remodelling now implicated in a variety of disease processes, from the structural changes seen in fistulisation and stricture formation, to providing direct pro-inflammatory stimulation

to the pathological response (Shimshoni et al., 2015, Petrey and de la Motte, 2017). It is in this latter role which tenascin-C is implicated as a driver and propagator of the inflammatory response. Animal models of disease have implicated tenascin-C in this role in variety of diverse IMIDs, from RA (Midwood et al., 2009) to multiple sclerosis (Momcilovic et al., 2017), with the work of this thesis adding IBD to this list as well. This includes the work of chapter 3 which demonstrated tenascin-C's upregulation in the damaged and inflamed mucosal tissue of the DSS colitis model. This was further corroborated by the work of chapter 4 which additionally provided evidence for tenascin-C's direct role in the inflammatory pathology as indicated by the partially protective phenotype seen in *Tnc*$^{-/-}$ mice.

While not addressed directly in this thesis a number of previous mechanisms for tenascin-C's pro-inflammatory activity have been reported and shown to have *in vivo* pathological relevance in other models of inflammatory disease. As such, with the apparent usage of the same or similar pathological mechanisms across different IMIDs (Rahman et al., 2010), it can be reasonably speculated that these same mechanisms may explain some of the observations made with the DSS colitis model in this thesis as well. This includes tenascin-C's ability to signal via the α9β1 and αVβ3 integrins (Kanayama et al., 2011, Shimojo et al., 2015), as well as the PRR TLR4 (Midwood et al., 2009). Indeed, links between these pathways and IBD already exist with the gene *ITGAV, which codes for* the αV subunit of the αVβ3 integrin, found to lie within in an IBD associated locus in a genetic association study (de Lange et al., 2017). Additionally, for TLR4 a significant body of work has already established this receptors link to the disease. This has similarly included genetic association studies which have found polymorphisms in the receptor associated with IBD in a number of diverse patient cohorts (Ao et al., 2015, Cheng et al., 2015). Furthermore, these associations have been found to have additional phenotypic correlations with some variants associated with more aggressive disease course and extraintestinal manifestations, such as arthritis (Dragasevic et al., 2017, Feki et al., 2017). TLR4 is found to be expressed at increased levels in both epithelial and lamina propria cells of IBD patients (Vamadevan et al., 2010). Additionally the macrophages in the latter population also show a hyperresponsiveness to TLR stimulation leading to production of a number of key IBD mediators, including TNF, IL-6, and IL-23 (Bain and

Schridde, 2018). Together these data indicate that the TLR4 signalling pathway, known to be activated by tenascin-C, displays a clear association with IBD pathogenesis which may explain the protective effects of tenascin-C's loss in DSS colitis.

It should be kept in mind however, that the role of tenascin-C in the inflammatory response has been shown to not always be so clear cut of a pathological nature. This has already been mentioned for the cases of chemically induced dermatitis (Koyama et al., 1998) and toxin induced glomerulonephritis (Nakao et al., 1998) in which *Tnc*$^{-/-}$ mice showed defective tissue regeneration. It is perhaps best exemplified in the case of osteoarthritis (OA) however, as it shares a similar localisation of pathology to the joint as RA, a disease in which tenascin-C's role in driving has been already highlighted (Midwood et al., 2009). OA is characterised as a degenerative disease of the whole joint in which structural alterations and breakdown of the articular cartilage and subchondral bone leads to pain and joint dysfunction (Hunter and Bierma-Zeinstra, 2019). In both spontaneous and surgical models of OA *Tnc*$^{-/-}$ mice showed slower cartilage repair and enhanced cartilage degeneration (Okamura et al., 2010). Furthermore, more recent studies have shown that injection of exogenous glioma cell line purified tenascin-C into the joints of a surgical OA model slowed joint degeneration (Matsui et al., 2018). This is surprising considering injection of similar amounts of recombinantly produced FBG domain of tenascin-C into joints has been shown to induce synovitis and joint damage (Midwood et al., 2009). This demonstrates the multifunctional nature of the different domains of tenascin-C and highlights its potential roles at different stages of the inflammatory response.

Indeed, this duplicitous nature in fact mirrors a similar phenomenon which has been found for TLR4 signalling in models of IBD as well in which the receptor has been found to have protective functions. This has been evidenced in several studies of TLR4 knockout (*Tlr4*$^{-/-}$) mice in the DSS colitis model which found, counterintuitively based on its pro-inflammatory nature, that TLR4 deficiency actually worsened colitis (Rakoff-Nahoum et al., 2004, Fukata et al., 2005, Shi et al., 2019). This was attributed to the fact that, while the *Tlr4*$^{-/-}$ mice exhibited reduced granulocyte infiltration, their mucosal healing was perturbed leading to increased tissue damage and associated

intestinal bleeding, and bacterial invasion. Furthermore, this was found to mimic the phenotype of *Myd88*$^{-/-}$ mice suggesting that there affects were mediated via the myddosome extracellular signalling pathway, rather than the alternative intracellular TRIF pathway, by which TLR4's protective signalling was acting (Rakoff-Nahoum et al., 2004, Araki et al., 2005). This was suggested to be due to TLR4's ability to induce production of signalling factors, including prostaglandin E2 (PGE2) and granulocyte-macrophage colony-stimulating factor (GM-CSF)(Shi et al., 2019), which have known roles in promoting intestinal tissue repair (Egea et al., 2013, Miyoshi et al., 2017). As the *Tnc*$^{-/-}$ mice did not show any deficiencies in mucosal healing, as evidenced in the DSS recovery model, this suggests that tenascin-C signalling does not contribute significantly to this pathway. Indeed, it could be argued that tenascin-C actually acts to tip the balance in TLR4 signalling towards a more pro-inflammatory and thus tissue damaging response, for example by its ability to promote TNF production in response to TLR4 stimulation (Piccinini and Midwood, 2012). Overall, this demonstrates the contrasting roles, factors, receptors, and signalling pathways can play at different stages of the inflammatory response and the importance of feedback loops and changes in signalling context. This is particularly important to consider when considering the possibility of targeting tenascin-C therapeutically.

6.1.2 Tenascin-C as a therapeutic target in inflammatory disease

In recent years great gains have been made with the introduction of antibody based biologic therapies targeting specific mediators of inflammatory disease and IBD is no different. Indeed, IBD was actually the first IMID to be targeted by these therapies with the trailblazer anti-TNF antibody infliximab first tested and shown efficacy in the treatment of a Crohn's disease patient in 1993 (Derkx et al., 1993). Infliximab subsequently received its first in class marketing approval by the American Food and Drug Administration (FDA) in 1998 (Melsheimer et al., 2019) and since then the biologics field has rapidly grown as research has expanded the list of potential targets and improved antibody technologies. Currently three major classes of biologics are approved for the treatment of IBD which target TNF, IL-12/23, and α4 integrin receptors respectively with all having demonstrated good efficacy in clinical trials (Paramsothy et al., 2018). However, while a significant breakthrough, these therapies

still have shortcomings with for example 30% of patients failing to respond to anti-TNF agents which increases further when accounting for patients who develop loss of responsiveness later in treatment (Yanai and Hanauer, 2011). Furthermore, these therapies also do not come without their downsides with an increased risk of infection or malignancy having been established for some of the therapies (Quezada et al., 2018).

With this current treatment landscape there is obviously clear unmet clinical need and thus opportunity for novel treatments to emerge. The work of this thesis would raise tenascin-C as one such potential candidate to pursue with chapter 4's work showing its ablation is protective of disease. Indeed, tenascin-C already has a long-established relationship as a target of biologic therapy in the field of oncology where anti-tenascin-C antibodies have been used to target radioactive iodine to gliomas in human patients as far back as 1988 (Lee et al., 1988, Spenle et al., 2015). Of greater relevance to IBD however is more recent efforts to develop an anti-tenascin-C therapy aimed at disrupting the FBG-TLR4 interaction and thus help dampen the proteins pro-inflammatory activity. These efforts are currently focused on applying this therapy to RA where the role of TLR4 signalling in disease is well known with anti-TLR4 biologic therapies also in development (Monnet et al., 2017) having shown efficacy in animal models (Kiyeko et al., 2016). These therapies raise concerns of potential adverse immunosuppression however, with a number of immunodeficiency syndromes associated with increased susceptibility to infection caused by defective TLR signalling (Maglione et al., 2015). Furthermore, this approach as was indicated by the findings in *Tlr4*$^{-/-}$ mice is unlikely to be efficacious in IBD. In regard to this a separate anti-TLR4 antibody used in a DSS colitis study has already demonstrated that this approach recapitulated the abrogated mucosal healing phenotype of the *Tlr4*$^{-/-}$ mice (Ungaro et al., 2009). As such, targeting the ligand tenascin-C presents itself as a potentially more amicable option for therapy.

This approach has already demonstrated efficacy in an animal model, with a rat collagen-induced RA model showing significant reductions in both clinical and histological disease scoring with anti-tenascin-C antibody treatment (Aungier et al., 2019). These early findings are promising and not just necessarily for RA with the

previous success of transfer of biologic therapies between IBD and RA seen with the anti-TNF therapies, attributed to common shared pathological mechanisms (Kuek et al., 2007). With the findings in this thesis of *Tnc*$^{-/-}$ mice protected in an IBD model similarly to how they were protected in a range of RA models this suggests that tenascin-C may be playing a role in another common disease mechanism. As such, therapies targeting this mechanism, diagrammatically summarised in figure 6.1, may have applicability across both conditions as well.

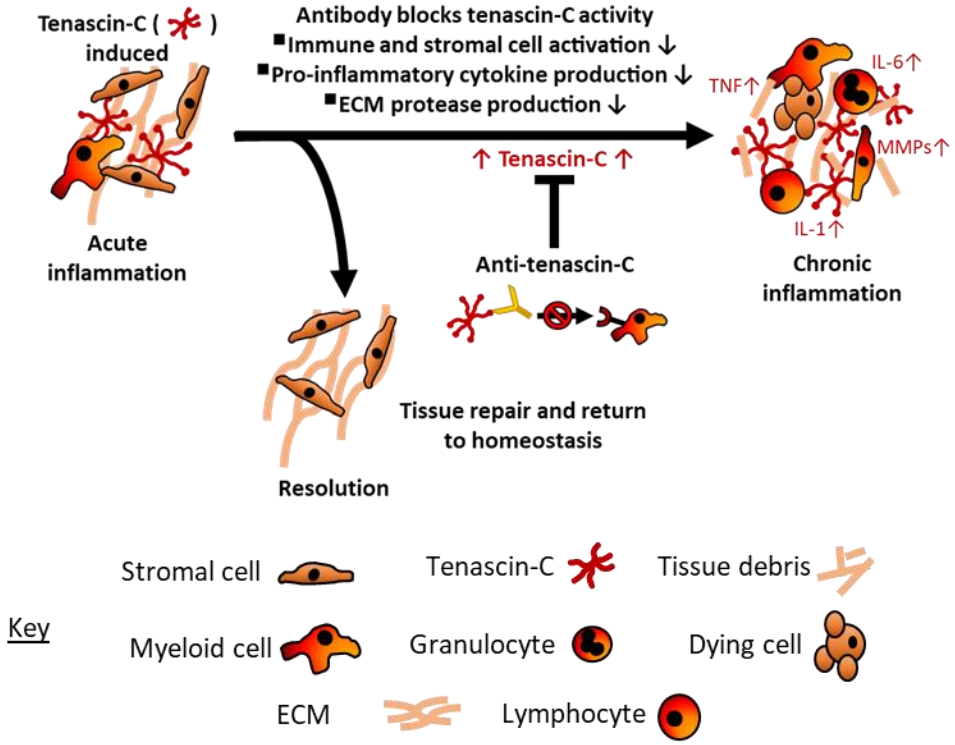

Figure 6.1 Model of targeting of tenascin-C as a therapy in inflammatory disease

Theoretical model for how a tenascin-C targeting therapy might function. Tenascin-C is induced in the initial acute inflammatory stage of inflammatory disease and deposited in the extracellular matrix (ECM). Left unchecked tenascin-C subsequently creates a self perpetuating pro-inflammatory niche at this site which helps drive the inflammatory response to chronicity leading to disease and tissue dysfunction. However, administration of therapeutic neutralising antibodies directed against tenascin-C aims to block this pathway by binding to tenascin-C. These antibodies epitopes lie within the pro-inflammatory signalling domains of tenascin-C, such as those within the fibrinogen-like globe domain required for TLR4 signalling. As such, antibody binding blocks these domains interactions with their cognate receptors. This disrupts the pro-inflammatory niche and breaks the positive feedback loop supporting its self-perpetuation with reduced pro-inflammatory signalling leading to a reduction in tenascin-C expression. Additionally, production of tissue damaging ECM proteases is likewise reduced resulting in reduced release of endogenous damage associated inflammatory inducers as well. With these drivers of chronicity blocked and tissue damage subsiding the inflammatory response is able to dampen down and resolve.

6.1.3 Clinical applicability of tenascin-C as a biomarker

As has been explored in this thesis therapy is not the only area in which tenascin-C has shown promise for clinical application with its systemic form and autoantibodies against it candidate biomarkers as well. Biomarkers are of increasing clinical importance as objective tests for diagnostic and prognostic management of patients become ever more important as medicine switches to a more personalised approach (Committee, 2011). This is particularly true of complex diseases like IMIDs whose combination of non-specific symptoms and often lack of objective diagnostic and prognostic tests, especially in the early stages of disease, leads to a delay in diagnosis and impaired clinical management (Alonso et al., 2016).

To this end tenascin-C has already been investigated as a biomarker in a variety of conditions, including cancer and heart disease (Midwood et al., 2011), as well as a range of IMIDs (Marzeda and Midwood, 2018). However, these analyses have been somewhat hamstrung by the lack of a simple, accurate, and robust assay for the measurement of total tenascin-C levels in biological samples. In chapter 5 of this thesis I have aimed to help address this issue with the development and characterisation two novel assays for measurement of tenascin-C and tenascin-C specific autoantibodies in human serum samples.

Both of these assays demonstrate some degree of clinical utility, with significantly elevated levels of tenascin-C and autoantibodies against it found in RA patient samples. However, the lack of disease specificity seen with the total tenascin-C ELISA and reduced sensitivity in comparison with the current gold standards for the autoantibody test, suggest these assays are unlikely to find diagnostic utility in a clinical setting. Instead, their utility is likely to be better realised in the stratification of patients with tenascin-C acting as a direct or proxy marker for specific disease mechanisms with potential clinical implications for patient management. Furthermore, as discussed earlier with the potential for these disease mechanisms to be shared between a range of IMIDs these tests could potentially also be applicable to a range of different IMIDs as well. Indeed, it could be envisaged that these tests might find use as companion diagnostics for anti-tenascin-C based therapies, allowing application of

the therapy to patients in which tenascin-C appears to be particularly elevated or involved in disease pathogenesis (Cutolo et al., 2019).

6.2 Directions for future research

Based on these as well as earlier conclusions on the roles and function of tenascin-C in inflammatory disease a number of key questions have arisen or remain to be answered.

6.2.1 Function of basal expression of tenascin-C and non-pathological roles

One key question, which has remained unanswered since the generation of the first *Tnc*$^{-/-}$ mouse, is what function basal expression of tenascin-C in tissues serves. Chapter 3 found a not insignificant amount of tenascin-C present in the resting colon which was found to localise to smooth muscle and a subepithelial band in the mucosa. Chapter 5 meanwhile found an equally not insignificant amount of tenascin-C present in normal healthy human serum. With the apparent health and normal tissue function of *Tnc*$^{-/-}$ mice no obvious function of either of these reservoirs of basal tenascin-C protein can be readily attributed. As such, is it safe to assume, as was postulated at the time of the generation of first *Tnc*$^{-/-}$ mouse, that this expression may simply be superfluous, perhaps a quirk of the evolution of the transcriptional regulation of genes (Erickson, 1993)? I would argue no, as was found back then, it may simply be the phenotypes are more subtle in locations or context yet to be examined or than can be readily detected utilising the current models and tools available.

In regard to this a number of experiments can be proposed to help tease out these functions. Firstly, further characterisation of tenascin-C producing cells and transcriptional programs, under basal conditions, may aid in inferring function. This could be studied in current transcriptomic datasets with the mapping of co-expression networks around tenascin-C potentially able to infer function based on the known functions of its co-expressors and their shared regulatory networks (Li et al., 2017). Additionally, a much more costly approach would be to apply lineage tracing, to label tenascin-C producing cells *in vivo*, and single cell transcriptional approaches to further dissect these cells functions once isolated (Kester and van Oudenaarden, 2018). Both of these approaches could help in the teasing out of tenascin-C's potential functions or

relevance in the colon. However, the source of the tenascin-C found in circulation proves a much more challenging prospect to determine, with its potential to be produced in any of the vascularised organs of the body. In this case generation of conditional tissue or cell type specific knockouts of tenascin-C combined with serum measurement of the protein may prove the only method of identifying the source. In particular, the smooth muscle cells of the vasculature as well as hepatocytes of the liver may prove prospective first targets with the former known to produce tenascin-C in close proximity to the circulation, and the latter known to produce the majority of serum proteins found within the blood.

The roles of both of these basal reservoirs of tenascin-C protein may turn out still to be related to the inflammatory or immune response albeit in a non-pathological context. Indeed, this is another area of research worth pursuing further as while much work has been done on tenascin-C's function in pathological inflammation it's physiological role in the process has been less closely scrutinised. Indeed some studies have already hinted at perhaps perturbed immunity with the reduction in TNF and IL-17 production by *Tnc*$^{-/-}$ mice (Piccinini and Midwood, 2012, Ruhmann et al., 2012). However, the exact impacts of these deficiencies in models of infection remains to be seen and dissected. Indeed, these studies themselves may prove important in evaluating the potential risks which tenascin-C targeting therapeutics might pose.

6.2.2 Further dissection of tenascin-C's specific roles in colonic inflammation

While the work of this thesis has descriptively profiled tenascin-Cs localisation in DSS colitis further work remains to identify its specific roles in intestinal inflammation. These can somewhat be inferred from the phenotypes of *Tnc*$^{-/-}$ mice as well as tenascin-C's proven roles in other inflammatory disease contexts. However, with the context of the inflammatory response shown to be so important and the GI immune system so specialised, especially in contrast to the sterile environment of an RA joint, further work is needed to more precisely characterise tenascin-C's role in intestinal inflammation. Indeed, in the studies undertaken in chapter 5 further analysis was planned with samples collected for the interrogation of colonic gene expression in both WT and *Tnc*$^{-/-}$ mice under basal and colitic conditions. Completion of this work would

give a first glimpse at the functional consequences of tenascin-C loss on specific inflammatory factors in the colon. Additionally, the DSS model is amendable to cell type specific analysis by applying flow cytometry to colon extracted cells (Weigmann et al., 2007). Again, by combining this technique with the *Tnc*$^{-/-}$ mouse a more comprehensive as well as quantifiable overview of the impacts of tenascin-C on the various cell indicated to be involved in IBD could be undertaken. Furthermore, isolation of cells types of interest by cell sorting would additionally allow for even more detailed analysis. This could come in the form of cell type specific transcriptional or proteomic analysis as well as *ex vivo* manipulation and experimentation, such as stimulation with exogenous tenascin-C. Another aspect of biology which could be probed with particular relevance to IBD is metabolomics, with the interaction between gut microbiome produced metabolites and immune cells a growing area of interest (Franzosa et al., 2019). Additionally, it is now well known that other inflammatory activation can produce profound changes in cell metabolism (O'Neill et al., 2016) and so it would be of interest to examine tenascin-C's impact on this aspect of biology and how it might interact with IBD associated bacterial dysbiosis in the gut.

Besides these experiments which can be carried out with the already established models future experiments could also look to expand upon these with additional IBD models. This could include the use of other inducible chemical models of colitis with different modes of pathogenesis. One example is trinitrobenzene sulfonic acid (TNBS) colitis which induces pathology by intra-rectal administration of the TNBS haptenizing agent which creates neo-antigens which induce an immunogenic reaction in the colon (Wirtz et al., 2017). Non-chemical models could also be investigated such as the T cell transfer model, in which a pro-inflammatory population of T cells depleted of Tregs are transferred to immunodeficient *Rag1*$^{-/-}$ mice which subsequently develop colitis (Ostanin et al., 2009). Both these models have greatly different mechanisms of action from DSS colitis, with different integral cell types and inflammatory mediators (Strober et al., 2002). These experiments could thus help unravel tenascin-C's role in other immune compartments in intestinal inflammation. The T cell transfer model, being adaptive immune driven in contrast to innate driven DSS colitis, could be of particular interest in *Tnc*$^{-/-}$ mice given tenascin-C's apparent immunosuppressive roles in terms of T cells (Mirzaei et al., 2018). Non-inducible

genetic models could also be investigated for tenascin-C involvement with *Il-10*$^{-/-}$ mice, deficient in the anti-inflammatory cytokine IL-10 required for gut immune homeostasis, probably the best known example (Kuhn et al., 1993). This model could additionally be further probed by generation of *Tnc*$^{-/-}$ *Il-10*$^{-/-}$ double knockout mice to examine tenascin-C's role in this spontaneous disease model.

Besides *Tnc*$^{-/-}$ mice, novel genetically engineered tenascin-C models could also be of benefit in teasing out tenascin-C's roles in IBD. In particular a conditional knockout system for tenascin-C would be of great utility in a variety of ways. For a start this model could be used to generate cell type specific knockouts and reporter systems of tenascin-C in the gut. These could be used to confirm the key tenascin-C producers *in vivo* and whether tenascin-C's impacts on certain cells is in an autocrine or paracrine manner during inflammation. Additionally, generation of inducible systems could allow for control of induction or ablation of tenascin-C expression which if carried out at different time points would allow for further picking apart tenascin-C's roles in the different stages of inflammatory response. Besides knocking out tenascin-C knock-in mutants of the protein could also potentially be generated with key signalling sites inactivated or modified to assess their individual contributions to driving the inflammatory process. Indeed, such inactivating mutants have already been generated during the validation of the TLR4 and integrin IDG binding sites and thus would just need to be integrated into full length tenascin-C targeting vector to be utilised (Yokosaki et al., 1998, Zuliani-Alvarez et al., 2017).

6.2.3 Comprehensive characterisation of the different forms of tenascin-C

To fully understand tenascin-C's functionality, in health as well as disease, a better understanding of its various forms and modifications will likely be necessary. Tenascin-C displays remarkable variety with variable splicing and a number of post-translational modifications which have already been shown to impact its functionality (Giblin and Midwood, 2015). Further elucidation of these mechanisms will potentially provide explanations for a range of questions, such as how basally expressed tenascin-C regulates its pro-inflammatory properties, with modifications modulating its functionality in different contexts. Much of the work thus far done in this regard has

been in *in vitro* settings particularly in models involving exposing cultured cell lines to purified tenascin-C or domain fragments derived from it. While proving informative these studies obviously lack important context including the exact forms of tenascin-C present in the *in vivo* context of a complex 3D ECM.

To answer these questions the immunoprecipitation assay developed in chapter 5 should prove useful in allowing for the simplified purification of tenascin-C from biological samples for subsequent analysis. This was already partly begun in chapter 5 for serum with molecular weight forms and binding partners probed for by mass spectrometry and western blotting. Far more detailed analysis is possible however with splice forms able to be probed with antibodies specific to the different alternatively spliced repeats. Additionally, PTM mapping by mass spectrometry looking at modifications such as glycosylation, phosphorylation, and citrullination would also be possible. Following the identification of these mapped modifications their functionality could then then be better explored. This might be best done initially *in vitro* with recombinant tenascin-C artificially modified to match *in vivo* forms before application to cell lines. Additionally, recombinant tenascin-C could itself be engineered to lack for example key modified residues to further establish their functionality by studying what occurs with their disruption.

As well as informing studies of tenascin-C's function probing its variation might also aid its further development as a biomarker as well by potentially identifying specific disease associated forms. In combination with the ELISAs developed in chapter 5 these could be further investigated in better described prospective cohorts and might provide an additional measure by which to stratify patients into clinical subgroups.

In summary these proposed additional investigations would help to further characterise tenascin-C's role in health and disease and provide further mechanistic insight into the diverse nature of a highly variable protein. This greater understanding it is hoped could aid in the potential development of clinical tools based on tenascin-C for the treatment and management of chronic inflammatory disease.

References

ABBADI, D., LAROUMANIE, F., BIZOU, M., POZZO, J., DAVIAUD, D., DELAGE, C., CALISE, D., GAITS-IACOVONI, F., DUTAUR, M., TORTOSA, F., RENAUD-GABARDOS, E., DOUIN-ECHINARD, V., PRATS, A. C., RONCALLI, J., PARINI, A. & PIZZINAT, N. 2017. Local production of tenascin-C acts as a trigger for monocyte/macrophage recruitment that provokes cardiac dysfunction. *Cardiovasc Res*.

ADAMS, J. C., CHIQUET-EHRISMANN, R. & TUCKER, R. P. 2015. The evolution of tenascins and fibronectin. *Cell Adh Migr,* 9**,** 22-33.

AIGNER, T., NEUREITER, D., MULLER, S., KUSPERT, G., BELKE, J. & KIRCHNER, T. 1997. Extracellular matrix composition and gene expression in collagenous colitis. *Gastroenterology,* 113**,** 136-43.

AKTAR, R., PEIRIS, M., FIKREE, A., CIBERT-GOTON, V., WALMSLEY, M., TOUGH, I. R., WATANABE, P., ARAUJO, E. J. A., MOHAMMED, S. D., DELALANDE, J. M., BULMER, D. C., SCOTT, S. M., COX, H. M., VOERMANS, N. C., AZIZ, Q. & BLACKSHAW, L. A. 2018. The extracellular matrix glycoprotein tenascin-X regulates peripheral sensory and motor neurones. *J Physiol,* 596**,** 4237-4251.

ALETAHA, D., NEOGI, T., SILMAN, A. J., FUNOVITS, J., FELSON, D. T., BINGHAM, C. O., 3RD, BIRNBAUM, N. S., BURMESTER, G. R., BYKERK, V. P., COHEN, M. D., COMBE, B., COSTENBADER, K. H., DOUGADOS, M., EMERY, P., FERRACCIOLI, G., HAZES, J. M., HOBBS, K., HUIZINGA, T. W., KAVANAUGH, A., KAY, J., KVIEN, T. K., LAING, T., MEASE, P., MENARD, H. A., MORELAND, L. W., NADEN, R. L., PINCUS, T., SMOLEN, J. S., STANISLAWSKA-BIERNAT, E., SYMMONS, D., TAK, P. P., UPCHURCH, K. S., VENCOVSKY, J., WOLFE, F. & HAWKER, G. 2010. 2010 rheumatoid arthritis classification criteria: an American College of Rheumatology/European League Against Rheumatism collaborative initiative. *Ann Rheum Dis,* 69**,** 1580-8.

ALLEN, A., CARVILLE, S. & MCKENNA, F. 2018. Diagnosis and management of rheumatoid arthritis in adults: summary of updated NICE guidance. *Bmj,* 362**,** k3015.

ALONSO, A., JULIA, A., VINAIXA, M., DOMENECH, E., FERNANDEZ-NEBRO, A., CANETE, J. D., FERRANDIZ, C., TORNERO, J., GISBERT, J. P., NOS, P., CASBAS, A. G., PUIG, L., GONZALEZ-ALVARO, I., PINTO-TASENDE, J. A., BLANCO, R., RODRIGUEZ, M. A., BELTRAN, A., CORREIG, X. & MARSAL, S. 2016. Urine metabolome profiling of immune-mediated inflammatory diseases. *BMC Med,* 14**,** 133.

ALVES, C., LUIME, J. J., VAN ZEBEN, D., HUISMAN, A. M., WEEL, A. E., BARENDREGT, P. J. & HAZES, J. M. 2011. Diagnostic performance of the ACR/EULAR 2010 criteria for rheumatoid arthritis and two diagnostic algorithms in an early arthritis clinic (REACH). *Ann Rheum Dis,* 70**,** 1645-7.

ALZOGHAIBI, M. A., AL-MOFLEH, I. A. & AL-JEBREEN, A. M. 2008. Neutrophil chemokines GCP-2 and GRO-alpha in patients with inflammatory bowel disease. *J Dig Dis,* 9**,** 144-8.

AMBORT, D., BRELLIER, F., BECKER-PAULY, C., STOCKER, W., ANDREJEVIC-BLANT, S., CHIQUET, M. & STERCHI, E. E. 2010. Specific processing of tenascin-C by the metalloprotease meprinbeta neutralizes its inhibition of cell spreading. *Matrix Biol,* 29**,** 31-42.

AMIN, K., LUDVIKSDOTTIR, D., JANSON, C., NETTELBLADT, O., GUDBJORNSSON, B., VALTYSDOTTIR, S., BJORNSSON, E., ROOMANS, G. M., BOMAN, G., SEVEUS, L. & VENGE, P. 2001. Inflammation and structural changes in the airways of patients with primary Sjogren's syndrome. *Respir Med,* 95**,** 904-10.

ANNESE, V., DAPERNO, M., RUTTER, M. D., AMIOT, A., BOSSUYT, P., EAST, J., FERRANTE, M., GOTZ, M., KATSANOS, K. H., KIESSLICH, R., ORDAS, I., REPICI, A., ROSA, B., SEBASTIAN, S., KUCHARZIK, T. & ELIAKIM, R. 2013. European evidence based consensus for endoscopy in inflammatory bowel disease. *J Crohns Colitis,* 7**,** 982-1018.

ANTONI, L., NUDING, S., WEHKAMP, J. & STANGE, E. F. 2014. Intestinal barrier in inflammatory bowel disease. *World J Gastroenterol,* 20**,** 1165-79.

AO, R., WANG, Y., ZHNAG, D. R. & DU, Y. Q. 2015. Role of TLR4 rs4986790A>G and rs4986791C>T Polymorphisms in the Risk of Inflammatory Bowel Disease. *Gastroenterol Res Pract,* 2015**,** 141070.

ARAKI, A., KANAI, T., ISHIKURA, T., MAKITA, S., URAUSHIHARA, K., IIYAMA, R., TOTSUKA, T., TAKEDA, K., AKIRA, S. & WATANABE, M. 2005. MyD88-deficient mice develop severe intestinal inflammation in dextran sodium sulfate colitis. *J Gastroenterol,* 40**,** 16-23.

ARTIS, D. 2008. Epithelial-cell recognition of commensal bacteria and maintenance of immune homeostasis in the gut. *Nat Rev Immunol,* 8**,** 411-20.

ASANO, T., IWASAKI, N., KON, S., KANAYAMA, M., MORIMOTO, J., MINAMI, A. & UEDE, T. 2014. alpha9beta1 integrin acts as a critical intrinsic regulator of human rheumatoid arthritis. *Rheumatology (Oxford),* 53**,** 415-24.

ASSAD, L., SCHWARTZ, M. M., VIRTANEN, I. & GOULD, V. E. 1993. Immunolocalization of tenascin and cellular fibronectins in diverse glomerulopathies. *Virchows Arch B Cell Pathol Incl Mol Pathol,* 63**,** 307-16.

AUFDERHEIDE, E., CHIQUET-EHRISMANN, R. & EKBLOM, P. 1987. Epithelial-mesenchymal interactions in the developing kidney lead to expression of tenascin in the mesenchyme. *J Cell Biol,* 105**,** 599-608.

AUFDERHEIDE, E. & EKBLOM, P. 1988. Tenascin during gut development: appearance in the mesenchyme, shift in molecular forms, and dependence on epithelial-mesenchymal interactions. *J Cell Biol,* 107**,** 2341-9.

AUMILLER, V., BALSARA, N., WILHELM, J., GUNTHER, A. & KONIGSHOFF, M. 2013. WNT/beta-catenin signaling induces IL-1beta expression by

alveolar epithelial cells in pulmonary fibrosis. *Am J Respir Cell Mol Biol,* 49**,** 96-104.

AUNGIER, S. R., CARTWRIGHT, A. J., SCHWENZER, A., MARSHALL, J. L., DYSON, M. R., SLAVNY, P., PARTHIBAN, K., KARATT-VELLATT, A., SAHBUDIN, I., CULBERT, E., HEXTALL, P., CLANCHY, F. I., WILLIAMS, R., MARSDEN, B. D., RAZA, K., FILER, A., BUCKLEY, C. D., MCCAFFERTY, J. & MIDWOOD, K. S. 2019. Targeting early changes in the synovial microenvironment: a new class of immunomodulatory therapy? *Ann Rheum Dis,* 78**,** 186-191.

BACK, W., HEUBNER, C., WINTER, J. & BLEYL, U. 1997. Expression of tenascin in lymphocytic autoimmune thyroiditis. *J Clin Pathol,* 50**,** 863-6.

BAIN, C. C. & SCHRIDDE, A. 2018. Origin, Differentiation, and Function of Intestinal Macrophages. *Front Immunol,* 9**,** 2733.

BALA, S., MARCOS, M., KODYS, K., CSAK, T., CATALANO, D., MANDREKAR, P. & SZABO, G. 2011. Up-regulation of microRNA-155 in macrophages contributes to increased tumor necrosis factor {alpha} (TNF{alpha}) production via increased mRNA half-life in alcoholic liver disease. *J Biol Chem,* 286**,** 1436-44.

BALKA, K. R. & DE NARDO, D. 2019. Understanding early TLR signaling through the Myddosome. *J Leukoc Biol,* 105**,** 339-351.

BALUK, P. & MCDONALD, D. M. 2008. Markers for microscopic imaging of lymphangiogenesis and angiogenesis. *Ann N Y Acad Sci,* 1131**,** 1-12.

BANKS, C., BATEMAN, A., PAYNE, R., JOHNSON, P. & SHERON, N. 2003. Chemokine expression in IBD. Mucosal chemokine expression is unselectively increased in both ulcerative colitis and Crohn's disease. *J Pathol,* 199**,** 28-35.

BANSARD, C., LEQUERRE, T., DAVEAU, M., BOYER, O., TRON, F., SALIER, J. P., VITTECOQ, O. & LE-LOET, X. 2009. Can rheumatoid arthritis responsiveness to methotrexate and biologics be predicted? *Rheumatology (Oxford),* 48**,** 1021-8.

BAPTISTA, A. P., OLIVIER, B. J., GOVERSE, G., GREUTER, M., KNIPPENBERG, M., KUSSER, K., DOMINGUES, R. G., VEIGA-FERNANDES, H., LUSTER, A. D., LUGERING, A., RANDALL, T. D., CUPEDO, T. & MEBIUS, R. E. 2013. Colonic patch and colonic SILT development are independent and differentially regulated events. *Mucosal Immunol,* 6**,** 511-21.

BARCZYK, M., CARRACEDO, S. & GULLBERG, D. 2010. Integrins. *Cell Tissue Res,* 339**,** 269-80.

BARTON, G. M. 2008. A calculated response: control of inflammation by the innate immune system. *J Clin Invest,* 118**,** 413-20.

BAUMGART, D. C., MISERY, L., NAEYAERT, S. & TAYLOR, P. C. 2019. Biological Therapies in Immune-Mediated Inflammatory Diseases: Can Biosimilars Reduce Access Inequities? *Front Pharmacol,* 10**,** 279.

BEAULIEU, J. F. 1997. Extracellular matrix components and integrins in relationship to human intestinal epithelial cell differentiation. *Prog Histochem Cytochem,* 31**,** 1-78.

BEAULIEU, J. F., JUTRAS, S., DURAND, J., VACHON, P. H. & PERREAULT, N. 1993. Relationship between tenascin and alpha-smooth muscle actin expression in the developing human small intestinal mucosa. *Anat Embryol (Berl),* 188**,** 149-58.

BELANGER, I. & BEAULIEU, J. F. 2000. Tenascin in the developing and adult human intestine. *Histol Histopathol,* 15**,** 577-85.

BERENS, H. M., POLINSKI, K. J., MIKULS, T. R., KHATTER, S., AUGUST, J., VISSER, A., MAHLER, M., WEISMAN, M., O'DELL, J. R., KEATING, R. M., BUCKNER, J. H., GREGERSEN, P. K., NORRIS, J. M., HOLERS, V. M., DEANE, K. D. & DEMORUELLE, M. K. 2019. Anti-CCP3.1 and Anti-CCP-IgA Are Associated with Increasing Age in Individuals Without Rheumatoid Arthritis. *J Rheumatol*.

BERNSTEIN, C. N. 2017. Review article: changes in the epidemiology of inflammatory bowel disease-clues for aetiology. *Aliment Pharmacol Ther,* 46**,** 911-919.

BERTENSHAW, G. P., YIP, P., SESHAIAH, P., ZHAO, J., CHEN, T. H., WIGGINS, W. S., MAPES, J. P. & MANSFIELD, B. C. 2008. Multianalyte profiling of serum antigens and autoimmune and infectious disease molecules to identify biomarkers dysregulated in epithelial ovarian cancer. *Cancer Epidemiol Biomarkers Prev,* 17**,** 2872-81.

BHATTACHARYYA, S., WANG, W., MORALES-NEBREDA, L., FENG, G., WU, M., ZHOU, X., LAFYATIS, R., LEE, J., HINCHCLIFF, M., FEGHALI-BOSTWICK, C., LAKOTA, K., BUDINGER, G. R., RAPARIA, K., TAMAKI, Z. & VARGA, J. 2016. Tenascin-C drives persistence of organ fibrosis. *Nat Commun,* 7**,** 11703.

BIZZARO, N., TONUTTI, E., TOZZOLI, R. & VILLALTA, D. 2007. Analytical and diagnostic characteristics of 11 2nd- and 3rd-generation immunoenzymatic methods for the detection of antibodies to citrullinated proteins. *Clin Chem,* 53**,** 1527-33.

BOETERS, D. M., MANGNUS, L., AJEGANOVA, S., LINDQVIST, E., SVENSSON, B., TOES, R. E. M., TROUW, L. A., HUIZINGA, T. W. J., BERENBAUM, F., MOREL, J., RANTAPAA-DAHLQVIST, S. & VAN DER HELM-VAN MIL, A. H. M. 2017. The prevalence of ACPA is lower in rheumatoid arthritis patients with an older age of onset but the composition of the ACPA response appears identical. *Arthritis Res Ther,* 19**,** 115.

BOON, K., OSORIO, E. C., GREENHUT, S. F., SCHAEFER, C. F., SHOEMAKER, J., POLYAK, K., MORIN, P. J., BUETOW, K. H., STRAUSBERG, R. L., DE SOUZA, S. J. & RIGGINS, G. J. 2002. An anatomy of normal and malignant gene expression. *Proc Natl Acad Sci U S A,* 99**,** 11287-92.

BOSCA-WATTS, M. M., TOSCA, J., ANTON, R., MORA, M., MINGUEZ, M. & MORA, F. 2015. Pathogenesis of Crohn's disease: Bug or no bug. *World J Gastrointest Pathophysiol,* 6**,** 1-12.

BOURDON, M. A., WIKSTRAND, C. J., FURTHMAYR, H., MATTHEWS, T. J. & BIGNER, D. D. 1983. Human glioma-mesenchymal extracellular matrix antigen defined by monoclonal antibody. *Cancer Res,* 43**,** 2796-805.

BRANCATO, S. K. & ALBINA, J. E. 2011. Wound macrophages as key regulators of repair: origin, phenotype, and function. *Am J Pathol,* 178**,** 19-25.

BRANDTZAEG, P. 1974. Mucosal and glandular distribution of immunoglobulin components: differential localization of free and bound SC in secretory epithelial cells. *J Immunol,* 112**,** 1553-9.

BRANT, S. R., OKOU, D. T., SIMPSON, C. L., CUTLER, D. J., HARITUNIANS, T., BRADFIELD, J. P., CHOPRA, P., PRINCE, J., BEGUM, F., KUMAR, A., HUANG, C., VENKATESWARAN, S., DATTA, L. W., WEI, Z., THOMAS, K., HERRINTON, L. J., KLAPPROTH, J. A., QUIROS, A. J., SEMINERIO, J., LIU, Z., ALEXANDER, J. S., BALDASSANO, R. N., DUDLEY-BROWN, S., CROSS, R. K., DASSOPOULOS, T., DENSON, L. A., DHERE, T. A., DRYDEN, G. W., HANSON, J. S., HOU, J. K., HUSSAIN, S. Z., HYAMS, J. S., ISAACS, K. L., KADER, H., KAPPELMAN, M. D., KATZ, J., KELLERMAYER, R., KIRSCHNER, B. S., KUEMMERLE, J. F., KWON, J. H., LAZAREV, M., LI, E., MACK, D., MANNON, P., MOULTON, D. E., NEWBERRY, R. D., OSUNTOKUN, B. O., PATEL, A. S., SAEED, S. A., TARGAN, S. R., VALENTINE, J. F., WANG, M. H., ZONCA, M., RIOUX, J. D., DUERR, R. H., SILVERBERG, M. S., CHO, J. H., HAKONARSON, H., ZWICK, M. E., MCGOVERN, D. P. & KUGATHASAN, S. 2017. Genome-Wide Association Study Identifies African-Specific Susceptibility Loci in African Americans With Inflammatory Bowel Disease. *Gastroenterology,* 152**,** 206-217.e2.

BRELLIER, F., HOSTETTLER, K., HOTZ, H. R., OZCAKIR, C., COLOGLU, S. A., TOGBE, D., RYFFEL, B., ROTH, M. & CHIQUET-EHRISMANN, R. 2011. Tenascin-C triggers fibrin accumulation by downregulation of tissue plasminogen activator. *FEBS Lett,* 585**,** 913-20.

BRELLIER, F., TUCKER, R. P. & CHIQUET-EHRISMANN, R. 2009. Tenascins and their implications in diseases and tissue mechanics. *Scand J Med Sci Sports,* 19**,** 511-9.

BRIATA, P., ILENGO, C., BOBOLA, N. & CORTE, G. 1999. Binding properties of the human homeodomain protein OTX2 to a DNA target sequence. *FEBS Lett,* 445**,** 160-4.

BRISSETT, M., VERALDI, K. L., PILEWSKI, J. M., MEDSGER, T. A., JR. & FEGHALI-BOSTWICK, C. A. 2012. Localized expression of tenascin in systemic sclerosis-associated pulmonary fibrosis and its regulation by insulin-like growth factor binding protein 3. *Arthritis Rheum,* 64**,** 272-80.

BRITTON, G. J., CONTIJOCH, E. J., MOGNO, I., VENNARO, O. H., LLEWELLYN, S. R., NG, R., LI, Z., MORTHA, A., MERAD, M., DAS, A., GEVERS, D., MCGOVERN, D. P. B., SINGH, N., BRAUN, J., JACOBS, J. P., CLEMENTE, J. C., GRINSPAN, A., SANDS, B. E., COLOMBEL, J. F., DUBINSKY, M. C. & FAITH, J. J. 2019. Microbiotas from Humans with Inflammatory Bowel Disease Alter the Balance of Gut Th17 and RORgammat(+) Regulatory T Cells and Exacerbate Colitis in Mice. *Immunity,* 50**,** 212-224.e4.

BROGGI, A. & GRANUCCI, F. 2015. Microbe- and danger-induced inflammation. *Mol Immunol,* 63**,** 127-33.

BRYANT, C. E., GAY, N. J., HEYMANS, S., SACRE, S., SCHAEFER, L. & MIDWOOD, K. S. 2015. Advances in Toll-like receptor biology: Modes of activation by diverse stimuli. *Crit Rev Biochem Mol Biol,* 50**,** 359-79.

BUCHMAN, T. G. 2002. The community of the self. *Nature,* 420**,** 246-51.

BUCKLEY, C. D., GILROY, D. W., SERHAN, C. N., STOCKINGER, B. & TAK, P. P. 2013. The resolution of inflammation. *Nat Rev Immunol,* 13**,** 59-66.

BUDHWAR, S., VERMA, P., VERMA, R., RAI, S. & SINGH, K. 2018. The Yin and Yang of Myeloid Derived Suppressor Cells. *Front Immunol,* 9**,** 2776.

BUETTNER, M. & LOCHNER, M. 2016. Development and Function of Secondary and Tertiary Lymphoid Organs in the Small Intestine and the Colon. *Front Immunol,* 7**,** 342.

BUJKO, A., ATLASY, N., LANDSVERK, O. J. B., RICHTER, L., YAQUB, S., HORNELAND, R., OYEN, O., AANDAHL, E. M., AABAKKEN, L., STUNNENBERG, H. G., BAEKKEVOLD, E. S. & JAHNSEN, F. L. 2018. Transcriptional and functional profiling defines human small intestinal macrophage subsets. *J Exp Med,* 215**,** 441-458.

BURCHARDT, E. R., HEIN, R. & BOSSERHOFF, A. K. 2003. Laminin, hyaluronan, tenascin-C and type VI collagen levels in sera from patients with malignant melanoma. *Clin Exp Dermatol,* 28**,** 515-20.

BURISCH, J., JESS, T. & EGEBERG, A. 2019. Incidence of Immune-Mediated Inflammatory Diseases Among Patients With Inflammatory Bowel Diseases in Denmark. *Clin Gastroenterol Hepatol*.

BURISCH, J., JESS, T., MARTINATO, M. & LAKATOS, P. L. 2013. The burden of inflammatory bowel disease in Europe. *J Crohns Colitis,* 7**,** 322-37.

CADER, M. Z., FILER, A., HAZLEHURST, J., DE PABLO, P., BUCKLEY, C. D. & RAZA, K. 2011. Performance of the 2010 ACR/EULAR criteria for rheumatoid arthritis: comparison with 1987 ACR criteria in a very early synovitis cohort. *Ann Rheum Dis,* 70**,** 949-55.

CAREY, W. A., TAYLOR, G. D., DEAN, W. B. & BRISTOW, J. D. 2010. Tenascin-C deficiency attenuates TGF- β -mediated fibrosis following murine lung injury. *Am J Physiol Lung Cell Mol Physiol,* 299**,** L785-93.

CELONA, B., WEINER, A., DI FELICE, F., MANCUSO, F. M., CESARINI, E., ROSSI, R. L., GREGORY, L., BABAN, D., ROSSETTI, G., GRIANTI, P., PAGANI, M., BONALDI, T., RAGOUSSIS, J., FRIEDMAN, N., CAMILLONI, G., BIANCHI, M. E. & AGRESTI, A. 2011. Substantial histone reduction modulates genomewide nucleosomal occupancy and global transcriptional output. *PLoS Biol,* 9**,** e1001086.

CHASSAING, B., AITKEN, J. D., MALLESHAPPA, M. & VIJAY-KUMAR, M. 2014. Dextran sulfate sodium (DSS)-induced colitis in mice. *Curr Protoc Immunol,* 104**,** Unit 15.25.

CHASSAING, B. & DARFEUILLE-MICHAUD, A. 2011. The commensal microbiota and enteropathogens in the pathogenesis of inflammatory bowel diseases. *Gastroenterology,* 140**,** 1720-28.

CHAUDHRY, A., SAMSTEIN, R. M., TREUTING, P., LIANG, Y., PILS, M. C., HEINRICH, J. M., JACK, R. S., WUNDERLICH, F. T., BRUNING, J. C., MULLER, W. & RUDENSKY, A. Y. 2011. Interleukin-10 signaling in

regulatory T cells is required for suppression of Th17 cell-mediated inflammation. *Immunity,* 34**,** 566-78.

CHEN, L., DENG, H., CUI, H., FANG, J., ZUO, Z., DENG, J., LI, Y., WANG, X. & ZHAO, L. 2018. Inflammatory responses and inflammation-associated diseases in organs. *Oncotarget,* 9**,** 7204-7218.

CHENG, Y., ZHU, Y., HUANG, X., ZHANG, W., HAN, Z. & LIU, S. 2015. Association between TLR2 and TLR4 Gene Polymorphisms and the Susceptibility to Inflammatory Bowel Disease: A Meta-Analysis. *PLoS One,* 10**,** e0126803.

CHIOVARO, F., CHIQUET-EHRISMANN, R. & CHIQUET, M. 2015. Transcriptional regulation of tenascin genes. *Cell Adh Migr,* 9**,** 34-47.

CHIQUET, M. 1992. Tenascin: an extracellular matrix protein involved in morphogenesis of epithelial organs. *Kidney Int,* 41**,** 629-31.

CHIQUET, M. & WEHRLE-HALLER, B. 1994. Tenascin-C in peripheral nerve morphogenesis. *Perspect Dev Neurobiol,* 2**,** 67-74.

CHIQUET-EHRISMANN, R., HAGIOS, C. & MATSUMOTO, K. 1994. The tenascin gene family. *Perspect Dev Neurobiol,* 2**,** 3-7.

CHIQUET-EHRISMANN, R., OREND, G., CHIQUET, M., TUCKER, R. P. & MIDWOOD, K. S. 2014. Tenascins in stem cell niches. *Matrix Biol,* 37**,** 112-23.

CHOCKALINGAM, P. S., GLASSON, S. S. & LOHMANDER, L. S. 2013. Tenascin-C levels in synovial fluid are elevated after injury to the human and canine joint and correlate with markers of inflammation and matrix degradation. *Osteoarthritis Cartilage,* 21**,** 339-45.

CHOMCZYNSKI, P. & SACCHI, N. 1987. Single-step method of RNA isolation by acid guanidinium thiocyanate-phenol-chloroform extraction. *Anal Biochem,* 162**,** 156-9.

CHOVATIYA, R. & MEDZHITOV, R. 2014. Stress, inflammation, and defense of homeostasis. *Mol Cell,* 54**,** 281-8.

CHRISTO, S. N., DIENER, K. R. & HAYBALL, J. D. 2015. The functional contribution of calcium ion flux heterogeneity in T cells. *Immunol Cell Biol,* 93**,** 694-704.

CHUNG, C. Y., MURPHY-ULLRICH, J. E. & ERICKSON, H. P. 1996. Mitogenesis, cell migration, and loss of focal adhesions induced by tenascin-C interacting with its cell surface receptor, annexin II. *Mol Biol Cell,* 7**,** 883-92.

CHUNG, C. Y., ZARDI, L. & ERICKSON, H. P. 1995. Binding of tenascin-C to soluble fibronectin and matrix fibrils. *J Biol Chem,* 270**,** 29012-7.

CLANCY, P., LINCZ, L. F., MAGUIRE, J., MCEVOY, M., KOBLAR, S. A. & GOLLEDGE, J. 2014. Tenascin-C is increased in atherothrombotic stroke patients and has an anti-inflammatory effect in the human carotid artery. *Biofactors,* 40**,** 448-57.

CLARK, R. A., ERICKSON, H. P. & SPRINGER, T. A. 1997. Tenascin supports lymphocyte rolling. *J Cell Biol,* 137**,** 755-65.

CLEYNEN, I., BOUCHER, G., JOSTINS, L., SCHUMM, L. P., ZEISSIG, S., AHMAD, T., ANDERSEN, V., ANDREWS, J. M., ANNESE, V., BRAND, S., BRANT, S. R., CHO, J. H., DALY, M. J., DUBINSKY, M., DUERR, R. H., FERGUSON, L. R., FRANKE, A., GEARRY, R. B., GOYETTE,

P., HAKONARSON, H., HALFVARSON, J., HOV, J. R., HUANG, H., KENNEDY, N. A., KUPCINSKAS, L., LAWRANCE, I. C., LEE, J. C., SATSANGI, J., SCHREIBER, S., THEATRE, E., VAN DER MEULEN-DE JONG, A. E., WEERSMA, R. K., WILSON, D. C., PARKES, M., VERMEIRE, S., RIOUX, J. D., MANSFIELD, J., SILVERBERG, M. S., RADFORD-SMITH, G., MCGOVERN, D. P., BARRETT, J. C. & LEES, C. W. 2016. Inherited determinants of Crohn's disease and ulcerative colitis phenotypes: a genetic association study. *Lancet,* 387**,** 156-67.

CLICK, B., LOPEZ, R., ARRIGAIN, S., SCHOLD, J., REGUEIRO, M. & RIZK, M. 2019. Shifting Cost-drivers of Health Care Expenditures in Inflammatory Bowel Disease. *Inflamm Bowel Dis*.

COHEN, J. 2002. The immunopathogenesis of sepsis. *Nature,* 420**,** 885-91.

COITO, A. J. 2011. Leukocyte transmigration across endothelial and extracellular matrix protein barriers in liver ischemia/reperfusion injury. *Curr Opin Organ Transplant,* 16**,** 34-40.

COMMITTEE, N. R. C. 2011. The National Academies Collection: Reports funded by National Institutes of Health. *Toward Precision Medicine: Building a Knowledge Network for Biomedical Research and a New Taxonomy of Disease.* Washington (DC): National Academies Press (US)National Academy of Sciences.

CONWAY, G., VELONIAS, G., ANDREWS, E., GARBER, J. J., YAJNIK, V. & ANANTHAKRISHNAN, A. N. 2017. The impact of co-existing immune-mediated diseases on phenotype and outcomes in inflammatory bowel diseases. *Aliment Pharmacol Ther,* 45**,** 814-823.

COPERTINO, D. W., EDELMAN, G. M. & JONES, F. S. 1997. Multiple promoter elements differentially regulate the expression of the mouse tenascin gene. *Proc Natl Acad Sci U S A,* 94**,** 1846-51.

COSIN-ROGER, J., ORTIZ-MASIA, D., CALATAYUD, S., HERNANDEZ, C., ESPLUGUES, J. V. & BARRACHINA, M. D. 2016. The activation of Wnt signaling by a STAT6-dependent macrophage phenotype promotes mucosal repair in murine IBD. *Mucosal Immunol,* 9**,** 986-98.

COSNES, J., GOWER-ROUSSEAU, C., SEKSIK, P. & CORTOT, A. 2011. Epidemiology and natural history of inflammatory bowel diseases. *Gastroenterology,* 140**,** 1785-94.

CUPPEN, B. V., WELSING, P. M., SPRENGERS, J. J., BIJLSMA, J. W., MARIJNISSEN, A. C., VAN LAAR, J. M., LAFEBER, F. P. & NAIR, S. C. 2016. Personalized biological treatment for rheumatoid arthritis: a systematic review with a focus on clinical applicability. *Rheumatology (Oxford),* 55**,** 826-39.

CUTOLO, M., PICASSO, M., PONASSI, M., SUN, M. Z. & BALZA, E. 1992. Tenascin and fibronectin distribution in human normal and pathological synovium. *J Rheumatol,* 19**,** 1439-47.

CUTOLO, M., SOLDANO, S. & PAOLINO, S. 2019. Potential roles for tenascin in (very) early diagnosis and treatment of rheumatoid arthritis. *Ann Rheum Dis*.

D'ANGELO, F., BERNASCONI, E., SCHAFER, M., MOYAT, M., MICHETTI, P., MAILLARD, M. H. & VELIN, D. 2013. Macrophages promote

epithelial repair through hepatocyte growth factor secretion. *Clin Exp Immunol,* 174**,** 60-72.

DANESE, S., VERMEIRE, S., HELLSTERN, P., PANACCIONE, R., ROGLER, G., FRASER, G., KOHN, A., DESREUMAUX, P., LEONG, R. W., COMER, G. M., CATALDI, F., BANERJEE, A., MAGUIRE, M. K., LI, C., RATH, N., BEEBE, J. & SCHREIBER, S. 2019. Randomised trial and open-label extension study of an anti-interleukin-6 antibody in Crohn's disease (ANDANTE I and II). *Gut,* 68**,** 40-48.

DE LANGE, K. M., MOUTSIANAS, L., LEE, J. C., LAMB, C. A., LUO, Y., KENNEDY, N. A., JOSTINS, L., RICE, D. L., GUTIERREZ-ACHURY, J., JI, S. G., HEAP, G., NIMMO, E. R., EDWARDS, C., HENDERSON, P., MOWAT, C., SANDERSON, J., SATSANGI, J., SIMMONS, A., WILSON, D. C., TREMELLING, M., HART, A., MATHEW, C. G., NEWMAN, W. G., PARKES, M., LEES, C. W., UHLIG, H., HAWKEY, C., PRESCOTT, N. J., AHMAD, T., MANSFIELD, J. C., ANDERSON, C. A. & BARRETT, J. C. 2017. Genome-wide association study implicates immune activation of multiple integrin genes in inflammatory bowel disease. *Nat Genet,* 49**,** 256-261.

DE LAPORTE, L., RICE, J. J., TORTELLI, F. & HUBBELL, J. A. 2013. Tenascin C promiscuously binds growth factors via its fifth fibronectin type III-like domain. *PLoS One,* 8**,** e62076.

DE ROOY, D. P., VAN DER LINDEN, M. P., KNEVEL, R., HUIZINGA, T. W. & VAN DER HELM-VAN MIL, A. H. 2011. Predicting arthritis outcomes--what can be learned from the Leiden Early Arthritis Clinic? *Rheumatology (Oxford),* 50**,** 93-100.

DE SOUZA, H. S. & FIOCCHI, C. 2016. Immunopathogenesis of IBD: current state of the art. *Nat Rev Gastroenterol Hepatol,* 13**,** 13-27.

DELVES, P., MARTIN, S., BURTON, D. & ROITT, I. 2006. *Roitt's Essential Immunology (Essentials)*, Wiley-Blackwell.

DEMORUELLE, M. K. & DEANE, K. 2011. Antibodies to citrullinated protein antigens (ACPAs): clinical and pathophysiologic significance. *Curr Rheumatol Rep,* 13**,** 421-30.

DEMORUELLE, M. K., PARISH, M. C., DERBER, L. A., KOLFENBACH, J. R., HUGHES-AUSTIN, J. M., WEISMAN, M. H., GILLILAND, W., EDISON, J. D., BUCKNER, J. H., MIKULS, T. R., O'DELL, J. R., KEATING, R. M., GREGERSEN, P. K., NORRIS, J. M., HOLERS, V. M. & DEANE, K. D. 2013. Performance of anti-cyclic citrullinated Peptide assays differs in subjects at increased risk of rheumatoid arthritis and subjects with established disease. *Arthritis Rheum,* 65**,** 2243-52.

DENDA, S., MULLER, U., CROSSIN, K. L., ERICKSON, H. P. & REICHARDT, L. F. 1998. Utilization of a soluble integrin-alkaline phosphatase chimera to characterize integrin alpha 8 beta 1 receptor interactions with tenascin: murine alpha 8 beta 1 binds to the RGD site in tenascin-C fragments, but not to native tenascin-C. *Biochemistry,* 37**,** 5464-74.

DERKX, B., TAMINIAU, J., RADEMA, S., STRONKHORST, A., WORTEL, C., TYTGAT, G. & VAN DEVENTER, S. 1993. Tumour-necrosis-factor antibody treatment in Crohn's disease. *Lancet,* 342**,** 173-4.

DESLOGES, N., SIMONEAU, A., JUTRAS, S. & BEAULIEU, J. F. 1994. Tenascin may not be required for intestinal villus development. *Int J Dev Biol,* 38**,** 737-9.

DIDEM, T., FARUK, T., SENEM, K., DERYA, D., MURAT, S., MURAT, G. & OZNUR, K. 2014. Clinical significance of serum tenascin-c levels in epithelial ovarian cancer. *Tumour Biol,* 35**,** 6777-82.

DIELEMAN, L. A., PALMEN, M. J., AKOL, H., BLOEMENA, E., PENA, A. S., MEUWISSEN, S. G. & VAN REES, E. P. 1998. Chronic experimental colitis induced by dextran sulphate sodium (DSS) is characterized by Th1 and Th2 cytokines. *Clin Exp Immunol,* 114**,** 385-91.

DIELEMAN, L. A., RIDWAN, B. U., TENNYSON, G. S., BEAGLEY, K. W., BUCY, R. P. & ELSON, C. O. 1994. Dextran sulfate sodium-induced colitis occurs in severe combined immunodeficient mice. *Gastroenterology,* 107**,** 1643-52.

DOAN, T. C., JEONG, B. M., CODEN, M. E., LOFFREDO, L. F., BHATTACHARYYA, S., CHIARELLA, S. E., VARGA, J., ABDALA-VALENCIA, H. & BERDNIKOVS, S. 2018. Matrix protein Tenascin C expands and reversibly blocks maturation of murine eosinophil progenitors. *J Allergy Clin Immunol*.

DOBIE, R., MACRAE, V. E., PASS, C., MILNE, E. M., AHMED, S. F. & FARQUHARSON, C. 2018. Suppressor of cytokine signaling 2 (Socs2) deletion protects bone health of mice with DSS-induced inflammatory bowel disease. *Dis Model Mech,* 11.

DOOLITTLE, R. F. 1992. A detailed consideration of a principal domain of vertebrate fibrinogen and its relatives. *Protein Sci,* 1**,** 1563-77.

DORIA, A., ZEN, M., BETTIO, S., GATTO, M., BASSI, N., NALOTTO, L., GHIRARDELLO, A., IACCARINO, L. & PUNZI, L. 2012. Autoinflammation and autoimmunity: bridging the divide. *Autoimmun Rev,* 12**,** 22-30.

DORRIES, U. & SCHACHNER, M. 1994. Tenascin mRNA isoforms in the developing mouse brain. *J Neurosci Res,* 37**,** 336-47.

DOS ANJOS, L. M., PEREIRA, I. A., D 'ORSI, E., SEAMAN, A. P., BURLINGAME, R. W. & MORATO, E. F. 2009. A comparative study of IgG second- and third-generation anti-cyclic citrullinated peptide (CCP) ELISAs and their combination with IgA third-generation CCP ELISA for the diagnosis of rheumatoid arthritis. *Clin Rheumatol,* 28**,** 153-8.

DRAGASEVIC, S., STANKOVIC, B., MILOSAVLJEVIC, T., SOKIC-MILUTINOVIC, A., LUKIC, S., ALEMPIJEVIC, T., ZUKIC, B., KOTUR, N., NIKCEVIC, G., PAVLOVIC, S. & POPOVIC, D. 2017. Genetic and environmental factors significant for the presentation and development of inflammatory bowel disease. *Eur J Gastroenterol Hepatol,* 29**,** 909-915.

EDELSTEIN, A. D., TSUCHIDA, M. A., AMODAJ, N., PINKARD, H., VALE, R. D. & STUURMAN, N. 2014. Advanced methods of microscope control using muManager software. *J Biol Methods,* 1.

EFTYCHI, C., SCHWARZER, R., VLANTIS, K., WACHSMUTH, L., BASIC, M., WAGLE, P., NEURATH, M. F., BECKER, C., BLEICH, A. & PASPARAKIS, M. 2019. Temporally Distinct Functions of the Cytokines

IL-12 and IL-23 Drive Chronic Colon Inflammation in Response to Intestinal Barrier Impairment. *Immunity,* 51**,** 367-380.e4.

EGEA, L., MCALLISTER, C. S., LAKHDARI, O., MINEV, I., SHENOUDA, S. & KAGNOFF, M. F. 2013. GM-CSF produced by nonhematopoietic cells is required for early epithelial cell proliferation and repair of injured colonic mucosa. *J Immunol,* 190**,** 1702-13.

EGGER, B., BAJAJ-ELLIOTT, M., MACDONALD, T. T., INGLIN, R., EYSSELEIN, V. E. & BUCHLER, M. W. 2000. Characterisation of acute murine dextran sodium sulphate colitis: cytokine profile and dose dependency. *Digestion,* 62**,** 240-8.

EL-BROLOSY, M. A., KONTARAKIS, Z., ROSSI, A., KUENNE, C., GUNTHER, S., FUKUDA, N., KIKHI, K., BOEZIO, G. L. M., TAKACS, C. M., LAI, S. L., FUKUDA, R., GERRI, C., GIRALDEZ, A. J. & STAINIER, D. Y. R. 2019. Genetic compensation triggered by mutant mRNA degradation. *Nature,* 568**,** 193-197.

EL-BROLOSY, M. A. & STAINIER, D. Y. R. 2017. Genetic compensation: A phenomenon in search of mechanisms. *PLoS Genet,* 13**,** e1006780.

EL-GABALAWY, H., GUENTHER, L. C. & BERNSTEIN, C. N. 2010. Epidemiology of immune-mediated inflammatory diseases: incidence, prevalence, natural history, and comorbidities. *J Rheumatol Suppl,* 85**,** 2-10.

END, P., PANAYOTOU, G., ENTWISTLE, A., WATERFIELD, M. D. & CHIQUET, M. 1992. Tenascin: a modulator of cell growth. *Eur J Biochem,* 209**,** 1041-51.

ENDERLIN VAZ DA SILVA, Z., LEHR, H. A. & VELIN, D. 2014. In vitro and in vivo repair activities of undifferentiated and classically and alternatively activated macrophages. *Pathobiology,* 81**,** 86-93.

ENNS, M. W., BERNSTEIN, C. N., KROEKER, K., GRAFF, L., WALKER, J. R., LIX, L. M., HITCHON, C. A., EL-GABALAWY, R., FISK, J. D. & MARRIE, R. A. 2018. The association of fatigue, pain, depression and anxiety with work and activity impairment in immune mediated inflammatory diseases. *PLoS One,* 13**,** e0198975.

ERDEM, E., KOCHAN, K., PAKER, N., GOKDEN, Y., DEGIRMENCI, A. S., KOCAK, F. & GONEN, C. 2014. The correlation between tenascin-C expression, and formation of intestinal stricture. *North Clin Istanb,* 1**,** 127-131.

ERICKSON, H. P. 1993. Gene knockouts of c-src, transforming growth factor beta 1, and tenascin suggest superfluous, nonfunctional expression of proteins. *J Cell Biol,* 120**,** 1079-81.

ESPINOZA, F., FABRE, S. & PERS, Y. M. 2016. Remission-induction therapies for early rheumatoid arthritis: evidence to date and clinical implications. *Ther Adv Musculoskelet Dis,* 8**,** 107-18.

FAISSNER, A. 1997. The tenascin gene family in axon growth and guidance. *Cell Tissue Res,* 290**,** 331-41.

FAN, Y., MAO, R. & YANG, J. 2013. NF-kappaB and STAT3 signaling pathways collaboratively link inflammation to cancer. *Protein Cell,* 4**,** 176-85.

FANG, K., BRUCE, M., PATTILLO, C. B., ZHANG, S., STONE, R., 2ND, CLIFFORD, J. & KEVIL, C. G. 2011. Temporal genomewide expression profiling of DSS colitis reveals novel inflammatory and angiogenesis genes similar to ulcerative colitis. *Physiol Genomics,* 43**,** 43-56.

FEKI, S., BOUZID, D., ABIDA, O., CHTOUROU, L., ELLOUMI, N., TOUMI, A., HACHICHA, H., AMOURI, A., TAHRI, N. & MASMOUDI, H. 2017. Genetic association and phenotypic correlation of TLR4 but not NOD2 variants with Tunisian inflammatory bowel disease. *J Dig Dis,* 18**,** 625-633.

FILSELL, W., RUDMAN, S., JENKINS, G. & GREEN, M. R. 1999. Coordinate upregulation of tenascin C expression with degree of photodamage in human skin. *Br J Dermatol,* 140**,** 592-9.

FISHER, B. A., PLANT, D., BRODE, M., VAN VOLLENHOVEN, R. F., MATHSSON, L., SYMMONS, D., LUNDBERG, K., RONNELID, J. & VENABLES, P. J. 2011. Antibodies to citrullinated alpha-enolase peptide 1 and clinical and radiological outcomes in rheumatoid arthritis. *Ann Rheum Dis,* 70**,** 1095-8.

FLUCK, M., TUNC-CIVELEK, V. & CHIQUET, M. 2000. Rapid and reciprocal regulation of tenascin-C and tenascin-Y expression by loading of skeletal muscle. *J Cell Sci,* 113 (Pt 20)**,** 3583-91.

FOLEY, K., MUTH, S., JAFFEE, E. & ZHENG, L. 2017. Hedgehog signaling stimulates Tenascin C to promote invasion of pancreatic ductal adenocarcinoma cells through Annexin A2. *Cell Adh Migr,* 11**,** 514-523.

FORBES, E., MURASE, T., YANG, M., MATTHAEI, K. I., LEE, J. J., LEE, N. A., FOSTER, P. S. & HOGAN, S. P. 2004. Immunopathogenesis of experimental ulcerative colitis is mediated by eosinophil peroxidase. *J Immunol,* 172**,** 5664-75.

FORSBERG, E., HIRSCH, E., FROHLICH, L., MEYER, M., EKBLOM, P., ASZODI, A., WERNER, S. & FASSLER, R. 1996. Skin wounds and severed nerves heal normally in mice lacking tenascin-C. *Proc Natl Acad Sci U S A,* 93**,** 6594-9.

FRANCESCHI, C. & CAMPISI, J. 2014. Chronic inflammation (inflammaging) and its potential contribution to age-associated diseases. *J Gerontol A Biol Sci Med Sci,* 69 Suppl 1**,** S4-9.

FRANTZ, C., STEWART, K. M. & WEAVER, V. M. 2010. The extracellular matrix at a glance. *J Cell Sci,* 123**,** 4195-200.

FRANZOSA, E. A., SIROTA-MADI, A., AVILA-PACHECO, J., FORNELOS, N., HAISER, H. J., REINKER, S., VATANEN, T., HALL, A. B., MALLICK, H., MCIVER, L. J., SAUK, J. S., WILSON, R. G., STEVENS, B. W., SCOTT, J. M., PIERCE, K., DEIK, A. A., BULLOCK, K., IMHANN, F., PORTER, J. A., ZHERNAKOVA, A., FU, J., WEERSMA, R. K., WIJMENGA, C., CLISH, C. B., VLAMAKIS, H., HUTTENHOWER, C. & XAVIER, R. J. 2019. Gut microbiome structure and metabolic activity in inflammatory bowel disease. *Nat Microbiol,* 4**,** 293-305.

FUJINO, S., ANDOH, A., BAMBA, S., OGAWA, A., HATA, K., ARAKI, Y., BAMBA, T. & FUJIYAMA, Y. 2003. Increased expression of interleukin 17 in inflammatory bowel disease. *Gut,* 52**,** 65-70.

FUKAMAUCHI, F., MATAGA, N., WANG, Y. J., SATO, S., YOUSHIKI, A. & KUSAKABE, M. 1996. Abnormal behavior and neurotransmissions of tenascin gene knockout mouse. *Biochem Biophys Res Commun,* 221**,** 151-6.

FUKATA, M., MICHELSEN, K. S., ERI, R., THOMAS, L. S., HU, B., LUKASEK, K., NAST, C. C., LECHAGO, J., XU, R., NAIKI, Y., SOLIMAN, A., ARDITI, M. & ABREU, M. T. 2005. Toll-like receptor-4 is required for intestinal response to epithelial injury and limiting bacterial translocation in a murine model of acute colitis. *Am J Physiol Gastrointest Liver Physiol,* 288**,** G1055-65.

GARRETT, W. S., GORDON, J. I. & GLIMCHER, L. H. 2010. Homeostasis and inflammation in the intestine. *Cell,* 140**,** 859-70.

GAWDA, A., MAJKA, G., NOWAK, B. & MARCINKIEWICZ, J. 2017. Air pollution, oxidative stress, and exacerbation of autoimmune diseases. *Cent Eur J Immunol,* 42**,** 305-312.

GEBOES, K., EL-ZINE, M. Y., DALLE, I., EL-HADDAD, S., RUTGEERTS, P. & VAN EYKEN, P. 2001. Tenascin and strictures in inflammatory bowel disease: an immunohistochemical study. *Int J Surg Pathol,* 9**,** 281-6.

GEBOES, K., RUTGEERTS, P., OPDENAKKER, G., OLSON, A., PATEL, K., WAGNER, C. L. & MARANO, C. W. 2005. Endoscopic and histologic evidence of persistent mucosal healing and correlation with clinical improvement following sustained infliximab treatment for Crohn's disease. *Curr Med Res Opin,* 21**,** 1741-54.

GEFFROTIN, C., GARRIDO, J. J., TREMET, L. & VAIMAN, M. 1995. Distinct tissue distribution in pigs of tenascin-X and tenascin-C transcripts. *Eur J Biochem,* 231**,** 83-92.

GERRITSEN, M. J., ELBERS, M. E., DE JONG, E. M. & VAN DE KERKHOF, P. C. 1997. Recruitment of cycling epidermal cells and expression of filaggrin, involucrin and tenascin in the margin of the active psoriatic plaque, in the uninvolved skin of psoriatic patients and in the normal healthy skin. *J Dermatol Sci,* 14**,** 179-88.

GHOSH, N. & PREMCHAND, P. 2015. A UK cost of care model for inflammatory bowel disease. *Frontline Gastroenterol,* 6**,** 169-174.

GIBLIN, S. 2018. *Investigating cell lineage specific biosynthesis of tenascin-C during inflammation - ORA - Oxford University Research Archive.* Doctor of Philosophy in Molecular and Cellular Medicine http://purl.org/dc/dcmitype/Text, University of Oxford.

GIBLIN, S. P. & MIDWOOD, K. S. 2015. Tenascin-C: Form versus function. *Cell Adh Migr,* 9**,** 48-82.

GIBLIN, S. P., MURDAMOOTHOO, D., DELIGNE, C., SCHWENZER, A., OREND, G. & MIDWOOD, K. S. 2018. How to detect and purify tenascin-C. *Methods Cell Biol,* 143**,** 371-400.

GOH, F. G., PICCININI, A. M., KRAUSGRUBER, T., UDALOVA, I. A. & MIDWOOD, K. S. 2010. Transcriptional regulation of the endogenous danger signal tenascin-C: a novel autocrine loop in inflammation. *J Immunol,* 184**,** 2655-62.

GOMOLLON, F., DIGNASS, A., ANNESE, V., TILG, H., VAN ASSCHE, G., LINDSAY, J. O., PEYRIN-BIROULET, L., CULLEN, G. J., DAPERNO,

M., KUCHARZIK, T., RIEDER, F., ALMER, S., ARMUZZI, A., HARBORD, M., LANGHORST, J., SANS, M., CHOWERS, Y., FIORINO, G., JUILLERAT, P., MANTZARIS, G. J., RIZZELLO, F., VAVRICKA, S. & GIONCHETTI, P. 2017. 3rd European Evidence-based Consensus on the Diagnosis and Management of Crohn's Disease 2016: Part 1: Diagnosis and Medical Management. *J Crohns Colitis,* 11**,** 3-25.

GONZALEZ-LOPEZ, L., ROCHA-MUNOZ, A. D., PONCE-GUARNEROS, M., FLORES-CHAVEZ, A., SALAZAR-PARAMO, M., NAVA, A., CARDONA-MUNOZ, E. G., FAJARDO-ROBLEDO, N. S., ZAVALETA-MUNIZ, S. A., GARCIA-COBIAN, T. & GAMEZ-NAVA, J. I. 2014. Anti-cyclic citrullinated peptide (anti-CCP) and anti-mutated citrullinated vimentin (anti-MCV) relation with extra-articular manifestations in rheumatoid arthritis. *J Immunol Res,* 2014**,** 536050.

GORDON, I. O., AGRAWAL, N., WILLIS, E., GOLDBLUM, J. R., LOPEZ, R., ALLENDE, D., LIU, X., PATIL, D. Y., YERIAN, L., EL-KHIDER, F., FIOCCHI, C. & RIEDER, F. 2018. Fibrosis in ulcerative colitis is directly linked to severity and chronicity of mucosal inflammation. *Aliment Pharmacol Ther,* 47**,** 922-939.

GREENWOOD-VAN MEERVELD, B., JOHNSON, A. C. & GRUNDY, D. 2017. Gastrointestinal Physiology and Function. *Handb Exp Pharmacol,* 239**,** 1-16.

GRIFFITHS, A. M., HERBERT, K. E., PERRETT, D. & SCOTT, D. L. 1989. Fragmented fibronectin and other synovial fluid proteins in chronic arthritis: their relation to immune complexes. *Clin Chim Acta,* 184**,** 133-46.

GROSSBERG, L. B. 2019. A Case Report of Successful Treatment of Crohn's Disease and Psoriasis With Guselkumab. *Inflamm Bowel Dis,* 25**,** e84.

GROUP, B. D. W. 2001. Biomarkers and surrogate endpoints: preferred definitions and conceptual framework. *Clin Pharmacol Ther,* 69**,** 89-95.

GRUMET, M., HOFFMAN, S., CROSSIN, K. L. & EDELMAN, G. M. 1985. Cytotactin, an extracellular matrix protein of neural and non-neural tissues that mediates glia-neuron interaction. *Proc Natl Acad Sci U S A,* 82**,** 8075-9.

GULCHER, J. R., NIES, D. E., MARTON, L. S. & STEFANSSON, K. 1989. An alternatively spliced region of the human hexabrachion contains a repeat of potential N-glycosylation sites. *Proc Natl Acad Sci U S A,* 86**,** 1588-92.

GULLBERG, D., VELLING, T., SJOBERG, G., SALMIVIRTA, K., GAGGERO, B., TIGER, C. F., EDSTROM, L. & SEJERSEN, T. 1997. Tenascin-C expression correlates with macrophage invasion in Duchenne muscular dystrophy and in myositis. *Neuromuscul Disord,* 7**,** 39-54.

GUPTA, L., BHATTACHARYA, S. & AGGARWAL, A. 2018. Tenascin-C, a biomarker of disease activity in early ankylosing spondylitis. *Clin Rheumatol*.

GUTOWSKI, N. J., NEWCOMBE, J. & CUZNER, M. L. 1999. Tenascin-R and C in multiple sclerosis lesions: relevance to extracellular matrix remodelling. *Neuropathol Appl Neurobiol,* 25**,** 207-14.

HAAGE, V., ELMADANY, N., ROLL, L., FAISSNER, A., GUTMANN, D. H., SEMTNER, M. & KETTENMANN, H. 2019. Tenascin C regulates multiple microglial functions involving TLR4 signaling and HDAC1. *Brain Behav Immun,* 81**,** 470-483.

HADIS, U., WAHL, B., SCHULZ, O., HARDTKE-WOLENSKI, M., SCHIPPERS, A., WAGNER, N., MULLER, W., SPARWASSER, T., FORSTER, R. & PABST, O. 2011. Intestinal tolerance requires gut homing and expansion of FoxP3+ regulatory T cells in the lamina propria. *Immunity,* 34**,** 237-46.

HAFSTROM, I., ENGVALL, I. L., RONNELID, J., BOONEN, A., VAN DER HEIJDE, D. & SVENSSON, B. 2014. Rheumatoid factor and anti-CCP do not predict progressive joint damage in patients with early rheumatoid arthritis treated with prednisolone: a randomised study. *BMJ Open,* 4**,** e005246.

HAIST, V., ULRICH, R., KALKUHL, A., DESCHL, U. & BAUMGARTNER, W. 2012. Distinct spatio-temporal extracellular matrix accumulation within demyelinated spinal cord lesions in Theiler's murine encephalomyelitis. *Brain Pathol,* 22**,** 188-204.

HALL, L. J., FAIVRE, E., QUINLAN, A., SHANAHAN, F., NALLY, K. & MELGAR, S. 2011. Induction and activation of adaptive immune populations during acute and chronic phases of a murine model of experimental colitis. *Dig Dis Sci,* 56**,** 79-89.

HALLING, M. L., KJELDSEN, J., KNUDSEN, T., NIELSEN, J. & HANSEN, L. K. 2017. Patients with inflammatory bowel disease have increased risk of autoimmune and inflammatory diseases. *World J Gastroenterol,* 23**,** 6137-6146.

HANAMURA, N., YOSHIDA, T., MATSUMOTO, E., KAWARADA, Y. & SAKAKURA, T. 1997. Expression of fibronectin and tenascin-C mRNA by myofibroblasts, vascular cells and epithelial cells in human colon adenomas and carcinomas. *Int J Cancer,* 73**,** 10-5.

HAO, J., LI, T. G., QI, X., ZHAO, D. F. & ZHAO, G. Q. 2006. WNT/beta-catenin pathway up-regulates Stat3 and converges on LIF to prevent differentiation of mouse embryonic stem cells. *Dev Biol,* 290**,** 81-91.

HARADA, M., KAMIMURA, D., ARIMA, Y., KOHSAKA, H., NAKATSUJI, Y., NISHIDA, M., ATSUMI, T., MENG, J., BANDO, H., SINGH, R., SABHARWAL, L., JIANG, J. J., KUMAI, N., MIYASAKA, N., SAKODA, S., YAMAUCHI-TAKIHARA, K., OGURA, H., HIRANO, T. & MURAKAMI, M. 2015. Temporal expression of growth factors triggered by epiregulin regulates inflammation development. *J Immunol,* 194**,** 1039-46.

HARDBOWER, D. M., SINGH, K., ASIM, M., VERRIERE, T. G., OLIVARES-VILLAGOMEZ, D., BARRY, D. P., ALLAMAN, M. M., WASHINGTON, M. K., PEEK, R. M., JR., PIAZUELO, M. B. & WILSON, K. T. 2016. EGFR regulates macrophage activation and function in bacterial infection. *J Clin Invest,* 126**,** 3296-312.

HASEGAWA, M., HIRATA, H., SUDO, A., KATO, K., KAWASE, D., KINOSHITA, N., YOSHIDA, T. & UCHIDA, A. 2004. Tenascin-C

concentration in synovial fluid correlates with radiographic progression of knee osteoarthritis. *J Rheumatol,* 31**,** 2021-6.

HASEGAWA, M., NAKOSHI, Y., MURAKI, M., SUDO, A., KINOSHITA, N., YOSHIDA, T. & UCHIDA, A. 2007. Expression of large tenascin-C splice variants in synovial fluid of patients with rheumatoid arthritis. *J Orthop Res,* 25**,** 563-8.

HASHIMOTO, H. & KUSAKABE, M. 1997. Three-dimensional distribution of extracellular matrix in the mouse small intestinal villi. Laminin and tenascin. *Connect Tissue Res,* 36**,** 63-71.

HASIBUAN, F. M., SHIRATORI, B., SENOPUTRA, M. A., CHAGAN-YASUTAN, H., KOESOEMADINATA, R. C., APRIANI, L., TAKAHASHI, Y., NIKI, T., ALISJAHBANA, B. & HATTORI, T. 2015. Evaluation of matricellular proteins in systemic and local immune response to Mycobacterium tuberculosis infection. *Microbiol Immunol*.

HEADLAND, S. E. & NORLING, L. V. 2015. The resolution of inflammation: Principles and challenges. *Semin Immunol,* 27**,** 149-60.

HEDIN, U., HOLM, J. & HANSSON, G. K. 1991. Induction of tenascin in rat arterial injury. Relationship to altered smooth muscle cell phenotype. *Am J Pathol,* 139**,** 649-56.

HEMESATH, T. J., MARTON, L. S. & STEFANSSON, K. 1994. Inhibition of T cell activation by the extracellular matrix protein tenascin. *J Immunol,* 152**,** 5199-207.

HENDAOUI, I., TUCKER, R. P., ZINGG, D., BICHET, S., SCHITTNY, J. & CHIQUET-EHRISMANN, R. 2014. Tenascin-C is required for normal Wnt/beta-catenin signaling in the whisker follicle stem cell niche. *Matrix Biol,* 40**,** 46-53.

HERLYN, M., GRAEVEN, U., SPEICHER, D., SELA, B. A., BENNICELLI, J. L., KATH, R. & GUERRY, D. T. 1991. Characterization of tenascin secreted by human melanoma cells. *Cancer Res,* 51**,** 4853-8.

HIBINO, S., KATO, K., KUDOH, S., YAGITA, H. & OKUMURA, K. 1998. Tenascin suppresses CD3-mediated T cell activation. *Biochem Biophys Res Commun,* 250**,** 119-24.

HUANG, J. Y., CHENG, Y. J., LIN, Y. P., LIN, H. C., SU, C. C., JULIANO, R. & YANG, B. C. 2010. Extracellular matrix of glioblastoma inhibits polarization and transmigration of T cells: the role of tenascin-C in immune suppression. *J Immunol,* 185**,** 1450-9.

HUDCOVIC, T., STEPANKOVA, R., CEBRA, J. & TLASKALOVA-HOGENOVA, H. 2001. The role of microflora in the development of intestinal inflammation: acute and chronic colitis induced by dextran sulfate in germ-free and conventionally reared immunocompetent and immunodeficient mice. *Folia Microbiol (Praha),* 46**,** 565-72.

HUGOT, J. P., CHAMAILLARD, M., ZOUALI, H., LESAGE, S., CEZARD, J. P., BELAICHE, J., ALMER, S., TYSK, C., O'MORAIN, C. A., GASSULL, M., BINDER, V., FINKEL, Y., CORTOT, A., MODIGLIANI, R., LAURENT-PUIG, P., GOWER-ROUSSEAU, C., MACRY, J., COLOMBEL, J. F., SAHBATOU, M. & THOMAS, G. 2001. Association of NOD2 leucine-rich repeat variants with susceptibility to Crohn's disease. *Nature,* 411**,** 599-603.

HUNTER, D. J. & BIERMA-ZEINSTRA, S. 2019. Osteoarthritis. *Lancet,* 393**,** 1745-1759.

HYNES, R. O. 2009. The extracellular matrix: not just pretty fibrils. *Science,* 326**,** 1216-9.

IMAI, K., KUSAKABE, M., SAKAKURA, T., NAKANISHI, I. & OKADA, Y. 1994. Susceptibility of tenascin to degradation by matrix metalloproteinases and serine proteinases. *FEBS Lett,* 352**,** 216-8.

IMANAKA-YOSHIDA, K., HIROE, M., YASUTOMI, Y., TOYOZAKI, T., TSUCHIYA, T., NODA, N., MAKI, T., NISHIKAWA, T., SAKAKURA, T. & YOSHIDA, T. 2002. Tenascin-C is a useful marker for disease activity in myocarditis. *J Pathol,* 197**,** 388-94.

INOUE, K., JINNIN, M., HARA, Y., MAKINO, K., KAJIHARA, I., MAKINO, T., SAKAI, K., FUKUSHIMA, S., INOUE, Y. & IHN, H. 2013. Serum levels of tenascin-C in collagen diseases. *J Dermatol,* 40**,** 715-9.

ISAACS, J. D. & FERRACCIOLI, G. 2011. The need for personalised medicine for rheumatoid arthritis. *Ann Rheum Dis,* 70**,** 4-7.

ISHIZAKI, J., TAKEMORI, A., SUEMORI, K., MATSUMOTO, T., AKITA, Y., SADA, K. E., YUZAWA, Y., AMANO, K., TAKASAKI, Y., HARIGAI, M., ARIMURA, Y., MAKINO, H., YASUKAWA, M., TAKEMORI, N. & HASEGAWA, H. 2017. Targeted proteomics reveals promising biomarkers of disease activity and organ involvement in antineutrophil cytoplasmic antibody-associated vasculitis. *Arthritis Res Ther,* 19**,** 218.

ISLAM, M. S., KUSAKABE, M., HORIGUCHI, K., IINO, S., NAKAMURA, T., IWANAGA, K., HASHIMOTO, H., MATSUMOTO, S., MURATA, T., HORI, M. & OZAKI, H. 2014. PDGF and TGF-beta promote tenascin-C expression in subepithelial myofibroblasts and contribute to intestinal mucosal protection in mice. *Br J Pharmacol,* 171**,** 375-88.

JACHETTI, E., CAPUTO, S., MAZZOLENI, S., BRAMBILLASCA, C. S., PARIGI, S. M., GRIONI, M., PIRAS, I. S., RESTUCCIA, U., CALCINOTTO, A., FRESCHI, M., BACHI, A., GALLI, R. & BELLONE, M. 2015. Tenascin-C Protects Cancer Stem-like Cells from Immune Surveillance by Arresting T-cell Activation. *Cancer Res,* 75**,** 2095-108.

JACOBS, P., BISSONNETTE, R. & GUENTHER, L. C. 2011. Socioeconomic burden of immune-mediated inflammatory diseases--focusing on work productivity and disability. *J Rheumatol Suppl,* 88**,** 55-61.

JANEWAY, C. A., JR. 1992. The immune system evolved to discriminate infectious nonself from noninfectious self. *Immunol Today,* 13**,** 11-6.

JARNEROT, G., HERTERVIG, E., FRIIS-LIBY, I., BLOMQUIST, L., KARLEN, P., GRANNO, C., VILIEN, M., STROM, M., DANIELSSON, A., VERBAAN, H., HELLSTROM, P. M., MAGNUSON, A. & CURMAN, B. 2005. Infliximab as rescue therapy in severe to moderately severe ulcerative colitis: a randomized, placebo-controlled study. *Gastroenterology,* 128**,** 1805-11.

JAYADEV, R. & SHERWOOD, D. R. 2017. Basement membranes. *Curr Biol,* 27**,** R207-r211.

JINNIN, M., IHN, H., ASANO, Y., YAMANE, K., TROJANOWSKA, M. & TAMAKI, K. 2004. Tenascin-C upregulation by transforming growth

factor-beta in human dermal fibroblasts involves Smad3, Sp1, and Ets1. *Oncogene,* 23**,** 1656-67.

JONES, F. S., CHALEPAKIS, G., GRUSS, P. & EDELMAN, G. M. 1992. Activation of the cytotactin promoter by the homeobox-containing gene Evx-1. *Proc Natl Acad Sci U S A,* 89**,** 2091-5.

JONES, F. S. & JONES, P. L. 2000. The tenascin family of ECM glycoproteins: structure, function, and regulation during embryonic development and tissue remodeling. *Dev Dyn,* 218**,** 235-59.

JONES, G. R., BAIN, C. C., FENTON, T. M., KELLY, A., BROWN, S. L., IVENS, A. C., TRAVIS, M. A., COOK, P. C. & MACDONALD, A. S. 2018. Dynamics of Colon Monocyte and Macrophage Activation During Colitis. *Front Immunol,* 9**,** 2764.

JONES, P. L., CRACK, J. & RABINOVITCH, M. 1997. Regulation of tenascin-C, a vascular smooth muscle cell survival factor that interacts with the alpha v beta 3 integrin to promote epidermal growth factor receptor phosphorylation and growth. *J Cell Biol,* 139**,** 279-93.

JORGENSEN, J. T. 2015. Clinical application of companion diagnostics. *Trends Mol Med,* 21**,** 405-7.

KAARTEENAHO-WIIK, R., KINNULA, V. L., HERVA, R., SOINI, Y., POLLANEN, R. & PAAKKO, P. 2002. Tenascin-C is highly expressed in respiratory distress syndrome and bronchopulmonary dysplasia. *J Histochem Cytochem,* 50**,** 423-31.

KAARTEENAHO-WIIK, R., LAKARI, E., SOINI, Y., POLLANEN, R., KINNULA, V. L. & PAAKKO, P. 2000. Tenascin expression and distribution in pleural inflammatory and fibrotic diseases. *J Histochem Cytochem,* 48**,** 1257-68.

KAARTEENAHO-WIIK, R., MERTANIEMI, P., SAJANTI, E., SOINI, Y. & PAAKKO, P. 1998. Tenascin is increased in epithelial lining fluid in fibrotic lung disorders. *Lung,* 176**,** 371-80.

KAARTEENAHO-WIIK, R., TANI, T., SORMUNEN, R., SOINI, Y., VIRTANEN, I. & PAAKKO, P. 1996. Tenascin immunoreactivity as a prognostic marker in usual interstitial pneumonia. *Am J Respir Crit Care Med,* 154**,** 511-8.

KAMADA, N., HISAMATSU, T., OKAMOTO, S., CHINEN, H., KOBAYASHI, T., SATO, T., SAKURABA, A., KITAZUME, M. T., SUGITA, A., KOGANEI, K., AKAGAWA, K. S. & HIBI, T. 2008. Unique CD14 intestinal macrophages contribute to the pathogenesis of Crohn disease via IL-23/IFN-gamma axis. *J Clin Invest,* 118**,** 2269-80.

KAMMERER, R. A., SCHULTHESS, T., LANDWEHR, R., LUSTIG, A., FISCHER, D. & ENGEL, J. 1998. Tenascin-C hexabrachion assembly is a sequential two-step process initiated by coiled-coil alpha-helices. *J Biol Chem,* 273**,** 10602-8.

KANAYAMA, M., KUROTAKI, D., MORIMOTO, J., ASANO, T., MATSUI, Y., NAKAYAMA, Y., SAITO, Y., ITO, K., KIMURA, C., IWASAKI, N., SUZUKI, K., HARADA, T., LI, H. M., UEHARA, J., MIYAZAKI, T., MINAMI, A., KON, S. & UEDE, T. 2009. Alpha9 integrin and its ligands constitute critical joint microenvironments for development of autoimmune arthritis. *J Immunol,* 182**,** 8015-25.

KANAYAMA, M., MORIMOTO, J., MATSUI, Y., IKESUE, M., DANZAKI, K., KUROTAKI, D., ITO, K., YOSHIDA, T. & UEDE, T. 2011. alpha9beta1 integrin-mediated signaling serves as an intrinsic regulator of pathogenic Th17 cell generation. *J Immunol,* 187**,** 5851-64.

KARATAS, Z., BAYSAL, T., SAP, F., ALTIN, H. & CICEKLER, H. 2013. The role of tenascin-C and oxidative stress in rheumatic and congenital heart valve diseases: an observational study. *Anadolu Kardiyol Derg,* 13**,** 350-6.

KASTBOM, A., STRANDBERG, G., LINDROOS, A. & SKOGH, T. 2004. Anti-CCP antibody test predicts the disease course during 3 years in early rheumatoid arthritis (the Swedish TIRA project). *Ann Rheum Dis,* 63**,** 1085-9.

KESTER, L. & VAN OUDENAARDEN, A. 2018. Single-Cell Transcriptomics Meets Lineage Tracing. *Cell Stem Cell,* 23**,** 166-179.

KIESLER, P., FUSS, I. J. & STROBER, W. 2015. Experimental Models of Inflammatory Bowel Diseases. *Cell Mol Gastroenterol Hepatol,* 1**,** 154-170.

KIM, J. J., SHAJIB, M. S., MANOCHA, M. M. & KHAN, W. I. 2012. Investigating intestinal inflammation in DSS-induced model of IBD. *J Vis Exp*.

KIMURA, S., ISHIDA, S., MATUNAGA, K., WASHIZU, K., HIRAIWA, H., TAKEUCHI, K., WAKABAYASHI, T., YOSHIDA, J. & KATO, K. 1993. Determination of tenascin-C in human serum by the use of a new enzyme immunoassay. *Biomedical Research,* 14**,** 203-208.

KIMURA, T., SHIRAISHI, K., FURUSHO, A., ITO, S., HIRAKATA, S., NISHIDA, N., YOSHIMURA, K., IMANAKA-YOSHIDA, K., YOSHIDA, T., IKEDA, Y., MIYAMOTO, T., UENO, T., HAMANO, K., HIROE, M., AONUMA, K., MATSUZAKI, M., IMAIZUMI, T. & AOKI, H. 2014. Tenascin C protects aorta from acute dissection in mice. *Sci Rep,* 4**,** 4051.

KIMURA, T., TAJIRI, K., SATO, A., SAKAI, S., WANG, Z., YOSHIDA, T., UEDE, T., HIROE, M., AONUMA, K., IEDA, M. & IMANAKA-YOSHIDA, K. 2019. Tenascin-C accelerates adverse ventricular remodelling after myocardial infarction by modulating macrophage polarization. *Cardiovasc Res,* 115**,** 614-624.

KINCHEN, J., CHEN, H. H., PARIKH, K., ANTANAVICIUTE, A., JAGIELOWICZ, M., FAWKNER-CORBETT, D., ASHLEY, N., CUBITT, L., MELLADO-GOMEZ, E., ATTAR, M., SHARMA, E., WILLS, Q., BOWDEN, R., RICHTER, F. C., AHERN, D., PURI, K. D., HENAULT, J., GERVAIS, F., KOOHY, H. & SIMMONS, A. 2018. Structural Remodeling of the Human Colonic Mesenchyme in Inflammatory Bowel Disease. *Cell,* 175**,** 372-386.e17.

KIYEKO, G. W., HATTERER, E., HERREN, S., CEGLIE, I. D., VAN LENT, P. L., REITH, W., KOSCO-VILBOIS, M., FERLIN, W. & SHANG, L. 2016. Spatiotemporal expression of endogenous TLR4 ligands leads to inflammation and bone erosion in mouse collagen-induced arthritis. *Eur J Immunol*.

KLAASEN, R., CANTAERT, T., WIJBRANDTS, C. A., TEITSMA, C., GERLAG, D. M., OUT, T. A., DE NOOIJER, M. J., BAETEN, D. & TAK, P. P. 2011.

The value of rheumatoid factor and anti-citrullinated protein antibodies as predictors of response to infliximab in rheumatoid arthritis: an exploratory study. *Rheumatology (Oxford),* 50**,** 1487-93.

KLEMENT, E. & MEDZIHRADSZKY, K. F. 2017. Extracellular Protein Phosphorylation, the Neglected Side of the Modification. *Mol Cell Proteomics,* 16**,** 1-7.

KOJOUHAROFF, G., HANS, W., OBERMEIER, F., MANNEL, D. N., ANDUS, T., SCHOLMERICH, J., GROSS, V. & FALK, W. 1997. Neutralization of tumour necrosis factor (TNF) but not of IL-1 reduces inflammation in chronic dextran sulphate sodium-induced colitis in mice. *Clin Exp Immunol,* 107**,** 353-8.

KOLIOS, G. 2016. Animal models of inflammatory bowel disease: how useful are they really? *Curr Opin Gastroenterol,* 32**,** 251-7.

KORPOS, E., WU, C. & SOROKIN, L. 2009. Multiple roles of the extracellular matrix in inflammation. *Curr Pharm Des,* 15**,** 1349-57.

KOYAMA, Y., KUSUBATA, M., YOSHIKI, A., HIRAIWA, N., OHASHI, T., IRIE, S. & KUSAKABE, M. 1998. Effect of tenascin-C deficiency on chemically induced dermatitis in the mouse. *J Invest Dermatol,* 111**,** 930-5.

KRAWISZ, J. E., SHARON, P. & STENSON, W. F. 1984. Quantitative assay for acute intestinal inflammation based on myeloperoxidase activity. Assessment of inflammation in rat and hamster models. *Gastroenterology,* 87**,** 1344-50.

KROL, A., GARRED, P., HEEGAARD, N. H., CHRISTENSEN, A. F., HETLAND, M. L., STENGAARD-PEDERSEN, K., JUNKER, P., MADSEN, H. O., LOTTENBURGER, T., ELLINGSEN, T., ANDERSEN, L. S., HANSEN, I., PEDERSEN, J. K., SVENDSEN, A. J., TARP, U., PODENPHANT, J., LINDEGAARD, H., OSTERGAARD, M., HORSLEV-PETERSEN, K. & JACOBSEN, S. 2015. Interactions between smoking, increased serum levels of anti-CCP antibodies, rheumatoid factors, and erosive joint disease in patients with early, untreated rheumatoid arthritis. *Scand J Rheumatol,* 44**,** 8-12.

KRUSE, J., KEILHAUER, G., FAISSNER, A., TIMPL, R. & SCHACHNER, M. 1985. The J1 glycoprotein--a novel nervous system cell adhesion molecule of the L2/HNK-1 family. *Nature,* 316**,** 146-8.

KUEK, A., HAZLEMAN, B. L. & OSTOR, A. J. 2007. Immune-mediated inflammatory diseases (IMIDs) and biologic therapy: a medical revolution. *Postgrad Med J,* 83**,** 251-60.

KUHN, R., LOHLER, J., RENNICK, D., RAJEWSKY, K. & MULLER, W. 1993. Interleukin-10-deficient mice develop chronic enterocolitis. *Cell,* 75**,** 263-74.

KURAHASHI, M., NAKANO, Y., PERI, L. E., TOWNSEND, J. B., WARD, S. M. & SANDERS, K. M. 2013. A novel population of subepithelial platelet-derived growth factor receptor alpha-positive cells in the mouse and human colon. *Am J Physiol Gastrointest Liver Physiol,* 304**,** G823-34.

KURIYAMA, N., DUARTE, S., HAMADA, T., BUSUTTIL, R. W. & COITO, A. J. 2011. Tenascin-C: a novel mediator of hepatic ischemia and reperfusion injury. *Hepatology,* 54**,** 2125-36.

LACOUR, J. P., VITETTA, A., CHIQUET-EHRISMANN, R., PISANI, A. & ORTONNE, J. P. 1992. Increased expression of tenascin in the dermis in scleroderma. *Br J Dermatol,* 127**,** 328-34.

LAKOS, G., SOOS, L., FEKETE, A., SZABO, Z., ZEHER, M., HORVATH, I. F., DANKO, K., KAPITANY, A., GYETVAI, A., SZEGEDI, G. & SZEKANECZ, Z. 2008. Anti-cyclic citrullinated peptide antibody isotypes in rheumatoid arthritis: association with disease duration, rheumatoid factor production and the presence of shared epitope. *Clin Exp Rheumatol,* 26**,** 253-60.

LAROUI, H., INGERSOLL, S. A., LIU, H. C., BAKER, M. T., AYYADURAI, S., CHARANIA, M. A., LAROUI, F., YAN, Y., SITARAMAN, S. V. & MERLIN, D. 2012. Dextran sodium sulfate (DSS) induces colitis in mice by forming nano-lipocomplexes with medium-chain-length fatty acids in the colon. *PLoS One,* 7**,** e32084.

LATIJNHOUWERS, M. A., BERGERS, M., KUIJPERS, A. L., VAN DER VLEUTEN, C. J., DIJKMAN, H., VAN DE KERKHOF, P. C. & SCHALKWIJK, J. 1998a. Tenascin-C is not a useful marker for disease activity in psoriasis. *Acta Derm Venereol,* 78**,** 331-4.

LATIJNHOUWERS, M. A., PFUNDT, R., DE JONGH, G. J. & SCHALKWIJK, J. 1998b. Tenascin-C expression in human epidermal keratinocytes is regulated by inflammatory cytokines and a stress response pathway. *Matrix Biol,* 17**,** 305-16.

LATTIN, J. E., SCHRODER, K., SU, A. I., WALKER, J. R., ZHANG, J., WILTSHIRE, T., SAIJO, K., GLASS, C. K., HUME, D. A., KELLIE, S. & SWEET, M. J. 2008. Expression analysis of G Protein-Coupled Receptors in mouse macrophages. *Immunome Res,* 4**,** 5.

LEBENSZTEJN, D. M., SOBANIEC-LOTOWSKA, M. E., KACZMARSKI, M., VOELKER, M. & SCHUPPAN, D. 2006. Matrix-derived serum markers in monitoring liver fibrosis in children with chronic hepatitis B treated with interferon alpha. *World J Gastroenterol,* 12**,** 3338-43.

LEE, E. Y., STENSON, W. F. & DESCHRYVER-KECSKEMETI, K. 1991. Thickening of muscularis mucosae in Crohn's disease. *Mod Pathol,* 4**,** 87-90.

LEE, Y., BULLARD, D. E., HUMPHREY, P. A., COLAPINTO, E. V., FRIEDMAN, H. S., ZALUTSKY, M. R., COLEMAN, R. E. & BIGNER, D. D. 1988. Treatment of intracranial human glioma xenografts with 131I-labeled anti-tenascin monoclonal antibody 81C6. *Cancer Res,* 48**,** 2904-10.

LEWIS, J. D., BRENSINGER, C., BILKER, W. B. & STROM, B. L. 2002. Validity and completeness of the General Practice Research Database for studies of inflammatory bowel disease. *Pharmacoepidemiol Drug Saf,* 11**,** 211-8.

LI, Y., CHEN, H., JIANG, X., LI, X., LV, J., PENG, H., TSIEN, J. Z. & LIU, T. 2017. Discover mouse gene coexpression landscapes using dictionary learning and sparse coding. *Brain Struct Funct,* 222**,** 4253-4270.

LIU, C. F., BREIDENBACH, A., ASCHBACHER-SMITH, L., BUTLER, D. & WYLIE, C. 2013. A role for hedgehog signaling in the differentiation of

the insertion site of the patellar tendon in the mouse. *PLoS One,* 8**,** e65411.

LIU, J. Z., VAN SOMMEREN, S., HUANG, H., NG, S. C., ALBERTS, R., TAKAHASHI, A., RIPKE, S., LEE, J. C., JOSTINS, L., SHAH, T., ABEDIAN, S., CHEON, J. H., CHO, J., DAYANI, N. E., FRANKE, L., FUYUNO, Y., HART, A., JUYAL, R. C., JUYAL, G., KIM, W. H., MORRIS, A. P., POUSTCHI, H., NEWMAN, W. G., MIDHA, V., ORCHARD, T. R., VAHEDI, H., SOOD, A., SUNG, J. Y., MALEKZADEH, R., WESTRA, H. J., YAMAZAKI, K., YANG, S. K., BARRETT, J. C., ALIZADEH, B. Z., PARKES, M., BK, T., DALY, M. J., KUBO, M., ANDERSON, C. A. & WEERSMA, R. K. 2015. Association analyses identify 38 susceptibility loci for inflammatory bowel disease and highlight shared genetic risk across populations. *Nat Genet,* 47**,** 979-986.

LIVAK, K. J. & SCHMITTGEN, T. D. 2001. Analysis of relative gene expression data using real-time quantitative PCR and the 2(-Delta Delta C(T)) Method. *Methods,* 25**,** 402-8.

LJUBIMOV, A. V., SAGHIZADEH, M., SPIRIN, K. S., KHIN, H. L., LEWIN, S. L., ZARDI, L., BOURDON, M. A. & KENNEY, M. C. 1998. Expression of tenascin-C splice variants in normal and bullous keratopathy human corneas. *Invest Ophthalmol Vis Sci,* 39**,** 1135-42.

LONNFORS, S., VERMEIRE, S., GRECO, M., HOMMES, D., BELL, C. & AVEDANO, L. 2014. IBD and health-related quality of life -- discovering the true impact. *J Crohns Colitis,* 8**,** 1281-6.

MA, C., JAIRATH, V., KHANNA, R. & FEAGAN, B. G. 2018. Investigational drugs in phase I and phase II clinical trials targeting interleukin 23 (IL23) for the treatment of Crohn's disease. *Expert Opin Investig Drugs***,** 1-12.

MACHINO-OHTSUKA, T., TAJIRI, K., KIMURA, T., SAKAI, S., SATO, A., YOSHIDA, T., HIROE, M., YASUTOMI, Y., AONUMA, K. & IMANAKA-YOSHIDA, K. 2014. Tenascin-C aggravates autoimmune myocarditis via dendritic cell activation and Th17 cell differentiation. *J Am Heart Assoc,* 3**,** e001052.

MACKIE, E. J., HALFTER, W. & LIVERANI, D. 1988. Induction of tenascin in healing wounds. *J Cell Biol,* 107**,** 2757-67.

MACKIE, E. J., SCOTT-BURDEN, T., HAHN, A. W., KERN, F., BERNHARDT, J., REGENASS, S., WELLER, A. & BUHLER, F. R. 1992. Expression of tenascin by vascular smooth muscle cells. Alterations in hypertensive rats and stimulation by angiotensin II. *Am J Pathol,* 141**,** 377-88.

MACKIE, E. J. & TUCKER, R. P. 1999. The tenascin-C knockout revisited. *J Cell Sci,* 112 (Pt 22)**,** 3847-53.

MAGLIONE, P. J., SIMCHONI, N. & CUNNINGHAM-RUNDLES, C. 2015. Toll-like receptor signaling in primary immune deficiencies. *Ann N Y Acad Sci,* 1356**,** 1-21.

MAGNUSSON, M. K., STRID, H., ISAKSSON, S., BAJOR, A., LASSON, A., UNG, K. A. & OHMAN, L. 2015. Response to infliximab therapy in ulcerative colitis is associated with decreased monocyte activation, reduced CCL2 expression and downregulation of Tenascin C. *J Crohns Colitis,* 9**,** 56-65.

MAGRO, F., GIONCHETTI, P., ELIAKIM, R., ARDIZZONE, S., ARMUZZI, A., BARREIRO-DE ACOSTA, M., BURISCH, J., GECSE, K. B., HART, A. L., HINDRYCKX, P., LANGNER, C., LIMDI, J. K., PELLINO, G., ZAGOROWICZ, E., RAINE, T., HARBORD, M. & RIEDER, F. 2017. Third European Evidence-based Consensus on Diagnosis and Management of Ulcerative Colitis. Part 1: Definitions, Diagnosis, Extra-intestinal Manifestations, Pregnancy, Cancer Surveillance, Surgery, and Ileo-anal Pouch Disorders. *J Crohns Colitis,* 11**,** 649-670.

MAGRO, F., LANGNER, C., DRIESSEN, A., ENSARI, A., GEBOES, K., MANTZARIS, G. J., VILLANACCI, V., BECHEANU, G., BORRALHO NUNES, P., CATHOMAS, G., FRIES, W., JOURET-MOURIN, A., MESCOLI, C., DE PETRIS, G., RUBIO, C. A., SHEPHERD, N. A., VIETH, M. & ELIAKIM, R. 2013. European consensus on the histopathology of inflammatory bowel disease. *J Crohns Colitis,* 7**,** 827-51.

MAI, J., SAMENI, M., MIKKELSEN, T. & SLOANE, B. F. 2002. Degradation of extracellular matrix protein tenascin-C by cathepsin B: an interaction involved in the progression of gliomas. *Biol Chem,* 383**,** 1407-13.

MANGAN, R. J., STAMPER, L., OHASHI, T., EUDAILEY, J. A., GO, E. P., JAEGER, F. H., ITELL, H. L., WATTS, B. E., FOUDA, G. G., ERICKSON, H. P., ALAM, S. M., DESAIRE, H. & PERMAR, S. R. 2019. Determinants of Tenascin-C and HIV-1 envelope binding and neutralization. *Mucosal Immunol*.

MAQBOOL, A., SPARY, E. J., MANFIELD, I. W., RUHMANN, M., ZULIANI-ALVAREZ, L., GAMBOA-ESTEVES, F. O., PORTER, K. E., DRINKHILL, M. J., MIDWOOD, K. S. & TURNER, N. A. 2016. Tenascin C upregulates interleukin-6 expression in human cardiac myofibroblasts via toll-like receptor 4. *World J Cardiol,* 8**,** 340-50.

MARTIN, J. C., CHANG, C., BOSCHETTI, G., UNGARO, R., GIRI, M., GROUT, J. A., GETTLER, K., CHUANG, L. S., NAYAR, S., GREENSTEIN, A. J., DUBINSKY, M., WALKER, L., LEADER, A., FINE, J. S., WHITEHURST, C. E., MBOW, M. L., KUGATHASAN, S., DENSON, L. A., HYAMS, J. S., FRIEDMAN, J. R., DESAI, P. T., KO, H. M., LAFACE, I., AKTURK, G., SCHADT, E. E., SALMON, H., GNJATIC, S., RAHMAN, A. H., MERAD, M., CHO, J. H. & KENIGSBERG, E. 2019. Single-Cell Analysis of Crohn's Disease Lesions Identifies a Pathogenic Cellular Module Associated with Resistance to Anti-TNF Therapy. *Cell*.

MARZEDA, A. M. & MIDWOOD, K. S. 2018. Internal Affairs: Tenascin-C as a Clinically Relevant, Endogenous Driver of Innate Immunity. *J Histochem Cytochem***,** 22155418757443.

MASAKI, T., YORIOKA, N., TANIGUCHI, Y., ODA, H. & YAMAKIDO, M. 1998. Tenascin expression may reflect the activity and chronicity of human IgA nephropathy. *Clin Nephrol,* 50**,** 205-13.

MASSON-BESSIERE, C., SEBBAG, M., GIRBAL-NEUHAUSER, E., NOGUEIRA, L., VINCENT, C., SENSHU, T. & SERRE, G. 2001. The major synovial targets of the rheumatoid arthritis-specific antifilaggrin

autoantibodies are deiminated forms of the alpha- and beta-chains of fibrin. *J Immunol,* 166**,** 4177-84.

MATHSSON ALM, L., FOUNTAIN, D. L., CADWELL, K. K., MADRIGAL, A. M., GALLO, G. & POORAFSHAR, M. 2018. The performance of anti-cyclic citrullinated peptide assays in diagnosing rheumatoid arthritis: a systematic review and meta-analysis. *Clin Exp Rheumatol,* 36**,** 144-152.

MATSUI, Y., HASEGAWA, M., IINO, T., IMANAKA-YOSHIDA, K., YOSHIDA, T. & SUDO, A. 2018. Tenascin-C Prevents Articular Cartilage Degeneration in Murine Osteoarthritis Models. *Cartilage,* 9**,** 80-88.

MATSUMOTO, K., NAKAI, Y., HOSHINO, M., YAMAZAKI, K., TAKIOTO, Y., TAKADERA, S., NAKAGAWA, T., NISHIMURA, R. & KUSAKABE, M. 2017. Comprehensive DNA microarray expression profiles of tumors in tenascin-C-knockout mice. *Biosci Biotechnol Biochem,* 81**,** 1926-1936.

MATSUMOTO, K., SAGA, Y., IKEMURA, T., SAKAKURA, T. & CHIQUET-EHRISMANN, R. 1994. The distribution of tenascin-X is distinct and often reciprocal to that of tenascin-C. *J Cell Biol,* 125**,** 483-93.

MATZINGER, P. 1994. Tolerance, danger, and the extended family. *Annu Rev Immunol,* 12**,** 991-1045.

MCCACHREN, S. S. & LIGHTNER, V. A. 1992. Expression of human tenascin in synovitis and its regulation by interleukin-1. *Arthritis Rheum,* 35**,** 1185-96.

MEDZHITOV, R. 2008. Origin and physiological roles of inflammation. *Nature,* 454**,** 428-435.

MEHTA, B. B., TIWARI, A., SHARMA, S., SHUKLA, A., SHARMA, M., VASISHTA, R. K., SEN, R. K., SHARMA, A. & LUTHRA-GUPTASARMA, M. 2018. Amelioration of collagen antibody induced arthritis in mice by an antibody directed against the fibronectin type III repeats of tenascin-C: Targeting fibronectin type III repeats of tenascin-C in rheumatoid arthritis. *Int Immunopharmacol,* 58**,** 15-23.

MELGAR, S., KARLSSON, L., REHNSTROM, E., KARLSSON, A., UTKOVIC, H., JANSSON, L. & MICHAELSSON, E. 2008. Validation of murine dextran sulfate sodium-induced colitis using four therapeutic agents for human inflammatory bowel disease. *Int Immunopharmacol,* 8**,** 836-44.

MELSHEIMER, R., GELDHOF, A., APAOLAZA, I. & SCHAIBLE, T. 2019. Remicade((R)) (infliximab): 20 years of contributions to science and medicine. *Biologics,* 13**,** 139-178.

MIDWOOD, K., SACRE, S., PICCININI, A. M., INGLIS, J., TREBAUL, A., CHAN, E., DREXLER, S., SOFAT, N., KASHIWAGI, M., OREND, G., BRENNAN, F. & FOXWELL, B. 2009. Tenascin-C is an endogenous activator of Toll-like receptor 4 that is essential for maintaining inflammation in arthritic joint disease. *Nat Med,* 15**,** 774-80.

MIDWOOD, K. S., CHIQUET, M., TUCKER, R. P. & OREND, G. 2016. Tenascin-C at a glance. *J Cell Sci,* 129**,** 4321-4327.

MIDWOOD, K. S., HUSSENET, T., LANGLOIS, B. & OREND, G. 2011. Advances in tenascin-C biology. *Cell Mol Life Sci,* 68**,** 3175-99.

MIDWOOD, K. S. & OREND, G. 2009. The role of tenascin-C in tissue injury and tumorigenesis. *J Cell Commun Signal,* 3**,** 287-310.

MIEHLKE, S., VERHAEGH, B., TONTINI, G. E., MADISCH, A., LANGNER, C. & MUNCH, A. 2019. Microscopic colitis: pathophysiology and clinical management. *Lancet Gastroenterol Hepatol,* 4**,** 305-314.

MIGHELL, A. J., THOMPSON, J., HUME, W. J., MARKHAM, A. F. & ROBINSON, P. A. 1997. Human tenascin-C: identification of a novel type III repeat in oral cancer and of novel splice variants in normal, malignant and reactive oral mucosae. *Int J Cancer,* 72**,** 236-40.

MILLS, J. T., SCHWENZER, A., MARSH, E. K., EDWARDS, M. R., SABROE, I., MIDWOOD, K. S. & PARKER, L. C. 2019. Airway Epithelial Cells Generate Pro-inflammatory Tenascin-C and Small Extracellular Vesicles in Response to TLR3 Stimuli and Rhinovirus Infection. *Front Immunol,* 10**,** 1987.

MIROSHNIKOVA, Y. A., MOUW, J. K., BARNES, J. M., PICKUP, M. W., LAKINS, J. N., KIM, Y., LOBO, K., PERSSON, A. I., REIS, G. F., MCKNIGHT, T. R., HOLLAND, E. C., PHILLIPS, J. J. & WEAVER, V. M. 2016. Tissue mechanics promote IDH1-dependent HIF1alpha-tenascin C feedback to regulate glioblastoma aggression. *Nat Cell Biol,* 18**,** 1336-1345.

MIRZAEI, R., SARKAR, S., DZIKOWSKI, L., RAWJI, K. S., KHAN, L., FAISSNER, A., BOSE, P. & YONG, V. W. 2018. Brain tumor-initiating cells export tenascin-C associated with exosomes to suppress T cell activity. *Oncoimmunology.* United States.

MIYOSHI, H., VANDUSSEN, K. L., MALVIN, N. P., RYU, S. H., WANG, Y., SONNEK, N. M., LAI, C. W. & STAPPENBECK, T. S. 2017. Prostaglandin E2 promotes intestinal repair through an adaptive cellular response of the epithelium. *Embo j,* 36**,** 5-24.

MOELLER, A. H., SUZUKI, T. A., PHIFER-RIXEY, M. & NACHMAN, M. W. 2018. Transmission modes of the mammalian gut microbiota. *Science,* 362**,** 453-457.

MOLLER, B., BENDER, P., EICK, S., KUCHEN, S., MALDONADO, A., POTEMPA, J., REICHENBACH, S., SCULEAN, A., SCHWENZER, A., VILLIGER, P. M., WONG, A. & MIDWOOD, K. S. 2019. Treatment of severe periodontitis may improve clinical disease activity in otherwise treatment-refractory rheumatoid arthritis patients. *Rheumatology (Oxford)*.

MOLODECKY, N. A., SOON, I. S., RABI, D. M., GHALI, W. A., FERRIS, M., CHERNOFF, G., BENCHIMOL, E. I., PANACCIONE, R., GHOSH, S., BARKEMA, H. W. & KAPLAN, G. G. 2012. Increasing incidence and prevalence of the inflammatory bowel diseases with time, based on systematic review. *Gastroenterology,* 142**,** 46-54.e42; quiz e30.

MOMCILOVIC, M., STAMENKOVIC, V., JOVANOVIC, M., ANDJUS, P. R., JAKOVCEVSKI, I., SCHACHNER, M. & MILJKOVIC, D. 2017. Tenascin-C deficiency protects mice from experimental autoimmune encephalomyelitis. *J Neuroimmunol,* 302**,** 1-6.

MONNET, E., LAPEYRE, G., POELGEEST, E. V., JACQMIN, P., GRAAF, K., REIJERS, J., MOERLAND, M., BURGGRAAF, J. & MIN, C. 2017. Evidence of NI-0101 pharmacological activity, an anti-TLR4 antibody,

in a randomized phase I dose escalation study in healthy volunteers receiving LPS. *Clin Pharmacol Ther,* 101**,** 200-208.

MONTGOMERY, A. B., VENABLES, P. J. & FISHER, B. A. 2013. The case for measuring antibodies to specific citrullinated antigens. *Expert Rev Clin Immunol,* 9**,** 1185-92.

MOPARTHI, L. & KOCH, S. 2019. Wnt signaling in intestinal inflammation. *Differentiation,* 108**,** 24-32.

MORGAN, A. R., HAN, D. Y., LAM, W. J., TRIGGS, C. M., FRASER, A. G., BARCLAY, M., GEARRY, R. B., MEISNER, S., STOKKERS, P., BOECKXSTAENS, G. E. & FERGUSON, L. R. 2011. Genetic variations in matrix metalloproteinases may be associated with increased risk of ulcerative colitis. *Hum Immunol,* 72**,** 1117-27.

MORIGGI, M., PASTORELLI, L., TORRETTA, E., TONTINI, G. E., CAPITANIO, D., BOGETTO, S. F., VECCHI, M. & GELFI, C. 2017. Contribution of Extracellular Matrix and Signal Mechanotransduction to Epithelial Cell Damage in Inflammatory Bowel Disease Patients: A Proteomic Study. *Proteomics,* 17.

MORIMOTO, S., IMANAKA-YOSHIDA, K., HIRAMITSU, S., KATO, S., OHTSUKI, M., UEMURA, A., KATO, Y., NISHIKAWA, T., TOYOZAKI, T., HISHIDA, H., YOSHIDA, T. & HIROE, M. 2005. Diagnostic utility of tenascin-C for evaluation of the activity of human acute myocarditis. *J Pathol,* 205**,** 460-7.

MORISE, J., TAKEMATSU, H. & OKA, S. 2017. The role of human natural killer-1 (HNK-1) carbohydrate in neuronal plasticity and disease. *Biochim Biophys Acta Gen Subj,* 1861**,** 2455-2461.

MOSSER, D. M. & EDWARDS, J. P. 2008. Exploring the full spectrum of macrophage activation. *Nat Rev Immunol,* 8**,** 958-69.

MOWAT, A. M. & AGACE, W. W. 2014. Regional specialization within the intestinal immune system. *Nat Rev Immunol,* 14**,** 667-85.

MOWAT, C., COLE, A., WINDSOR, A., AHMAD, T., ARNOTT, I., DRISCOLL, R., MITTON, S., ORCHARD, T., RUTTER, M., YOUNGE, L., LEES, C., HO, G. T., SATSANGI, J. & BLOOM, S. 2011. Guidelines for the management of inflammatory bowel disease in adults. *Gut,* 60**,** 571-607.

MULLER, S., NEUREITER, D., STOLTE, M., VERBEKE, C., HEUSCHMANN, P., KIRCHNER, T. & AIGNER, T. 2001. Tenascin: a sensitive and specific diagnostic marker of minimal collagenous colitis. *Virchows Arch,* 438**,** 435-41.

MULLER-FELBER, W., TOEPFER, M., MULLER, T., MULLER-HOCKER, J., FISCHER, P., LOCHMULLER, H. & PONGRATZ, D. 1998. Tenascin is a useful marker in the diagnosis of inflammatory myopathies. *Eur J Med Res,* 3**,** 281-7.

MURAI, M., TUROVSKAYA, O., KIM, G., MADAN, R., KARP, C. L., CHEROUTRE, H. & KRONENBERG, M. 2009. Interleukin 10 acts on regulatory T cells to maintain expression of the transcription factor Foxp3 and suppressive function in mice with colitis. *Nat Immunol,* 10**,** 1178-84.

MURAKAMI, R., YAMAOKA, I. & SAKAKURA, T. 1989. Appearance of tenascin in healing skin of the mouse: possible involvement in seaming of wounded tissues. *Int J Dev Biol,* 33**,** 439-44.

MURPHY, D., MATTEY, D. & HUTCHINSON, D. 2017. Anti-citrullinated protein antibody positive rheumatoid arthritis is primarily determined by rheumatoid factor titre and the shared epitope rather than smoking per se. *PLoS One,* 12**,** e0180655.

MURPHY-ULLRICH, J. E. & SAGE, E. H. 2014. Revisiting the matricellular concept. *Matrix Biol,* 37**,** 1-14.

NAITO, Y., TAKAGI, T., UCHIYAMA, K., KURODA, M., KOKURA, S., ICHIKAWA, H., YANAGISAWA, R., INOUE, K., TAKANO, H., SATOH, M., YOSHIDA, N., OKANOUE, T. & YOSHIKAWA, T. 2004. Reduced intestinal inflammation induced by dextran sodium sulfate in interleukin-6-deficient mice. *Int J Mol Med,* 14**,** 191-6.

NAKAHARA, H., GABAZZA, E. C., FUJIMOTO, H., NISHII, Y., D'ALESSANDRO-GABAZZA, C. N., BRUNO, N. E., TAKAGI, T., HAYASHI, T., MARUYAMA, J., MARUYAMA, K., IMANAKA-YOSHIDA, K., SUZUKI, K., YOSHIDA, T., ADACHI, Y. & TAGUCHI, O. 2006. Deficiency of tenascin C attenuates allergen-induced bronchial asthma in the mouse. *Eur J Immunol,* 36**,** 3334-45.

NAKAO, N., HIRAIWA, N., YOSHIKI, A., IKE, F. & KUSAKABE, M. 1998. Tenascin-C promotes healing of Habu-snake venom-induced glomerulonephritis: studies in knockout congenic mice and in culture. *Am J Pathol,* 152**,** 1237-45.

NAKOSHI, Y., HASEGAWA, M., SUDO, A., YOSHIDA, T. & UCHIDA, A. 2008. Regulation of tenascin-C expression by tumor necrosis factor-alpha in cultured human osteoarthritis chondrocytes. *J Rheumatol,* 35**,** 147-52.

NATHAN, C. 2002. Points of control in inflammation. *Nature,* 420**,** 846-52.

NATHAN, C. & DING, A. 2010. Nonresolving inflammation. *Cell,* 140**,** 871-82.

NEURATH, M. F. 2014. Cytokines in inflammatory bowel disease. *Nat Rev Immunol,* 14**,** 329-42.

NEURATH, M. F. 2019. Targeting immune cell circuits and trafficking in inflammatory bowel disease. *Nat Immunol,* 20**,** 970-979.

NG, S. C., SHI, H. Y., HAMIDI, N., UNDERWOOD, F. E., TANG, W., BENCHIMOL, E. I., PANACCIONE, R., GHOSH, S., WU, J. C. Y., CHAN, F. K. L., SUNG, J. J. Y. & KAPLAN, G. G. 2018. Worldwide incidence and prevalence of inflammatory bowel disease in the 21st century: a systematic review of population-based studies. *Lancet,* 390**,** 2769-2778.

NIELEN, M. M., VAN SCHAARDENBURG, D., REESINK, H. W., VAN DE STADT, R. J., VAN DER HORST-BRUINSMA, I. E., DE KONING, M. H., HABIBUW, M. R., VANDENBROUCKE, J. P. & DIJKMANS, B. A. 2004. Specific autoantibodies precede the symptoms of rheumatoid arthritis: a study of serial measurements in blood donors. *Arthritis Rheum,* 50**,** 380-6.

NIESS, J. H., BRAND, S., GU, X., LANDSMAN, L., JUNG, S., MCCORMICK, B. A., VYAS, J. M., BOES, M., PLOEGH, H. L., FOX, J. G., LITTMAN, D. R. & REINECKER, H. C. 2005. CX3CR1-mediated dendritic cell

access to the intestinal lumen and bacterial clearance. *Science,* 307**,** 254-8.

NISSINEN, L. & KAHARI, V. M. 2014. Matrix metalloproteinases in inflammation. *Biochim Biophys Acta,* 1840**,** 2571-80.

NOVAK, M. L. & KOH, T. J. 2013. Macrophage phenotypes during tissue repair. *J Leukoc Biol,* 93**,** 875-81.

NUNES, N. S., KIM, S., SUNDBY, M., CHANDRAN, P., BURKS, S. R., PAZ, A. H. & FRANK, J. A. 2018. Temporal clinical, proteomic, histological and cellular immune responses of dextran sulfate sodium-induced acute colitis. *World J Gastroenterol,* 24**,** 4341-4355.

O'BRYANT, S. E., LISTA, S., RISSMAN, R. A., EDWARDS, M., ZHANG, F., HALL, J., ZETTERBERG, H., LOVESTONE, S., GUPTA, V., GRAFF-RADFORD, N., MARTINS, R., JEROMIN, A., WARING, S., OH, E., KLING, M., BAKER, L. D. & HAMPEL, H. 2016. Comparing biological markers of Alzheimer's disease across blood fraction and platforms: Comparing apples to oranges. *Alzheimers Dement (Amst),* 3**,** 27-34.

O'NEILL, L. A., KISHTON, R. J. & RATHMELL, J. 2016. A guide to immunometabolism for immunologists. *Nat Rev Immunol,* 16**,** 553-65.

O'SULLIVAN, S., GILMER, J. F. & MEDINA, C. 2015. Matrix metalloproteinases in inflammatory bowel disease: an update. *Mediators Inflamm,* 2015**,** 964131.

OCKLIND, G., TALTS, J., FASSLER, R., MATTSSON, A. & EKBLOM, P. 1993. Expression of tenascin in developing and adult mouse lymphoid organs. *J Histochem Cytochem,* 41**,** 1163-9.

OHTA, M., SAKAI, T., SAGA, Y., AIZAWA, S. & SAITO, M. 1998. Suppression of hematopoietic activity in tenascin-C-deficient mice. *Blood,* 91**,** 4074-83.

OKADA, H., KUHN, C., FEILLET, H. & BACH, J. F. 2010. The 'hygiene hypothesis' for autoimmune and allergic diseases: an update. *Clin Exp Immunol,* 160**,** 1-9.

OKAMURA, N., HASEGAWA, M., NAKOSHI, Y., IINO, T., SUDO, A., IMANAKA-YOSHIDA, K., YOSHIDA, T. & UCHIDA, A. 2010. Deficiency of tenascin-C delays articular cartilage repair in mice. *Osteoarthritis Cartilage,* 18**,** 839-48.

OKAYASU, I., HATAKEYAMA, S., YAMADA, M., OHKUSA, T., INAGAKI, Y. & NAKAYA, R. 1990. A novel method in the induction of reliable experimental acute and chronic ulcerative colitis in mice. *Gastroenterology,* 98**,** 694-702.

OKIN, D. & MEDZHITOV, R. 2012. Evolution of inflammatory diseases. *Curr Biol,* 22**,** R733-40.

OKUMA, Y., SUDA, K., NAKAOKA, H., KATSUBE, Y., MITANI, Y., YOSHIKANE, Y., ICHIDA, F., MATSUSHITA, T., SHICHINO, H., SHIRAISHI, I., ABE, J., HIROE, M., YOSHIDA, T. & IMANAKA-YOSHIDA, K. 2016. Serum Tenascin-C as a Novel Predictor for Risk of Coronary Artery Lesion and Resistance to Intravenous Immunoglobulin in Kawasaki Disease- A Multicenter Retrospective Study. *Circ J,* 80**,** 2376-2381.

ORAK, U., CELIK, E., KAVAK, S. B., DEMIREL, I., ATILGAN, R., AYDIN, S. & SAPMAZ, E. 2016. Tenascin C levels in patients with mild and severe preeclampsia. *J Matern Fetal Neonatal Med,* 29**,** 270-3.

ORTEGA-GOMEZ, A., PERRETTI, M. & SOEHNLEIN, O. 2013. Resolution of inflammation: an integrated view. *EMBO Mol Med,* 5**,** 661-74.

OSTANIN, D. V., BAO, J., KOBOZIEV, I., GRAY, L., ROBINSON-JACKSON, S. A., KOSLOSKI-DAVIDSON, M., PRICE, V. H. & GRISHAM, M. B. 2009. T cell transfer model of chronic colitis: concepts, considerations, and tricks of the trade. *Am J Physiol Gastrointest Liver Physiol,* 296**,** G135-46.

OWENS, B. M., STEEVELS, T. A., DUDEK, M., WALCOTT, D., SUN, M. Y., MAYER, A., ALLAN, P. & SIMMONS, A. 2013. CD90(+) Stromal Cells are Non-Professional Innate Immune Effectors of the Human Colonic Mucosa. *Front Immunol,* 4**,** 307.

PAGE, T. H., CHARLES, P. J., PICCININI, A. M., NICOLAIDOU, V., TAYLOR, P. C. & MIDWOOD, K. S. 2012. Raised circulating tenascin-C in rheumatoid arthritis. *Arthritis Res Ther,* 14**,** R260.

PAHWA, R. & JIALAL, I. 2019. *Chronic Inflammation*, StatPearls Publishing.

PAPIN, S., CUENIN, S., AGOSTINI, L., MARTINON, F., WERNER, S., BEER, H.-D., GRÜTTER, C., GRÜTTER, M. & TSCHOPP, J. 2007. The SPRY domain of Pyrin, mutated in familial Mediterranean fever patients, interacts with inflammasome components and inhibits proIL-1|[beta]| processing. *Cell Death & Differentiation,* 14**,** 1457-1466.

PARAMSOTHY, S., ROSENSTEIN, A. K., MEHANDRU, S. & COLOMBEL, J. F. 2018. The current state of the art for biological therapies and new small molecules in inflammatory bowel disease. *Mucosal Immunol,* 11**,** 1558-1570.

PARANKO, J., HAAVISTO, M., CHIQUET-EHRISMANN, R., AUKHIL, I. & KAIPIA, A. 1995. Sex-dependent expression of tenascin-C in the differentiating fetal rat testis and ovary. *Differentiation,* 58**,** 329-39.

PAREKH, K., RAMACHANDRAN, S., COOPER, J., BIGNER, D., PATTERSON, A. & MOHANAKUMAR, T. 2005. Tenascin-C, over expressed in lung cancer down regulates effector functions of tumor infiltrating lymphocytes. *Lung Cancer,* 47**,** 17-29.

PATEL, L., SUN, W., GLASSON, S. S., MORRIS, E. A., FLANNERY, C. R. & CHOCKALINGAM, P. S. 2011. Tenascin-C induces inflammatory mediators and matrix degradation in osteoarthritic cartilage. *BMC Musculoskelet Disord,* 12**,** 164.

PATEL, R., FILER, A., BARONE, F. & BUCKLEY, C. D. 2014. Stroma: fertile soil for inflammation. *Best Pract Res Clin Rheumatol,* 28**,** 565-76.

PATTERSON, A. M. & WATSON, A. J. M. 2017. Deciphering the Complex Signaling Systems That Regulate Intestinal Epithelial Cell Death Processes and Shedding. *Front Immunol,* 8**,** 841.

PENG, R., DAI, W. & LI, Y. 2018. High serum levels of tenascin-C are associated with suicide attempts in depressed patients. *Psychiatry Res,* 268**,** 60-64.

PERREAULT, N., HERRING-GILLAM, F. E., DESLOGES, N., BELANGER, I., PAGEOT, L. P. & BEAULIEU, J. F. 1998. Epithelial vs mesenchymal

contribution to the extracellular matrix in the human intestine. *Biochem Biophys Res Commun,* 248**,** 121-6.

PERSE, M. & CERAR, A. 2012. Dextran sodium sulphate colitis mouse model: traps and tricks. *J Biomed Biotechnol,* 2012**,** 718617.

PERSSON, E. K., SCOTT, C. L., MOWAT, A. M. & AGACE, W. W. 2013. Dendritic cell subsets in the intestinal lamina propria: ontogeny and function. *Eur J Immunol,* 43**,** 3098-107.

PETREY, A. C. & DE LA MOTTE, C. A. 2017. The extracellular matrix in IBD: a dynamic mediator of inflammation. *Curr Opin Gastroenterol,* 33**,** 234-238.

PICCININI, A. M. & MIDWOOD, K. S. 2010. DAMPening inflammation by modulating TLR signalling. *Mediators Inflamm,* 2010.

PICCININI, A. M. & MIDWOOD, K. S. 2012. Endogenous control of immunity against infection: tenascin-C regulates TLR4-mediated inflammation via microRNA-155. *Cell Rep,* 2**,** 914-26.

PICCININI, A. M., ZULIANI-ALVAREZ, L., LIM, J. M. & MIDWOOD, K. S. 2016. Distinct microenvironmental cues stimulate divergent TLR4-mediated signaling pathways in macrophages. *Sci Signal,* 9**,** ra86.

PONCHEL, F., TOOMES, C., BRANSFIELD, K., LEONG, F. T., DOUGLAS, S. H., FIELD, S. L., BELL, S. M., COMBARET, V., PUISIEUX, A., MIGHELL, A. J., ROBINSON, P. A., INGLEHEARN, C. F., ISAACS, J. D. & MARKHAM, A. F. 2003. Real-time PCR based on SYBR-Green I fluorescence: an alternative to the TaqMan assay for a relative quantification of gene rearrangements, gene amplifications and micro gene deletions. *BMC Biotechnol,* 3**,** 18.

PROBSTMEIER, R., MARTINI, R. & SCHACHNER, M. 1990a. Expression of J1/tenascin in the crypt-villus unit of adult mouse small intestine: implications for its role in epithelial cell shedding. *Development,* 109**,** 313-21.

PROBSTMEIER, R., MARTINI, R., TACKE, R. & SCHACHNER, M. 1990b. Expression of the adhesion molecules L1, N-CAM and J1/tenascin during development of the murine small intestine. *Differentiation,* 44**,** 42-55.

PROUD, D., TURNER, R. B., WINTHER, B., WIEHLER, S., TIESMAN, J. P., REICHLING, T. D., JUHLIN, K. D., FULMER, A. W., HO, B. Y., WALANSKI, A. A., POORE, C. L., MIZOGUCHI, H., JUMP, L., MOORE, M. L., ZUKOWSKI, C. K. & CLYMER, J. W. 2008. Gene expression profiles during in vivo human rhinovirus infection: insights into the host response. *Am J Respir Crit Care Med,* 178**,** 962-8.

PUENTE NAVAZO, M. D., VALMORI, D. & RUEGG, C. 2001. The alternatively spliced domain TnFnIII A1A2 of the extracellular matrix protein tenascin-C suppresses activation-induced T lymphocyte proliferation and cytokine production. *J Immunol,* 167**,** 6431-40.

QIAO, Y. C., PAN, Y. H., LING, W., TIAN, F., CHEN, Y. L., ZHANG, X. X. & ZHAO, H. L. 2017. The Yin and Yang of regulatory T cell and therapy progress in autoimmune disease. *Autoimmun Rev,* 16**,** 1058-1070.

QUEZADA, S. M., MCLEAN, L. P. & CROSS, R. K. 2018. Adverse events in IBD therapy: the 2018 update. *Expert Rev Gastroenterol Hepatol,* 12**,** 1183-1191.

QUIROS, M., NISHIO, H., NEUMANN, P. A., SIUDA, D., BRAZIL, J. C., AZCUTIA, V., HILGARTH, R., O'LEARY, M. N., GARCIA-HERNANDEZ, V., LEONI, G., FENG, M., BERNAL, G., WILLIAMS, H., DEDHIA, P. H., GERNER-SMIDT, C., SPENCE, J., PARKOS, C. A., DENNING, T. L. & NUSRAT, A. 2017. Macrophage-derived IL-10 mediates mucosal repair by epithelial WISP-1 signaling. *J Clin Invest,* 127**,** 3510-3520.

RADWANSKA, A., GRALL, D., SCHAUB, S., DIVONNE, S. B. F., CIAIS, D., REKIMA, S., RUPP, T., SUDAKA, A., OREND, G. & VAN OBBERGHEN-SCHILLING, E. 2017. Counterbalancing anti-adhesive effects of Tenascin-C through fibronectin expression in endothelial cells. *Sci Rep,* 7**,** 12762.

RAHMAN, P., INMAN, R. D., EL-GABALAWY, H. & KRAUSE, D. O. 2010. Pathophysiology and pathogenesis of immune-mediated inflammatory diseases: commonalities and differences. *J Rheumatol Suppl,* 85**,** 11-26.

RAKOFF-NAHOUM, S., PAGLINO, J., ESLAMI-VARZANEH, F., EDBERG, S. & MEDZHITOV, R. 2004. Recognition of commensal microflora by toll-like receptors is required for intestinal homeostasis. *Cell,* 118**,** 229-41.

RAMOS, D. M., CHEN, B., REGEZI, J., ZARDI, L. & PYTELA, R. 1998. Tenascin-C matrix assembly in oral squamous cell carcinoma. *Int J Cancer,* 75**,** 680-7.

RANDALL, T. D. & MEBIUS, R. E. 2014. The development and function of mucosal lymphoid tissues: a balancing act with micro-organisms. *Mucosal Immunol,* 7**,** 455-66.

RAYEGO-MATEOS, S., RODRIGUES-DIEZ, R., MORGADO-PASCUAL, J. L., VALENTIJN, F., VALDIVIELSO, J. M., GOLDSCHMEDING, R. & RUIZ-ORTEGA, M. 2018. Role of Epidermal Growth Factor Receptor (EGFR) and Its Ligands in Kidney Inflammation and Damage. *Mediators Inflamm,* 2018**,** 8739473.

RAZA, K., SCHWENZER, A., JUAREZ, M., VENABLES, P., FILER, A., BUCKLEY, C. D. & MIDWOOD, K. S. 2016. Detection of antibodies to citrullinated tenascin-C in patients with early synovitis is associated with the development of rheumatoid arthritis. *RMD Open,* 2**,** e000318.

REKVIG, O. P., PUTTERMAN, C., CASU, C., GAO, H. X., GHIRARDELLO, A., MORTENSEN, E. S., TINCANI, A. & DORIA, A. 2012. Autoantibodies in lupus: culprits or passive bystanders? *Autoimmun Rev,* 11**,** 596-603.

RICARD-BLUM, S. & SALZA, R. 2014. Matricryptins and matrikines: biologically active fragments of the extracellular matrix. *Exp Dermatol,* 23**,** 457-63.

RIEDL, S., BODENMULLER, H., HINZ, U., HOLLE, R., MOLLER, P., SCHLAG, P., HERFARTH, C. & FAISSNER, A. 1995. Significance of tenascin serum level as tumor marker in primary colorectal carcinoma. *Int J Cancer,* 64**,** 65-9.

RIEDL, S., TANDARA, A., REINSHAGEN, M., HINZ, U., FAISSNER, A., BODENMULLER, H., BUHR, H. J., HERFARTH, C. & MOLLER, P. 2001. Serum tenascin-C is an indicator of inflammatory bowel disease activity. *Int J Colorectal Dis,* 16**,** 285-91.

RIEDL, S. E., FAISSNER, A., SCHLAG, P., VON HERBAY, A., KORETZ, K. & MOLLER, P. 1992. Altered content and distribution of tenascin in colitis, colon adenoma, and colorectal carcinoma. *Gastroenterology,* 103**,** 400-6.

RILEY, G. P., HARRALL, R. L., CAWSTON, T. E., HAZLEMAN, B. L. & MACKIE, E. J. 1996. Tenascin-C and human tendon degeneration. *Am J Pathol,* 149**,** 933-43.

ROBINSON, W. H., LINDSTROM, T. M., CHEUNG, R. K. & SOKOLOVE, J. 2013. Mechanistic biomarkers for clinical decision making in rheumatic diseases. *Nat Rev Rheumatol,* 9**,** 267-76.

ROBINSON, W. H. & MAO, R. 2016. Biomarkers to guide clinical therapeutics in rheumatology? *Curr Opin Rheumatol,* 28**,** 168-75.

RODRIGUES, M., YATES, C. C., NUSCHKE, A., GRIFFITH, L. & WELLS, A. 2013. The matrikine tenascin-C protects multipotential stromal cells/mesenchymal stem cells from death cytokines such as FasL. *Tissue Eng Part A,* 19**,** 1972-83.

ROPERS, T., KROLL, W., BECKA, M., VOELKER, M., BURCHARDT, E. R., SCHUPPAN, D. & GEHRMANN, M. 2000. Enzyme immunoassay for the measurement of human tenascin-C on the Bayer Immuno 1 analyzer. *Clin Biochem,* 33**,** 7-13.

ROSENSTEIN, E. D., GREENWALD, R. A., KUSHNER, L. J. & WEISSMANN, G. 2004. Hypothesis: the humoral immune response to oral bacteria provides a stimulus for the development of rheumatoid arthritis. *Inflammation,* 28**,** 311-8.

ROSSHART, S. P., VASSALLO, B. G., ANGELETTI, D., HUTCHINSON, D. S., MORGAN, A. P., TAKEDA, K., HICKMAN, H. D., MCCULLOCH, J. A., BADGER, J. H., AJAMI, N. J., TRINCHIERI, G., PARDO-MANUEL DE VILLENA, F., YEWDELL, J. W. & REHERMANN, B. 2017. Wild Mouse Gut Microbiota Promotes Host Fitness and Improves Disease Resistance. *Cell,* 171**,** 1015-1028.e13.

RUBIO, C. A., LANGNER, C. & SCHMIDT, P. T. 2018. Partial to complete abrogation of the subepithelial macrophage barrier against the gut microbiota in patients with ulcerative colitis and Crohn's colitis. *Histopathology,* 72**,** 580-587.

RUEDEN, C. T., SCHINDELIN, J., HINER, M. C., DEZONIA, B. E., WALTER, A. E., ARENA, E. T. & ELICEIRI, K. W. 2017. ImageJ2: ImageJ for the next generation of scientific image data. *BMC Bioinformatics,* 18**,** 529.

RUEGG, C. R., CHIQUET-EHRISMANN, R. & ALKAN, S. S. 1989. Tenascin, an extracellular matrix protein, exerts immunomodulatory activities. *Proc Natl Acad Sci U S A,* 86**,** 7437-41.

RUEL, J., RUANE, D., MEHANDRU, S., GOWER-ROUSSEAU, C. & COLOMBEL, J. F. 2014. IBD across the age spectrum: is it the same disease? *Nat Rev Gastroenterol Hepatol,* 11**,** 88-98.

RUHMANN, M. & MIDWOOD, K. 2013. The pro-inflammatory niche: how the extracellular matrix drives rheumatoid arthritis?OA Arthritis. *OA Arthritis,* 1(1)**,** 6.

RUHMANN, M., PICCININI, A. M., KONG, P. L. & MIDWOOD, K. S. 2012. Endogenous activation of adaptive immunity: tenascin-C drives interleukin-17 synthesis in murine arthritic joint disease. *Arthritis Rheum,* 64**,** 2179-90.

RUSSELL, A. S., GULLIVER, W. P., IRVINE, E. J., ALBANI, S. & DUTZ, J. P. 2011. Quality of life in patients with immune-mediated inflammatory diseases. *J Rheumatol Suppl,* 88**,** 7-19.

SAADA, J. I., PINCHUK, I. V., BARRERA, C. A., ADEGBOYEGA, P. A., SUAREZ, G., MIFFLIN, R. C., DI MARI, J. F., REYES, V. E. & POWELL, D. W. 2006. Subepithelial myofibroblasts are novel nonprofessional APCs in the human colonic mucosa. *J Immunol,* 177**,** 5968-79.

SAGA, Y., TSUKAMOTO, T., JING, N., KUSAKABE, M. & SAKAKURA, T. 1991. Murine tenascin: cDNA cloning, structure and temporal expression of isoforms. *Gene,* 104**,** 177-85.

SAGA, Y., YAGI, T., IKAWA, Y., SAKAKURA, T. & AIZAWA, S. 1992. Mice develop normally without tenascin. *Genes Dev,* 6**,** 1821-31.

SAITO, Y., IMAZEKI, H., MIURA, S., YOSHIMURA, T., OKUTSU, H., HARADA, Y., OHWAKI, T., NAGAO, O., KAMIYA, S., HAYASHI, R., KODAMA, H., HANDA, H., YOSHIDA, T. & FUKAI, F. 2007. A peptide derived from tenascin-C induces beta1 integrin activation through syndecan-4. *J Biol Chem,* 282**,** 34929-37.

SAKAI, T., KAWAKATSU, H., HIROTA, N., YOKOYAMA, T., SAKAKURA, T. & SAITO, M. 1993. Specific expression of tenascin in human colonic neoplasms. *Br J Cancer,* 67**,** 1058-64.

SALAS, A., FERNANDEZ-BANARES, F., CASALOTS, J., GONZALEZ, C., TARROCH, X., FORCADA, P. & GONZALEZ, G. 2003. Subepithelial myofibroblasts and tenascin expression in microscopic colitis. *Histopathology,* 43**,** 48-54.

SALTER, D. M. 1993. Tenascin is increased in cartilage and synovium from arthritic knees. *Br J Rheumatol,* 32**,** 780-6.

SATHALIYAWALA, T., KUBOTA, M., YUDANIN, N., TURNER, D., CAMP, P., THOME, J. J., BICKHAM, K. L., LERNER, H., GOLDSTEIN, M., SYKES, M., KATO, T. & FARBER, D. L. 2013. Distribution and compartmentalization of human circulating and tissue-resident memory T cell subsets. *Immunity,* 38**,** 187-97.

SAUPE, F., SCHWENZER, A., JIA, Y., GASSER, I., SPENLE, C., LANGLOIS, B., KAMMERER, M., LEFEBVRE, O., HLUSHCHUK, R., RUPP, T., MARKO, M., VAN DER HEYDEN, M., CREMEL, G., ARNOLD, C., KLEIN, A., SIMON-ASSMANN, P., DJONOV, V., NEUVILLE-MECHINE, A., ESPOSITO, I., SLOTTA-HUSPENINA, J., JANSSEN, K. P., DE WEVER, O., CHRISTOFORI, G., HUSSENET, T. & OREND, G. 2013. Tenascin-C downregulates wnt inhibitor dickkopf-1, promoting tumorigenesis in a neuroendocrine tumor model. *Cell Rep,* 5**,** 482-92.

SCALDAFERRI, F., VETRANO, S., SANS, M., ARENA, V., STRAFACE, G., STIGLIANO, E., REPICI, A., STURM, A., MALESCI, A., PANES, J.,

YLA-HERTTUALA, S., FIOCCHI, C. & DANESE, S. 2009. VEGF-A links angiogenesis and inflammation in inflammatory bowel disease pathogenesis. *Gastroenterology,* 136**,** 585-95.e5.

SCHAEFER, L. 2014. Complexity of danger: the diverse nature of damage-associated molecular patterns. *J Biol Chem,* 289**,** 35237-45.

SCHALKWIJK, J., VAN VLIJMEN, I., OOSTERLING, B., PERRET, C., KOOPMAN, R., VAN DEN BORN, J. & MACKIE, E. J. 1991. Tenascin expression in hyperproliferative skin diseases. *Br J Dermatol,* 124**,** 13-20.

SCHENK, S., MUSER, J., VOLLMER, G. & CHIQUET-EHRISMANN, R. 1995. Tenascin-C in serum: a questionable tumor marker. *Int J Cancer,* 61**,** 443-9.

SCHERBERICH, A., TUCKER, R. P., SAMANDARI, E., BROWN-LUEDI, M., MARTIN, D. & CHIQUET-EHRISMANN, R. 2004. Murine tenascin-W: a novel mammalian tenascin expressed in kidney and at sites of bone and smooth muscle development. *J Cell Sci,* 117**,** 571-81.

SCHINDELIN, J., ARGANDA-CARRERAS, I., FRISE, E., KAYNIG, V., LONGAIR, M., PIETZSCH, T., PREIBISCH, S., RUEDEN, C., SAALFELD, S., SCHMID, B., TINEVEZ, J. Y., WHITE, D. J., HARTENSTEIN, V., ELICEIRI, K., TOMANCAK, P. & CARDONA, A. 2012. Fiji: an open-source platform for biological-image analysis. *Nat Methods,* 9**,** 676-82.

SCHWENZER, A., JIANG, X., MIKULS, T. R., PAYNE, J. B., SAYLES, H. R., QUIRKE, A. M., KESSLER, B. M., FISCHER, R., VENABLES, P. J., LUNDBERG, K. & MIDWOOD, K. S. 2015. Identification of an immunodominant peptide from citrullinated tenascin-C as a major target for autoantibodies in rheumatoid arthritis. *Ann Rheum Dis*.

SCHWENZER, A., QUIRKE, A. M., MARZEDA, A. M., WONG, A., MONTGOMERY, A. B., SAYLES, H. R., EICK, S., GAWRON, K., CHOMYSZYN-GAJEWSKA, M., LAZARZ-BARTYZEL, K., DAVIS, S., POTEMPA, J., KESSLER, B. M., FISCHER, R., VENABLES, P. J., PAYNE, J. B., MIKULS, T. R. & MIDWOOD, K. S. 2017. Association of Distinct Fine Specificities of Anti-Citrullinated Peptide Antibodies With Elevated Immune Responses to Prevotella intermedia in a Subgroup of Patients With Rheumatoid Arthritis and Periodontitis. *Arthritis Rheumatol*.

SCHWENZER, A., QUIRKE, A. M., MONTGOMERY, A. B., VENABLES, P. J., SAYLES, H. R., SCHLUMBERGER, W., PAYNE, J. B., MIKULS, T. R. & MIDWOOD, K. S. 2019. Time to Include Fine Specificity Anti-Citrullinated Protein Antibodies in the Routine Diagnosis and Management of Rheumatoid Arthritis? *Arthritis Rheumatol,* 71**,** 476-478.

SCOTT, A., KHAN, K. M., COOK, J. L. & DURONIO, V. 2004. What is "inflammation"? Are we ready to move beyond Celsus? *Br J Sports Med,* 38**,** 248-9.

SERHAN, C. N. & SAVILL, J. 2005. Resolution of inflammation: the beginning programs the end. *Nat Immunol.* United States.

SEYGER, M. M., VAN DEN HOOGEN, F. H., VAN VLIJMEN-WILLEMS, I. M., VAN DE KERKHOF, P. C. & DE JONG, E. M. 2001. Localized and systemic scleroderma show different histological responses to methotrexate therapy. *J Pathol,* 193**,** 511-6.

SHI, Y. J., GONG, H. F., ZHAO, Q. Q., LIU, X. S., LIU, C. & WANG, H. 2019. Critical role of toll-like receptor 4 (TLR4) in dextran sulfate sodium (DSS)-Induced intestinal injury and repair. *Toxicol Lett,* 315**,** 23-30.

SHIMOJO, N., HASHIZUME, R., KANAYAMA, K., HARA, M., SUZUKI, Y., NISHIOKA, T., HIROE, M., YOSHIDA, T. & IMANAKA-YOSHIDA, K. 2015. Tenascin-C May Accelerate Cardiac Fibrosis by Activating Macrophages via the Integrin alphaVbeta3/Nuclear Factor-kappaB/Interleukin-6 Axis. *Hypertension,* 66**,** 757-66.

SHIMSHONI, E., AFIK, R., SOLOMONOV, I., ADIR, I., SHENOY, A., ADLER, M., PURICELLI, L., GHINI, V., MOUHADEB, O., GLUCK, N., FISHMAN, S., WERNER, L., SHOUVAL, D., VAROL, C., PODESTÀ, A., TURANO, P., GEIGER, T., MILANI, P., LUCHINAT, C., ALON, U. & SAGI, I. 2019. Unraveling the state-specific nature of the native extracellular matrix via multidimensional characterization of its material properties. *bioRxiv*.

SHIMSHONI, E., YABLECOVITCH, D., BARAM, L., DOTAN, I. & SAGI, I. 2015. ECM remodelling in IBD: innocent bystander or partner in crime? The emerging role of extracellular molecular events in sustaining intestinal inflammation. *Gut,* 64**,** 367-72.

SHUKLA, A., GAUR, P. & AGGARWAL, A. 2015. Tenascin-C Levels, A Toll-like Receptor 4 Ligand, in Enthesitis-related Arthritis Category of Juvenile Idiopathic Arthritis: A Cross-sectional and Longitudinal Study. *J Rheumatol,* 42**,** 891-6.

SIEGHART, D., PLATZER, A., STUDENIC, P., ALASTI, F., GRUNDHUBER, M., SWINIARSKI, S., HORN, T., HASLACHER, H., BLUML, S., SMOLEN, J. & STEINER, G. 2018. Determination of Autoantibody Isotypes Increases the Sensitivity of Serodiagnostics in Rheumatoid Arthritis. *Front Immunol,* 9**,** 876.

SIEVERS, F., WILM, A., DINEEN, D., GIBSON, T. J., KARPLUS, K., LI, W., LOPEZ, R., MCWILLIAM, H., REMMERT, M., SODING, J., THOMPSON, J. D. & HIGGINS, D. G. 2011. Fast, scalable generation of high-quality protein multiple sequence alignments using Clustal Omega. *Mol Syst Biol,* 7**,** 539.

SIHVONEN, S., KORPELA, M., MUSTILA, A. & MUSTONEN, J. 2005. The predictive value of rheumatoid factor isotypes, anti-cyclic citrullinated peptide antibodies, and antineutrophil cytoplasmic antibodies for mortality in patients with rheumatoid arthritis. *J Rheumatol,* 32**,** 2089-94.

SILVERBERG, M. S., SATSANGI, J., AHMAD, T., ARNOTT, I. D., BERNSTEIN, C. N., BRANT, S. R., CAPRILLI, R., COLOMBEL, J. F., GASCHE, C., GEBOES, K., JEWELL, D. P., KARBAN, A., LOFTUS, E. V., JR., PENA, A. S., RIDDELL, R. H., SACHAR, D. B., SCHREIBER, S., STEINHART, A. H., TARGAN, S. R., VERMEIRE, S. & WARREN, B. F. 2005. Toward an integrated clinical, molecular and serological

classification of inflammatory bowel disease: report of a Working Party of the 2005 Montreal World Congress of Gastroenterology. *Can J Gastroenterol,* 19 Suppl A**,** 5a-36a.

SIRI, A., CARNEMOLLA, B., SAGINATI, M., LEPRINI, A., CASARI, G., BARALLE, F. & ZARDI, L. 1991. Human tenascin: primary structure, pre-mRNA splicing patterns and localization of the epitopes recognized by two monoclonal antibodies. *Nucleic Acids Res,* 19**,** 525-31.

SIRI, A., KNAUPER, V., VEIRANA, N., CAOCCI, F., MURPHY, G. & ZARDI, L. 1995. Different susceptibility of small and large human tenascin-C isoforms to degradation by matrix metalloproteinases. *J Biol Chem,* 270**,** 8650-4.

SMITH, H. F., FISHER, R. E., EVERETT, M. L., THOMAS, A. D., BOLLINGER, R. R. & PARKER, W. 2009. Comparative anatomy and phylogenetic distribution of the mammalian cecal appendix. *J Evol Biol,* 22**,** 1984-99.

SOKOLOVE, J., BRENNAN, M. J., SHARPE, O., LAHEY, L. J., KAO, A. H., KRISHNAN, E., EDMUNDOWICZ, D., LEPUS, C. M., WASKO, M. C. & ROBINSON, W. H. 2013. Brief report: citrullination within the atherosclerotic plaque: a potential target for the anti-citrullinated protein antibody response in rheumatoid arthritis. *Arthritis Rheum,* 65**,** 1719-24.

SONG, Y. W. & KANG, E. H. 2010. Autoantibodies in rheumatoid arthritis: rheumatoid factors and anticitrullinated protein antibodies. *Qjm,* 103**,** 139-46.

SOROKIN, L. 2010. The impact of the extracellular matrix on inflammation. *Nat Rev Immunol,* 10**,** 712-23.

SPENLE, C., SAUPE, F., MIDWOOD, K., BURCKEL, H., NOEL, G. & OREND, G. 2015. Tenascin-C: Exploitation and collateral damage in cancer management. *Cell Adh Migr,* 9**,** 141-53.

SRIRAMARAO, P., MENDLER, M. & BOURDON, M. A. 1993. Endothelial cell attachment and spreading on human tenascin is mediated by alpha 2 beta 1 and alpha v beta 3 integrins. *J Cell Sci,* 105 (Pt 4)**,** 1001-12.

STANICH, J. A., CARTER, J. D., WHITTUM-HUDSON, J. & HUDSON, A. P. 2009. Rheumatoid arthritis: Disease or syndrome? *Open Access Rheumatol,* 1**,** 179-192.

STEINDLER, D. A., SETTLES, D., ERICKSON, H. P., LAYWELL, E. D., YOSHIKI, A., FAISSNER, A. & KUSAKABE, M. 1995. Tenascin knockout mice: barrels, boundary molecules, and glial scars. *J Neurosci,* 15**,** 1971-83.

STRAUB, R. H. & SCHRADIN, C. 2016. Chronic inflammatory systemic diseases - an evolutionary trade-off between acutely beneficial but chronically harmful programs. *Evol Med Public Health*.

STROBER, W., FUSS, I. J. & BLUMBERG, R. S. 2002. The immunology of mucosal models of inflammation. *Annu Rev Immunol,* 20**,** 495-549.

SUZUKI, C., NAKAMURA, A., MIURA, N., FUKAI, K., OHNO, N., YAHATA, T., OKAMOTO-HAMAOKA, A., FUJII, M., YOSHIOKA, A., KUCHITSU, Y., IKEDA, K. & HAMAOKA, K. 2017. Non-receptor type, proline-rich protein tyrosine kinase 2 (Pyk2) is a possible therapeutic target for Kawasaki disease. *Clin Immunol,* 179**,** 17-24.

SVARD, A., SKOGH, T., ALFREDSSON, L., ILAR, A., KLARESKOG, L., BENGTSSON, C. & KASTBOM, A. 2015. Associations with smoking and shared epitope differ between IgA- and IgG-class antibodies to cyclic citrullinated peptides in early rheumatoid arthritis. *Arthritis Rheumatol,* 67**,** 2032-7.

SWINDLE, C. S., TRAN, K. T., JOHNSON, T. D., BANERJEE, P., MAYES, A. M., GRIFFITH, L. & WELLS, A. 2001. Epidermal growth factor (EGF)-like repeats of human tenascin-C as ligands for EGF receptor. *J Cell Biol,* 154**,** 459-68.

SZEKANECZ, Z., SZABO, Z., ZEHER, M., SOOS, L., DANKO, K., HORVATH, I. & LAKOS, G. 2013. Superior performance of the CCP3.1 test compared to CCP2 and MCV in the rheumatoid factor-negative RA population. *Immunol Res,* 56**,** 439-43.

TAKEUCHI, O. & AKIRA, S. 2010. Pattern recognition receptors and inflammation. *Cell,* 140**,** 805-20.

TASNIM, N., ABULIZI, N., PITHER, J., HART, M. M. & GIBSON, D. L. 2017. Linking the Gut Microbial Ecosystem with the Environment: Does Gut Health Depend on Where We Live? *Front Microbiol,* 8**,** 1935.

TASTEKIN, D., TAS, F., KARABULUT, S., DURANYILDIZ, D., SERILMEZ, M., GUVELI, M. & VATANSEVER, S. 2014. Clinical significance of serum tenascin-C levels in breast cancer. *Tumour Biol,* 35**,** 6619-25.

TATO, C. M. & O'SHEA, J. J. 2006. Immunology: what does it mean to be just 17? *Nature.* England.

TAUTZ, D. 1992. Redundancies, development and the flow of information. *Bioessays,* 14**,** 263-6.

TAYLOR, H. C., LIGHTNER, V. A., BEYER, W. F., JR., MCCASLIN, D., BRISCOE, G. & ERICKSON, H. P. 1989. Biochemical and structural studies of tenascin/hexabrachion proteins. *J Cell Biochem,* 41**,** 71-90.

TE VELDE, A. A., DE KORT, F., STERRENBURG, E., PRONK, I., TEN KATE, F. J., HOMMES, D. W. & VAN DEVENTER, S. J. 2007. Comparative analysis of colonic gene expression of three experimental colitis models mimicking inflammatory bowel disease. *Inflamm Bowel Dis,* 13**,** 325-30.

TECCHIO, C., MICHELETTI, A. & CASSATELLA, M. A. 2014. Neutrophil-derived cytokines: facts beyond expression. *Front Immunol,* 5**,** 508.

TERVO, K., TERVO, T., VAN SETTEN, G. B., TARKKANEN, A. & VIRTANEN, I. 1989. Demonstration of tenascin-like immunoreactivity in rabbit corneal wounds. *Acta Ophthalmol (Copenh),* 67**,** 347-50.

THEOCHARIS, A. D., SKANDALIS, S. S., GIALELI, C. & KARAMANOS, N. K. 2016. Extracellular matrix structure. *Adv Drug Deliv Rev,* 97**,** 4-27.

TIITTA, O., LUOMANEN, M., HIETANEN, J. & VIRTANEN, I. 1995. Tenascin expression in mucocutaneous diseases and related lesions of human oral mucosa. *Arch Oral Biol,* 40**,** 1039-45.

TIITTA, O., SIPPONEN, P., GOULD, V. & VIRTANEN, I. 1994. Tenascin expression in inflammatory, dysplastic and neoplastic lesions of the human stomach. *Virchows Arch,* 425**,** 369-74.

TIITTA, O., WAHLSTROM, T., PAAVONEN, J., LINNALA, A., SHARMA, S., GOULD, V. E. & VIRTANEN, I. 1992. Enhanced tenascin expression in cervical and vulvar koilocytotic lesions. *Am J Pathol,* 141**,** 907-13.

TO, W. S. & MIDWOOD, K. S. 2010. Cryptic domains of tenascin-C differentially control fibronectin fibrillogenesis. *Matrix Biol,* 29**,** 573-85.

TO, W. S. & MIDWOOD, K. S. 2011a. Identification of novel and distinct binding sites within tenascin-C for soluble and fibrillar fibronectin. *J Biol Chem,* 286**,** 14881-91.

TO, W. S. & MIDWOOD, K. S. 2011b. Plasma and cellular fibronectin: distinct and independent functions during tissue repair. *Fibrogenesis Tissue Repair,* 4**,** 21.

TOJYO, I., YAMAGUCHI, A., NITTA, T., YOSHIDA, H., FUJITA, S. & YOSHIDA, T. 2008. Effect of hypoxia and interleukin-1beta on expression of tenascin-C in temporomandibular joint. *Oral Dis,* 14**,** 45-50.

TOO, C. L., MURAD, S., HANSSON, M., ALM, L. M., DHALIWAL, J. S., HOLMDAHL, R., JAKOBSSON, P. J., ALFREDSSON, L., KLARESKOG, L., RONNELID, J. & PADYUKOV, L. 2017. Differences in the Spectrum of Anti-Citrullinated Protein Antibody Fine Specificities Between Malaysian and Swedish Patients With Rheumatoid Arthritis: Implications for Disease Pathogenesis. *Arthritis Rheumatol,* 69**,** 58-69.

TOUSSIROT, E. 2012. The IL23/Th17 pathway as a therapeutic target in chronic inflammatory diseases. *Inflamm Allergy Drug Targets,* 11**,** 159-68.

TRAVIS, S. P., SCHNELL, D., KRZESKI, P., ABREU, M. T., ALTMAN, D. G., COLOMBEL, J. F., FEAGAN, B. G., HANAUER, S. B., LEMANN, M., LICHTENSTEIN, G. R., MARTEAU, P. R., REINISCH, W., SANDS, B. E., YACYSHYN, B. R., BERNHARDT, C. A., MARY, J. Y. & SANDBORN, W. J. 2012. Developing an instrument to assess the endoscopic severity of ulcerative colitis: the Ulcerative Colitis Endoscopic Index of Severity (UCEIS). *Gut,* 61**,** 535-42.

TREMAROLI, V. & BACKHED, F. 2012. Functional interactions between the gut microbiota and host metabolism. *Nature,* 489**,** 242-9.

TREMBLE, P., CHIQUET-EHRISMANN, R. & WERB, Z. 1994. The extracellular matrix ligands fibronectin and tenascin collaborate in regulating collagenase gene expression in fibroblasts. *Mol Biol Cell,* 5**,** 439-53.

TSUKADA, B., TERASAKI, F., SHIMOMURA, H., OTSUKA, K., KATASHIMA, T., FUJITA, S., IMANAKA-YOSHIDA, K., YOSHIDA, T., HIROE, M. & KITAURA, Y. 2009. High prevalence of chronic myocarditis in dilated cardiomyopathy referred for left ventriculoplasty: expression of tenascin C as a possible marker for inflammation. *Hum Pathol,* 40**,** 1015-22.

TSUNODA, T., INADA, H., KALEMBEYI, I., IMANAKA-YOSHIDA, K., SAKAKIBARA, M., OKADA, R., KATSUTA, K., SAKAKURA, T., MAJIMA, Y. & YOSHIDA, T. 2003. Involvement of large tenascin-C splice variants in breast cancer progression. *Am J Pathol,* 162**,** 1857-67.

TUCKER, R. P. & CHIQUET-EHRISMANN, R. 2009. The regulation of tenascin expression by tissue microenvironments. *Biochim Biophys Acta,* 1793**,** 888-92.

TUCKER, R. P., DRABIKOWSKI, K., HESS, J. F., FERRALLI, J., CHIQUET-EHRISMANN, R. & ADAMS, J. C. 2006. Phylogenetic analysis of the tenascin gene family: evidence of origin early in the chordate lineage. *BMC Evol Biol,* 6**,** 60.

UDALOVA, I. A., RUHMANN, M., THOMSON, S. J. & MIDWOOD, K. S. 2011. Expression and immune function of tenascin-C. *Crit Rev Immunol,* 31**,** 115-45.

UNGARO, R., FUKATA, M., HSU, D., HERNANDEZ, Y., BREGLIO, K., CHEN, A., XU, R., SOTOLONGO, J., ESPANA, C., ZAIAS, J., ELSON, G., MAYER, L., KOSCO-VILBOIS, M. & ABREU, M. T. 2009. A novel Toll-like receptor 4 antagonist antibody ameliorates inflammation but impairs mucosal healing in murine colitis. *Am J Physiol Gastrointest Liver Physiol,* 296**,** G1167-79.

USHER-SMITH, J. A., SHARP, S. J. & GRIFFIN, S. J. 2016. The spectrum effect in tests for risk prediction, screening, and diagnosis. *Bmj,* 353**,** i3139.

VAMADEVAN, A. S., FUKATA, M., ARNOLD, E. T., THOMAS, L. S., HSU, D. & ABREU, M. T. 2010. Regulation of Toll-like receptor 4-associated MD-2 in intestinal epithelial cells: a comprehensive analysis. *Innate Immun,* 16**,** 93-103.

VAN DEN BRINK, G. R., BLEUMING, S. A., HARDWICK, J. C., SCHEPMAN, B. L., OFFERHAUS, G. J., KELLER, J. J., NIELSEN, C., GAFFIELD, W., VAN DEVENTER, S. J., ROBERTS, D. J. & PEPPELENBOSCH, M. P. 2004. Indian Hedgehog is an antagonist of Wnt signaling in colonic epithelial cell differentiation. *Nat Genet,* 36**,** 277-82.

VAN DEN HAM, H. J., COOPER, J. D., TOMASIK, J., BAHN, S., AERTS, J. L., OSTERHAUS, A., GRUTERS, R. A. & ANDEWEG, A. C. 2018. Dendritic cell immunotherapy followed by cART interruption during HIV-1 infection induces plasma protein markers of cellular immunity and neutrophil recruitment. *PLoS One,* 13**,** e0192278.

VAN DONGEN, H., VAN AKEN, J., LARD, L. R., VISSER, K., RONDAY, H. K., HULSMANS, H. M., SPEYER, I., WESTEDT, M. L., PEETERS, A. J., ALLAART, C. F., TOES, R. E., BREEDVELD, F. C. & HUIZINGA, T. W. 2007. Efficacy of methotrexate treatment in patients with probable rheumatoid arthritis: a double-blind, randomized, placebo-controlled trial. *Arthritis Rheum,* 56**,** 1424-32.

VAN HEEMST, J., TROUW, L. A., NOGUEIRA, L., VAN STEENBERGEN, H. W., VAN DER HELM-VAN MIL, A. H., ALLAART, C. F., SERRE, G., HOLMDAHL, R., HUIZINGA, T. W., TOES, R. E. & VAN DER WOUDE, D. 2015. An investigation of the added value of an ACPA multiplex assay in an early rheumatoid arthritis setting. *Arthritis Res Ther,* 17**,** 276.

VAN OOSTERHOUT, M., BAJEMA, I., LEVARHT, E. W., TOES, R. E., HUIZINGA, T. W. & VAN LAAR, J. M. 2008. Differences in synovial tissue infiltrates between anti-cyclic citrullinated peptide-positive rheumatoid arthritis and anti-cyclic citrullinated peptide-negative rheumatoid arthritis. *Arthritis Rheum,* 58**,** 53-60.

VAN VENROOIJ, W. J., VAN BEERS, J. J. & PRUIJN, G. J. 2011. Anti-CCP antibodies: the past, the present and the future. *Nat Rev Rheumatol,* 7**,** 391-8.

VAN VENROOIJ, W. J. & ZENDMAN, A. J. 2008. Anti-CCP2 antibodies: an overview and perspective of the diagnostic abilities of this serological marker for early rheumatoid arthritis. *Clin Rev Allergy Immunol,* 34**,** 36-9.

VAUGHAN, L., HUBER, S., CHIQUET, M. & WINTERHALTER, K. H. 1987. A major, six-armed glycoprotein from embryonic cartilage. *Embo j,* 6**,** 349-53.

VEIGA-FERNANDES, H., COLES, M. C., FOSTER, K. E., PATEL, A., WILLIAMS, A., NATARAJAN, D., BARLOW, A., PACHNIS, V. & KIOUSSIS, D. 2007. Tyrosine kinase receptor RET is a key regulator of Peyer's patch organogenesis. *Nature,* 446**,** 547-51.

VERPOORT, K. N., JOL-VAN DER ZIJDE, C. M., PAPENDRECHT-VAN DER VOORT, E. A., IOAN-FACSINAY, A., DRIJFHOUT, J. W., VAN TOL, M. J., BREEDVELD, F. C., HUIZINGA, T. W. & TOES, R. E. 2006. Isotype distribution of anti-cyclic citrullinated peptide antibodies in undifferentiated arthritis and rheumatoid arthritis reflects an ongoing immune response. *Arthritis Rheum,* 54**,** 3799-808.

VERSINI, M., JEANDEL, P. Y., ROSENTHAL, E. & SHOENFELD, Y. 2014. Obesity in autoimmune diseases: not a passive bystander. *Autoimmun Rev,* 13**,** 981-1000.

VERSTRAETEN, A. A., MACKIE, E. J., HAGEMAN, P. C., HILGERS, J., SCHOL, D. J., DE JONGH, G. J. & SCHALKWIJK, J. 1992. Tenascin expression in basal cell carcinoma. *Br J Dermatol,* 127**,** 571-4.

VON LAMPE, B., BARTHEL, B., COUPLAND, S. E., RIECKEN, E. O. & ROSEWICZ, S. 2000. Differential expression of matrix metalloproteinases and their tissue inhibitors in colon mucosa of patients with inflammatory bowel disease. *Gut,* 47**,** 63-73.

VOSSENAAR, E. R., DESPRES, N., LAPOINTE, E., VAN DER HEIJDEN, A., LORA, M., SENSHU, T., VAN VENROOIJ, W. J. & MENARD, H. A. 2004. Rheumatoid arthritis specific anti-Sa antibodies target citrullinated vimentin. *Arthritis Res Ther,* 6**,** R142-50.

WALLNER, K., LI, C., SHAH, P. K., WU, K. J., SCHWARTZ, S. M. & SHARIFI, B. G. 2004. EGF-Like domain of tenascin-C is proapoptotic for cultured smooth muscle cells. *Arterioscler Thromb Vasc Biol,* 24**,** 1416-21.

WASHIZU, K., KIMURA, S., HIRAIWA, H., MATSUNAGA, K., KUWABARA, M., ARIYOSHI, Y., KATO, K. & TAKEUCHI, K. 1993. Development and application of an enzyme immunoassay for tenascin. *Clin Chim Acta,* 219**,** 15-22.

WEIGMANN, B., TUBBE, I., SEIDEL, D., NICOLAEV, A., BECKER, C. & NEURATH, M. F. 2007. Isolation and subsequent analysis of murine lamina propria mononuclear cells from colonic tissue. *Nat Protoc,* 2**,** 2307-11.

WEISMANN, M., GUSE, A. H., SOROKIN, L., BROKER, B., FRIESER, M., HALLMANN, R. & MAYR, G. W. 1997. Integrin-mediated intracellular Ca2+ signaling in Jurkat T lymphocytes. *J Immunol,* 158**,** 1618-27.

WELLER, A., BECK, S. & EKBLOM, P. 1991. Amino acid sequence of mouse tenascin and differential expression of two tenascin isoforms during embryogenesis. *J Cell Biol,* 112**,** 355-62.

WELLS, C. A., RAVASI, T. & HUME, D. A. 2005. Inflammation suppressor genes: please switch out all the lights. *J Leukoc Biol,* 78**,** 9-13.

WEVERS-DE BOER, K., VISSER, K., HEIMANS, L., RONDAY, H. K., MOLENAAR, E., GROENENDAEL, J. H., PEETERS, A. J., WESTEDT, M. L., COLLEE, G., DE SONNAVILLE, P. B., GRILLET, B. A., HUIZINGA, T. W. & ALLAART, C. F. 2012. Remission induction therapy with methotrexate and prednisone in patients with early rheumatoid and undifferentiated arthritis (the IMPROVED study). *Ann Rheum Dis,* 71**,** 1472-7.

WILLEMZE, A., BOHRINGER, S., KNEVEL, R., LEVARHT, E. W., STOEKEN-RIJSBERGEN, G., HOUWING-DUISTERMAAT, J. J., VAN DER HELM-VAN MIL, A. H., HUIZINGA, T. W., TOES, R. E. & TROUW, L. A. 2012. The ACPA recognition profile and subgrouping of ACPA-positive RA patients. *Ann Rheum Dis,* 71**,** 268-74.

WIRTZ, S., NEUFERT, C., WEIGMANN, B. & NEURATH, M. F. 2007. Chemically induced mouse models of intestinal inflammation. *Nat Protoc,* 2**,** 541-6.

WIRTZ, S., POPP, V., KINDERMANN, M., GERLACH, K., WEIGMANN, B., FICHTNER-FEIGL, S. & NEURATH, M. F. 2017. Chemically induced mouse models of acute and chronic intestinal inflammation. *Nat Protoc,* 12**,** 1295-1309.

WU, C., OROZCO, C., BOYER, J., LEGLISE, M., GOODALE, J., BATALOV, S., HODGE, C. L., HAASE, J., JANES, J., HUSS, J. W., 3RD & SU, A. I. 2009. BioGPS: an extensible and customizable portal for querying and organizing gene annotation resources. *Genome Biol,* 10**,** R130.

XIE, K., LIU, Y., HAO, W., WALTER, S., PENKE, B., HARTMANN, T., SCHACHNER, M. & FASSBENDER, K. 2013. Tenascin-C deficiency ameliorates Alzheimer's disease-related pathology in mice. *Neurobiol Aging,* 34**,** 2389-98.

YAGI, H., YANAGISAWA, M., SUZUKI, Y., NAKATANI, Y., ARIGA, T., KATO, K. & YU, R. K. 2010. HNK-1 epitope-carrying tenascin-C spliced variant regulates the proliferation of mouse embryonic neural stem cells. *J Biol Chem,* 285**,** 37293-301.

YAMAMOTO, K., DANG, Q. N., KENNEDY, S. P., OSATHANONDH, R., KELLY, R. A. & LEE, R. T. 1999. Induction of tenascin-C in cardiac myocytes by mechanical deformation. Role of reactive oxygen species. *J Biol Chem,* 274**,** 21840-6.

YAMAUCHI, M., MIZUHARA, Y., MAEZAWA, Y. & TODA, G. 1994. Serum tenascin levels in chronic liver disease. *Liver,* 14**,** 148-53.

YAN, Y., KOLACHALA, V., DALMASSO, G., NGUYEN, H., LAROUI, H., SITARAMAN, S. V. & MERLIN, D. 2009. Temporal and spatial analysis of clinical and molecular parameters in dextran sodium sulfate induced colitis. *PLoS One,* 4**,** e6073.

YANAI, H. & HANAUER, S. B. 2011. Assessing response and loss of response to biological therapies in IBD. *Am J Gastroenterol,* 106**,** 685-98.

YASUDA, M., HARADA, N., HARADA, S., ISHIMORI, A., KATSURA, Y., ITOIGAWA, Y., MATSUNO, K., MAKINO, F., ITO, J., ONO, J., TOBINO, K., AKIBA, H., ATSUTA, R., IZUHARA, K. & TAKAHASHI, K. 2018. Characterization of tenascin-C as a novel biomarker for asthma: utility of tenascin-C in combination with periostin or immunoglobulin E. *Allergy Asthma Clin Immunol,* 14**,** 72.

YE, B. D. & MCGOVERN, D. P. 2016. Genetic variation in IBD: progress, clues to pathogenesis and possible clinical utility. *Expert Rev Clin Immunol,* 12**,** 1091-107.

YE, J., COULOURIS, G., ZARETSKAYA, I., CUTCUTACHE, I., ROZEN, S. & MADDEN, T. L. 2012. Primer-BLAST: a tool to design target-specific primers for polymerase chain reaction. *BMC Bioinformatics,* 13**,** 134.

YLATUPA, S., MERTANIEMI, P., HAGLUND, C. & PARTANEN, P. 1995. Enzyme immunoassay for quantification of tenascin in biologic samples. *Clin Biochem,* 28**,** 263-8.

YOKOSAKI, Y., MATSUURA, N., HIGASHIYAMA, S., MURAKAMI, I., OBARA, M., YAMAKIDO, M., SHIGETO, N., CHEN, J. & SHEPPARD, D. 1998. Identification of the ligand binding site for the integrin alpha9 beta1 in the third fibronectin type III repeat of tenascin-C. *J Biol Chem,* 273**,** 11423-8.

YOKOSAKI, Y., MONIS, H., CHEN, J. & SHEPPARD, D. 1996. Differential effects of the integrins alpha9beta1, alphavbeta3, and alphavbeta6 on cell proliferative responses to tenascin. Roles of the beta subunit extracellular and cytoplasmic domains. *J Biol Chem,* 271**,** 24144-50.

YOKOSAKI, Y., PALMER, E. L., PRIETO, A. L., CROSSIN, K. L., BOURDON, M. A., PYTELA, R. & SHEPPARD, D. 1994. The integrin alpha 9 beta 1 mediates cell attachment to a non-RGD site in the third fibronectin type III repeat of tenascin. *J Biol Chem,* 269**,** 26691-6.

YOKOUCHI, Y., OHARASEKI, T., ENOMOTO, Y., SATO, W., IMANAKA-YOSHIDA, K. & TAKAHASHI, K. 2019. Expression of tenascin C in cardiovascular lesions of Kawasaki disease. *Cardiovasc Pathol,* 38**,** 25-30.

YOKOYAMA, K., ERICKSON, H. P., IKEDA, Y. & TAKADA, Y. 2000. Identification of amino acid sequences in fibrinogen gamma -chain and tenascin C C-terminal domains critical for binding to integrin alpha vbeta 3. *J Biol Chem,* 275**,** 16891-8.

YOSHIDA, J., WAKABAYASHI, T., OKAMOTO, S., KIMURA, S., WASHIZU, K., KIYOSAWA, K. & MOKUNO, K. 1994. Tenascin in cerebrospinal fluid is a useful biomarker for the diagnosis of brain tumour. *J Neurol Neurosurg Psychiatry,* 57**,** 1212-5.

YOUNG, S. L., CHANG, L. Y. & ERICKSON, H. P. 1994. Tenascin-C in rat lung: distribution, ontogeny and role in branching morphogenesis. *Dev Biol,* 161**,** 615-25.

ZAVADA, J., UHER, M., SVOBODOVA, R., OLEJAROVA, M., HUSAKOVA, M., CIFERSKA, H., HULEJOVA, H., TOMCIK, M., SENOLT, L. & VENCOVSKY, J. 2015. Serum tenascin-C discriminates patients with active SLE from inactive patients and healthy controls and predicts the

need to escalate immunosuppressive therapy: a cohort study. *Arthritis Res Ther,* 17**,** 341.

ZENDEDEL, A., KASHANI, I. R., AZIMZADEH, M., PASBAKHSH, P., OMIDI, N., GOLESTANI, A., BEYER, C. & CLARNER, T. 2016. Regulatory effect of triiodothyronine on brain myelination and astrogliosis after cuprizone-induced demyelination in mice. *Metab Brain Dis,* 31**,** 425-33.

ZHANG, C., HE, A., LIU, S., HE, Q., LUO, Y., HE, Z., CHEN, Y., TAO, A. & YAN, J. 2019. Inhibition of HtrA2 alleviated dextran sulfate sodium (DSS)-induced colitis by preventing necroptosis of intestinal epithelial cells. *Cell Death Dis,* 10**,** 344.

ZHAO, X., OKEKE, N. L., SHARPE, O., BATLIWALLA, F. M., LEE, A. T., HO, P. P., TOMOOKA, B. H., GREGERSEN, P. K. & ROBINSON, W. H. 2008. Circulating immune complexes contain citrullinated fibrinogen in rheumatoid arthritis. *Arthritis Res Ther,* 10**,** R94.

ZHEN, E. Y., BRITTAIN, I. J., LASKA, D. A., MITCHELL, P. G., SUMER, E. U., KARSDAL, M. A. & DUFFIN, K. L. 2008. Characterization of metalloprotease cleavage products of human articular cartilage. *Arthritis Rheum,* 58**,** 2420-31.

ZIGMOND, E., BERNSHTEIN, B., FRIEDLANDER, G., WALKER, C. R., YONA, S., KIM, K. W., BRENNER, O., KRAUTHGAMER, R., VAROL, C., MULLER, W. & JUNG, S. 2014. Macrophage-restricted interleukin-10 receptor deficiency, but not IL-10 deficiency, causes severe spontaneous colitis. *Immunity,* 40**,** 720-33.

ZIZZO, G., HILLIARD, B. A., MONESTIER, M. & COHEN, P. L. 2012. Efficient clearance of early apoptotic cells by human macrophages requires M2c polarization and MerTK induction. *J Immunol,* 189**,** 3508-20.

ZULIANI-ALVAREZ, L., MARZEDA, A. M., DELIGNE, C., SCHWENZER, A., MCCANN, F. E., MARSDEN, B. D., PICCININI, A. M. & MIDWOOD, K. S. 2017. Mapping tenascin-C interaction with toll-like receptor 4 reveals a new subset of endogenous inflammatory triggers. *Nat Commun,* 8**,** 1595.

Appendix

Appendix I - Commercial buffer recipes

TE buffer

1mM EDTA, 10mM Tris-HCl pH8

1x TAE buffer

1mM EDTA, 0.1 % acetic acid, 40mM Tris

10x PCR buffer

500mM KCl, 200mM Tris-HCl pH 8.4

5X First-Strand Buffer

75mM KCl, 15mM $MgCl_2$, 250mM Tris-HCl, pH 8.3

Radioimmunoprecipitation assay (RIPA) buffer

150mM NaCl, 1% NP-40, 1% sodium deoxycholate, 0.1% SDS, 25mM Tris-HCl pH7.6

Ponceau S Solution

0.1% Ponceau S, 5% Acetic Acid

Appendix II - Primary antibodies

Immunofluorescence

Target	Antibody Name	Supplier	Species and isotype	Working concentration
Tenascin-C	MTn-12	Sigma-Aldrich	Rat monoclonal IgG1	1µg/ml
	NSCT-121	Nascient Ltd	Human monoclonal IgG4	1µg/ml
CD3	17A2	Biolegend	Rat monoclonal IgG2b	10µg/ml
B220	RA3-6B2	Biolegend	Rat monoclonal IgG2a	1µg/ml
CD11c	HL3	Biolegend	Armenian Hamster monoclonal IgG	10µg/ml
CD31	MEC13.3	Biolegend	Rat monoclonal IgG2a	1µg/ml
CD326	G8.8	Biolegend	Rat monoclonal IgG2a	1µg/ml
LYVE-1	ab14917	Abcam	Rabbit polyclonal	10µg/ml
Collagen IV	ab6586	Abcam	Rabbit polyclonal	1µg/ml
αSMA	ab21027	Abcam	Goat polyclonal	1µg/ml

Western blotting

Target	Antibody Name	Supplier	Species and isotype	Working concentration or dilution
Tenascin-C	MTn-12	Sigma-Aldrich	Rat monoclonal IgG1	1µg/ml
	NSCT-121	Nascient Ltd	Human monoclonal IgG4	1µg/ml
	B12	Nascient Ltd	Mouse monoclonal IgG2a	10µg/ml
	BC-24	Sigma-Aldrich	Mouse monoclonal IgG1	1µg/ml
Fibronectin	F14	Abcam	Rabbit monoclonal IgG	0.27µg/ml
β-Actin	13E5	Cell Signalling Technology	Rabbit monoclonal IgG	1 in 5000

Appendix III - Secondary antibodies and reagents

Immunofluorescence

Target	Antibody Name	Supplier	Conjugate	Working concentration
Anti-rat IgG	A-11006	Sigma-Aldrich	Alexa Fluor 488	2µg/ml
Anti-rat IgG	112-065-167	Jackson Immunoresearch	Biotin	2µg/ml
Anti-rat IgG1	MRG1-58	Biolegend	FITC	2µg/ml
Anti-rat IgG2a	MRG2a-83	Biolegend	Alexa Fluor 594	2µg/ml
Anti-rat IgG2b	MRG2b-85	Biolegend	Alexa Fluor 594	2µg/ml
Anti-rabbit IgG	A-11012	Biolegend	Alexa Fluor 594	2µg/ml
Anti-Armenian hamster IgG	Poly4055	Biolegend	Alexa Fluor 594	2µg/ml
Anti-goat IgG	SA5-10080	Thermo Fisher	DyLight 594	2µg/ml
Anti-human IgG	A-11014	Thermo Fisher	Alexa Fluor 594	2µg/ml
Streptavidin	405240	Biolegend	Alexa Fluor 594	2µg/ml

Western blotting

Target	Antibody Name	Supplier	Conjugate	Working concentration
Anti-human IgG	926-32232	LI-COR Biosciences	IRDye 800CW	0.3µg/ml
Anti-mouse IgG	926-32212	LI-COR Biosciences	IRDye 800CW	0.3µg/ml
Anti-rat IgG	926-32219	LI-COR Biosciences	IRDye 800CW	0.3µg/ml
Anti-rabbit IgG	926-68073	LI-COR Biosciences	IRDye 680RD	0.3µg/ml

Appendix IV - Genotyping and qPCR primers

Target Gene	Supplier	Pair	Sequence (5'-3')
Genotyping			
Tnc	Sigma-Aldrich	F	GAAGTCACTAGAAACTAGTGGACAACTC
		R	AAGATGCCTGGCAGTAGCCAGGTCAC
LacZ	Sigma-Aldrich	F	GAAGTCACTAGAAACTAGTGGACAACTC
		R	CTCCATGCTTGGAACAACGAGCGCAGC
qPCR			
Tnc	PrimerDesign	F	GCCACAGCCTGCCTACTG
		R	GGTTAAGCCACAACGAGTTCC
18S rRNA	Sigma-Aldrich	F	GTAACCCGTTGAACCCCATT
		R	CCATCCAATCGGTAGTAGCG
Il-6	Sigma-Aldrich	F	TTCCATCCAGTTGCCTTCTTG
		R	AGGTCTGTTGGGAGTGGTATC
Il-10	Sigma-Aldrich	F	CCCTTTGCTATGGTGTCCTTTC
		R	GATCTCCCTGGTTTCTCTTCCC
TNFα	Sigma-Aldrich	F	CAGACCCTCACACTCAGATCATC
		R	GGCTACAGGCTTGTCACTCG
Il-12a (p35)	Sigma-Aldrich	F	TATCTCTATGGTCAGCGTTCC
		R	TGGTCTTCAGCAGGTTTCG
Il-1β	Sigma-Aldrich	F	GACGGACCCCAAAAGATGAAGG
		R	GTGATACTGCCTGCCTGAAGC
Il-23a	Sigma-Aldrich	F	CAACTTCACACCTCCCTAC
		R	CCACTGCTGACTAGAACTC
Il-17a	Sigma-Aldrich	F	TTTAACTCCCTTGGCGCAAAA
		R	CTTTCCCTCCGCATTGACAC
TGF-β1	Sigma-Aldrich	F	CCACCTGCAAGACCATCGAC
		R	CTGGCGAGCCTTAGTTTGGAC
Cxcl1	Sigma-Aldrich	F	ACTGCACCCAAACCGAAGTC
		R	TGGGGACACCTTTTAGCATCTT
IFNγ	Sigma-Aldrich	F	TCAAGTGGCATAGATGTGGAAGAA
		R	TGGCTCTGCAGGATTTTCATG
Il-22	Sigma-Aldrich	F	ATGAGTTTTTCCCTTATGGGGAC
		R	GCTGGAAGTTGGACACCTCAA

Appendix V - DSS study health monitoring scoring sheet

DSS Study Scoring Sheet

Mouse ID:

Cage ID (DSS%): DSS OFF

Date:

APPEARANCE											
Coat lost sheen											
Coat staring											
Hair loss											
Failure to groom											
Discharge from eyes or nose											
Hunched body											
Change in gait											
BEHAVIOR											
Change in temperament											
Isolated, away from others											
Restless											
Reluctant to move											
Recumbent											
DSS Symptoms											
Stool Consistency											
Fecal Blood											
CLINICAL SIGNS											*Minimum Weight*
Weight (g)											
Cold to touch											
Breathing abnormal											

H2O Consumption: (g)						

Score System

Normal (no fecal blood/Normal well formed feaces) = 0

Slightly abnormal (blood visible in stool/soft pasty stool) = 1

Significant change (gross rectal bleeding/diarrhea liquid stool) = 2

Euthanasia will be performed when the following criteria are met:

- A score of 2 is given to 3 or more parameters (except for “clinical signs”)
- A total score of 5 is reached from any parameters
- Both cold to touch/abnormal breathing clinical signs receive a score of 1
- An overall weight loss of over 20% is observed

Appendix VI - Supplementary images of WT and *Tnc*$^{-/-}$ colon sections

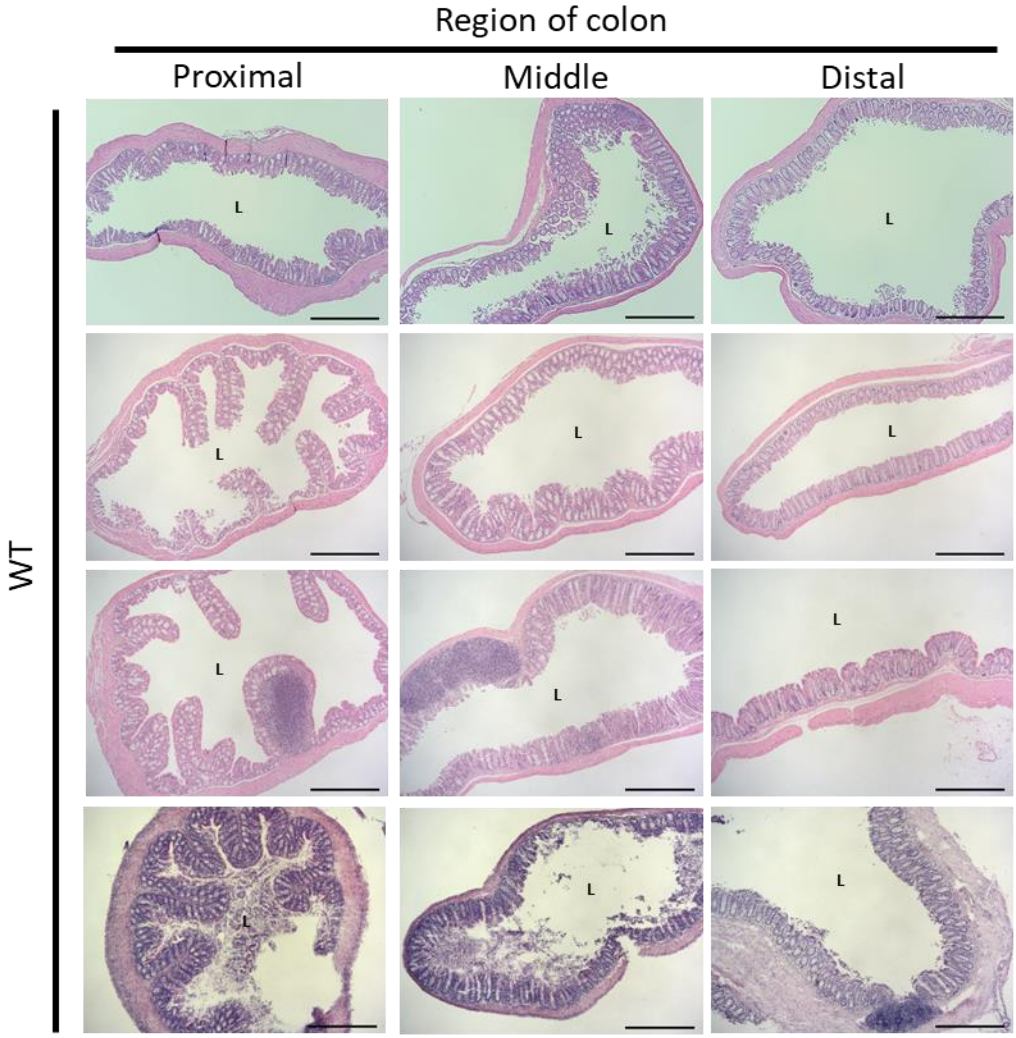

Representative H&E stained colon sections from WT(Ox) and *Tnc*$^{-/-}$ mice

Representative H&E stained transverse proximal, middle, and distal colon sections from 7-9 week-old WT(Ox) (above) and *Tnc*$^{-/-}$ mice (following page). Histologically along it's full length the colon tissue from *Tnc*$^{-/-}$ mice appears the same as that from WT(Ox) mice. No abnormalities were observed in the tissue taken from either genotype.
Images captured using a Nikon E600 brightfield microscope. Scale bars = 1000µm. L = lumen.

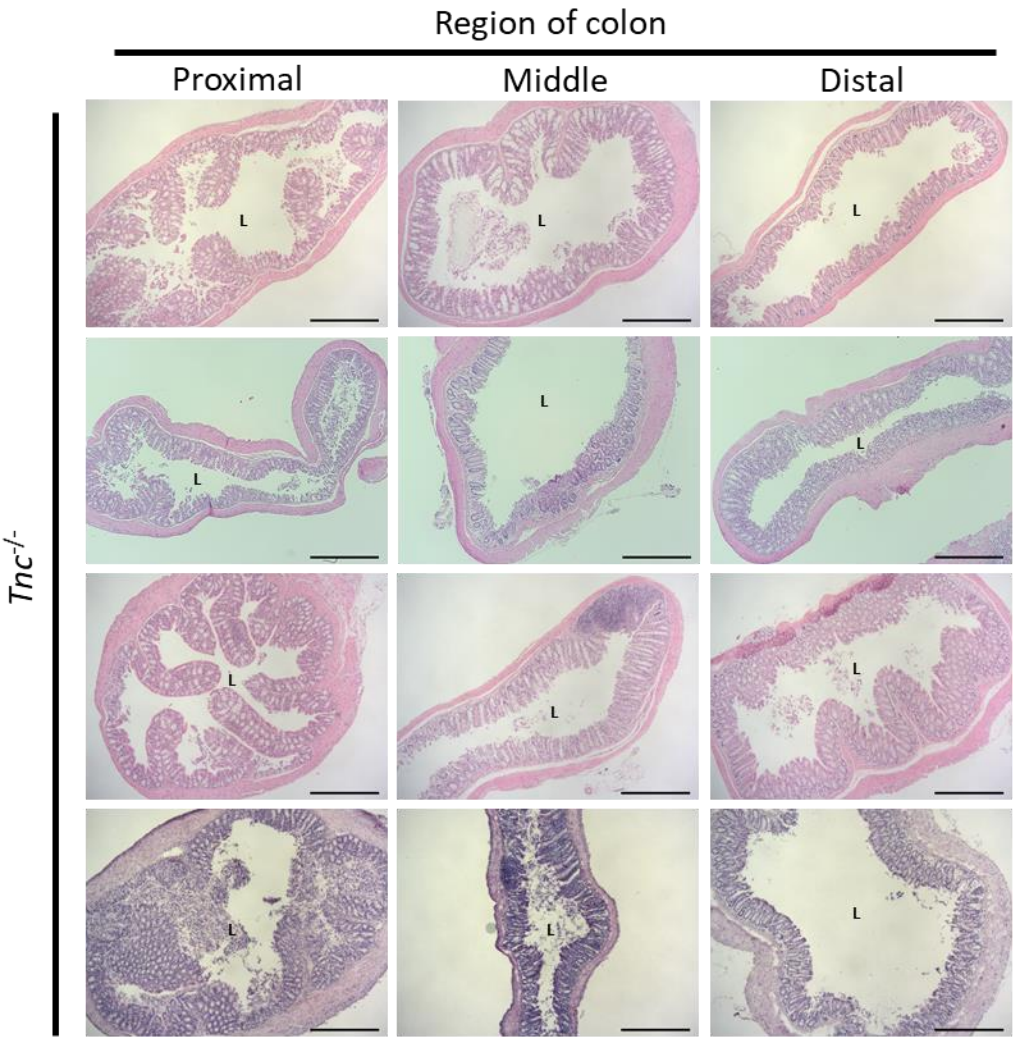

Representative H&E stained colon sections from WT(Ox) and *Tnc*$^{-/-}$ mice Contd.

Images captured using a Nikon E600 brightfield microscope. Scale bars = 1000µm. L = lumen.